CONFIDENTIAL

C70-448

CLASSIFICATION CHANGED
UNCLASSIFIED
TO
By Authority of Date 6-28-72

NASA-CR-72627
GA-8956

(NASA-CR-72627) STUDIES OF THERMIONIC MATERIALS FOR SPACE POWER APPLICATIONS Summary Report, 1 Feb. 1967 - 31 Jul. 1969 (Gulf General Atomic) 9 Dec. 1969 324 p
N72-74679
Unclas
00/99 38174

(THRU)
(CODE)
(CATEGORY)
(ACCESSION NUMBER)
(PAGES)
(NASA CR OR TMX OR AD NUMBER)
FF No. 602(D)
AVAILABLE TO U.S. GOVERNMENT AGENCIES AND CONTRACTORS ONLY
X70-19027

(Title Unclassified)

STUDIES OF THERMIONIC MATERIALS FOR SPACE POWER APPLICATIONS

SUMMARY REPORT

FEBRUARY 1, 1967 THROUGH JULY 31, 1969

By Authority of Date
TO
CLASSIFICATION CHANGED
UNCLASSIFIED

Prepared for
National Aeronautics and Space Administration
Lewis Research Center
under Contract NAS 3-8504

GROUP-1
Excluded from automatic downgrading and declassification

RESTRICTED DATA
ATOMIC ENERGY ACT 1954

Gulf General Atomic
Incorporated

Issued: December 9, 1969

CONFIDENTIAL

NOTICE

This report was prepared as an account of Government sponsored work. Neither the United States, nor the National Aeronautics and Space Administration (NASA), nor any person acting on behalf of NASA:

A. Makes any warranty or representation, expressed or implied, with respect to the accuracy, completeness, or usefulness of the information contained in this report, or that the use of any information, apparatus, method, or process disclosed in this report may not infringe privately owned rights; or

B. Assumes any liabilities with respect to the use of, or for damages resulting from the use of any information, apparatus, method or process disclosed in this report.

As used above, "person acting on behalf of NASA" includes any employee or contractor of NASA, or employee of such contractor, to the extent that such employee or contractor of NASA, or employee of such contractor prepares, disseminates, or provides access to, any information pursuant to his employment or contract with NASA, or his employment with such contractor.

Requests for copies of this report should be referred to:

National Aeronautics and Space Administration
Office of Scientific and Technical Information
Attention: AFSS-A
Washington, D. C. 20546

CONFIDENTIAL

C70-448

Copy No. 27

Gulf General Atomic
Incorporated
P. O. Box 608, San Diego, California 92112

NASA-CR-72627
GA-8956

(Title Unclassified)

STUDIES OF THERMIONIC MATERIALS FOR SPACE POWER APPLICATIONS

SUMMARY REPORT

FEBRUARY 1, 1967 THROUGH JULY 31, 1969

Sponsored by
National Aeronautics and Space Administration
Lewis Research Center

Technical Management
NASA-Lewis Research Center
Reactor Irradiation Branch
J. W. R. Creagh

During the period of this report, the following "reportable items" as defined by the article "Report of New Technology" evolved:

(1) Preparation of {110} oriented tungsten emitters for high performance converter application.

(2) Preparation of UC-ZrC of stable open pore structures as high temperature fuel materials.

GROUP-1
Excluded from automatic downgrading and declassification

RESTRICTED DATA
ATOMIC ENERGY ACT 1954

Project: 552
Contract: NAS 3-8504

Issued: December 9, 1969

CONFIDENTIAL

PREVIOUS SUMMARY REPORT IN THIS SERIES

Contract NAS 5-1253	GA-3523, Final Report for the Period Ending August 31, 1962. (U)
Contract NAS 3-2301	GA-3642, Final Report for the Period Ending August 31, 1962. (U)
Contract NAS 3-2532	GA-4769, Final Report for the Period Ending August 31, 1963. Part I (U), Part II (C/RD).
Contract NAS 3-4165	NASA CR-54322, GA-5665, Summary Report for the Period September 1, 1963 through August 31, 1964. (C/RD)
Contract NAS 3-6471	NASA CR-54980, GA-6860, Summary Report for the Period September 1, 1964, through November 23, 1965. (C/RD)
Contract NAS 3-8504	NASA CR-72315, GA-7682, Summary Report for the Period November 23, 1965 through January 31, 1967. (C/RD)
Contract NAS 3-6471	NASA CR-72517, GA-8974, Summary Report for the Period November 23, 1965 through September 30, 1968. (C/RD)

(This page is Unclassified)

RESTRICTED DATA
ATOMIC ENERGY ACT 1954
GROUP 1

CONFIDENTIAL

CONTENTS

INTRODUCTION 1

PART I. 2

SUMMARY 2

1.1. VACUUM EMISSION STABILITY OF TUNGSTEN CLAD 90UC-10ZrC AT 1800°C 5

1.1.1. Vacuum Work Function Measurements. 6
1.1.2. Post-test Chemical Analysis of Collector Condensate, Tungsten Cladding and Carbide Fuel . . 6
1.1.3. Metallographic and Electron Microprobe Examinations 11
1.1.4. Conclusions and Discussions 11

1.2. PREPARATION OF PLANAR TUNGSTEN EMITTER STRUCTURES 16

1.2.1. B_5 Series Emitter Structures 16
1.2.2. B_6 Series Emitter Structures 16
1.2.3. B_7 Series Emitter Structures 30
1.2.4. B_8 Series Emitter Structures 30
1.2.5. C_1 Series Emitter Structures 36
1.2.6. C_2 Series Emitter Structures 46
1.2.7. C_3 Series Emitter Structures 46
1.2.8. D_1 Series Emitter Structures 47

1.3. POST OPERATIONAL EXAMINATION OF EMITTER STRUCTURES 53

1.3.1. B_6-2 Emitter Structure 53
1.3.2. C_1-2 Emitter Structure 67
1.3.3. Emitter Structures C_1-4 and C_1-5 72
1.3.4. C_3-3 Emitter Structure 85
1.3.5. D_1-1 Emitter Structure 89

REFERENCES. 100

PART II. POST-OPERATIONAL ANALYSIS OF CESIUM CONTENTS IN OUT-OF-PILE LIFE TESTING CONVERTER COMPONENTS. 101

SUMMARY 101

2.1. INTRODUCTION 102

2.2. SAMPLE ACQUISITION 102

CONFIDENTIAL

RESTRICTED DATA
ATOMIC ENERGY ACT 1954
GROUP 1

CONFIDENTIAL

CONTENTS (Continued)

2.3. ANALYTICAL TECHNIQUES 105

2.4. ANALYTICAL RESULTS 107

2.4.1. Blank Samples 107
2.4.2. Results for Components of LC-3, LC-4 and LC-5 . . 108

2.5. CONCLUSIONS AND DISCUSSIONS 113

REFERENCES 114

PART III. CHEMICAL VAPOR-DEPOSITION OF CHLORIDE TUNGSTEN 115

SUMMARY 115

3.1. ESTABLISHMENT OF CONDITIONS FOR DEPOSITING {110} ORIENTED TUNGSTEN OF HIGH VACUUM WORK FUNCTION BY HYDROGEN REDUCTION OF TUNGSTEN CHLORIDE 116

3.1.1. WCl_6 Powder as Source of Tungsten Chloride 116

3.1.1.1. Experimental Arrangement 116
3.1.1.2. Experimental Procedures 119
3.1.1.3. Experimental Results 120

3.1.2. Source Material Provided by "In Situ" Chlorination of Tungsten Chips 120

3.1.2.1. Experimental Arrangement 120
3.1.2.2. Experimental Procedures 123
3.1.2.3. Experimental Results 124

3.2. EVALUATION OF REPRODUCIBILITY AND STABILITY OF DEGREE OF {110} PREFERRED ORIENTATION AND VACUUM WORK FUNCTION OF TUNGSTEN DEPOSITED UNDER CONDITIONS ESTABLISHED IN SECTION 3.1 129

3.2.1. Reproducibility Test 129

3.2.1.1. Chloride Tungsten Samples 1L Through 10L 130
3.2.1.2. Duplex Tungsten Samples 1DL Through 10DL 130

3.2.2. Emission Stability Test. 144
3.2.3. Cesiated Emission Test 159

REFERENCES. 182

CONFIDENTIAL

RESTRICTED DATA
ATOMIC ENERGY ACT 1954
GROUP 1

CONFIDENTIAL

CONTENTS (Continued)

PART IV. UC-ZrC SINTERING STUDIES 183

SUMMARY 183

4.1. PREPARATION OF UC-ZrC SAMPLES 185

4.1.1. Physical and Chemical Characteristics of Samples . . 185
4.1.2. Procedures for Preparation of Samples. 186
4.1.3. Selection of Sintering Temperatures for 90UC-10ZrC and 50UC-50ZrC Samples. 187

4.2. SAMPLE CHARACTERIZATION. 190

4.3. EVALUATION OF STABILITY OF OPEN POROSITY 194

4.4. POST-TEST EVALUATION 201

4.4.1. Microstructures 201
4.4.2. Compositions, Stoichiometries and Impurity Contents. 210

REFERENCES. 210

PART V. PERFORMANCE STABILITY TESTS ON FUELED AND UNFUELED CESIUM THERMIONIC CONVERTERS 212

SUMMARY 212

5.1. INTRODUCTION 214

5.2. LC-7 TEST (UNFUELED CONVERTER) 217

5.2.1. LC-7 Initial Performance 218
5.2.2. LC-7 Operating History 223
5.2.3. LC-7 Diagnostic Data 231
5.2.4. Interpretation of the LC-7 Results 234

5.3. LC-8 TEST (90UC-10ZrC) 234

5.3.1. LC-8 Initial Performance 235
5.3.2. LC-8 Operating History 235
5.3.3. LC-8 Diagnostic Data 248
5.3.4. Interpretation of the LC-8 Results 251

5.4. LC-9 TEST (UNFUELED HIGH-WORK-FUNCTION EMITTER). 253

5.4.1. LC-9 Initial Performance 253
5.4.2. LC-9 Operating History 260
5.4.3. LC-9 Diagnostic Data 267
5.4.4. Interpretation of the LC-9 Results 270

REFERENCES. 273

CONFIDENTIAL

RESTRICTED DATA
ATOMIC ENERGY ACT 1954
GROUP 1

CONTENTS (Continued)

APPENDIX 5A. EMITTER TEMPERATURE PROFILE AND VACUUM WORK FUNCTIONS 274

REFERENCE 288

APPENDIX 5B. STABILITY OF HIGH TEMPERATURE THERMOCOUPLES 289

APPENDIX 5C. POST-OPERATIONAL METALLOGRAPHIC EXAMINATION OF LC-7 CONVERTER 292

RESTRICTED DATA
ATOMIC ENERGY ACT 1954
GROUP 1

FIGURES

1.1 (U) Effective work function of Sample 2A-1 (vapor-deposited fluoride tungsten clad 90UC-10ZrC) as a function of time at 1800°C 7

1.2 (U) Effective work function of Sample 2A-2 (vapor-deposited fluoride tungsten clad 90UC-10ZrC) as a function of time at 1800°C 8

1.3 (U) Effective work function of Sample 2A-2 (vapor-deposited fluoride tungsten clad 90UC-10ZrC) as a function of time during thermal cycling between 1800°C and 1300°C after 10,000 hours at 1800°C 9

1.4 (U) Stabilized effective work function as a function of temperature for Sample 2A-2 (W clad 90UC-10ZrC) following the 10,000 hour life test at 1800°C 10

1.5 (U) Appearance of the fuel-clad interface of Sample 2A-1 after the test 13

1.6 (U) Microstructures of one of the Ta-10W discs used for the preparation of B_6 series emitter structures after annealing for 15 hours at 1850°C in 5 x 10^{-8} torr vacuum. Note clean grain structures 27

1.7 (U) Microstructures of a cross section of the Ta-10W region of B_6-4 emitter structure. Note clean grain structures. 28

1.8 (U) Spatial distribution of the <100> axes in emitter structure B_6-2 before delivery to NASA 31

1.9 (U) Surface microstructures of emitter structure B_6-2 before delivery to NASA 32

1.10 (U) Effective work function as a function of time at 1650°C for Sample B_7-1 33

1.11 (U) Appearance of W-Ta interface of B_7-1 after vacuum work function study at 1650°C for 400 hours. Note numerous Kirkendall voids on Ta side near the interface 34

RESTRICTED DATA
ATOMIC ENERGY ACT 1954
GROUP 1

FIGURES (Continued)

1.12 (U) Appearance of W-Ta interface of B_8-1 after 100 hour heat treatment at 2200°C, followed by thermal cycling 15 times between 1650°C and room temperature. Note the number of Kirkendall voids is much less than that of B_7-1 (see Fig. 1.10) 37

1.13 (U) Spatial distribution of the <110> axes in the tungsten discs used for the preparation of emitter structures C_1-1, C_1-2, C_1-4 and C_1-5 38

1.14 (U) Spatial distribution of the <110> axes in C_1-2 39

1.15 (U) Spatial distribution of the <110> axes in C_1-4 40

1.16 (U) Spatial distribution of the <110> axes in C_1-5 41

1.17 (U) Surface appearance of emitter structure C_1-2 after electropolishing 42

1.18 (U) Surface appearance of emitter structure C_1-4 after electropolishing 42

1.19 (U) Surface appearance of emitter structure C_1-5 after electropolishing 43

1.20 (U) Emitter surface of emitter structure C_1-3 after the thermal cycling test. 45

1.21 (U) Spatial distribution of the <110> axes in C_3-2 48

1.22 (U) Spatial distribution of the <110> axes in C_3-3 49

1.23 (U) Surface appearance of emitter structure C_3-2 after electropolishing 50

1.24 (U) Surface appearance of emitter structure C_3-3 after electropolishing and stress-relieving at 1800°C 50

1.25 (U) Spatial distribution of the <100> axes in D_1-1 51

1.26 (U) Appearance of the chemically etched surface of the emitter of D_1-1 52

1.27 (U) Appearance of the exterior of the B_6-2 emitter structure, as-received from NASA after operation in a cesiated converter 54

RESTRICTED DATA
ATOMIC ENERGY ACT 1954
GROUP 1

FIGURES (Continued)

1.28 (U) Presence of cracks in the vicinity of the weld between the Ta-10W lip of the emitter structure and the tantalum emitter stem in post-test B_6-2 emitter assembly. 55-57

1.29 (U) Appearance near the Ta-10W lip of the weld region in post-test B_6-2 emitter structure. The thin lip fell apart when the emitter structure was removed mechanically from the tantalum stem, and only the base of the lip is left. Note the presence of grain boundary cracks and one grain was lost. 58

1.30 (U) Post-test surface microstructure of the tungsten emitter of B_6-2 60

1.31 (U) Electron micrograph of the post-test B_6-2 emitter surface 61

1.32 (U) Spatial distribution of the <100> axes in post-tested B_6-2 62

1.33 (U) Appearance of Ta-10W substrate surface which has been subjected to electron bombardment heating during converter operation 63

1.34 (U) Magnified appearance of one of the dark patches of the Ta-10W substrate surface shown in Fig. 1.33 64

1.35 (U) Appearance of the W-(Ta-10W) interface in post-test emitter structure B_6-2 66

1.36 (U) Post-test appearance of surface of the chloride tungsten emitter of emitter structure C_1-2 68

1.37 (U) Electron micrographs of the replica of the post-test surface of the chloride tungsten emitter of emitter structure C_1-2 69-70

1.38 (U) Post-test appearance of the surface of the Ta-10W substrate of emitter structure C_1-2 71

1.39 (U) Post-test appearance of the tungsten-(Ta-10W) interface of emitter structure C_1-2 (Note: the black line at the interface is due to relief polishing, not cracks) 74-75

1.40 (U) Macroscopic appearance of the post-test surface of the chloride tungsten emitter of emitter structure C_1-4 77

RESTRICTED DATA
ATOMIC ENERGY ACT 1954
GROUP 1

FIGURES (Continued)

1.41 (U) Macroscopic appearance of the post-test surface of the chloride tungsten emitter of emitter structure C_1-5. 77

1.42 (U) Appearance of the "pimple" on the post-test surface of the chloride tungsten emitter of emitter structure C_1-4 78

1.43 (U) Distribution of <110> axes in chloride tungsten emitter structures C_1-4 and C_1-5 79

1.44 (U) Macroscopic appearance of the post-test surface of the Ta-10W substrate of the emitter structure of C_1-4 80

1.45 (U) Macroscopic appearance of the post-test surface of the Ta-10W substrate of the emitter structure of C_1-5 80

1.46 (U) Typical post-test appearance of the tungsten-(Ta-10W) interface of emitter structure C_1-4 83

1.47 (U) Typical post-test appearance of the tungsten-(Ta-10W) interface of emitter structure C_1-5 83

1.48 (U) Post-test microstructures of the Ta-10W substrate of emitter structure C_1-4 84

1.49 (U) Post-test microstructures of the Ta-10W substrate of emitter structure C_1-5 84

1.50 (U) Macroscopic appearance of the post-test duplex tungsten emitter surface of emitter structure C_3-3 86

1.51 (U) Microscopic appearance of the post-test duplex tungsten emitter surface of emitter structure C_3-3 86

1.52 (U) Distribution of <110> axes in post-test chloride tungsten emitter structure C_3-3 87

1.53 (U) Macroscopic appearance of the post-test Ta-10W substrate surface of emitter structure C_3-3. 90

1.54 (U) Post-test microstructures of the fluoride tungsten-(Ta-10W) interface of emitter structure C_3-3 90

1.55 (U) Post-test microstructures of the chloride tungsten-fluoride tungsten interface of emitter structure C_3-3 . . . 91

1.56 (U) Post-test grain structures of the Ta-10W substrate of emitter structure C_3-3 91

RESTRICTED DATA
ATOMIC ENERGY ACT 1954
GROUP 1

FIGURES (Continued)

1.57 (U) Macroscopic appearance of the post-test chemically etched fluoride tungsten emitter surface of emitter structure D_1-1 92

1.58 (U) Appearance of the surface shown in Fig. 1.57 at a higher magnification 92

1.59 (U) Electron micrograph of a replica of the post-test emitter surface of emitter structure D_1-1 93

1.60 (U) Spatial distribution of the <100> axes in the chemically etched fluoride tungsten emitter of emitter structure D_1-1 after test in a cesiated converter 94

1.61 (U) Vacuum work function of emitter structure D_1-1 as a function of time at 1600°C 96

1.62 (U) Post-test macroscopic appearance of the Ta-10W substrate surface of emitter structure D_1-1 97

1.63 (U) Unetched appearance of the tungsten-(Ta-10W) interface of emitter structure D_1-1 after test in a cesiated converter 99

1.64 (U) Etched appearance of the tungsten-(Ta-10W) interface of emitter structure D_1-1 after test in a cesiated converter 99

2.1 (U) Mark VI out-of-pile converter schematic, illustrating the nature and the locations of the samples taken for the determination of their cesium contents 104

2.2 (U) Appearance of vanadium braze region in LC-4 converter. Note pores in vanadium braze 112

2.3 (U) Cs Lα scan of the pores in the vanadium braze of Fig. 2.2. Note high concentration of cesium in pores. . . .112

3.1 (U) Chloride tungsten deposition apparatus using WCl_6 powder to provide tungsten source material 117

3.2 (U) Chloride tungsten deposition apparatus using chlorination of tungsten chips to provide tungsten source material 122

3.3 (U) Macroscopic appearance of {110} oriented chloride tungsten deposit on molybdenum mandrel 128

RESTRICTED DATA
ATOMIC ENERGY ACT 1954
GROUP 1

FIGURES (Continued)

3.4 (U) Microstructure of a cross section {110} oriented chloride tungsten deposit. 128

3.5 (U) Preferred orientation and vacuum work function in chloride tungsten as a function of deposition conditions 128

3.6 (U) Typical microstructures of a cross section of as-deposited chloride tungsten deposit 131-133

3.7 (U) Spatial distribution of <110> axes in ten chloride tungsten samples 134-143

3.8 (U) Typical microstructures of a cross section of as-deposited duplex tungsten deposit 145-147

3.9 (U) Spatial distribution of the <110> axes in ten duplex tungsten samples. 148-157

3.10 (U) Emission stability test results for five chloride tungsten samples at 1800°C 158

3.11 (U) Richardson plots for five chloride tungsten samples as a function of time at 1800°C 160-164

3.12 (U) Emission stability test results for five duplex tungsten samples at 1800°C. 165

3.13 (U) Richardson plots for five duplex tungsten samples as a function of time at 1800°C 166-170

3.14 (U) Rasor-Warner plots for five selected (110) oriented tungsten emitters 172-176

3.15 (U) Thermionic emission patterns of the five selected tungsten emitters after emission test (200X) 177-178

3.16(a)(U) Electron micrograph of the surface of Sample 5L after emission test. 179

3.16(b)(U) Electron micrograph of the surface of Sample 7DL after emission test. 180

3.17 (U) Microstructures of the cross sections of five tungsten emitters after emission test 181

4.1 (U) Surface roughness factor as a function of time at 1600°C and 1800°C for 90UC-10ZrC samples sintered at 1950°C 189

RESTRICTED DATA
ATOMIC ENERGY ACT 1954
GROUP 1

FIGURES (Continued)

4.2 (C-RD)(Gp-1) Microstructures of unetched hyperstoichiometric 90UC-10ZrC containing tungsten addition. 192

4.3 (C-RD)(Gp-1) Microstructures of unetched hyperstoichiometric 50UC-50ZrC containing tungsten addition. 193

4.4 (C-RD)(Gp-1) Etched microstructures of hyperstoichiometric 90UC-10ZrC containing tungsten addition. Sample obtained from carbide cylinder "b' " of Table 4.2 195

4.5 (C-RD)(Gp-1) Etched microstructures of hyperstoichiometric 50UC-50ZrC containing tungsten addition. Sample obtained from carbide cylinder "d" of Table 4.2 196

4.6 (U) Surface roughness factor as a function of time at 1800°C for 90UC-10ZrC and 50UC-50ZrC samples 197

4.7 (U) Surface roughness factor as a function of time at 1700°C for 90UC-10ZrC and 50UC-50ZrC samples 198

4.8 (U) Surface roughness factor as a function of time at 1600°C for 90UC-10ZrC and 50UC-50ZrC samples 199

4.9 (U) Microstructures of 90UC-10ZrC samples prepared from -44/+20 micron powder after 5000 hours at 1800°C, 1700°C and 1600°C. 202-203

4.10 (U) Microstructures of 90UC-10ZrC samples prepared from -62/+20 micron powder after 5000 hours at 1800°C, 1700°C and 1600°C. 204-205

4.11 (U) Microstructures of 50UC-50ZrC samples prepared from -44/+20 micron powder after 5000 hours at 1800°C, 1700°C and 1600°C. 206-207

4.12 (U) Microstructures of 50UC-50ZrC samples prepared from -62/+20 micron powder after 5000 hours at 1800°C, 1700°C and 1600°C. 208-209

5.1 (U) Converter design of LC-7, 8 and 9 216

5.2 (U) LC-7 cesium reservoir temperature optimization initial data. Emitter temperature 1805°C, collector temperature 750°C 219

5.3 (U) Envelope of I-V characteristics for LC-7 initial data. Emitter temperature 1805°C, collector temperature 750°C. 220

RESTRICTED DATA
ATOMIC ENERGY ACT 1954
GROUP 1

FIGURES (Continued)

5.4 (U) Maximum output power and optimum current determination for LC-7 initial data. Emitter temperature 1805°C, collector temperature 750°C 221

5.5 (U) LC-7 emitter temperature profile and thermocouple distribution in converter compared with pre-converter-assembly data 222

5.6 (U) LC-7 performance history 225

5.7 (U) LC-7 performance history 226

5.8 (U) Envelope of I-V characteristics for LC-7 228

5.9 (U) Maximum output power and optimum current determinations for LC-7 229

5.10 (U) LC-7 collector temperature optimization 232

5.11 (U) LC-7 emitter and collector work function 233

5.12 (U) LC-8 performance history 236

5.13 (U) LC-8 performance history 237

5.14 (U) LC-8 cesium reservoir temperature optimization initial data. Emitter temperature 1400°C, collector temperature 775°C, time 353 hours 238

5.15 (U) LC-8 cesium reservoir temperature optimization initial data. Emitter temperature 1400°C, collector temperature 790°C, time 1458 hours 239

5.16 (U) LC-8 cesium reservoir temperature optimization initial data. Emitter temperature 1600°C, collector temperature 800°C, time 1722 hours. 240

5.17 (U) LC-8 cesium reservoir temperature optimization initial data. Emitter temperature 1600°C, collector temperature 800°C, time 2683 hours. 241

5.18 (U) LC-8 cesium reservoir temperature optimization initial data. Emitter temperature 1800°C, collector temperature 800°C, time 3306 hours. 242

5.19 (U) LC-8 cesium reservoir temperature optimization initial data. Emitter temperature 1800°C, collector temperature 800°C, time 5987 hours. 243

RESTRICTED DATA
ATOMIC ENERGY ACT 1954
GROUP 1

FIGURES (Continued)

5.20 (U) Envelope of I-V characteristics for LC-8. 244

5.21 (U) Maximum output power and optimum current determination for LC-8 245

5.22 (U) Emitter and collector work function 249

5.23 (U) LC-8 collector temperature optimization 250

5.24 (U) Maximum output power and optimum current determination for LC-7 and LC-8 at 1800°C 252

5.25 (U) LC-9 initial cesium reservoir temperature optimization data 254

5.26 (U) Envelope of I-V characteristics for LC-9 255

5.27 (U) Maximum output power and optimum current determination for LC-9 256

5.28 (U) LC-9 collector temperature optimization 258

5.29 (U) LC-9 emitter temperature profile and thermocouple distribution in converter compared with pre-converter-assembly data. 259

5.30 (U) LC-9 performance history. 261

5.31 (U) LC-9 performance history. 262

5.32 (U) Envelope of I-V characteristics for LC-9. 264

5.33 (U) Maximum output power and optimum current determination for LC-9 265

5.34 (U) LC-9 emitter temperature profile (power mode) 266

5.35 (U) Maximum output power and optimum current determination for LC-9 268

5.36 (U) LC-9 work function data 269

5.37 (U) Performance comparison between LC-9 and OC-5 271

5A.1 (U) Vacuum emission test assembly 275

5A.2 (U) LC-7 emitter temperature profiles prior to converter assembly 277

RESTRICTED DATA
ATOMIC ENERGY ACT 1954
GROUP 1

FIGURES (Continued)

5A.3 (U) LC-7 post operational emitter profiles 279

5A.4 (U) LC-7 vacuum emitter work function (post operative) 280

5A.5 (U) LC-8 emitter temperature profile and thermocouple reading prior to converter assembly 281

5A.6 (U) LC-8 vacuum emitter work function 282

5A.7 (U) LC-9 emitter temperature profiles prior to converter assembly. 283

5A.8 (U) LC-9 emitter vacuum work function 285

5A.9 (U) LC-6 emitter profile data 286

5A.10 (U) LC-5 and LC-6 emitter vacuum emission determinations 287

5B.1 (U) Calibration and test assembly schematic 290

5B.2 (U) 1000 hour test of three tungsten rhenium thermocouples 291

5C.1 (U) Post-test macroscopic appearance of LC-7 emitter 293

5C.2 (U) Post-test microstructures of a cross section of the fluoride tungsten emitter of LC-7 converter 294

5C.3 (U) Post-test macroscopic appearance of LC-7 collector surface 295

5C.4 (U) Post-test microstructures of the niobium collector of LC-7 converter 296

5C.5 (U) Post-test appearance of the final closure braze of LC-7 converter 298

5C.6 (U) Post-test appearance of the Al_2O_3-niobium interface of the insulator seal of LC-7 converter 299

5C.7 (U) Post-test appearance of the cesium reservoir tube of LC-7 converter. 300

5C.8(a)(U) Grain boundary oxide inclusions in the LC-7 copper cesium reservoir to niobium lead tube weld. Note the niobium-copper interface integrity 302

RESTRICTED DATA
ATOMIC ENERGY ACT 1954
GROUP 1

FIGURES (Continued)

5C.8(b)(U) Same area as in Fig. 5C.8(a) at higher magnification. The oxide inclusions in the copper grain boundary are visable. In the lower left and upper right hand portions of the view, porosity is apparent. 303

5C.8(c)(U) Etched microstructure of a portion of Fig. 5C.8(b). Evidence of plastic deformation is shown by the structure of the twins 304

TABLES

1.1 (U) Analytical Results for Samples 2A-1 and 2A-2. 12

1.2 (U) Summary of Fabrication, Characterization and Thermal Cycling Results for Emitter Structures Prepared During this Reporting Period (Sheet 1 of 2). 17/18

1.2 (U) Summary of Fabrication, Characterization and Thermal Cycling Results for Emitter Structures Prepared During this Reporting Period (Sheet 2 of 2). 19/20

1.3 (U) Dimensions of Emitter Structure Prepared for Delivery to NASA 21

1.4 (U) Optical Micrometer Measurement of W and Ta-10W Surface Contours of Emitter Structures Prepared for Delivery to NASA. d = Distance Between Tungsten Emitter Surface and Top of Ta-10W Lip. 22/23

1.5 (U) Optical Micrometer Measurements (Mils) of W and Ta-10W Surface Contours of Emitter Structures Subjected to Thermal Cycling Tests. 24/25

1.6 (U) Microhardness at Different Equally-Spaced Locations Along the Diameter of a Cross Section of One of the Ta-10W Discs Used for the Preparation of the B_6 Series Emitter Structures After Annealing for 15 Hours at 1850°C in 5×10^{-8} Torr Vacuum 29

1.7 (U) Microhardness at Different Equally Spaced Locations Along the Diameter of a Cross Section of B_6-4 Emitter Structure in the Ta-10W Region 29

1.8 (U) Effective Vacuum Work Function of Emitter Structure C_1-3 Between 1600°C and 1800°C After 175 Hours at 1800°C 44

RESTRICTED DATA
ATOMIC ENERGY ACT 1954
GROUP 1

TABLES (Continued)

1.9 (U) Optical Micrometer Measurements of W and Ta-10W Surface Contours of Emitter Structure C_1-2 After Testing at TECO 73

1.10 (U) Optical Micrometer Measurements of W and Ta-10W Surface Contours of Emitter Structures C_1-4 and C_1-5 After Receipt From NASA 82

1.11 (U) Optical Micrometer Measurements of W and Ta-10W Surface Contours of Emitter Structure C_3-3 After Receipt From NASA 88

1.12 (U) Optical Micrometer Measurements of W and Ta-10W Surface Contours of Emitter Structure D_1-1 After Testing at TECO 98

2.1 (U) Analytical Results on Blank Samples 108

2.2 (U) Cesium Contents in Components of LC-3, LC-4 and LC-5 109

3.1 (U) Results of Vapor-Deposition of Tungsten Using WCl_6 Powder 121

3.2 (U) Results of Vapor-Deposition of Tungsten Using Chlorination of Tungsten Chips. 125/126

3.3 (U) Impurity Contents of Five Selected Tungsten Emitters After Emission Test 171

4.1 (C-RD)(Gp-1) Surface Roughness Factors of UC-ZrC Samples Sintered at Various Temperatures and Effect of Annealing at 1800°C for 233 Hours 188

4.2 (U) Characteristics of UC-ZrC Samples Prepared 191

4.3 (U) Compositions, Stoichiometries and Impurity Contents of UC-ZrC Samples After 5000 Hours Sintering Study 211

5.1 (U) Characteristics of Converters LC-7, LC-8 and LC-9 212

5.2 (U) Converter Characteristics and Status 215

5.3 (U) Converter LC-7 (Unfueled) at beginning of life test 224

5.4 (U) LC-7 Performance and Operating Parameters 227

5.5 (U) LC-8 Performance and Operating Parameters 246

5.6 (U) LC-9 Performance and Operating Parameters 263

RESTRICTED DATA
ATOMIC ENERGY ACT 1954
GROUP 1

INTRODUCTION

(U) This report describes the work carried out under Contract NAS 3-8504 during the period February 1, 1967 through July 31, 1969 for the development of thermionic materials for nuclear space power application. Five tasks were included under Contract NAS 3-8504 during this period. These are:

1. Vacuum emission studies.
2. Post-operational determination of cesium contents in the components of three life-testing converters, LC-3, LC-4 and LC-5.
3. Chemical vapor-deposition of tungsten by the hydrogen reduction of tungsten chloride.
4. UC-ZrC sintering studies.
5. Converter testing.

(U) In addition to these five tasks, converter fabrication and thermionic fuel and cladding material research and development work were continued under Contracts NAS 3-6471, NAS 3-11822 and NAS 3-12980.

(U) A list of reports published previously on thermionic work sponsored by NASA at Gulf General Atomic is shown on the page next to the title page.

PART I. VACUUM EMISSION STUDIES

(L. Yang, R. G. Hudson)

SUMMARY

(U) A 10,000 hour test of the vacuum emission stability of two vapor-deposited fluoride tungsten clad $U_{0.90}$ $Zr_{0.10}$ $C_{1.02}$ planar samples at 1800°C was completed. Both samples were capable of maintaining stable vacuum work functions at this temperature, which were higher than the vacuum work function of unfueled fluoride tungsten (4.7-4.75 eV versus 4.5-4.6 eV), presumably due to the presence of adsorbed carbon atoms on the emitting surface. The vacuum work function of one of the samples was measured at lower temperatures after the completion of the 1800°C test. The sample was cooled in 100°C steps from 1800°C to 1300°C and then brought back to 1800°C in a similar fashion. It was found that between 1800°C and 1500°C, the vacuum work function decreased gradually with time at each of the testing temperatures during the cooling, and increased gradually with time at each of the testing temperatures during the heating, and that it took about 50-100 hours before the work function reached a steady value which was always lower than that at 1800°C. Below 1400°C, the change in the vacuum work function of the sample was slight, and remained at about the same value as that at 1400°C during a testing period of about 100 hours. Post-test examinations of the carbides in these samples showed that their compositions changed from $U_{.090}$ $Zr_{0.10}$ $C_{1.02}$ to $U_{.0875}$ $Zr_{0.098}$ $W_{0.026}$ $C_{0.992}$ and $U_{0.881}$ $Zr_{0.097}$ $W_{0.020}$ $C_{0.998}$ respectively because of the dissolution of the tungsten cladding into the carbide, which occurred unevenly along the fuel-clad interface. Post-test analysis of the tungsten claddings and the condensate on the collectors by neutron activation and gas chromatographic methods showed that the claddings contained about 20 μgs of uranium in the outer 30 mils and that the average uranium and carbon fluxes through the 40 mil thick fluoride tungsten cladding at 1800°C during the 10,000 hour tests were of the order of 10^{-8} and 10^{-9}

gm/cm^2, hour respectively. It is believed that at 1800°C, the uranium atoms arriving at the emitting surface by diffusion were mostly lost by vaporization, while a large part of the carbon atoms, because of their high affinity for tungsten, stayed on the emitting surface with the result that the observed vacuum work function at 1800°C was higher than that of the unfueled fluoride tungsten. At lower temperatures, the uranium atoms arriving at the emitting surface began to accumulate presumably because their rate of evaporation was less than their rate of diffusion through the cladding. Apparently the uranium effect outweighed the carbon effect and the vacuum work function was reduced. Pre-saturation of the carbide with tungsten together with its carbon share may help to prevent the increase of the uranium activity of the fuel due to tungsten dissolution and thus may improve the stability of the vacuum work function of the tungsten cladding when its temperature is lowered. Fabrication development of such carbide materials is being undertaken under Task IV of this report.

(U) Twenty-one planar emitter structures, consisting of fluoride tungsten, chloride tungsten or duplex tungsten diffusion bonded to tantalum-10 tungsten or tantalum, were prepared for the study of fabrication variables and for delivery to NASA for the evaluation of their performance in parallel plate cesiated converters. It was found that the increase of the tungsten emitter thickness from 40 mils to 60 mils and the decrease of the tantalum-10 tungsten substrate thickness from 150 mils to 110 mils did not improve the dimensional stability of the emitter structure upon rapid thermal cycling. At 1650°C and a vacuum of 4×10^{-9} torr, it took about 200 hours to clean an electropolished tungsten emitter surface, either in the as-prepared state or after the cleaned surface was exposed to air for 18 hours. Heat treatment of a fluoride tungsten emitter bonded to a tantalum substrate at 2200°C for 100 hours helped to build a diffusion zone at the tungsten-tantalum interface without the formation of an excessive number of Kirkendall voids. Such heat treatment, however, did not improve the dimensional stability of the emitter structure upon rapid thermal cycling between 1800°C and room temperature.

(U) Thermal cycling study of a chloride tungsten emitter bonded to a Ta-10W substrate showed that excessive deformation of the surface of the

emitter structure occurred, although the vacuum work function of the chloride tungsten emitting surface was not affected. Heat treatment of a chloride tungsten bonded to a tantalum substrate at 2200°C for 100 hours did not improve the dimensional stability of the emitter structure upon thermal cycling between 1650°C and room temperature. The use of a duplex tungsten emitter did not improve the dimensional stability of an emitter structure containing a Ta-10W substrate upon thermal cycling between 1800°C and room temperature. A total of nine emitter structures containing Ta-10W substrates were delivered to NASA. Of these eight emitter structures, two contained electropolished fluoride tungsten emitters (B_6-1 and B_6-2), four contained chloride tungsten emitters (C_1-1, C_1-2, C_1-4, and C_1-5), two contained chloride-fluoride duplex tungsten emitters (C_3-2 and C_3-3) and one contained chemically etched fluoride tungsten emitter (D_1-1). Six of these eight emitter structures (B_6-2, C_1-2, C_1-4, C_1-5, C_3-3 and D_1-1) incorporated into cesiated converters have been tested successfully for long periods of time at high temperatures. Post-test examinations showed that B_6-2 and C_1-2 failed at the weld between the Ta-10W lip of the emitter structure and the tantalum stem. Chemical analysis results indicated oxygen contamination of these emitter structures. No leak was detected in the other four emitter structures and the interstitial impurity concentrations were of the same order of magnitude as that of the component materials used for the fabrication of these emitter structures. Measurements of the surface contours indicated that the chloride tungsten emitter structures exhibited more deformation than the others. X-ray pole figure studies showed that for those with grain size small enough to allow a good pole figure plot to be constructed, the change of the degree of preferred crystal orientation in the emitter was not significant. Metallographic examinations of the cross section of each tungsten-(Ta-10W) interface revealed no gross defects, although Kirkendall voids were observed on the Ta-10W side of the interface. The width of the diffusion zone varied between 15-60 microns but the vacuum work functions obtained were similar to that of the same types of emitter materials. The vacuum work function of the chemically etched fluoride tungsten emitter remained higher than that of fluoride tungsten, indicating that at least part of the gain in vacuum work function by chemically etching

can be retained if the etched emitter is not operated at excessively high temperatures.

1.1. VACUUM EMISSION STABILITY OF TUNGSTEN CLAD 90UC-10ZrC AT 1800°C

(U) Previously[1] the vacuum work functions of two samples, 2A-1 and 2A-2, consisting of 40 mil thick vapor deposited fluoride tungsten clad $U_{0.10}$ $Zr_{0.90}$ $C_{1.02}$, were studied at 1800°C for periods of 7090 and 6800 hours respectively before the tests were shut down for the replacement of the electron bombardment filaments. At the beginning of this reporting period, these tests were resumed at 1800°C after the condensates on the collectors were analyzed for their carbon and uranium contents.

(U) Test for Sample 2A-1 was terminated at 10146 hours. The carbon and uranium contents of the collector condensate were again determined. Layers of the tungsten cladding were obtained from the outer 30 mils of the cladding by electrolytical dissolution in NaOH for the determination of their uranium contents. The sample was then broken into two halves. One half of the sample was mounted and examined metallographically and by electron microprobe analysis for the microstructures and compositions of the phases present at the fuel-clad interface. The carbide fuel from the other half of the sample was recovered and analyzed for its uranium, zirconium, tungsten and carbon contents.

(U) Test for Sample 2A-2 was continued at 1800°C for a total of 10,000 hours before the temperature was lowered to 1300°C at 100°C steps and then brought back to 1800°C in the same manner. The sample stayed at each temperature until a stable vacuum work function was reached. Post-test analysis of the collector condensate, the cladding and the fuel material was carried out in the same manner as that for Sample 2A-1.

(U) The results obtained in vacuum work function measurements, chemical analysis, and metallographical and electron microprobe examinations for these two samples are described below.

1.1.1. Vacuum Work Function Measurements

(U) Figures 1.1 and 1.2 show respectively the vacuum work functions of Samples 2A-1 and 2A-2 as a function of time at 1800°C. It can be seen that the vacuum work functions of both samples stayed essentially constant at 4.7-4.75 eV after the first 1000 hours. These values are higher than that of the vapor-deposited fluoride tungsten (4.5-4.6 eV), presumably due to the presence of adsorbed carbon on the emitter surface.

(U) Figure 1.3 shows the vacuum work functions of Sample 2A-2 as a function of time at various temperatures during the cooling and heating cycle. In the temperature range between 1800°C and 1500°C, the work function decreased gradually with time at each of the testing temperatures during the cooling, and increased gradually with time at each of the testing temperatures during the heating. In general, it took about 50-100 hours to reach a steady value at each temperature. In the temperature range between 1400°C and 1300°C, the changes in work function were not significant. Figure 1.4 shows the stabilized work function values at each temperature both during the cooling and during the heating. There seems to be a slight hysterisis effect. However, for a given temperature the difference between the work function value on the cooling curve and that on the heating curve is within the limit of experimental error.

1.1.2. Post-test Chemical Analysis of Collector Condensate, Tungsten Cladding and Carbide Fuel

(U) The collector-guard ring assembly was taken out of the diffusion-emission test cell under helium protection and joined by means of an Ultek vacuum seal to a stainless steel can which was connected to a gas chromatograph through a Cu_2O column. The can was evacuated and heated to about 350°C. Oxygen was then admitted into the can to convert the carbon in the collector condensate to CO_2. The gas mixture was flushed by helium into

UNCLASSIFIED

UNCLASSIFIED

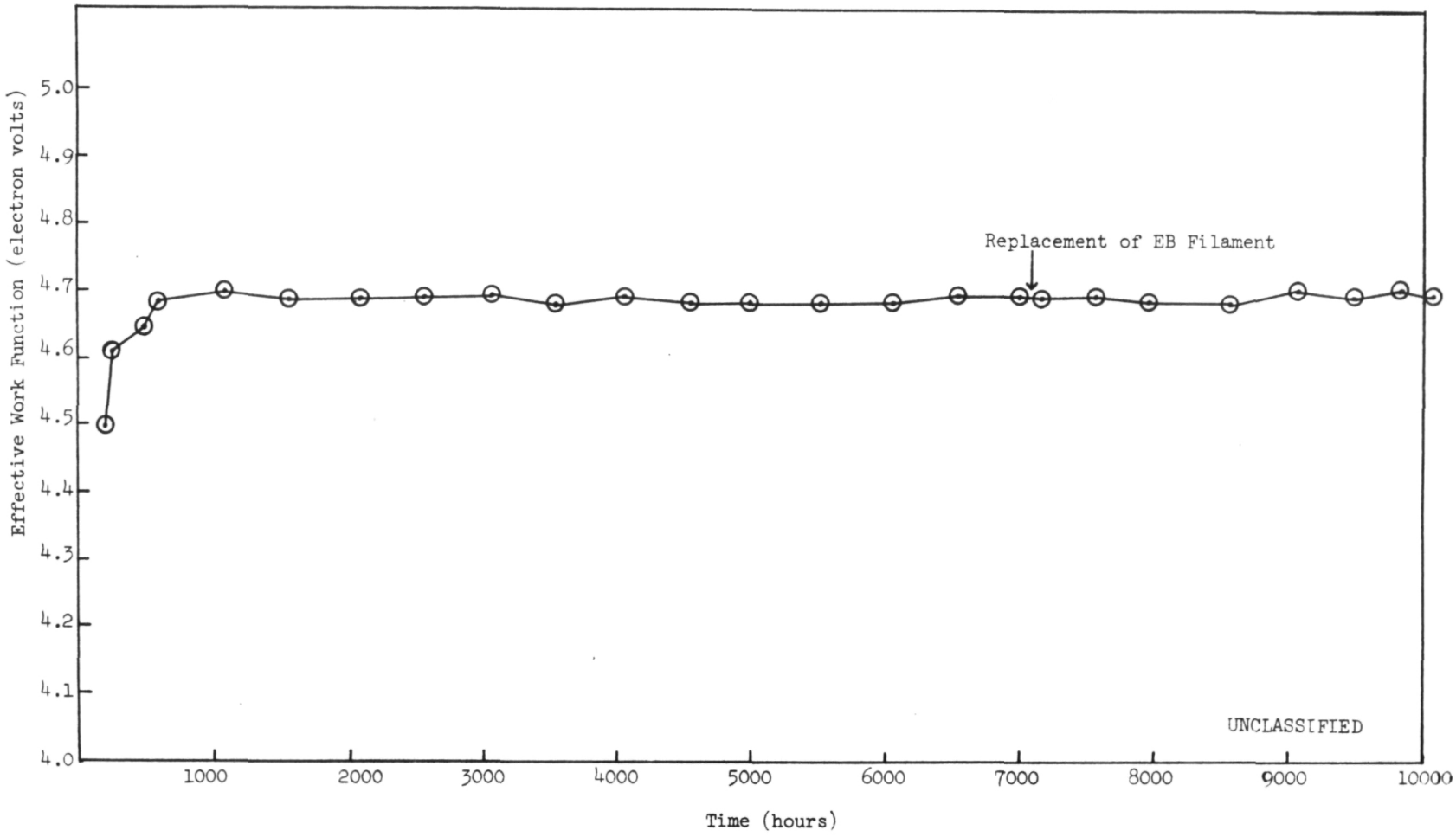

Fig. 1.1--(U) Effective work function of Sample 2A-1 (vapor-deposited fluoride tungsten clad 90UC-10ZrC) as a function of time at 1800°C

UNCLASSIFIED

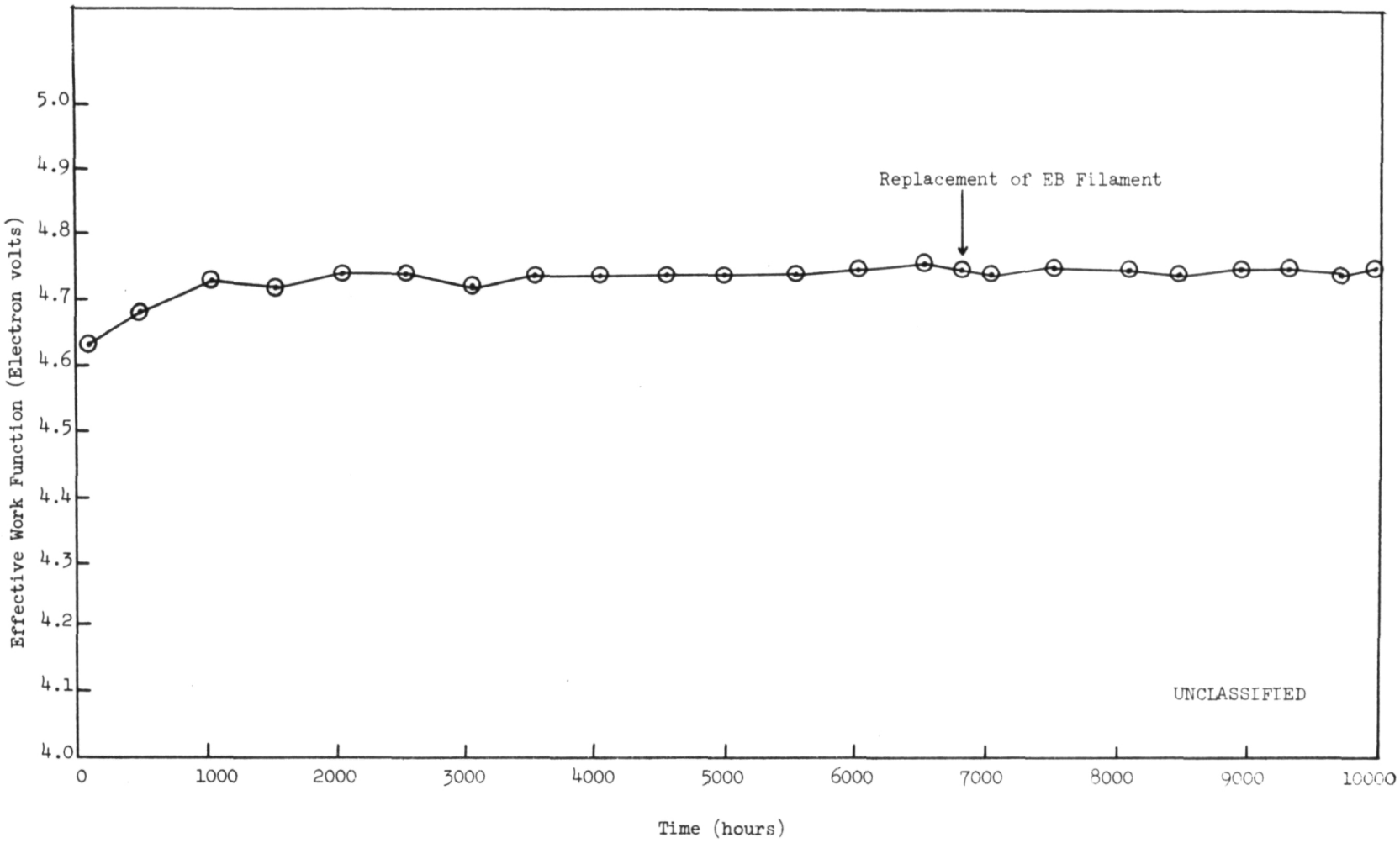

Fig. 1.2--(U) Effective work function of Sample 2A-2 (vapor-deposited fluoride tungsten clad 90UC-10ZrC) as a function of time at 1800°C

UNCLASSIFIED

UNCLASSIFIED

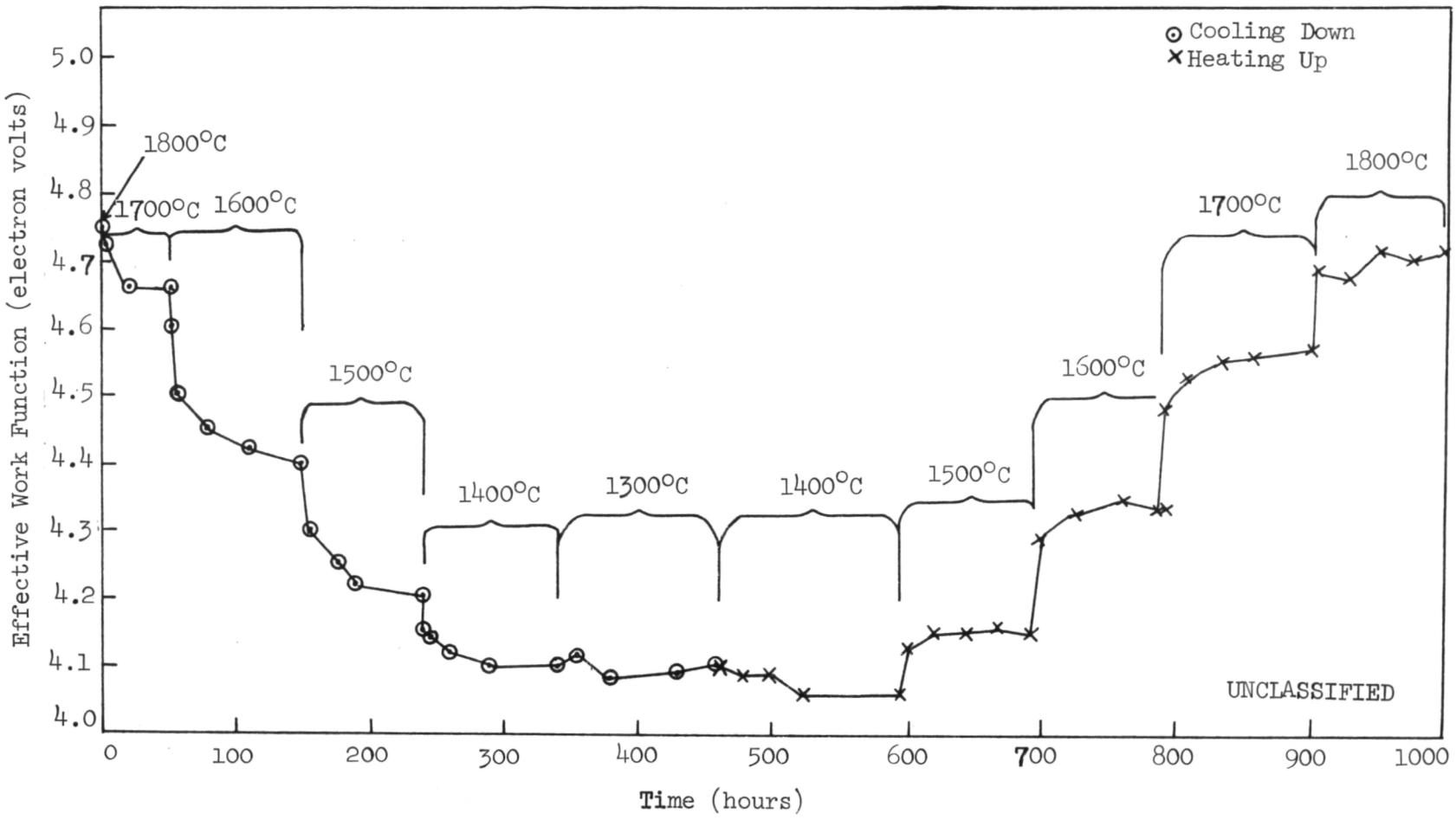

Fig. 1.3--(U) Effective work function of Sample 2A-2 (vapor-deposited fluoride tungsten clad 90UC-10ZrC) as a function of time during thermal cycling between 1800°C and 1300°C after 10,000 hours at 1800°C

UNCLASSIFIED

UNCLASSIFIED

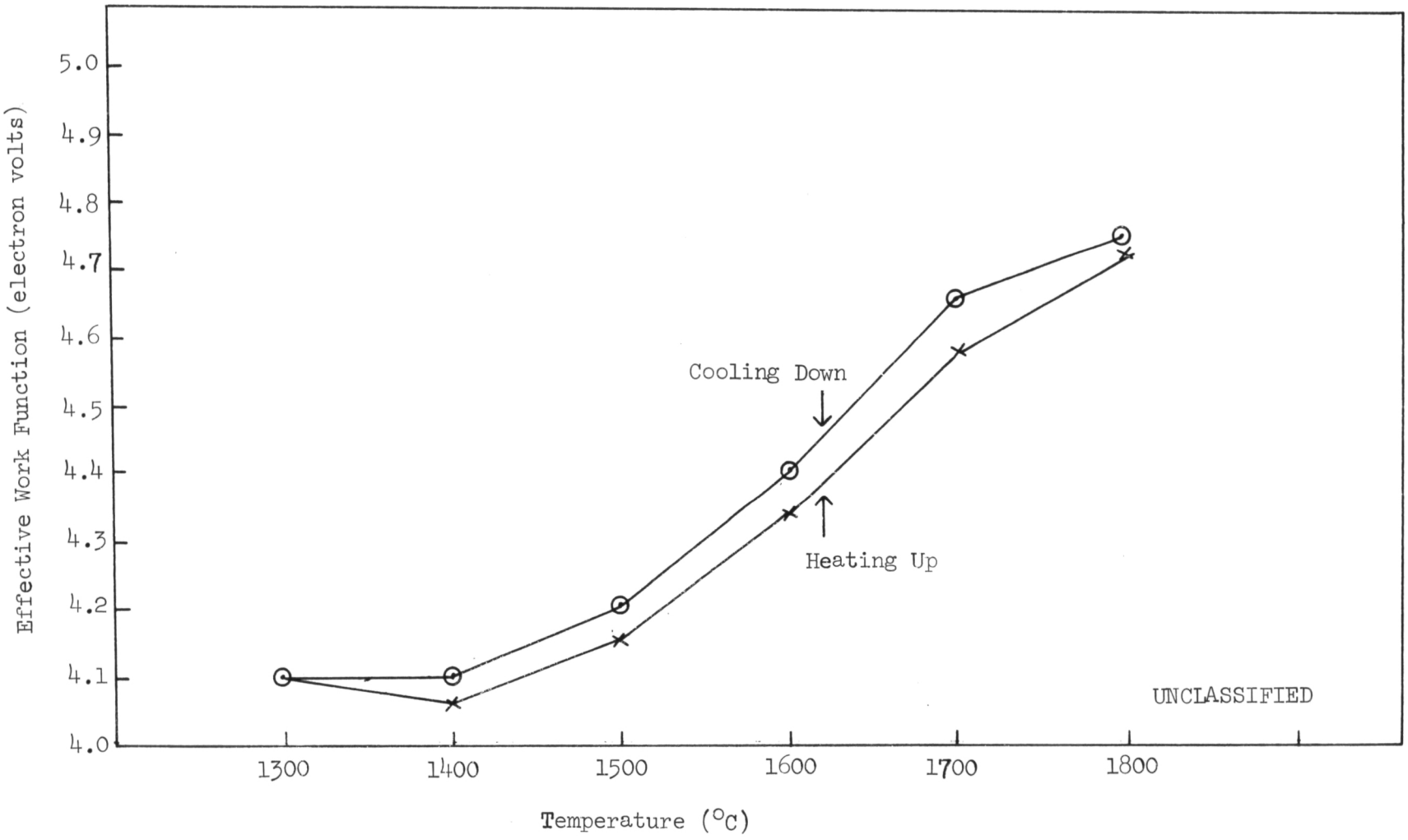

Fig. 1.4--(U) Stabilized effective work function as a function of temperature for Sample 2A-2 (W clad 90UC-10ZrC) following the 10,000 hour life test at 1800°C

UNCLASSIFIED

the absorption column of the gas chromatograph and the CO_2 content in the gas mixture determined by the standard gas chromatographic technique. The presence of a Cu_2O column in the path of the gas flow insures any CO in the gas mixture would be converted to CO_2. The carbon content in the collector condensate was calculated from the amount of CO_2 found after a blank correction was made. After the completion of the carbon analysis, the residue on the collector-guard ring assembly was dissolved in dilute HNO_3 and analyzed for its uranium content by neutron activation techniques.

(U) Dissolution of successive layers from the outer 30 mils of the tungsten cladding was carried out electrolytically in an aqueous solution of 10 wt% of NaOH. The uranium content in each layer was determined by neutron activation techniques.

(U) The uranium, zirconium, tungsten and carbon contents of the post-test carbide fuel were determined by X-ray fluorescence spectrometry and combustion technique.

(U) Table 1.1 summarizes all the analytical results for Samples 2A-1 and 2A-2.

1.1.3. Metallographic and Electron Microprobe Examinations

(U) The results obtained from Samples 2A-1 and 2A-2 are quite similar. In each case no gross interaction was observed at the fuel-clad interface. However, the tungsten side of the interface appeared jagged, as shown in Fig. 1.5 for Sample 2A-1, probably by the non-uniform dissolution of the tungsten into the carbide. Electron microprobe study showed no uranium (in excess of 0.1 wt%) in the cladding but about 1-2 wt% of tungsten was present throughout the carbide fuel.

1.1.4. Conclusions and Discussions

(U) The results indicate that emitters consisting of 40 mil thick fluoride tungsten clad $U_{0.90}\ Zr_{0.10}\ C_{1.02}$ (initial composition) could maintain stable vacuum work functions at 1800°C even though both the uranium and the carbon fluxes through the tungsten cladding were measurable and a finite

Table 1.1

(U) ANALYTICAL RESULTS FOR SAMPLES 2A-1 AND 2A-2

(This table is Unclassified)

(a) Collector Condensate

Sample	Testing Time* (hr)	Average Uranium Flux (gm/cm^2 - hr)	Average Carbon Flux (gm/cm^2 - hr)
2A-1	0-7090	1.1×10^{-8}	1.7×10^{-9}
	7090-10146	1.4×10^{-8}	1.2×10^{-9}
2A-2	0-6800	1.0×10^{-8}	2.0×10^{-9}
	6800-10000	1.2×10^{-8}	1.5×10^{-9}

(b) Uranium Content in Cladding

Sample	Total Testing Time* (hr)	Distance from Emitting Surface (mils)	Cumulative Uranium Content (μg)
2A-1	10146	3.0	0.6
		6.5	2.2
		10.7	4.2
		15.5	6.7
		19.2	9.2
		23.0	12.5
		26.5	15.8
		30.2	18.3
2A-2	10000	2.8	0.5
		6.2	1.8
		9.7	4.8
		14.1	6.3
		17.9	8.6
		20.8	10.1
		24.5	14.5
		28.2	17.1
		30.5	20.5

(c) Composition of Carbide Fuel

Sample	Total Testing Time* (hr)	Carbide Composition	
		Before Testing	After Testing
2A-1	10146	$U_{0.90}Zr_{0.10}C_{1.02}$	$U_{0.875}Zr_{0.098}W_{0.026}C_{0.992}$, C/U** = 1.007
2A-2	10000	$U_{0.90}Zr_{0.10}C_{1.02}$	$U_{0.881}Zr_{0.097}W_{0.020}C_{0.998}$, C/U** = 1.01

*The time for the thermal cycling test of Sample 2A-2 is not included.

**Assume 1 C for each Zr and 1 C for every 2W.

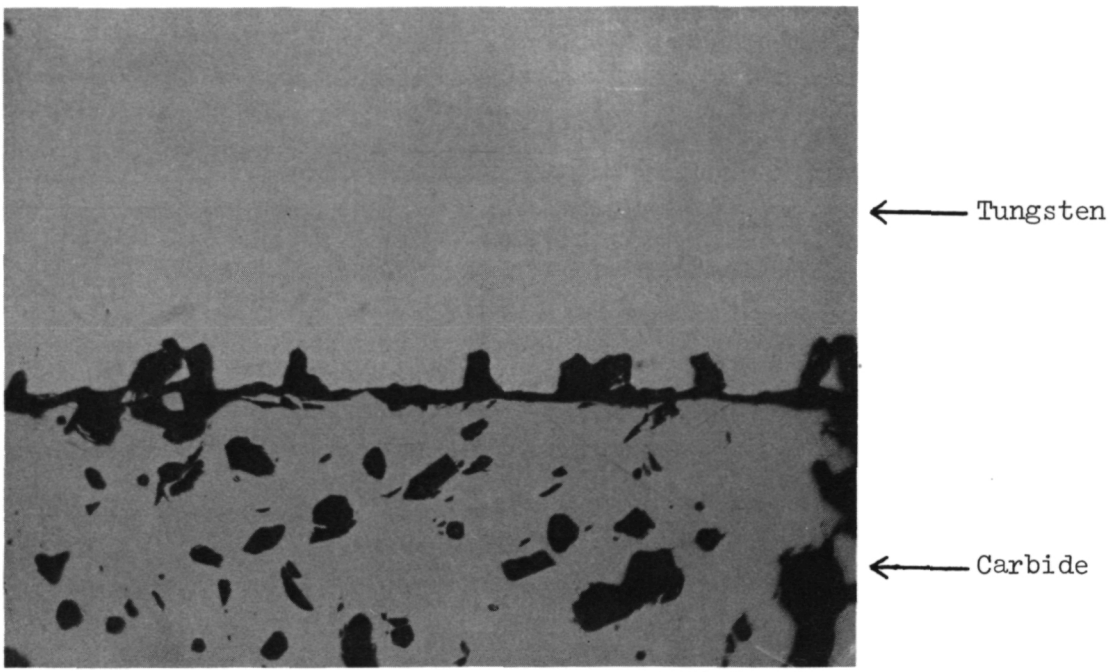

Fig. 1.5--(U) Appearance of the fuel-clad interface of Sample 2A-1 after the test

amount of uranium was present in the cladding. The observed vacuum work function at 1800°C, however, was higher than that of fluoride tungsten (4.7-4.75 eV versus 4.5-4.6 eV), presumably due to the presence of carbon atoms adsorbed on the emitting surface. Most of the uranium atoms arriving at the emitting surface were apparently lost by vaporization because of its high volatility at 1800°C and therefore no significant effect on the vacuum work function was observed at this temperature.

(U) During long term operation at 1800°C, however, the carbide fuel dissolved about 2 wt% of tungsten from the cladding. The dissolution which occurred non-uniformly along the fuel-clad interface, changed the composition of the carbide fuel. Thus the chemical analysis data indicated that while the initial composition of the fuel material was $U_{0.90}\ Zr_{0.10}\ C_{1.02}$, the post test compositions were $U_{0.875}\ Zr_{0.098}\ W_{0.026}\ C_{0.992}$ and $U_{0.881}\ Zr_{0.097}\ W_{0.022}\ C_{0.998}$ respectively for Samples 2A-1 and 2A-2. This decrease of the carbon to metal atom ratio should lead to an increase in the uranium activity and thus the diffusion rate of uranium through the tungsten cladding.

(U) While the vacuum work function data indicated that for the uranium activity prevailing in the fuel materials of these two test samples, no appreciable amount of uranium accumulated on their emitting surfaces at 1800°C because of the volatility of uranium at high temperatures, this apparently was not true when the temperature was lowered, as shown by the results obtained on Sample 2A-2. In the temperature range of 1700-1500°C, the arrival rate of uranium atoms at the emitting surface seemed to outweigh their vaporization rate, and the uranium atoms accumulated there led to the lowering of the vacuum work function by an amount increasing with the decrease of the temperature. As the temperature was further lowered to 1400°C and then to 1300°C, the rate of accumulation of uranium atoms was probably so slow that no further reduction of vacuum work function was observed in about 100 hours and the work function became "apparently stabilized" at a value of about 4.05 eV. No such temperature effect on the carbon accumulation on the emitting surface was indicated by the vacuum work function data of Sample 2A-2. This could be because the accumulation of carbon, due to its high affinity with tungsten, was already high on the

emitting surface even at 1800°C; therefore, no significant increase in carbon accumulation occurred when the temperature was lowered. It is also possible that the accumulation of carbon on the emitting surface was increased significantly at lower temperatures but the uranium effect outweighed the carbon effect.

(U) Similar temperature effect on vacuum work function was observed in the case of the emitter of the out-of-pile converter LC-5.[1] This emitter was fueled with $U_{0.87}\ Zr_{0.11}\ W_{0.02}\ C_{0.965}$ which had a lower carbon to metal atom ratio than that of Sample 2A-2 and therefore should possess a higher uranium activity and a lower carbon activity than that of the carbide fuel in Sample 2A-2. The vacuum work function of this emitter, after testing for 7558 hours in cesium at 1800°C, was 4.6 eV at 1800°C, which was about the same as that of fluoride tungsten, but "stabilized" at a value of 3.5 eV at temperatures below about 1400°C, as compared to a value of 4.05 eV for Sample 2A-2. Thus with a fuel material of lower carbon to metal atom ratio than that of Sample 2A-2, the carbon effect of raising the vacuum work function was not observed at 1800°C and the uranium effect of lowering the vacuum work function was enhanced. The results obtained on LC-5 emitter and that observed on Sample 2A-2 are consistent among themselves, and demonstrated the importance of the control of the carbon to metal atom ratio in UC-ZrC fuel materials in order to achieve stable performance of emitter fueled with UC-ZrC. A two prong approach has been adopted to exercise control of the carbon to metal ratio in UC-ZrC fuel materials. These are: (1) the addition of about 4 wt% of tungsten and its share of carbon (1 C to 2 W) to UC-ZrC fuel to prevent the lowering of carbon activity and the increase of uranium activity through the dissolution of tungsten cladding into the fuel material, and (2) the improvement of fabrication methods for achieving a carbon to uranium atom ratio of 1.03 to 1.05 (allowing one carbon atom to each zirconium atom and one carbon atom to every two tungsten atoms) in UC-ZrC fuel materials. The details of the fabrication method for UC-ZrC fuels containing tungsten additions will be described in Task 4 of this report.

1.2. PREPARATION OF PLANAR TUNGSTEN EMITTER STRUCTURES

(U) The objective of this work is to prepare planar tungsten emitter structures for the evaluation of their performance in cesiated converters. Previous work on this subject has been described in the Summary Report of Contract NAS 3-8504 for the period November 23, 1965 through January 31, 1967.[1]

(U) During this reporting period, twenty-one emitter structures were prepared. Of these twenty-one emitter structures, ten were for delivery to NASA while the rest were for the evaluation of fabrication variables on the dimensional stability of the emitter structure upon thermal cycling. Table 1.2 summarizes the fabrication variables and the studies carried out on these emitter structures. Tables 1.3 and 1.4 show respectively the dimension and the surface contour measurements made on emitter structures prepared for delivery to NASA. Table 1.5 presents the surface contour measurements carried out on emitter structures prepared for thermal cycling tests. The details about the work carried out on each series of emitter structures are described as follows.

1.2.1. B_5 Series Emitter Structures

(U) B_5-1 and P_5-2 were prepared for the purpose of evaluating whether the dimensional stability of emitter structures upon thermal cycling could be improved if the thickness of the vapor-deposited tungsten emitter was increased from 40 mils to 60 mils and that of the Ta-10W substrate was decreased from 150 mils to 110 mils.

(U) B_5-1 was heated in 10^{-6} torr vacuum for 200 hours at 1750°C and then thermal cycled between 1650°C and room temperature for 20 cycles, using the slow heating scheme. The results are shown in Table 1.5. Since the deformation of the emitter structure was in excess of 2 mils after 20 cycles, this approach was abandoned.

1.2.2. B_6 Series Emitter Structures

(U) For the B_6 series emitter structures, the fabrication method was improved in two respects in order to minimize contamination by interstitial elements. First, all heat treatments were carried out in 5×10^{-8}

Table 1.2

(U) SUMMARY OF FABRICATION, CHARACTERIZATION AND THERMAL CYCLING RESULTS FOR EMITTER STRUCTURES PREPARED DURING THIS REPORTING PERIOD

(This table is Unclassified)

Emitter Structure Designation	Nominal Configuration [a]	W Emitter Material [b]	(Ta-10W) or Ta Substrate Material [c]	Fabrication Conditions			Post-Fabrication Heat Treatment				Post-Fabrication Characterization	Thermal Cycling Test								Status
									Average Dimension Change [d] (mil)				Average Deformation Observed [d] (mils)							
													Tungsten Emitter Side				Opposite Side			
				Temp (°C)	Time (hr)	Pressure (psi)	Temp (°C)	Time (hr)	Tungsten Side	Opposite Side		Scheme [e]	After 10 Cycles	After 15 Cycles	After 20 Cycles	After 30 Cycles	After 10 Cycles	After 15 Cycles	After 20 Cycles	After 30 Cycles	
B_5-1	60W-110(Ta-10W)	2C-4 fluoride W	NRC(Ta-10W)-1	1850	3	3000	1750	200	0.45	0.5	None	Slow heating, fast cooling between 1650°C and room temp.	-	-	2.1	-	-	-	2.5	-	Hold
B_5-2	60W-110(Ta-10W)	2C-4 fluoride W	NRC(Ta-10W)-1	1850	3	3000	None	None	None	None	None	None	-	-	-	-	-	-	-	-	Hold
B_6-1	40W-150(Ta-10W)	2C-4 fluoride W	NRC(Ta-10W)-2	1850	3	3000	1800	4	0.2	0.1	None	None	-	-	-	-	-	-	-	-	Delivered to NASA
B_6-2	40W-150(Ta-10W)	2C-4 fluoride W	NRC(Ta-10W)-2	1850	3	3000	1800	4	0.25	0.1	Pole Figure	None	-	-	-	-	-	-	-	-	Delivered to NASA
B_6-3	40W-150(Ta-10W)	2C-4 fluoride W	NRC(Ta-10W)-2	1850	3	3000	1800	4	0.1	0.1	None	None	-	-	-	-	-	-	-	-	After chemical etch, became D_1-1
B_6-4	40W-150(Ta-10W)	2C-4 fluoride W	NRC(Ta-10W)-2	1850	3	3000	None	None	None	None	None	None	-	-	-	-	-	-	-	-	Sectioned for chemical analysis and microstructure examination
B_7-1	40W-150 Ta	2C-5 fluoride W	Wah Chang EB melted capacitor grade Ta	1850	1	1250	1650	430	-	-	Vacuum work function	None	-	-	-	-	-	-	-	-	Sectioned for microstructure examination
B_7-2	40W-150 Ta	2C-5 fluoride W	Wah Chang EB melted capacitor grade Ta	1850	1	1250	None	None	None	None	None	None	-	-	-	-	-	-	-	-	Rejected because of microcracks in tungsten
B_7-3	40W-150 Ta	2C-5 fluoride W	Wah Chang EB melted capacitor grade Ta	1850	1	1250	None	None	None	None	None	None	-	-	-	-	-	-	-	-	Rejected because of microcracks in tungsten
B_8-1	40W-150 Ta	2C-6 fluoride W	Wah Chang EB melted capacitor grade Ta	1850	1	1250	2200	100	0.1	0.4	None	Slow heating, fast cooling between 1650°C and room temp.	1.0	1.7	-	-	0.3	0.9	-	-	Sectioned for microstructure examination
B_8-2	40W-150 Ta	2C-6 fluoride W	Wah Chang EB melted capacitor grade Ta	1850	1	1250	None	None	None	None	None	None	-	-	-	-	-	-	-	-	Hold
C_1-1	40W-150(Ta-10W)	2C-7 chloride W	NRC(Ta-10W)-2	1850	3	3000	1800	4	0.2	0.4	None	None	-	-	-	-	-	-	-	-	Delivered to NASA
C_1-2	40W-150(Ta-10W)	2C-7 chloride W	NRC (Ta-10W)-2	1850	3	3000	1800	4	0.3	0.1	Pole Figure	None	-	-	-	-	-	-	-	-	Delivered to NASA
C_1-3	40W-150(Ta-10W)	2C-7 chloride W	NRC(Ta-10W)-2	1850	3	3000	1600-1800	180	0.2	0.3	Vacuum work function	Slow heating, fast cooling between 1800°C and room temp.	1.4	-	-	5.6	1.5	-	-	5.1	Hold
C_1-4	40W-150(Ta-10W)	2C-8 chloride W	NRC(Ta-10W)-2	1850	3	3000	1800	4	0.1	0.1	Pole Figure	None	-	-	-	-	-	-	-	-	Delivered to NASA
C_1-5	40W-150(Ta-10W)	2C-8 chloride W	NRC(Ta-10W)-2	1850	3	3000	1800	4	0.2	0.1	Pole Figure	None	-	-	-	-	-	-	-	-	Delivered to NASA

Table 1.2 (Continued)

(U) SUMMARY OF FABRICATION, CHARACTERIZATION AND THERMAL CYCLING RESULTS FOR EMITTER STRUCTURES PREPARED DURING THIS REPORTING PERIOD

(This table is Unclassified)

Emitter Structure Designation	Nominal Configuration[a]	W Emitter Material[b]	(Ta-10W) or Ta Substrate Material[c]	Fabrication Conditions			Post-Fabrication Heat Treatment				Post-Fabrication Characterization	Thermal Cycling Test								Status
									Average Dimension Change[d] (mil)			Scheme[g]	Average Deformation Observed[d] (mils)							
													Tungsten Emitter Side				Opposite Side			
				Temp (°C)	Time (hr)	Pressure (psi)	Temp (°C)	Time (hr)	Tungsten Side	Opposite Side			After 10 Cycles	After 15 Cycles	After 20 Cycles	After 30 Cycles	After 10 Cycles	After 15 Cycles	After 20 Cycles	After 30 Cycles	
C_2-1	40W-150 Ta	2C-8 chloride W	Wah Chang EB melted capacitor grade Ta	1850	1	1250	2200	100	0.5	4.4[f]	None	Slow heating, fast cooling between 1650°C and room temp.	0.6	-	1.5	2.9	1.8	-	2.3	2.2	Hold
C_3-1	40W-150(Ta-10W)	2B-8 duplex W[e]	NRC(Ta-10W)-2	1850	3	3000	1800	4	0.1	0.25	None	Slow heating, fast cooling between 1800°C and room temp.	1.0	-	2.6	1.9	1.5	-	2.0	2.7	Hold
C_3-2	40W-150(Ta-10W)	2B-8 duplex W	NRC(Ta-10W)-2	1850	3	3000	1800	4	0.2	0.15	Pole Figure	None	-	-	-	-	-	-	-	-	Delivered to NASA
C_3-3	40W-150(Ta-10W)	2B-9 duplex W	NRC(Ta-10W)-2	1850	3	3000	1800	4	0.4	0	Pole Figure	None	-	-	-	-	-	-	-	-	Delivered to NASA
D_1-1	Obtained by chemical etching of B_6-3 after 4 hours at 1800°C						None	None	None	None	Pole Figure	None	-	-	-	-	-	-	-	-	Delivered to NASA
D_1-2	40W-150(Ta-10W)	2C-6 fluoride W	NRC(Ta-10W)-2	1850	3	3000	1800	4	0.15	0.15	None	None	-	-	-	-	-	-	-	-	Hold

Foot Notes

[a] Numbers indicated are thickness in mils. For other dimensions of the emitter structure, see Reference (1)

[b] The sources and the impurity contents (in ppm) of the fluoride tungsten discs (after outgassing 200 hours at 1800°C), the chloride tungsten discs (after outgassing 100 hours at 1800°C), and the duplex tungsten discs (after outgassing 100 hours at 1800°C) are as follows:

Sample	2C-4	2C-5	2C-6	2C-7	2C-8	2B-8	2B-9
Source	SFL	SFL	SFL	SFL	SFL	SFL	GGA
C	5	8	7	15	18	9	3
O	10	5	8	10	9	5	5
N	<1	<1	<1	<1	<1	<1	<1
F	20	15	18	10	15	10	5
Cl	5	3	2	7	5	3	2

[c] The impurity contents (in ppm) of the NRC(Ta-10W) and the Wah Chang Ta after annealing for 15 hours at 1800-1850°C are:

Sample	NRC(Ta-10W)-1	NRC(Ta-10W)-2	Wah Chang Ta
C	8	13	26
N	37	31	12
O	7.9	16	15
H	-	-	3.2

[d] Deduced from data shown in Tables 1.4 and 1.5 after they were normalized to the condition that X_5 and X_7 are at the same level and that X_6 and X_8 are at the same level. The maximum deviations along X_5-X_7 and X_6-X_8 directions are averaged to obtain values given here.

[e] Duplex tungsten consists of 10 mil {110} oriented chloride tungsten deposited over 30 mil {100} oriented fluoride tungsten.

[f] Deformations observed on the Ta side are not reliable due to etching by electron bombardment.

[g] Details on thermal cycling scheme are described under Table 1.5.

UNCLASSIFIED

Table 1.3

(U) DIMENSIONS OF EMITTER STRUCTURES PREPARED FOR DELIVERY TO NASA

(This table is Unclassified)

Dimensions Required* (Inch)	Dimensions Observed (Inch)									
	B_6-1	B_6-2	C_1-1	C_1-2	C_1-4	C_1-5	C_3-2	C_3-3	D_1-1	D_1-2
$0.630^{+0.0000}_{-0.0005}$	0.6300	0.6300	0.6296	0.6299	0.6296	0.6295	0.6295	0.6300	0.6300	0.6297
$0.606^{+0.000}_{-0.002}$	0.606	0.606	0.606	0.606	0.606	0.606	0.606	0.606	0.605	0.606
0.570 ± 0.005	0.570	0.569	0.570	0.568	0.571	0.570	0.569	0.571	0.568	0.570
0.600 ± 0.002	0.602	0.602	0.600	0.600	0.601	0.600	0.599	0.601	0.600	0.601
0.190 ± 0.005	0.193	0.195	0.192	0.195	0.191	0.194	0.193	0.192	0.195	0.192
0.130 ± 0.005	0.131	0.130	0.129	0.131	0.130	0.130	0.129	0.132	0.129	0.131
0.105 ± 0.001	0.106	0.106	0.104	0.105	0.105	0.105	0.105	0.104	0.105	0.106
0.090 ± 0.005	0.091	0.090	0.094	0.087	0.089	0.090	0.085	0.092	0.092	0.091
0.060 ± 0.005	0.061	0.061	0.061	0.056	0.058	0.059	0.059	0.057	0.057	0.056
0.040 ± 0.002	0.040	0.040	0.040	0.040	0.040	0.040	0.040	0.040	0.040	0.040
0.28 ± 0.01	0.29	0.28	0.28	0.28	0.28	0.28	0.28	0.28	0.29	0.28
W emitter surface flat within 0.0002 inch TIR	See table 1.4	See table 1.4	See table 1.4	See table 1.4	See table 1.4	See table 1.4	See table 1.4	See table 1.4	See table 1.4	See table 1.4
Ta-10W lip top ∥ W emitter surface within 0.002 inch TIR	See table 1.4	See table 1.4	See table 1.4	See table 1.4	See table 1.4	See table 1.4	See table 1.4	See table 1.4	See table 1.4	See table 1.4
Ta-10W surface ∥ W emitter surface within 0.0002 inch TIR	See table 1.4	See table 1.4	See table 1.4	See table 1.4	See table 1.4	See table 1.4	See table 1.4	See table 1.4	See table 1.4	See table 1.4

*The detailed drawing of the emitter structure was shown in Fig. 2.89 of the Summary Report for the period November 23, 1966 through January 31, 1967 for Contract NAS 3-8504, NASA-CR-72315, GA-7682.(C/RD)

UNCLASSIFIED

Table 1.4

(U) OPTICAL MICROMETER MEASUREMENT OF W AND Ta-10W SURFACE CONTOURS OF EMITTER STRUCTURES PREPARED FOR DELIVERY TO NASA. d = DISTANCE BETWEEN TUNGSTEN EMITTER SURFACE AND TOP OF Ta-10W LIP

(This table is Unclassified)

	B_6-1			B_6-2			C_1-1			C_1-2			C_1-4			C_1-5			C_3-2			C_3-3			D_1-1			D_1-2		
Surface Position	W Surface (Mil)	Ta-10W Surface (Mil)	d (Inch)	W Surface (Mil)	Ta-10W Surface (Mil)	d (Inch)	W Surface (Mil)	Ta-10W Surface (Mil)	d (Inch)	W Surface (Mil)	Ta-10W Surface (Mil)	d (Inch)	W Surface (Mil)	Ta-10W Surface (Mil)	d (Inch)	W Surface (Mil)	Ta-10W Surface (Mil)	d (Inch)	W Surface (Mil)	Ta-10W Surface (Mil)	d (Inch)	W Surface (Mil)	Ta-10W Surface (Mil)	d (Inch)	W Surface (Mil)	Ta-10W Surface (Mil)	d (Inch)	W Surface (Mil)	Ta-10W Surface (Mil)	d (Inch)
X_0	0	0		0	0		0	0		0	0		0	0		0	0		0	0		0	0		0	0		0	0	
X_1	0	+0.2		-0.1	-0.1		+0.1	+0.2		0	-0.1		+0.1	0		+0.2	+0.2		-0.1	+0.2		0	-0.1		0	+0.1		+0.1	+0.1	
X_2	0	+0.2		+0.1	+0.1		-0.1	+0.2		0	-0.2		-0.2	+0.1		0	0		+0.2	+0.1		0	-0.1		0	0		+0.1	0	
X_3	0	-0.2		+0.1	0		-0.1	+0.1		+0.1	0		0	+0.1		0	-0.1		+0.2	-0.2		0	+0.1		0	0		-0.1	0	
X_4	+0.2	-0.2		+0.1	-0.1		+0.1	+0.1		+0.1	+0.2		+0.1	0		0	0		-0.1	-0.1		-0.1	+0.1		-0.1	+0.1		-0.1	0	
X_5	+0.2	+0.3	0.1060	+0.1	-0.1	0.1057	+0.2	+0.4	0.1040	+0.2	0	0.1050	+0.3	0	0.1052	+0.3	+0.3	0.1050	+0.1	+0.3	0.1050	+0.5	-0.2	0.1040	+0.1	+0.1	0.1057	+0.4	+0.2	0.1060
X_6	+0.1	+0.4	0.1059	+0.1	+0.2	0.1057	-0.4	+0.5	0.1040	+0.2	-0.3	0.1055	-0.3	+0.3	0.1046	+0.2	0	0.1053	+0.4	+0.1	0.1046	+0.3	-0.2	0.1041	+0.1	+0.1	0.1058	+0.2	+0.1	0.1052
X_7	+0.2	-0.3	0.1060	+0.3	0	0.1057	-0.3	+0.3	0.1040	+0.4	+0.1	0.1050	0	+0.2	0.1052	+0.1	-0.2	0.1048	+0.5	-0.1	0.1048	+0.2	+0.2	0.1041	+0.1	0	0.1058	-0.1	0	0.1052
X_8	+0.3	-0.3	0.1058	+0.3	-0.2	0.1058	+0.1	+0.3	0.1040	+0.4	+0.4	0.1050	+0.3	0	0.1056	-0.2	0	0.1049	-0.1	-0.1	0.1048	+0.1	+0.2	0.1040	0	+0.1	0.1057	-0.2	+0.2	0.1056

NOTE: On the W and Ta-W surface contours, the surface position designations represent the locations indicated below. All dimensions are in mils, with X_0 as the reference point. Positions with a "+" sign are lower than X_0 and positions with a "-" sign are higher than X_0.

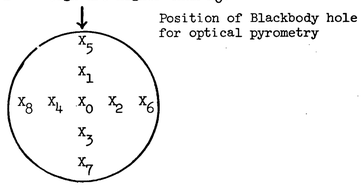

Table 1.5

(U) OPTICAL MICROMETER MEASUREMENTS (MILS) OF W AND Ta-10W SURFACE CONTOURS OF EMITTER STRUCTURES SUBJECTED TO THERMAL CYCLING TESTS

(This table is Unclassified)

	B_5-1				B_8-1						C_1-3								C_2-1*								C_3-1							
	After 200 hrs. at 1750°C		After 20 Cycles		After 100 hrs. at 2200°C		After 10 Cycles From 1650°C		After 15 Cycles From 1650°C		As Prepared		After 180 hrs. At 1600-1800°C		After 10 Cycles From 1800°C		After 30 Cycles From 1800°C		After 100 hrs. at 2200°C		After 10 Cycles From 1650°C		After 20 Cycles From 1650°C		After 30 Cycles From 1650°C		After 4 hrs. at 1800°C		After 10 Cycles From 1800°C		After 20 Cycles From 1800°C		After 30 Cycles From 1800°C	
Surface Position	W Surface	Ta-10W Surface	W Surface	Ta-10W Surface	W Surface	Ta Surface	W Surface	Ta Surface	W Surface	Ta Surface	W Surface	Ta-10W Surface	W Surface	Ta-10W Surface	W Surface	Ta-10W Surface	W Surface	Ta-10W Surface	W Surface	Ta Surface	W Surface	Ta Surface	W Surface	Ta Surface	W Surface	Ta Surface	W Surface	Ta-10W Surface	W Surface	Ta-10W Surface	W Surface	Ta-10W Surface	W Surface	Ta-10W Surface
X_0	0	0	0	0	0	0	0	0	0	0	0	0	0	0	0	0	0	0	0	0	0	0	0	0	0	0	0	0	0	0	0	0	0	0
X_1	-0.2	+0.2	-0.9	+0.9	-0.1	+0.3	-0.3	+0.3	-0.3	+0.1	0	0	-0.1	0	-1.5	+0.1	-3.4	+0.5	-0.3	-3.0	-1.2	-0.8	-1.3	-0.8	-1.5	-2.5	-0.1	+0.1	-0.1	+0.2	0	+0.3	-0.2	+1.2
X_2	-0.2	+0.1	-0.3	+1.0	-0.3	-0.5	-0.4	-0.3	-0.3	+0.1	+0.2	+0.1	0	+0.1	-0.5	+0.3	-1.5	+0.4	-0.4	-3.5	-0.3	-0.7	-0.1	-1.4	-0.6	-2.1	-0.1	0	-0.2	+0.3	-0.4	0	-1.4	+1.5
X_3	0	+0.1	0	+0.8	+0.1	-0.3	-0.4	-0.4	-0.7	-0.4	+0.1	+0.1	-0.2	+0.1	-0.4	+0.4	-2.4	+0.6	+0.5	-3.6	+1.0	+0.3	-0.1	-1.5	-1.4	-2.5	0	+0.1	-0.3	+0.3	0	0	-1.8	+1.2
X_4	-0.2	+0.2	-0.5	+0.8	+0.3	-0.5	-0.2	-0.4	-0.5	-0.3	-0.1	0	-0.2	+0.2	-0.5	+0.7	-4.3	+2.3	+0.1	-3.5	+2.4	-2.4	0	+1.2	-0.6	-2.1	0	+0.2	-0.3	+0.3	-0.5	0	-0.5	+1.5
X_5	-0.4	+0.5	-3.1	+2.5	0	-0.6	-1.0	+0.2	-0.5	+0.8	0	-0.1	-0.2	+0.2	-1.5	+1.5	-4.4	+6.4	0	-4.0	-1.8	-1.1	-2.5	-1.8	-3.0	-1.6	-0.1	+0.2	-0.4	+1.4	-3.5	+2.2	-1.4	+3.1
X_6	-0.5	+0.5	-1.5	+2.5	-0.5	-0.3	-1.0	0	-1.5	0.7	+0.5	+0.1	-0.1	+0.3	-1.5	+1.5	-3.5	+3.4	-0.1	-4.4	-0.4	-1.8	-0.6	-2.2	-1.9	-2.4	-0.2	0	-1.2	+1.3	-1.8	+2.4	-2.0	+3.0
X_7	-0.3	+0.5	-0.9	+2.5	0	-1.0	-1.0	-0.2	-1.9	+0.4	0	+0.3	-0.2	+0.4	-1.3	+1.5	-3.8	+3.5	+0.2	-4.3	+1.4	-1.5	-0.4	-2.7	-2.7	-2.7	-0.1	+0.3	-1.1	+1.3	-1.4	+2.0	-1.8	+2.4
X_8	-0.4	+0.5	-2.6	+2.2	+0.5	-0.9	-0.9	-0.2	-1.9	+0.4	-0.1	+0.1	-0.2	+0.3	-1.2	+1.5	-6.8	+6.7	+0.2	-4.4	+1.5	-2.7	-0.3	+1.1	-0.8	+2.5	-0.1	+0.5	-1.2	+1.9	-2.4	+0.2	-2.2	+2.3

Note: In the above table on the W and Ta-10W surface contours, the surface position designations represent the locations indicated below. All dimensions are in mils with X_0 as the reference point. Positions with "+" sign are lower than X_0 and positions with "-" sign are higher than X_0.

Thermal Cycling Scheme

(1) Room temperature to testing temperature - 1 hour
(2) At temperature - 5 minutes
(3) Power off instantaneously
(4) Time before power off and power on again - 20 minutes

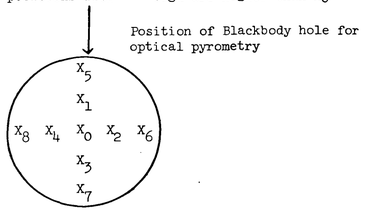

*Severe thermal etching of Ta surface by electron bombardment heating occurred. Observed readings on Ta surface are believed to be unreliable.

torr vacuum. Secondly the dimensions of the tungsten emitter disc and that of the Ta-10W substrate used for the diffusion bonding were such that after the bonding operation at least 15 mils could be removed from the surfaces exposed to the environment of the diffusion bonding chamber.

(U) Five discs of 0.200 inch thickness were cut from a Ta-10W alloy rod of 3/4 inch diameter and annealed for 15 hours at 1850°C and 5×10^{-8} torr. One disc was then cut into two halves and one half was analyzed for its N, O and C contents, which were found to be 31, 16 and 13 ppm respectively. Metallographic examination of the cross section of the other half showed clean grain structures (Fig. 1.6). Microhardness measurements were then made on this cross section and the results are shown in Table 1.6. The hardness near the exterior surface region is slightly higher but the difference is considered as insignificant.

(U) The other four discs were bonded to 0.630 inch diameter vapor deposited fluoride tungsten discs of {100} orientation by hot pressing at 1850°C and 3000 psi for 3 hours, using the arrangement shown in a previous report.(1) All four emitter structures, designated as B_6-1 through B_6-4, were stress relieved at 1800°C for 4 hours in 5×10^{-8} torr vacuum. B_6-4 was ground to the diametrical dimensions shown in the drawing of a previous report(1) and then sectioned into two halves. One half was analyzed for its N, O, C and H contents, which were found to be 12, 13, 9 and 2.1 ppm respectively. Metallographic examination of the cross section of the other half showed clean grain structures in the Ta-10W region (Fig. 1.7). Microhardness measurements made on this cross section yielded the results shown in Table 1.7. The slightly higher hardness near the end region could be due to the grinding operation. However, the difference is believed to be insignificant.

(U) B_6-1, B_6-2 and B_6-3 were ground to the required dimensions. The diameter of the tungsten side and the 12 mil wide Ta-10W lip were then prepared by electrical discharge machining. After the tungsten surface was polished with 1-micron diamond paste and electropolished, each was annealed for 4 hours at 1800°C. B_6-1 and B_6-2 were delivered to NASA, and

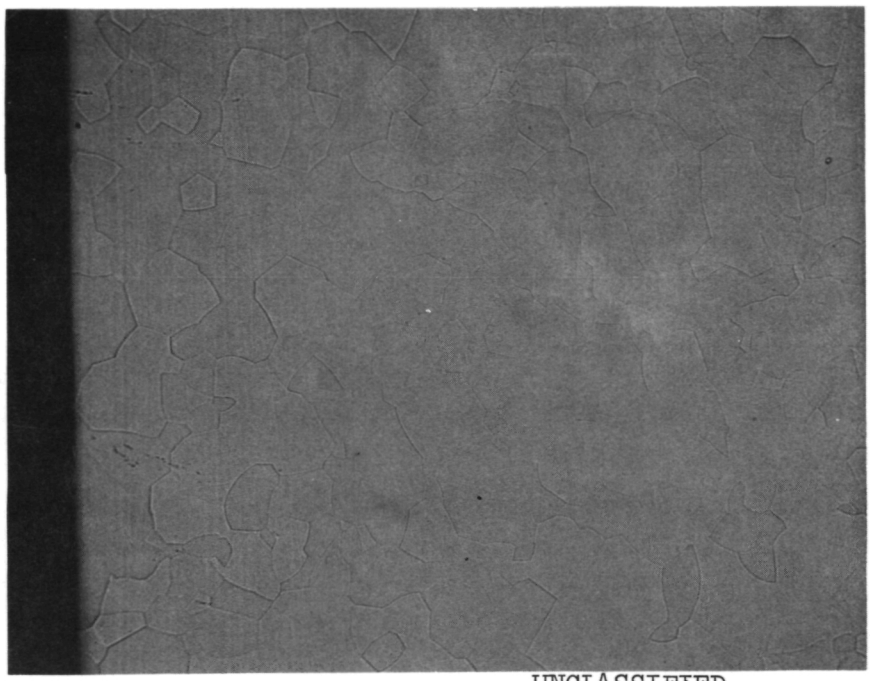

UNCLASSIFIED

M-19588-2 50X

Fig. 1.6--(U) Microstructures of one of the Ta-10W discs used for the preparation of B_6 series emitter structures after annealing for 15 hours at 1850°C in 5×10^{-8} torr vacuum. Note clean grain structures

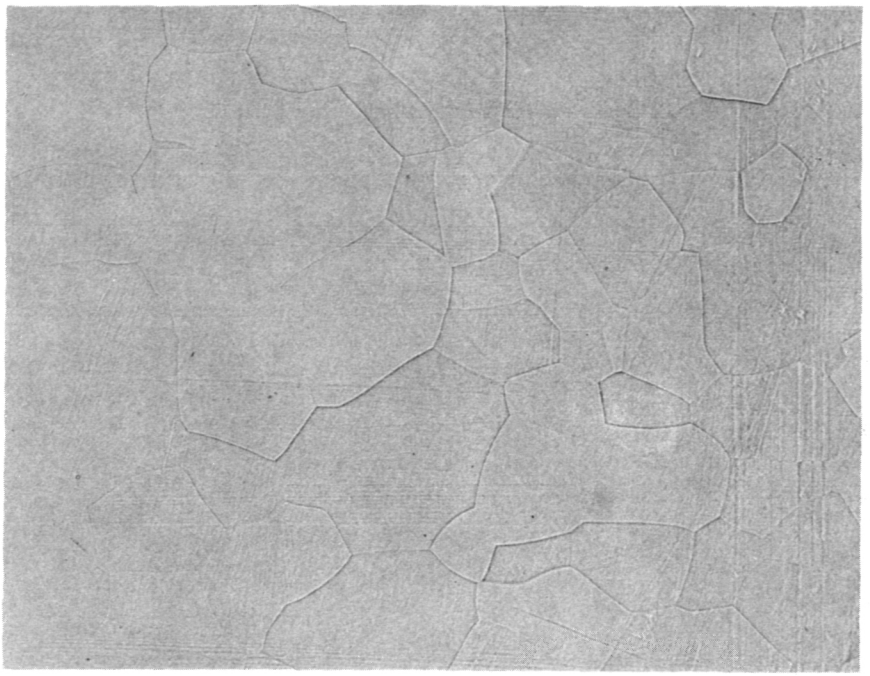

M 19718-2 UNCLASSIFIED 100X

Fig. 1.7--(U) Microstructures of a cross section of the Ta-10W region of B_6-4 emitter structure. Note clean grain structures

Table 1.6

(U) MICROHARDNESS AT DIFFERENT EQUALLY-SPACED LOCATIONS ALONG THE DIAMETER OF A CROSS SECTION OF ONE OF THE Ta-10W DISCS USED FOR THE PREPARATION OF THE B_6 SERIES EMITTER STRUCTURES AFTER ANNEALING FOR 15 HOURS AT 1850°C IN 5 x 10^{-8} TORR VACUUM

(This table is Unclassified)

Locations	DPH Hardness	Rockwell Hardness (RC)
1	274	26
2	254	24
3	245	22
4	236	20
5	245	22
6	245	22
7	245	22
8	254	24

Table 1.7

(U) MICROHARDNESS AT DIFFERENT EQUALLY SPACED LOCATIONS ALONG THE DIAMETER OF A CROSS SECTION OF B_6-4 EMITTER STRUCTURE IN THE Ta-10W REGION

(This table is Unclassified)

Locations	DPH Hardness	Rockwell Harness (RC)
1	264	25
2	264	25
3	250	23
4	245	22
5	245	22
6	245	22
7	237	20
8	254	24

B_6-3 was chemically etched before delivery to NASA as emitter structure D_1-1 (see Section 1.2.8 for D series). The finished dimensions and surface contours for B_6-1 and B_6-2 are shown respectively in Tables 1.3 and 1.4. Figure 1.8 shows the spatial distribution of the <100> axes in B_6-2 and Fig. 1.9 represents its surface microstructures before delivery to NASA.

1.2.3. B_7 Series Emitter Structures

(U) The B_7 series emitter structures were prepared for the purpose of studying the effect of using a tantalum instead of a Ta-10W substrate on the dimensional stability of the emitter structure upon thermal cycling. In addition, cleaning of the emitter surface by heating at 1650°C instead of at 1800°C was monitored by vacuum work function measurements.

(U) The B_7 series emitter structures were prepared by bonding fluoride tungsten emitters to Wah Chang capacitor grade tantalum at 1850°C and 1250 psi for 1 hour. The fabrication procedures were similar to that used for the B_6 series emitter structures. B_7-1 was installed in a vacuum emission cell and its vacuum work function ϕ was followed as a function of time at 1650°C. After 230 hours at 1650°C, a ϕ value of 4.56 eV was obtained at a vacuum of 4×10^{-9} torr. B_7-1 was then exposed to air for 18 hours and then its ϕ value was again followed as a function of time in vacuum at 1650°C. It took another 160 hours before ϕ returned to 4.57 eV at 4×10^{-9} torr vacuum (see Fig. 1.10). Metallographic examination of the emitter surface of B_7-1 after the test and that of the as-prepared B_7-2 and B_7-3 revealed the presence of microcracks presumably caused by defects present in the fluoride tungsten stock used. The study of the B_7 series emitter structures was therefore discontinued. Figure 1.11 shows the Ta interface of B_7-1 after the vacuum emission study. Numerous Kirkendall voids were observed on the tantalum side of the interface.

1.2.4. B_8 Series Emitter Structures

(U) The B_8 series emitter structures were prepared by using tantalum as the substrates, for the specific purpose of confirming the previous finding[2] that thermal treatment at 2200°C for 100 hours would help to

UNCLASSIFIED

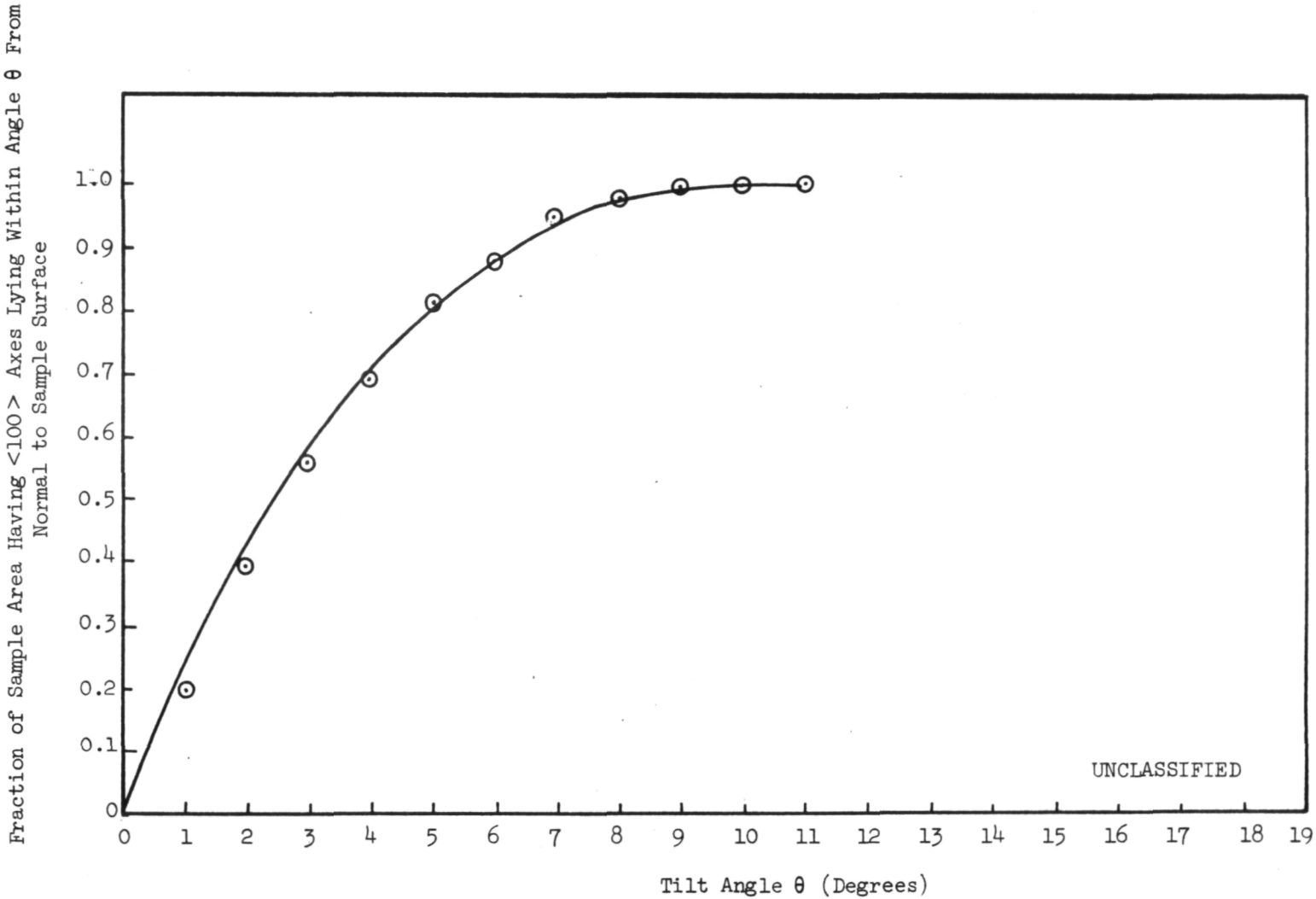

Fig. 1.8--(U) Spatial distribution of the <100> axes in emitter structure B_6-2 before delivery to NASA

UNCLASSIFIED

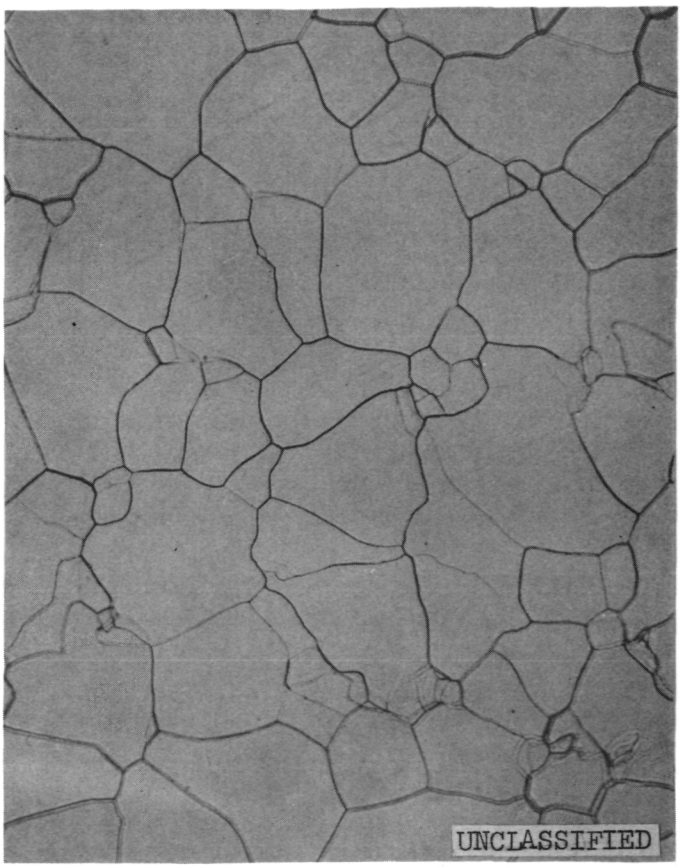

M 22974-1 250X

Fig. 1.9--(U) Surface microstructures of emitter structure B_6-2 before delivery to NASA

UNCLASSIFIED

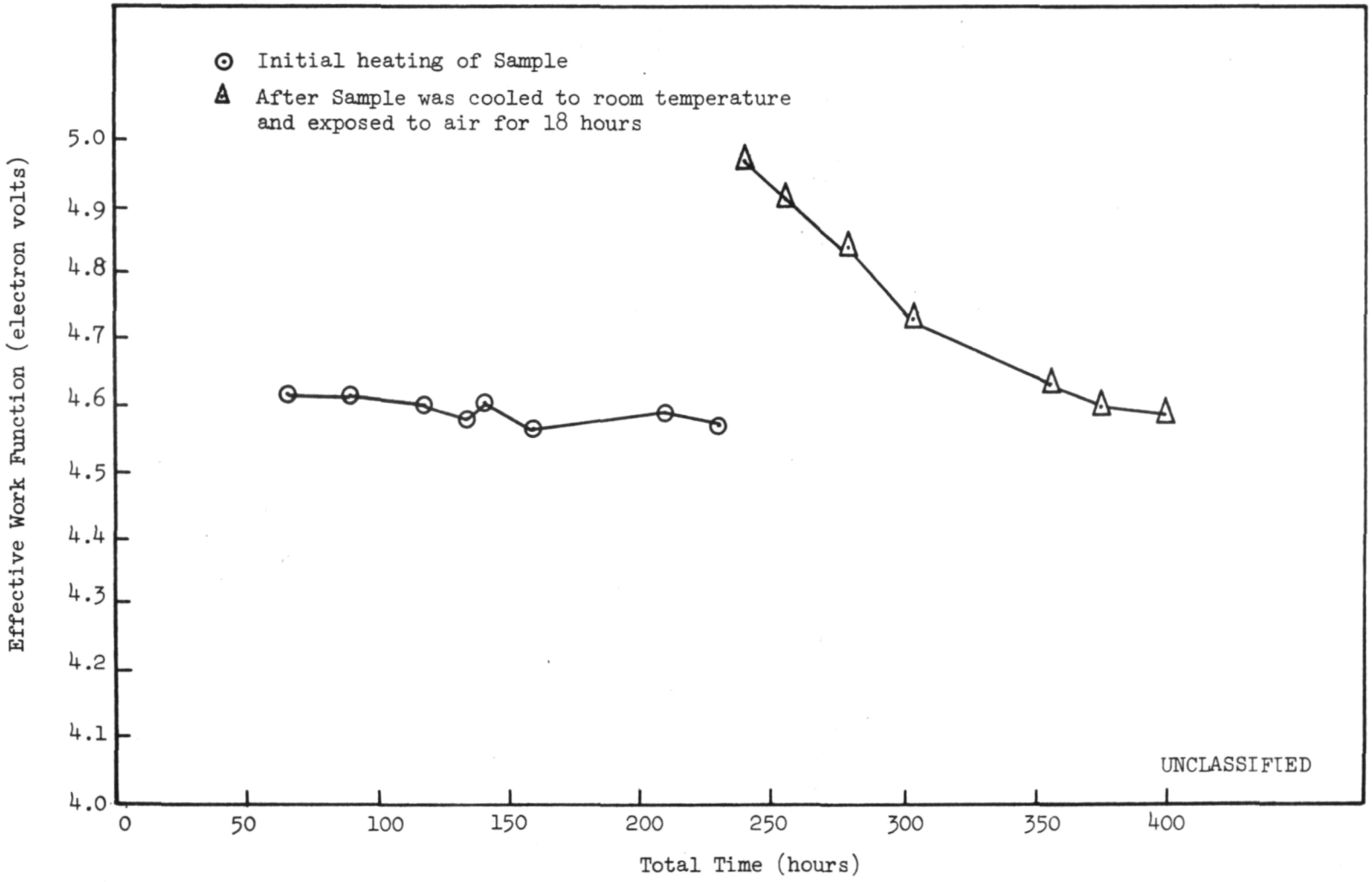

Fig. 1.10--(U) Effective work function as a function of time at 1650°C for Sample B_7-1

UNCLASSIFIED

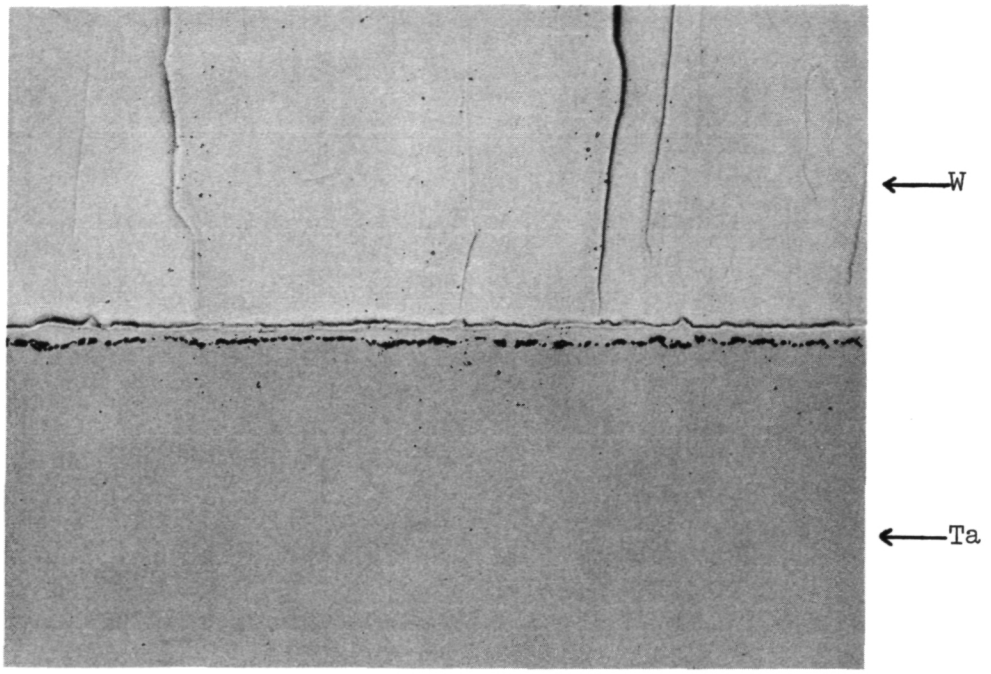

M 20471-1 UNCLASSIFIED 100X

Fig. 1.11--(U) Appearance of W-Ta interface of B_7-1 after vacuum work function study at 1650°C for 400 hours. Note numerous Kirkendall voids on Ta side near the interface

build up a diffusion zone at the tungsten-tantalum interface without the formation of numerous Kirkendall voids. Another objective was to find out whether such a heat treatment would improve the dimensional stability of the emitter structure upon thermal cycling.

(U) B_8-1 and B_8-2 were prepared by bonding fluoride tungsten emitters to Wah Chang capacitor grade tantalum at 1850°C and 1250 psi for 1 hour. Prior to bonding, the tantalum and tungsten were processed as follows. The large fluoride tungsten disc received from San Fernando Laboratories was stress-relieved for 4 hours at 1800°C in 2 x 10^{-6} torr vacuum. It was then ground to a 4 microinch finish. Examination under a microscope showed the absence of any surface defect. Emitter specimens were then cored from this large disc by electrical discharge machining and ground to 0.630 inch diameter and 0.043 inch thickness. Each of these emitter specimens was re-examined under a microscope and proved to be free from any surface defect. They were then annealed for 50 hours at 1800°C in 2 x 10^{-6} torr vacuum. Tantalum discs of 0.200 inch thickness were machined from the 0.75 inch diameter Wah Chang capacitor grade rod and annealed for 15 hours at 1850°C in 5 x 10^{-8} torr vacuum.

(U) After the bonding operation, B_8-1 and B_8-2 were stress-relieved for 4 hours at 1800°C in 5 x 10^{-8} torr vacuum and ground to the required diametrical dimensions. B_8-2 was kept in reserve and B_8-1 was heated for 100 hours at 2200°C in a vacuum emission cell. Following this high temperature treatment it was examined for any change in the contours of the tungsten and tantalum surfaces. The sample was then thermal cycled 10 times between 1650°C and room temperature in a vacuum emission cell according to the following scheme: 1 hour heating period from room temperature to 1650°C, at temperature for 5 minutes, power turned off instantaneously, and a cooling period of 20 minutes. After thermal cycling, the sample was examined again for contour changes. Following this the sample was again thermal cycled for 5 times and reexamined for contour changes. The results of these treatments are shown in Table 1.5. It can be seen that the maximum deformation of the tungsten emitter contour was about 1 mil after 10 cycles and about 1.7 mils after 15 cycles. These results do not differ significantly from those observed on tungsten emitters bonded to Ta-10W, which were not

heated at 2200°C. Thus the 2200°C heat treatment does not seem to have any appreciable effect in reducing emitter deformation upon thermal cycling.

(U) B_8-1 was then sectioned across the W-Ta interface. One of the sections was polished and examined under a microscope (Fig. 1.12). A good bond existed between the tungsten and the tantalum. The presence of some Kirkendall voids was observed on the tantalum side near the tungsten-tantalum interface but the number was much less than that present in B_7-1 (see Fig. 1.11) which was heated at 1650°C for 400 hours in a vacuum emission cell.

1.2.5. C_1 Series Emitter Structures

(U) The C_1 Series emitter structure consist of {110} oriented chloride tungsten emitters bonded to Ta-10W substrates. Five C_1 series emitter structures, C_1-1, C_1-2, C_1-3, C_1-4 and C_1-5 were prepared by diffusion bonding {110} oriented chloride tungsten emitters to Ta-10W discs at 1850°C and 3000 psi for 3 hours. The chloride tungsten emitters for C_1-1, C_1-2 and C_1-3 were cored out of one large chloride tungsten disc, while that for C_1-4 and C_1-5 were cored out of another large chloride tungsten disc. Both discs were procurred from San Fernando Laboratories. These emitters were outgassed at 1800°C for 100 hours in a vacuum of 2×10^{-6} torr. Figure 1.13 shows the spatial distributions of the <110> axes in these emitter discs before they were diffusion bonded to their Ta-10W substrate. The Ta-10W discs were obtained from the same rod used for the preparation of the B_6 series emitter structures and were heated at 1850°C for 15 hours in 5×10^{-8} torr vacuum before they were used. After diffusion bonding, all five emitter structures were stress-relieved at 1800°C for 4 hours in 5×10^{-8} torr vacuum. C_1-1, C_1-2, C_1-4 and C_1-5 were then ground and electrical discharge machined to the required dimensions, polished with 1-micron diamond paste, electropolished in an aqueous solution of NaOH and then annealed at 1800°C for 4 hours in 5×10^{-8} torr vacuum before delivery to NASA. Figures 1.14, 1.15 and 1.16 show respectively the spatial distributions of the <110> axes for the emitter surface by the emitter structures C_1-2, C_1-4 and C_1-5. Their finished dimensions and surface contours are shown respectively in Tables 1.3 and 1.4. Figures 1.17, 1.18 and 1.19 represent the surface appearances of C_1-2, C_1-4 and C_1-5 respectively after

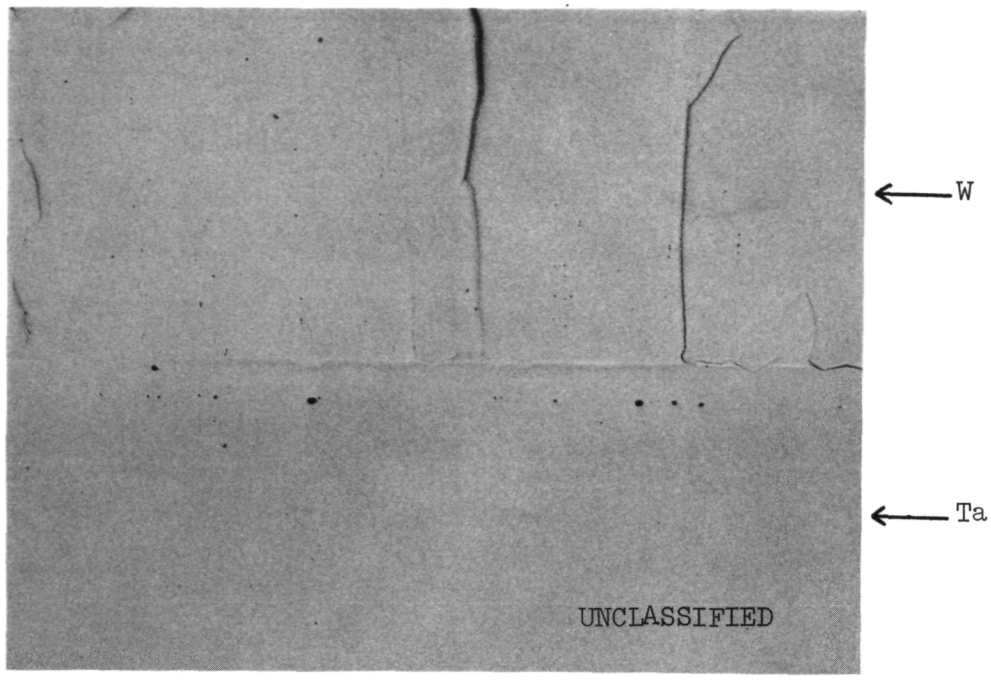

M 20923-5 (a) Unetched 100X

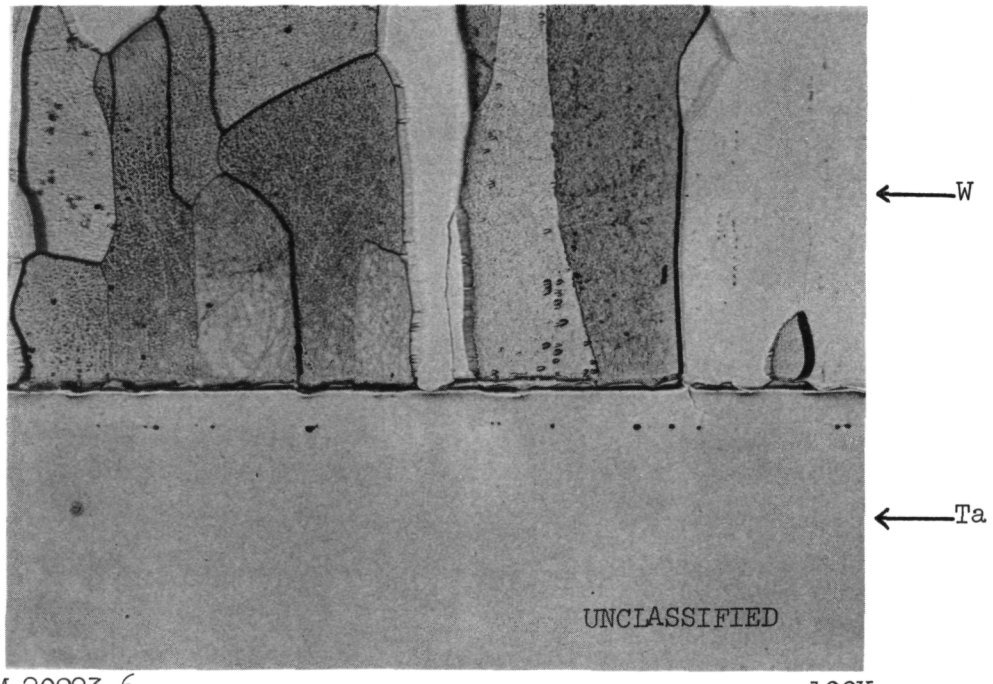

M 20923-6 (b) Etched 100X

Fig. 1.12--(U) Appearance of W-Ta interface of B_8-1 after 100 hour heat treatment at 2200°C, followed by thermal cycling 15 times between 1650°C and room temperature. Note the number of Kirkendall voids is much less than that of B_7-1 (see Fig. 1.10)

UNCLASSIFIED

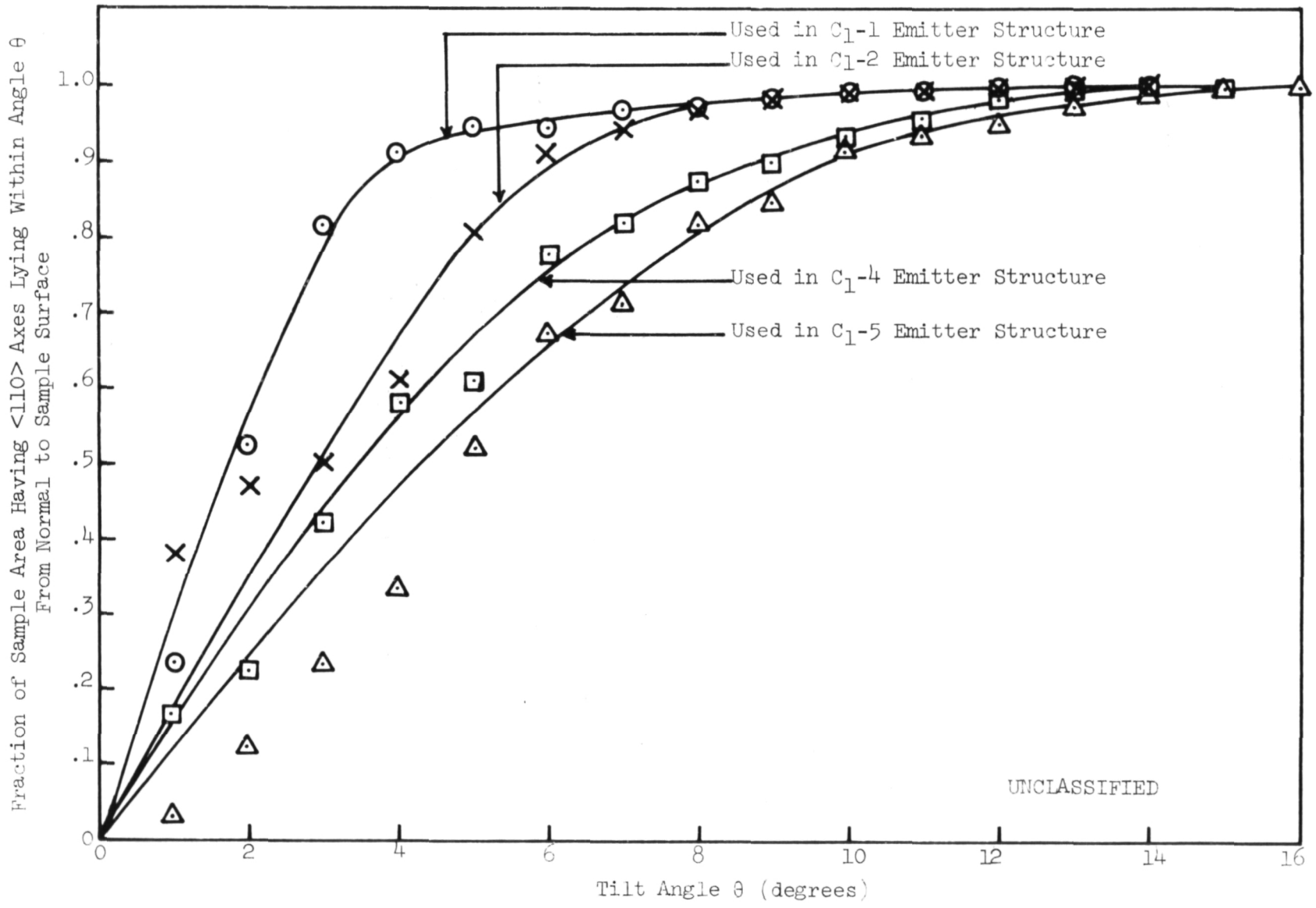

Fig. 1.13--(U) Spatial distribution of the <110> axes in the tungsten discs used for the preparation of emitter structures C_1-1, C_1-2, C_1-4 and C_1-5

UNCLASSIFIED

UNCLASSIFIED

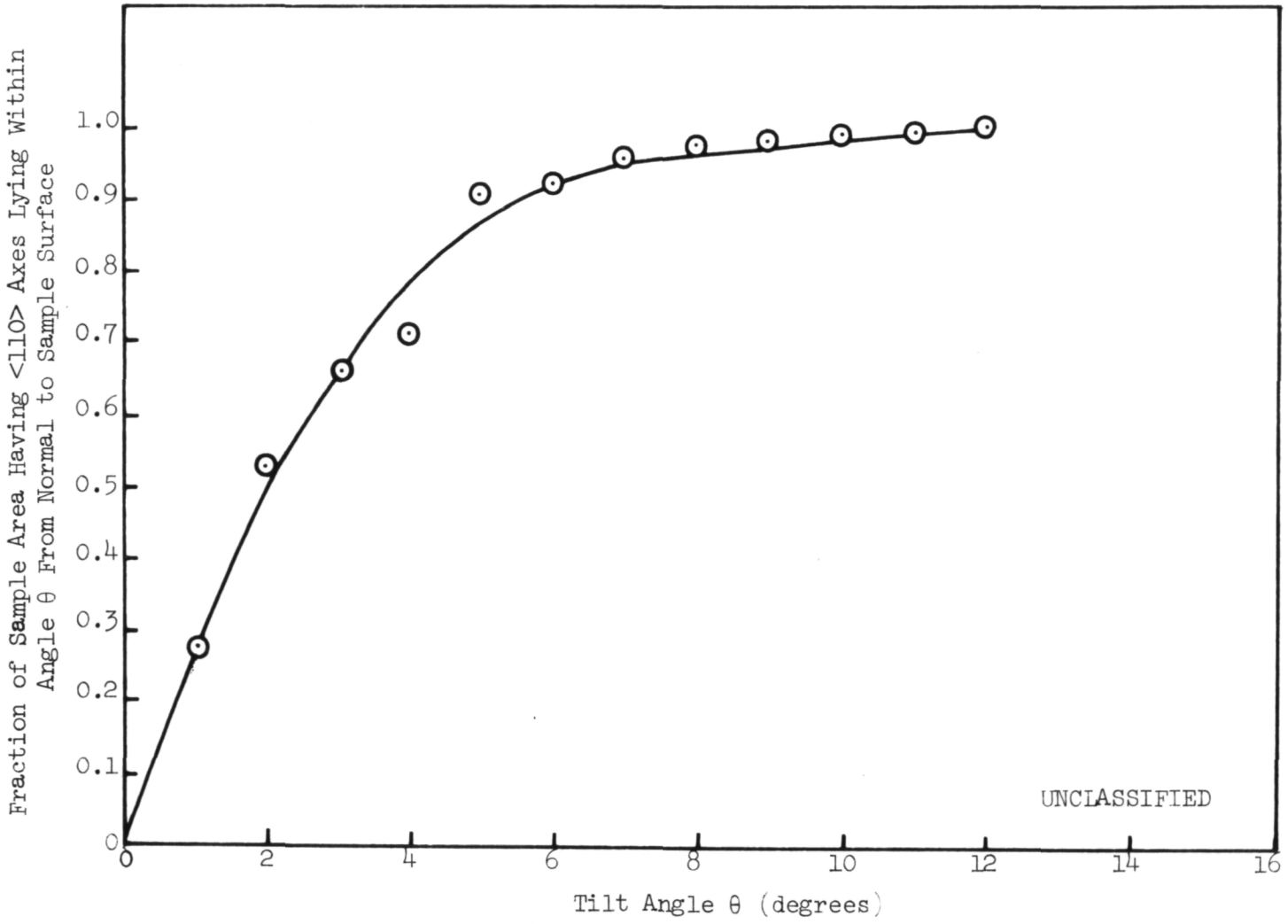

Fig. 1.14--(U) Spatial distribution of the <110> axes in C_1-2

UNCLASSIFIED

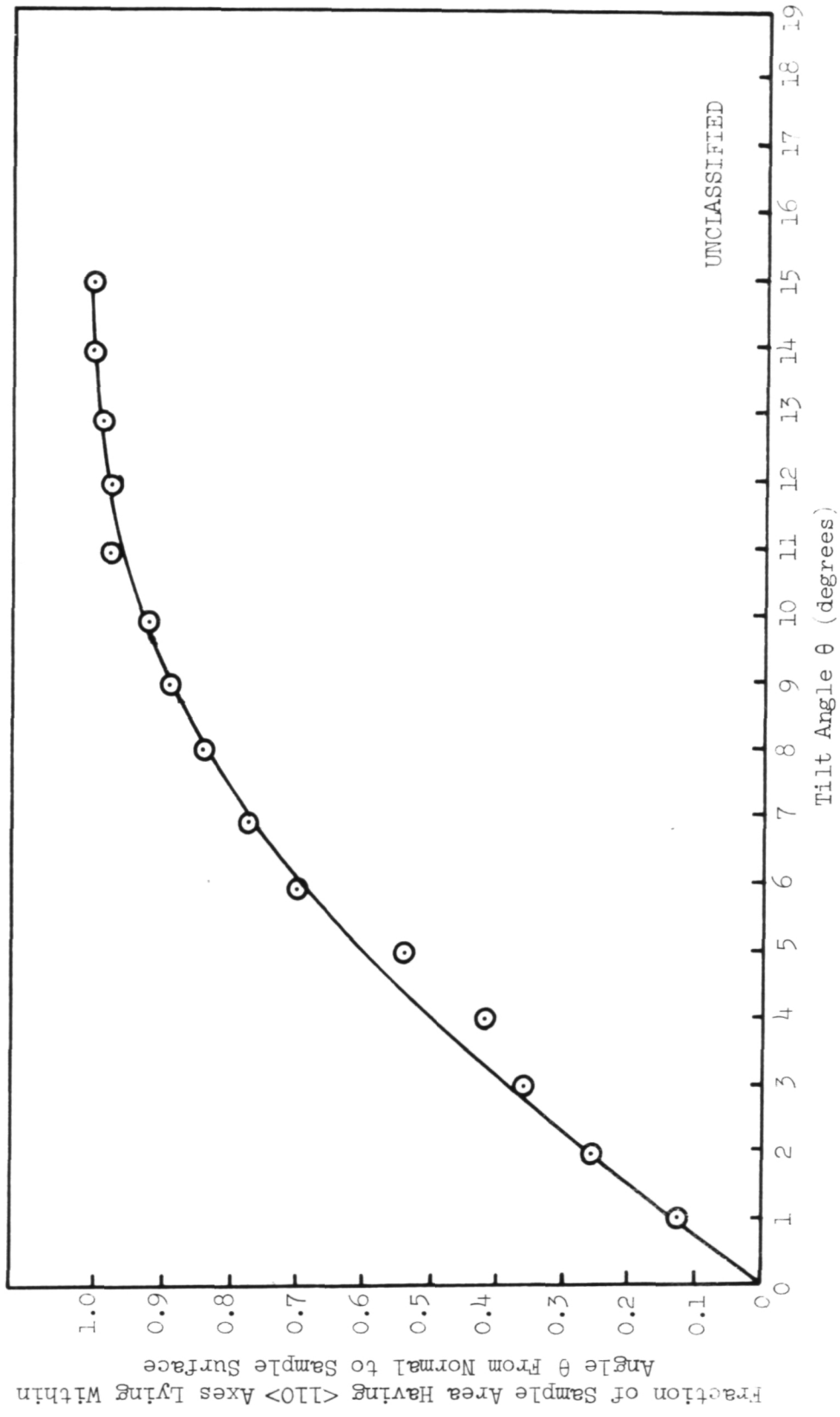

Fig. 1.15--(U) Spatial distribution of the <110> axes in C_1-4

UNCLASSIFIED

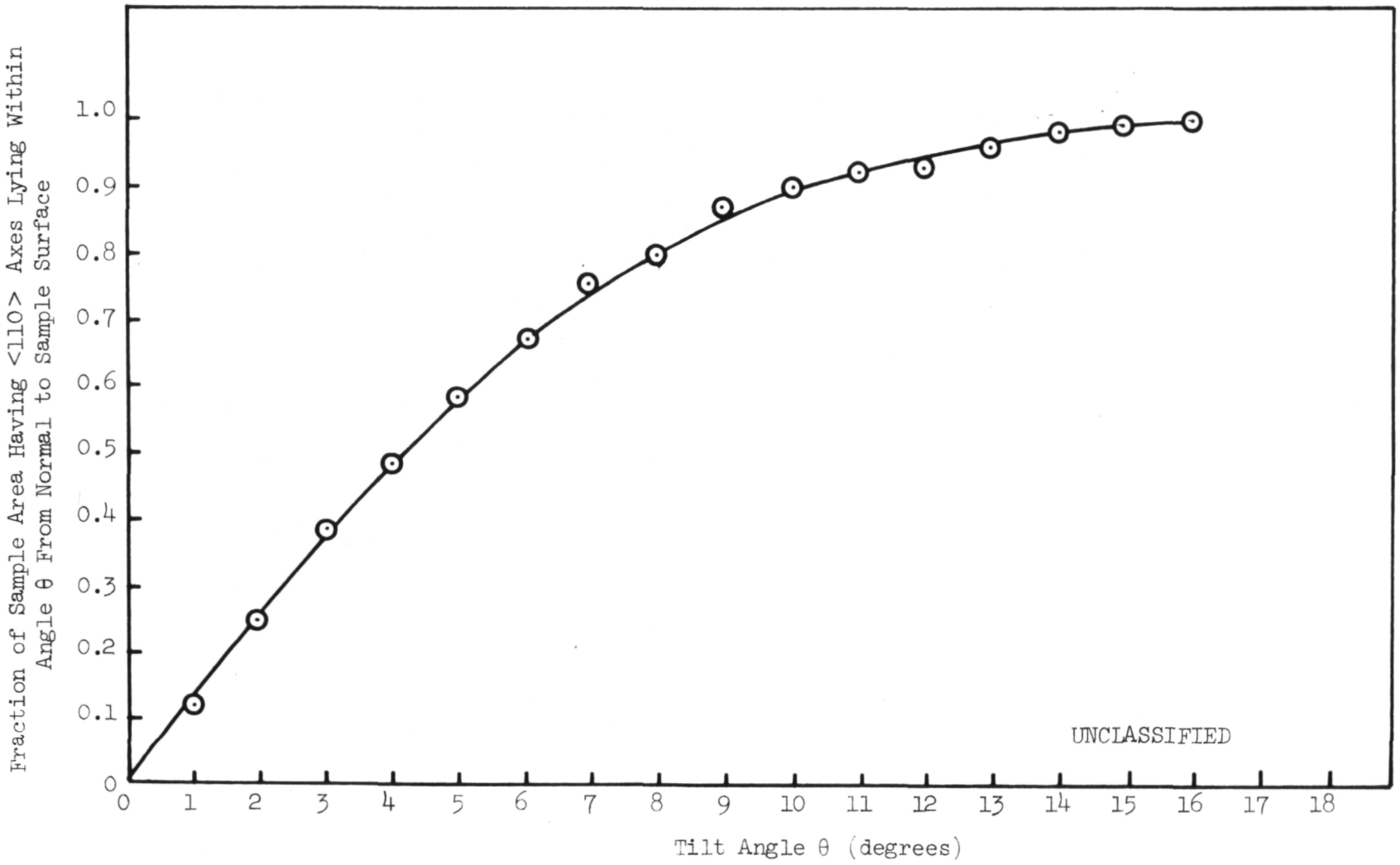

Fig. 1.16--(U) Spatial distribution of the <110> axes in C_1-5

UNCLASSIFIED

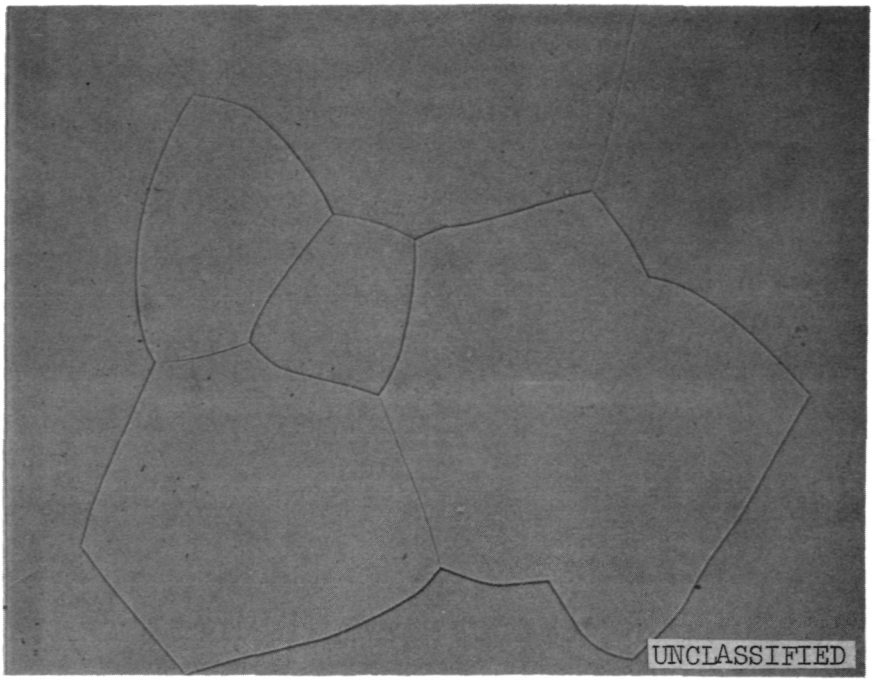

M 22875-2 100X

Fig. 1.17--(U) Surface appearance of emitter structure C_1-2 after electropolishing

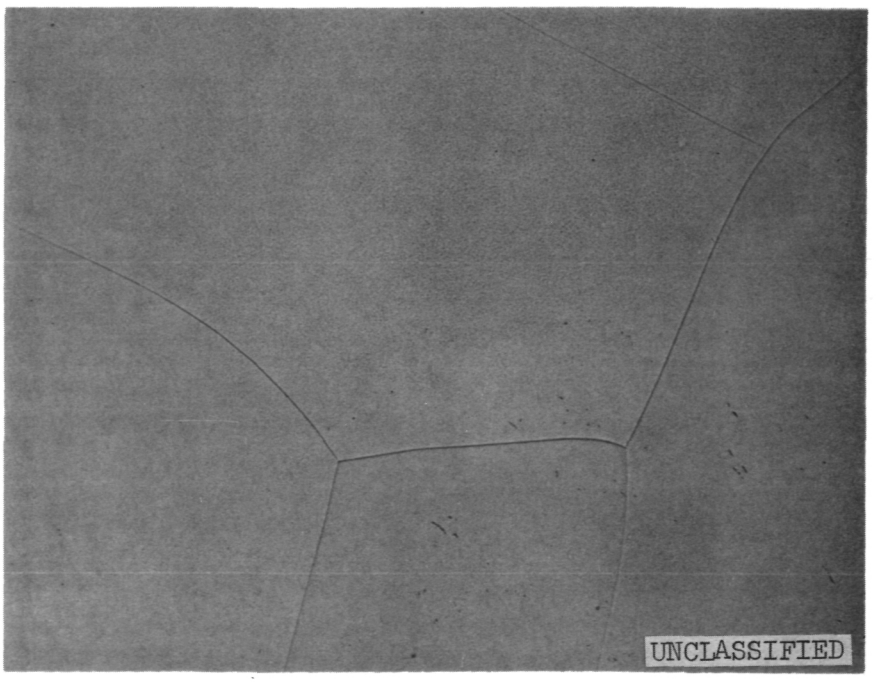

M 22985-3 100X

Fig. 1.18--(U) Surface appearance of emitter structure C_1-4 after electropolishing

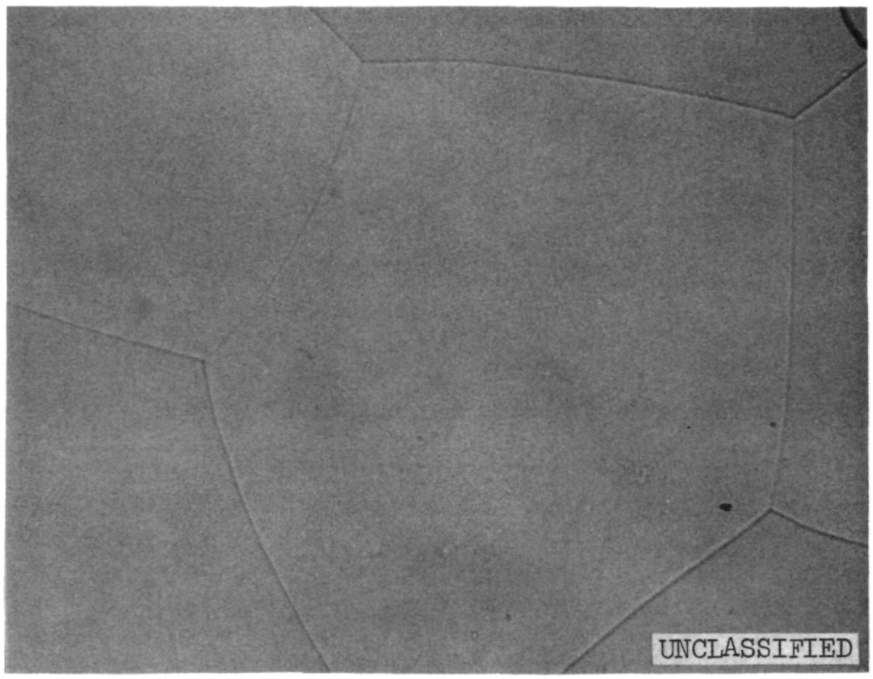

M 23275-1 100X

Fig. 1.19--(U) Surface appearance of emitter structure C_1-5 after electropolishing

electropolishing but before the final heat treatment. The large grain size of these chloride tungsten emitters is clearly indicated.

(U) C_1-3 was ground to the required diametrical dimensions, polished with 1-micron diamond paste and electropolished in an aqueous solution of NaOH. The contours of both the tungsten surface and the Ta-10W surface were then measured before C_1-3 was installed in a vacuum emission cell for vacuum work function measurements. In the vacuum emission cell, C_1-3 was heated at 1800°C for 175 hours before its work function was measured in the temperature range of 1600°C to 1800°C. After the completion of the work function measurements, the contours of the tungsten surface and Ta-10W surface were again measured. The surface contour measurements are given in Table 1.5 and the vacuum work function measurements are shown in Table 1.8. Visual observation indicated that excessive grain growth had occurred in the chloride tungsten emitter, and numerous slip lines were present on the surface of the emitter. C_1-3 was thermal cycled between 1800°C and room temperature according to the same scheme used for the thermal cycling of B_8-1. Optical micrometer measurements of the surface contours made after 10 and 30 cycles are included in Table 1.5. It can be seen that excessive deformation of the emitter structure surfaces occurred even after 10 cycles. Prior to lowering the emitter to room temperature during the thirtieth cycle, the vacuum work function at 1800°C was again determined. A value of 4.82 eV was obtained, which is the same as that obtained before the thermal cycling test (see Table 1.8). Figure 1.20 shows the emitter surface of C_1-3 after the thermal cycling test. The large grain size and the presence of numerous slip lines are apparent.

Table 1.8

(U) EFFECTIVE VACUUM WORK FUNCTION OF EMITTER STRUCTURE C_1-3 BETWEEN 1600°C AND 1800°C AFTER 175 HOURS AT 1800°C

(This table is Unclassified)

Temperature °C	Effective Vacuum Work Function (eV)
1800	4.82
1750	4.77
1700	4.78
1650	4.78
1600	4.77

100X

Fig. 1.20--(U) Emitter surface of emitter structure C_1-3 after the thermal cycling test

1.2.6. C_2 Series Emitter Structure

(U) One C_2 series emitter structure, C_2-1, was prepared for the evaluation of the effect of heat treatment at 2200°C on the dimensional stability of an emitter structure consisting of {110} oriented chloride tungsten emitter bonded to a tantalum substrate upon thermal cycling. The emitter disc was cored out of a large chloride tungsten disc from which the emitters of C_1-4 and C_1-5 were obtained. The tantalum disc was cut from the same Wah Chang capacitor grade tantalum rod from which the tantalum substrates for the B_7 and the B_8 series emitter structures were taken. Diffusion bonding was carried out at 1850°C and 1250 psi for 1 hour. After machining to the required dimensions, the emitter structure was heated at 2200°C for 100 hours at $< 2 \times 10^{-8}$ torr in a diffusion-emission cell. After the surface contours of the heat treated emitter structure were measured with an optical micrometer, the emitter structure was re-inserted in the diffusion-emission cell and thermal cycled for 30 times between room temperature and 1650°C. The thermal cycling scheme and the surface contour measurements after each 10 thermal cycles are shown in Table 1.5. The results indicate that the 2200°C heat treatment did not eliminate the deformation of the surface contours of such an emitter structure upon thermal cycling to any significant extent.

1.2.7. C_3 Series Emitter Structures

(U) The C_3 series emitter structures consist of duplex tungsten emitters (10 mil thick chloride tungsten emitting layer over 30 mil thick fluoride tungsten base material) diffusion-bonded to Ta-10W substrates at 1850°C and 3000 psi for 3 hours. Three emitter structures, C_3-1, C_3-2 and C_3-3 were prepared. The duplex tungsten emitter discs for C_3-1 and C_3-2 were obtained from the duplex tungsten disc 2B-8 which had been used in previous studies on the vacuum emission properties of duplex tungsten emitters,[1] while the duplex tungsten emitter disc for C_3-3 was prepared at Gulf General Atomic according to the procedures described under Task III of this report. The Ta-10W substrates were the same material and heat treated in the same way as that for the B_6 and the C_1 series emitter structures. Diffusion bonding between the duplex tungsten emitters and the

the Ta-10W substrates were carried out at 1850°C and 3000 psi for 3 hours. Subsequently they were machined to the required dimensions.

(U) C_3-1 was used to study the dimensional stability of duplex tungsten emitter structures upon thermal cycling. It was thermal cycled 30 times between room temperature and 1800°C and its surface contours were examined with an optical micrometer after each 10 cycles. The results are shown in Table 1.5. It can be seen that the use of a duplex tungsten emitter does not lead to significant improvement of the dimensional stability of the emitter structure upon thermal cycling.

(U) C_3-2 and C_3-3 were polished with 1 micron diamond paste, electropolished and stress relieved for 4 hours at 1800°C before delivery to NASA. Their dimensions and surface contour measurements are given in Tables 1.3 and 1.4 respectively. Figures 1.21 and 1.22 show the spatial distributions of the <110> axes in these two emitter structures. Figures 1.23 and 1.24 are the surface appearance of C_3-2 after electropolishing and the surface appearance of C_3-3 after electropolishing and stress-relieving at 1800°C. While the electropolished surface was highly smooth, the 1800°C heat treatment brought out grain boundaries and slip lines and yielded surface structures closer to the true equilibrium surface structures under these conditions.

1.2.8. D_1 Series Emitter Structures

(U) The D_1 series emitter structures consist of chemically etched fluoride tungsten emitters diffusion bonded to Ta-10W substrates. These emitter structures were prepared to determine whether the increase in vacuum work function of fluoride tungsten emitter, by chemical etching could benefit converter performance if the operating temperature of the emitter were not excessively high. Two D_1 series emitter structures, D_1-1 and D_1-2, were prepared. D_1-1 was obtained by chemical etching the emitter surface of the emitter structure B_6-3 in a solution of 100 parts saturated $K_3Fe(CN)_6$, 5 parts saturated KOH, and 95 parts of H_2O, for 2 hours at room temperature, after B_6-3 was stress-relieved for 4 hours at 1800°C. D_1-1 was delivered to NASA without any further heat treatment. Figure 1.25 shows the spatial distribution of the <100> axes in D_1-1, and Fig. 1.26 shows the appearance of the

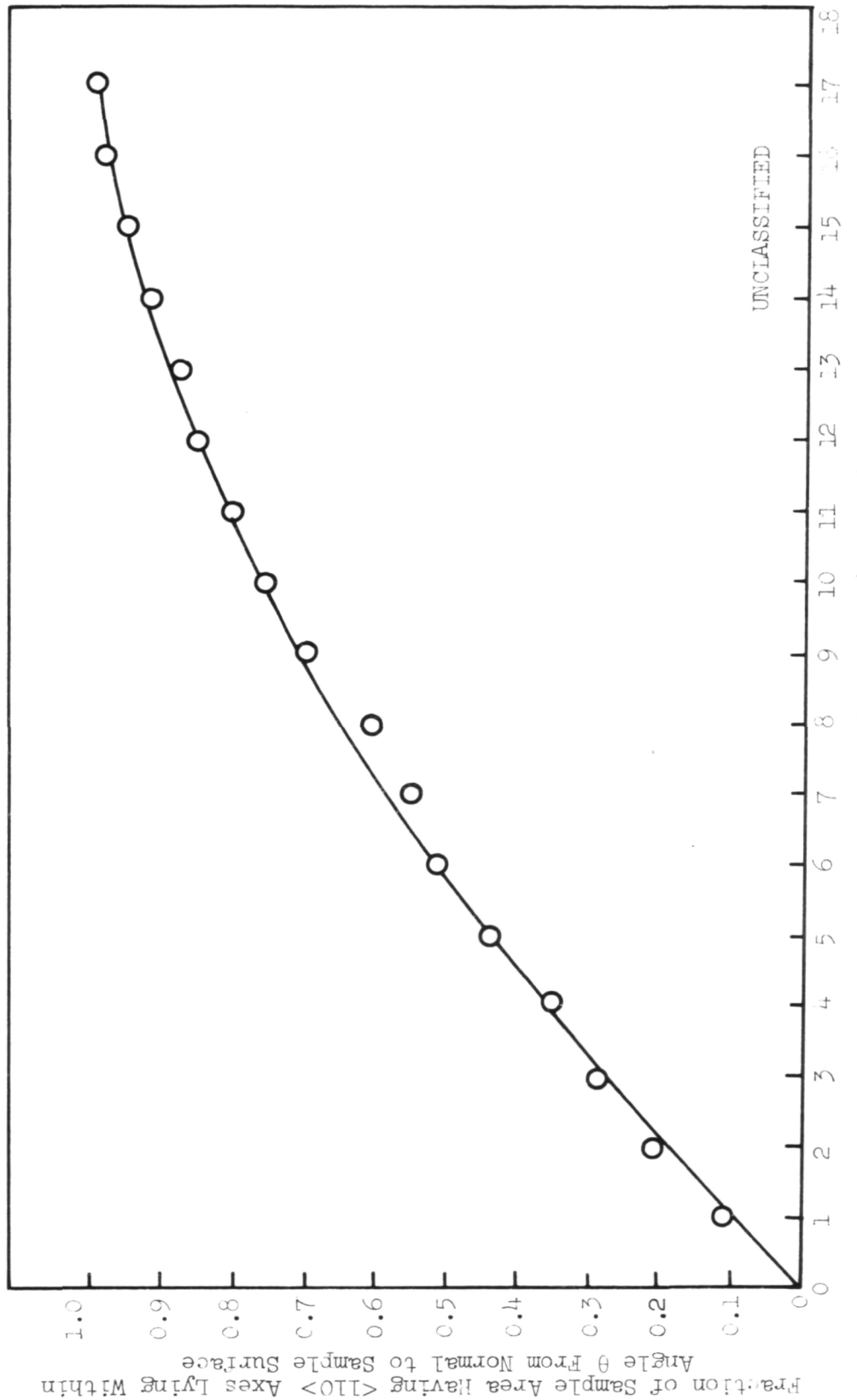

Fig. 1.21--(U) Spatial distribution of the <110> axes in C_3-2

UNCLASSIFIED

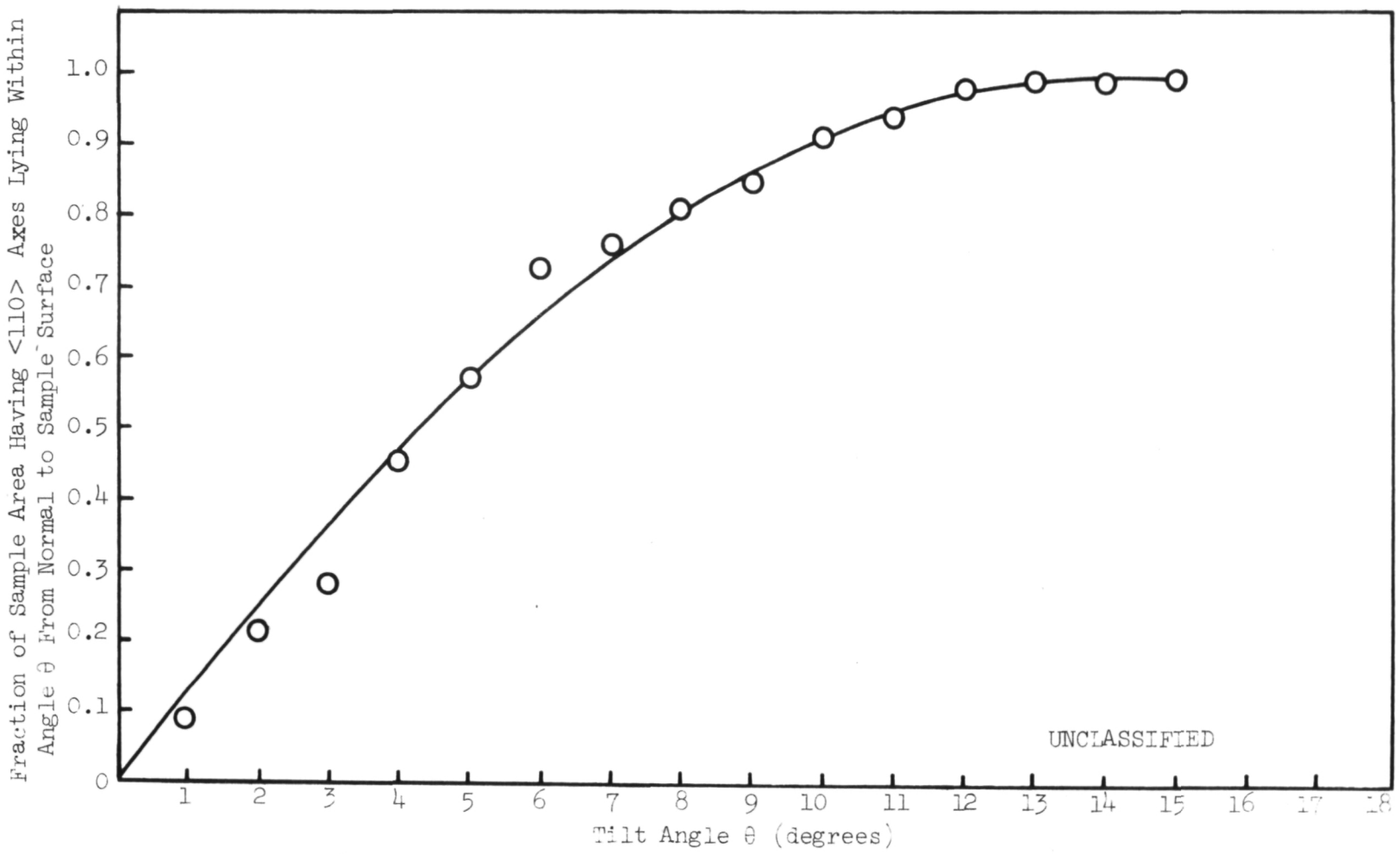

Fig. 1.22--(U) Spatial distribution of the <110> axes in C_3-3

UNCLASSIFIED

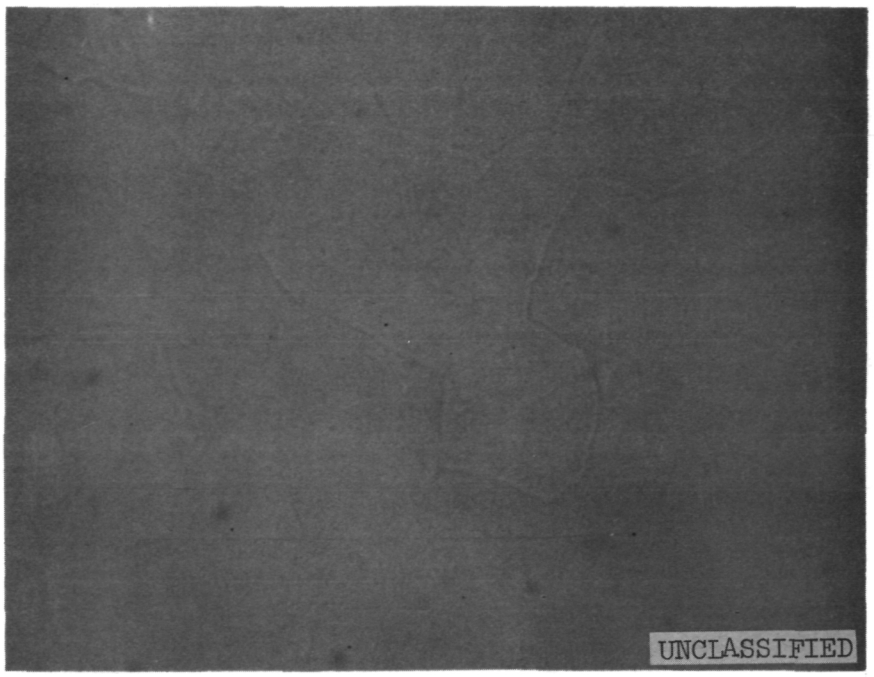

M 23998-1 250X

Fig. 1.23--(U) Surface appearance of emitter structure C_3-2 after electropolishing

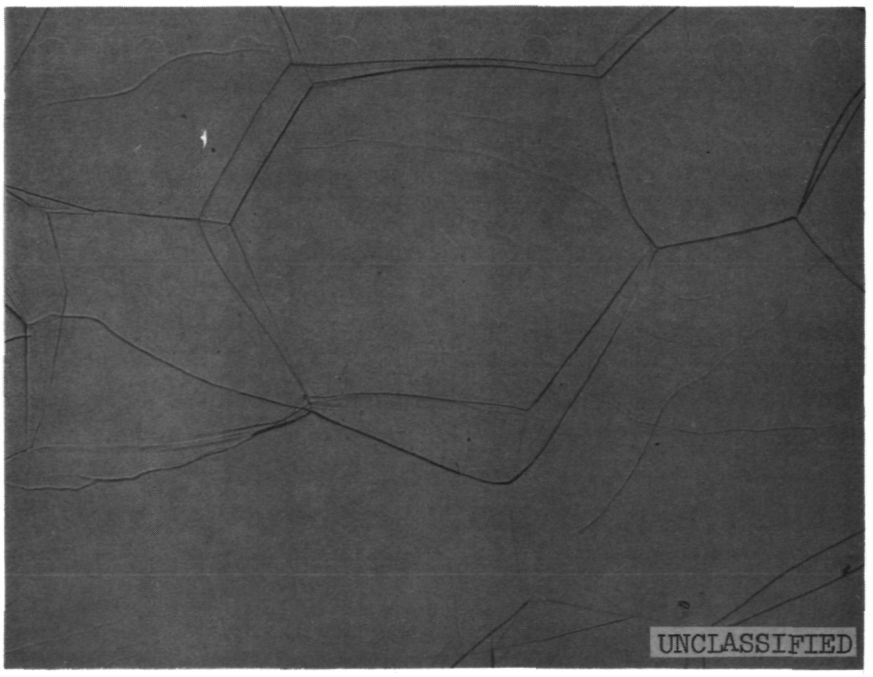

250X

Fig. 1.24--(U) Surface appearance of emitter structure C_3-3 after electropolishing and stress-relieving at 1800°C

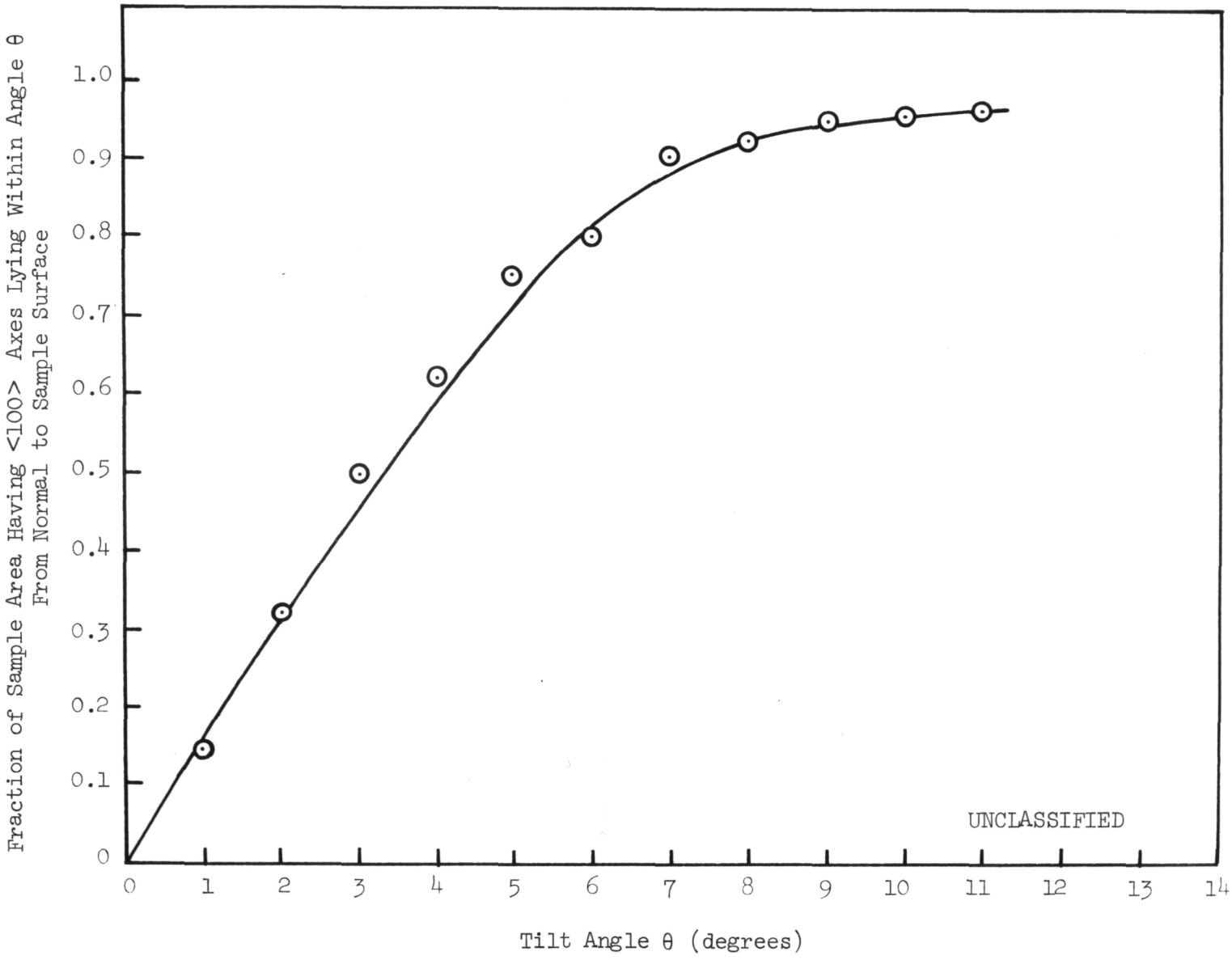

Fig. 1.25--(U) Spatial distribution of the <100> axes in D_1-1

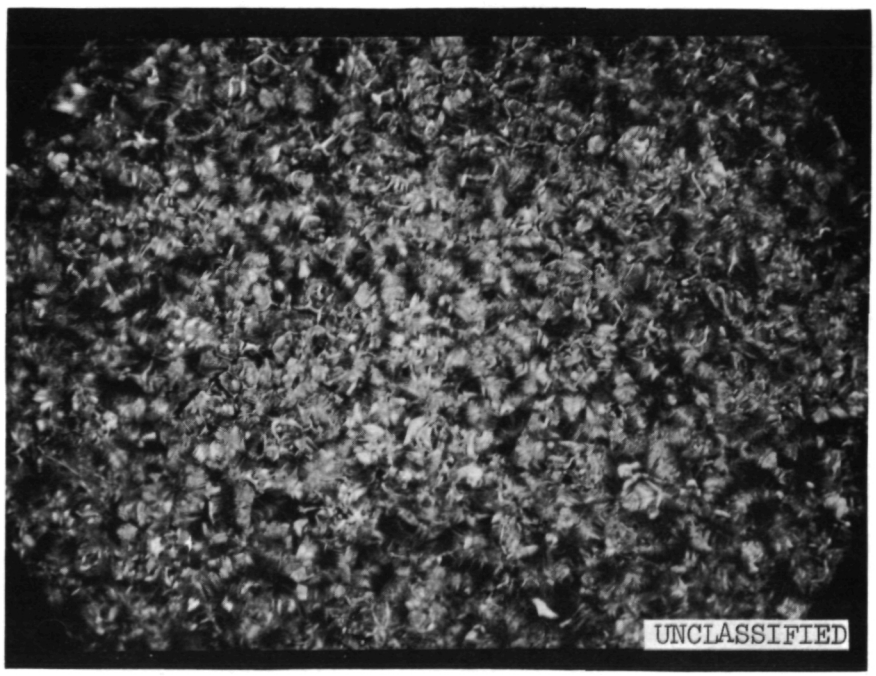

100X

Fig. 1.26--(U) Appearance of the chemically etched surface of the emitter D_1-1

chemically etched surface of the emitter of D_1-1. The dimensions and surface contour measurements of D_1-1 are shown in Tables 1.3 and 1.4 respectively. D_1-2 was prepared as a backup for D_1-1 under the same conditions as B_6-3. The dimensions and the surface contour measurements of D_1-2 in its pre-etching condition are shown respectively in Tables 1.3 and 1.4.

1.3. POST-OPERATIONAL EXAMINATION OF EMITTER STRUCTURES

1.3.1. B_6-2 Emitter Structure

(U) The B_6-2 emitter structure, attached to its tantalum stem and insulator structures, was received from NASA after 3000 hour operation in cesiated environment at 1727°C. Figure 1.27 is a macrophotograph of the as-received piece showing the Ta-10W substrate of the emitter structure, the weld between the Ta-10W thin lip, the tantalum emitter stem, and the insulator structure.

(U) Examination of the weld region between the Ta-10W lip of the emitter structure and the tantalum emitter stem revealed the presence of cracks across the weld (Fig. 1.28(a)), at the Ta-10W side of the weld (Fig. 1.28(b)), and in the groove between the Ta-10W lip and the Ta-10W emitter structure substrate (Fig. 1.28(c)). The development of such cracks is believed to be the principal cause of the failure of the converter. The tantalum stem was then separated from the emitter structure at the weld. Metallographic examination of the regions in the Ta-10W near the weld showed numerous grain boundary cracks (Fig. 1.29), but no precipitates of secondary phases were observed. Chemical analysis of the emitter structure (after the completion of post-test examinations) and the tantalum stem yielded the following results (in ppm):

	Emitter Structure	Tantalum Stem
O	277	932
N	22	21
C	30	240

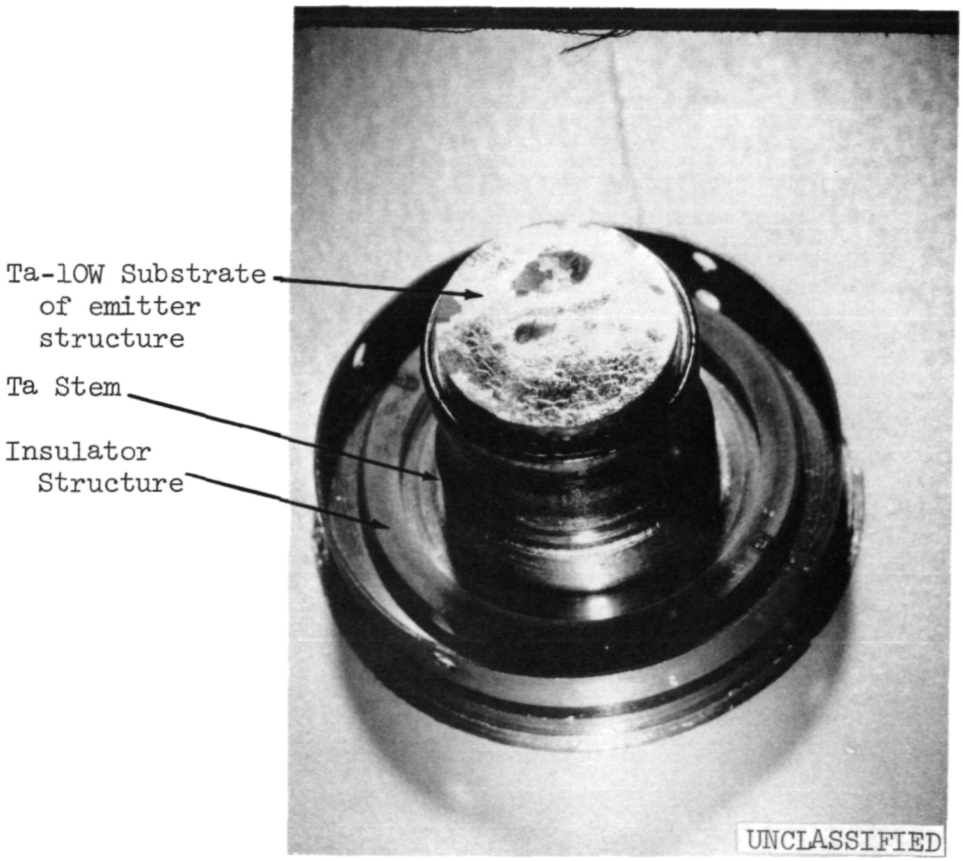

M 23279-3 ~1.5X

Fig. 1.27--(U) Appearance of the exterior of the B_6-2 emitter structure, as-received from NASA after operation in a cesiated converter

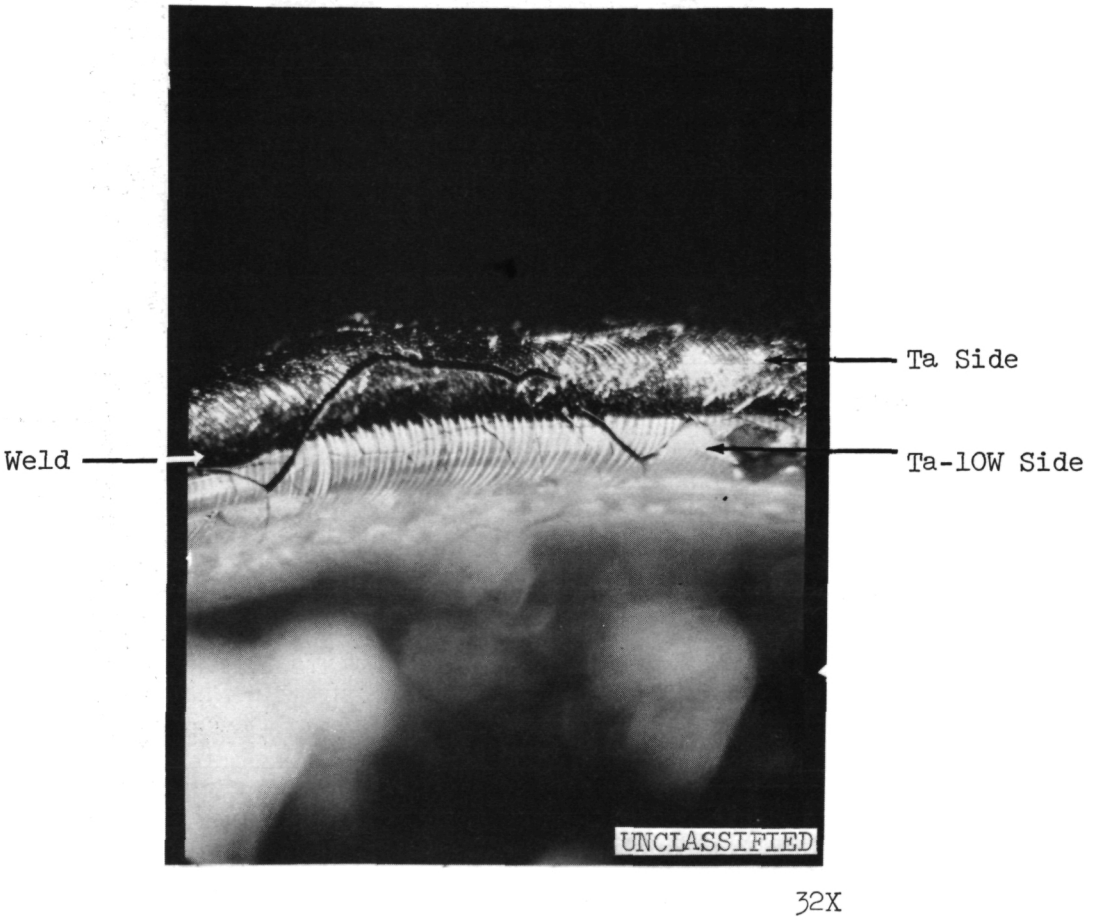

(a) Crack across the weld

Fig. 1.28--(U) Presence of cracks in the vicinity of the weld between the Ta-10W lip of the emitter structure and the tantalum emitter stem in post-test B_6-2 emitter assembly (page 1 of 3)

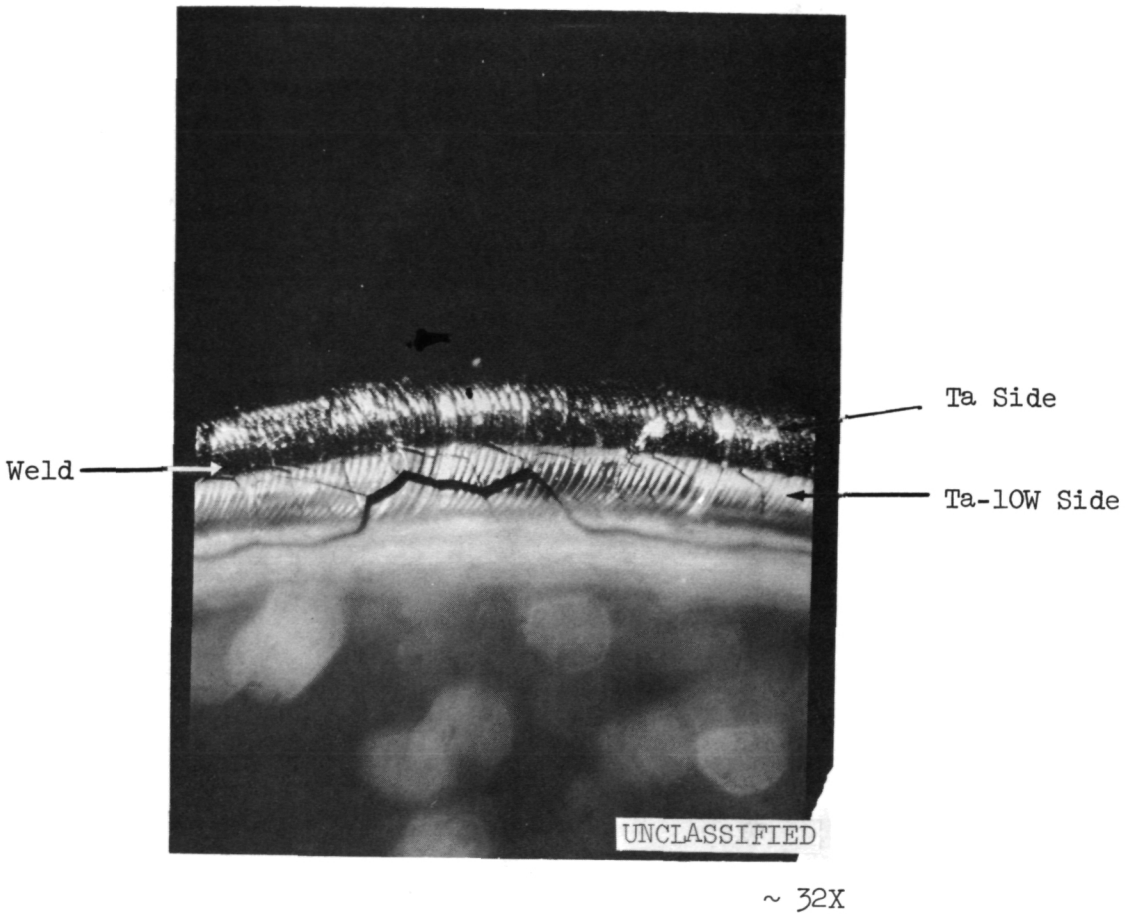

(b) Crack on Ta-10W side of the weld

Fig. 1.28--(U) Presence of cracks in the vicinity of the weld between the Ta-10W lip of the emitter structure and the tantalum emitter stem in post-test B_6-2 emitter assembly (page 2 of 3)

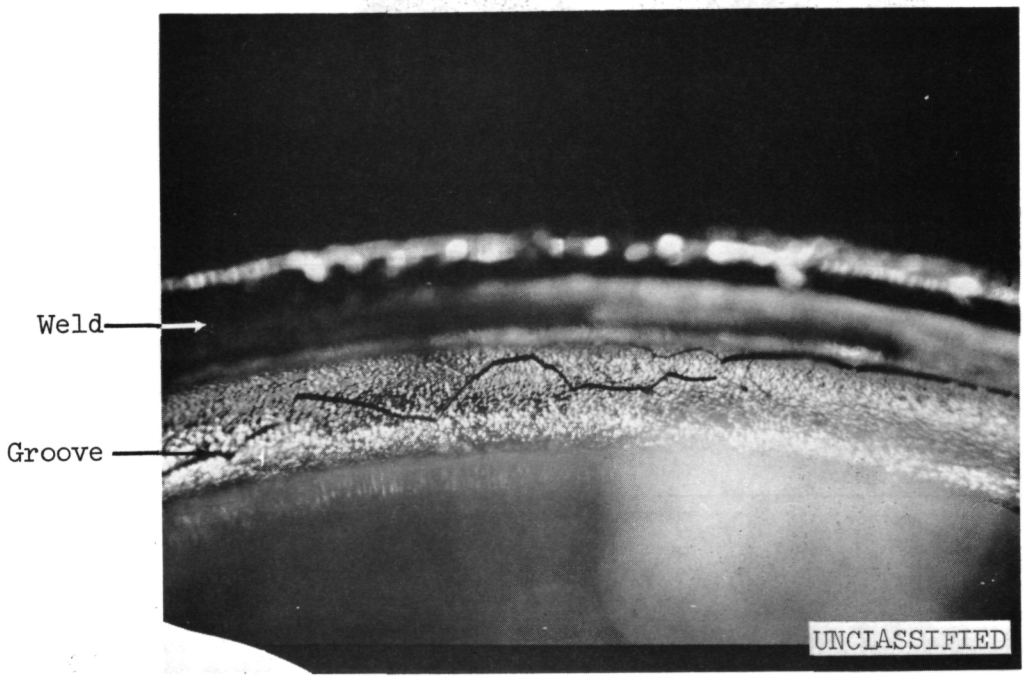

~32X

(c) Crack in the groove between the Ta-10W lip and the Ta-10W emitter substrate

Fig. 1.28--(U) Presence of cracks in the vicinity of the weld between the Ta-10W lip of the emitter structure and the tantalum emitter stem in post-test B_6-2 emitter assembly (page 3 of 3)

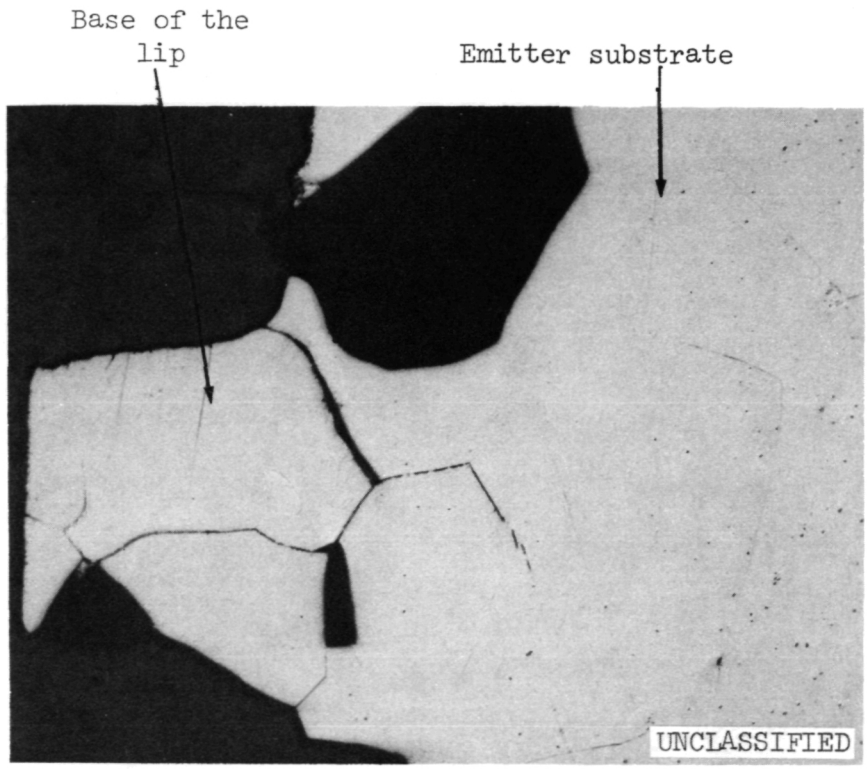

M 24107-9 75X

Fig. 1.29--(U) Appearance near the Ta-10W lip of the weld region in post-test B_6-2 emitter structure. The thin lip fell apart when the emitter structure was removed mechanically from the tantalum stem, and only the base of the lip is left. Note the presence of grain boundary cracks and one grain was lost

The oxygen content of the post-test emitter structure is much higher than that of the tungsten emitter and that of the Ta-10W substrate used for the preparation of B_6-2 emitter structure (see Table 1.2 footnote). The oxygen content and the carbon content of the post-test tantalum stem are also much higher than that of high purity tantalum (e.g. Wah Chang EB melted tantalum shown in Table 1.2). The thin lip weld was expected to be subjected to a high degree of stress when the emitter structure was thermal cycled because of the thermal gradient and the differential thermal expansion between the tantalum stem and the Ta-10W substrate of the emitter structure. Such stress concentration and high oxygen content in the Ta-10W probably both contribute to the formation of the grain boundary cracks shown in Fig. 1.29.

(U) After the emitter structure was removed mechanically from the tantalum emitter stem, the tungsten emitter surface was examined under a microscope. Figure 1.30 shows the surface microstructure of the tungsten emitter. When compared with the pretest surface microstructure shown in Fig. 1.9 (after normalized to the same magnification), it can be seen that no significant change has occurred during the operation in cesium at 1727°C for 3000 hours. Figure 1.31 is an electron micrograph taken of a replica of the post-test tungsten emitter surface, indicating that the surface was microscopically smooth, in agreement with observations made previously[1] on other heat-treated fluoride tungsten samples. Figure 1.32 shows the spatial distribution of the <100> axes in the post-test tungsten emitter of B_6-2. No appreciable difference seems to exist between this plot and a similar plot for the pre-test state (Fig. 1.8). Thus both the surface microstructure and the bulk preferred crystal orientation of the tungsten emitter of B_6-2 did not seem to be affected by operation in a cesiated environment at 1727°C for 3000 hours.

(U) Figure 1.33 is a macrophotograph of the surface of the Ta-10W substrate, which was subjected to electron bombardment during converter operation. A few dark patches were present, which were caused by contact with the electron bombardment filament before converter shutdown. Examination of these dark patches under higher magnification (Fig. 1.34) revealed no local melting. The grain boundaries were deeply grooved and sub-grain

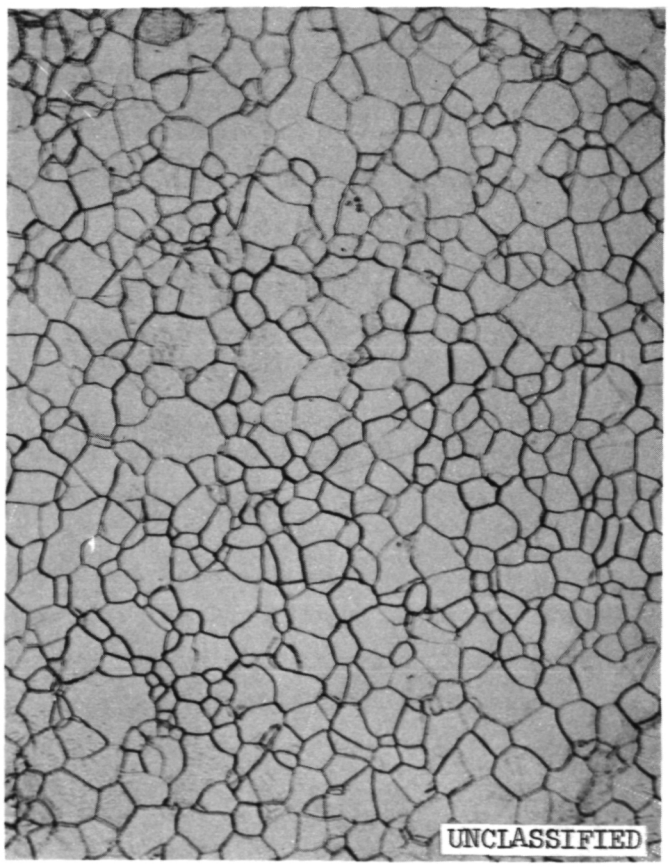

M 23516-6 50X

Fig. 1.30--(U) Post-test surface microstructure of the tungsten emitter of B_6-2

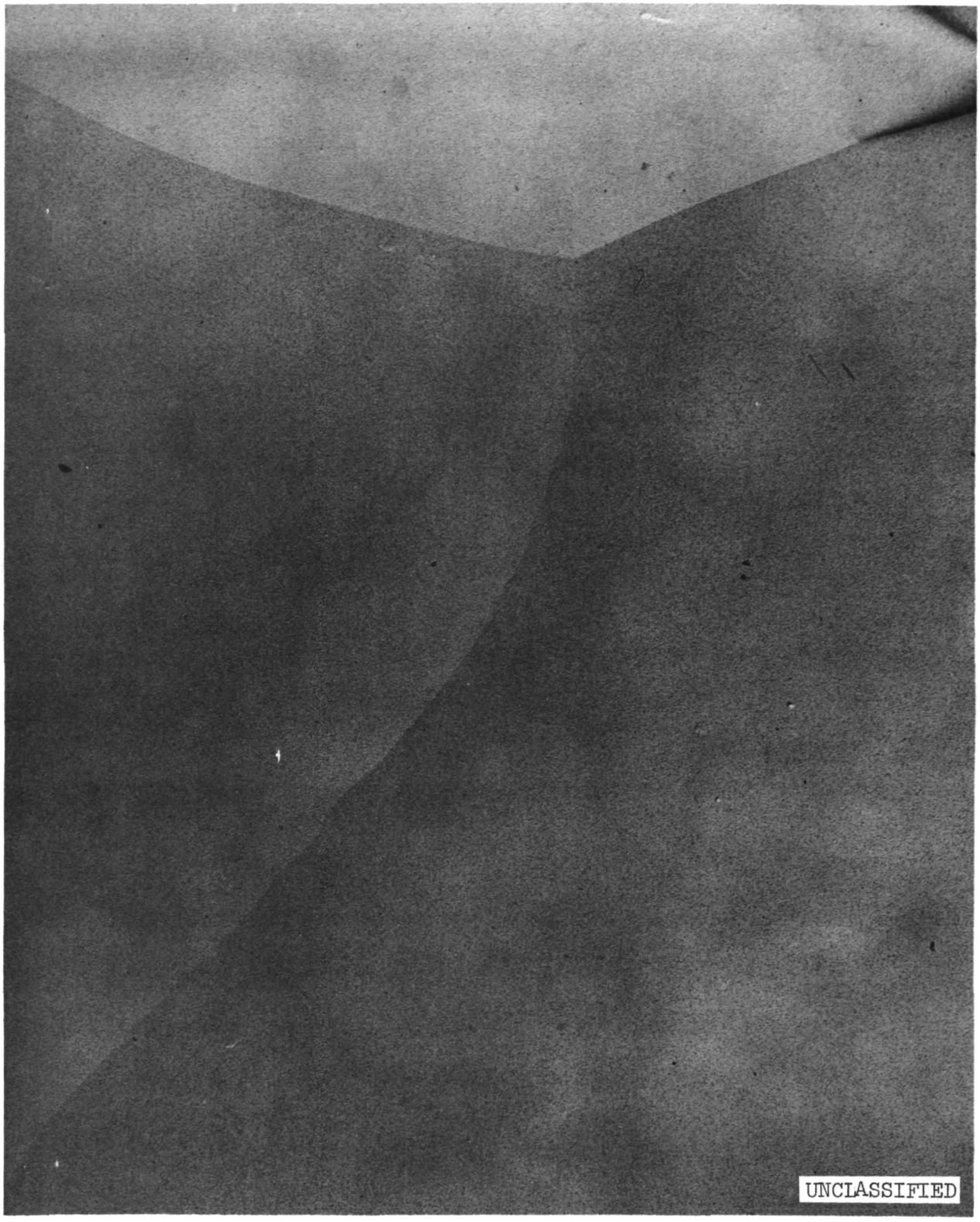

~18500X

Fig. 1.31--(U) Electron micrograph of the post-test B6-2 emitter surface

UNCLASSIFIED

Fig. 1.32--(U) Spatial distribution of the <100> axes in post-tested B_6-2 emitter

UNCLASSIFIED

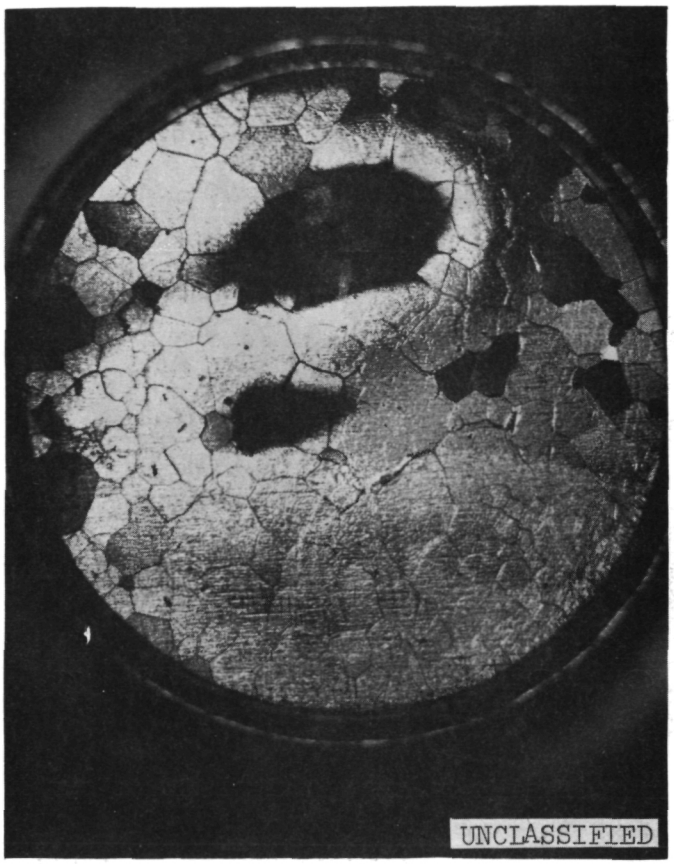

M 23516-4 ~6X

Fig. 1.33--(U) Appearance of Ta-10W substrate surface which has been subjected to electron bombardment heating during converter operation

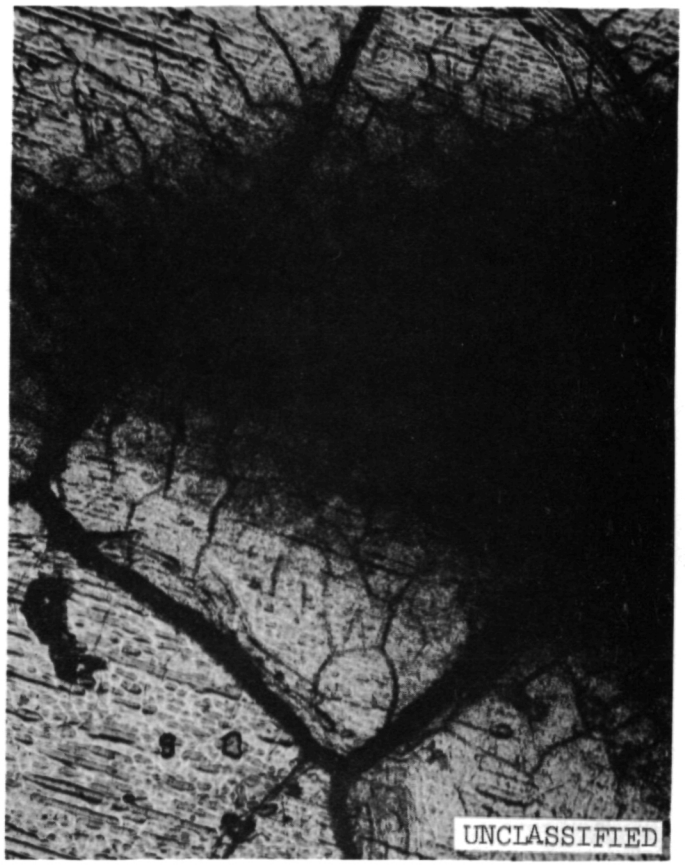

M 23516-1 50X

Fig. 1.34--(U) Magnified appearance of one of the dark patches of the Ta-10W substrate surface shown in Fig. 1.33

boundaries were clearly visible. Compared with Fig. 1.6 and Fig. 1.7, it can be seen that considerable grain growth has occurred during the converter operation.

(U) After the examinations of the tungsten emitter and the Ta-10W substrate were completed, the emitter structure was mounted in plastic and polished across the W-(Ta-10W) interface until the diameter of the emitter structure was reached. Metallographic examination revealed (Fig. 1.35) the following essential features:

(1) Good bond existed at the interface.

(2) Kirkendall voids were present near the interface on the (Ta-10W) side.

(3) No porosity was observed in the tungsten and no secondary phase precipitates were observed in the Ta-10W.

(4) Cracks and grain boundary separation were observed in Ta-10W near the base of the lip for welding to the tantalum emitter stem. The causes for such cracks and grain boundary separation have been discussed in the early part of this section.

(U) Electron microprobe scan across the W-(Ta-10W) interface showed that the width of the diffusion zone was 50 microns at the center, 42 microns at a location halfway between the center and the edge, and 58 microns at a location about 300 microns from the edge. The diffusion zone was wider at the center than at halfway from the center to the edge, probably because the temperature at the center was higher. Near the edge where the temperature was cooler but the stress in the material was higher, the increase in diffusion rate by stress probably had outweighed the decrease in diffusion rate by being at a lower temperature. If an average value of 50 microns is taken as the width of the diffusion zone formed in 3000 hours at 1727°C, then, since the diffusion distance is proportional to $\sqrt{\text{time}}$, the width of the diffusion zone in the emitter structure is expected to be 167 microns for 10,000 hour operation at 1727°C. Although the electron microprobe

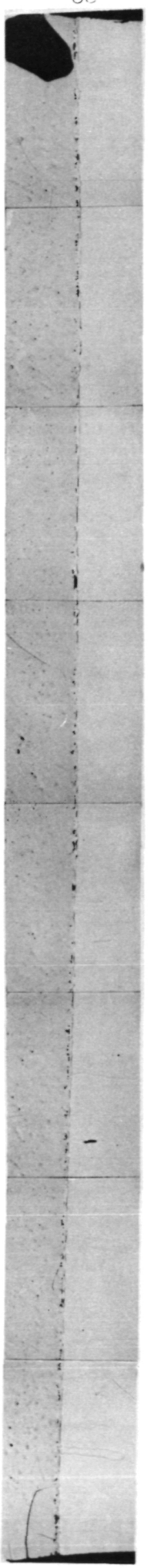

Fig. 1.35--(U) Appearance of the W-(Ta-10) interface in post test emitter structure B_6-2

results indicated that the amount of tantalum concentration at the emitter surface was negligible even at the end of the 3000 hour test, question remains whether trace of tantalum could be present at the emitter surface (either through grain boundary diffusion or surface diffusion) to affect its work function. To resolve this problem, vacuum work function measurement were carried out on all the other emitters examined (see below).

1.3.2. C_1-2 Emitter Structure

(U) The C_1-2 emitter structure consisted of a chloride tungsten emitter diffusion bonded to a Ta-10W substrate. It was operated in a cesiated converter for 3600 hours at 1757°C before being removed from the converter for post-operation examination. The emitter structure as received from NASA already had its tantalum stem removed. Leak test revealed the presence of a crack in the weld of the Ta-10W substrate to the tantalum stem, similar to the type shown in Fig. 1.28(b) for the emitter structure B_6-2.

(U) Figure 1.36(a) shows the macroscopic appearance of the emitter surface. It can be seen that the grains of the chloride tungsten have grown to very large sizes and covered with slip lines formed by the mechanical deformation of the emitter structure when it was thermal cycled during the operation of the converter. The grain boundaries were deeply grooved; however, no cracks were observed under a microscope. These features are brought out more clearly in Fig. 1.36(b) which shows the surface structures of the emitter at a higher magnification. Figures 1.37(a) and (b) are electron micrographs taken of a replica of the emitter surface, illustrating respectively the groove at a grain boundary and the slip lines originating from a grain boundary. Attempts were made to take the X-ray pole figure of the emitter surface, but no meaningful one could be obtained because the grain size of the emitter was too large. Vacuum emission study at 1800°C for 200 hours yielded an effective work function of 5.0 eV.

(U) Figure 1.38 shows the macroscopic appearance of the Ta-10W substrate surface which was subject to electron bombardment heating. The dark

M 26862-2

(a) ~5X

M 28406-1

(b) 75X

Fig. 1.36--(U) Post-test appearance of surface of the chloride tungsten emitter of emitter structure C_1-2

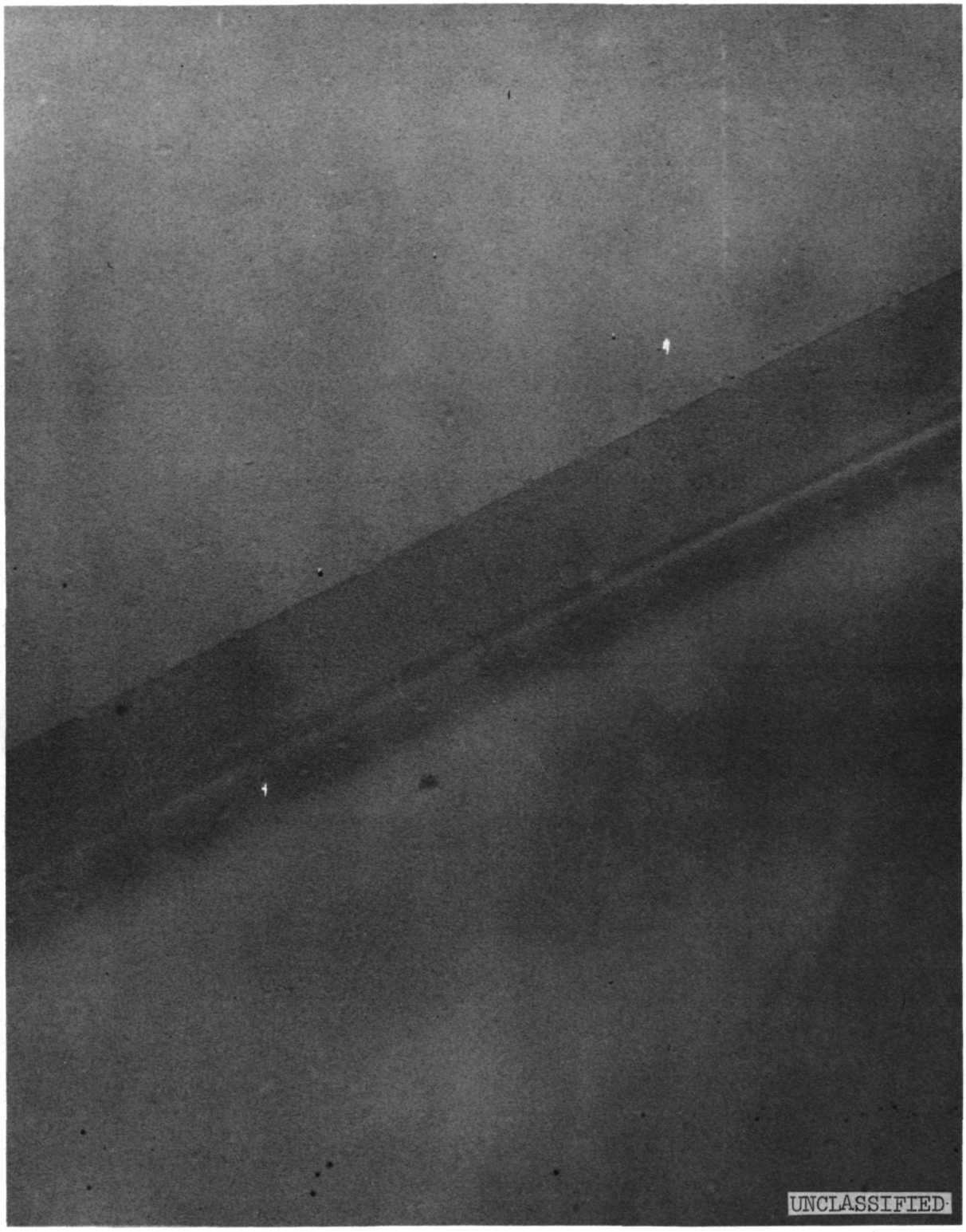

P 1504-6 10,500X

(a) Showing groove at grain boundary

Fig. 1.37--(U) Electron micrographs of the replica of the post-test surface of the chloride tungsten emitter of emitter structure C_1-2 (Page 1 of 2)

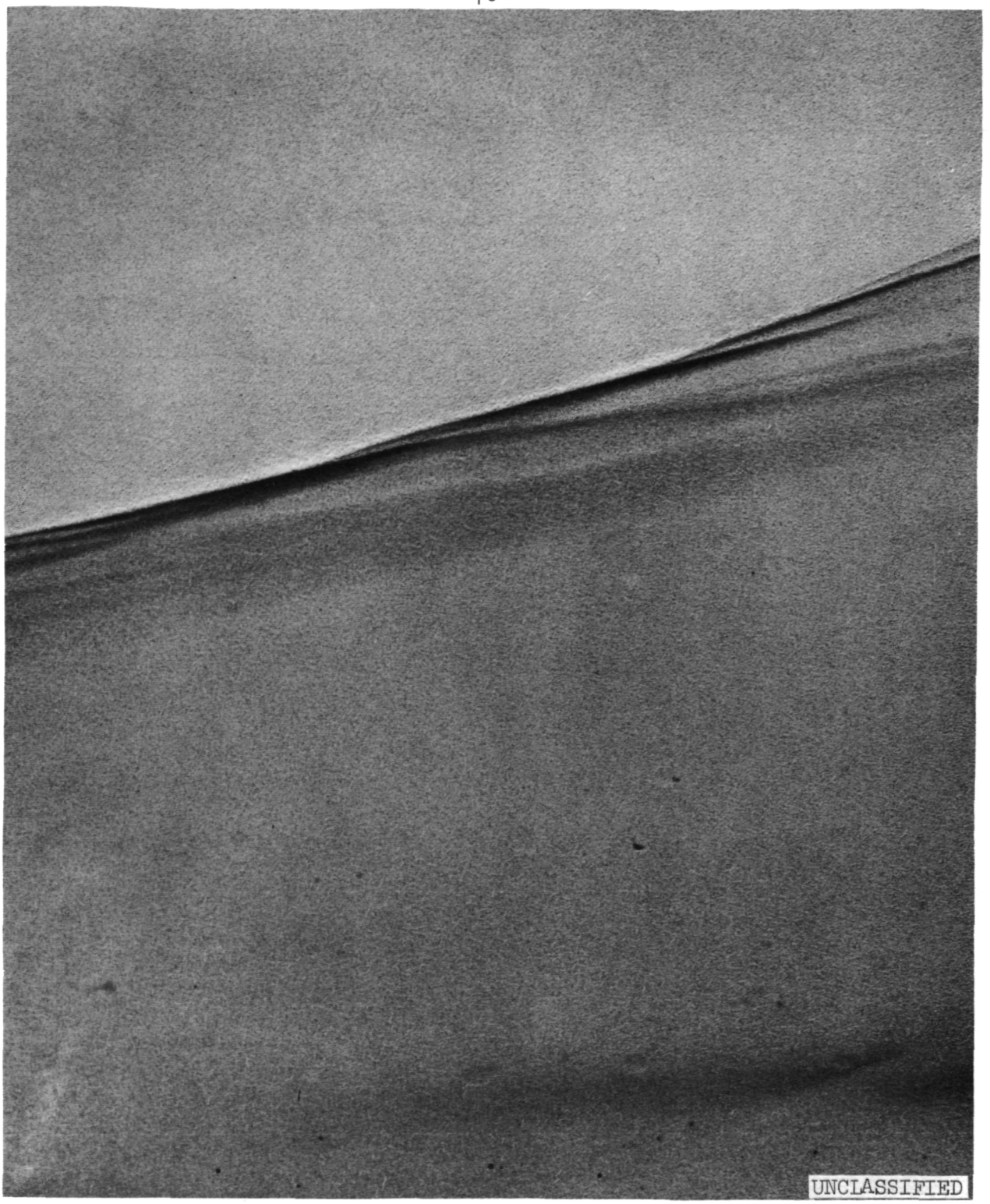

P 1504-5 10,500X

(b) Showing slip lines originating at grain boundary

Fig. 1.37--(U) Electron micrographs of the replica of the post-test surface of the chloride tungsten emitter of emitter structure C_1-2 (Page 2 of 2)

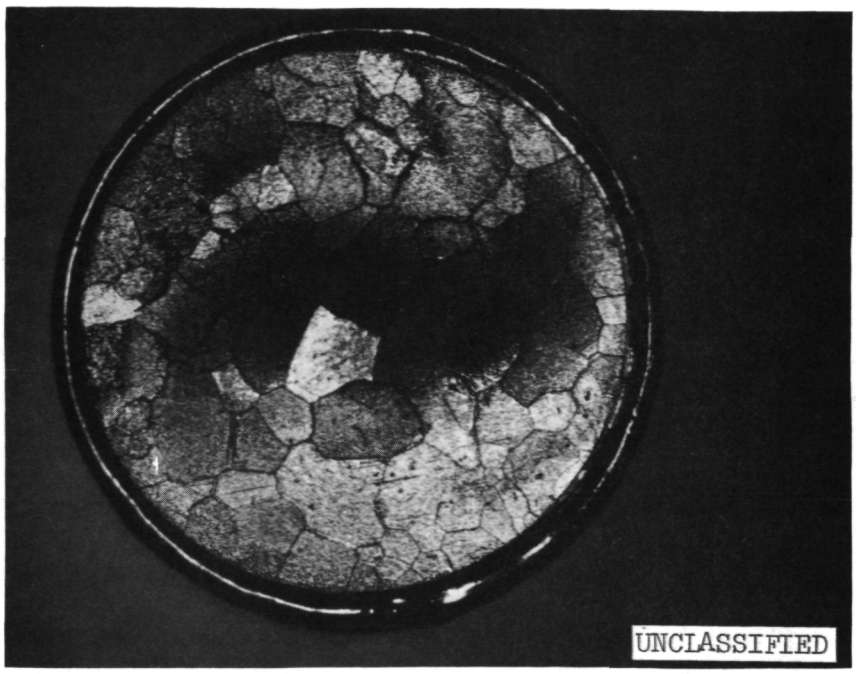

M 26862-3 ~ 5X

Fig. 1.38--(U) Post-test appearance of the surface of the Ta-10W substrate of emitter structure C_1-2

region shown is probably due to thermal etching of the area closer to the electron bombardment filament.

(U) The surface contours of the tungsten emitter and the Ta-10W substrate were measured with an optical micrometer. The results are shown in Table 1.9. However, it must be noted that in view of the highly non-uniform appearance of the emitter surface, the data taken at individual locations cannot be used to describe the overall contour of the emitter surface.

(U) Figures 1.39(a), (b) and (c) are photomicrographs taken of the two ends and the middle of the tungsten to Ta-10W interface across the diameter of the emitter structure. It can be seen that the bond between the tungsten emitter and the Ta-10W substrate is good in spite of the Kirkendall voids formed at the Ta-10W side of the interface by the inter-diffusion between the tungsten and the Ta-10W. Electron microprobe examination of the interface showed that the diffusion zone width varied randomly from 70 to 85 microns. Since the measured vacuum work function is about what would be expected from an {110} oriented chloride tungsten emitter, it appears that for a chloride tungsten emitter of 40 mil thickness, its vacuum work function was not significantly affected by the interdiffusion with Ta-10W to the extent observed for the emitter structure C_1-2.

(U) Chemical analysis of the emitter structure yielded the following interstitial contents (in ppm): O, 155; N, 30; C, 25. The higher oxygen content than that of the Ta-10W used for the preparation of the emitter indicates there has been some contamination of the emitter structure, which probably led to the formation of cracks in the weld of the (Ta-10W) substrate to the tantalum stem. The amount of tantalum stem left on the emitter structure received for the post-test examination was too short to provide enough material needed for chemical analysis; therefore analysis of the O, N and C could not be performed.

1.3.3. Emitter Structures C_1-4 and C_1-5

(U) Both emitter structures were prepared by diffusion bonding chloride tungsten emitters of the same origin to Ta-10W substrates, and

Table 1.9

(U) OPTICAL MICROMETER MEASUREMENTS OF W AND Ta-10W SURFACE CONTOURS OF EMITTER STRUCTURE C_1-2 AFTER TESTING AT TECO

(This table is Unclassified)

Surface Position	W Surface	Ta-10W Surface
X_0	0	0
X_1	-2.5	+1.0
X_2	-1.5	+2.0
X_3	0	+2.0
X_4	+1.8	+1.0
X_5	-4.5	+4.5
X_6	-5.0	+4.8
X_7	-3.7	+5.0
X_8	- .3	+4.5

Note: In the above table the W and W-10W surface contours, the surface position designations represent the locations indicated below. All dimensions are in mils with X_0 as the reference point. Positions with "+" sign are lower than X_0 and positions with "-" sign are higher than X_0.

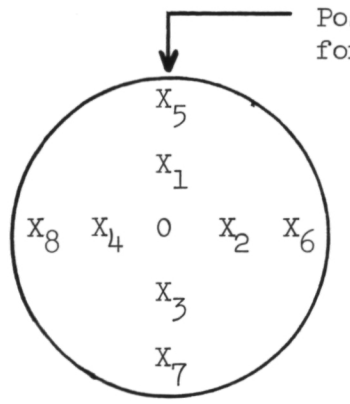

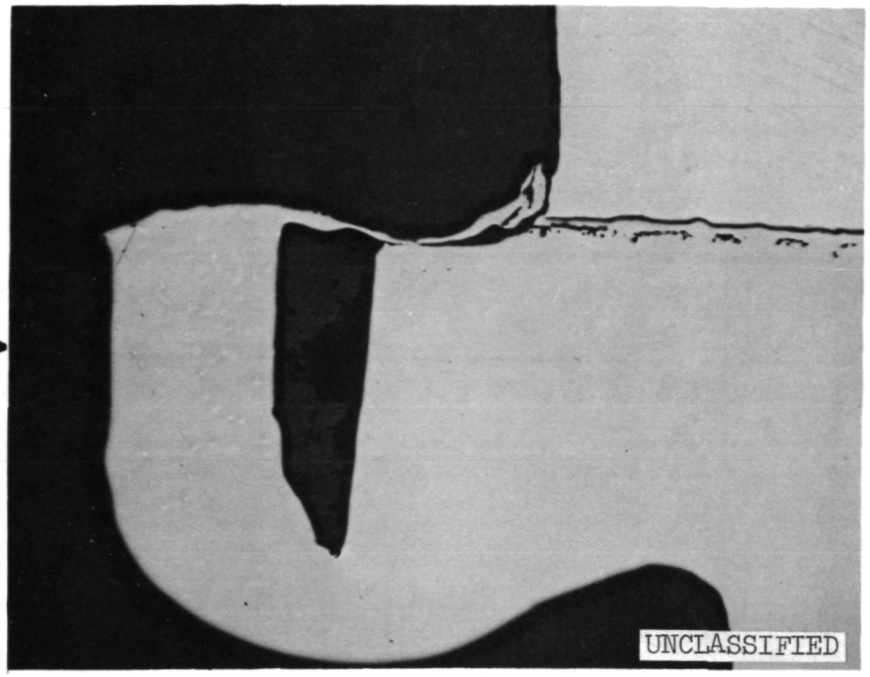

M 28451-7 50X

(a) Left end

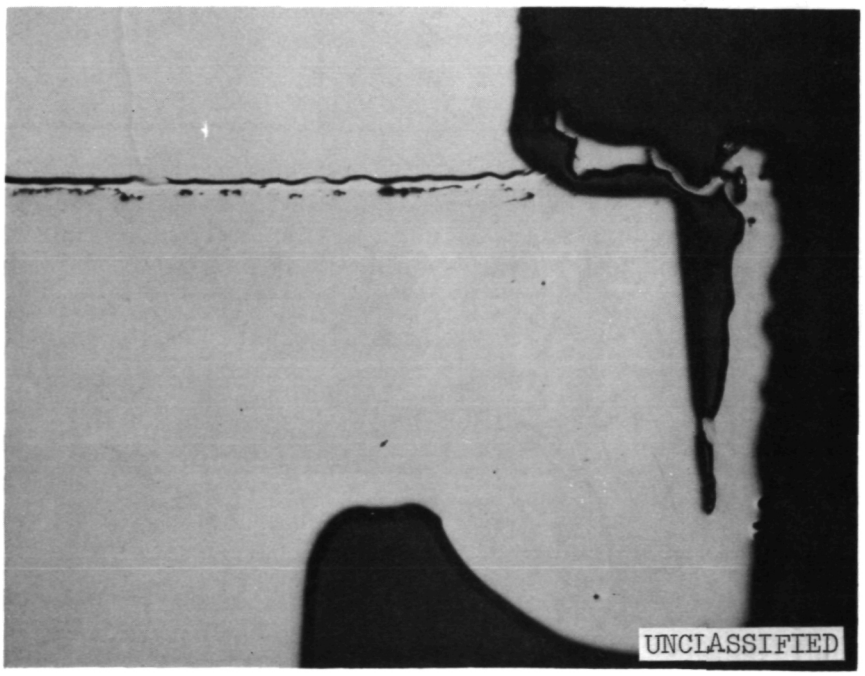

M 28451-6 50X

(b) Right end

Fig. 1.39--(U) Post-test appearance of the tungsten-(Ta-10W) interface of emitter structure C_1-2 (Note: the black line at the interface is due to relief polishing, not cracks.) (Page 1 of 2)

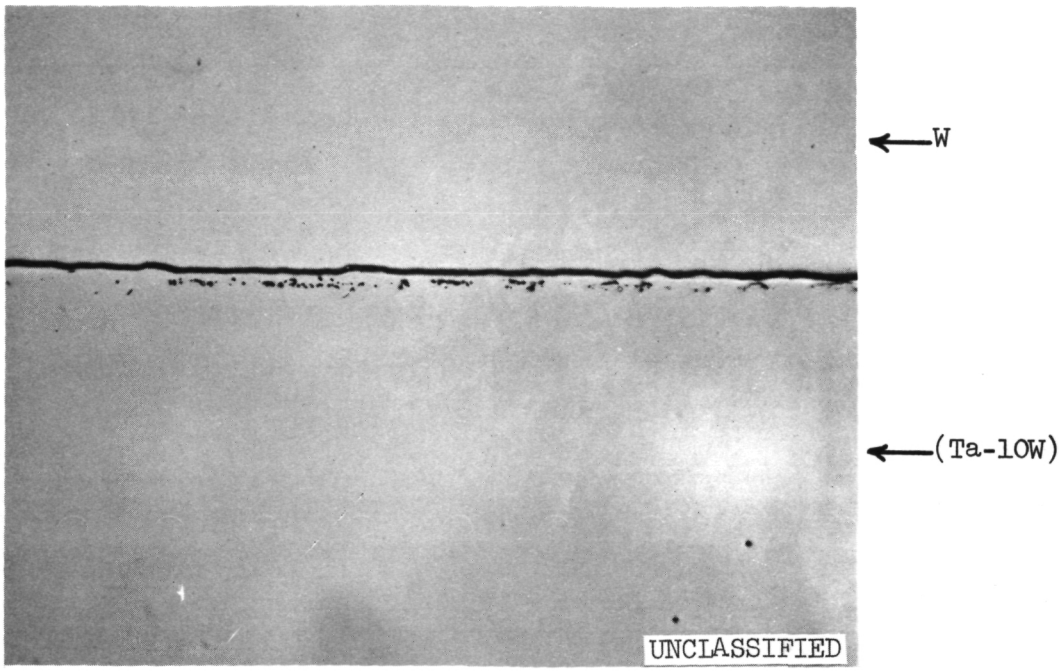

M 28451-3 50X

(c) Middle

Fig. 1.39--(U) Post-test appearance of the tungsten-(Ta-10W) interface of emitter structure C_1-2 (Note: the black line at the interface is due to relief polishing, not cracks.) (Page 2 of 2)

both were operated at 1727°C for 4000 hours in cesiated converters. Leak test showed no defects at the weld between the (Ta-10W) substrate and the tantalum stem in each case, or in the emitter structure proper.

(U) Figures 1.40 and 1.41 show the macroscopic appearances of the post-test surfaces of the chloride tungsten emitters of C_1-4 and C_1-5 respectively. The grain growth of these emitters was not as excessive as that for C_1-2, but slip lines, similar to that observed for C_1-2 were present on the surfaces of these emitters. In addition, the emitter of C_1-4 shows two distinct features. First, the slip lines ran across the grain boundaries in the central portion of the emitter surface. Secondly, a "pimple" about 40 mils in diameter and less than a few mils in height was present on its surface. Figure 1.42 shows the "pimple" at a higher magnification. It appears the "pimple" is situated in the middle of a crystal grain, with slip lines around its circumference as well as across its top surface. Metallographic examination of a cross section cutting through the "pimple" showed no porosity or inclusions. It appears that the presence of the slip lines on the surfaces of these emitters are associated with the mechanical deformation of the emitter structure due to thermal cyclings during the operation of the converters, but the exact reasons for the two special features observed for C_1-4 emitter are unknown. Electron micrographs obtained from the replicas of the post-test emitter surfaces of C_1-4 and C_1-5 are similar to that of C_1-2 (see Figs. 1.37(a) and (b)). X-ray analysis of the degree of (110) orientation yielded the results shown in Fig. 1.43. The irregularity of the shape of the curves may be attributed to the large grain size of these emitters, with the effect more pronounced in C_1-4. Vacuum emission measurements at 1800°C for 250 hours yielded a steady effective vacuum work function of 4.91 eV in each case.

(U) Figures 1.44 and 1.45 show the post-test macroscopic appearances of the Ta-10W substrates of C_1-4 and C_1-5 respectively. The surface of the C_1-4 substrate had a normal appearance but the surface of the C_1-5 substrate was highly matted, probably due to differences in the electron bombardment heating of these surfaces during the operation of the converters.

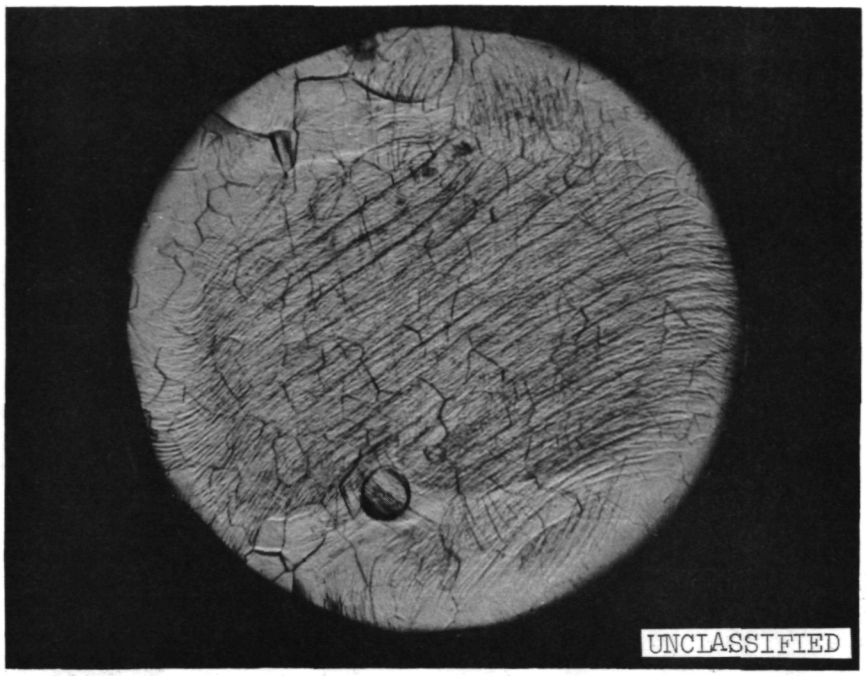

M 29239-4 ~5X

Fig. 1.40--(U) Macroscopic appearance of the post-test surface of the chloride tungsten emitter of emitter structure C_1-4

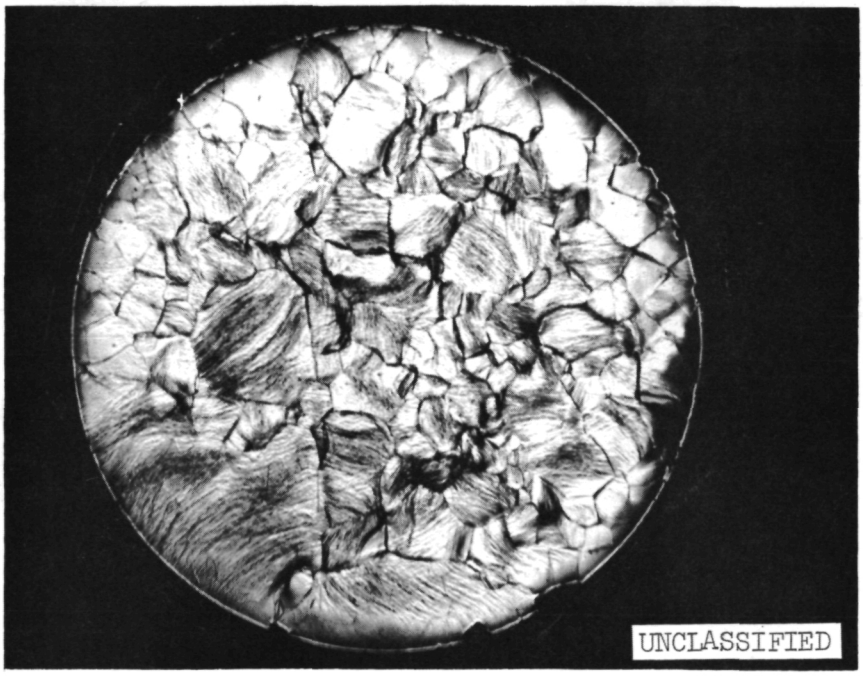

M 29239-3 ~5X

Fig. 1.41--(U) Macroscopic appearance of the post-test surface of the chloride tungsten emitter of emitter structure C_1-5

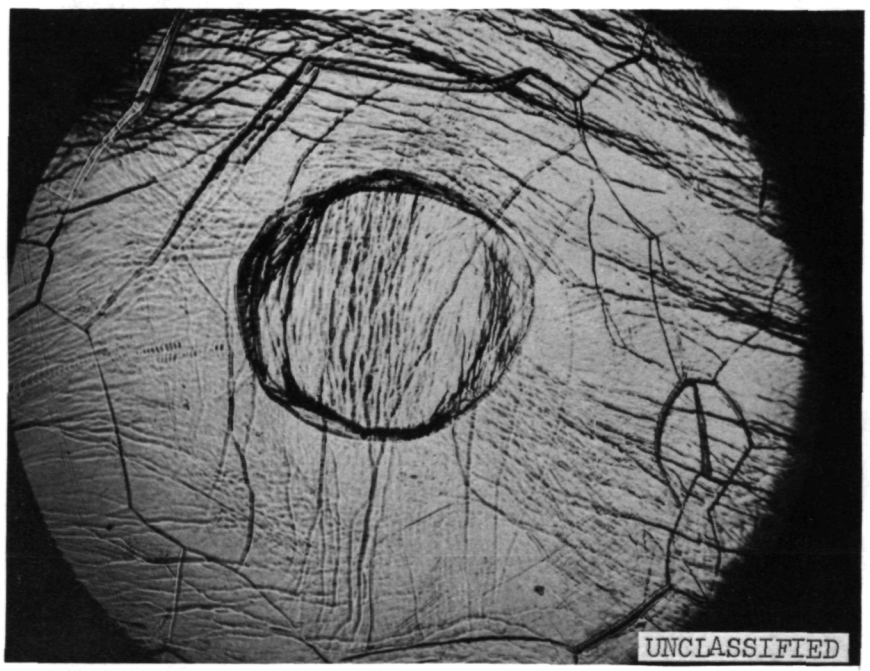

M 29239-6 35X

Fig. 1.42--(U) Appearance of the "pimple" on the post-test surface of the chloride tungsten emitter of emitter structure C_1-4

UNCLASSIFIED

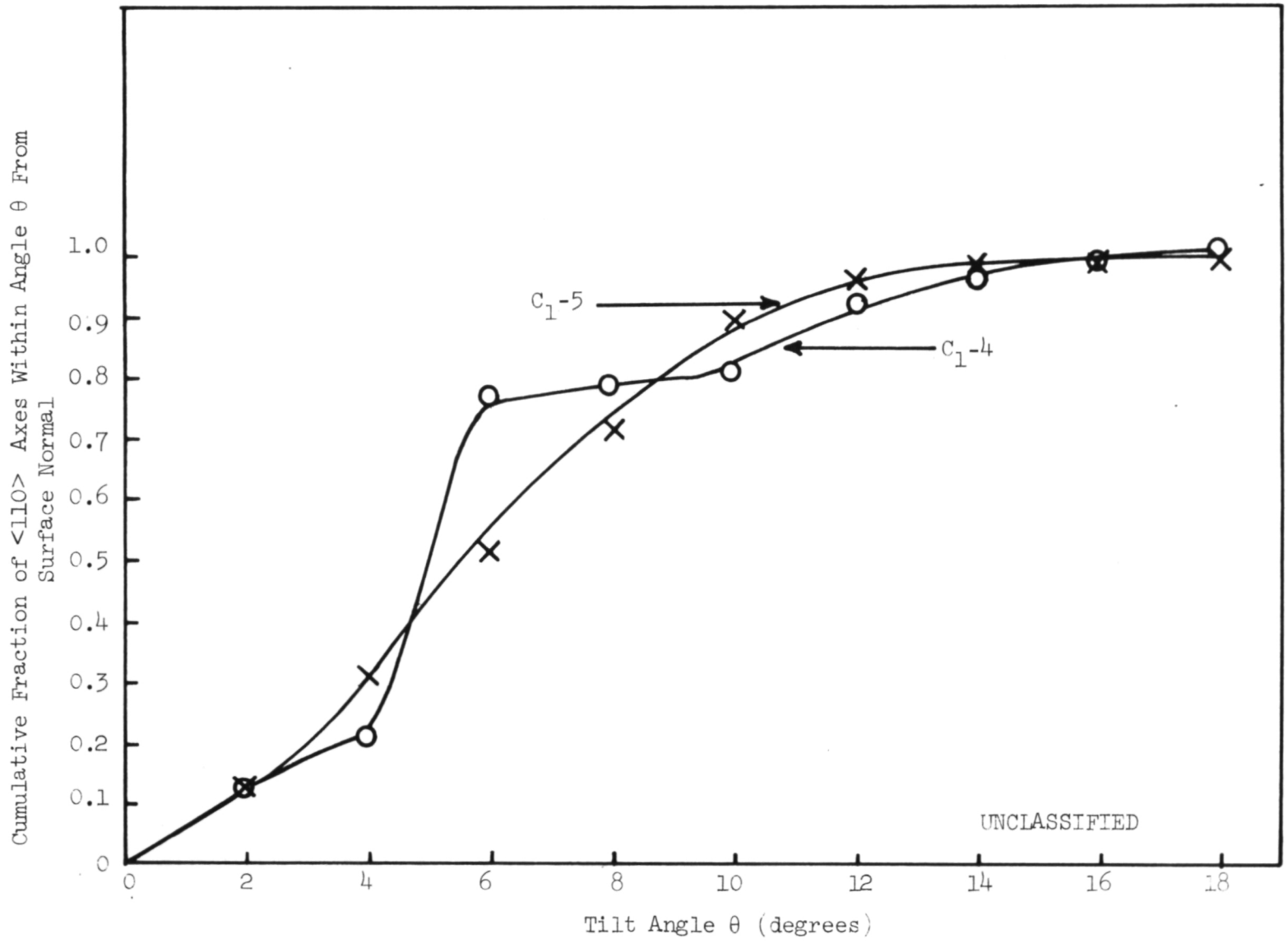

Fig. 1.43--(U) Distribution of <110> axes in chloride tungsten emitter structures C_1-4 and C_1-5

UNCLASSIFIED

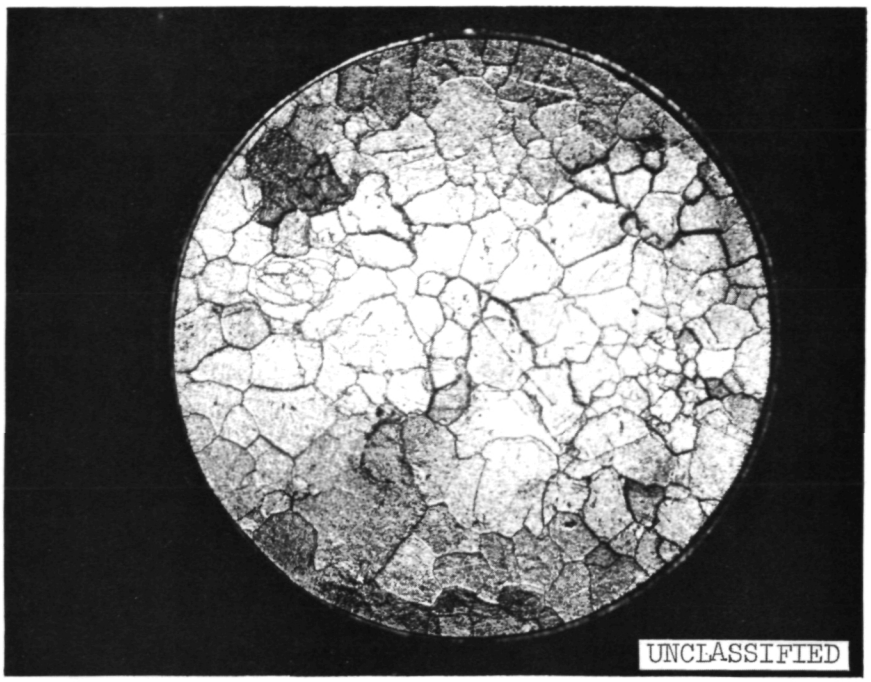

M 29239-5 ~5X

Fig. 1.44-(U) Macroscopic appearance of the post-test surface of the Ta-10W substrate of the emitter structure of C_1-4

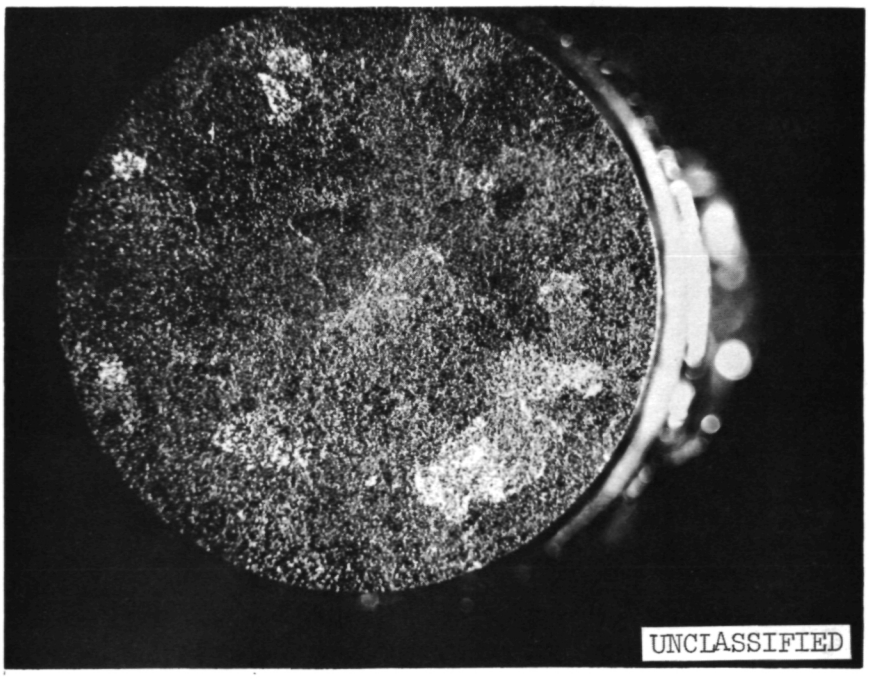

M 29239-1 ~5X

Fig. 1.45--(U) Macroscopic appearance of the post-test surface of the Ta-10W substrate of the emitter structure of C_1-5

(U) The post-test surface contours of the emitter and the substrate surfaces of the these emitter structures were measured with an optical micrometer. The results are shown in Table 1.10. It appears that of the three emitter structures containing chloride tungsten emitters, the deformation of the emitter surface is the least for C_1-5, and the most for C_1-2, with the deformation of the emitter surface of C_1-4 slightly higher than that for C_1-5. It is possible that these differences are related to the thermal history of each emitter structure in the operating converter. It is also possible that the difference in the degree of (110) orientation of the emitter material affects the degree of deformation of the emitter under stress, and thus its grain growth characteristics. It is interesting to note that in spite of the mechanical deformation observed for these emitters at room temperatures, their vacuum effective work functions at 1800°C do not seem to differ significantly from that of a (110) oriented tungsten emitter.

(U) Figures 1.46 and 1.47 show respectively the typical post-test appearances of the tungsten - (Ta-10W) interfaces of C_1-4 and C_1-5. Figures 1.48 and 1.49 show respectively the clean grain structures of the Ta-10W substrates of C_1-4 and C_1-5. Electron microprobe studies of the tungsten - (Ta-10W) interface indicate a diffusion zone width of 50-60 microns for C_1-4 and a diffusion zone width of 44-56 microns for C_1-5. Again, such interdiffusion does not seem to affect the vacuum effective work function of the chloride tungsten emitter.

(U) Chemical analysis yielded the following interstitial contents (in ppm): C_1-4 – O, 30; N, 27; C, 20; C_1-5 – O, 25; N, 25; C, 18. These do not deviate significantly from that of the Ta-10W used for the preparation of these emitter structures, indicating no significant contamination of these emitter structures during their operation in cesiated converters. No analysis was performed on the interstitial contents of the tantalum stems because the latter were already removed from the emitter structures prior to delivery for the post-operation examinations.

Table 1.10

(U) OPTICAL MICROMETER MEASUREMENTS OF W AND Ta-10W SURFACE CONTOURS OF EMITTER STRUCTURES C_1-4 AND C_1-5 AFTER RECEIPT FROM NASA

(This table is Unclassified)

Surface Position	C_1-4		C_1-5	
	W Surface	Ta-10W Surface	W Surface	Ta-10W Surface
X_0	0	0	0	0
X_1	- .8	+ .2	0	+ .4
X_2	- .3	+ .8	- .5	+ .3
X_3	+ .2	+ .3	- .2	- .2
X_4	+ .7	- .1	- .5	+ .2
X_5	-1.2	+1.8	+ .2	+1.2
X_6	- .5	+2.6	- .4	+ .9
X_7	- .1	+1.5	- .3	+1.0
X_8	+ .3	+1.6	0	+1.2

Note: On the W and Ta-10W surface contours, the surface position designations represent the locations indicated below. All dimensions are in mils, with X_0 as the reference point. Positions with a "+" sign are lower than X_0 and positions with a "-" sign are higher than X_0.

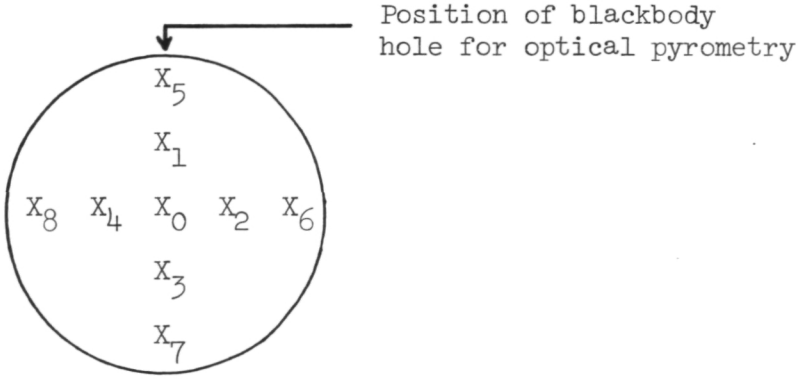

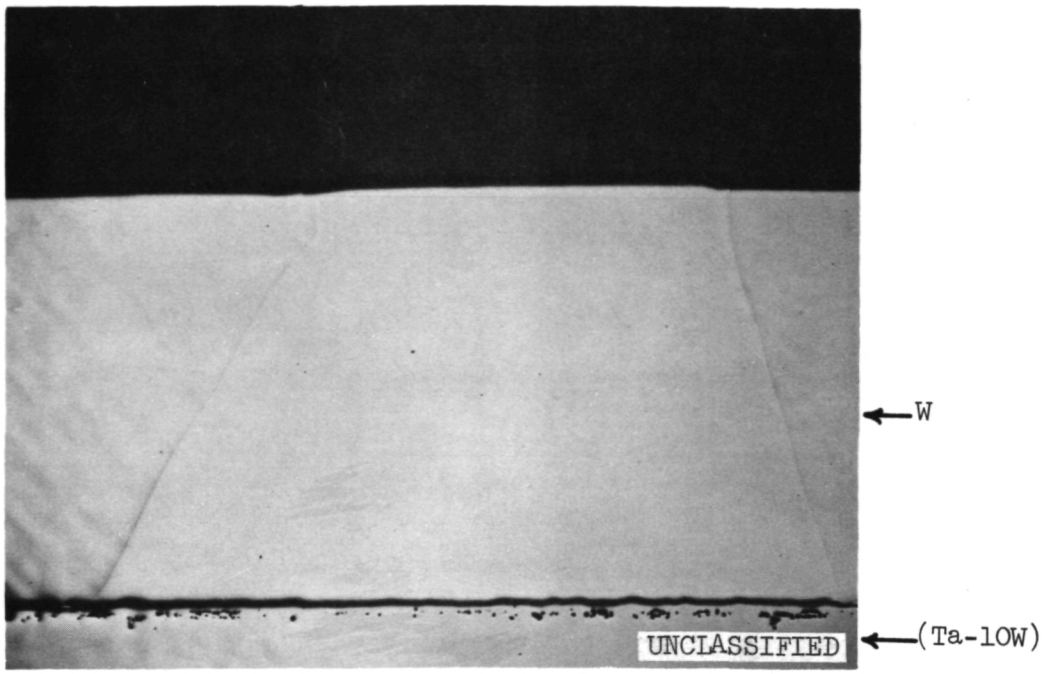

M 29919-3A 50X

Fig. 1.46--(U) Typical post-test appearance of the tungsten-(Ta-10W) interface of emitter structure C_1-4

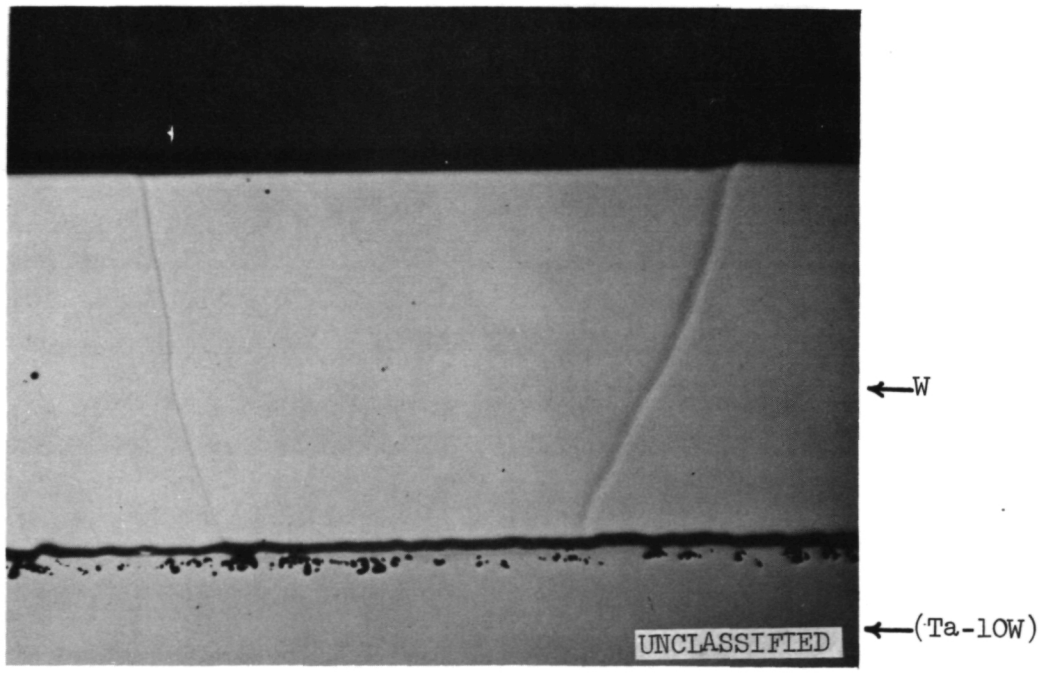

M 29920-1 50X

Fig. 1.47--(U) Typical post-test appearance of the tungsten-(Ta-10W) interface of emitter structure C_1-5

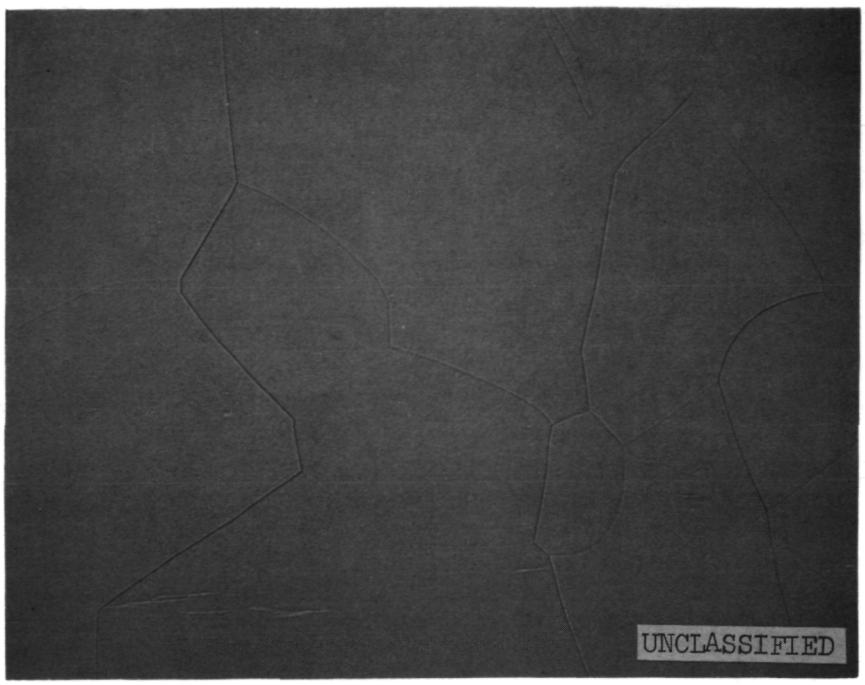

M 29919-4 50X

Fig. 1.48--(U) Post-test microstructures of the Ta-10W substrate of emitter structure C_1-4

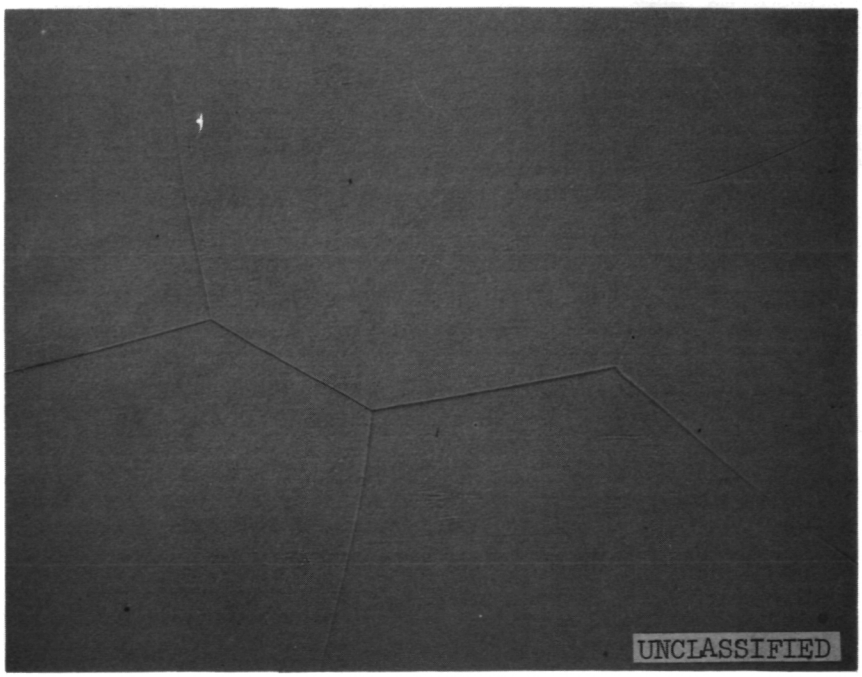

M 29920-4 50X

Fig. 1.49--(U) Post-test microstructures of the Ta-10W substrate of emitter structure C_1-5

1.3.4. C_3-3 Emitter Structure

(U) The C_3-3 emitter structure consisted of a duplex tungsten emitter (10 mil (110) oriented chloride tungsten over 30 mil (100) oriented fluoride tungsten) diffusion bonded to a Ta-10W substrate. It was operated in a cesiated converter for 4000 hours at 1727°C prior to being removed from the converter for post-operation examinations. When received from NASA, the tantalum stem was already removed. Leak test failed to detect any defect at the weld between the Ta-10W substrate and the tantalum stem or in the emitter structure proper.

(U) Figures 1.50 and 1.51 show respectively the macroscopic and the microscopic appearances of the post-test tungsten emitter surface. The grains appear to be smaller than that of the chloride tungsten emitters of emitter structures C_1-4 and C_1-5, but the grain boundary grooves and the presence of slip lines in each grain are typical of that for all the emitter structures containing chloride tungsten emitters. When a replica of the emitter surface was examined under an electron microscope, patterns similar to that for the chloride tungsten emitter of emitter structure C_1-2 were obtained. Figure 1.52 shows the post-test distribution of the <110> axes in the chloride tungsten emitter, which does not differ significantly from that obtained prior to the test in the cesiated converter (Fig. 1.22). Vacuum emission study at 1800°C for 200 hours yielded a vacuum effective work function of 4.84 eV.

(U) Figure 1.53 shows the post-test macroscopic appearance of the Ta-10W substrate. Like the Ta-10W substrate of emitter structure C_1-5, the surface seems to be highly matted, probably due to some thermal etching effects from the bombardment of the electron gun.

(U) The post-test surface contours of the tungsten emitter and the Ta-10W substrate were measured with an optical micrometer. The results are shown in Table 1.11. The deformation of the duplex emitter surface is much smaller than that observed for the chloride tungsten emitter of emitter structures C_1-2 and C_1-4, but does not differ significantly from that of the emitter structure C_1-5.

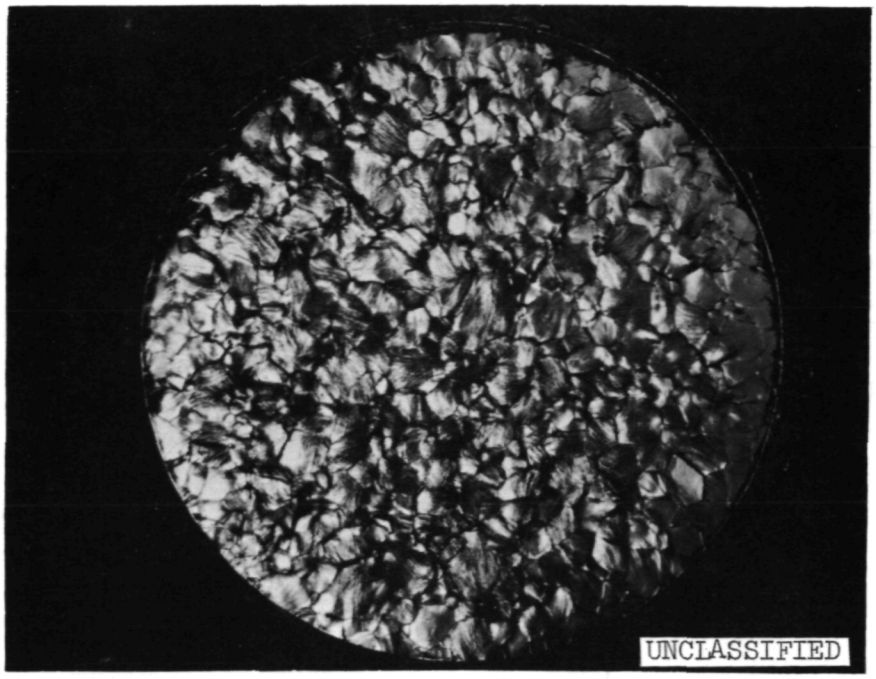

M 29939-1 ~5X

Fig. 1.50--(U) Macroscopic appearance of the post-test duplex tungsten emitter surface of emitter structure C_3-3

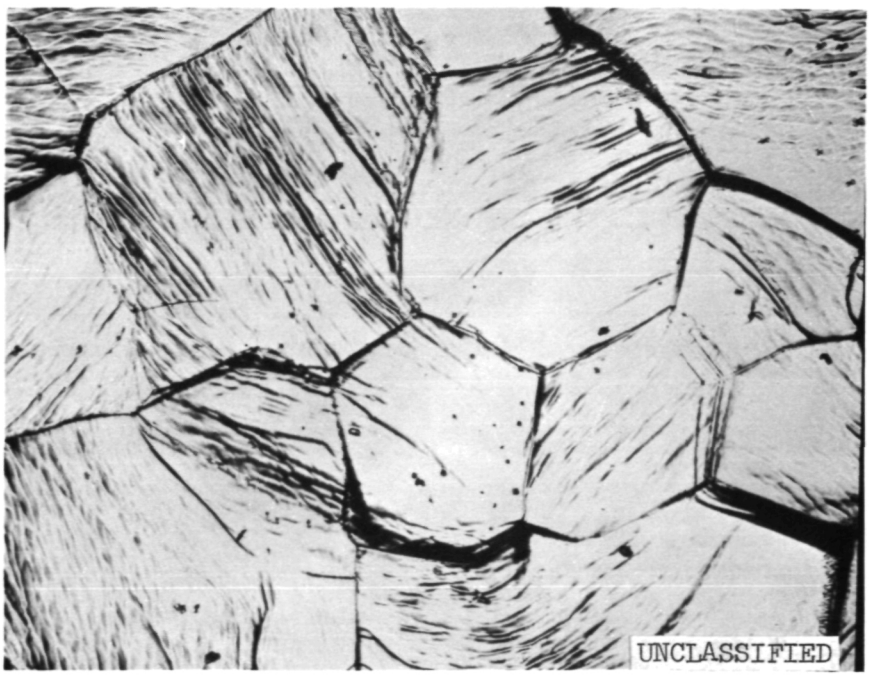

M 29939-3 50X

Fig. 1.51--(U) Microscopic appearance of the post-test duplex tungsten emitter surface of emitter structure C_3-3

UNCLASSIFIED

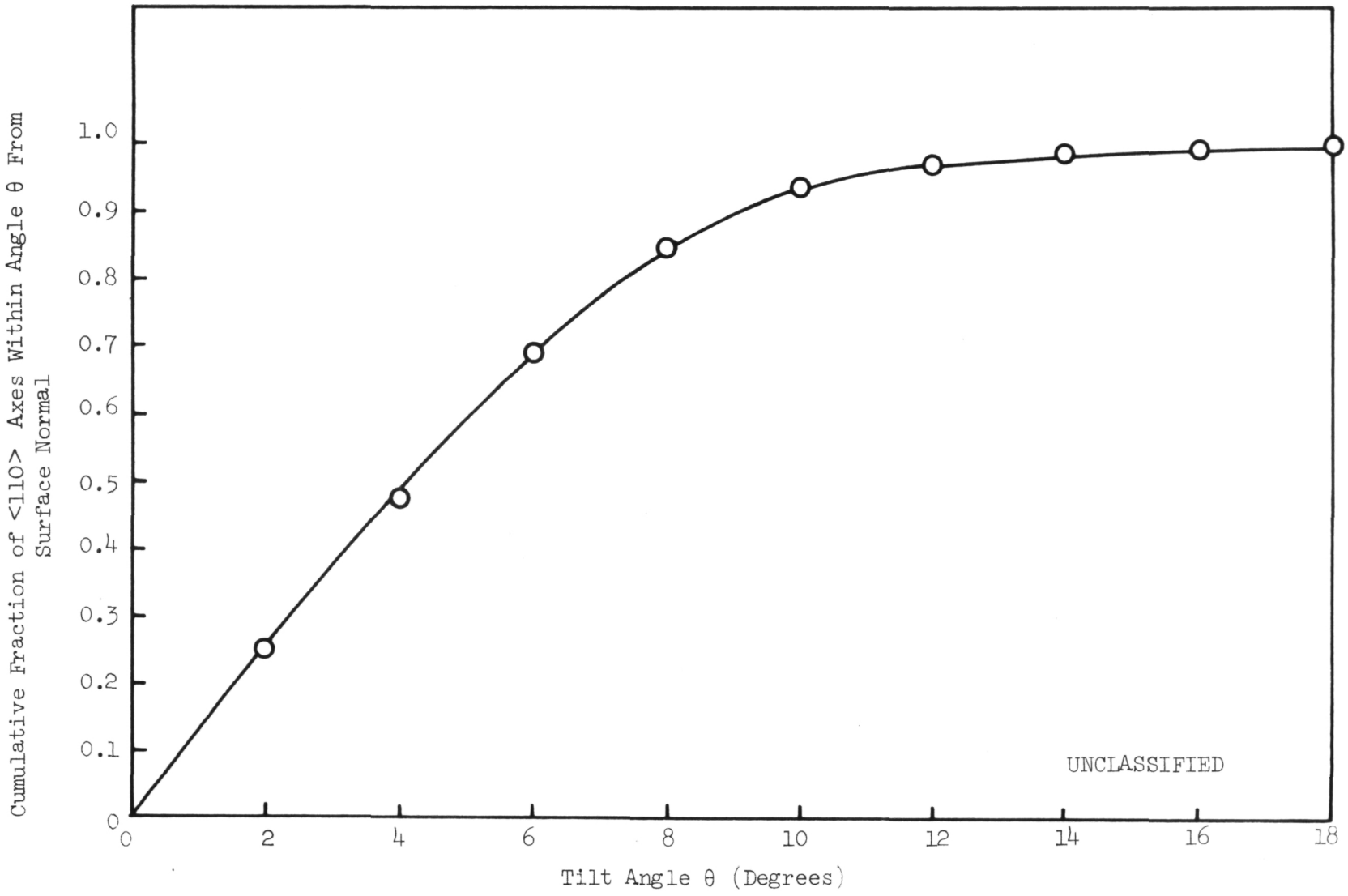

Fig. 1.52--(U) Distribution of <110> axes in post-test chloride tungsten emitter structure C_3-3

UNCLASSIFIED

Table 1.11

(U) OPTICAL MICROMETER MEASUREMENTS OF W AND Ta-10W SURFACE CONTOURS OF EMITTER STRUCTURE C_3-3 AFTER RECEIPT FROM NASA

(This table is Unclassified)

Surface Position	W Surface	Ta-10W Surface
X_0	0	0
X_1	-.2	+ .4
X_2	0	+ .5
X_3	-.3	+ .6
X_4	-.1	+ .6
X_5	-.1	+1.1
X_6	-.4	+1.1
X_7	-.5	+1.1
X_8	-.6	+1.1

Note: On the W and Ta-10W surface contours, the surface position designations represent the locations indicated below. All dimensions are in mils, with X_0 as the reference point. Positions with a "+" sign are lower than X_0 and positions with a "-" sign are higher than X_0.

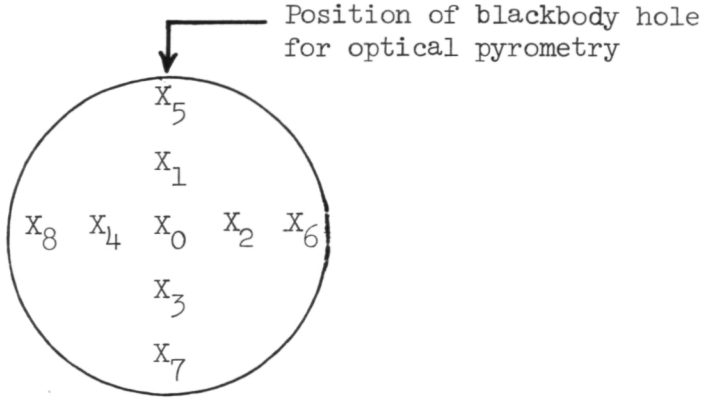

(U) Figure 1.54 shows the post-test microstructures of the tungsten-(Ta-10W) interface. Electron microprobe study indicated that the width of the diffusion zone varied between 55 to 65 microns. Figure 1.55 is a photomicrograph of the post-test interface between the chloride tungsten layer and the fluoride tungsten support. The bond appears to be excellent. Figure 1.56 shows the microstructures of the Ta-10W substrate, showing a clean grain structure.

(U) Chemical analysis of the interstitial contents of the emitter structure yielded the following results (in ppm): O, 15; N, 22; C, 20. The similarity of these data to that for the O, N and C contents of the Ta-10W used in the preparation of the emitter structure implies that the emitter structure was not significantly contaminated during the cesiated converter test.

1.3.5. D_1-1 Emitter Structure

(U) The D_1-1 emitter structure consists of a chemically etched fluoride tungsten emitter diffusion-bonded to a Ta-10W substrate. Its operating thermal history in a cesiated converter is as follows: 1427°C, 250 hours; 1527°C, 350 hours; 1627°C, 1600 hours. Although the converter test was terminated because of the presence of a leak, none was detected in the emitter structure received from NASA.

(U) Figures 1.57 and 1.58 represent the appearance of the post-test tungsten emitter surface under a microscope at different magnifications. Figure 1.59 is an electron micrograph taken of the replica of the emitter surface. It can be seen that although the emitter surface is macroscopically rough, it is free from the micro-facets shown in Fig. 1.26 for the as-etched surface. This is in agreement with the observation made previously[3] that while the chemically etched surface is covered with microfacets, thermal treatment at high temperatures will remove them even though the surface is still macroscopically rough. Figure 1.60 shows the spatial distribution of the <100> axes in the emitter in its post-test state, which does not

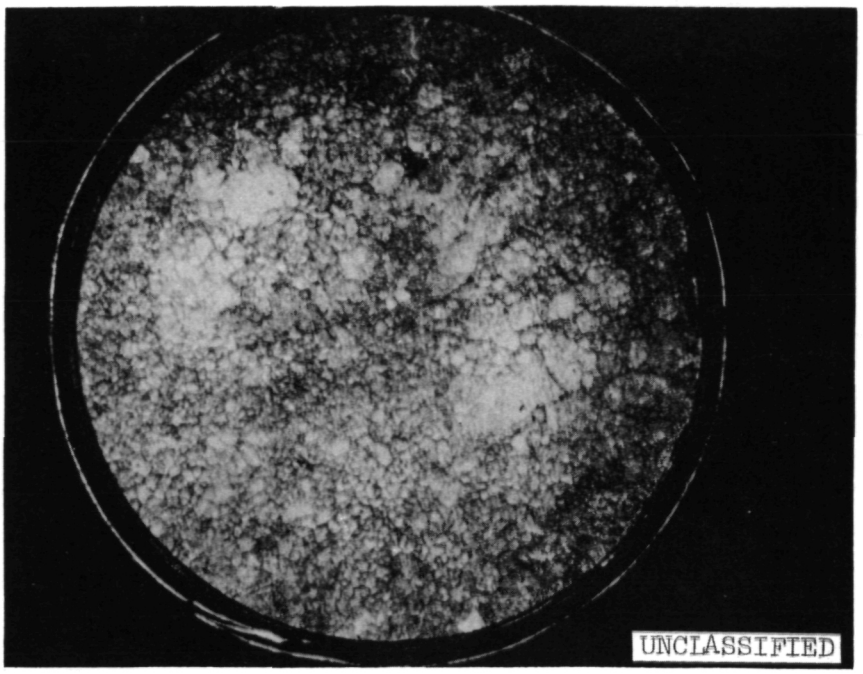

M 29939-2 ~5X

Fig. 1.53--(U) Macroscopic appearance of the post-test Ta-10W substrate surface of emitter structure C_3-3

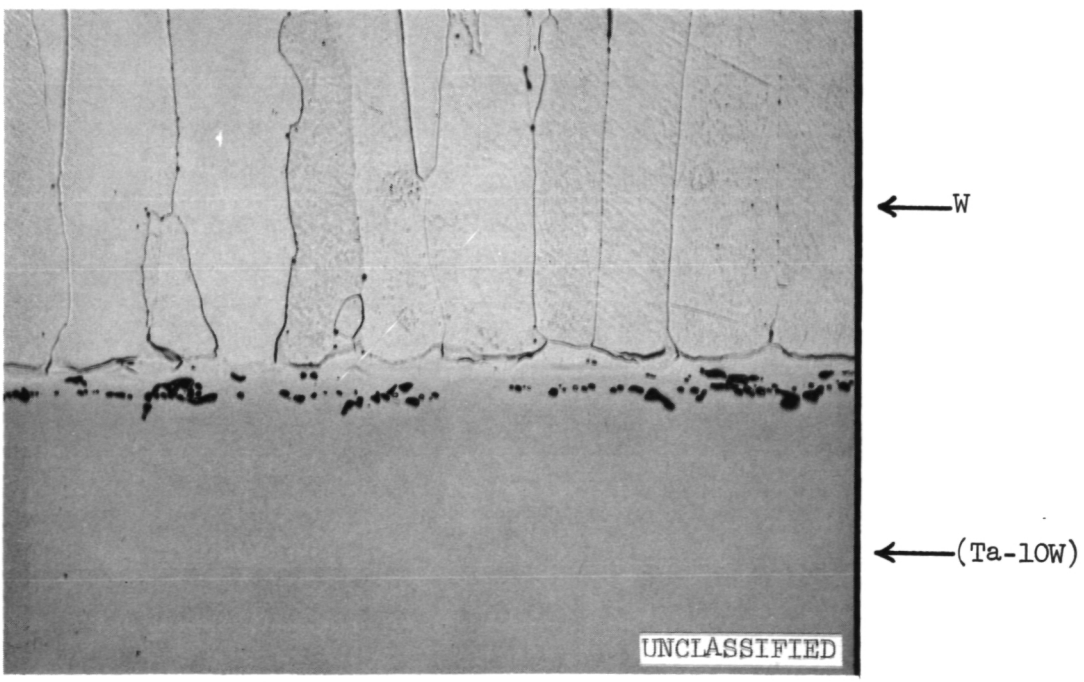

M 30860-2 100X

Fig. 1.54--(U) Post-test microstructures of the fluoride tungsten-(Ta-10W) interface of emitter structure C_3-3

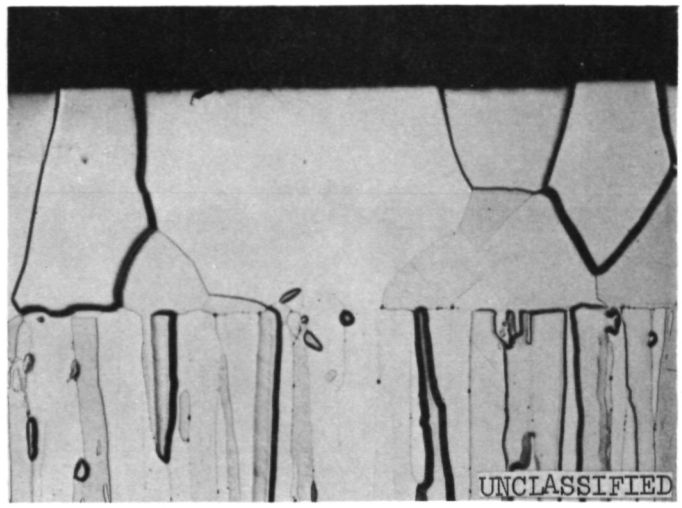

M 31383-2 35X

Fig. 1.55--(U) Post-test microstructures of the chloride tungsten-fluoride tungsten interface of emitter structure C_3-3

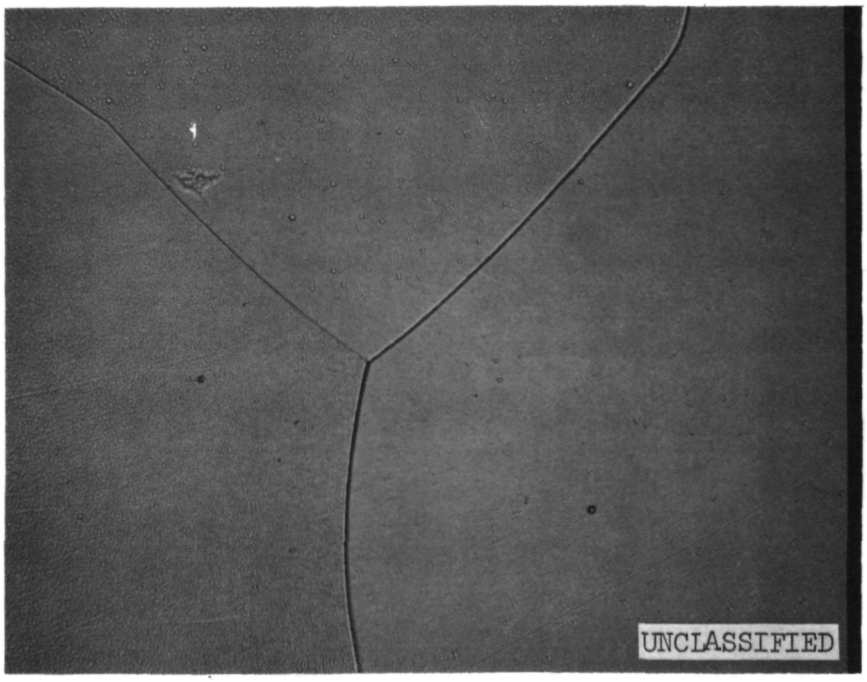

M 30860-5 100X

Fig. 1.56--(U) Post-test grain structures of the Ta-10W substrate of emitter structure C_3-3

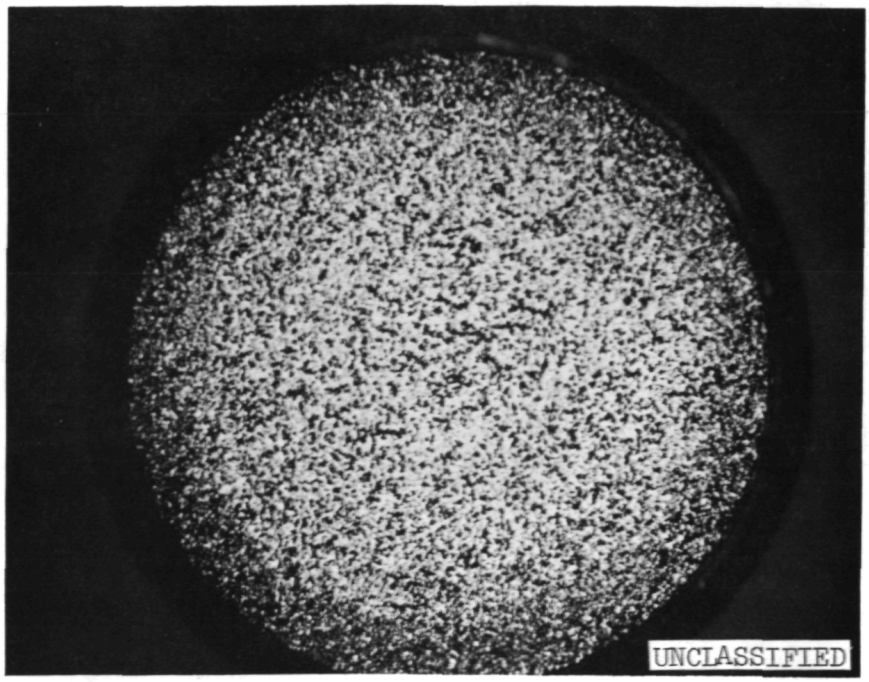

M 26643-1 ~5X

Fig. 1.57--(U) Macroscopic appearance of the post-test chemically etched fluoride tungsten emitter surface of emitter structure D_1-1

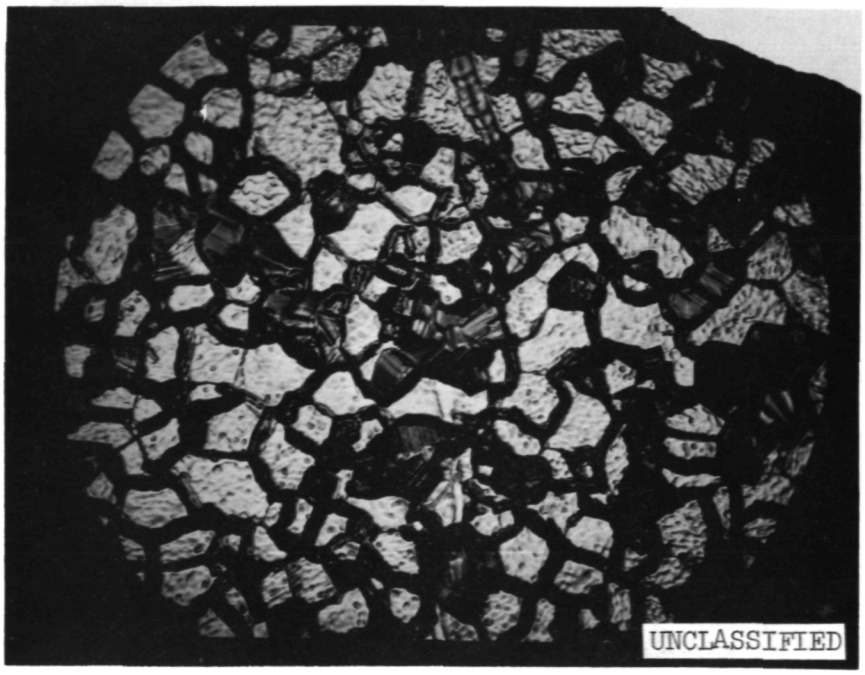

125X

Fig. 1.58--(U) Appearance of the surface shown in Fig. 1.57 at a higher magnification

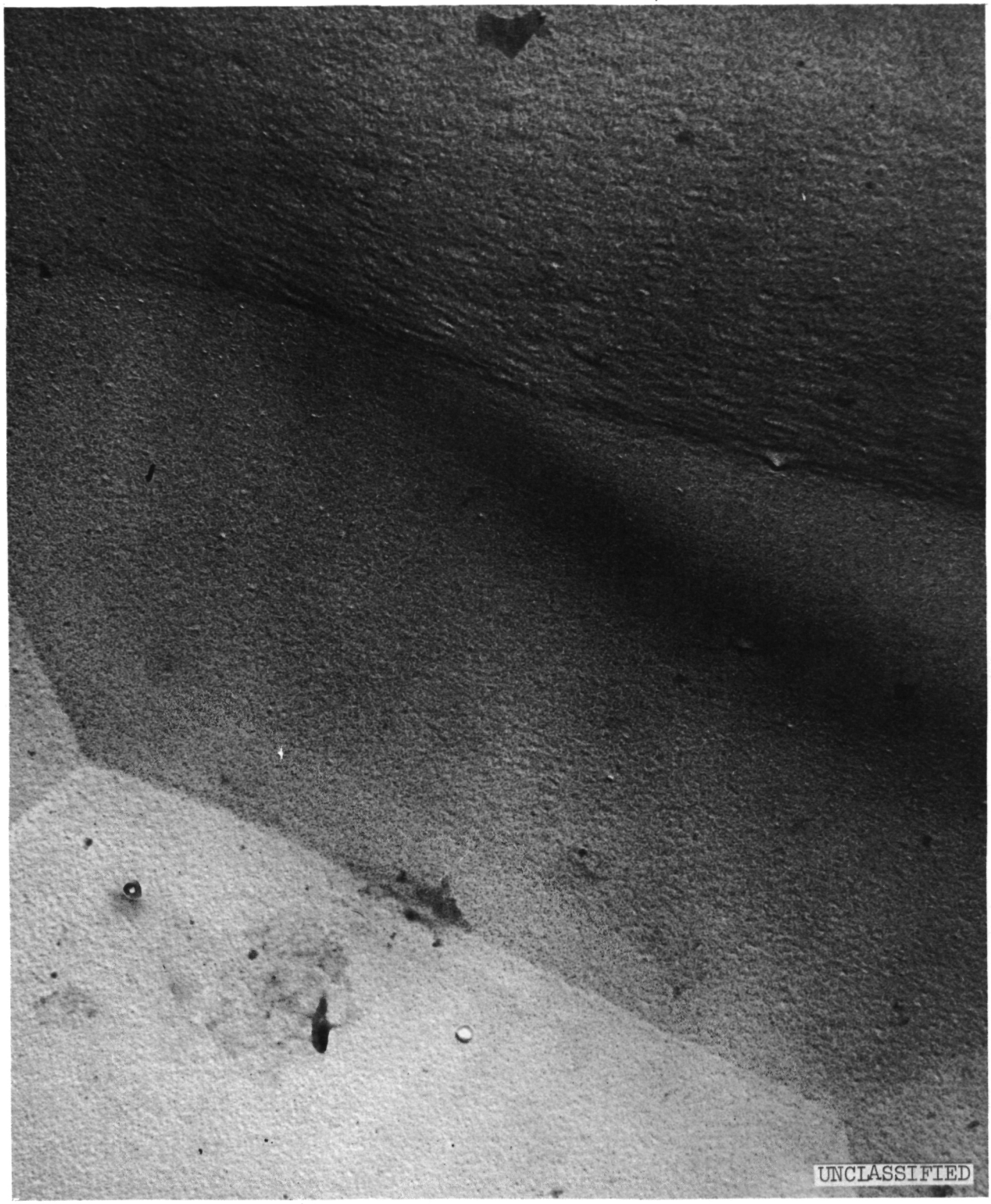

P 1464-5 10,500X

Fig. 1.59--(U) Electron micrograph of a replica of the post-test emitter surface of emitter structure D_1-1

Fig. 1.60-- (U) Spatial distribution of the <100> axes in the chemically etched fluoride tungsten emitter of emitter structure D_1-1 after test in a cesiated converter

seem to differ significantly from that obtained from the as-fabricated emitter (Fig. 1.25). Vacuum work function measurement was made of the received emitter at 1600°C for 650 hours. The results are shown in Fig. 1.61. It can be seen that a steady value of 4.77 eV was obtained after 380 hours which is higher than that of fluoride tungsten (~ 4.5-4.6 eV). Since the operation of this emitter in the cesiated converter was carried out at a temperature below 1623°C, it appears that at least part of the gain in vacuum work function by the chemical etching of fluoride tungsten emitters can be maintained for long periods of time at low temperatures. The trade-off between time and temperature for maintaining such gains in vacuum work function has been discussed and studied by various authors.(4) However, more long-term test data are needed to establish a reliable quantitative relationship for predicting the performance of converters containing chemically etched fluoride tungsten emitters.

(U) Figure 1.62 is a macrophotograph of the post-test appearance of the Ta-10W substrate surface. The dark marks present seem to be in the shape of the electron bombardment filament. Its formation could be related to thermal etching. However, the exact reason for its presence is unknown. Table 1.12 contains the optical micrometer data of the surface contours of the tungsten emitter and the Ta-10W substrate. It can be seen that the deformation of the emitter surface is fairly symmetrical and less than 1 mil.

(U) Figures 1.63 and 1.64 show respectively the post-test appearance of the tungsten-(Ta-10W) interface in the unetched and the etched states. The formation of the Kirkendall voids is less severe than that for the other emitter structures studied, presumably because of the lower operating temperature and thus less interdiffusion between the tungsten and the Ta-10W. Electron microprobe study indicated a diffusion zone width of 25-28 microns, which is about a factor of two less than that observed for the other emitter structures studied above. The post-test interstitial contents (O, 45; N, 20; C, 15) of the emitter structure are of the same order of magnitude as that of the Ta-10W used for the preparation of the emitter structures studied, indicating no significant contamination of the emitter structure during converter testing.

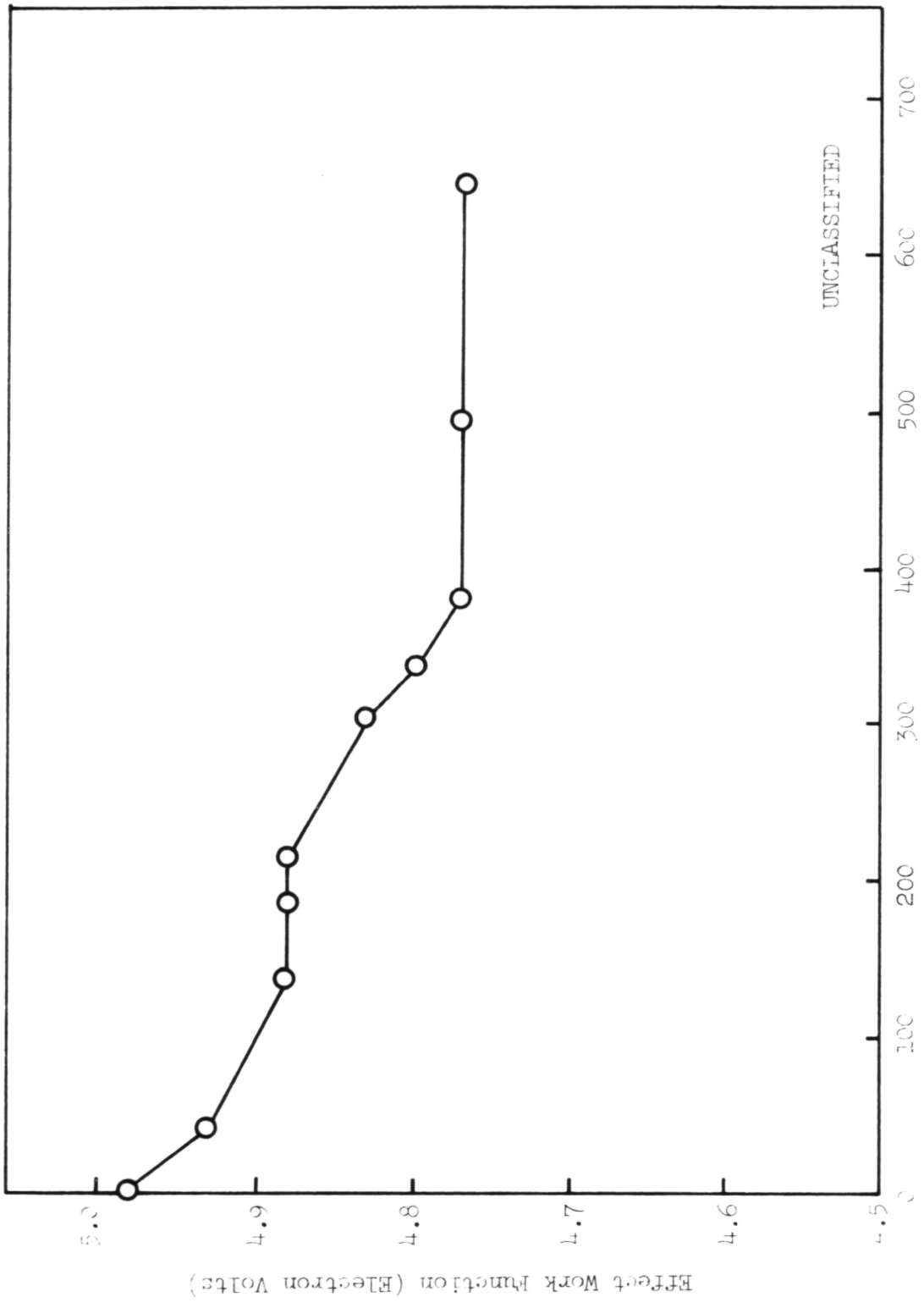

Fig. 1.61--(U) Vacuum work function of emitter structure D_1-1 as a function of time at 1600°C

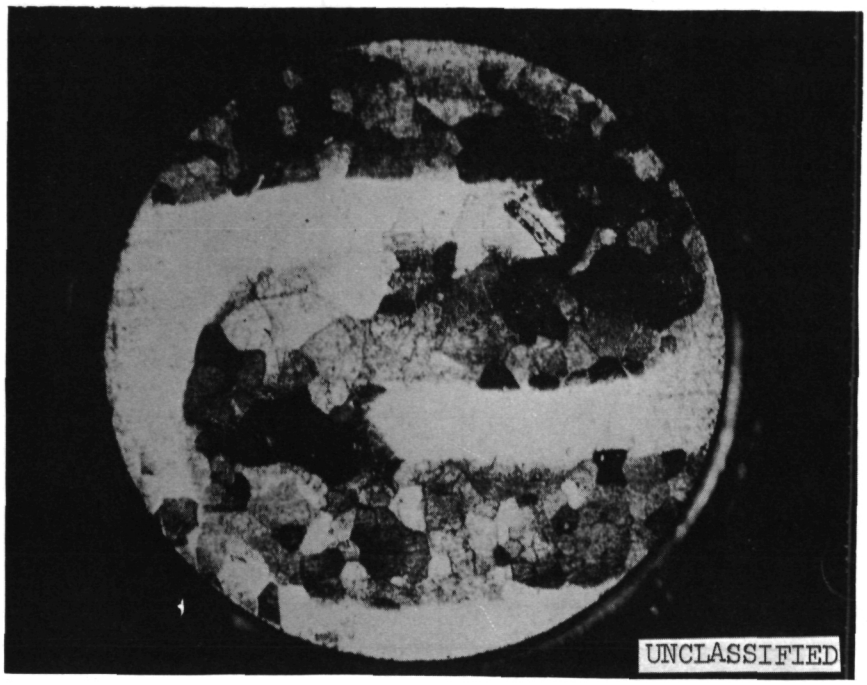

M 26643-2 ~5X

Fig. 1.62--(U) Post-test macroscopic appearance of the Ta-10W substrate surface of emitter structure D_1-1

Table 1.12

(U) OPTICAL MICROMETER MEASUREMENTS OF W AND Ta-10W SURFACE CONTOURS OF EMITTER STRUCTURE D_1-1 AFTER TESTING AT TECO

(This table is Unclassified)

Surface Position	W Surface	Ta-10W Surface
X_0	0	0
X_1	-.7	+ .2
X_2	-.3	+ .3
X_3	-.3	+ .4
X_4	-.3	+ .4
X_5	-.7	+1.0
X_6	-.9	+1.0
X_7	-.7	+1.0
X_8	-.9	+1.0

Note: In the above table the W and W-10W surface contours, the surface position designations represent the locations indicated below. All dimensions are in mils with X_0 as the reference point. Positions with "+" sign are lower than X_0 and positions with "-" sign are higher than X_0.

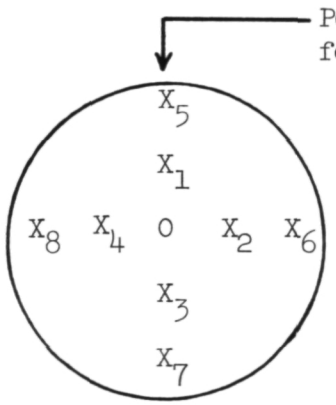

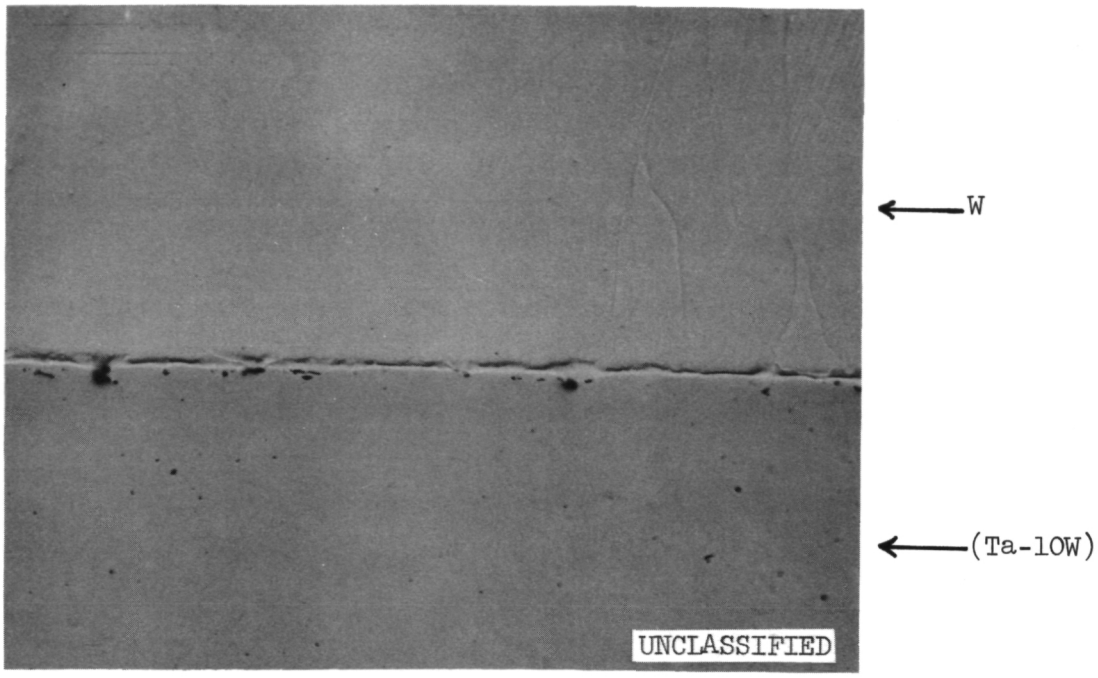

M 27647-3 100X

Fig. 1.63--(U) Unetched appearance of the tungsten-(Ta-10W) interface of emitter structure D_1-1 after test in a cesiated converter

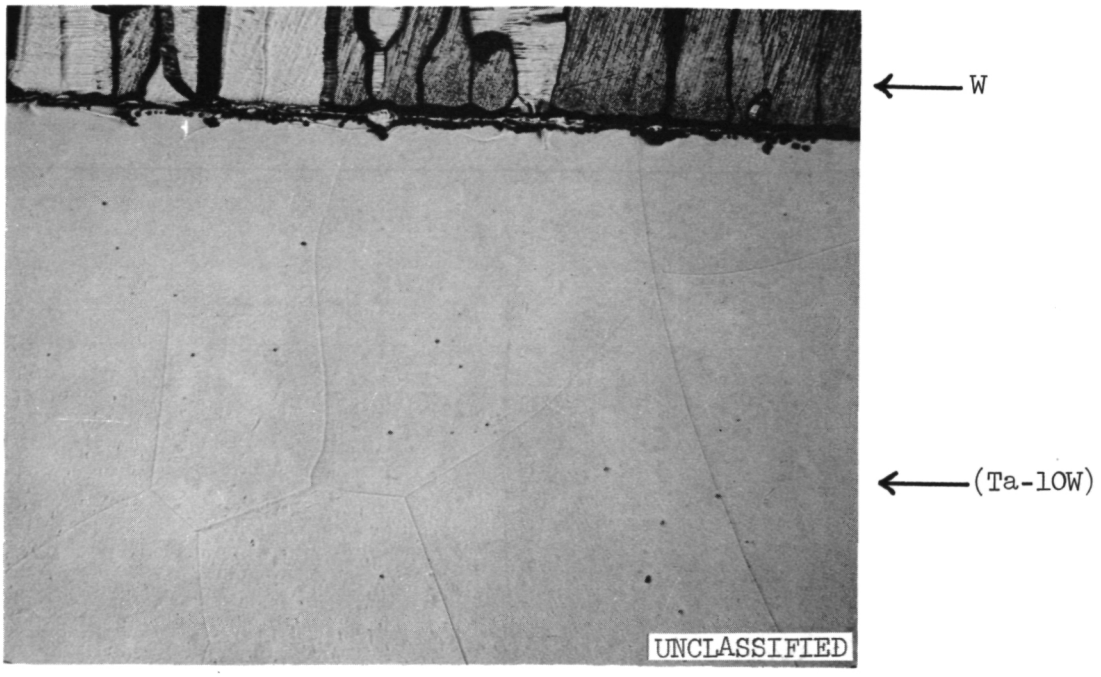

M 27647-13 100X

Fig. 1.64--(U) Etched appearance of the tungsten-(Ta-10W) interface of emitter structure D_1-1 after test in a cesiated converter

REFERENCES

1. "Studies of Thermionic Materials for Space Power Applications," (U) Summary Report for the Period November 23, 1965 through January 31, 1967, Contract NAS 3-8504, NASA CR-72315, GA-7682. (C/RD)

2. "Study of Thermionic Materials for Space Power Applications," (U) Annual Summary Report for the Period September 1, 1963 through August 31, 1964, Contract NAS 3-4165, NASA CR-54322, GA-5665. (C/RD)

3. Yang, L., and R. G. Hudson, "Effect of Preferred Crystal Orientation and Surface Treatment on the Work Function of Vapor-Deposited Tungsten," (U), Proceedings of the 1966 Thermionic Specialist Conference, p. 395. Houston, Texas, (November 2-4, 1966) GA-7343

4. Batzies, D., J. Demy and H. E. Schmid, "Preparation and Investigation on Tungsten Surfaces with Preferred Orientation," Presented at the Second International Conference on Thermionic Electrical Power Generation, May 27-31, 1968, Stresa, Italy.

PART II. POST-OPERATIONAL ANALYSIS OF CESIUM CONTENTS IN OUT-OF-PILE LIFE TESTING CONVERTER COMPONENTS

(R. G. Hudson, G. Buzzelli, L. Yang)

SUMMARY

(U) The cesium contents of the components of three life-testing cesiated converters, LC-3, LC-4 and LC-5 were analyzed by neutron-activation techniques. Among all the components studied, the most important cesium sink was the metallizing layer of the Litton insulator. The principal converter materials, namely tungsten, molybdenum, tantalum, niobium and Al_2O_3 did not hold appreciably amounts of cesium at their operating temperatures, although for tantalum and niobium rigid control of the concentrations of interstitial impurity contents may be needed in order to minimize their cesium uptakes. The cesium contents found in the vanadium brazes examined were shown to consist largely of cesium mechanically occluded in the porosity of the braze, rather than being dissolved in the braze.

2.1. INTRODUCTION

(U) If the conventional liquid cesium reservoir in a thermionic converter could be replaced by a cesium source capable of operating at temperatures between the emitter temperature and the collector temperature, the design and the operation of a thermionic reactor core might be simplified. One of the concepts for developing such an integral cesium reservoir involves the use of a cesium source consisting of cesium atoms adsorbed in monolayer form on a porous refractory metal substrate (e.g. tungsten). While the attractiveness of this concept is evident since it introduces no foreign material into the converter, it suffers from the disadvantage that the total cesium reserve in such an adsorption integral reservoir is very limited. For the specific surface areas currently achievable in refractory

metal bodies which are stable at about 1000°C, the total cesium reserve is less than 1 mg of cesium per each cm^3 of the porous substrate material. Thus the feasibility of this concept requires that the cesium loss in an operating converter be kept to a minimum. One of the major sources of cesium loss, which is inherently present, involves diffusion and interaction between cesium and the converter components. Since such diffusion and interaction even in trace amounts will affect a significant percentage of this limited amount of cesium reserve, measurements of the cesium losses to life test converter components by using the sensitive neutron activation techniques represent the best means to provide a direct answer to the feasibility of this concept.

2.2. SAMPLE ACQUISITION

(U) Three out-of-pile Mark VI type life-testing converters, designated as LC-3, LC-4 and LC-5 were available for such investigations. LC-3 and LC-5 emitters contained W-UO_2 cermet and 90UC-10ZrC respectively, and LC-4 emitter was unfueled. The testing time was 10,406 hours for LC-3, 7345 hours for LC-4, and 7558 hours for LC-5. Typical operating temperatures for the converter components at a cesium pressure of about 10 torr were: tungsten emitter, 1750-1800°C; molybdenum collector, 700°C; Al_2O_3 insulator, 750-800°C; tantalum transition piece and vanadium braze between the transition piece and the tungsten emitter, 900°C. Figure 2.1 is a schematic of Mark VI out-of-pile converter, illustrating the nature and the locations of the samples taken. These samples (each sample indentified by numbers in Fig. 2.1) are:

(1) Vapor-deposited fluoride tungsten emitter. – The sample was a half cylinder of about 1/2 inch in length, taken over the fueled regions of LC-3 and LC-5 and at a similar location for LC-4. The fuel material and the wall of the electron bombardment filament cavity was removed by electrical discharge machining, leaving only the 40 mil thick cladding.

(2) Molybdenum collector. – The sample was also a half cylinder of about 1/2 inch in length and 40 mil in thickness, taken from a position opposite to that of the emitter sample. For LC-3 and LC-5, the collector samples were leached with dilute HNO_3 to remove the collector condensates for the determination of their uranium contents prior to being used as samples for the determination of cesium contents in the collector material. About 0.5 mil was dissolved from the LC-5 sample and 1.1 mil was dissolved from the LC-3 sample during this operation.

(3) Tantalum transition piece. – The whole tantalum transition piece was used. Successive layers were machined off from "Surface A" in Fig. 2.1 as the samples for cesium determination. Care was taken to leave the vanadium braze region intact. This pre-irradiation machining was necessary because of the strong radioactivity of irradiated tantalum.

(4) Upper niobium insulator sleeve. – One quarter of the upper sleeve was taken as the sample for cesium determination.

(5) Lower niobium insulator sleeve. – One quarter of the lower sleeve was taken as the sample for cesium determination.

(6) Vanadium braze. – The tantalum transition piece of (3), after machining off successive layers from "Surface A", was cut into two halves. One half was used as the sample for cesium determination.

(7) Insulator. – One half of the insulator ring, including the Al_2O_3, the metallizing layer, the braze and the Nb attached to the braze was taken as the sample for cesium determination.

(U) Each of these samples was washed thoroughly with distilled water to remove any cesium contamination prior to irradiation in the Gulf General Atomic TRIGA reactor. In addition to these samples taken from the

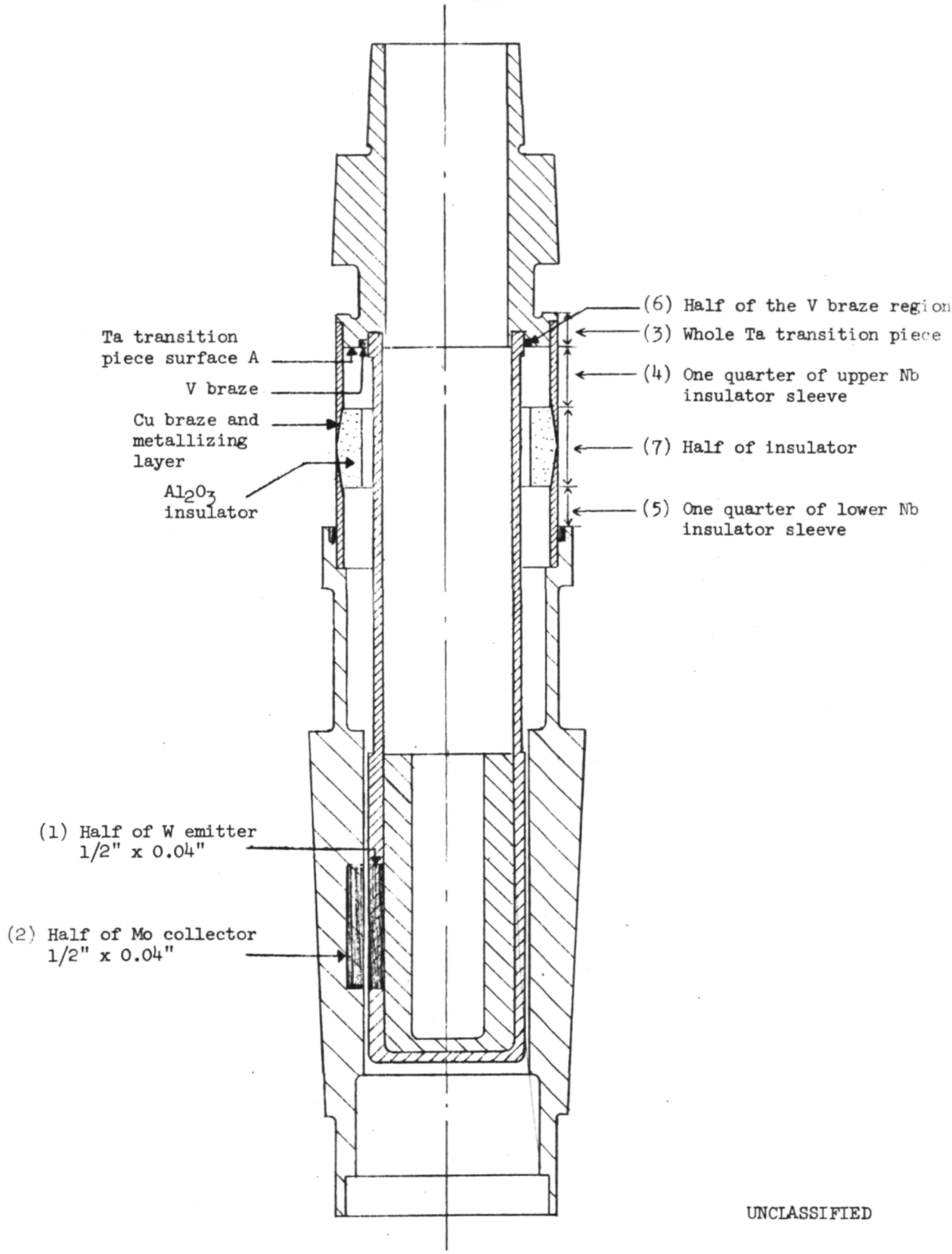

Fig. 2.1--(U) Mark VI out-of-pile converter schematic, illustrating the nature and the locations of the samples taken for the determination of their cesium contents

converter components, a sample of each of the types listed above, which had not been exposed to cesium, was analyzed to provide blank corrections.

2.3. ANALYTICAL TECHNIQUES

(U) Thermal neutron activation analysis was used to determine the cesium contents of the above described samples. Elementary cesium consists of the single isotope Cs^{133} which has a thermal neutron activation cross section of about 30 barns. Upon adsorption of a thermal neutron, Cs^{133} transmutes to Cs^{134}, which exists in two isomeric forms, a 2.9 hour half-life form and a 2.06 year half-life form. For this work, counting of the γ-activity of the 2.06 year half-life form was used to determine the cesium content of a sample. The sensitivity via the activation technique to form the Cs^{134} of 2.06 year half-life is 0.05 to 0.10 μg in the absence of other interferences. This limit of detection, however, may be raised if interfering activities are present.

(U) The activation technique consists of irradiating the samples together with a cesium standard in the Gulf General Atomic TRIGA reactor for about one hour at 250 kW (neutron flux = $2 \times 10^{12}/cm^2$ sec). A cooling period of about two weeks is needed to decay the matrix (e.g. tungsten, tantalum) activity to a level suitable for handling. If the matrix activity introduces a high background or interfering radioactivity, a chemical separation of the Cs^{134} formed is necessary. Otherwise the sample is counted for its Cs^{134} activity directly. Quantitative values are obtained by reference to a Cs^{134} standard counted in the same counting geometry. In case a radiochemical separation of Cs^{134} has to be performed, milligram quantity of non-radioactive cesium carrier is added when the sample is brought into solution. Chemical separation of the matrix and the cesium in the solution is then carried out. For instance, for the tantalum and niobium samples, these elements can be precipitated as the hydrated oxides in strong acid solution, leaving the cesium in solution. Then the cesium can be purified by repeated precipitation as $CsSnCl_6$. If the degree of decontamination is adequate, the Cs precipitate is weighed for chemical yield to correct for any loss. This precipitate is then counted with a

gamma spectrometer. Quantitative results are obtained by reference to the irradiated cesium standard prepared and counted in the same form as the sample.

(U) After the samples listed in Section 2.2 were irradiated, they were treated as follows:

(1) Tungsten emitter. – Successive layers of the irradiated sample were dissolved electrolytically in 10% NaOH. The solutions were then counted directly.

(2) Molybdenum collector. – The irradiated sample was sectioned into a number of layers by machining. The material in each layer was counted directly.

(3) Tantalum transition piece. – The layers of tantalum machined off from the transition piece were dissolved in HNO_3 + HF. Radiochemical separation was performed on each of the solutions obtained according to the procedures described above prior to the counting of the Cs^{134} activity.

(4) Upper niobium insulator sleeve. – The irradiated sample was machined into a number of layers. The material in each of the layers obtained was dissolved in HNO_3 + HF. Radiochemical separation was performed on each of the solutions obtained according to the procedures described above prior to the counting of the Cs^{134} activity.

(5) Lower niobium insulator sleeve. – The sample was treated in the same way as the upper niobium insulator sleeve.

(6) Vanadium braze. – After irradiation, the vanadium braze contained in the well formed by the tantalum transition piece and the tungsten emitter stem was dissolved in HNO_3 + HCl and the solution obtained was counted for its Cs^{134} content. For samples obtained from LC-3 and LC-5, extraction with hot water was

performed to remove any cesium occluded in fine crevices prior to dissolution in HNO_3 + HCl.

(7) Insulator. – The irradiated insulator sample was treated with dilute HNO_3 to dissolve the copper braze and some of the metallizing layer. The solution obtained was counted directly for its Cs^{134} content. The Nb pieces attached to the Al_2O_3, (plus some metallizing layer) were then removed by mechanical means and dissolved in HNO_3 + HF. Radiochemical separation was performed according to the procedures described above prior to the counting of the Cs^{134} activity. The Al_2O_3 piece, together with some metallizing layer attached to it, was counted directly.

2.4. ANALYTICAL RESULTS

(U) The analytical results for the blank samples and the samples from LC-3, LC-4 and LC-5 are shown in Table 2.1 and Table 2.2 respectively. The essential findings are described as follows.

2.4.1. Blank Samples

(U) No cesium was detected in any of the blank samples studied. The detection limits for cesium in each of these samples were deduced from the counting backgrounds and included in Table 2.1.

2.4.2. Results for Components of LC-3, LC-4 and LC-5

(U)

(1) Tungsten emitter. – No cesium (> 0.26 μg) was detected in each case. Counting was stopped at the second layer for each emitter since the cesium content was below the detection limit.

(2) Molybdenum collector. – No cesium (> 0.15 μg) was detected for all the samples studied for LC-3 and LC-5. Although the initial acid leaching solutions for the collector condensate (see Section 2.2) prior to the irradiation yielded 25.6 μg cesium in 1.1 mil of molybdenum dissolved for LC-3 and 1.33 μg cesium in 0.5 mil of molybdenum dissolved for LC-5, it is believed

Table 2.1

(U) ANALYTICAL RESULTS ON BLANK SAMPLES

(This table is Unclassified)

Sample	Amount	Cesium Content (Detection Limit)
Tungsten emitter	0.6055 gm	< 0.25 ppm
Molybdenum collector	0.4263 gm	< 0.40 ppm
Niobium insulator sleeve	0.0575 gm	< 0.36 ppm
Solution of insulator braze plus some metallizing layer	From half of insulator	< 0.085 μg
Al_2O_3 plus some metallizing layer	From half of insulator 2.4809 gm	< 0.034 ppm
Nb attached to insulator plus some metallizing layer	From half of insulator 0.5895 gm	< 0.5 ppm
Ta transition piece	0.1089	< 1 ppm
V braze	0.0653	< 1 ppm

that the cesium observed represented contaminants in the collector condensate and not cesium diffused into the molybdenum collector. Contrary to the results for LC-3 and LC-5, the molybdenum collector in the unfueled converter LC-4 contained 2.5 μg of cesium in 18.4 mils. It is possible that the presence of fuel components on the collector surface suppress the diffusion of cesium into the collector. However, more experimental data are needed to substantiate this.

Table 2.2

(U) CESIUM CONTENTS IN COMPONENTS OF LC-3, LC-4 AND LC-5

(This table is Unclassified)

	LC-3			LC-4			LC-5		
	Thickness* of Layer or Weight of Piece	Cesium Content (10^{-6} gm)	Total Observed Cesium Content in Each Item (10^{-6} gm)	Thickness of Layer or Weight of Piece	Cesium Content (10^{-6} gm)	Total Observed Cesium Content in Each Item (10^{-6} gm)	Thickness of Layer or Weight of Piece	Cesium Content (10^{-6} gm)	Total Observed Cesium Content in Each Item (10^{-6} gm)
1. Half W emitter 1/2 in. long	5.0 mil 5.0 mil	0 0	0	5.0 mil 5.2 mil	0 0	0	5.0 mil 5.1 mil	0 0	0
2. Half Mo collector 1/2 in. long	4.8 mil 4.2 mil 4.9 mil	0 0 0	0	3.7 mil 1.0 mil 4.1 mil 4.8 mil 4.8 mil 5.0 mil	1.3 0.3 0.3 0.3 0.3 0	2.5	6.2 mil 4.0 mil 5.2 mil	0 0 0	0
3. Whole Ta transition piece	5.9 mil 8.3 mil 7.3 mil 7.5 mil 8.8 mil 5.2 mil	1.5 0.8 0.2 0 0 0	2.5	5.9 mil 4.1 mil 10.7 mil 6.0 mil 7.1 mil 5.2 mil	22.2 13.4 30.5 2.7 1.8 0	70.6	2.4 3.3 3.9 10.0 12.9 6.8	1.7 1.0 0.5 1.2 1.5 0	5.9
4. One quarter of upper Nb insulator sleeve	2.2 mil 2.0 mil 21.2 mil	1.2 0.7 0	1.9	5.6 mil 3.0 mil 2.0 mil	0.9 0 0	0.9	1.0 mil 1.1 mil 20.5 mil	0 0 0	0
5. One quarter of lower Nb insulator sleeve	19.9 mil	1.2	1.2	3.8 mil 1.5 mil 15.7 mil	0.7 0.3 2.1	3.1	17.5 mil	0	0
6. Half of V braze**	0.0039 gm	66	66	0.0052 gm	3160	3160	0.0045 gm	1	1
7. Half of insulator**									
(1) Braze + metallizing layer	-	470		-	400		-	1060	
(2) Al_2O_3 + some metallizing layer	2.3632 gm	5.7		2.3066 gm	20.1		2.3236 gm	43	
(3) Nb attached to Al_2O_3 + some metallizing layer	0.6166 gm	3.0	478.7	0.6149 gm	4.3	424.4	0.7461 gm	12	1115

*Starting from surface facing cesium vapor

**No sectioning was performed. The whole sample was analyzed.

Note: The cesium detection limits for the particular samples shown in the table are: 0.26 μg for W, 0.15 μg for Mo, 0.1 μg for Ta and Nb, 0.07 μg for Al_2O_3.

(3) Tantalum transition piece. – Cesium was found in the tantalum transition piece in all three converters. The amount of cesium (70.6 μg) in the LC-4 tantalum transition piece, however, far exceeded that in the LC-3 (2.5 μg) and the LC-5 (5.9 μg) tantalum transition pieces. Analysis of the C, N, and O concentrations in samples taken from the tantalum transition pieces of LC-3, LC-4 and LC-5 yielded the following results: LC-3, 41 ppm C, 41 ppm O, 5 ppm N; LC-4, 43 ppm C, 71 ppm O, 35 ppm N; and LC-5, 47 ppm C, 44 ppm O, 5 ppm N. Whether the higher O and N contents in the LC-4 tantalum transition piece were responsible for its higher cesium content remains to be proved by controlled experiments.

(4) Niobium insulator sleeves. – Samples from LC-3 and LC-4 contained a total of 3 and 4 μg of cesium respectively, while samples from LC-5 contained no detectable (< 0.1 μg) of cesium.

(5) Vanadium braze. – Excessive amount of cesium was found in the LC-4 vanadium braze. It is believed that the cesium observed represented cesium occluded mechanically in fine crevices or porosities in the vanadium braze, not cesium dissolved or reacted with the vanadium braze. To resolve this point, the other half of the LC-4 tantalum transition piece containing the vanadium braze was polished and examined under a microscope. Figure 2.2 is a photomicrograph taken of the region where the tungsten emitter stem was brazed to the tantalum transition piece. It can be seen that the vanadium braze contained a large number of pores. Electron microprobe scan showed that a high concentration of cesium was present in these pores (Fig. 2.3). Thus, the cesium observed in the vanadium braze of LC-4 was indeed mechanically occluded in the defects of the braze.

(C-RD)(Gp-1) In view of these findings, the vanadium braze samples for LC-3 and LC-5 were leached repeatedly in hot distilled water to remove the mechanically occluded cesium as far as possible. A total of 30 μgs of cesium was obtained from the LC-3 braze and less than 1 μg of cesium was obtained from the LC-5 braze. Subsequent acid leaching yielded 66 μgs of cesium in 3.9 mgs of dissolved material for the LC-3 braze and about 1 μg of cesium in 4.5 mgs of dissolved material for the LC-5 braze. Metallographic examination of the other half of the LC-3 braze indicated that there were still some pores present in the braze, while similar examination on the other half of the LC-5 braze detected no pores in the braze. These results seem to indicate that the solubility of cesium in vanadium is very small and that most of the cesium observed in the LC-3 and LC-4 vanadium brazes owes its origin to mechanical occlusion in the defects of the braze rather than the dissolution of cesium in vanadium. A vanadium wire weighing 61.32 mgs was exposed to Cs^{134} tagged cesium vapor at 1000°C and 1 x 10^{-5} atm for 70 hours. Counting of the exposed wire yielded a cesium content of 5.1 ppm of which 2.7 ppm could not be washed off with water. This observation indicates that although cesium does seem to possess a finite solubility in vanadium, the amount of cesium loss to the vanadium braze in a thermionic converter is negligible.

(6) (U) Insulator. – The solution obtained by the dissolution of the copper braze and part of the metallizing layer of the Litton insulator contained a large amount of cesium (400-1060 μgs) in all three cases. It is believed that the cesium observed, unlike that in the vanadium braze as described above, was not caused by mechanical occlusion of cesium in the braze but due to the interaction of cesium with components of the metallizing layer, probably the silica impurity in the metallizing compound. Metallographic examination reported elsewhere(1) revealed the attack of the metallizing layer of the Litton insulator in a number of out-of-pile life-testing converters. The cesium present in the

RESTRICTED DATA
ATOMIC ENERGY ACT 1954
GROUP 1

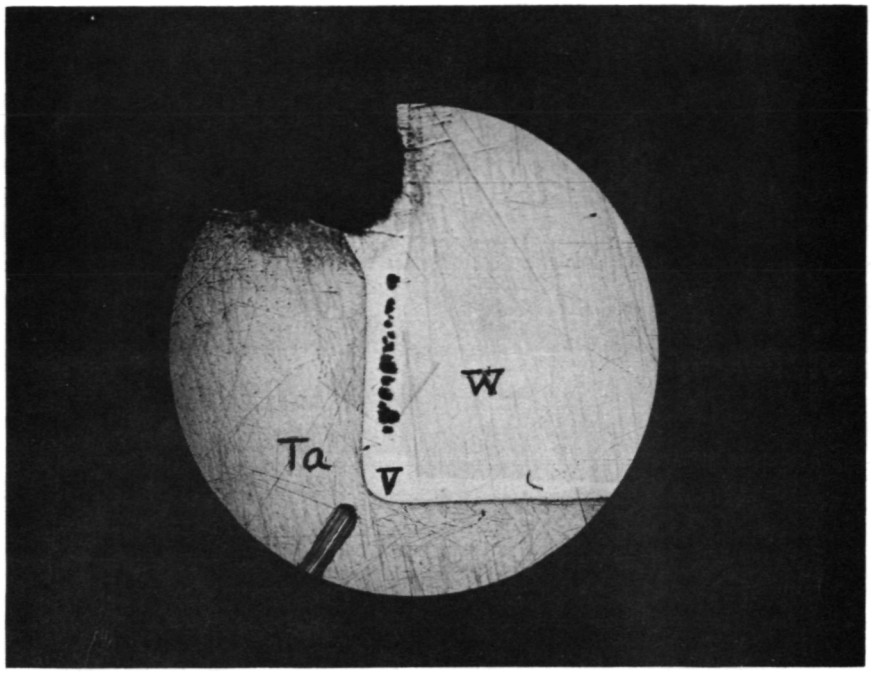

45X

Fig. 2.2--(U) Appearance of vanadium braze region in LC-4 converter. Note pores in vanadium braze

250 μ

Fig. 2.3--(U) CS Lα scan of the pores in the vanadium braze of Fig. 2.2. Note high concentration of cesium in pores

Al_2O_3 piece and the niobium attached to the insulator owe its origin mostly to the metallizing layer left on these materials. When the metallizing layer was ground off from the Al_2O_3 pieces of LC-3, LC-4 and LC-5 together with about 4 mils of Al_2O_3 adjacent to the metallizing layer, the cesium content dropped from 5.7 μg to 1.5 μg for LC-3, from 20.1 μg to 1.8 μg for LC-4, and from 43 μg to 2.5 μg for LC-5. Further removal of 5 mils of Al_2O_3 from the inner cylindrical surface of the Al_2O_3 of LC-3 and LC-5, which was exposed to cesium vapor during the operation of the converter, lowered the cesium contents of the Al_2O_3 to background level (< 0.07 μg). Similar results were obtained with LC-4 when 7.2 mils were removed from the Al_2O_3 surface which was exposed to the cesium vapor during converter testing. Thus the cesium present in the Al_2O_3 pieces of these life-testing converters amounted to only a few micrograms in the outer 5-7 mil region of the surface facing the cesium vapor. Al_2O_3 is thus not a cesium sink at its operating temperature (750-800°C) in these converters.

2.5 CONCLUSIONS AND DISCUSSIONS

(C-RD)(Gp-1) These results indicate that among all the converter components studied the most important cesium sink is the metallizing layer of the Litton insulator. An insulator containing tungsten-yttria metallizing layer (with strict control of silica contamination) is currently under evaluation. Unless complete inertness toward cesium vapor is demonstrated by neutron activation analysis for this type of metallizing, the feasibility of an adsorption integral cesium reservoir using porous refractory metal substrates is questionable.

(U) The basic converter components, namely tungsten, molybdenum, tantalum, niobium, and Al_2O_3, are not important cesium sinks at their operating temperatures. Tantalum and niobium, which showed variable results among the three converters studied, may need rigid control of the concentrations of their intersititial impurities to minimize their cesium solubilities. Vanadium braze, which is not a cesium sink, may have to be

RESTRICTED DATA
ATOMIC ENERGY ACT 1954
GROUP 1

excluded from future converters for reasons of structural integrity rather than cesium solubility.

(U) Previous analysis[1] showed that in an adsorption integral reservoir converter using a porous tungsten substrate, the maximum change in cesium reserve which can be tolerated if the converter output is to be maintained within 90% of its optimum value is 2%. With a cesium reserve of about 1 mg, the total loss of cesium during long term converter operation has to be kept below 20 μgs in order to achieve this goal. Although the total cesium found in LC-3 or LC-5 components is somewhat less than this value, if the cesium in the metallizing layer of the insulator is neglected, the adsorption integral reservoir concept is rather marginal. Its success demands very strict control of material purity and converter outgassing conditions.

REFERENCE

1. "Studies of Thermionic Materials for Space Power Applications," (U) Summary Report, November 23, 1965 through January 31, 1967. GA-7682, Contract NAS 3-8504. (C/RD)

PART III. CHEMICAL VAPOR-DEPOSITION OF CHLORIDE TUNGSTEN

(R. G. Hudson and L. Yang)

SUMMARY

(U) Chemical vapor deposition of tungsten by the hydrogen reduction of tungsten chloride has been studied in order to define the conditions under which {110} oriented deposits could be reproducibly obtained. The tungsten chloride used was provided either from WCl_6 powder or by the chlorination of fluoride tungsten chips. The latter was preferred as the source of the tungsten chloride because it provided better purity and process variable control. Exploratory studies indicated that the principal controlling factors of the degree of {110} orientation and the vacuum work function of the deposit were the mandrel temperature and the H_2/W ratio in the gaseous reactants, with the latter governed by the tungsten chip temperature and column height in the chlorinator, and the chlorine flow rate. Typical deposition conditions for the preparation of chloride tungsten deposits of 4.9 - 5.0 eV vacuum work functions were: mandrel temperature 1100-1150°C, hydrogen flow rate 140-160 c.c./min., chlorine flow rate 115-135 c.c./min., tungsten chip temperature 830-875°C, tungsten chip column height 7-1/2 inches, and residual gas pressure 4-6 torr. The H_2/W ratio corresponding to these conditions fell in the range of 2 to 3. The reproducibility of the stability of the emission characteristics of samples prepared under these conditions were demonstrated.

3.1. ESTABLISHMENT OF CONDITIONS FOR DEPOSITING {110} ORIENTED TUNGSTEN OF HIGH VACUUM WORK FUNCTION BY HYDROGEN REDUCTION OF TUNGSTEN CHLORIDE

(U) Previously under the 1966 NASA Thermionic Program at General Atomic,[1] it was shown that flat plate specimens having {110} oriented tungsten surfaces with vacuum work function as high as 5 eV could be obtained by hydrogen reduction of tungsten chloride. Long-term (1000 hours) test using thermally stabilized disc-shaped samples demonstrated the stability of such high work function surfaces at 1800°C. An unfueled converter containing a 12.5 mil {110} oriented chloride tungsten emitter of vacuum work function equal to 4.78 eV deposited on a 30 mil {100} oriented fluoride tungsten substrate has exhibited stable and superior performance over that containing a {100} oriented fluoride tungsten emitter (see Part V of this report).

(U) While the advantage of using {110} oriented tungsten emitters in cesiated converters has been proven, the conditions under which {110} oriented tungsten deposits can be reproducibly obtained remained obscure. The purpose of this task is thus two fold, to determine the conditions under which flat plate specimens of {110} oriented tungsten having high vacuum work function (> 4.8 eV) can be deposited, and to establish the reproducibility and stability of the degree of {110} orientation and the vacuum work function of the deposits obtained under these deposition conditions. The work carried out and the results obtained are described below.

3.1.1. WCl_6 Powder As Source of Tungsten Chloride

3.1.1.1. Experimental arrangement

(U) The experimental arrangement, shown schematically in Fig. 3.1, consisted of the following major components.

(1) Molybdenum mandrel (3/4 inch in diameter and 1/4 inch in thickness) supported on a McDanel tube and heated by high frequency induction. The temperature of the mandrel was determined by

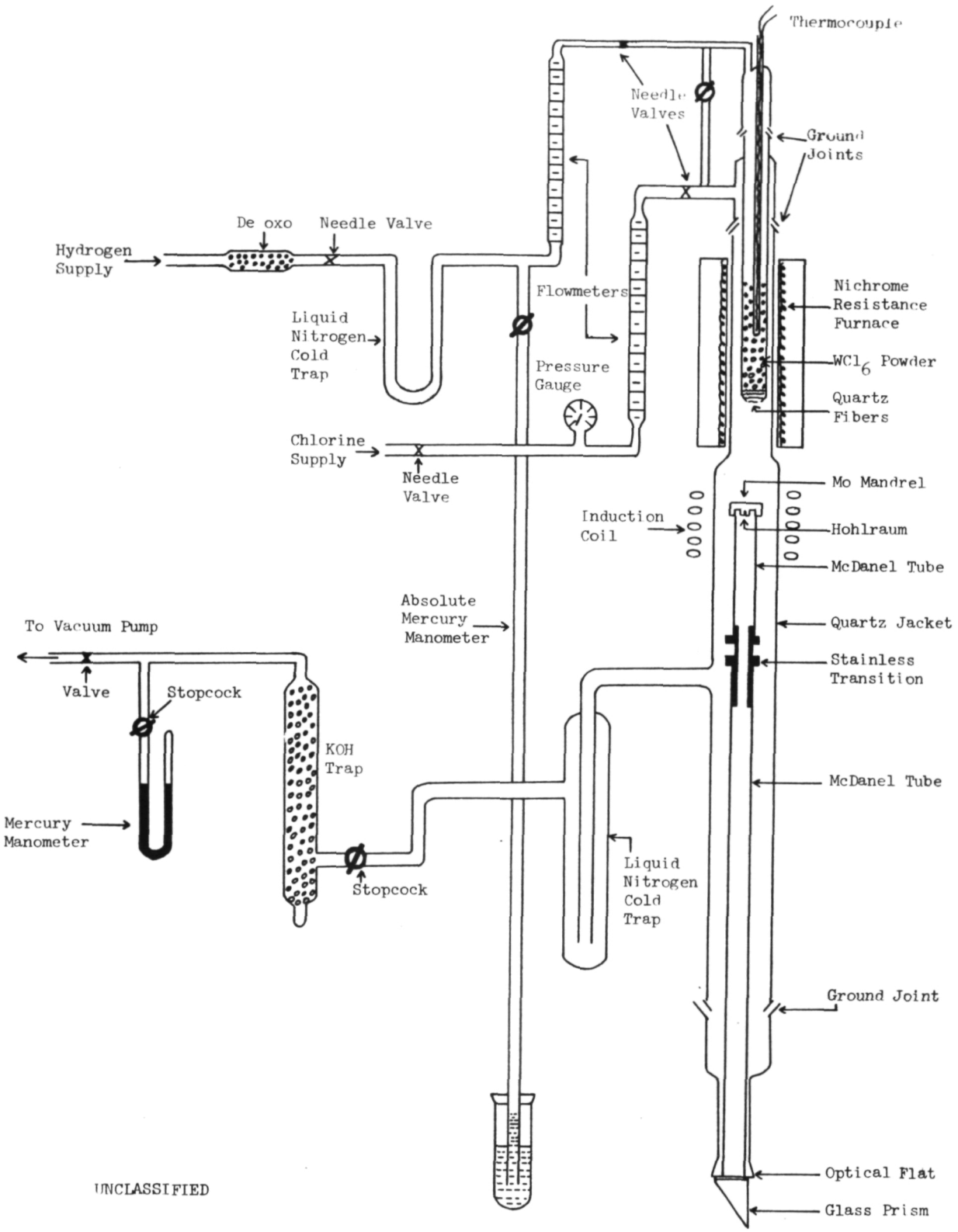

Fig. 3.1--(U) Chloride tungsten deposition apparatus using WCl_6 powder to provide tungsten source material

sighting an optical pyrometer into a hohlraum of 0.030 inch in diameter and 0.21 inch in depth, drilled into the center of the back side of the mandrel.

(2) Quartz WCl_6 reservoir containing about 40 grams of WCl_6. The WCl_6 powder used was obtained from Shwayder Chemical Metallurgy Corporation of Detroit, Michigan, and sublimated into a pyrex glass container for storage. Chemical analysis yielded a W/Cl value of 5.98. About 40 gms of the sublimated powder was loaded into the quartz reservoir in a glove box for each run. No redistillation was carried out in the deposition appratus.

(3) Quartz jacket containing the molybdenum mandrel and the gaseous reactants.

(4) Hydrogen supply the rate of flow of which was determined with a flowmeter at a pressure (usually one atmosphere) indicated by a mercury manometer and regulated with a stainless steel needle valve.

(5) Chlorine supply the rate of flow of which was determined with a flowmeter at a pressure (usually one atmosphere) indicated by a Monel pressure gage and regulated with a Monel needle valve. Chlorine was added to the gaseous reactants to prevent the formation of metal films on the inner wall of the quartz.

(6) Exhaust system consisting of a mechanical pump, a KOH trap, a liquid nitrogen trap and a stainless steel valve for controlling the gas pressure in the deposition chamber. The latter was measured with an absolute mercury manometer and maintained at less than 10 torr.

3.1.1.2. Experimental procedures

(U) The experimental procedures consist of the following steps.

(1) Outgas the molybdenum mandrel at 1600°C for 15 hours before installation into the deposition chamber.

(2) Load the WCl_6 reservoir with about 40 grams of WCl_6 powder and insert the reservoir into the deposition chamber. The WCl_6 column was about 5 inches in height.

(3) Evacuate the deposition chamber and start hydrogen flow at the desired rate and pressure.

(4) Heat the molybdenum mandrel to the desired temperature and maintain the temperature for a period of one hour for the cleaning of any surface oxide layer.

(5) Heat the WCl_6 reservoir to the desired temperature in about 5 minutes.

(6) Start chlorine flow at the desired rate and pressure.

(7) Bring the gas pressure in the deposition chamber to the desired value (< 10 torr) by adjusting the valve in the exhaust line.

(8) Continue the deposition for a pre-determined period of time.

(9) Separate the mandrel containing the tungsten deposit from the McDanel support after the completion of the deposition and determine the thickness of the deposit on the top surface of the mandrel with a micrometer. The preferred orientation of the deposit was determined by X-ray pole figure analysis after the deposit surface was polished with fine emery paper and electro-polished in 10% NaOH solution.

(10) Transfer the WCl_6 left in the reservoir into a closed glass container for weighing. The weight of WCl_6 used during the deposition was calculated from the amount of WCl_6 in the initial loading and that left in the reservoir after the completion of the experiment.

3.1.1.3. Experimental results

(U) The experimental results are summarized in Table 3.1. The data in the ten columns shown are either measured directly or deduced from the measured data according to the procedures described in the footnotes of Table 3.1. For the deposition conditions shown in this table, (100) preferred orientation was observed in deposits prepared at mandrel temperatures of 1150-1325°C, and (111) and (211) preferred orientations were observed in deposits prepared at 1400°C. The efficiency of deposition fell in general in the range of 40-60% but dropped to very low value (~ 4%) when the hydrogen flow rate was reduced to a low value (Run No. 7). At low WCl_6 reservoir temperature and thus low WCl_6 concentration in the gaseous reactants, the molybdenum mandrel was attacked by the chlorine added to the system. Attempts to vary the hydrogen to WCl_6 ratio in a systematic fashion ran into several difficulties. First, since hydrogen was used as a carrier gas for the WCl_6, the hydrogen concentration and the WCl_6 concentration in the gaseous reactants were not independent of each other. Secondly, the variation of WCl_6 concentration in the gaseous reactants with WCl_6 reservoir temperature is irregular and therefore difficult to control, (see Column III and Column VI), indicating a strong effect of the packing configuration of the WCl_6 powder in the reservoir on the WCl_6 flux in the deposition chamber. In addition, the hygroscopic and reactive nature of the WCl_6 powder makes the handling of this tungsten source material very inconvenient. As a result, the effort was shifted to experiments using the chlorination of tungsten chips to provide the tungsten source material.

3.1.2. Source Material Provided by "In Situ" Chlorination of Tungsten Chips

3.1.2.1. Experimental arrangement

(U) The experimental arrangement, as shown schematically in Fig. 3.2 is similar to that shown in Fig. 3.1 when WCl_6 powder was used as the source material except in two respects. First the reservoir was loaded with vapor-deposited fluoride tungsten chips instead of WCl_6 powder. Typical analysis of the fluoride tungsten chips used yielded: C, 10 ppm; O, 12 ppm; N, 1 ppm; and F, 25 ppm. Secondly, chlorine instead of hydrogen was directed through

UNCLASSIFIED

Table 3.1

(U) RESULTS OF VAPOR-DEPOSITION OF TUNGSTEN USING WCl_6 POWDER

(This table is Unclassified)

	I	II		III	IV	V	VI	VII	VIII	IX	X
Run No.	Mo Mandrel Temperature (°C)	H_2 Flow Rate (a) (c.c./min)	(b) (mole/min)	WCl_6 Reservoir Temperature (°C)	Time (min)	Rate of Removal of WCl_6 From Reservoir (mole/min.)	Mole of WCl_6 Removed From Reservoir per c.c. of Gas Flowing Through Reservoir (10^{-5} mole/c.c.)	Molar Ratio of H_2 to W in Vapor $\left(\frac{\text{mole } H_2}{\text{mole W}}\right)$	Thickness of Deposit on Surface of Mo Mandrel (mils)	Efficiency of Deposition (%)	Preferred Crystal Orientation in Deposit
1	1150	70	0.00284	200	120	0.00063	9.00	4.51	10	40	(100)
2	1325	140	0.00569	150	60	0.00126	9.00	4.51	13	52	(211)
3	1175	140	0.00569	170	45	0.00157	9.00	3.62	10	43	(100)
4	1150	140	0.00569	170	60	0.00134	7.67	4.25	14	53	(100)
5	1250	140	0.00569	170	35	0.00216	15.45	2.63	11	44	(100)
6	1275	140	0.00569	170	30	0.00252	18.00	2.25	10	40	(100)
7	1260	50	0.00203	250	15	0.00504	108	0.40	1	4	-
8	1225	140	0.00569	110	45	0.00112	0.80	50.70	Mandrel Attacked by Chlorine	-	-
9	1400	140	0.00569	175	20	0.00290	20.70	1.96	12	60	(111)
10	1400	70	0.00284	150	60	0.00102	14.70	2.76	8	40	(211)

NOTE: 1. Column II(a) refers to flow rate of hydrogen at 1 atm. and 300°K. Column II(b) was calculated from Column II(a) by using perfect gas law.

2. A chlorine flow rate of 50 c.c./min was maintained during all the runs to prevent metal film formation on the quartz container. For Run No. 3 and Run No. 4, both the hydrogen and the chlorine passed through the WCl_6 reservoir. For other runs, only hydrogen passed through the WCl_6 reservoir.

3. Column V was obtained by dividing the weight loss of the WCl_6 (in mole) in the WCl_6 reservoir by the time of the run.

4. Column VI was obtained by dividing Column V by the flow rate of hydrogen (Column II(a)) for all runs except Run No. 3 and Run No. 4, and by the flow rate of hydrogen plus the flow rate of chlorine for Run No. 3 and Run No. 4.

5. Column VII was obtained by dividing Column II(b) by Column V.

6. Column IX was obtained according to the following formula:

$$\text{Efficiency of deposition} = \frac{\text{Weight of tungsten deposited on Mo mandrel surface}}{\text{Total weight of tungsten intersected by the Mo mandrel surface during the run}} \times 100$$

$$= \frac{\frac{\pi}{4}(1.9)^2 \times \text{Column VIII} \times 0.00254 \times 19.3}{\text{Column V} \times \text{Column IV} \times 183.92 \times \frac{\frac{\pi}{4}(1.9)^2}{\frac{\pi}{4}(3.8)^2}} \times 100$$

where 1.9 cm = diameter of Mo mandrel

3.8 cm = inner diameter of quartz jacket

0.00254 cm/mil = conversion factor from mil to cm

19.3 gm/c.c. = density of tungsten

183.92 gm/atom = atomic weight of tungsten

UNCLASSIFIED

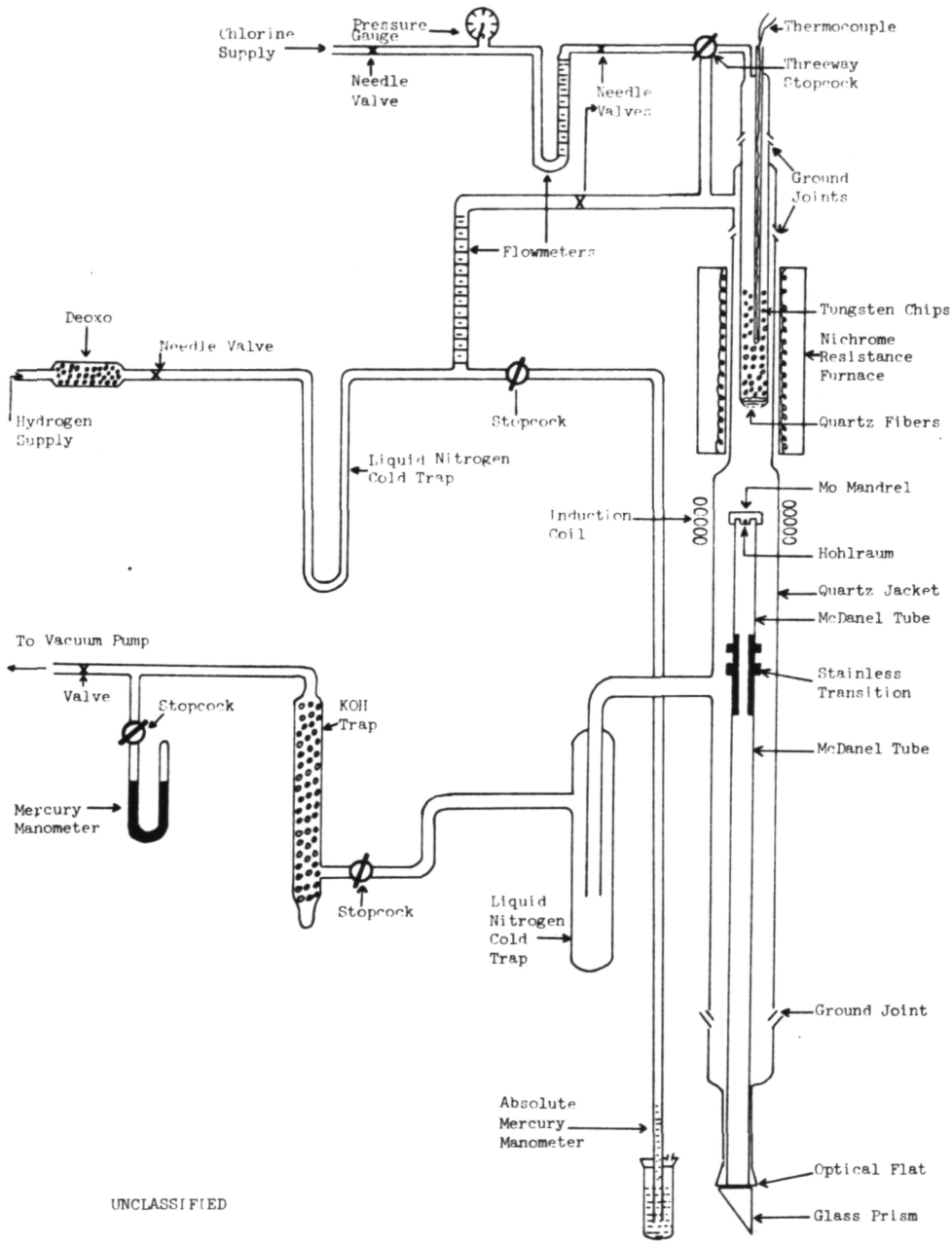

Fig. 3.2--(U) Chloride tungsten deposition apparatus using chlorination of tungsten chips to provide tungsten source material

the reservoir while hydrogen instead of chlorine entered into the deposition chamber through the annular space between the reservoir and the quartz jacket. To remove any surface contamination from the tungsten chips used, however, hydrogen was directed by using a three way stopcock through the reservoir at the beginning of each experiment for 1 hour with the chips maintained at 900°C. Afterwards, the hydrogen flow was switched through the annular space between the reservoir and the quartz jacket and chlorine was let into the reservoir for the initiation of the deposition experiment.

3.1.2.2. Experimental proced ures

(U) The experimental procedures consist of the following steps:

(1) Outgas the molybdenum mandrel at 1600°C for 15 hours before installing into the deposition chamber.

(2) Load the reservoir with about 300 grams of fluoride tungsten chips and insert the reservoir into the deposition chamber. The tungsten column containing tungsten chips of about 1 millimeter thickness and a few millimeters in other dimensions was about 7-1/2 inches in height.

(3) Evacuate the deposition chamber and start the hydrogen flow through the tungsten reservoir at the desired rate and pressure.

(4) Heat the tungsten reservoir to a temperature of 900 ± 25°C and continue the hydrogen flow for a period of one hour to clean off any oxide layer which might be present on the surface of the tungsten chips used.

(5) Heat the molybdenum mandrel to the desired temperature and maintain the temperature for a period of one hour to clean off any surface oxide layer.

(6) Divert the hydrogen flow from the tungsten reservoir to the annular space between the reservoir and the quartz jacket.

(7) Let in chlorine through the tungsten reservoir at the desired rate and pressure.

(8) Bring the gas pressure in the deposition chamber to the desired value (4-6 torr) by adjusting the valve in the exhaust line.

(9) Continue the deposition for a pre-determined period of time.

(10) Separate the mandrel containing the tungsten deposit from the McDanel support after the completion of the deposition, and determine the thickness of the deposit on the top surface of the mandrel with a micrometer. The preferred orientation of the deposit was determined by X-ray pole figure analysis after the deposit surface was polished with fine emery paper and electropolished in 10% NaOH solution.

(11) Determine the weight of tungsten chips used during the experiment from the weight of the initial loading and the weight of the tungsten chips left in the reservoir at the completion of the experiment.

(12) Core out a disc of 0.575 inch diameter from the deposit by electrical discharge machining. Remnants from the coring operation were used for determining the impurity contents and the microstructure of the deposit. The disc was ground to 40 mil thickness, polished with 1 micron diamond paste and then electropolished in 10% NaOH solution. After outgassing at 1850°C for a period of 200 hours, the vacuum work function of the disc was measured at 1800°C for a period of 200 hours.

3.1.2.3. Experimental results

(U) The experimental results are summarized in Table 3.2. The data in the columns shown are either measured directly or deduced from the measured data according to the procedures described in the footnotes of Table 3.2.

Table 3.2

(U) RESULTS OF VAPOR-DEPOSITION OF TUNGSTEN USING CHLORINATION OF TUNGSTEN CHIPS

(This table is Unclassified)

	I	II		III		IV	V	VI	VII	VIII	IX	X	XI	XII	XIII
Run No.	Mo Mandrel Temperature (°C)	H_2 Flow Rate (a) (c.c./min)	(b) (mole/min)	Cl_2 Flow Rate (a) (c.c./min)	(b) (mole/min)	Time (Min)	W Chip Temperature (°C)	Tungsten Reacted With Cl_2 (gm)	Rate of Tungsten Reaction With Cl_2 (mole/min)	Atom Ratio of Cl to W in Vapor	Mole Ratio of H_2 to W in Vapor	Thickness of Deposit on Top of Mandrel (mil)	Efficiency of Deposition (%)	Preferred Crystal Orientation in Deposit	Vacuum Work Function (eV)
1	1350	70	.00285	350	.01423	180	850	77	.00233	12.24	1.22	33	24	(100)	4.55
2	1150	70	.00285	200	.00814	180	825	58	.00175	9.30	1.63	24	23	(110)	4.85
3	1250	70	.00285	200	.00814	180	850	68	.00205	7.92	1.39	39	32	(110)	4.80
4	1150	70	.00285	115	.00468	255	850	96	.00205	4.56	1.39	31	18	(110)	4.87
5	1150	140	.00570	115	0.00468	240	830	88	.00199	4.70	2.86	68	43	(110)	4.88
6	1200	140	.00570	115	.00468	240	840	96	.00217	4.32	2.61	115	67	Random	4.57
7	1150	140	.00570	115	.00468	240	850	115	.00261	3.60	2.19	87	42	(110)	4.92
8	1200	100	.00407	60	.00244	180	820	48	.00145	3.36	2.80	53	61	Random	4.53
9	1200	100	.00407	60	.00244	240	825	67	.00151	3.23	2.61	80	66	(100)	4.52
10	1100	140	.00570	115	.00468	240	850	114	.00258	3.64	2.19	86	42	(110)	5.01
11	1050	140	.00570	115	.00468	240	875	125	.00283	3.32	2.01	46	20	(110)	4.85
12	1100	200	.00812	115	.00468	180	875	88	.00266	3.53	3.05	58	37	(110)	4.83
13	1100	160	.00652	115	.00468	180	875	94	.00284	3.32	2.29	60	36	(110)	4.89
14	1100	160	.00652	115	.00468	180	875	95	.00289	3.26	2.25	60	35	(110)	4.97
15	1100	140	.00570	115	.00468	180	850	79	.00240	3.93	2.37	46	33	(110)	5.00
16	1100	140	.00570	135	.00550	210	830	78	.00204	5.45	2.79	41	29	(110)	4.92
17	1100	280	.01140	115	.00468	72	850	34	.00250	3.71	4.55	31	52	Random	4.52
18	1100	140	.00570	115	.00468	200	750	15	.00041	22.7	13.89	1	0.4	-	-

Note:
1. Column II(a) refers to flow rate of hydrogen at 1 atm. and 300°K. Column II(b) was calculated from Column II(a) by using perfect gas law.
2. Column III(a) refers to flow rate of chlorine at 1 atm. and 300°K. Column III(b) was calculated from Column III(a) by using perfect gas law.
3. Column VII was calculated from the formula $\frac{\text{Column VI}}{\text{Column IV} \times 183.92}$
4. Column VIII was calculated from the formula $\frac{\text{Column III(b)} \times 2}{\text{Column VII}}$
5. Column IX was calculated from the formula $\frac{\text{Column II(b)}}{\text{Column VII}}$
6. Column XI was calculated from the formula:

$$\text{Efficiency of deposition} = \frac{\text{Weight of tungsten deposited on Mo mandrel surface}}{\text{Total weight of tungsten intersected by the Mo mandrel surface during the run}} \times 100$$

$$= \frac{\frac{\pi}{4}(1.9)^2 \times \text{Column X} \times 0.00254 \times 19.3}{\text{Column VI} \times \frac{\frac{\pi}{4}(1.9)^2}{\frac{\pi}{4}(3.8)^2}}$$

where 1.9 cm = diameter of Mo mandrel
3.8 cm = inner diameter of quartz jacket
0.00254 cm/mil = conversion factor from mil to cm
19.3 gm/c.c. = density of tungsten
183.92 gm/atom = atomic weight of tungsten

Figures 3.3 and 3.4 show respectively the macroscopic appearance and the microstructures of the cross section of a {110} oriented chloride tungsten deposit. Analysis of these deposits yielded the following ranges of major impurity contents: O, 0.5-1 ppm; N, < 1 ppm; C, 2-8 ppm; F, 9-17 ppm; Cl, 5-10 ppm; Al, 4-20 ppm; Fe, 10-20 ppm; Cu, 1-2 ppm; Mg, 0.4-0.6 ppm; Si, 3-20 ppm. In Fig. 3.5, the preferred orientation and the vacuum work function of each deposit obtained are shown together with corresponding values of deposition temperature and the mole ratio of hydrogen to tungsten in the vapor phase. From Fig. 3.5 and the data shown in Table 3.2, the following conclusions can be drawn for the deposition conditions studied.

1. Lower deposition temperature and lower H_2/W mole ratio in the vapor phase favor the development of {110} preferred orientation in the deposit.

2. Higher deposition temperature and higher H_2/W mole ratio in the vapor phase increase the deposition efficiency and favor the development of random or {100} oriented deposits.

3. The Cl/W atom ratio in the vapor emerging from the tungsten chip reservoir is usually less than 6, indicating that the reaction product contains significant amounts of tungsten sub-halides. At high chlorine flow rate, the Cl/W atom ratio becomes higher than 6, implying that a part of the chlorine gas passes through the tungsten column without reacting with the tungsten. The Cl/W atom ratio, however, does not seem to be a critical factor in determining the nature of the preferred crystal orientation in the deposit.

4. The temperature of the tungsten chips is the principal controlling factor for the tungsten flux and thus the Cl/W ratio and the H_2/W ratio in the gaseous reactant mixture. When the temperature of the tungsten chips is too low (e.g. 750°C), the efficiency of deposition is almost reduced to zero because of the low tungsten flux in the vapor surrounding the molybdenum mandrel.

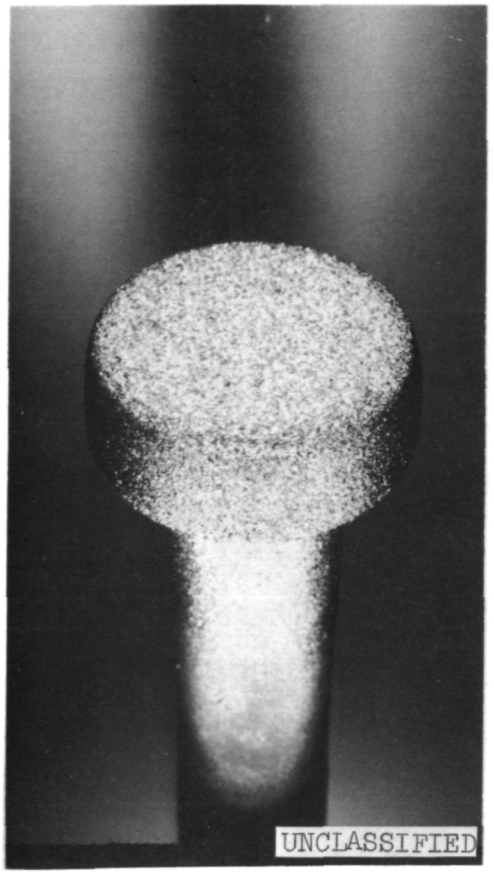

Fig. 3.3--(U) Macroscopic appearance of {110} oriented chloride tungsten deposit on molybdenum mandrel

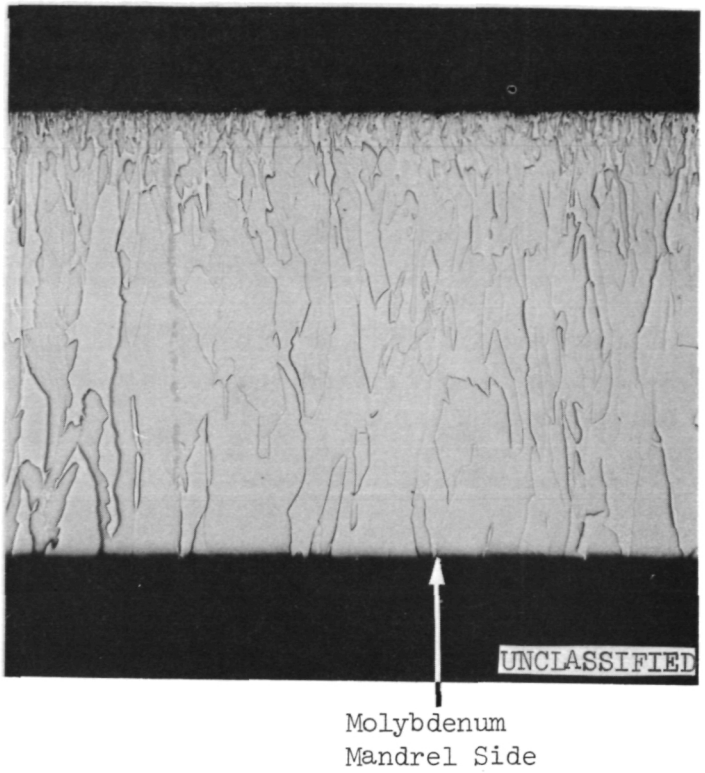

Fig. 3.4--(U) Microstructure of a cross section {110} oriented chloride tungsten deposit

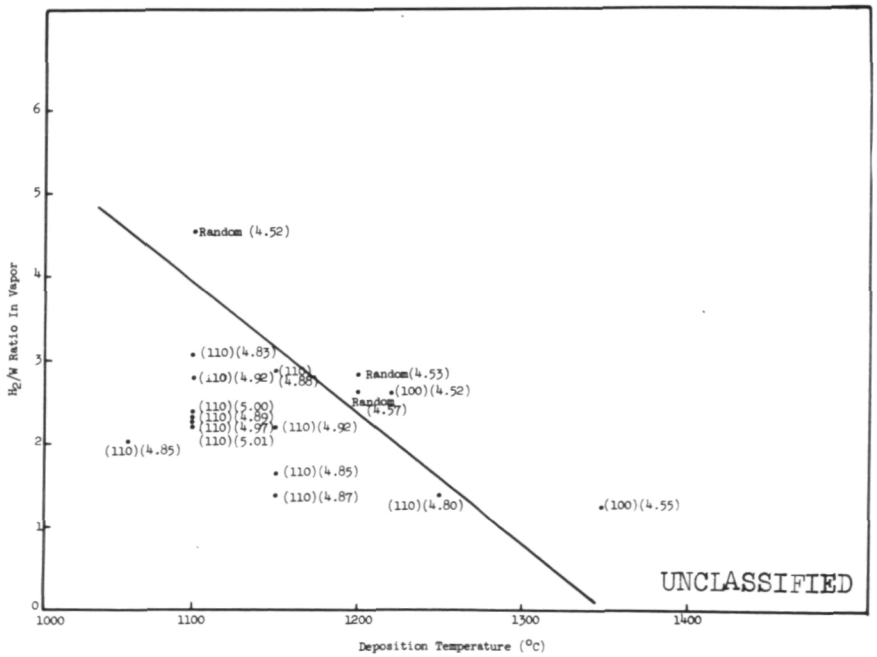

Fig. 3.5--(U) Preferred orientation and vacuum work function in chloride tungsten as a function of deposition conditions
The numbers in parentheses represent the lattice planes of preferred orientation and the vacuum work functions

5. Chloride tungsten deposits of vacuum work functions between 4.9 and 5.0 eV can be obtained at the following deposition conditions: mandrel temperature 1100-1150°C, hydrogen flow rate 140-160 c.c./min., chlorine flow rate 115-135 c.c./min., and tungsten chip temperature 830-875°C.

3.2. EVALUATION OF REPRODUCIBILITY AND STABILITY OF DEGREE OF {110} PREFERRED ORIENTATION AND VACUUM WORK FUNCTION OF TUNGSTEN DEPOSITED UNDER CONDITIONS ESTABLISHED IN SECTION 3.1

3.2.1. Reproducibility Test

(U) To test the reproducibility of the results obtained under the deposition conditions established in Section 3.1, twenty tungsten deposits were prepared at a mandrel temperature of 1100°C, a hydrogen flow rate of 140 c.c./min., a chlorine flow rate of 115 c.c./min., and a tungsten chip temperature of 850°C. Ten of these deposits designated as chloride tungsten 1L through 10L, were deposited on molybdenum mandrels which were subsequently removed by dissolution in HNO_3 + HCl. The other ten of these deposits, designated as duplex tungsten 1DL through 10DL, were deposited on fluoride tungsten substrates.* The procedures for the deposition on fluoride tungsten substrate were similar to those for deposition on molybdenum mandrel. The fluoride tungsten surface was ground to 4 microinch finish, cleaned and annealed in hydrogen at 1000°C for 1 hour before the deposition was initiated.

(U) From each of these deposits, a sample of 0.575 inch diameter was cored out, polished and electropolished to a thickness of 40 mils. For samples 1L through 10L, all the 40 mil thickness consists of chloride tungsten deposit; while for samples 1DL through 10DL, the 40 mil thickness consists of 10 mils (± 2 mils) of chloride tungsten deposit over 30 mils of fluoride tungsten substrate. Chemical analysis and microstructure examination were made on remnants of the coring operation, and X-ray study of the degree of preferred orientation and vacuum work function measurements were carried out

*The fluoride tungsten substrates were obtained from a large disc procurred from San Fernando Laboratories. After outgassing for 200 hours at 1800°C, the disc contained 10 ppm C, 8 ppm O, 1 ppm N, 12 ppm F and 3 ppm Cl.

on each sample after outgassing for 200 hours at 1850°C, in 10^{-6} torr vacuum. The results are described as follows.

3.2.1.1. Chloride tungsten samples 1L through 10L

(U) Chemical analysis. The ranges of the major impurity contents detected in the ten chloride tungsten samples 1L through 10L are: O, 0.5-2 ppm; N, < 1 ppm; C, 5-10 ppm; F, 5-12 ppm; Cl, 3-10 ppm; Al, 1-5 ppm; Fe, < 4-10 ppm; Cu, < 0.3-1 ppm; Mg 0.1-0.5 ppm; Si, 2-5 ppm. These results do not differ significantly with those obtained on the exploratory samples of {110} preferred orientation under Section 3.1.

(U) Microstructures of cross section. The essential features of the microstructures of the cross sections of sample 1L through 10L consist of a thin layer of small crystallities on the side near the mandrel surface, which grow bigger and wider with the increase of the thickness of the deposit. Typical examples are shown in Fig. 3.6(a) through (f).

(U) Degree of {110} preferred orientation. The spatial distributions of the {110} axes in sample 1L through 10L are shown in Fig. 3.7(a) through (j). For the ten samples studied, 90% of the <110> axes were located between 6° - 11° from the normals to their surfaces.

(U) Vacuum work function. The stabilized vacuum work functions of sample 1L through 10L are also indicated in Fig. 3.7(a) through (j). For samples with 90% of the <110> axes located within 7° from the surface normal, the vacuum work functions are about 5 eV, while for samples with 90% of the <110> axes located within 11° from the surface normal, the vacuum work functions are about 4.9 eV.

3.2.1.2. Duplex tungsten samples 1DL through 10DL

(U) Chemical analysis. The ranges of the major impurity contents detected in the chloride tungsten deposits of the ten duplex tungsten samples 1DL through 10DL are: O, 1-7 ppm; N, < 1 ppm; C, 3-10 ppm; F, < 3-4 ppm; Cl, 3-17 ppm; Al, < 0.3-0.9 ppm; Fe, < 4-5.5 ppm; Cu, < 0.3-4 ppm; Mg, 0.1-0.3 ppm; Si, < 1.0 - 3 ppm. These results do not differ significantly with those observed for the chloride tungsten sample 1L through 10L.

UNCLASSIFIED

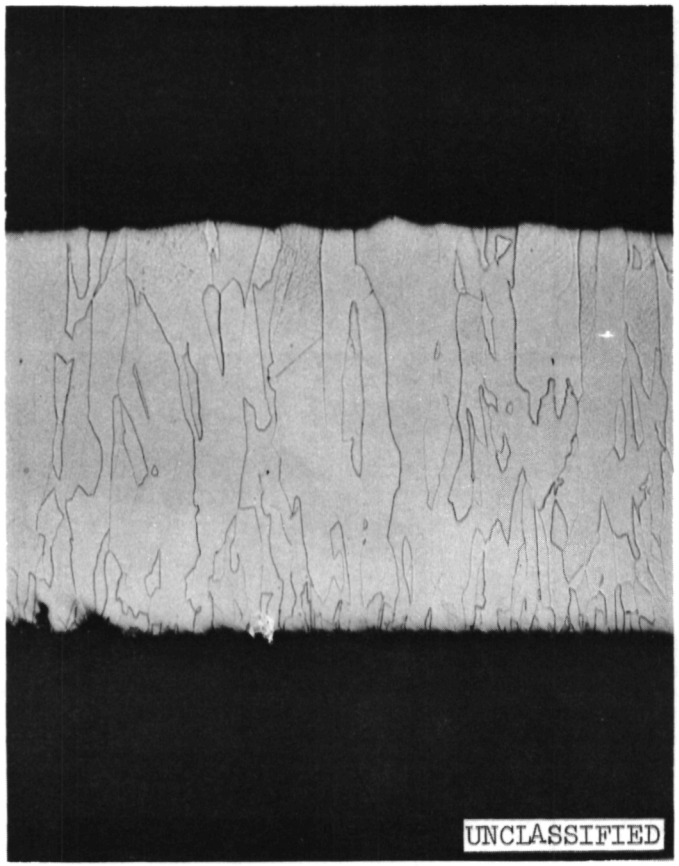

M 25990-1 35X

(a) Sample 2L

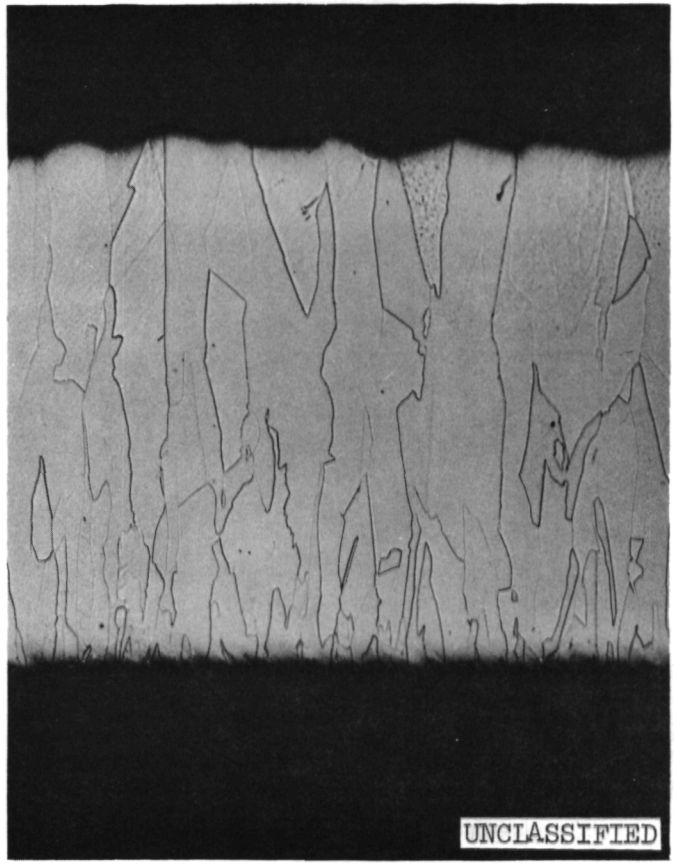

M 25991-1 35X

(b) Sample 3L

Fig. 3.6--(U) Typical microstructures of a cross section of as-deposited chloride tungsten deposit (Page 1 of 3)

UNCLASSIFIED

UNCLASSIFIED

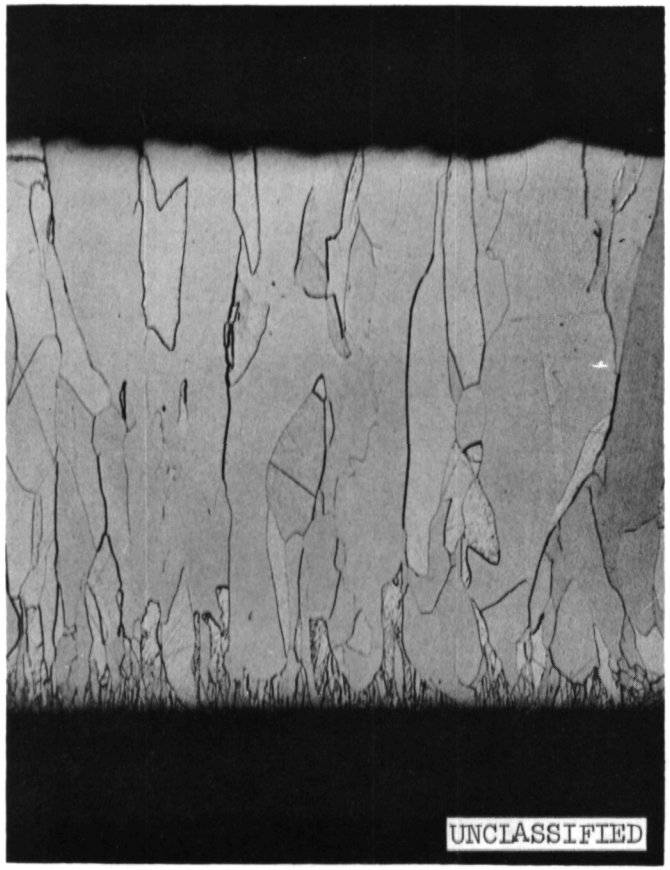

M 25992-2 50X

(c) Sample 4L

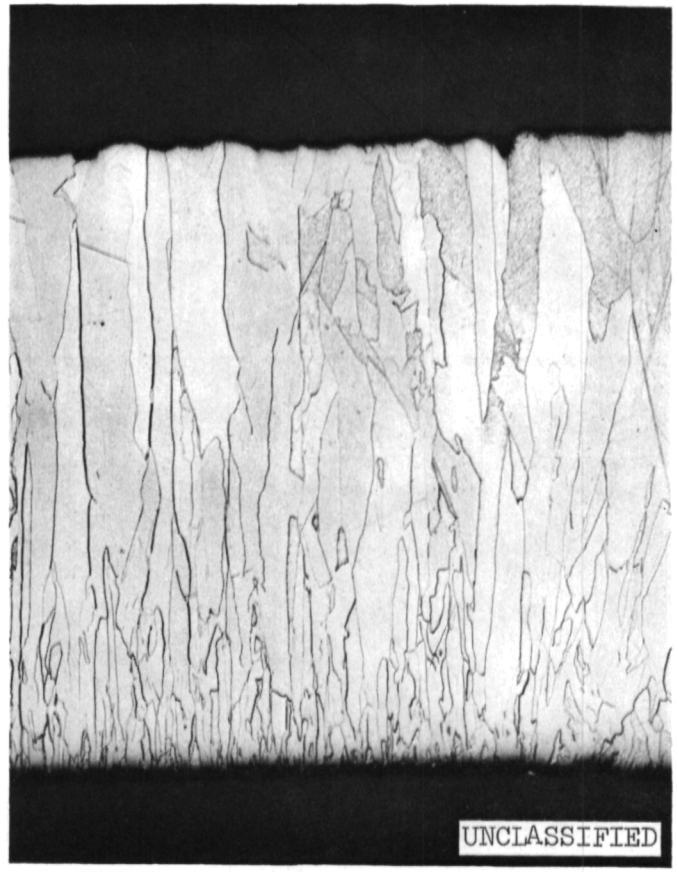

M 25993-1 50X

(d) Sample 5L

Fig. 3.6--(U) Typical microstructures of a cross section of as-deposited chloride tungsten deposit (Page 2 of 3)

UNCLASSIFIED

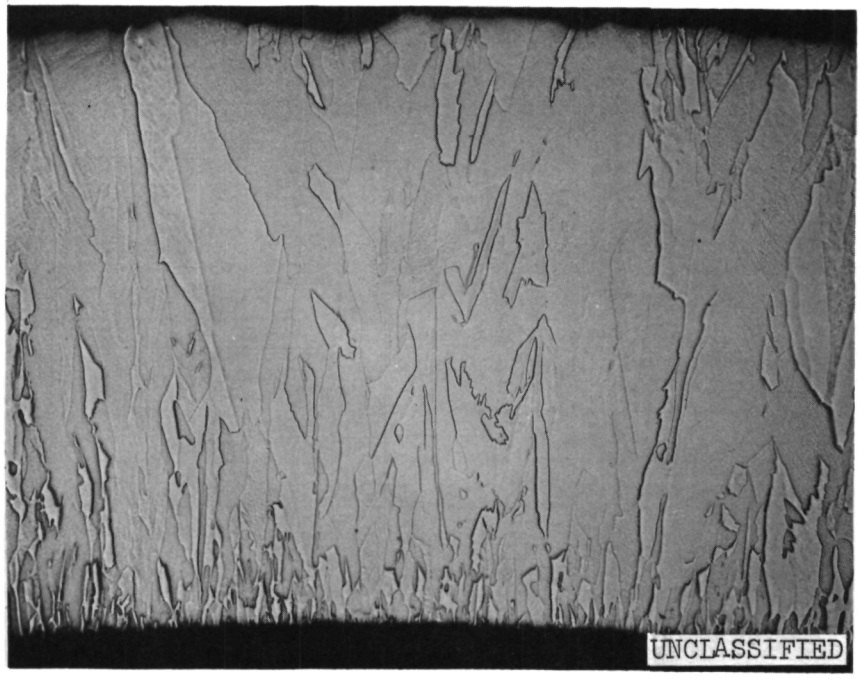

M 23847-1 50X

(e) Sample 7L

(taken from deposition on cylindrical surface of mandrel)

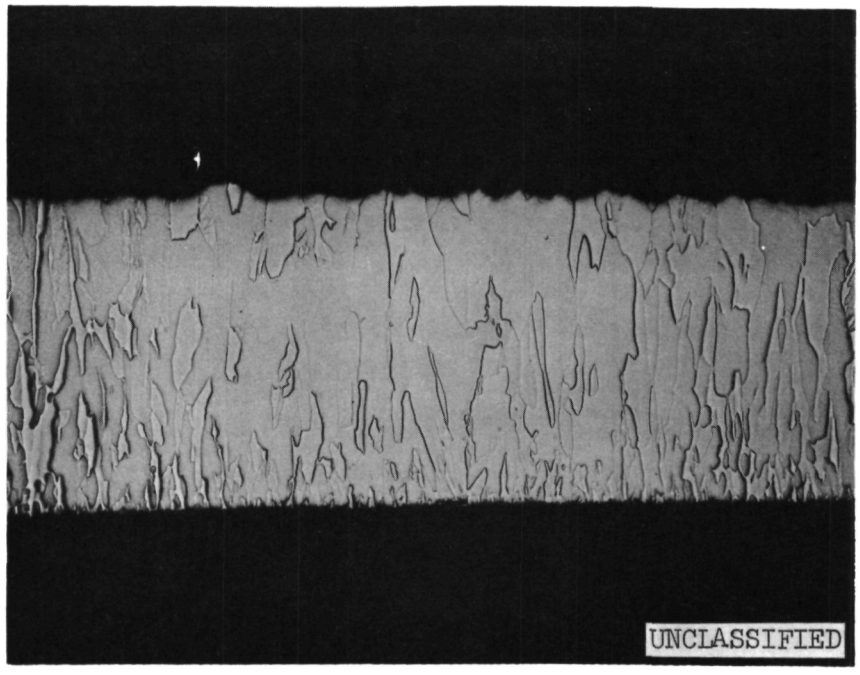

M 23849-1 35X

(f) Sample 9L

Fig. 3.6--(U) Typical microstructures of a cross section of as-deposited chloride tungsten deposit (Page 3 of 3)

UNCLASSIFIED

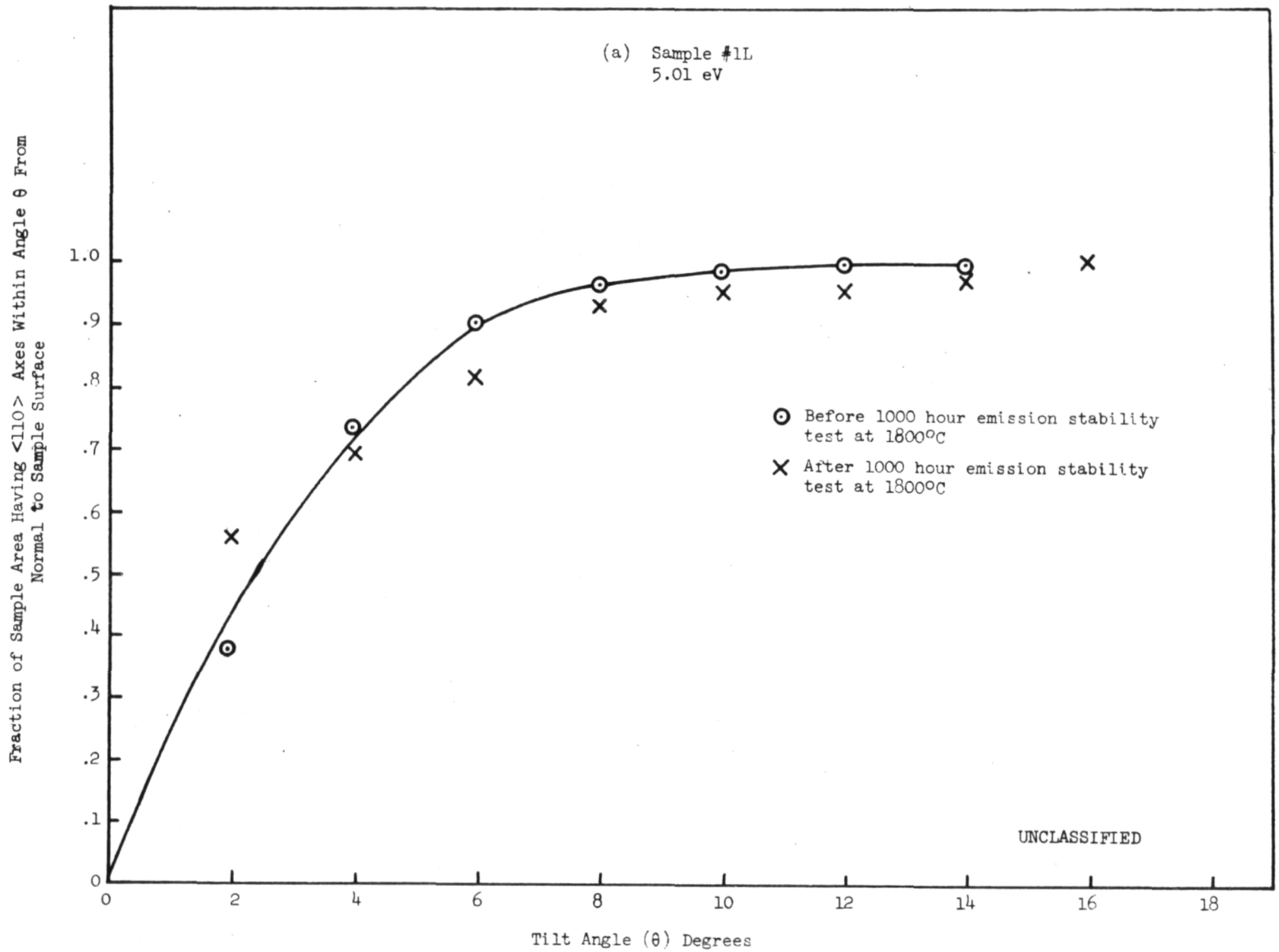

Fig. 3.7--(U) Spatial distribution of <110> axes in ten chloride tungsten samples (Page 1 of 10)

UNCLASSIFIED

UNCLASSIFIED

UNCLASSIFIED

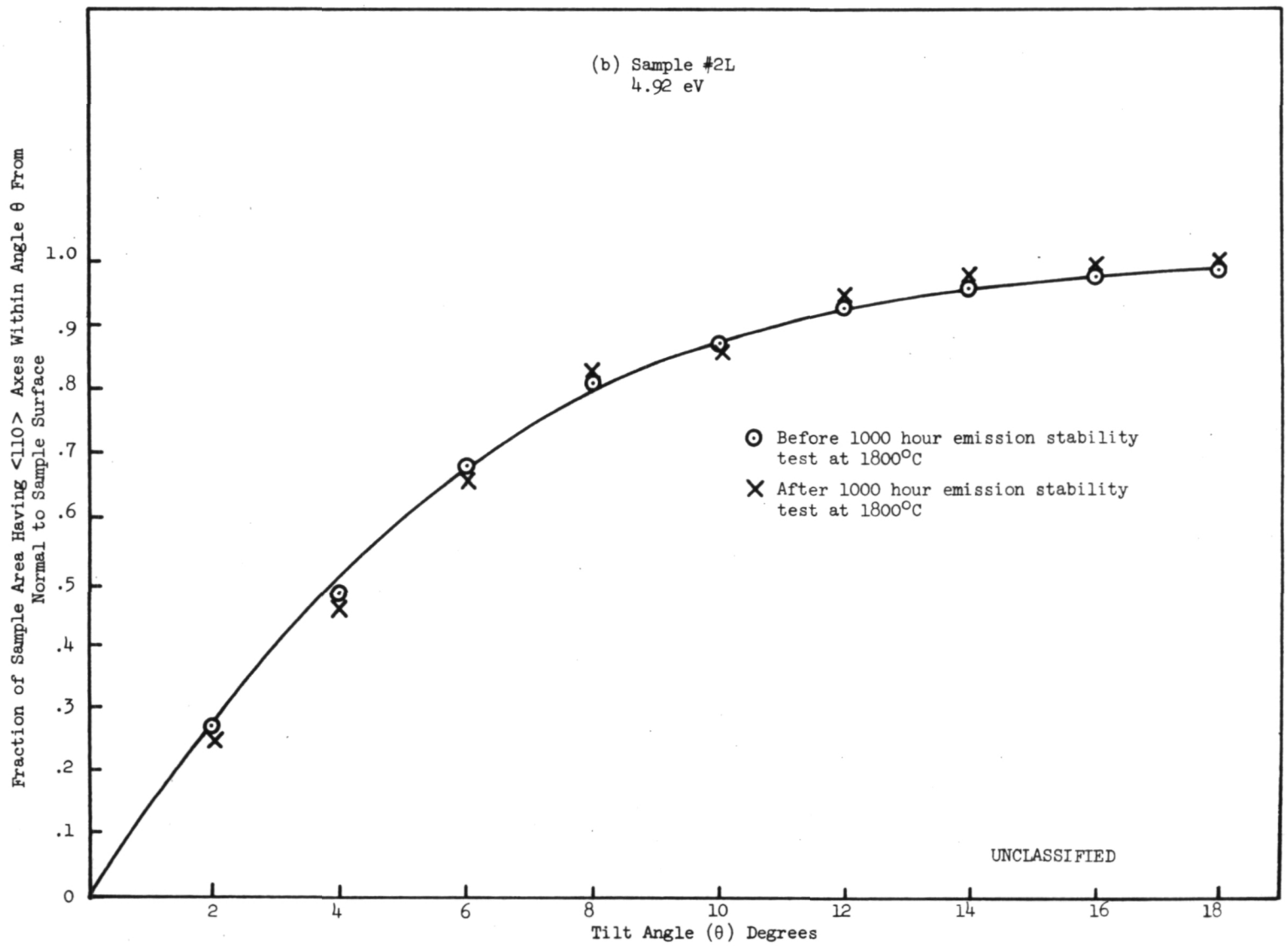

Fig. 3.7--(U) Spatial distribution of <110> axes in ten chloride tungsten samples (Page 2 of 10)

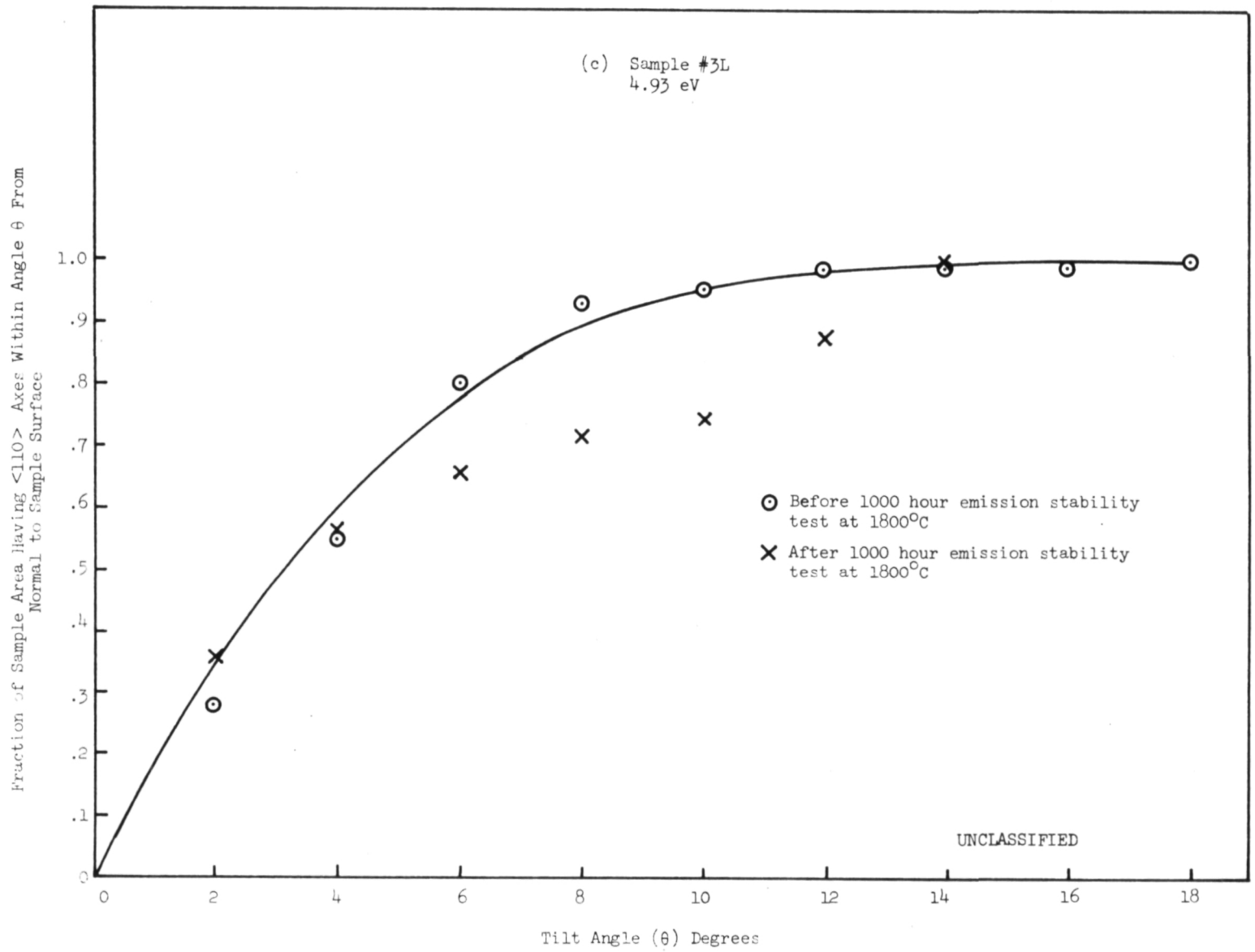

Fig. 3.7--(U) Spatial distribution of <110> axes in ten chloride tungsten samples (Page 3 of 10)

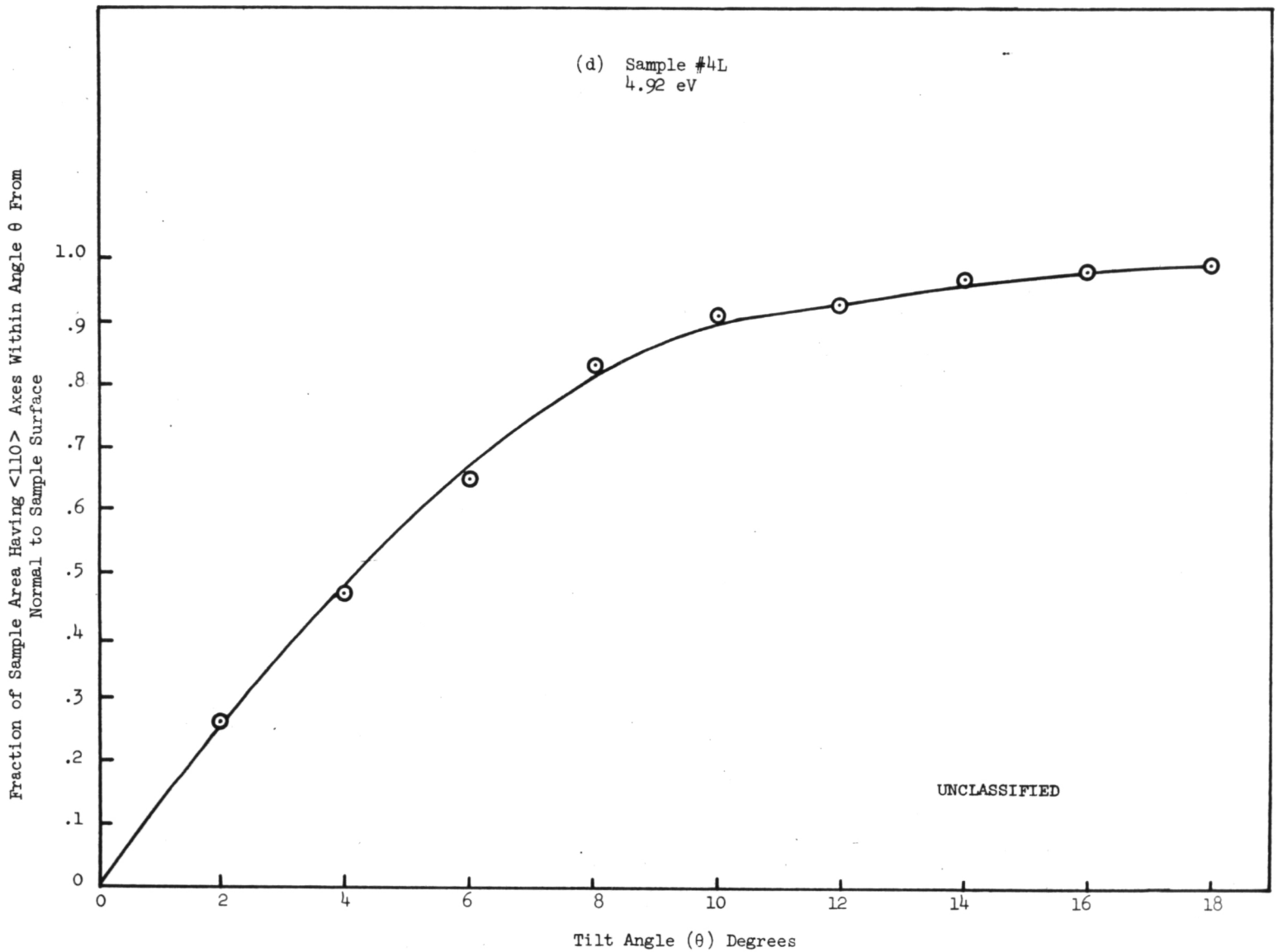

Fig. 3.7--(U) Spatial distribution of <110> axes in ten chloride tungsten samples (Page 4 of 10)

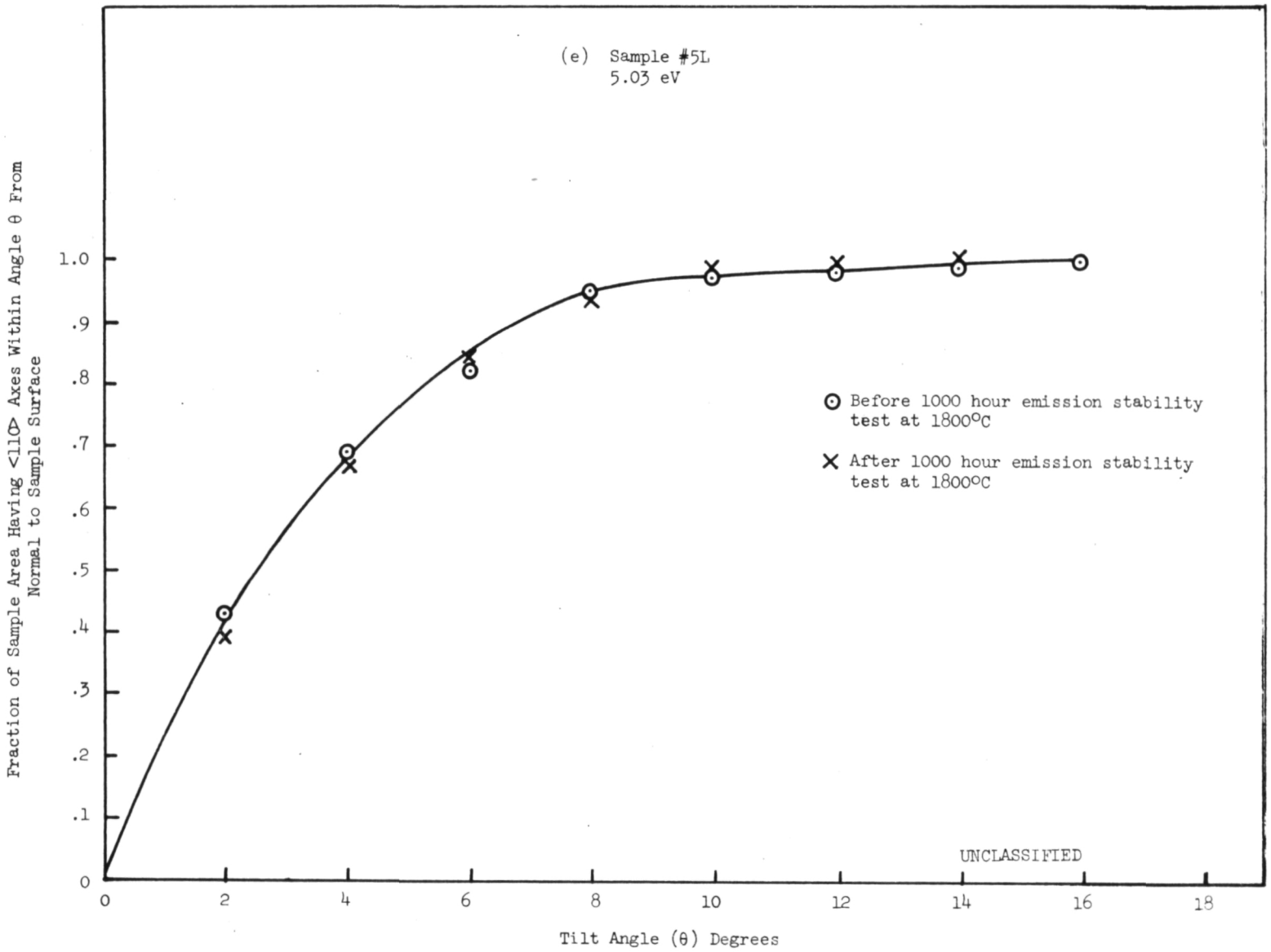

Fig. 3.7--(U) Spatial distribution of <110> axes in ten chloride tungsten samples (Page 5 of 10)

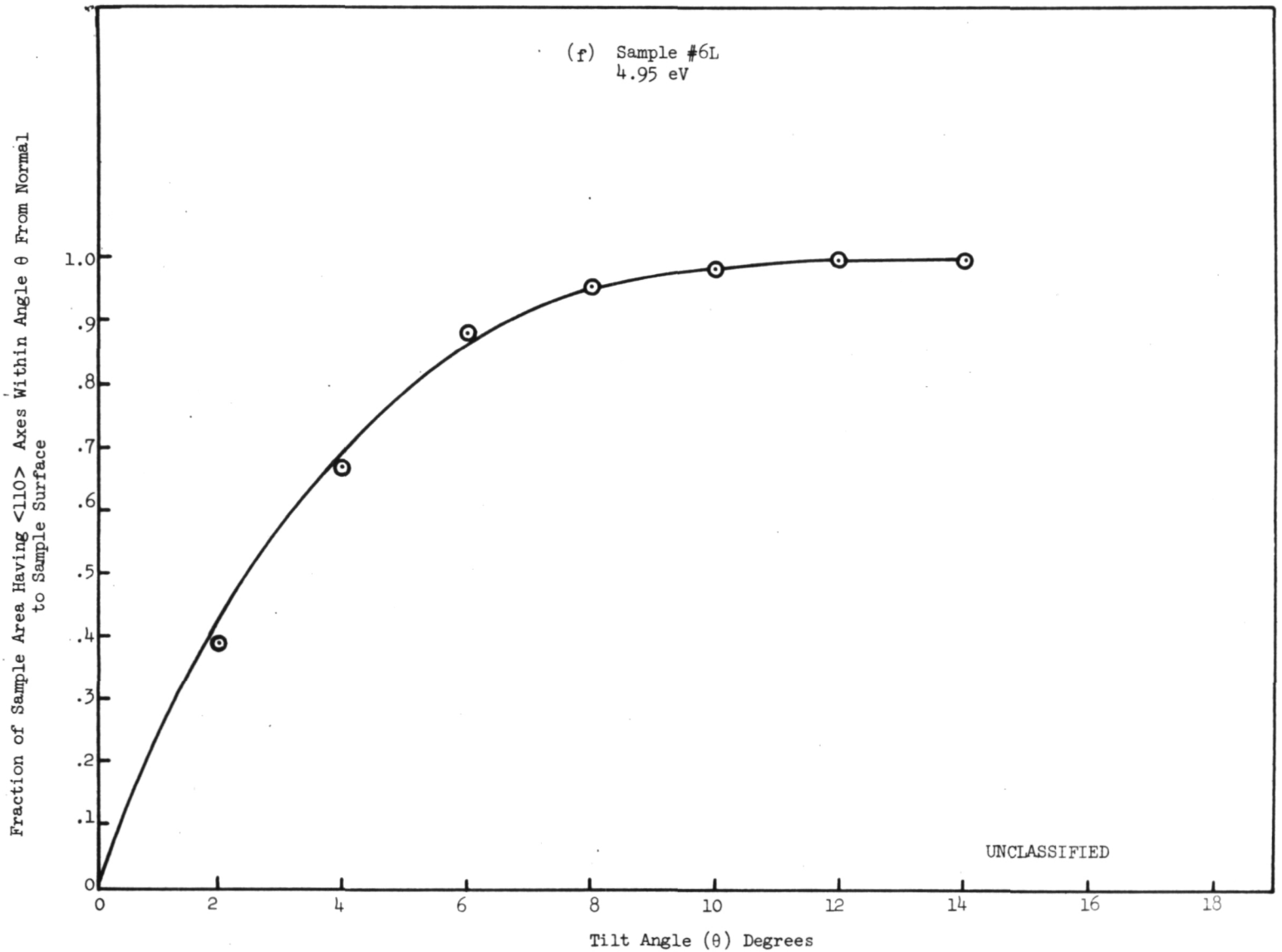

Fig. 3.7--(U) Spatial distribution of <110> axes in ten chloride tungsten samples (Page 6 of 10)

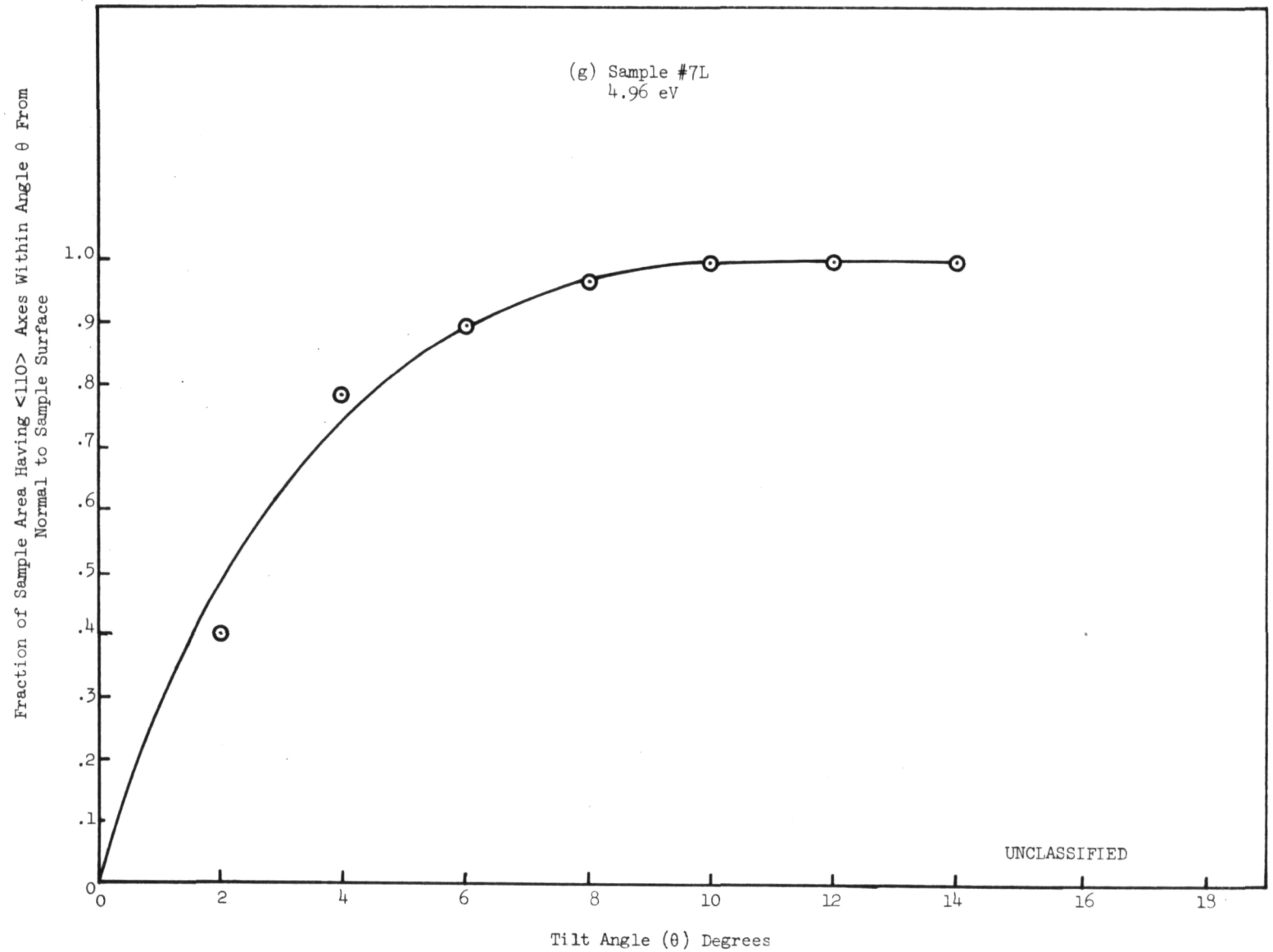

Fig. 3.7--(U) Spatial distribution of <110> axes in ten chloride tungsten samples (Page 7 of 10)

UNCLASSIFIED

UNCLASSIFIED

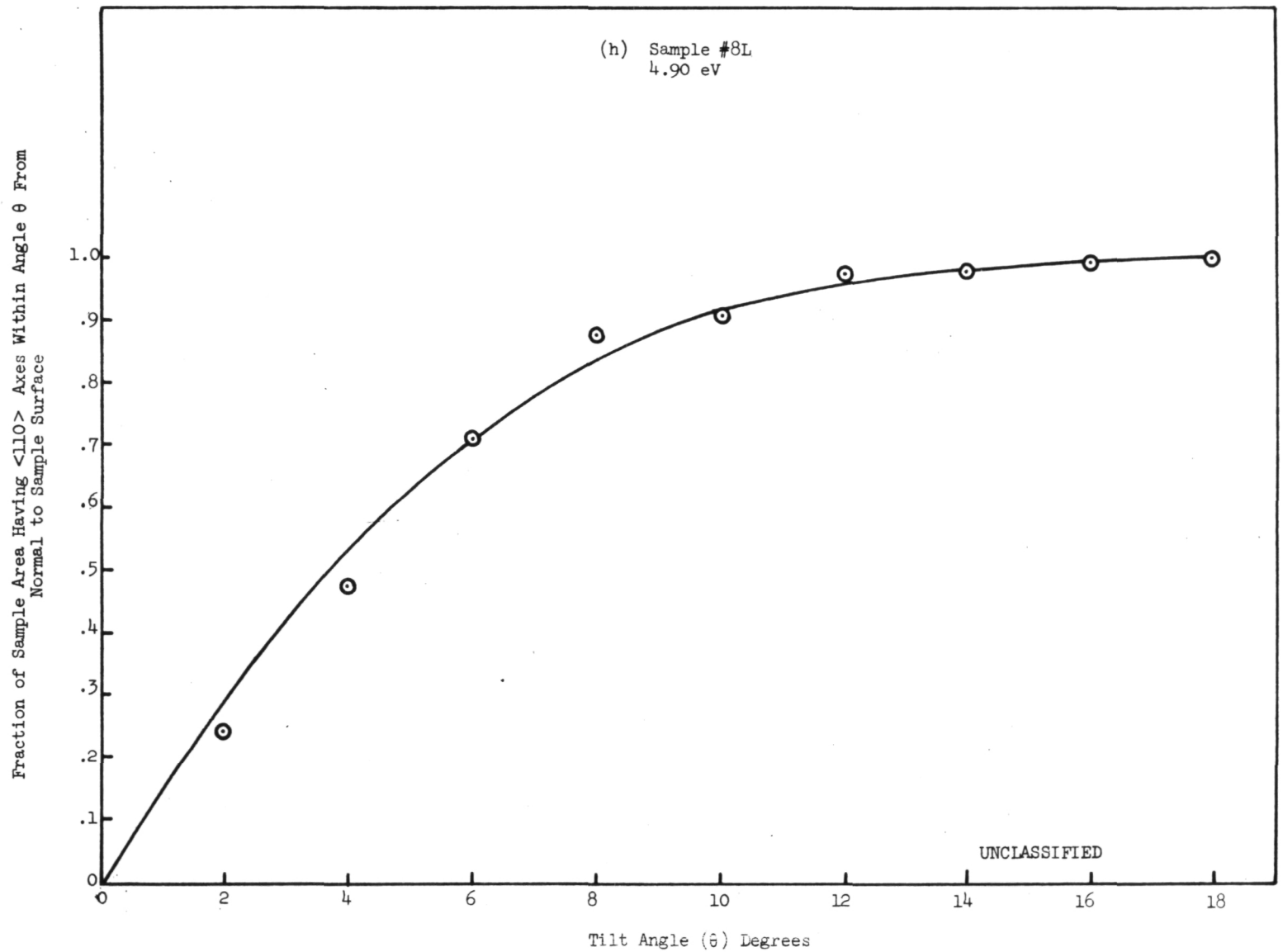

Fig. 3.7--(U) Spatial distribution of <110> axes in ten chloride tungsten samples (Page 8 of 10)

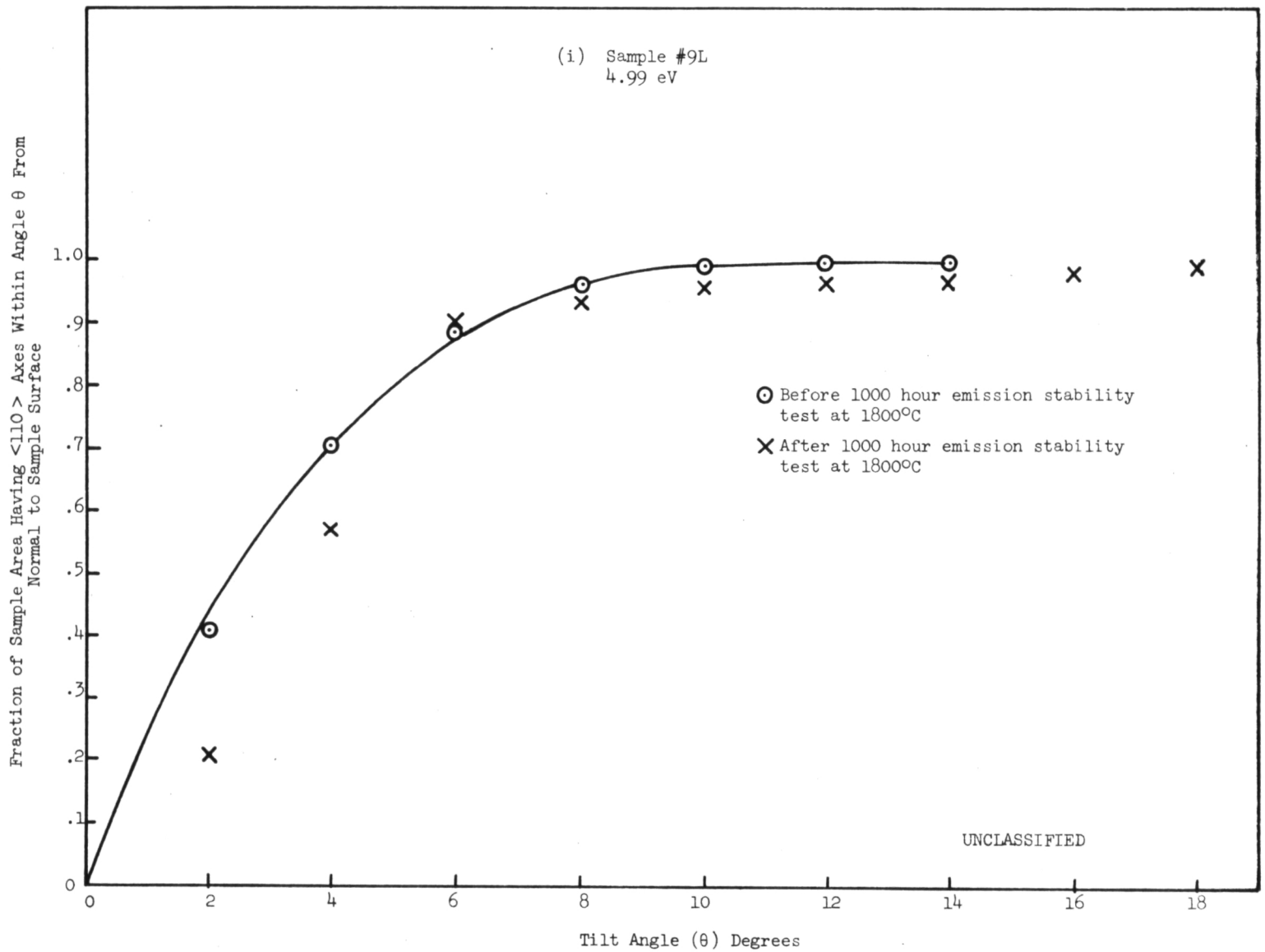

Fig. 3.7--(U) Spatial distribution of <110> axes in ten chloride tungsten samples (Page 9 of 10)

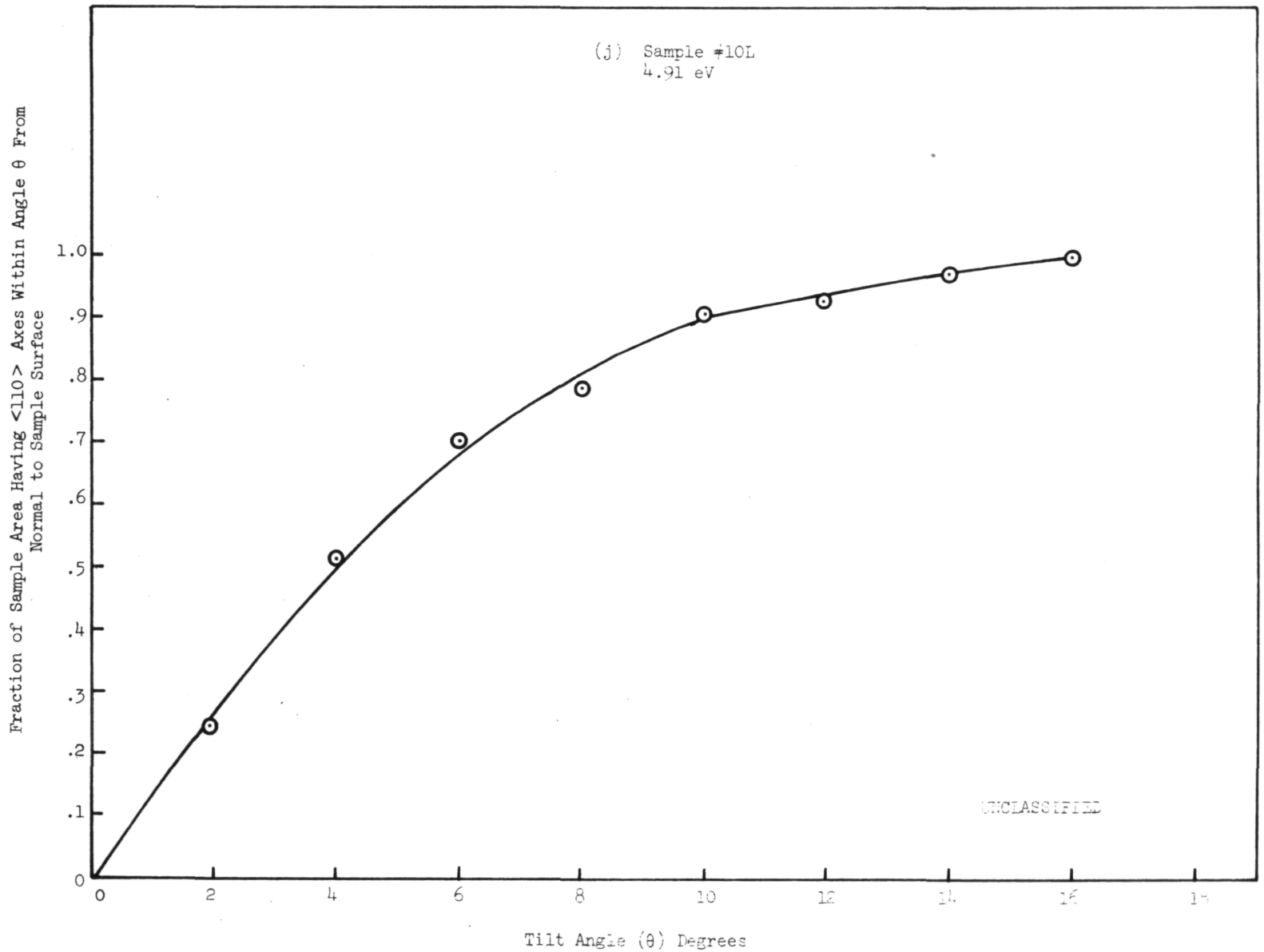

Fig. 3.7--(U) Spatial distribution of <110> axes in ten chloride tungsten samples (Page 10 of 10)

(U) Microstructures of cross section. Typical examples of the microstructures of the cross sections of the as-deposited duplex tungsten samples are shown in Figs. 3.8(a) through (f). The interruption of the grain structures between the chloride tungsten layer and the fluoride tungsten substrate is evident in each of the cases shown.

(U) Degree of {110} preferred orientation. The spatial distributions of the {110} axes in Sample 1DL through 10DL are shown in Fig. 3.9(a) through (j). For the ten samples studied, 90% of the <110> axes were located between 4° - 8° from the normals to their surfaces.

(U) Vacuum work function. The stabilized vacuum work functions of Sample 1DL through 10DL are also indicated in Fig. 3.9(a) through (j). For samples with 90% of the <110> axes located within 6.5° from the surface normal, the vacuum work functions are about 5 eV, while for samples with 90% of the <110> axes located within 8° from the surface normal, the vacuum work functions are about 4.9 eV.

(U) From the results described above, it can be seen that by following the deposition conditions established in Section 3.1, chloride tungsten deposits of vacuum work functions between 4.9-5.0 eV can be reproducibly obtained.

3.2.2. Emission Stability Test

(U) Ten samples, five (1L, 2L, 3L, 5L, and 9L) from the chloride tungsten deposit group and five (1DL, 3DL, 4DL, 7DL, and 9DL) from the duplex tungsten deposit group, were selected for tests of their vacuum emission stability at $1800^{\circ}C$ for 1000 hours in a vacuum of less than 10^{-7} torr residual gas pressure. The effective work functions were calculated from the emission data at $1800^{\circ}C$ and the Richardson work functions were deduced from the emission data in the temperature range 1600-$1800^{\circ}C$, both at about 200 hour intervals. The temperature of the sample was brought back to $1800^{\circ}C$ after each vacuum work function (effective and Richardson) determination and then cooled to room temperature by turning off the power to the electron bombardment heater, and then heated back to $1800^{\circ}C$ in one hour.

(U) Figure 3.10 shows the effective work functions of the five chloride tungsten test samples as a function of time. The stability of the

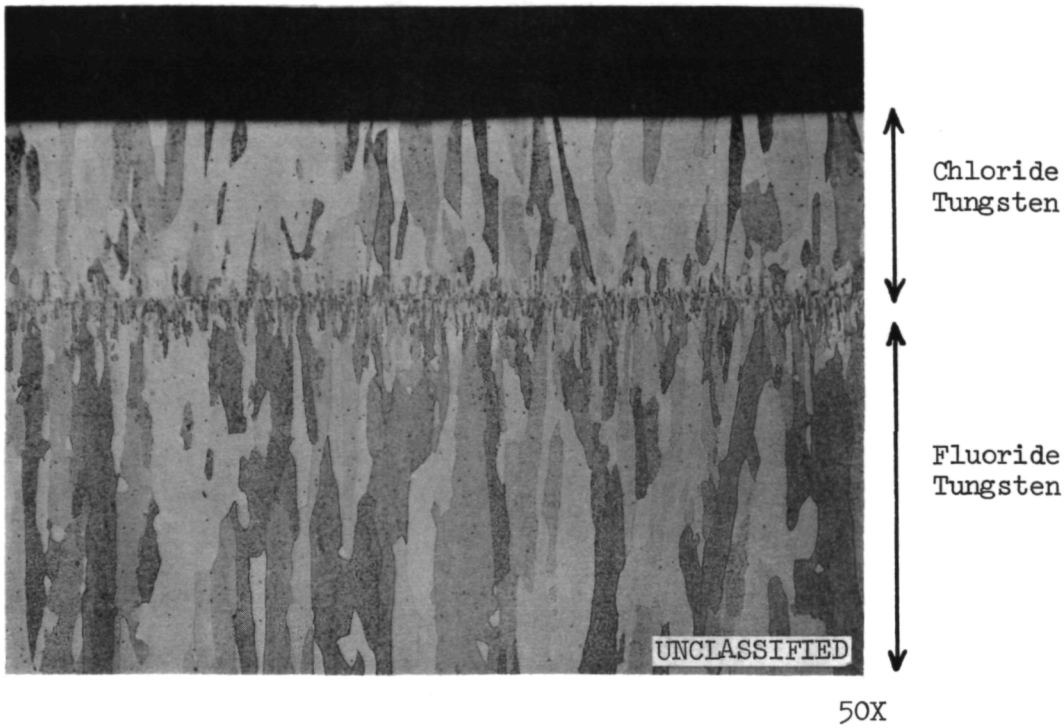

50X

(a) Sample 3DL

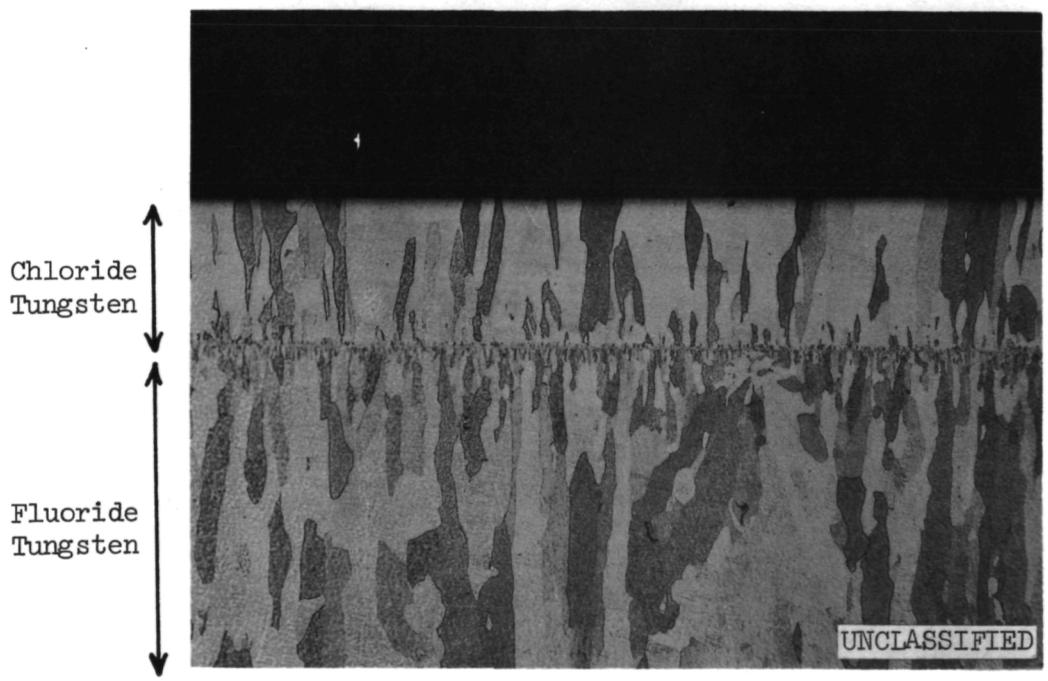

50X

(b) Sample 4DL

Fig. 3.8--(U) Typical microstructures of a cross section of as-deposited duplex tungsten deposit (Page 1 of 3)

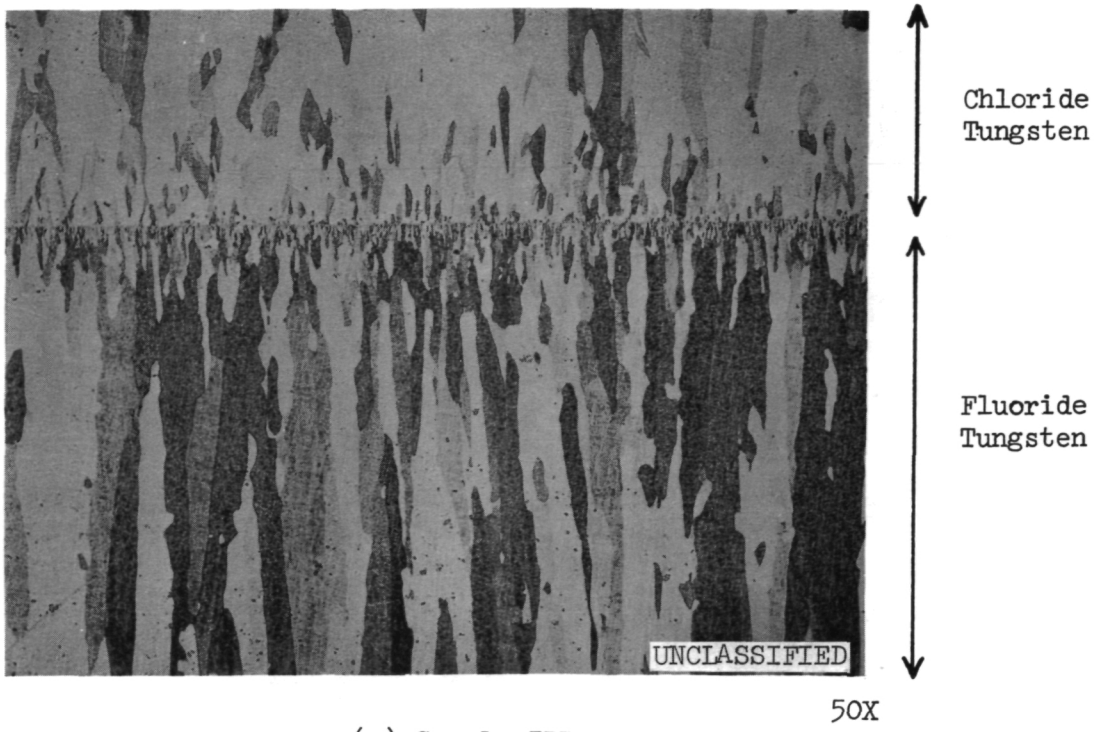

(c) Sample 5DL

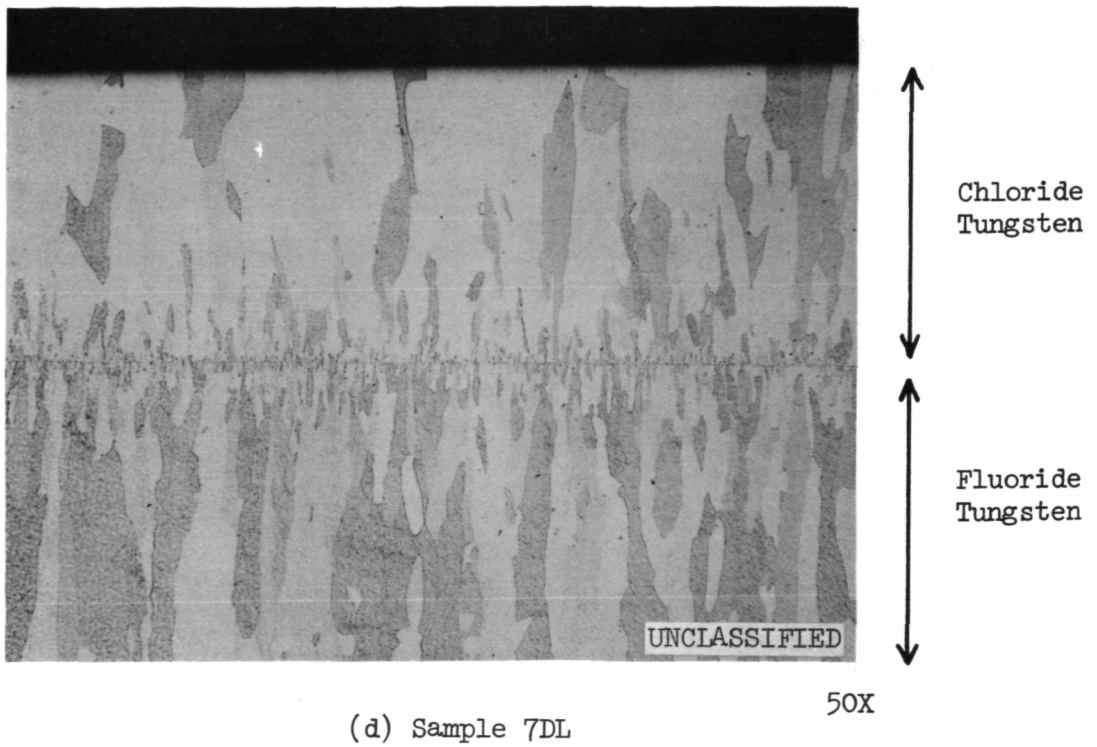

(d) Sample 7DL

Fig. 3.8--(U) Typical microstructures of a cross section of as-deposited duplex tungsten deposit (Page 2 of 3)

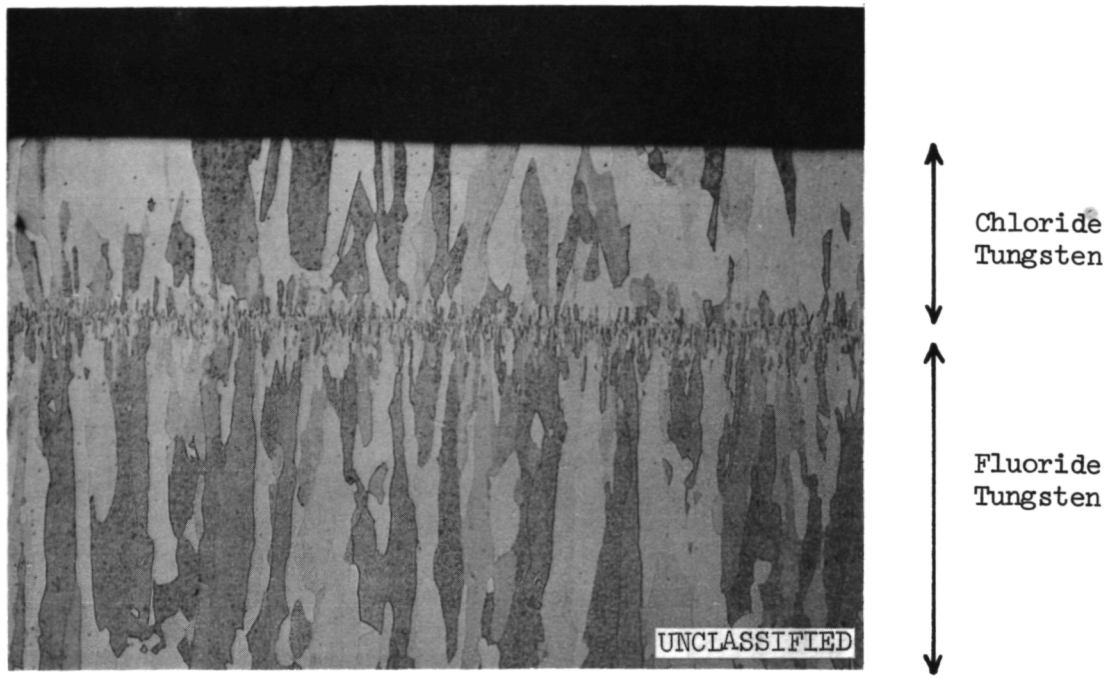

50X

(e) Sample 9DL

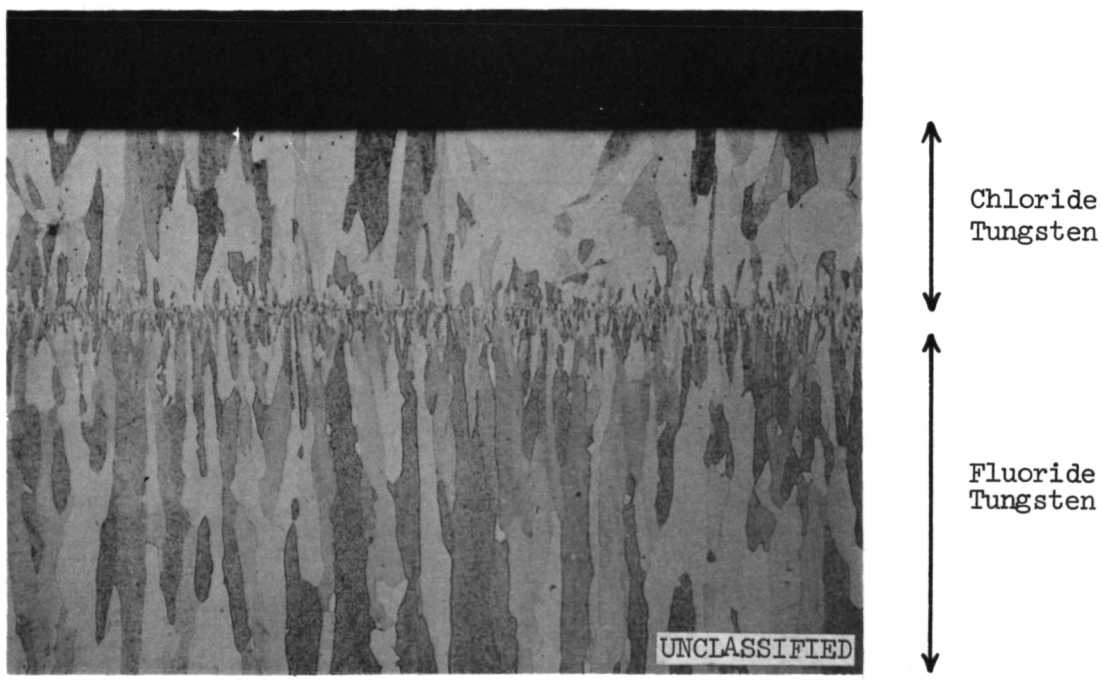

50X

(f) Sample 10DL

Fig. 3.8--(U) Typical microstructures of a cross section of as-deposited duplex tungsten deposit (Page 3 of 3)

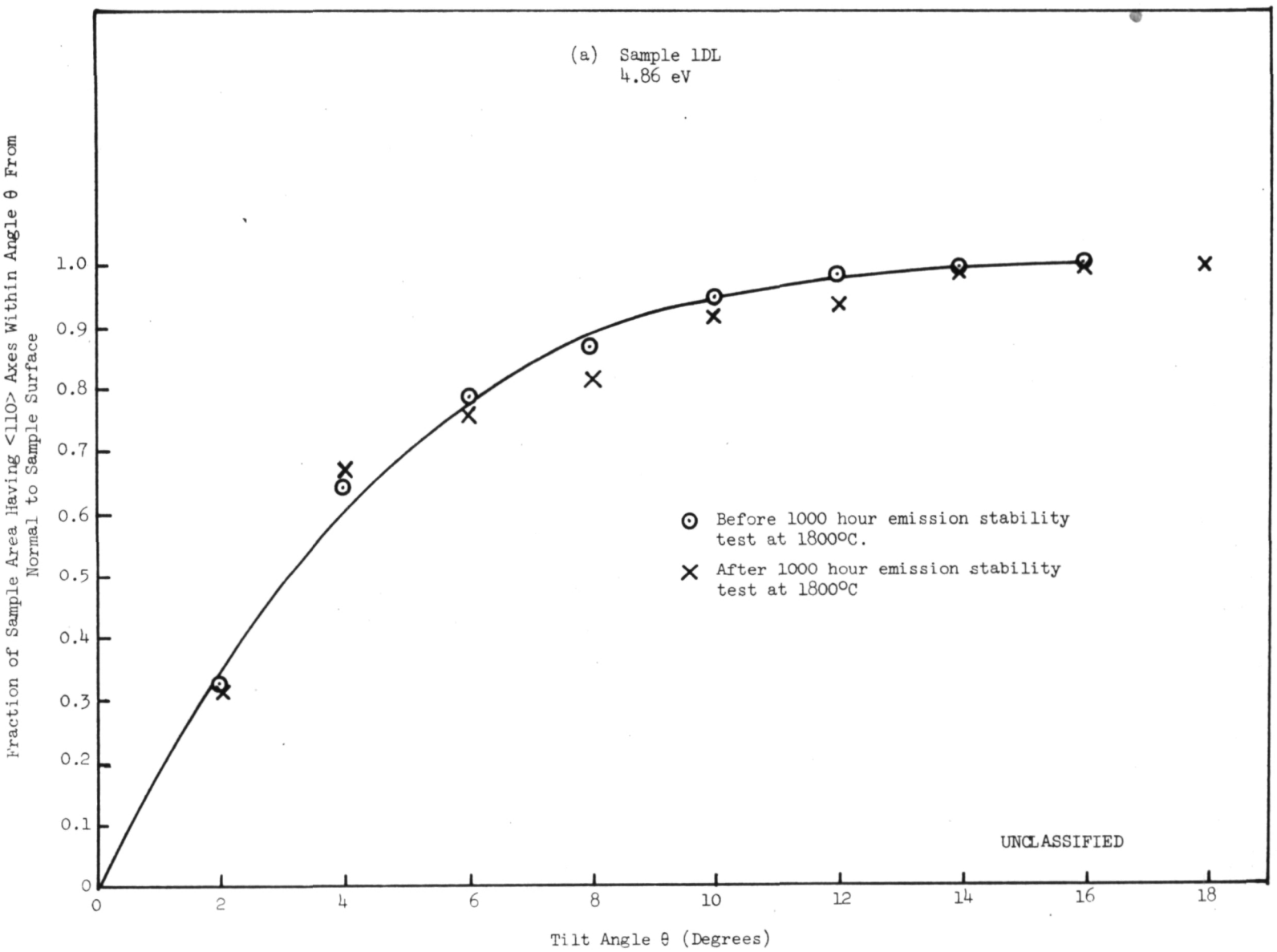

Fig. 3.9--(U) Spatial distribution of the <110> axes in ten duplex tungsten samples (Page 1 of 10)

UNCLASSIFIED

UNCLASSIFIED

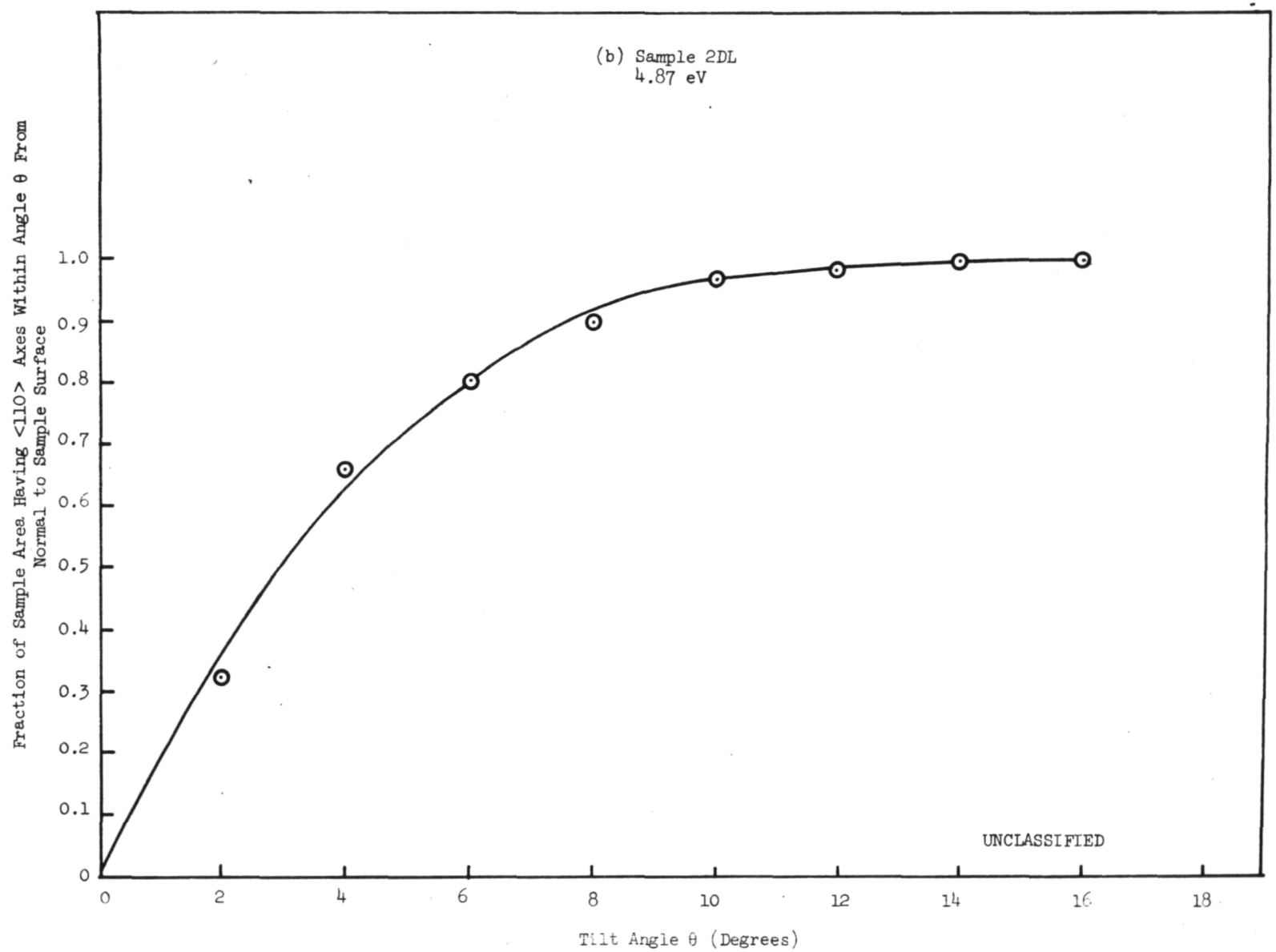

Fig. 3.9--(U) Spatial distribution of the <110> axes in ten duplex tungsten samples (Page 2 of 10)

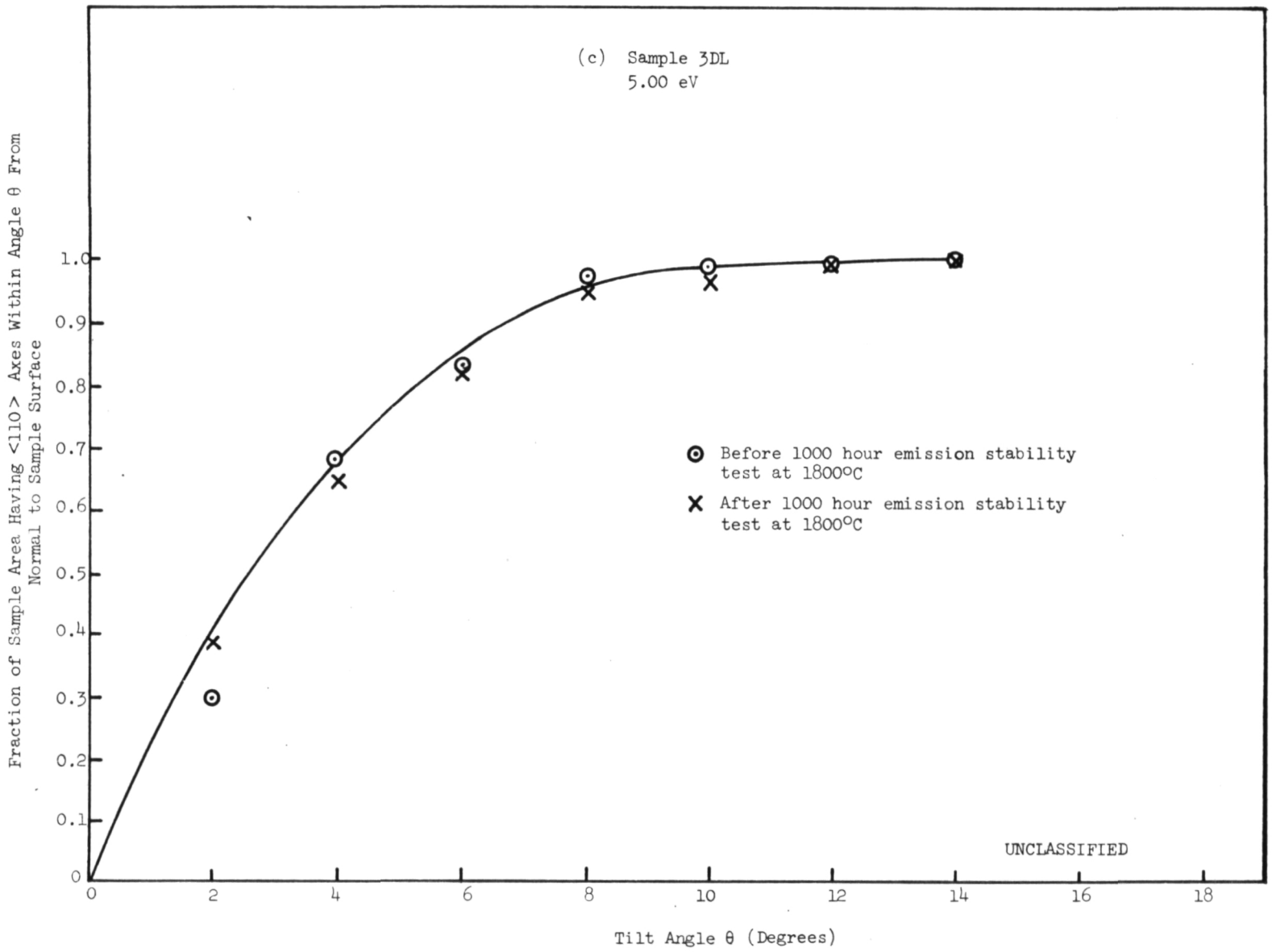

Fig. 3.9--(U) Spatial distribution of the <110> axes in ten duplex tungsten samples (Page 3 of 10)

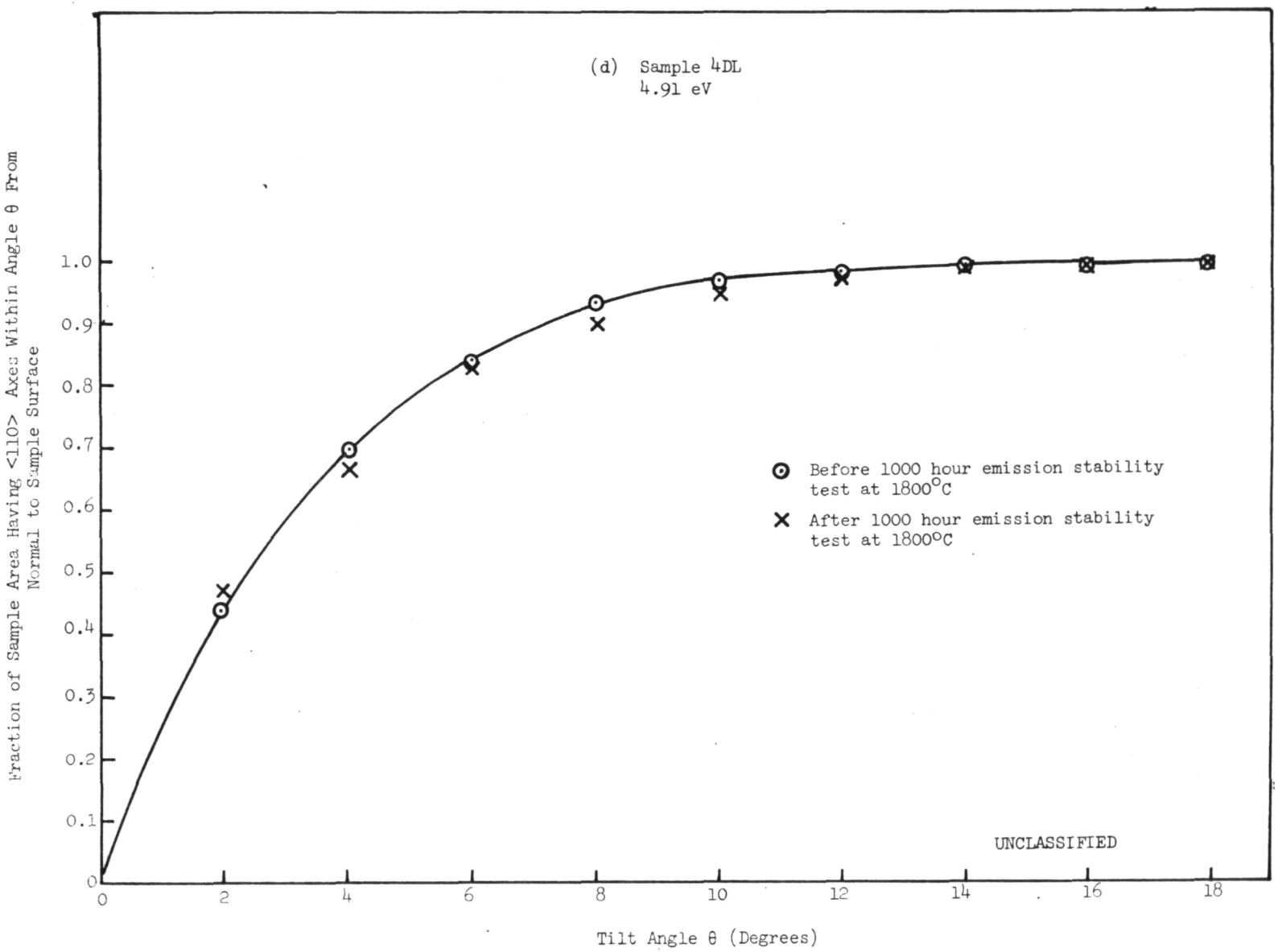

Fig. 3.9--(U) Spatial distribution of the <110> axes in ten duplex tungsten samples (Page 4 of 10)

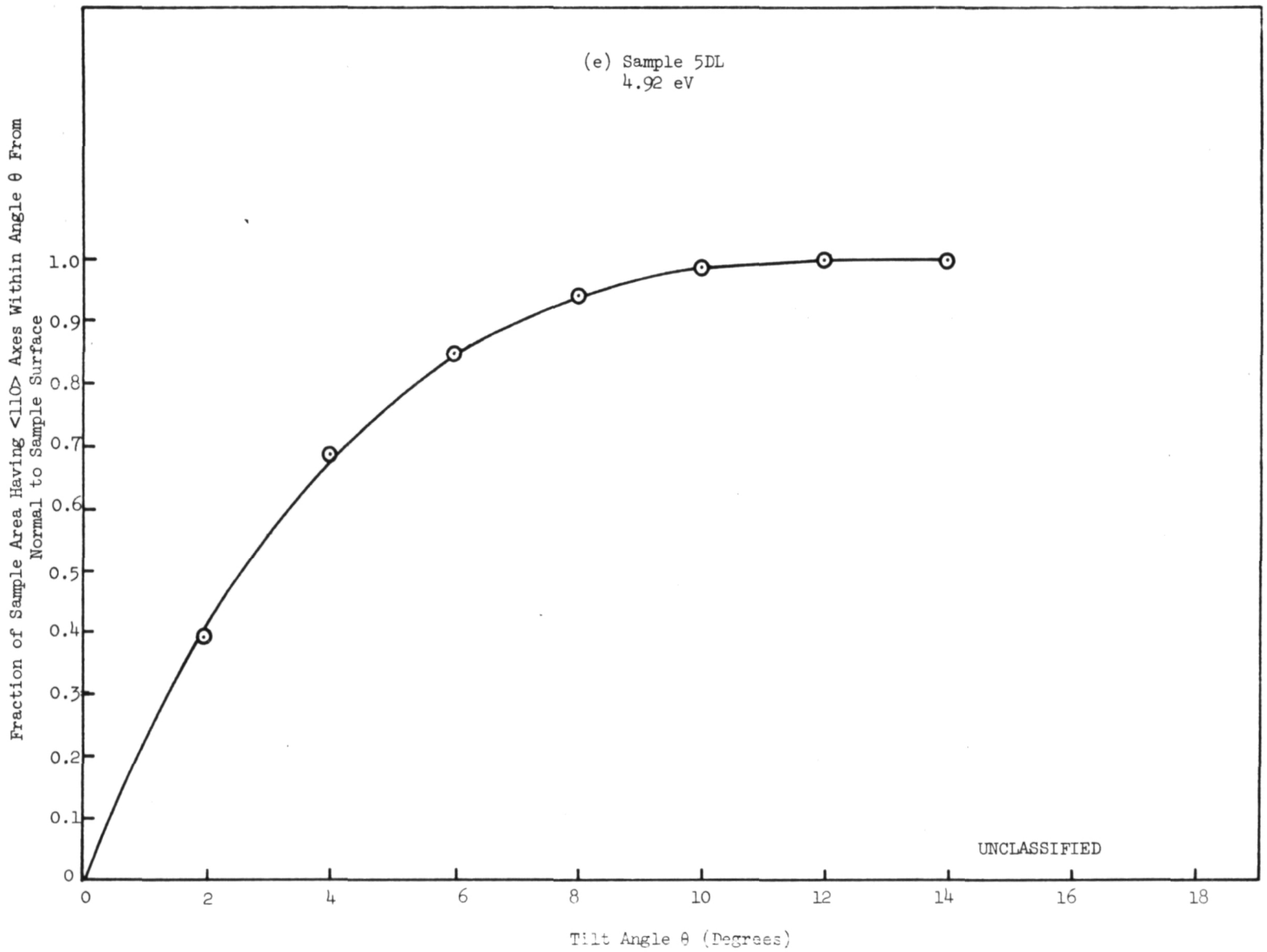

Fig. 3.9--(U) Spatial distribution of the <110> axes in ten duplex tungsten samples (Page 5 of 10)

UNCLASSIFIED

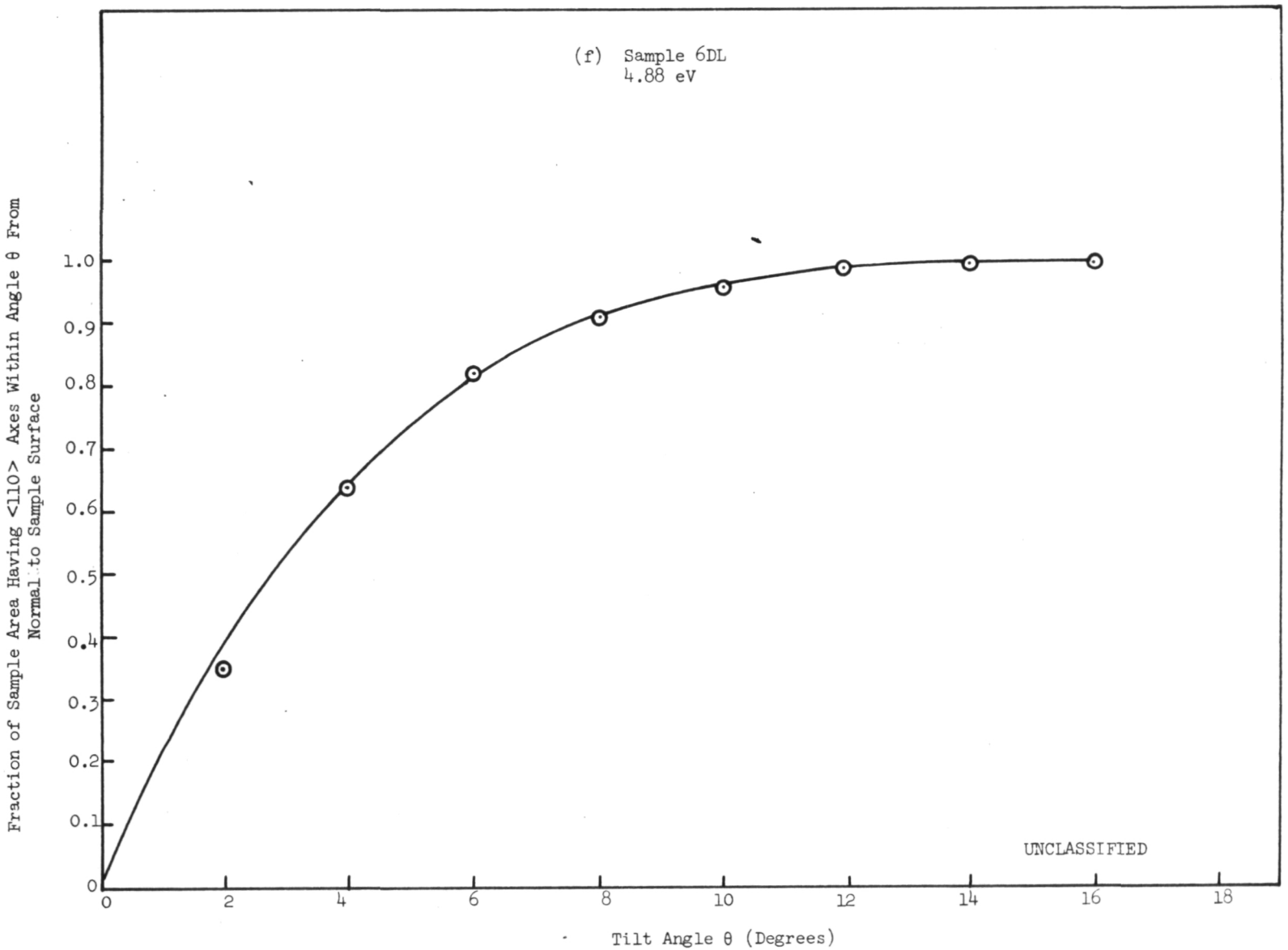

Fig. 3.9--(U) Spatial distribution of the <110> axes in ten duplex tungsten samples (Page 6 of 10)

UNCLASSIFIED

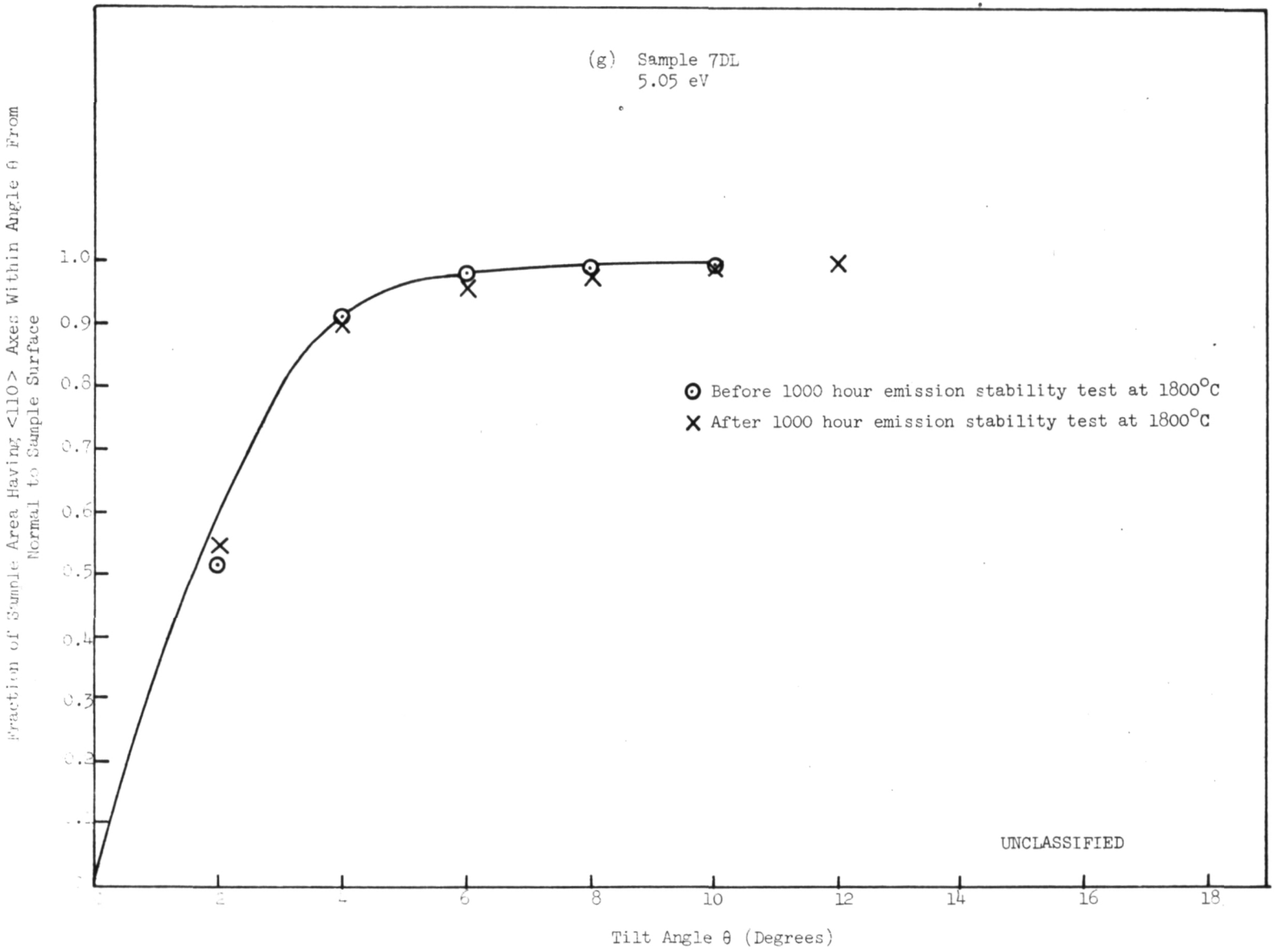

Fig. 3.9--(U) Spatial distribution of the <110> axes in ten duplex tungsten samples (Page 7 of 10)

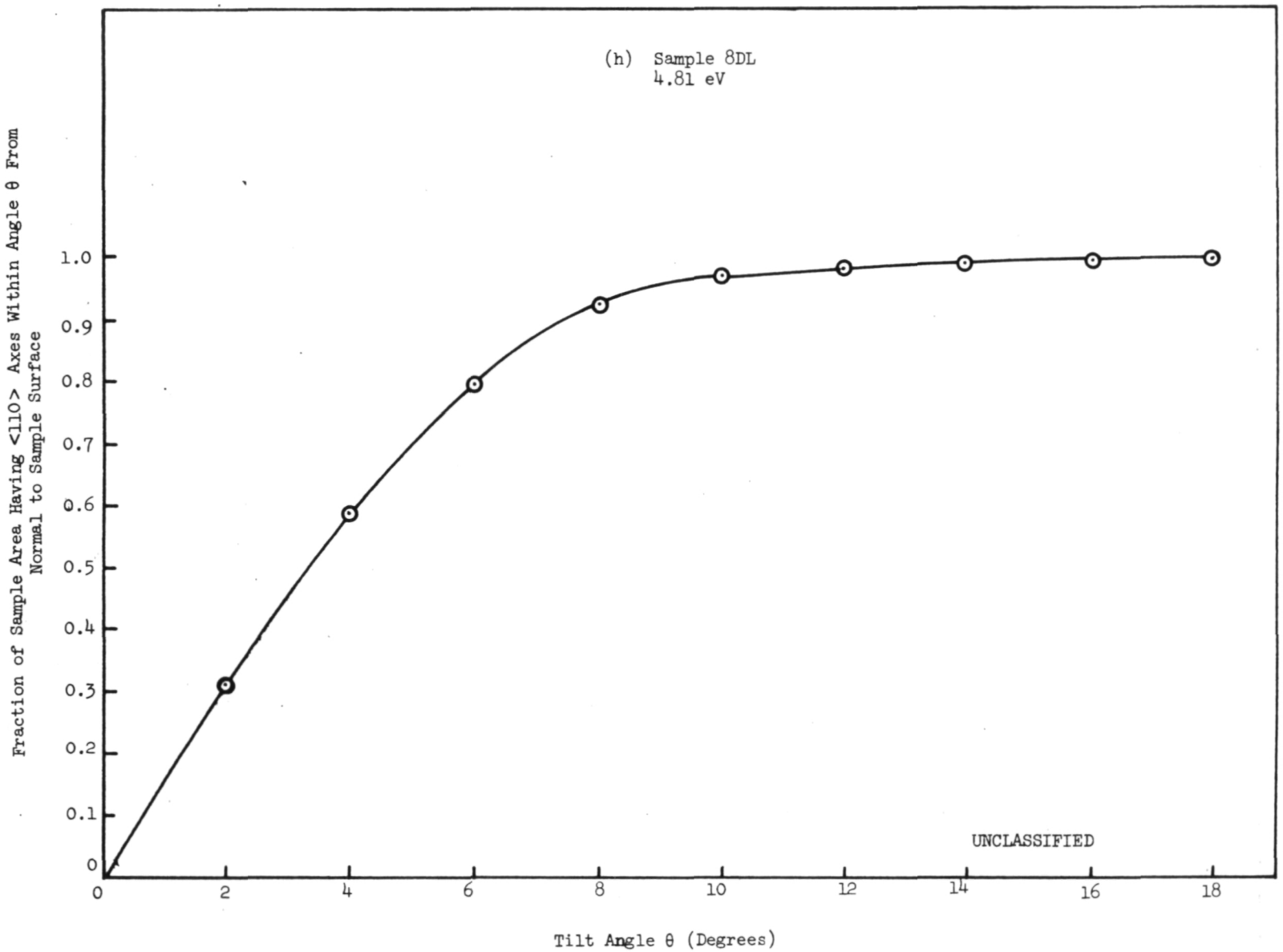

Fig. 3.9--(U) Spatial distribution of the <110> axes in ten duplex tungsten samples (Page 8 of 10)

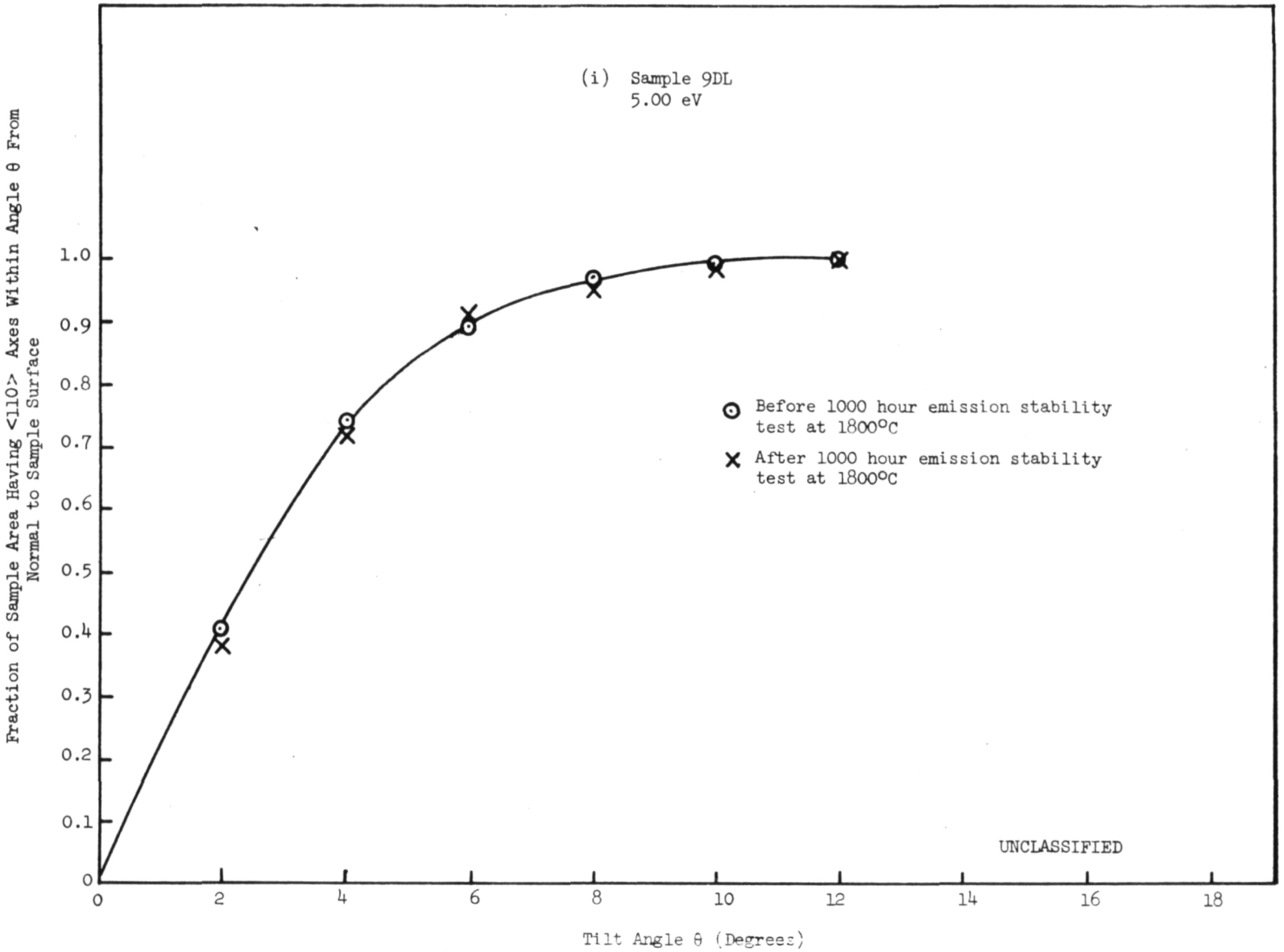

Fig. 3.9--(U) Spatial distribution of the <110> axes in ten duplex tungsten samples (Page 9 of 10)

UNCLASSIFIED

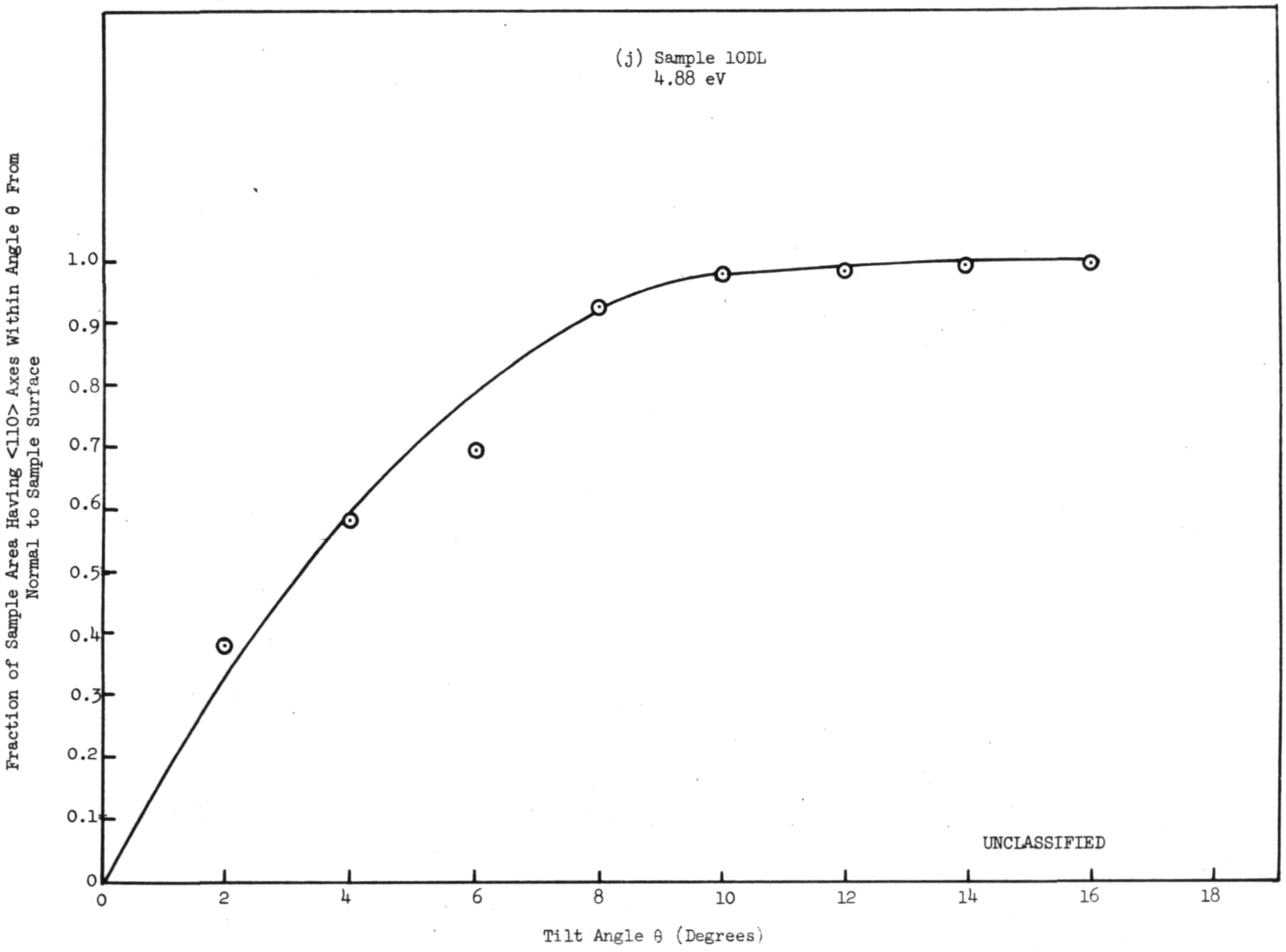

Fig. 3.9--(U) Spatial distribution of the <110> axes in ten duplex tungsten samples (Page 10 of 10)

UNCLASSIFIED

UNCLASSIFIED

UNCLASSIFIED

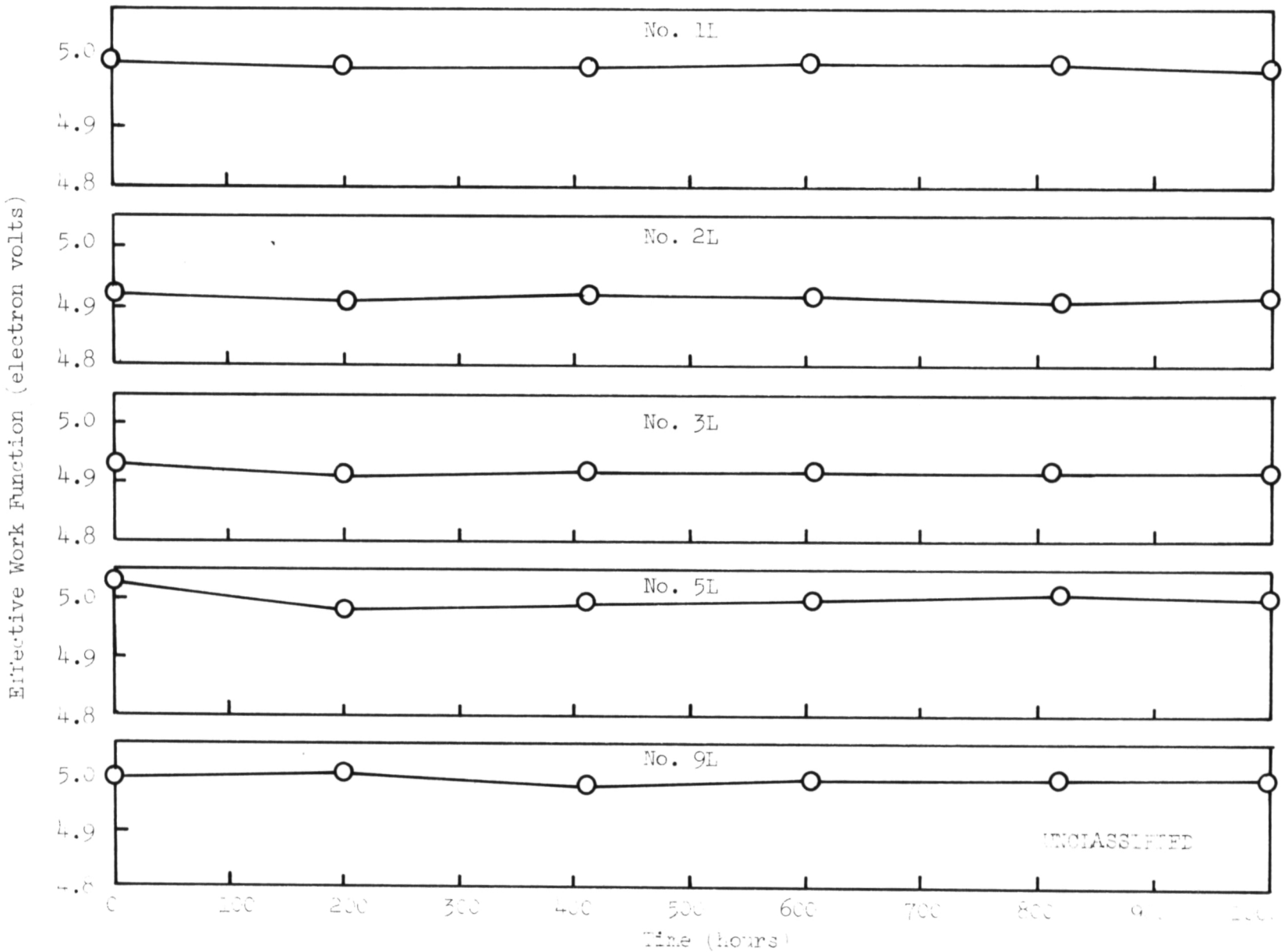

Fig. 3.10--(U) Emission stability test results for five chloride tungsten samples at 1800°C

effective work functions of these samples is evident. Figures 3.11(a) through (e) show the emission results of these samples in the temperature range 1600-1800°C as a function of testing time at 1800°C. The variation of these results with testing time at 1800°C is insignificant. From the Richardson lines drawn through the experimental points, the Richardson work functions (ϕ_R) and the pre-exponential factors "A" were deduced and shown in Figs. 3.11(a) through (e). The "A" values are all less than 120 amp/$cm^2/°K^2$, indicating non-uniformity in emission characteristics over the sample surface. After the emission test, the spatial distributions of the <110> axes in the five test samples were again determined. The results are included in Figs. 3.7(a) through (j). Except for some changes observed for Sample 3L, there are no significant differences between the results obtained before and after the emission stability test of the other four samples.

(U) Figure 3.12 shows the effective work functions of the five duplex tungsten test samples as a function of time. The changes with time during the 1000 hour tests were insignificant. Figures 3.13(a) through (e) are the Richardson plots for these samples in the temperature range 1600-1800°C as a function of testing time at 1800°C, with the deduced Richardson work function (ϕ_R) and the pre-exponential factors "A" values included in each figure. Here again, the "A" values are all less than 120 amp/$cm^2/°K^2$, implying non-uniformity in emission characteristics over the surfaces of these samples. Results on the spatial distributions of the <110> axes in these samples after the emission stability test are included in Fig. 3.9(a) through (j). It can be seen that no significant changes occurred in the degree of (110) orientation in these samples during the emission stability test.

3.2.3. Cesiated Emission Test

(U) Five of the ten samples, (2L, 5L, 3DL, 7DL and 9DL) studied in Section 3.2.2 were selected for the determination of their cesiated work functions in an emission-diffusion cell which has provision for operation in cesium vapor, using the techniques described in a previous report.(1) Studies of these five samples were carried out in the emitter temperature range 1000°-1150°C and cesium temperature range 47-127°C. The results are

UNCLASSIFIED

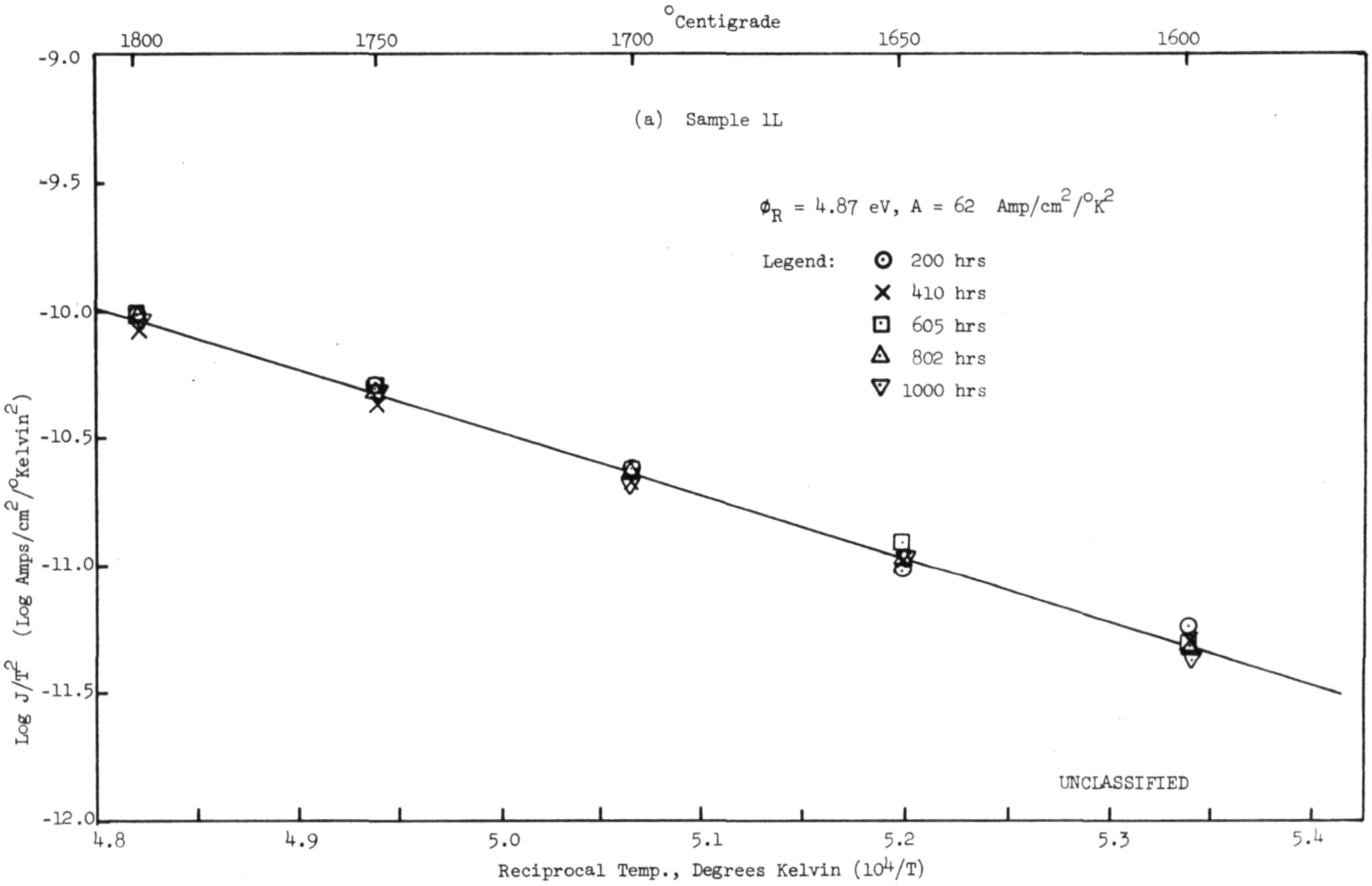

Fig. 3.11-(U) Richardson plots for five chloride tungsten samples as a function of time at 1800°C
(Page 1 of 5)

UNCLASSIFIED

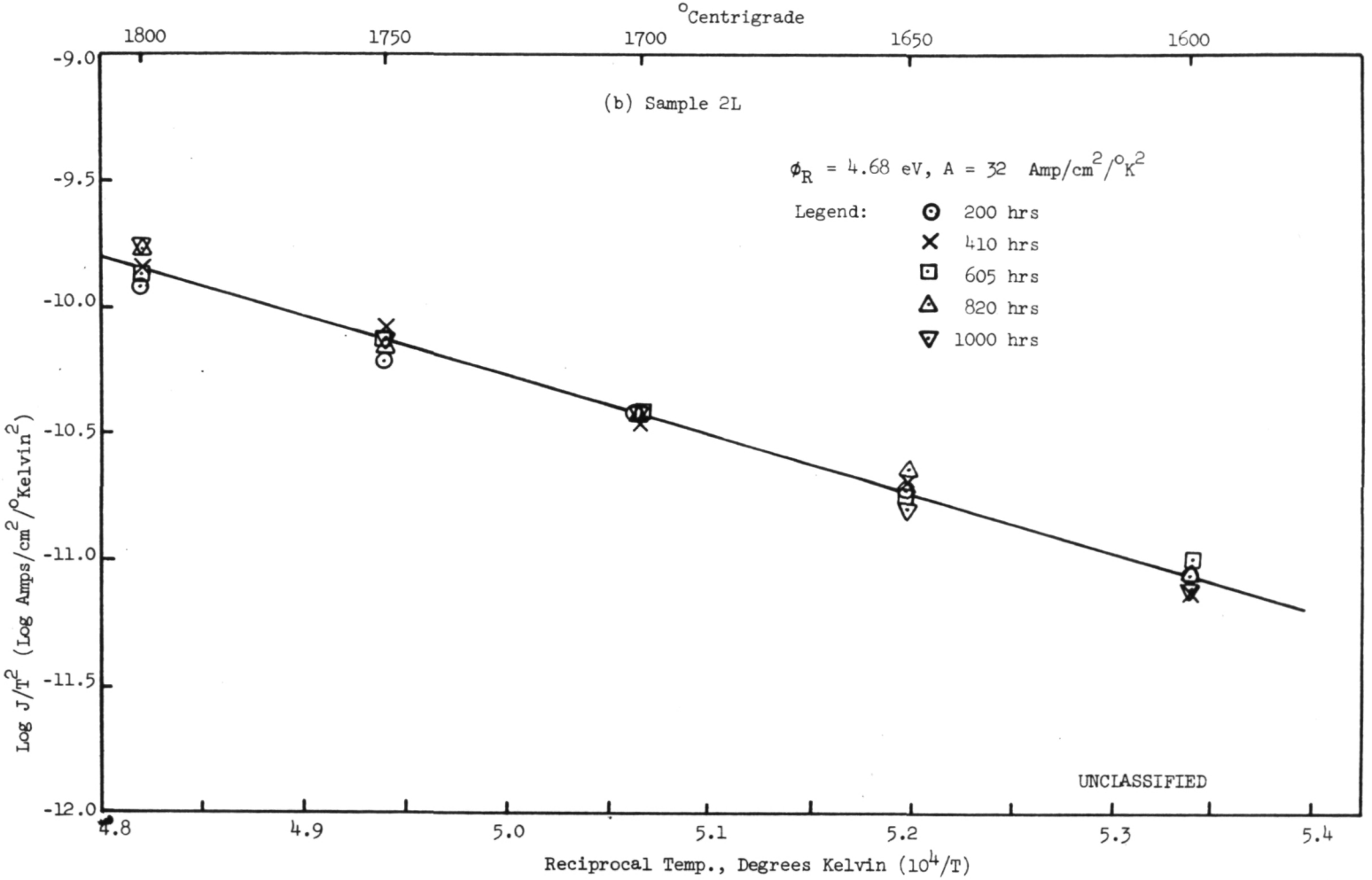

Fig. 3.11--(U) Richardson plots for five chloride tungsten samples as a function of time at 1800°C
(Page 2 of 5)

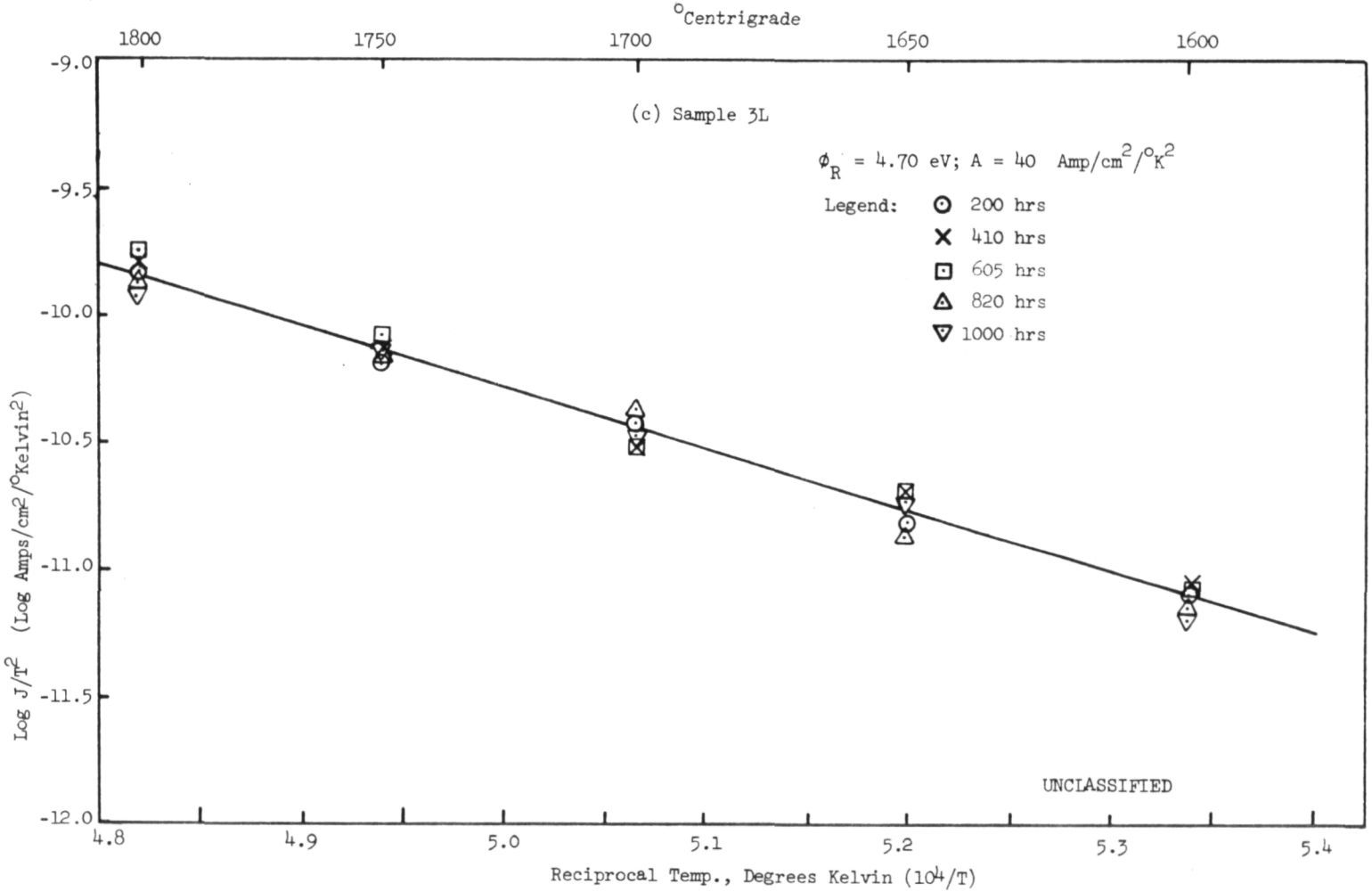

Fig. 3.11--(U) Richardson plots for five chloride tungsten samples as a function of time at 1800°C
(Page 3 of 5)

UNCLASSIFIED

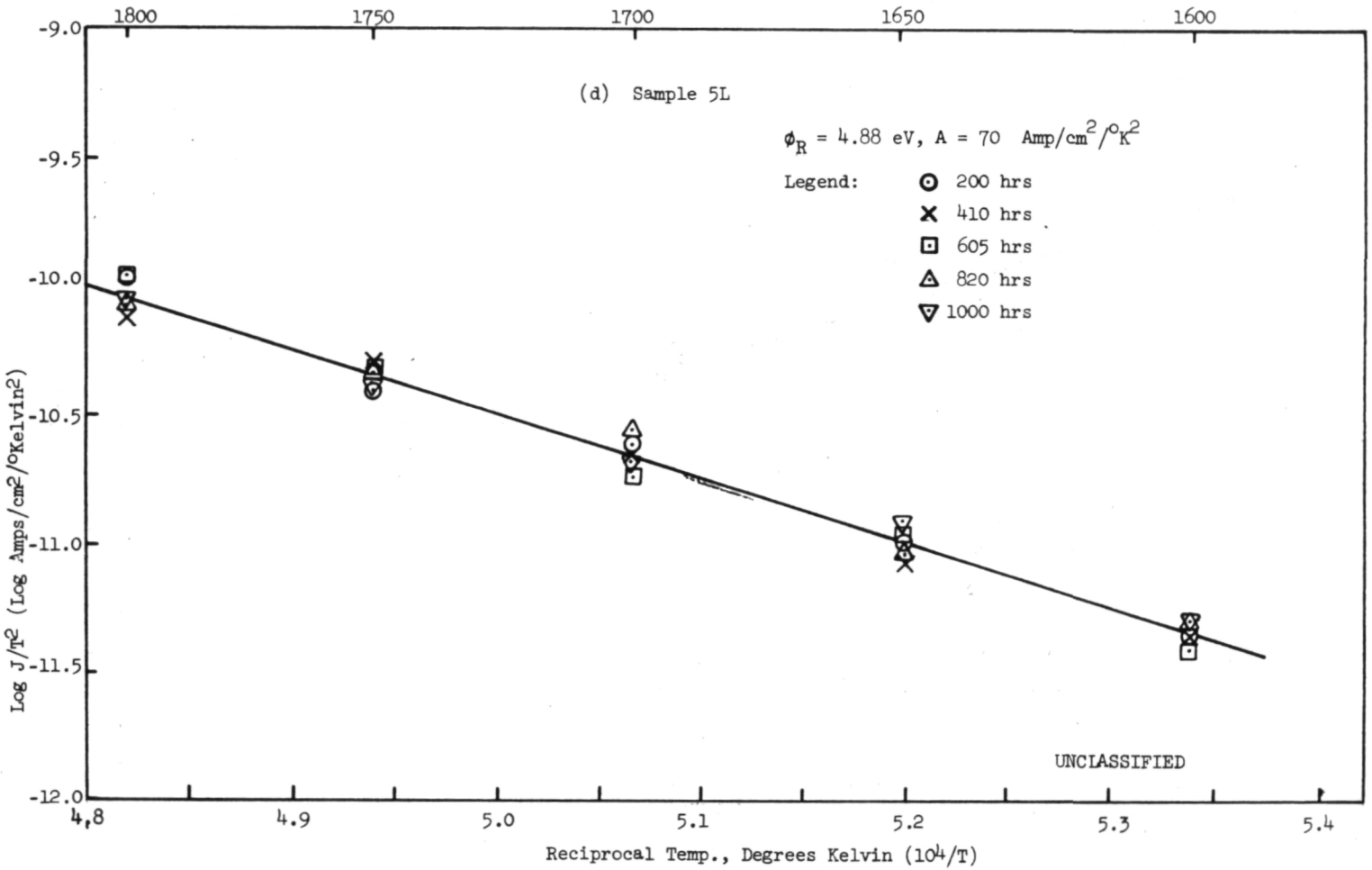

Fig. 3.11--(U) Richardson plots for five chloride tungsten samples as a function of time at 1800°C
(Page 4 of 5)

UNCLASSIFIED

UNCLASSIFIED

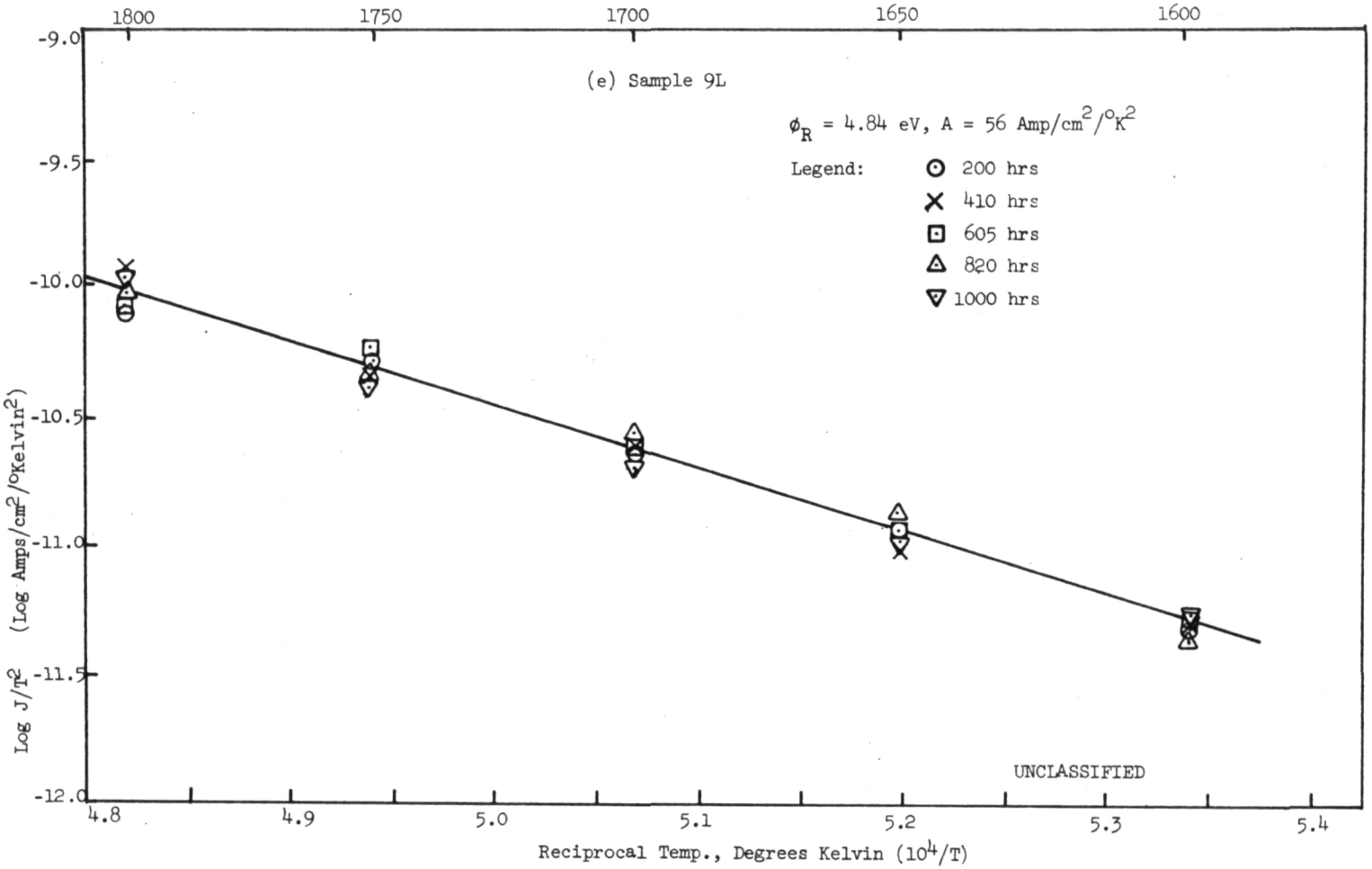

Fig. 3.11--(U) Richardson plots for five chloride tungsten samples as a function of time at 1800°C
(Page 5 of 5)

UNCLASSIFIED

UNCLASSIFIED

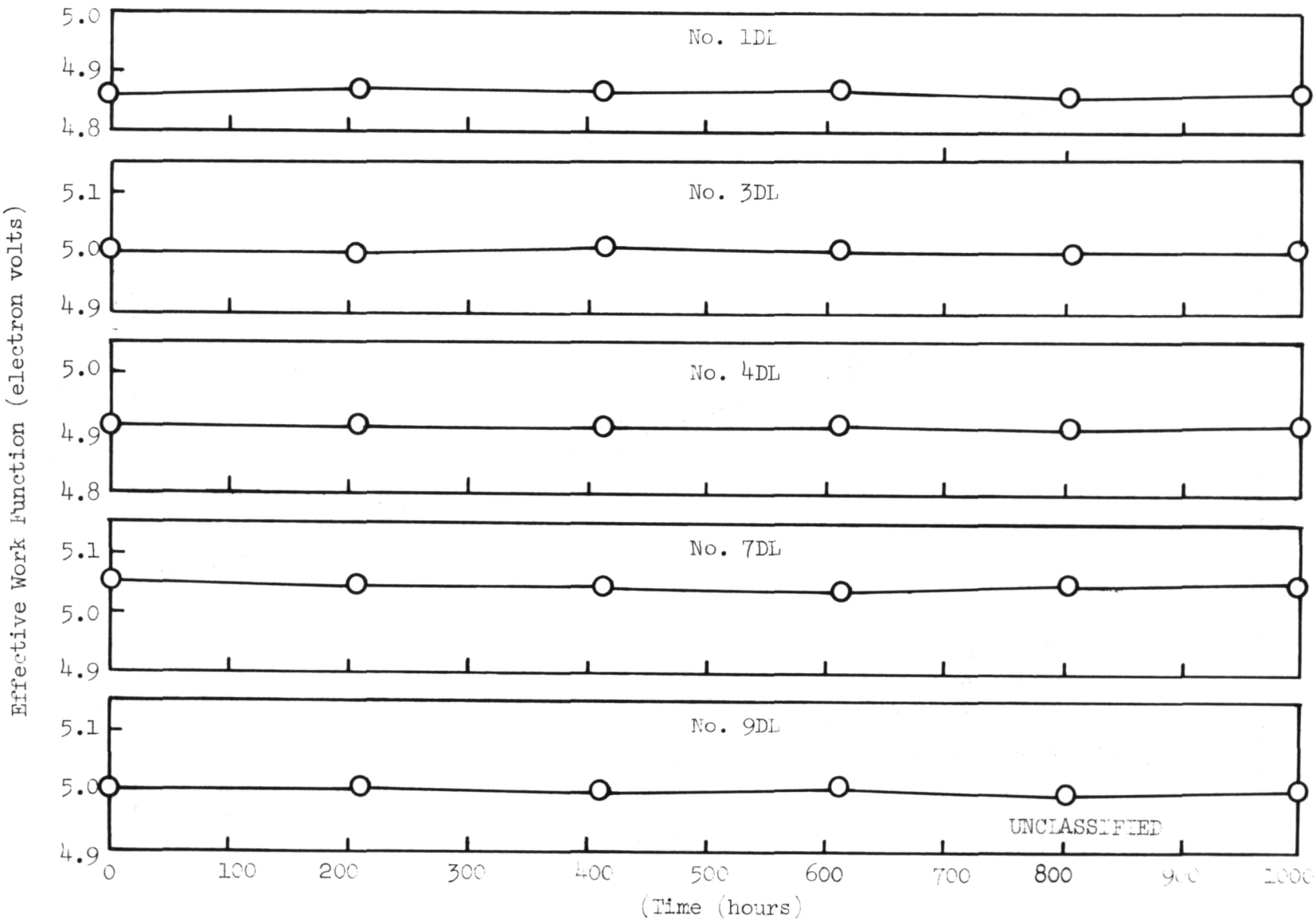

Fig. 3.12--(U) Emission stability test results for five duplex tungsten samples at 1800°C

UNCLASSIFIED

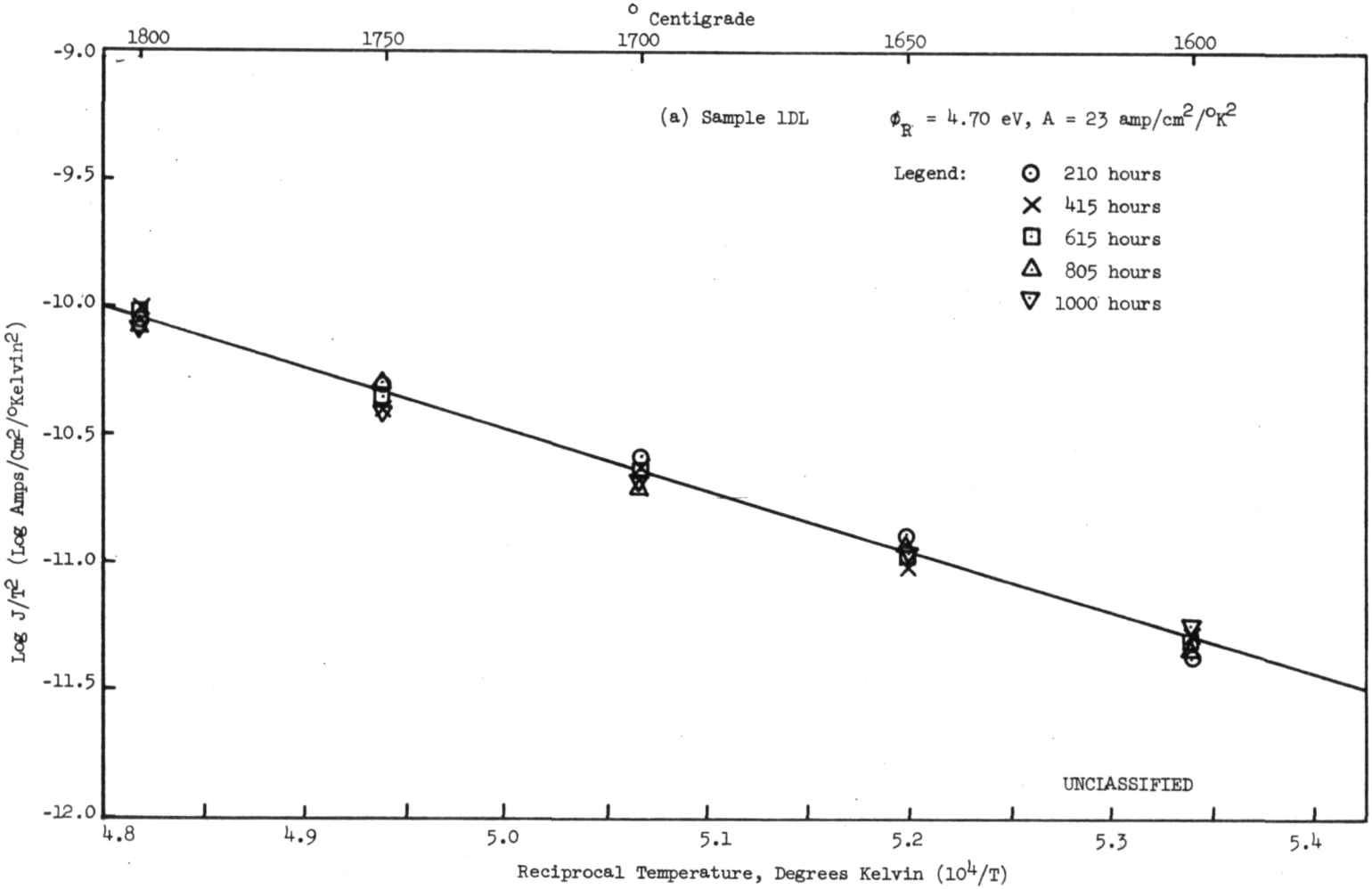

Fig. 3.13--(U) Richardson plots for five duplex tungsten samples as a function of time at 1800°C
(Page 1 of 5)

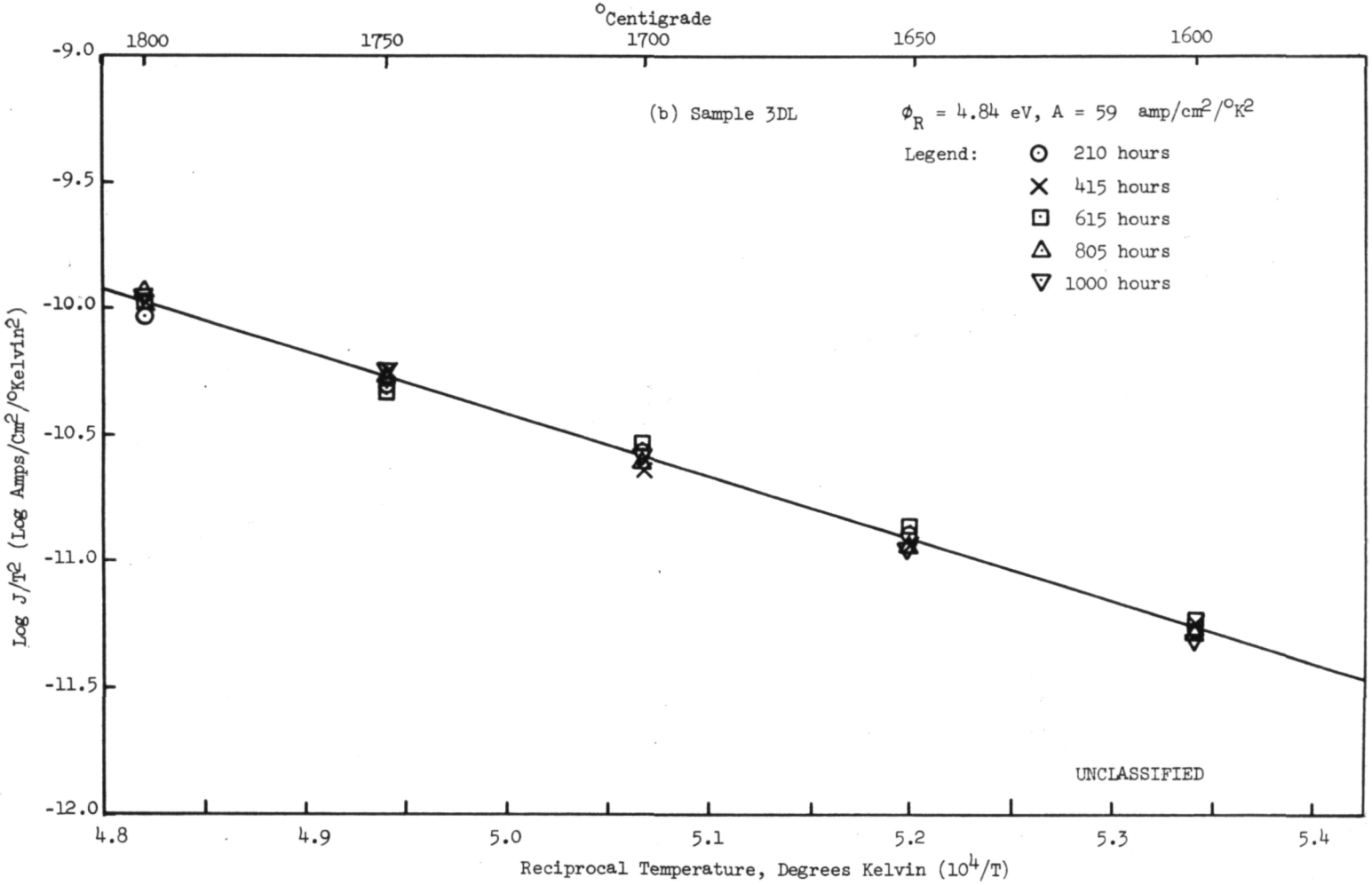

Fig. 3.13--(U) Richardson plots for five duplex tungsten samples as a function of time at 1800°C
(Page 2 of 5)

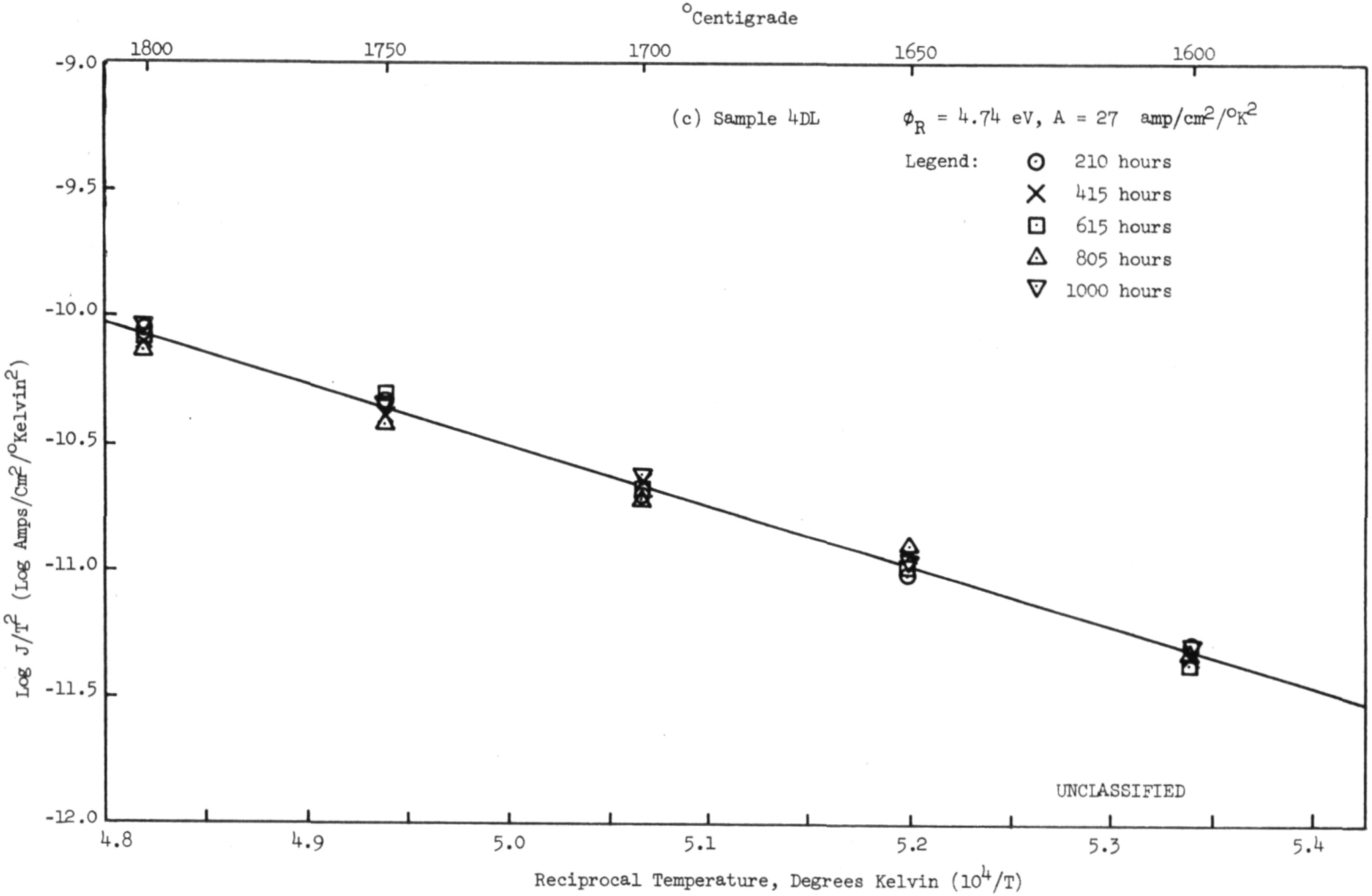

Fig. 3.13--(U) Richardson plots for five duplex tungsten samples as a function of time at 1800°C
(Page 3 of 5)

UNCLASSIFIED

UNCLASSIFIED

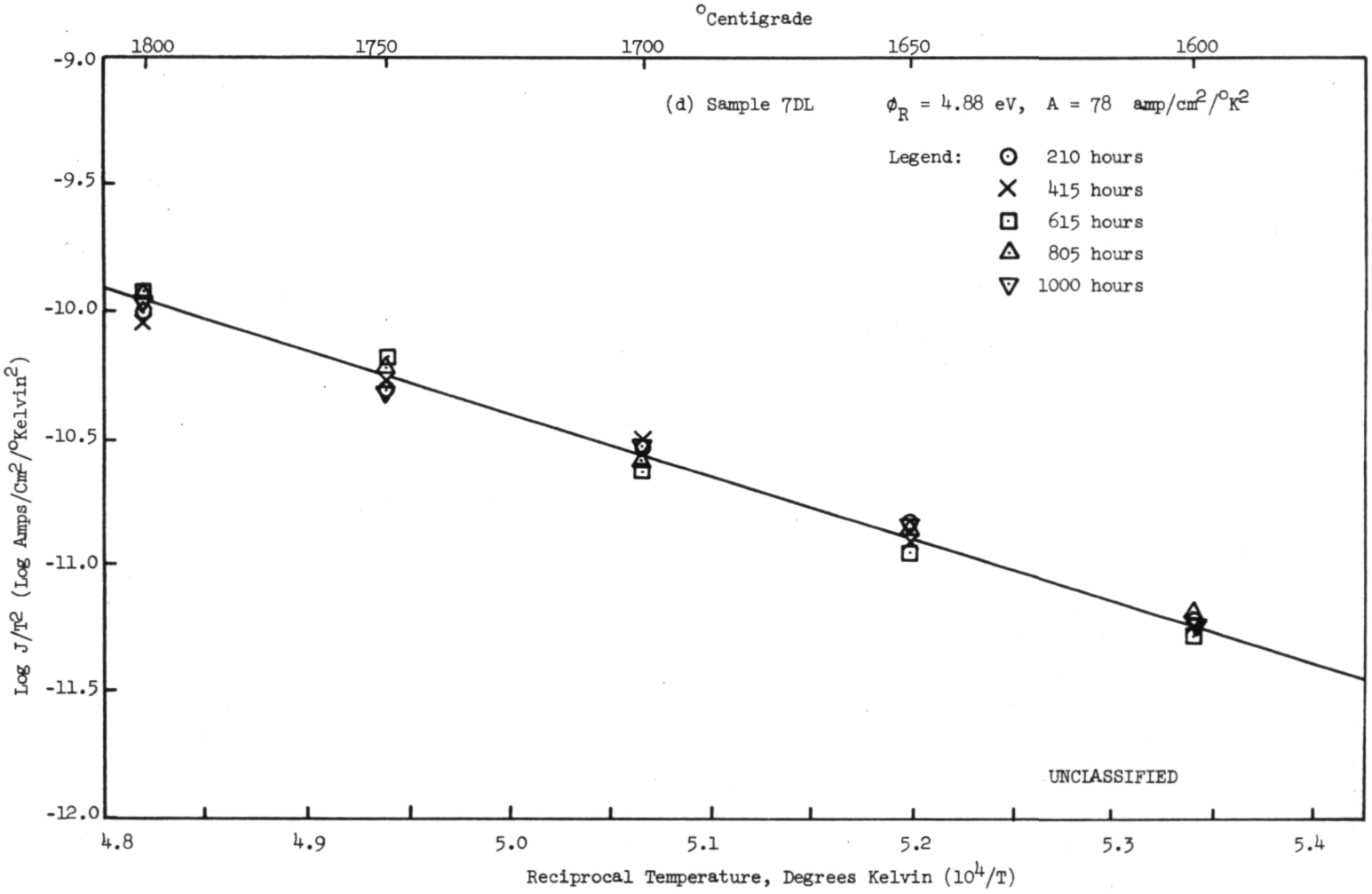

Fig. 3.13--(U) Richardson plots for five duplex tungsten samples as a function of time at 1800°C
(Page 4 of 5)

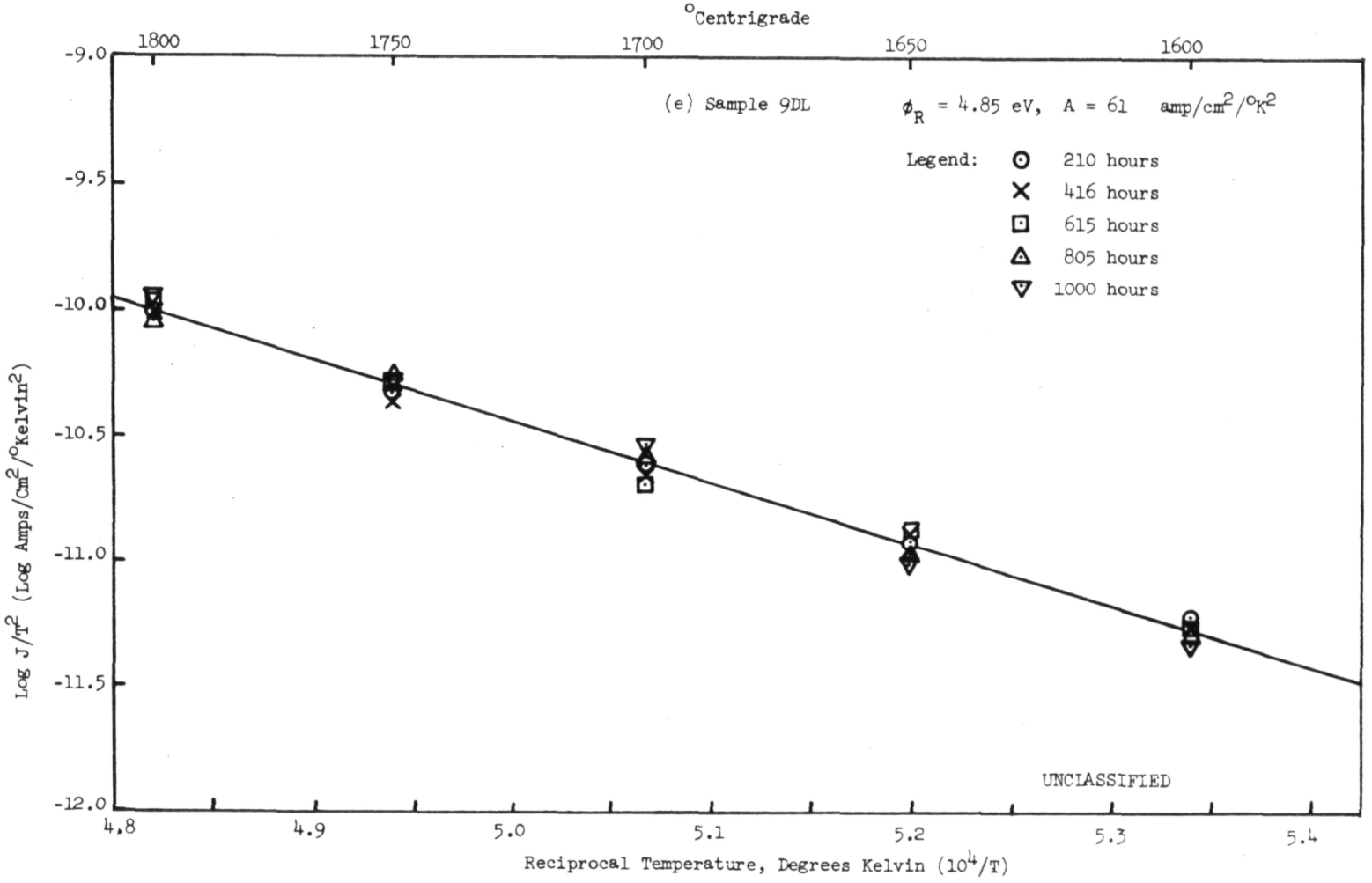

Fig. 3.13--(U) Richardson plots for five duplex tungsten samples as a function of time at 1800°C
(Page 5 of 5)

expressed as the Rasor-Warner plots in Figs. 3.14(a) through (e). It can be seen that the experimental points in each plot stay near the line for a vacuum work function value equal to 5.0 eV which agrees with the vacuum emission results. Similar agreement has been observed in previous studies[1] of the emission characteristics of oriented tungsten emitters.

(U) All five samples were examined in a thermionic emission microscope. The patterns obtained indicate that in each case the emission characteristics are not uniform over the whole emitter surface. Typical thermionic emission patterns are shown in Figs. 3.15(a) through (e). This is probably the reason that the effective work functions of these samples differ from their Richardson work functions and the Richardson "A" values are less than 120 amp/cm^2/$^\circ$K^2. The surface morphology of these samples was then studied by examining the replica taken from their surfaces in an electron microscope. In each case, the surface was found to be microscopically smooth and was free from micro-facets. Examples of the electron micrographs are shown in Figs. 3.16(a) and (b). Figures 3.17(a) through (e) illustrate the bulk microstructures of these samples. It can be seen that the grain sizes of the chloride tungsten samples are bigger than that of the chloride tungsten layers in the duplex tungsten samples, and that for the duplex tungsten samples the bond between the chloride tungsten layer and the fluoride tungsten substrate is good. Chemical analysis of these five samples yielded the results shown in Table 3.3.

Table 3.3
(U) IMPURITY CONTENTS OF FIVE SELECTED TUNGSTEN EMITTERS AFTER EMISSION TEST
(This table is Unclassified)

Sample	Impurity Contents (ppm)									
	O	N	C	F	Cl	Al	Fe	Cu	Mg	Si
2L	3	<1	7	<3	8	1	<4	<0.3	0.1	1.5
5L	2	<1	5	<3	3	<0.3	<4	<0.3	0.2	2
3DL	5	<1	3	5	5	<0.3	<4	<0.3	0.1	<1
7DL	3	<1	5	<3	3	0.5	<4	<0.3	0.3	<1
9DL	7	<1	8	4	7	<0.3	<4	<0.3	0.1	2

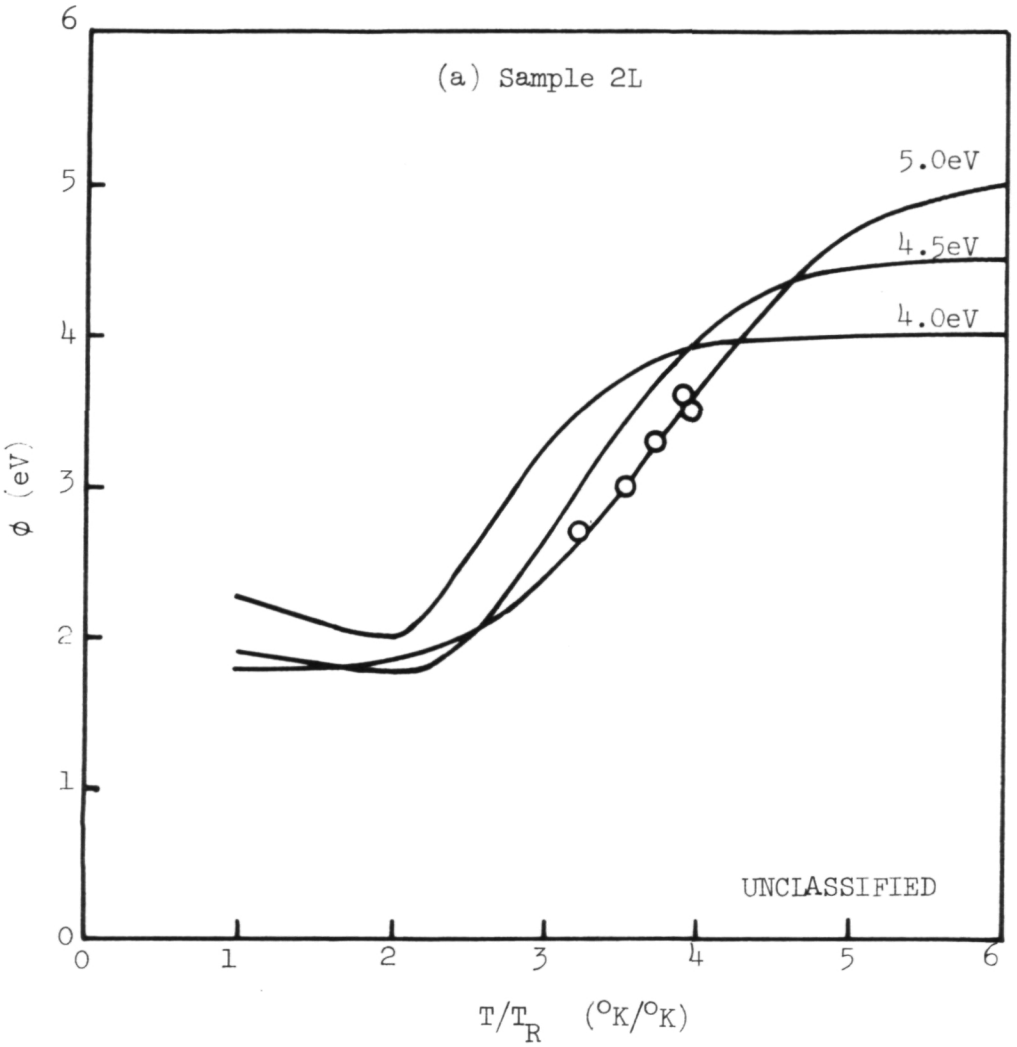

Fig. 3.14--(U) Rasor-Warner plots for five selected (110) oriented tungsten emitters (Page 1 of 5)

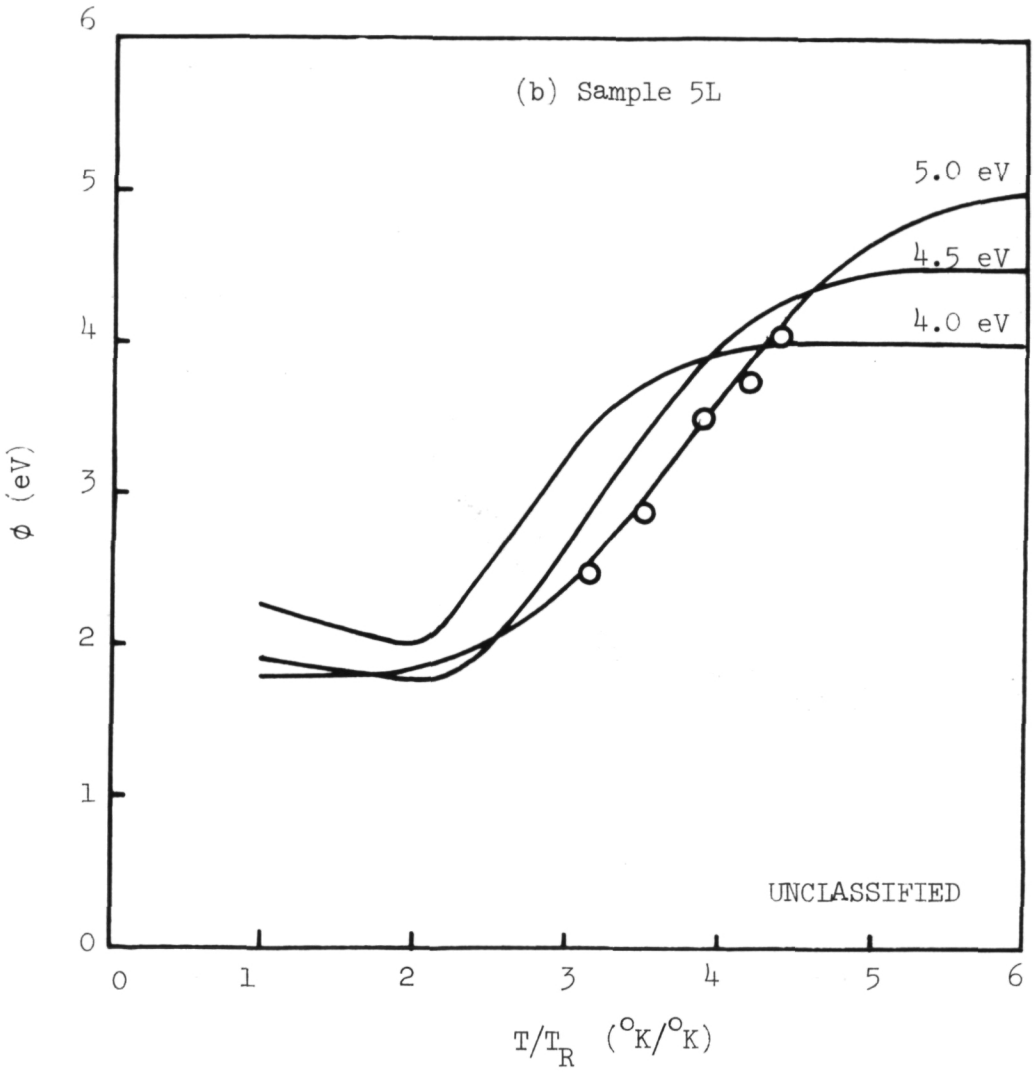

Fig. 3.14--(U) Rasor-Warner plots for five selected (110) oriented tungsten emitters (Page 2 of 5)

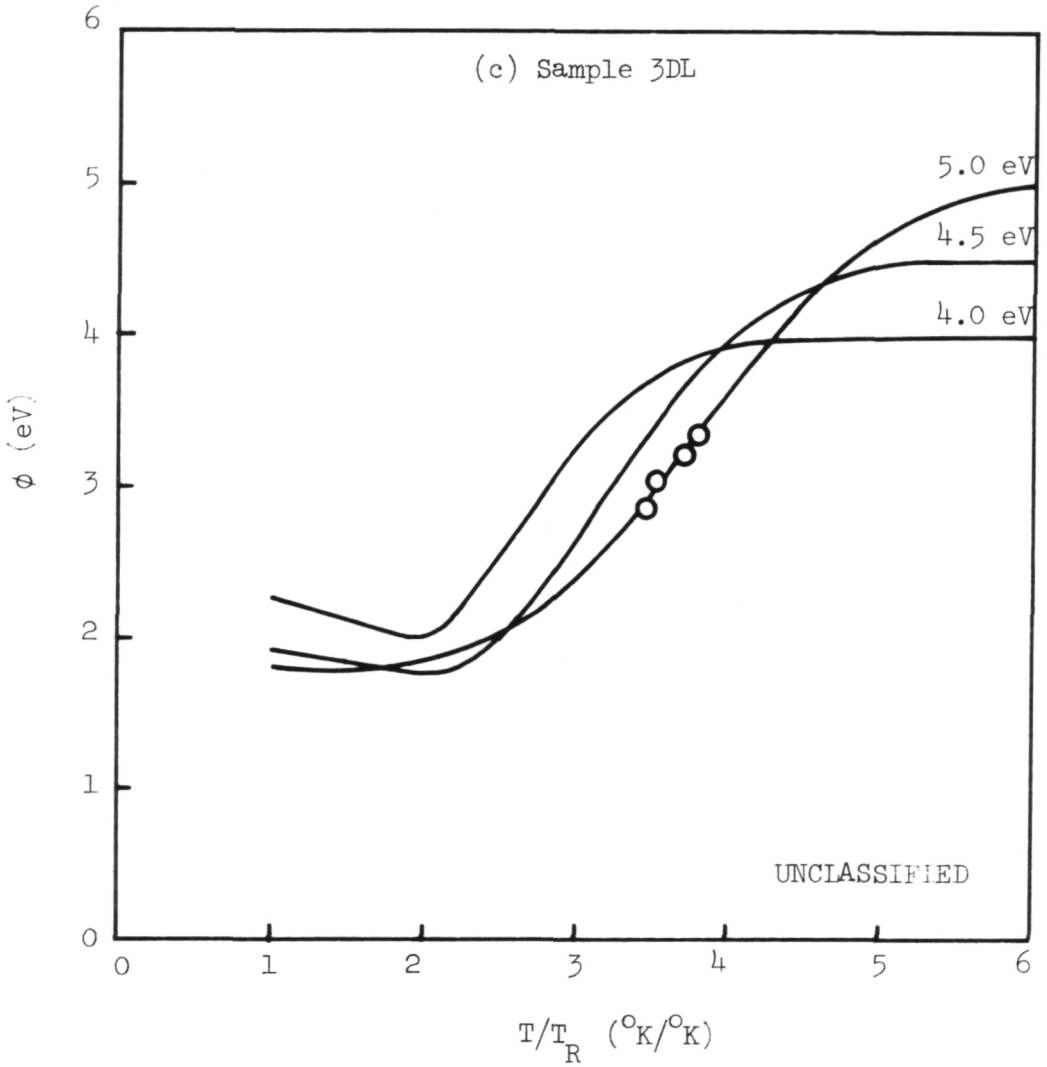

Fig. 3.14--(U) Rasor-Warner plots for five selected (110) oriented tungsten emitters (Page 3 of 5)

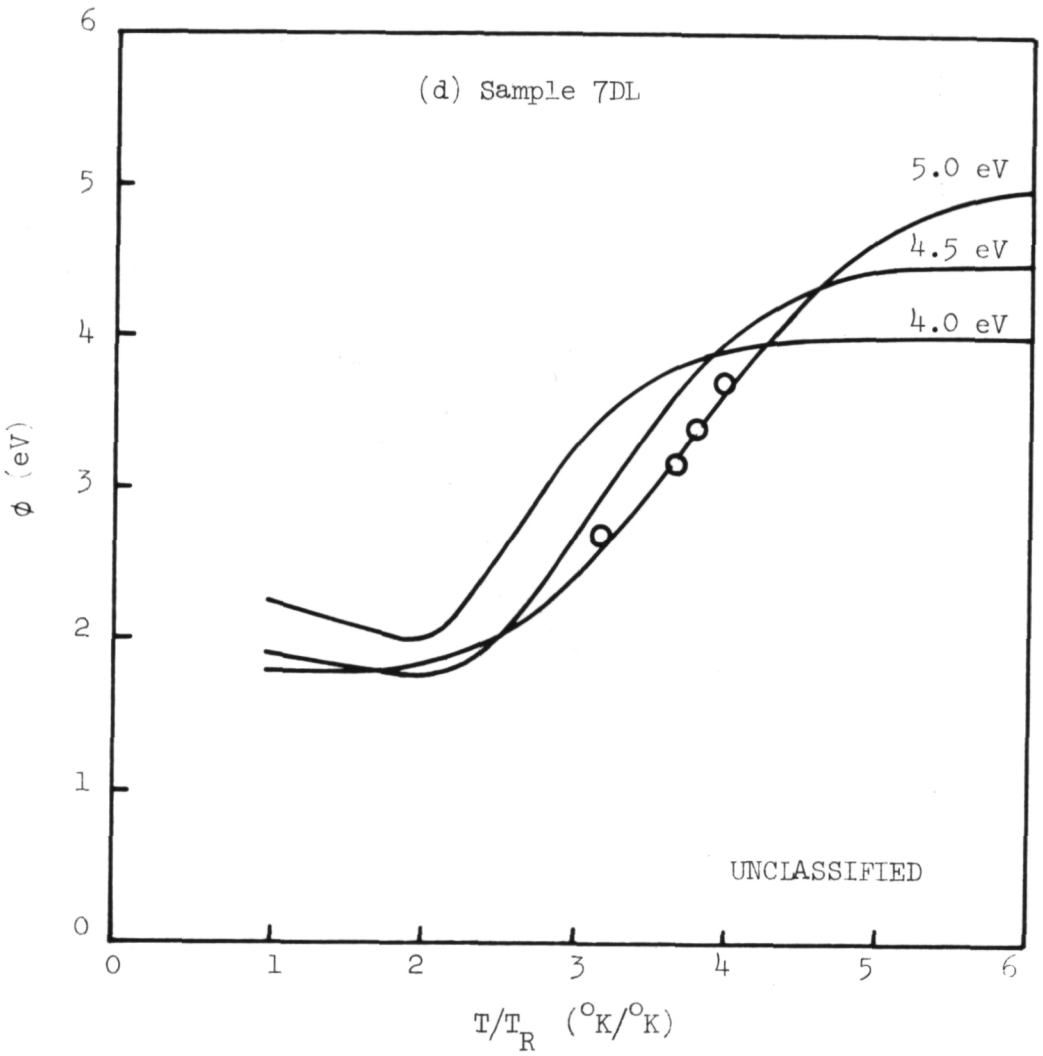

Fig. 3.14--(U) Rasor-Warner plots for five selected (110) oriented tungsten emitters (Page 4 of 5)

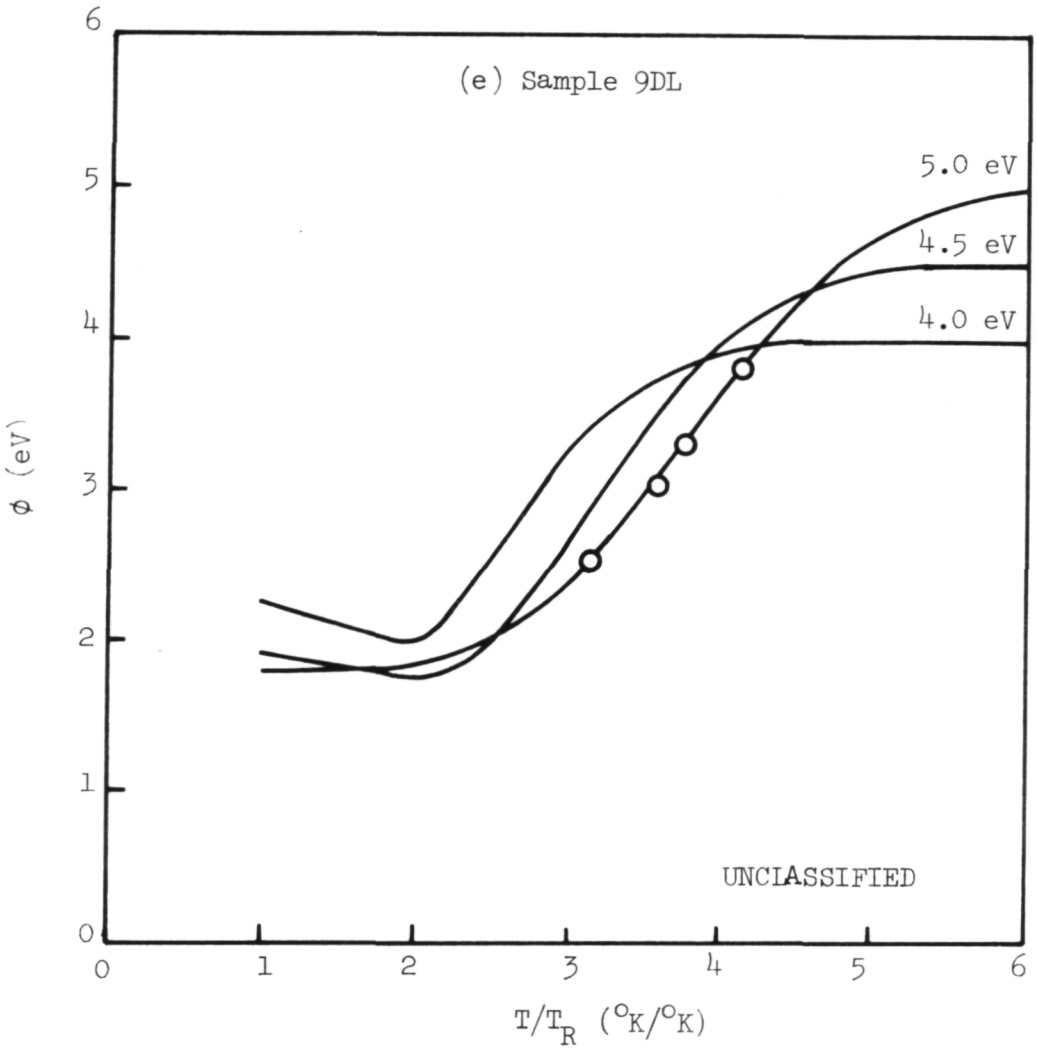

Fig. 3.14--(U) Rasor-Warner plots for five selected (110) oriented tungsten emitters (Page 5 of 5)

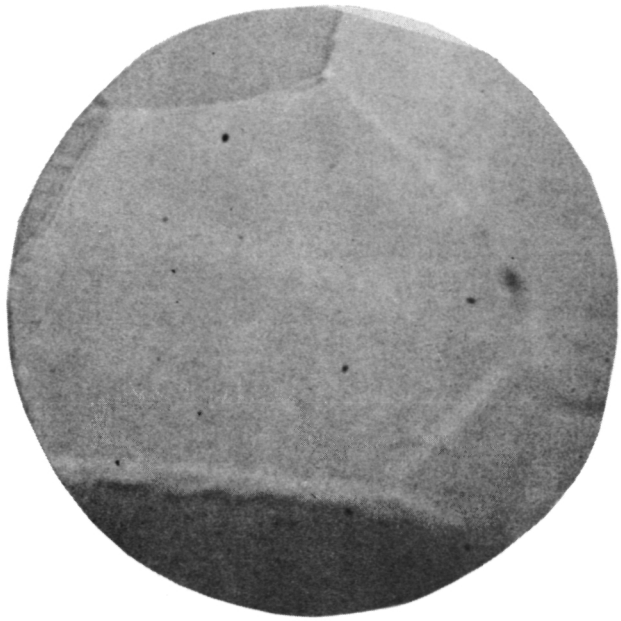

(a) Sample 2L

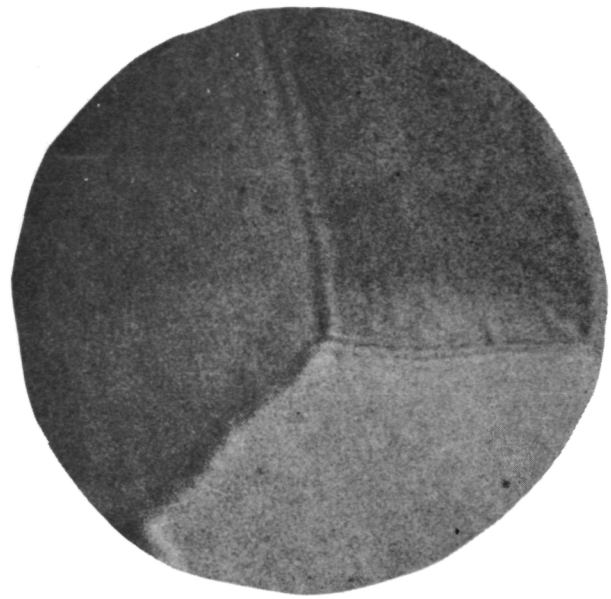

(b) Sample 5L

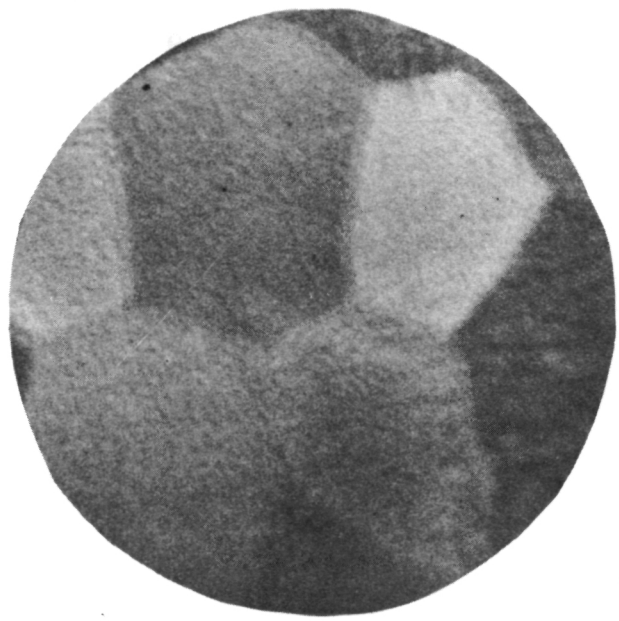

UNCLASSIFIED

(c) Sample 3DL

Fig. 3.15--(U) Thermionic emission patterns of the five selected tungsten emitters after emission test. 200X (Page 1 of 2)

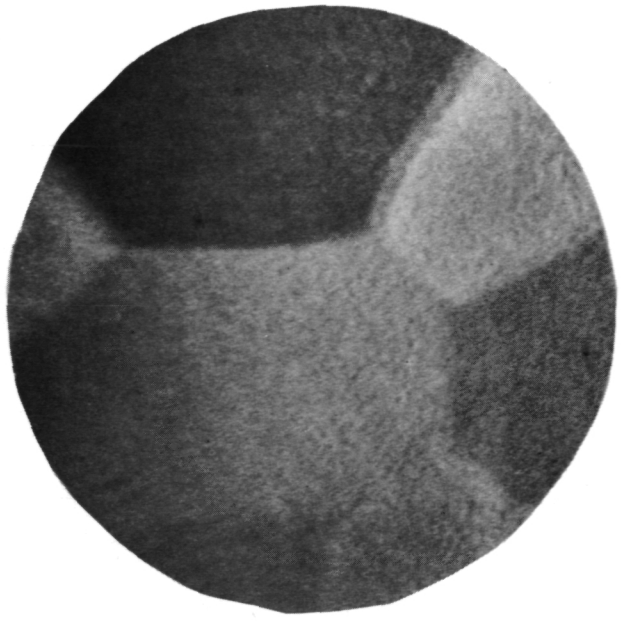

(d) Sample 7DL

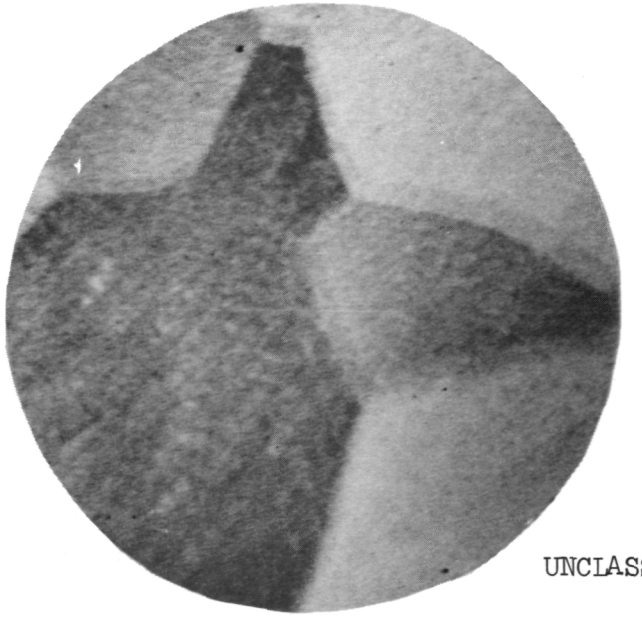

UNCLASSIFIED

(e) Sample 9DL

Fig. 3.15--(U) Thermionic emission patterns of the five selected tungsten emitters after emission test. 200X (Page 2 of 2)

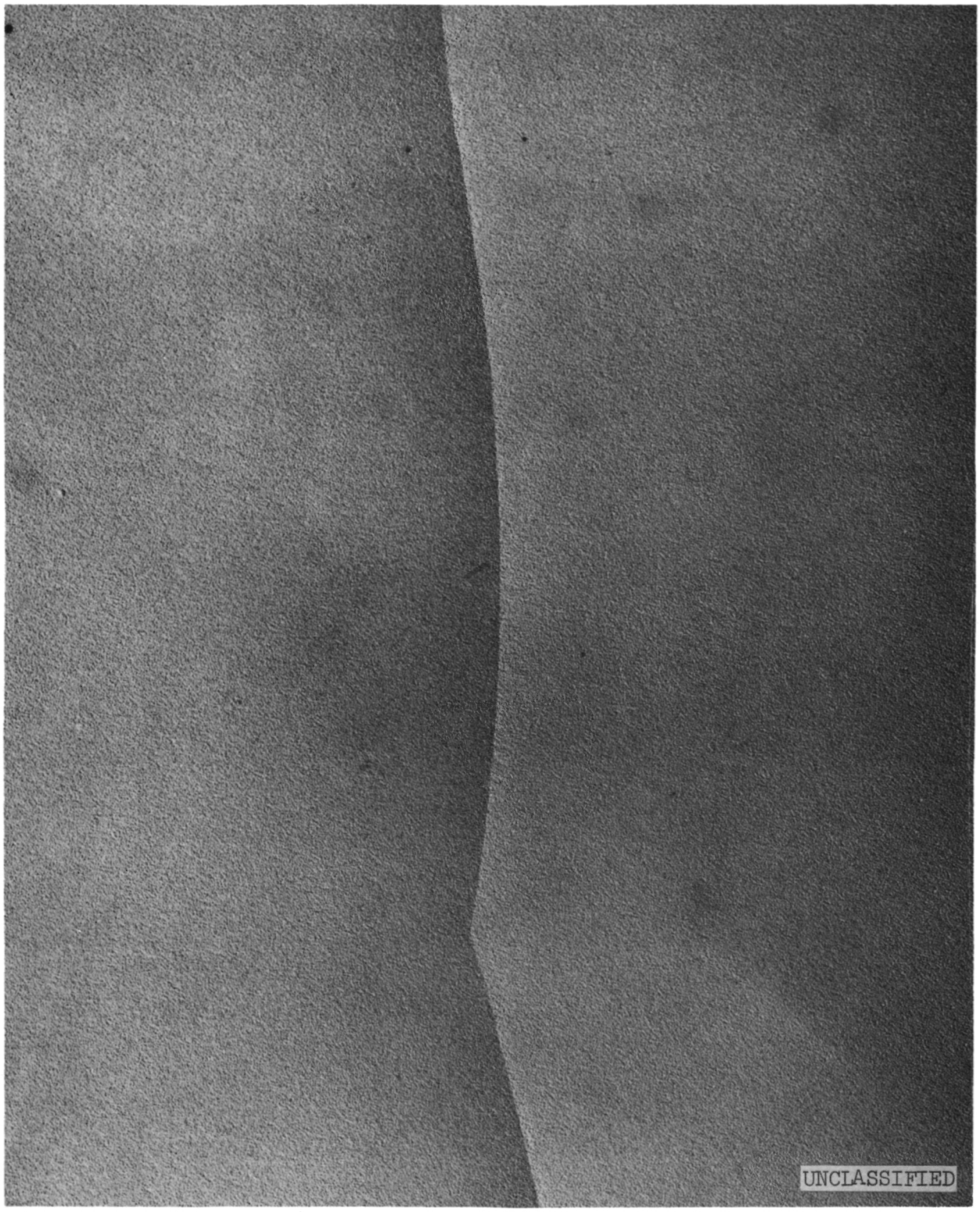

P 7879 17000X

Fig. 3.16(a)--(U) Electron micrograph of the surface of Sample 5L after emission test

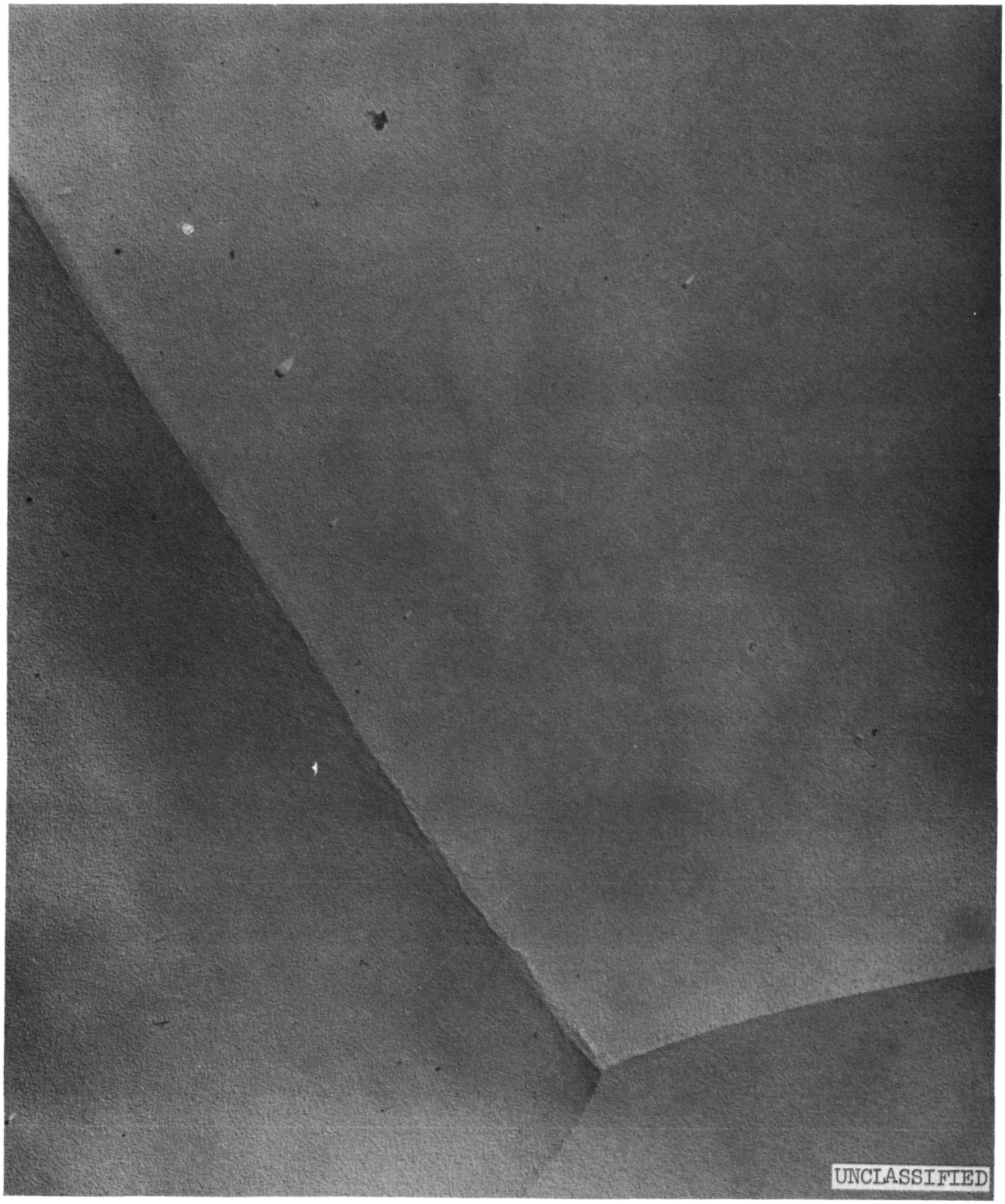

P 8890 17,000X

Fig. 3.16(b)--(U) Electron micrograph of the surface of Sample 7DL after emission test

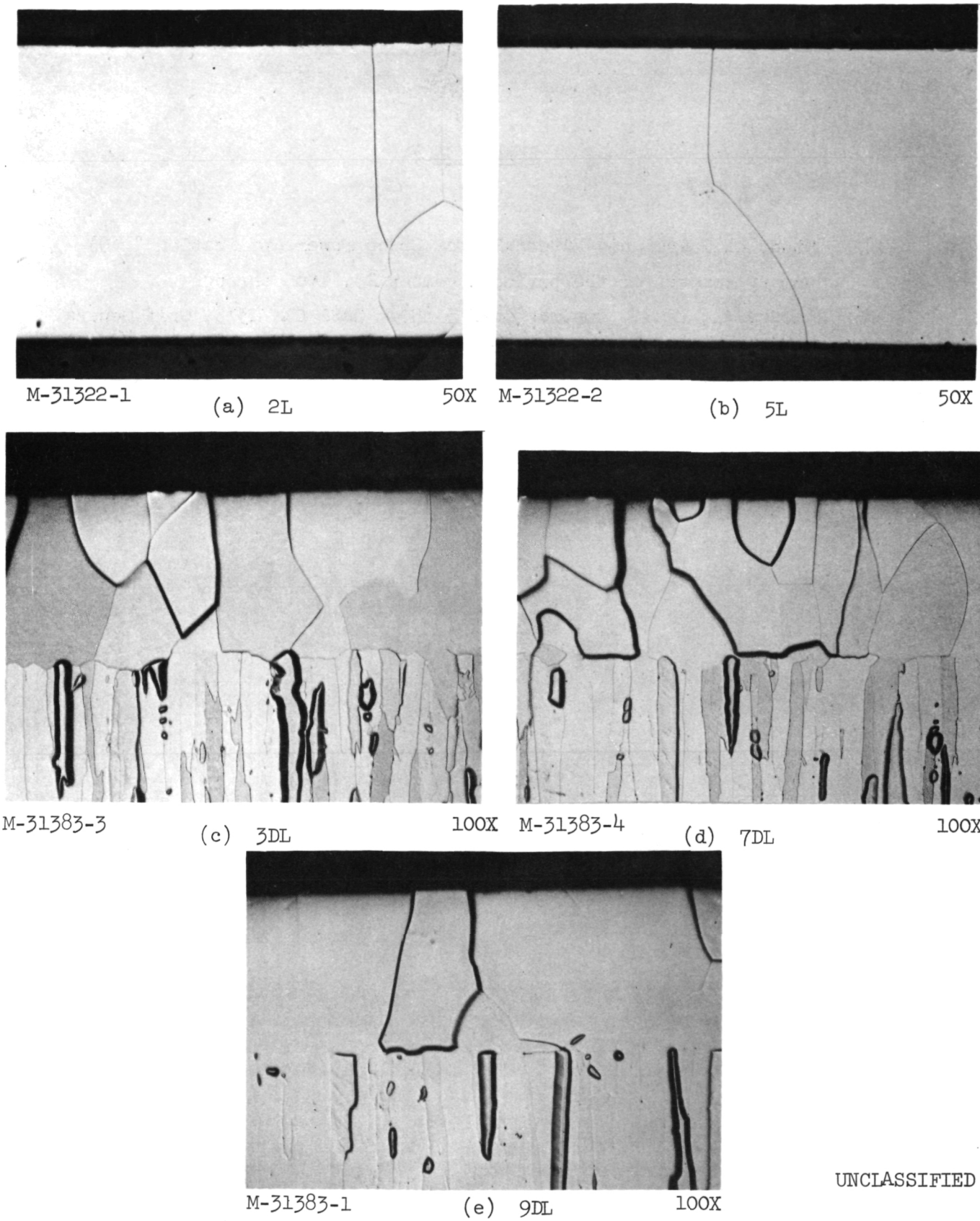

Fig. 3.17--(U) Microstructures of the cross sections of five tungsten emitters after emission test

REFERENCE

(1) "Study of Thermionic Materials for Space Power Application," (U) Summary Report for the period November 23, 1965 through January 31, 1967. Contract NAS 3-8504, NASA CR-72315, Gulf General Atomic Report, GA-7682. (C/RD)

CONFIDENTIAL

PART IV. UC-ZrC SINTERING STUDIES

(R. G. Hudson, M. H. Horner, L. Yang)

SUMMARY

(C-RD)(Gp-1) Fabrication procedures were established for the rigid control of the carbon to uranium ratio (C/U = 1.03-1.05) of 90UC-10ZrC and 50UC-50ZrC and the incorporation of 4-5 wt% tungsten into these carbide materials. The stability of the open pore structures of samples prepared with carbide powder size fractions of -44/+20 microns and -62/+20 microns was studied at 1600, 1700 and 1800°C for periods of 5000 hours by following the change of the ratio of their total surface areas to geometric surface areas (the SRF value) as a function of time, using the low pressure krypton adsorption technique. It was found that most of the decrease in the SRF values of these samples occurred during the first 500-1000 hours of heating time and that at the end of the 5000 hour test, their SRF values were still higher than that believe needed for efficient fission gas release. Post-test examinations indicated no significant change in the microstructures and chemical compositions of the samples studied. Some UWC_2 phases were observed along the grain boundaries and along the surfaces of some pores. This may be the contributing factor to the high temperature stability of the open pore structures of the samples studied.

CONFIDENTIAL
RESTRICTED DATA
ATOMIC ENERGY ACT 1954
GROUP 1

CONFIDENTIAL

INTRODUCTION

(C-RD)(Gp-1) The work carried out under this task represents a continuing effort to develop UC-ZrC as a fuel material for nuclear thermionic applications. Previous capsule irradiation studies[1] showed that the swelling of UC-ZrC at high temperatures could be minimized if a large amount of open porosity was incorporated into the fuel body to facilitate fission gas release. An isostatic cold pressing and sintering method was therefore developed for the preparation of such porous fuel bodies.[2] Subsequently long-term diffusion-emission studies[3] made on vapor-deposited fluoride tungsten clad UC-ZrC and metallurgical examinations of life tested thermionic emitters composed of these materials[4] indicated the need of the presence of a few mole percent of excess carbon and about a few weight percent of tungsten in UC-ZrC in order to maintain electron emission and chemical stability of the tungsten cladding at high temperatures. The fabrication method for such tungsten-containing hyperstoichiometric porous UC-ZrC fuel materials was described at the 1968 Palo Alto Thermionic Specialist Meeting.[5] In spite of such improvements, however, the usefulness of UC-ZrC as a thermionic fuel still depends upon whether the open pore structures could be maintained for long periods of time at high temperatures for efficient fission gas release. Experiments were therefore conducted to evaluate the stability of open pore structures of tungsten-containing hyperstoichiometric porous UC-ZrC samples by following the change of their total surface areas as a function of time during isothermal out-of-pile annealing in the temperature range 1600-1800°C. Such out-of-pile qualification constitutes a pre-requisite for in-pile application, since fuel bodies which cannot maintain open pore structures under out-of-pile isothermal conditions are not expected to do so under in-pile conditions where, in addition to thermal sintering, radiation induced sintering and vapor transport along the radial temperature gradient in a fuel body may further lead to the blockage of open porosities.

CONFIDENTIAL
RESTRICTED DATA
ATOMIC ENERGY ACT 1954
GROUP 1

CONFIDENTIAL

4.1. PREPARATION OF UC-ZrC SAMPLES

4.1.1. Physical and Chemical Characteristics of Samples

(C-RD)(Gp-1) The physical and chemical characteristics of the samples prepared for this study are listed below:

(1) Composition. – Both 90UC-10ZrC and 50UC-50ZrC samples were included in order to cover a range of uranium concentrations which are of nuclear thermionic interest.

(2) Size. – All samples studied were in the shape of right cylinders of 0.550 inch diameter and 0.2 inch thickness.

(3) Concentration of tungsten additions. – 4 wt% of tungsten was added to the carbide samples to insure that ample amount of tungsten would be available to satisfy the solubility of tungsten (~ 2 wt%) in these fuel materials.

(4) Degree of open porosity. – All samples had a high degree of open porosity. Surface roughness factor (SRF), defined as the ratio of true surface area to geometric surface area, of all samples were higher than 200. For the size of samples used this corresponded to a surface to volume ratio greater than 1360 cm^2 per c.c. of fuel body.

(5) Carbon to uranium ratio. – A carbon to uranium atom ratio of 1.03 to 1.05 was selected, allowing one carbon atom to each zirconium atom and one carbon atom to every two tungsten atoms. A lower bound of 1.03 was chosen to insure that the fuel was carbon rich after taking into account the analytical uncertainty which amounts to a carbon to uranium atom ratio of 0.02. An upper bound of 1.05 was chosen in order to prevent the carburization of the tungsten cladding.(5)

CONFIDENTIAL

RESTRICTED DATA
ATOMIC ENERGY ACT 1954
GROUP 1

(6) Ranges of carbide particle size used for preparing the samples. – Two particle size range, -44/+20 microns and -62/+20 microns were used to study the effect of particle size range on the stability of the open porosity in the samples prepared.

4.1.2. Procedures for Preparation Samples

(C-RD)(Gp-1) The following procedures were used for carbon control and incorporation of tungsten into samples used for this study. Special attention was paid to minimizing the loss of carbon by atmospheric contamination.

(1) Arc-melting weighed amounts of U, Zr, and C into carbide buttons in an argon atmosphere.

(2) Grinding the carbide buttons to -44μ size in an argon atmosphere in a glove box, the moisture content of which was kept below 10 ppm.

(3) Blending the required amount (~ 4 wt%) of W powder with the carbide powder in an argon atmosphere in a glove box.

(4) Cold pressing the blended powder to carbide cylinders in a steel die and homogenizing the pressed carbide cylinders at 2285°C for 6 hours in vacuum.

(5) Analyzing the composition of the homogenized carbide cylinder to insure that it contained the required uranium to carbon atom ratio.

(6) Grinding the homogenized carbide cylinder and sieving out the required powder size fraction in argon.

(7) Isostatically cold pressing the sieved out carbide powder fraction at 90,000 psi and sintering the pressed body at the selected sintering temperature for 16 hours. The selection of the sintering temperature is described in the next section.

RESTRICTED DATA
ATOMIC ENERGY ACT 1954
GROUP 1

(8) Grinding the sintered carbide body to 0.550 inch diameter and cutting the ground cylinder to discs of about 0.2 inch thickness.

(9) Annealing and outgassing the machined carbide discs in vacuum at 1800°C for 50 hours before determining the physical and chemical characteristics of these samples.

4.1.3. Selection of Sintering Temperature for 90UC-10ZrC and 50UC-50ZrC Samples

(C-RD)(Gp-1) Four 90UC-10ZrC samples and one 50UC-50ZrC sample were prepared according to the procedures described above. Of the 90UC-10ZrC samples, one was sintered at 2185°C, one was sintered at 2070°C and two were sintered at 1950°C. The 50UC-50ZrC sample was sintered at 2285°C. The SRF values of these samples were determined by the low pressure adsorption of Kr gas.(6) The results obtained are shown in Table 4.1 together with the physical and chemical characteristics of these samples. It can be seen that the 90UC-10ZrC sample sintered at 2185°C had a SRF value of only 143, which is below the specification set (SRF = 200) on the basis of post-irradiation annealing studies for efficient fission gas release(6) from samples of similar size and configuration, indicating that a sintering temperature of 2185°C is too high for achieving a high degree of open porosity in 90UC-10ZrC. The other three 90UC-10ZrC samples were heated at 1800°C for 233 hours and their SRF values were again determined. The results are also shown in Table 4.1. The 90UC-10ZrC samples, sintered either at 1950°C or at 2070°C all had SRF values higher than 200, both in the outgassed state and after an additional 233 hours at 1800°C. The 1800°C heat treatment, however, introducted a smaller percentage decrease in the SRF value of the 90UC-10ZrC sample sintered at 2070°C than that of the 90UC-10ZrC samples sintered at 1950°C. The two samples sintered at 1950°C, 50009B and 50009B and C, were heated at 1800°C and 1600°C respectively for longer periods of time. The changes of SRF values with time of heating are shown in Fig. 4.1. It can be seen that although the change of SRF with time at 1600°C was insignificant in 2000 hours, yet at 1800°C, the SRF value dropped by a factor of three in the same period of time. On the basis of these observations, a sintering temperature of 2070°C was selected for the 90UC-10ZrC sample.

RESTRICTED DATA
ATOMIC ENERGY ACT 1954
GROUP 1

Table 4.1

(C-RD)(Gp-1) SURFACE ROUGHNESS FACTORS OF UC-ZrC SAMPLES SINTERED AT VARIOUS TEMPERATURES AND EFFECT OF ANNEALING AT 1800°C FOR 233 HOURS

(This table is classified Confidential-Restricted Data-Group 1)

Sample Number	Composition	Carbon to Uranium Ratio (C/U)	Powder Size Fraction (Microns)	Sintering Temperature (°C)	Density (% Theorectical)	Surface Roughness Factor (cm^2/cm^2)	Density (% Theoretical) After 233 hrs at 1800°C	Surface Roughness Factor (cm^2/cm^2) After 233 hrs at 1800°C
50005D (90/10, 4% W)	$U_{0.873}Zr_{0.097}W_{0.0302}C_{1.021}$	1.042	-44/+20	2185	87.2	143	--	--
50009A (90/10, 4% W)	$U_{0.876}Zr_{0.099}W_{0.0249}C_{1.035}$	1.057	-62/+20	2070	81.0	294	80.7	251
50009 B & C (90/10, 4% W)	$U_{0.875}Zr_{0.100}W_{0.0251}C_{1.027}$	1.053	-62/+20	1950	75.4	404	76.0	335
50009B (90/10, 4% W)	$U_{0.876}Zr_{0.0975}W_{0.0268}C_{1.034}$	1.042	-44/+20	1950	77.8	496	81.4	345
50002 (50/50, 5% W)	$U_{0.496}Zr_{0.482}W_{0.0235}C_{1.010}$	1.038	-44/+20	2285	82.2	447	81.9	394

Note: The compositions, densities, and surface roughness factors were determined after the samples were annealed and outgassed for 50 hours in vacuum at 1800°C

CONFIDENTIAL
CONFIDENTIAL
RESTRICTED DATA
ATOMIC ENERGY ACT 1954
GROUP 1

CONFIDENTIAL

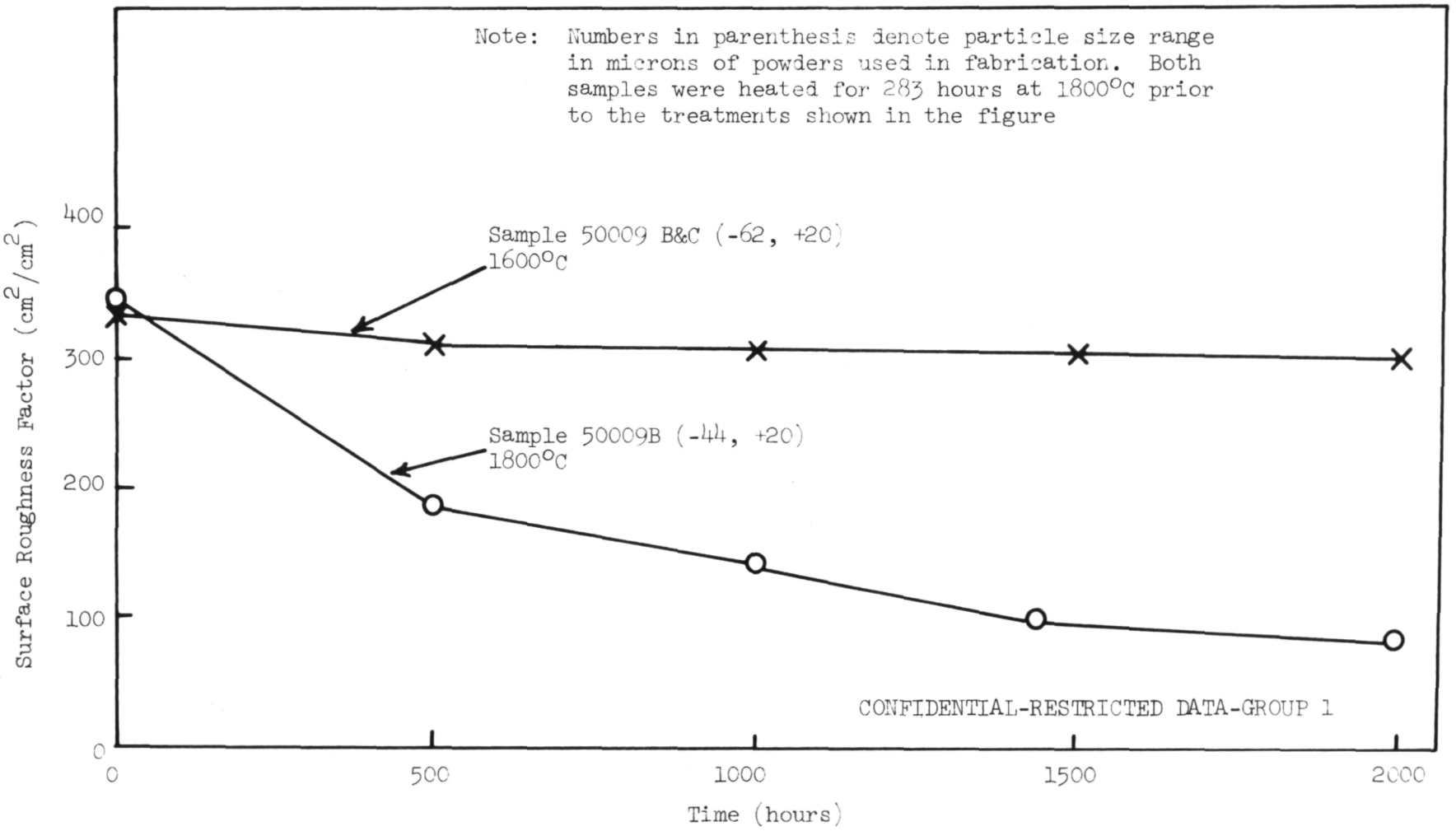

Fig. 4.1--(U) Surface roughness factor as a function of time at 1600°C and 1800°C for 90UC-10ZrC samples sintered at 1950°C

RESTRICTED DATA
ATOMIC ENERGY ACT 1954
GROUP 1

CONFIDENTIAL

(C-RD)(Gp-1) For the 50UC-50ZrC sample sintered at 2285°C, the change of SRF value was small after 233 hours at 1800°C, and was substantially higher than 200. No attempt was therefore made to vary the sintering temperature, and 2285°C was selected as the sintering temperature for all 50UC-50ZrC samples.

4.2. SAMPLE CHARACTERIZATION

(C-RD)(Gp-1) Sample characterization includes determination of: (1) uranium, zirconium and tungsten contents by X-ray fluorescence spectroscopy, (2) carbon content by combustion, (3) oxygen, nitrogen and hydrogen contents by fusion analysis, (4) density from weight and dimensions, (5) true surface area by low pressure krypton adsorption, and (6) microstructure details by metallographic and electron microprobe examinations.

(C-RD)(Gp-1) As shown in Table 4.2, a total of eight carbide cylinders (a, a', b, b', c, c', d, d') were prepared for this study, with a, b, c, and d being duplicates of a', b', c', and d' respectively (i.e. prepared from the same batch of carbide powder). Samples obtained from the same carbide cylinder, (such as carbide cylinder "a") are represented by designations indicating this common source (such as S_1a and S_2a).

(C-RD)(Gp-1) The compositions, stoichiometries, interstitial impurity contents, initial densities (expressed as percentage of the theoretical values) and initial SRF values of the samples used in this study are included in Table 4.2. It is interesting to see that while the change of the carbide powder size fraction from -44/+20 microns to -62/+20 microns did not appreciably affect the density and the SRF values of the 90UC-10ZrC samples, the same change in carbide powder size fraction increased the density of the 50UC-50ZrC samples by as much as 7% and reduced its SRF values by almost a factor of two. Figures 4.2(a) and (b), and Figs. 4.3(a) and (b) show respectively the microstructures of unetched 90UC-10ZrC and 50UC-50ZrC prepared from the -44/+20 and -62/+20 micron powder fractions. It is apparent that the -44/+20 powder size fraction yielded much finer pore structures in both the 90UC-10ZrC and the 50UC-50ZrC samples. Since the pore structures, density and SRF value are determined by both the range of the powder size and the distribution of the size within the range specified, an understanding

RESTRICTED DATA
ATOMIC ENERGY ACT 1954
GROUP 1

Table 4.2

(U) CHARACTERISTICS OF UC-ZrC SAMPLES PREPARED

(This table is classified Confidential-Restricted Data-Group 1)

Set Designation	Carbide Cylinder Designation	Carbide Particle Size Range	Sintering Temperature (°C)	Composition*	Gaseous Impurity Content (ppm)			Carbide Sample Designation	% Theoretical Density	SRF (cm^2/cm^2)
					N	O	H			
I	a	-44μ/+20μ	2070	$U_{0.844}Zr_{0.104}W_{0.052}C_{1.002}$ C/U = 1.03	125	294	4	S_1a S_2a S_3a	76.7 77.4 76.4	403 394 403
	a'	-44μ/+20μ	2070	$U_{0.845}Zr_{0.105}W_{0.050}C_{1.015}$ C/U = 1.05	287	246	7	S_1a' S_2a' S_3a'	76.4 77.5 77.5	400 374 394
II	b	-62μ/+20μ	2070	$U_{0.850}Zr_{0.098}W_{0.052}C_{1.018}$ C/U = 1.05	122	290	25	S_1b S_2b S_3b	76.1 77.4 77.2	380 356 394
	b'	-62μ/+20μ	2070	$U_{0.837}Zr_{0.102}W_{0.061}C_{1.020}$ C/U = 1.05	120	283	11	S_1b' S_2b' S_3b'	73.4 71.9 73.6	473 436 468
III	c	-44μ/+20μ	2285	$U_{0.487}Zr_{0.475}W_{0.038}C_{1.001}$ C/U = 1.04	188	219	8	S_1c S_2c S_3c	79.3 79.4 78.4	516 464 476
	c'	-44μ/+20μ	2285	$U_{0.498}Zr_{0.468}W_{0.034}C_{1.002}$ C/U = 1.05	267	343	17	S_1c' S_2c' S_3c'	76.9 76.9 78.5	509 498 482
IV	d	-62μ/+20μ	2285	$U_{0.477}Zr_{0.475}W_{0.048}C_{1.000}$ C/U = 1.05	259	159	5	S_1d S_2d S_3d	81.8 81.4 82.7	247 277 263
	d'	-62μ/+20μ	2285	$U_{0.474}Zr_{0.475}W_{0.051}C_{1.000}$ C/U = 1.05	174	186	4	S_1d' S_2d' S_3d'	83.4 83.8 83.0	271 282 270

*Determined after annealing and outgassing for 50 hours at 1800°C

Note: Samples of the S_1 series were studied at 1800°C
Samples of the S_2 series were studied at 1600°C
Samples of the S_3 series were studied at 1700°C

CONFIDENTIAL
RESTRICTED DATA
ATOMIC ENERGY ACT 1954
GROUP 1
CONFIDENTIAL

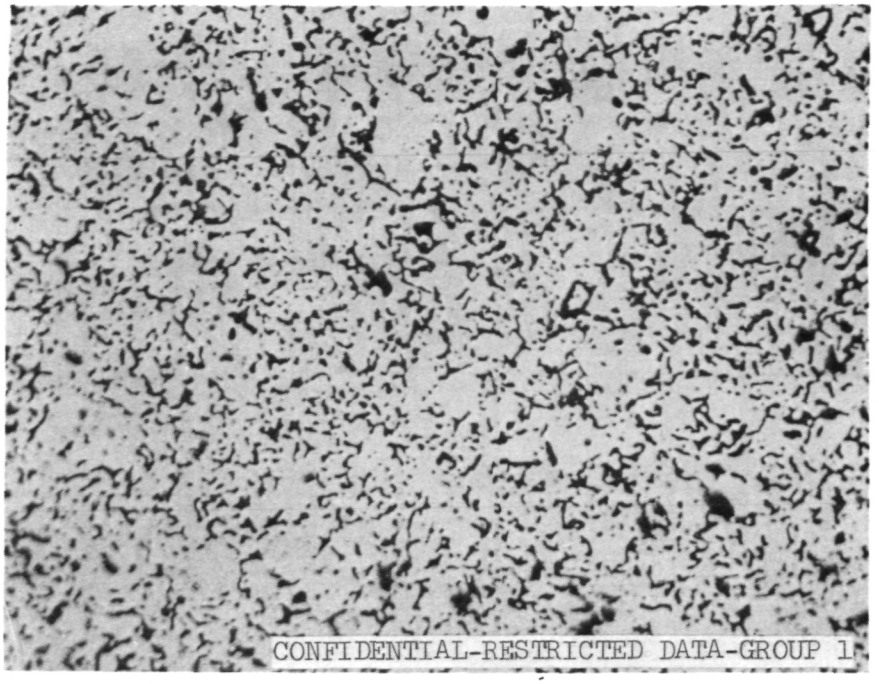

M 21488-1 250X

(a) Prepared from -44/+20 micron powder. Obtained from carbide cylinder (a) of Table 4.2

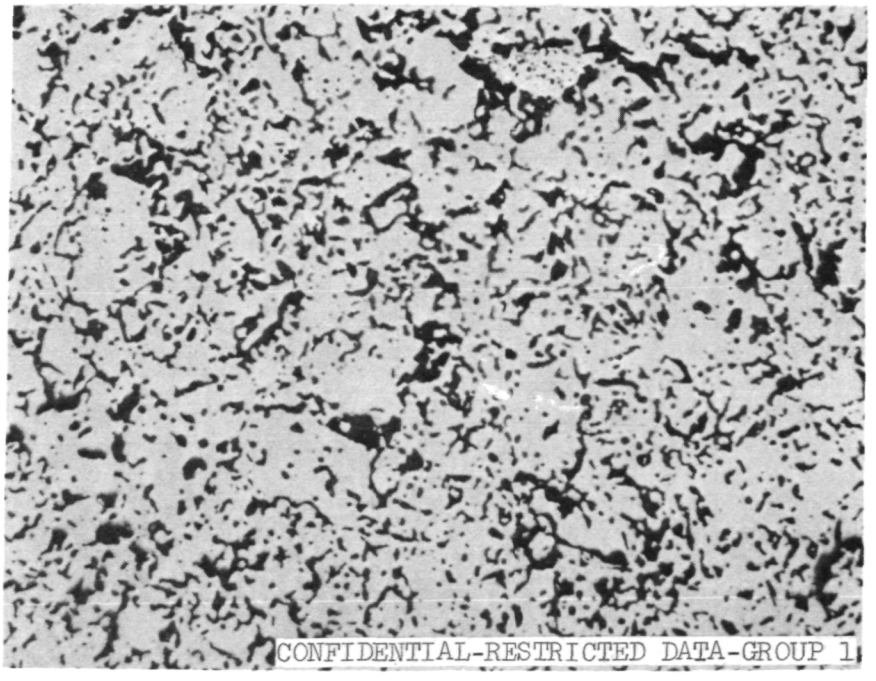

M 21490-1 250X

(b) Prepared from -62/+20 micron powder. Obtained from carbide cylinder (b) of Table 4.2

Fig. 4.2--(C-RD)(Gp-1) Microstructures of unetched hyperstoichiometric 90UC-10ZrC containing tungsten addition

RESTRICTED DATA
ATOMIC ENERGY ACT 1954
GROUP 1

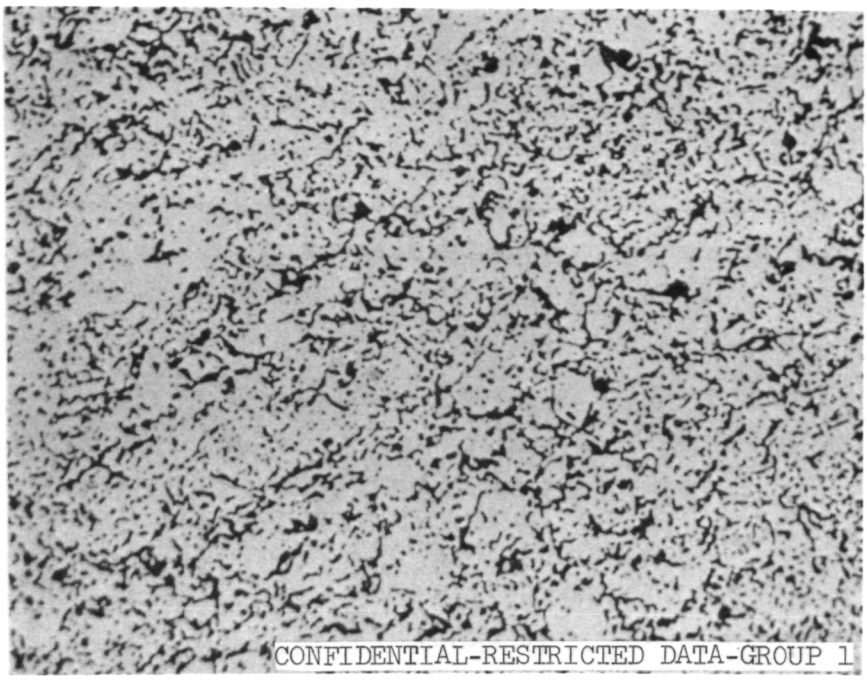

M 21492-1 250X

(a) Prepared from -44/+20 micron powder. Obtained from carbide cylinder "c" of Table 4.2

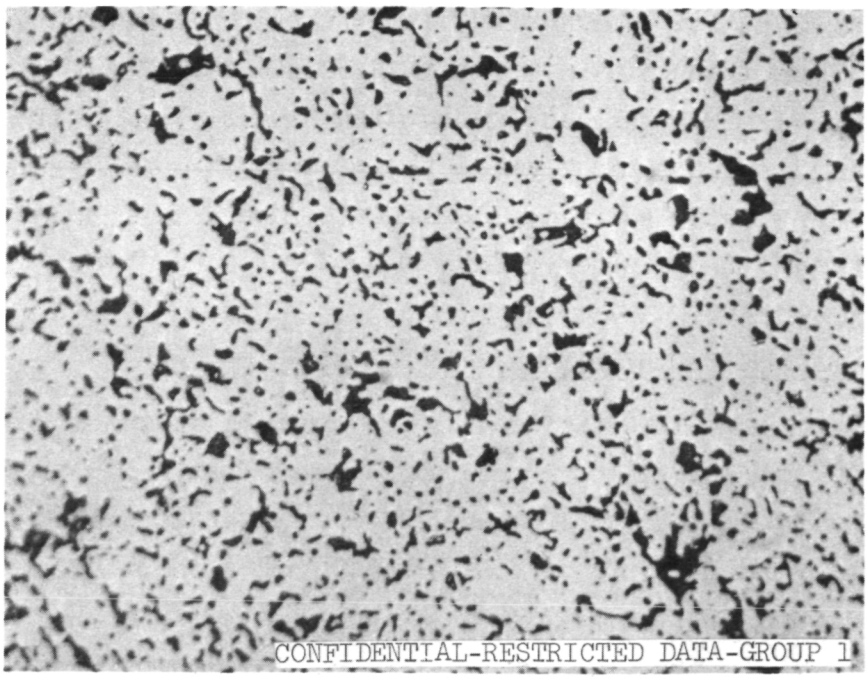

M 21494-1 250X

(b) Prepared from -62/+20 micron powder. Obtained from carbide cylinder "d" of Table 4.2

Fig. 4.3--(C-RD)(Gp-1) Microstructures of unetched hyperstoichiometric 50UC-50ZrC containing tungsten addition

RESTRICTED DATA
ATOMIC ENERGY ACT 1954
GROUP 1

of the observed changes in these properties would have to wait for the analysis of the size spectrum of the carbide powder used. Figure 4.4 shows the etched microstructures of a 90UC-10ZrC sample taken from the carbide cylinder "b' " from which Samples S_1b', S_2b' and S_3b' were obtained. Electron microprobe examinations revealed that there existed two kinds of secondary phase precipitates in the 90UC-10ZrC matrix containing a few percent of dissolved tungsten. One of them was a high tungsten phase having a composition close to that of the UWC_2 phase, while the other contained about the same tungsten concentration as that of the 90UC-10ZrC matrix but lower uranium concentration (~55-70% by weight) and higher zirconium concentration (~20-30% by weight) than that of the 90UC-10ZrC matrix. High zirconium phase precipitates were less prevalent than high tungsten phase precipitates and both tend to be small (<20-30 microns). X-ray study also indicated the presence of a very small amount of pure tungsten particles which were probably too small to be detected by the electron microprobe. Figure 4.5 shows the etched microstructures of a 50UC-50ZrC sample taken from the carbide cylinder "d" from which Samples S_1d, S_2d and S_3d were obtained. Electron microprobe examinations showed that the amount of secondary phase precipitates was much smaller than that in the 90UC-10ZrC sample. The 50UC-50ZrC carbide matrix contained a few percent of dissolved tungsten, while the small amount of secondary phase appeared to be UWC_2 containing about a few percent of zirconium. More detailed investigations are needed to elucidate the phase relationship of the quaternery system U-Zr-W-C.

4.3. EVALUATION OF STABILITY OF OPEN POROSITY

(C-RD)(Gp-1) The stability of the open porosities in the 90UC-10ZrC and the 50UC-50ZrC samples prepared was evaluated at 1600°C, 1700°C and 1800°C for periods of 5000 hours. The samples were heated at the planned temperature in a vacuum resistance furnace controlled to ±15°C for various pre-determined periods of time. Their densities were then deduced from weight and dimension data and the true surface areas were measured by using the low pressure krypton adsorption technique after each heating period. In Figs. 4.6, 4.7 and 4.8, the SRF values of the samples studied are plotted as a function of heating time at 1600°C, 1700°C and 1800°C respectively, and the densities

RESTRICTED DATA
ATOMIC ENERGY ACT 1954
GROUP 1

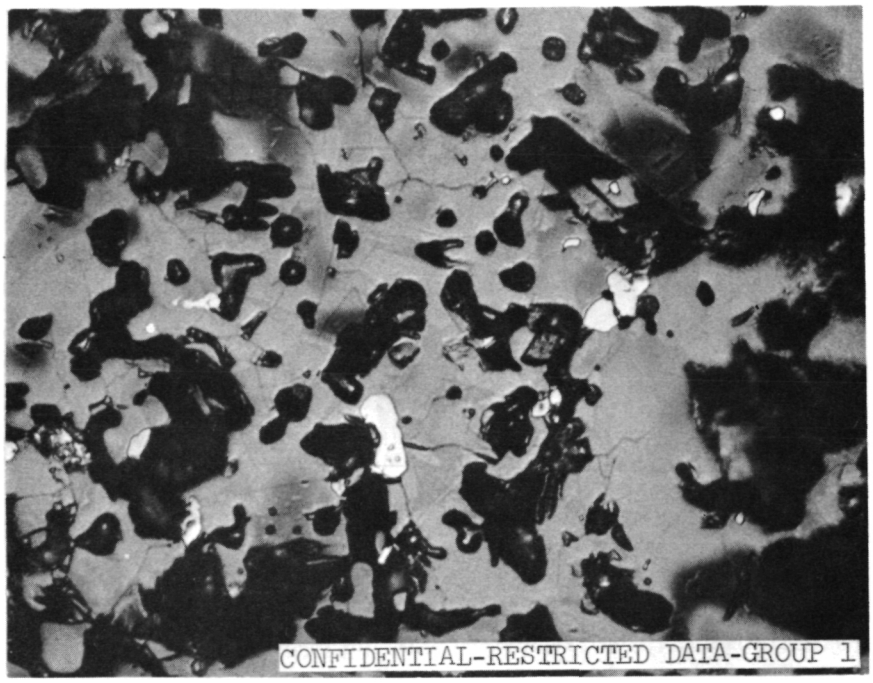

M 21491-2 1000X

Fig. 4.4--(C-RD)(Gp-1) Etched microstructures of hyperstoichiometric 90UC-10ZrC containing tungsten addition. Sample obtained from carbide cylinder "b'" of Table 4.2

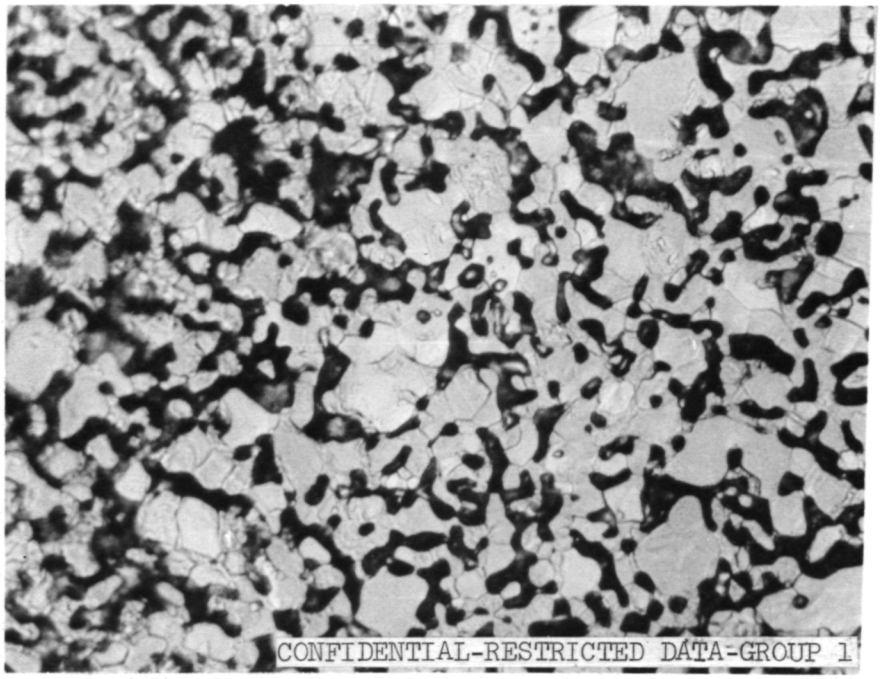

M 20977-1 1000X

Fig. 4.5--(C-RD)(Gp-1) Etched microstructures of hyperstoichiometric 50UC-50ZrC containing tungsten addition. Sample obtained from carbide cylinder "d" of Table 4.2

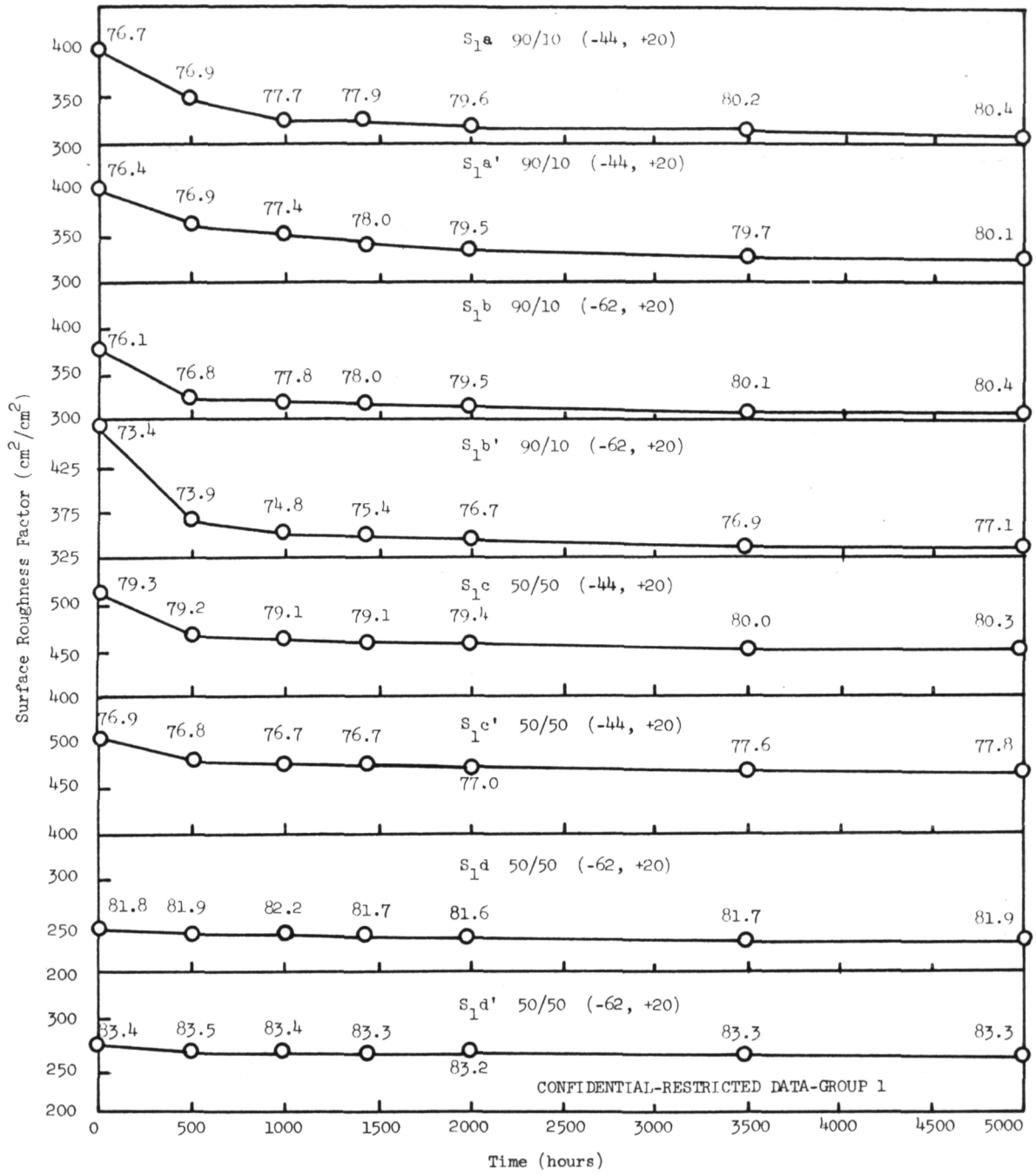

Fig. 4.6--(U) Surface roughness factor as a function of time at 1800°C for 90UC-10ZrC and 50UC-50ZrC samples

Note: Numbers in parenthesis denote particle size range in microns of powders used in fabrication. Numbers beside each data point represent percentage of theoretical density of the sample

RESTRICTED DATA
ATOMIC ENERGY ACT 1954
GROUP 1

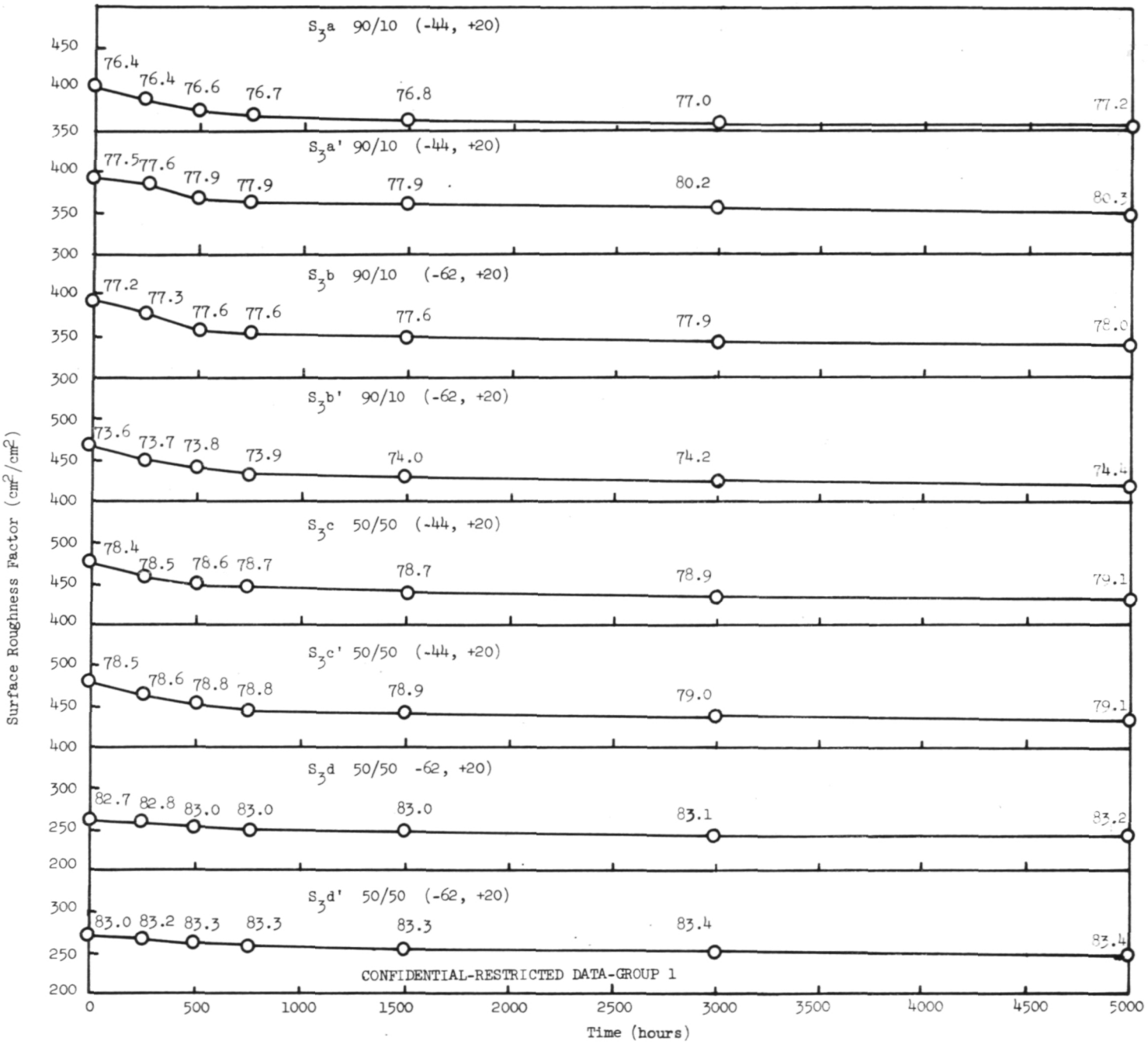

Fig. 4.7--(U) Surface roughness factor as a function of time at 1700°C for 90UC-10ZrC and 50UC-50ZrC samples

Note: Numbers in parenthesis denote particle size range in microns of power used in fabrication. Numbers beside each data point represent percentage of theoretical density of the sample.

RESTRICTED DATA
ATOMIC ENERGY ACT 1954
GROUP 1

CONFIDENTIAL

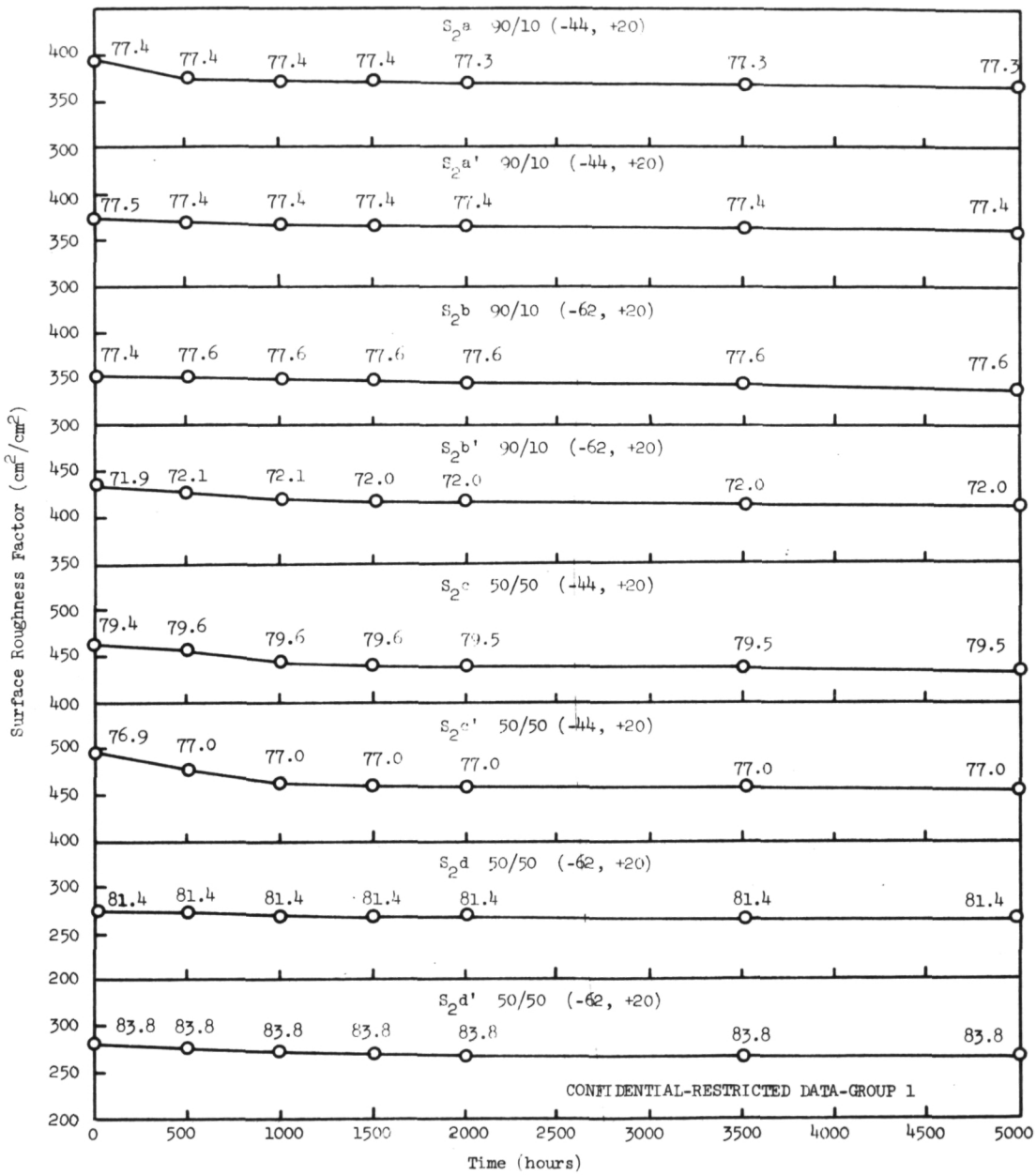

Fig. 4.8--(U) Surface roughness factor as a function of time at 1600°C for 90UC-10ZrC and 50UC-50ZrC samples

Note: Numbers in parenthesis denote particle size range in microns of powders used in fabrication. Numbers beside each data point represent percentage of theoretical density of the sample.

CONFIDENTIAL
RESTRICTED DATA
ATOMIC ENERGY ACT 1954
GROUP 1

are shown beside the data points. From these results, the following conclusions can be drawn.

(1) The initial SRF values of the 90UC-10ZrC samples were in the range of 320-450, and the initial SRF values of the 50UC-50ZrC samples were in the range of 250-520. (250-275 for samples derived from -62/+20 micron carbide powder and 470-520 for samples derived from -44/+20 micron carbide powder.) These values were in general higher than the SRF values of 90UC-10ZrC (170-360 for samples derived from -44/+20 micron carbide powder) and 50UC-50ZrC (200-400 for samples derived from -44/+20 micron carbide powder) samples prepared previously without the addition of tungsten.[2]

(2) Most of the decreases in SRF values occurred during the first 500-1000 hours of heating time. For a given carbide composition and a given temperature, the rate of decrease during this period was higher for samples with higher initial SRF values.

(3) After this initial period of adjustment, the change of SRF values with further heating was slight. The average "steady state" SRF values for the 90UC-10ZrC samples studied were: 1600°C, 370; 1700°C, 350; 1800°C, 320. For 50UC-50ZrC, the "steady state" SRF values were about 450 at 1600°C, 1700°C or 1800°C for samples prepared from -44/+20 micron powder, and about 250 at 1600°C, 1700°C or 1800°C for samples prepared from -62/+20 micron powder. These values are equal or higher than the specified SRF value (200) set on the basis of post-irradiation annealing studies of fission gas release rates from porous UC-ZrC fuel bodies. This indicates that the 90UC-10ZrC and the 50UC-50ZrC samples studied in this work may be capable of maintaining open porosities for efficient fission gas release for long periods of time in the temperature range studied. Since the "steady-state" SRF values of 90UC-10ZrC and 50UC-50ZrC for 1600°C, 1700°C and 1800°C are all higher than 200, there is no incentive in operating these carbide fuels at temperatures below 1800°C from the point of view of maintaining

RESTRICTED DATA
ATOMIC ENERGY ACT 1954
GROUP 1

CONFIDENTIAL

open pore structures. On the contrary, an operating temperature of 1800°C is preferred over 1600°C because the fission gas diffusion rates in the carbide matrix increase exponentially with temperature. Such considerations, however, are based mainly on the sintering results. Other material properties, such as fuel transport rates through the cladding and creep strength of the fuel and the cladding materials, would have to be taken into consideration in the selection of the operating temperature of an emitter for nuclear thermionic application.

4.4. POST-TEST EVALUATION

4.4.1. Microstructures

(C-RD)(Gp-1) Figures 4.9 through 4.12 show the typical etched and unetched microstructures of the test samples after the sintering study. Generally speaking, the change in pore structures of these samples before and after the 5000 hour tests, if any, is slight (compare Figs. 4.9 through 4.12 with Figs. 4.2 and 4.3). This is in agreement with the findings that the maximum observed change in bulk density was about 4%, which occurred in the case of the 90UC-10ZrC samples tested at 1800°C. It seems that the major portion of the change in the total surface area was due to the local blockage of the open pores at narrow passages during the high temperature treatment, which converted some of the open pores to closed pores but contributed very little to the change in the bulk density. When the samples were etched and examined with electron microprobe, it was found that both the 90UC-10ZrC and the 50UC-50ZrC samples contained about a few percent of dissolved tungsten and precipitates of UWC_2 and tungsten phases. The UWC_2 precipitates in the 50UC-50ZrC samples, however, were much smaller than that in the 90UC-90ZrC samples. Small amounts of UWC_2 phase were also detected in the grain boundaries and along the surfaces of some pores. The presence of such UWC_2 phase along the surfaces of the pores may be the reason why the tungsten-containing UC-ZrC fuel material can maintain stability of their pore structures at high temperatures.

CONFIDENTIAL
RESTRICTED DATA
ATOMIC ENERGY ACT 1954
GROUP 1

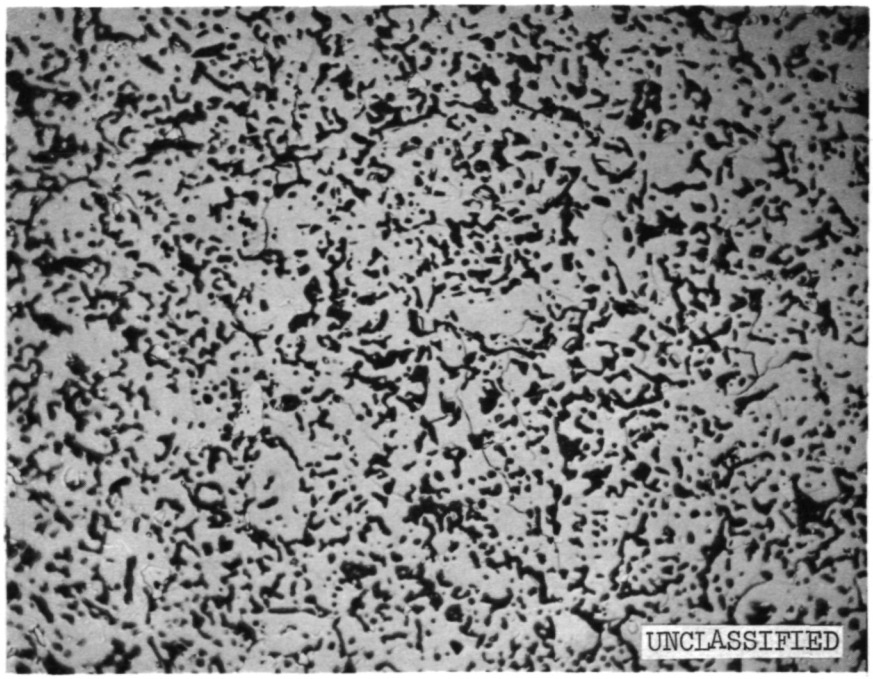

M 31150-2 250X

(a) Sample S_1a, unetched
Tested at 1800°C

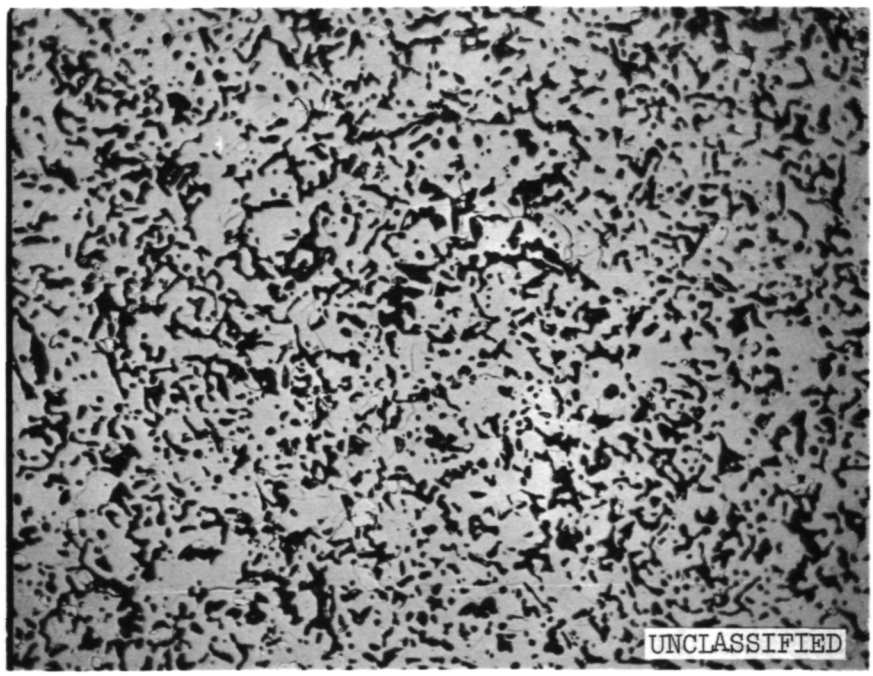

M 31150-1 250X

(b) Sample S_3a, unetched
Tested at 1700°C

Fig. 4.9--(U) Microstructures of 90UC-10ZrC samples prepared from -44/+20 micron powder after 5000 hours at 1800°C, 1700°C and 1600°C (page 1 of 2)

(This page is Unclassified)

RESTRICTED DATA
ATOMIC ENERGY ACT 1954
GROUP 1

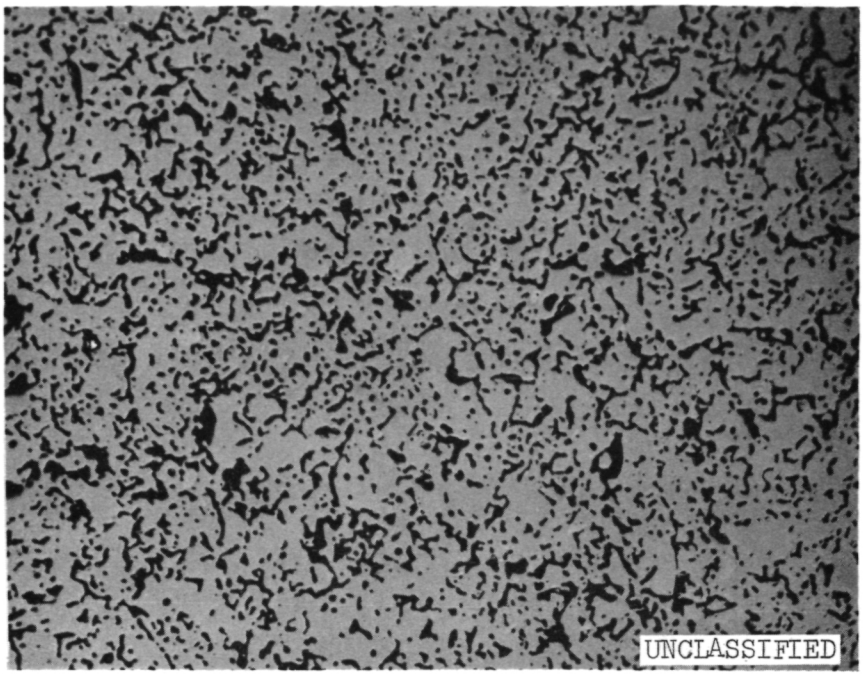

M 31150-3 250X

(c) Sample S_2a, unetched
Tested at 1600°C

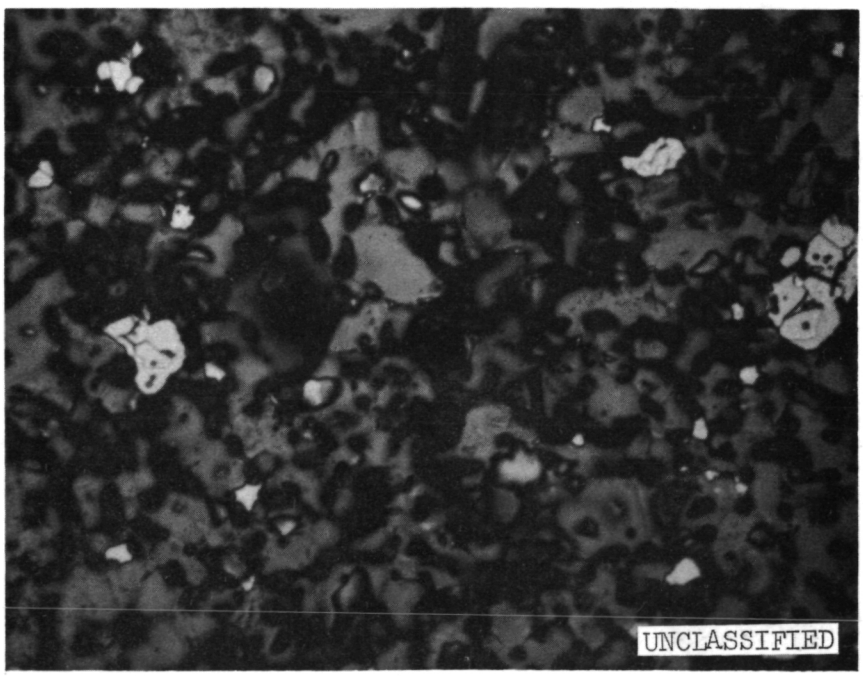

M 31148-6 750X

(d) Sample S_1a, etched
Tested at 1800°C

Fig. 4.9--(U) Microstructures of 90UC-10ZrC samples prepared from -44/+20 micron powder after 5000 hours at 1800°C, 1700°C and 1600°C (page 2 of 2)

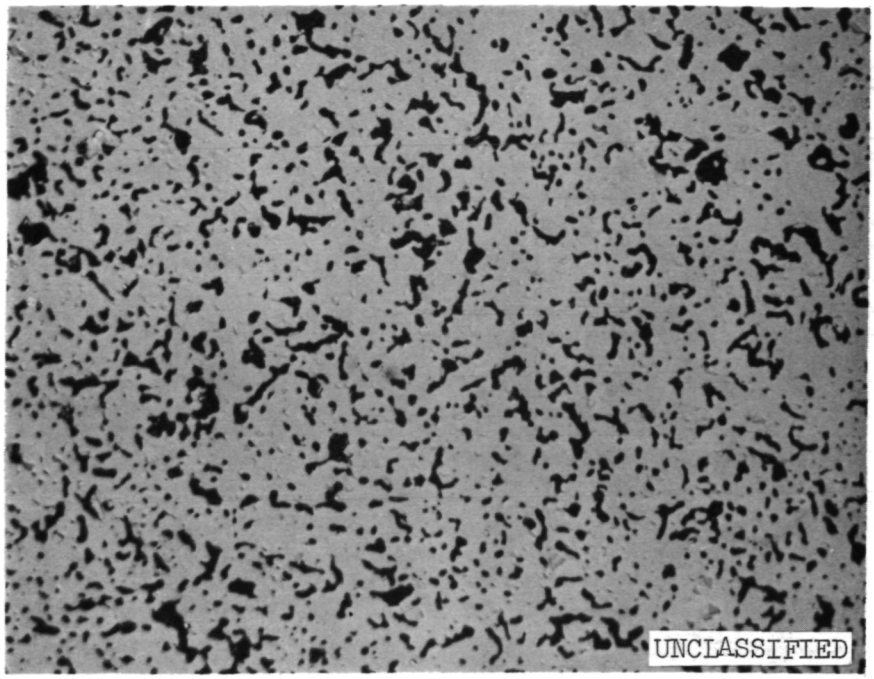

M 31151-2 250X

(a) Sample S_1b, unetched
Tested at 1800°C

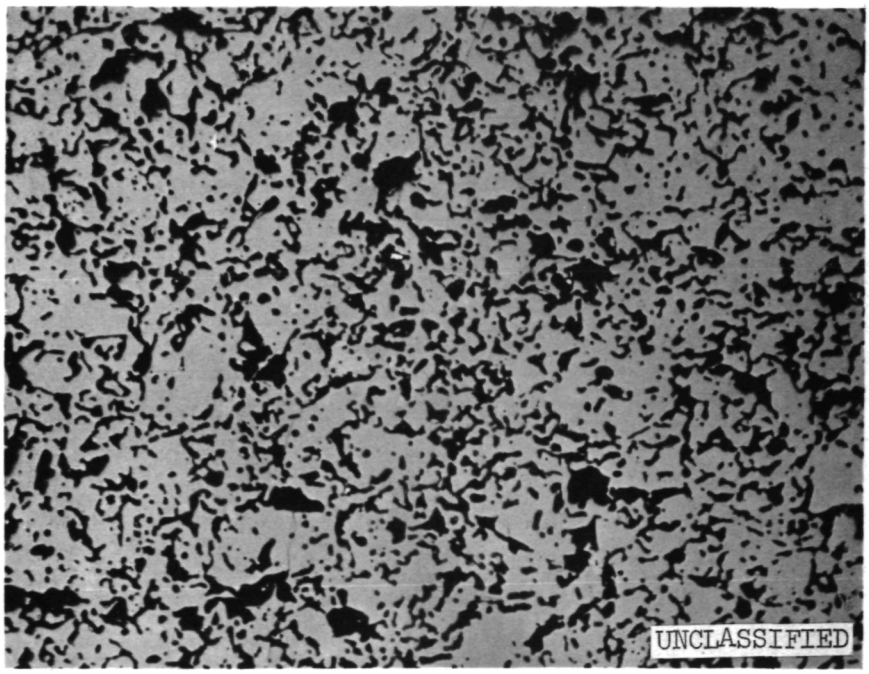

M 31154-2 250X

(b) Sample S_3b, unetched
Tested at 1700°C

Fig. 4.10--(U) Microstructures of 90UC-10ZrC samples prepared from -62/+20 micron powder after 5000 hours at 1800°C, 1700°C and 1600°C (page 1 of 2)

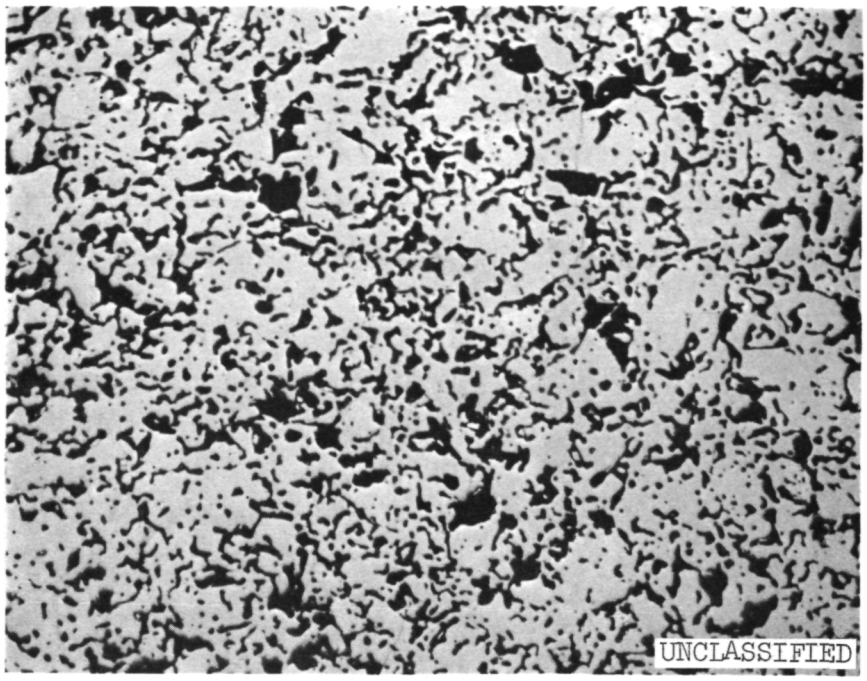

M 31154-3 250X

(c) Sample S_2b, unetched
Tested at 1600°C

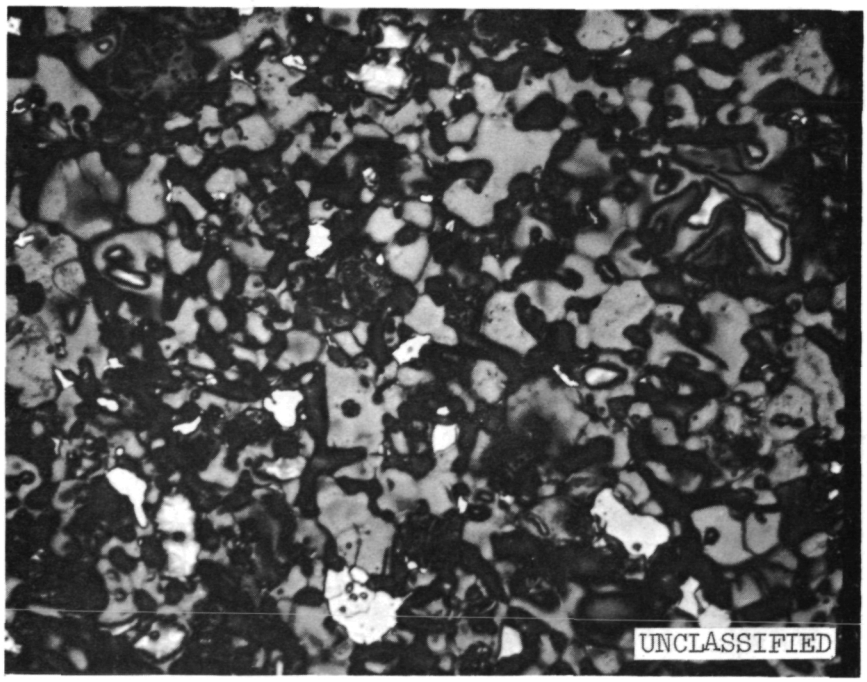

M 31148-7 750X

(d) Sample S_1b, etched
Tested at 1800°C

Fig. 4.10--(U) Microstructures of 90UC-10ZrC samples prepared from -62/+20 micron powder after 5000 hours at 1800°C, 1700°C and 1600°C (page 2 of 2)

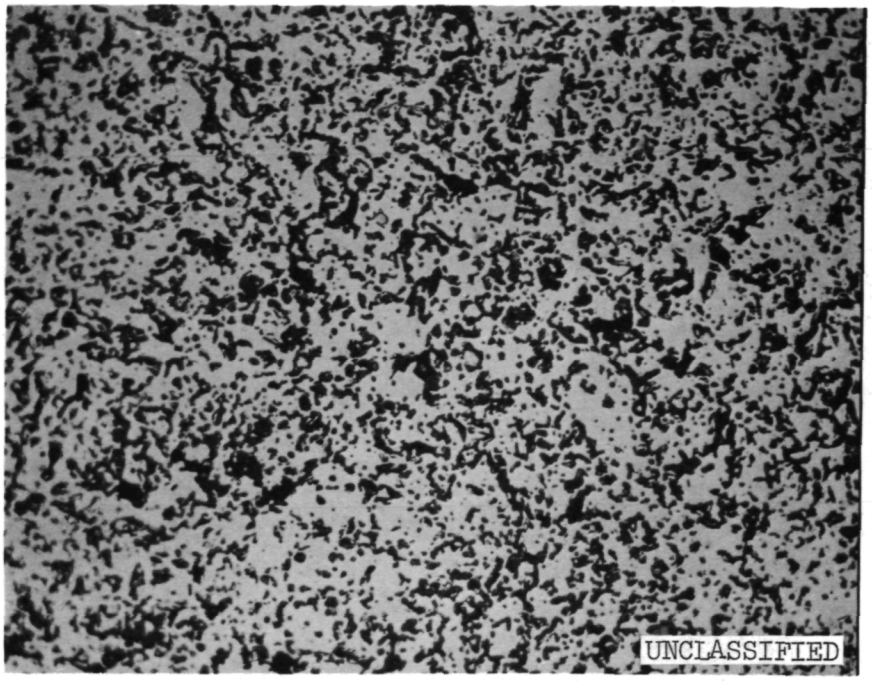

M 31147-3 250X

(a) Sample S_1c, unetched
Tested at 1800°C

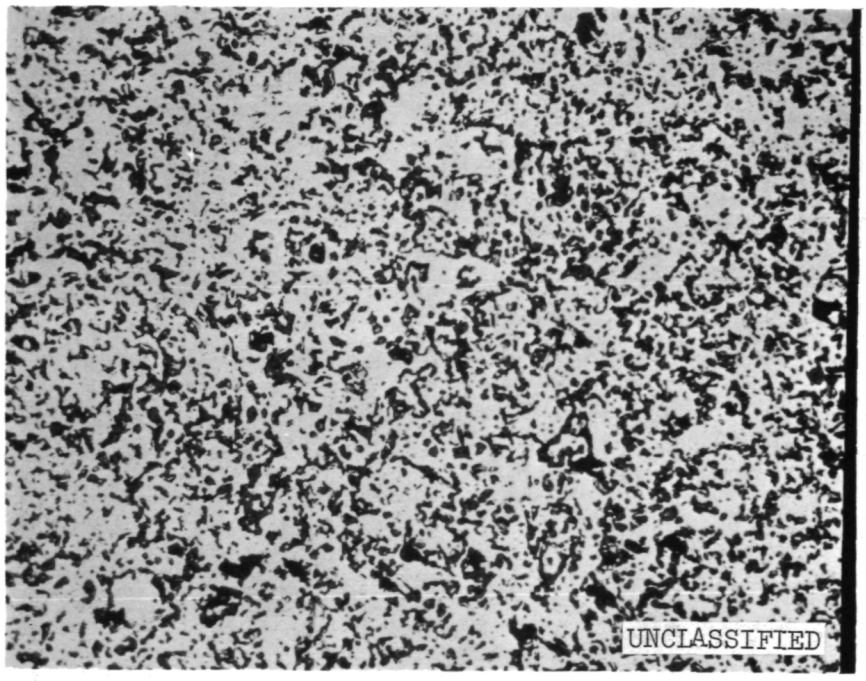

M 31147-1 250X

(b) Sample S_3c, unetched
Tested at 1700°C

Fig. 4.11--(U) Microstructures of 50UC-50ZrC samples prepared from -44/+20 micron powder after 5000 hours at 1800°C, 1700°C and 1600°C (page 1 of 2)

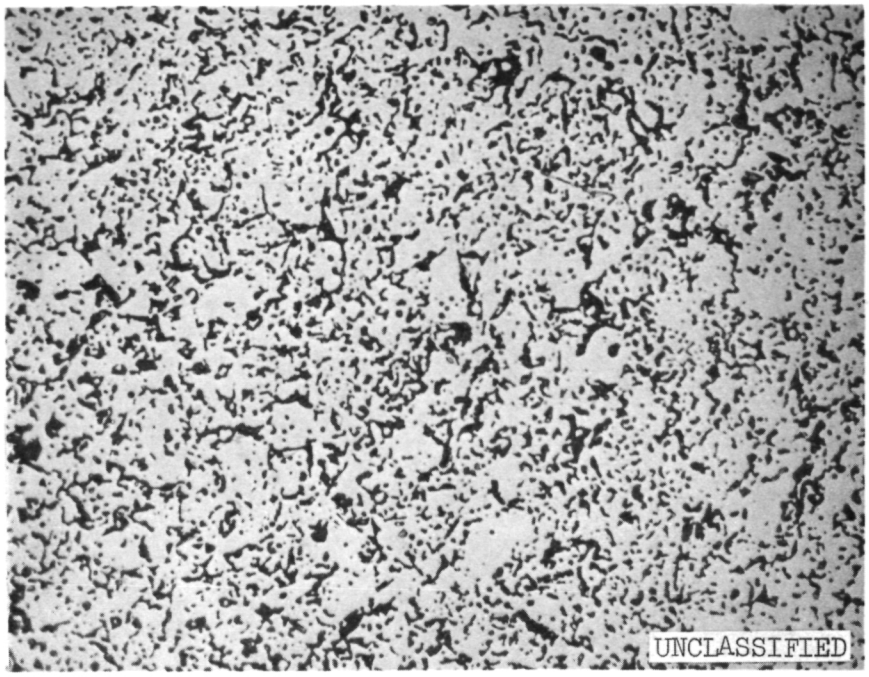

M 31153-1 250X

(c) Sample S_2c, unetched
Tested at 1600°C

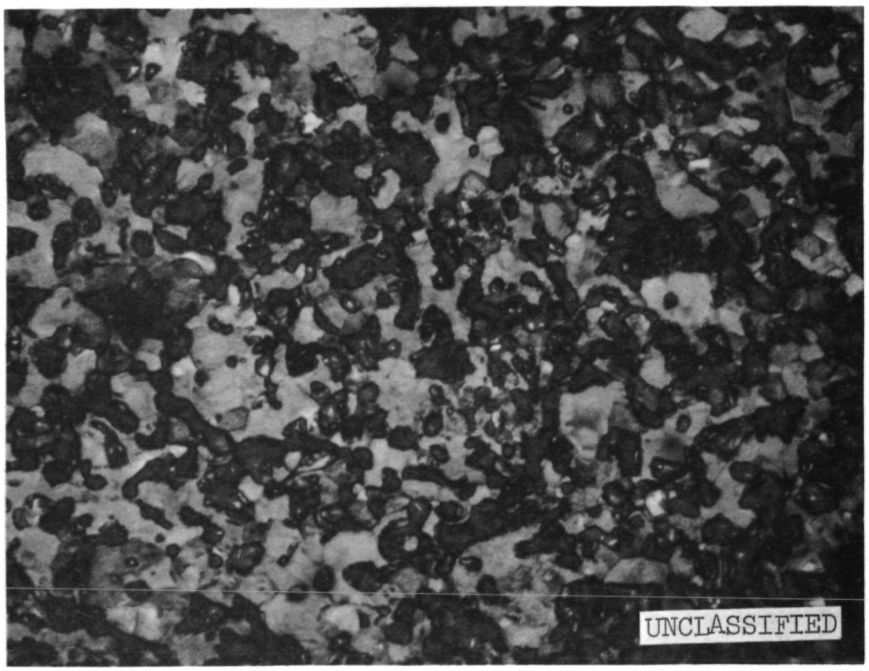

M 31147-4 750X

(d) Sample S_1c, etched
Tested at 1800°C

Fig. 4.11--(U) Microstructures of 50UC-50ZrC samples prepared from -44/+20 micron powder after 5000 hours at 1800°C, 1700°C and 1600°C (page 2 of 2)

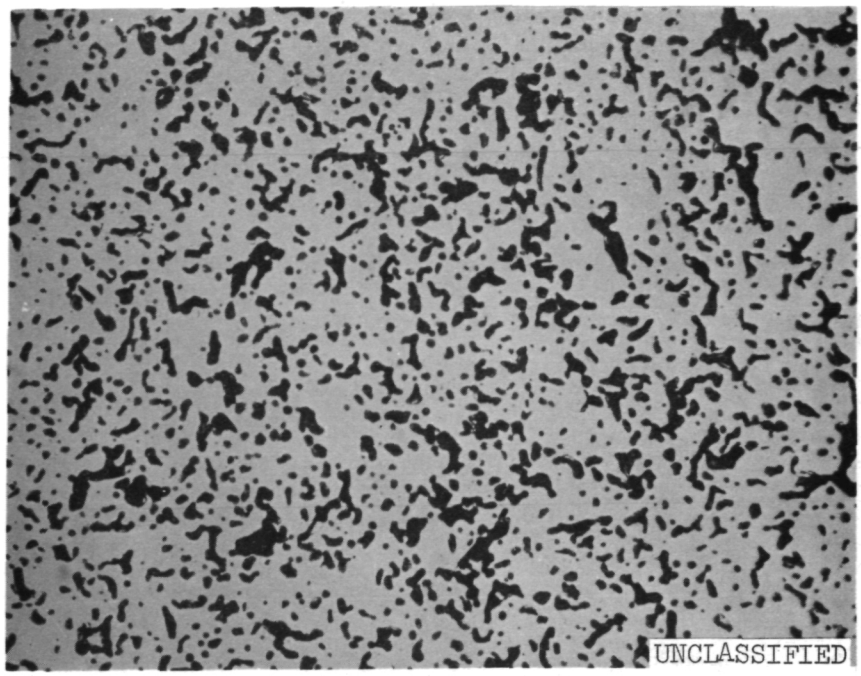

M 31149-5 250X

(a) Sample S_1d, unetched
Tested at 1800°C

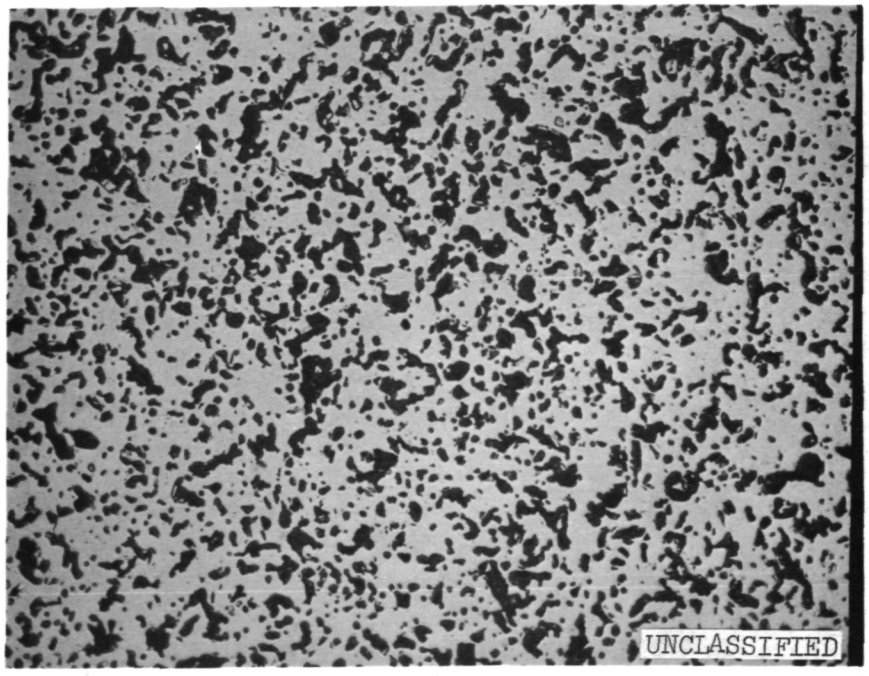

M 311491-1 250X

(b) Sample S_3d, unetched
Tested at 1700°C

Fig. 4.12--(U) Microstructures of 50UC-50ZrC samples prepared from -62/+20 micron powder after 5000 hours at 1800°C, 1700°C and 1600°C (page 1 of 2)

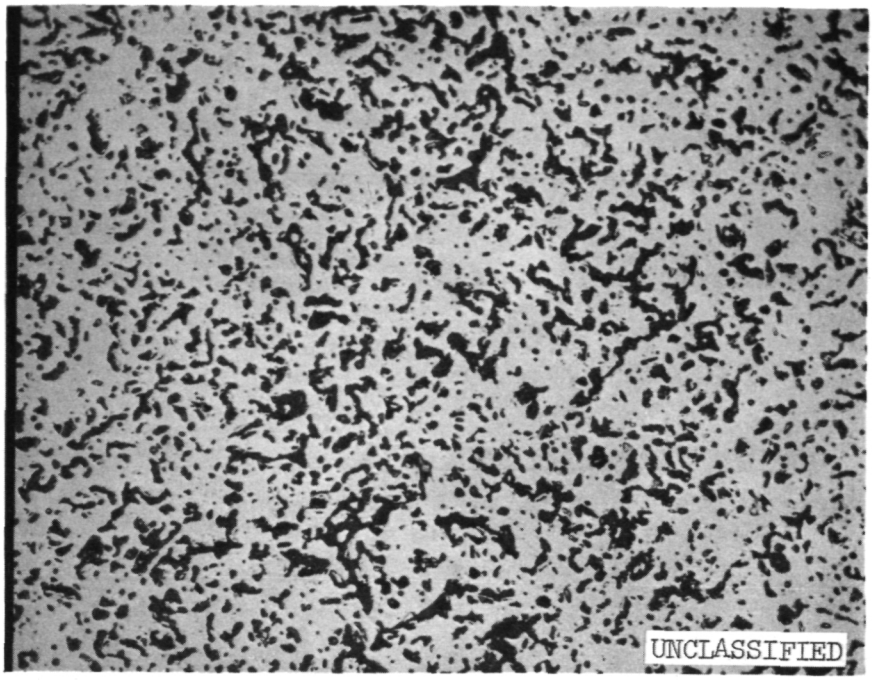

M 31152-2 250X

(c) Sample S_2d, unetched
Tested at 1600°C

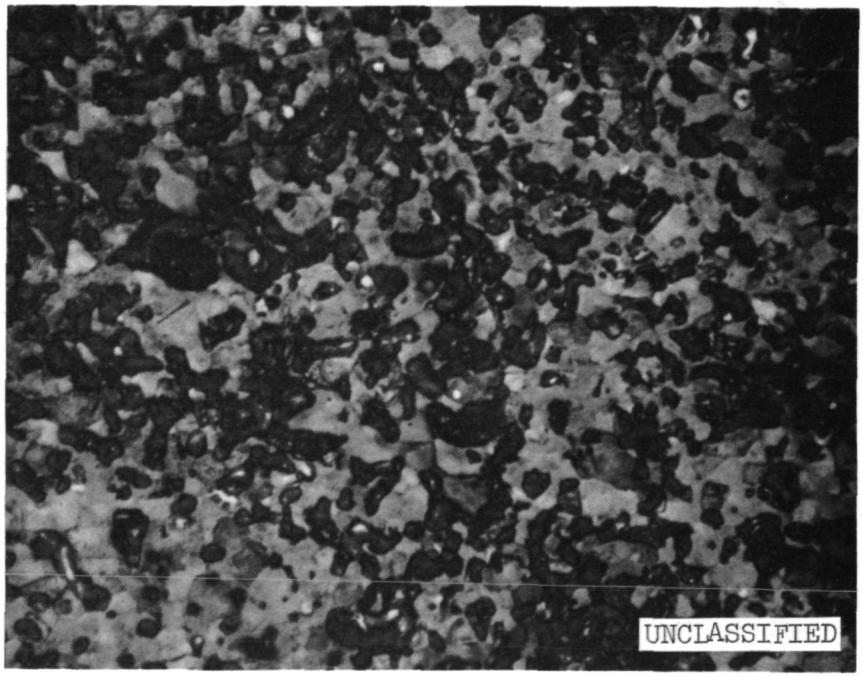

M 31147-2 750X

(d) Sample S_1d, etched
Tested at 1800°C

Fig. 4.12--(U) Microstructures of 50UC-50ZrC samples prepared from -62/+20 micron powder after 5000 hours at 1800°C, 1700°C and 1600°C (page 2 of 2)

4.4.2. Compositions, Stoichiometries and Impurity Contents

(C-RD)(Gp-1) The compositions, stoichiometries and impurity contents of the twenty-four samples subjected to the 5000 hour sintering test are shown in Table 4.3. Compared with the data shown in Table 4.2, the results indicate a slight decrease in the N, O and H contents but no significant change in compositions and C/U ratios.

REFERENCES

(1) "Investigations of Carbides as Cathodes for Thermionic Space Reactors," (U) Final Report, Part II, GA-4769 (C/RD).

(2) Lindgren, J. R. and A. F. Weinberg, "Fabrication Development of U-ZrC Fuels," (U) NASA CR-54381, GA-5790. (C/RD)

(3) Yang, L., R. G. Hudson and F. D. Carpenter, "Physico-Chemical Properties of Carbide Fuel for Thermionics," (U) Presented at the AIME Symposium on High Temperature Nuclear Fuels, Delevan, Wisconsin (October 3-5, 1966).

(4) Horner, M. H., "Post Operational Examinations of Thermionic Converters," (U) Presented at the Palo Alto Thermionic Specialist Meeting, Palo Alto, California, October 30-November 2, 1967, GA-7748.(C/RD)

(5) Horner, M. H. "Uranium Zirconium Carbide Fuel Fabrication Development," (U) Presented at the Palo Alto Thermionic Specialist Meeting, Palo Alto, California, October 30 - November 2, 1967, GA-7749 (C/RD)

(6) "Studies of Thermionic Materials for Space Power Applications," (U) Annual Summary Report for the Period September 1, 1963 through August 31, 1964. NASA CR-54322, GA-5665. (C/RD)

Table 4.3

(U) COMPOSITIONS, STOICHIOMETRIES AND IMPURITY CONTENTS OF UC-ZrC SAMPLES AFTER 5000 HOURS SINTERING STUDY

(This table is classified Confidential-Restricted Data-Group 1)

Set Designation	Carbide Cylinder Designation	Carbide Particle Size Range	Carbide Sample Designation	Testing Temperature (°C)	Composition				Stoichiometry (C/U)	Impurity Content (ppm)		
					U	Zr	W	C		N	O	H
I	a	-44μ/+20μ	S_1a	1800	0.845	0.102	0.053	1.000	1.03	94	180	2
			S_2a	1600	0.853	0.105	0.042	1.009	1.04	115	212	3
			S_3a	1700	0.840	0.110	0.050	1.005	1.04	105	195	1
	a'	-44μ/+20μ	S_1a'	1800	0.851	0.100	0.049	1.006	1.04	87	210	1
			S_2a'	1600	0.848	0.105	0.047	1.013	1.04	195	245	3
			S_3a'	1700	0.842	0.102	0.056	1.010	1.05	90	205	1
II	b	-62μ/+20μ	S_1b	1800	0.850	0.101	0.049	1.011	1.04	75	170	1
			S_2b	1600	0.845	0.095	0.060	1.012	1.05	117	215	1
			S_3b	1700	0.839	0.099	0.062	1.010	1.05	95	185	1
	b'	-62μ/+20μ	S_1b'	1800	0.835	0.105	0.060	1.007	1.05	85	155	2
			S_2b'	1600	0.842	0.110	0.048	1.009	1.04	88	197	1
			S_3b'	1700	0.838	0.108	0.054	1.005	1.04	78	183	2
III	c	-44μ/+20μ	S_1c	1800	0.490	0.470	0.040	1.000	1.04	125	145	2
			S_2c	1600	0.480	0.475	0.045	1.001	1.05	158	188	3
			S_3c	1700	0.483	0.470	0.047	1.002	1.05	118	173	1
	c'	-62μ/+20μ	S_1c'	1800	0.482	0.478	0.040	1.001	1.04	152	171	1
			S_2c'	1600	0.487	0.475	0.038	1.002	1.04	187	210	4
			S_3c'	1700	0.485	0.472	0.043	1.000	1.04	149	181	2
IV	d	-44μ/+20μ	S_1d	1800	0.475	0.474	0.051	1.000	1.05	155	125	1
			S_2d	1600	0.481	0.475	0.044	1.002	1.05	192	153	3
			S_3d	1700	0.478	0.480	0.042	1.005	1.04	174	150	1
	d'	-62μ/+20μ	S_1d'	1800	0.473	0.478	0.049	1.001	1.05	105	102	1
			S_2d'	1600	0.475	0.482	0.043	1.002	1.05	156	175	1
			S_3d'	1700	0.470	0.485	0.045	1.000	1.05	115	125	1

CONFIDENTIAL
RESTRICTED DATA
ATOMIC ENERGY ACT 1954
GROUP 1
CONFIDENTIAL

PART V. PERFORMANCE STABILITY TESTS ON FUELED AND UNFUELED ELECTRICALLY HEATED CESIATED THERMIONIC CONVERTERS

(J. Kay and M. Yates)

SUMMARY

(U) Three electrically heated cesiated thermionic converters were tested from November 1966 to July 1969. Table 5.1 lists the essential characteristics of each converter.

Table 5.1

(U) CHARACTERISTICS OF CONVERTERS LC-7, LC-8 AND LC-9

(This table is classified Confidential-Restricted Data-Group 1)

	LC-7	LC-8	LC-9
Emitter			
Material	W	W	W
Orientation	(100)	(100)	(110)
Collector	Nb	Nb	Nb
Fuel	None	90UC-10ZrC[a]	None
Hours tested (7-31-69)	3672	7089	20,696
Electrode avg power density, watts/cm^2	6.7	variable	7.9
Emitter avg temp. ^{o}C	1800	variable	1700
Status (7-31-69)	Test Ended	Test Continuing	Test Continuing

[a] Mole percent.

(C-RD)(Gp-1) The design of LC-7, LC-8 and LC-9 was altered as an evolutionary step in the upgrading of the converter as a test vehicle. The collector material was changed to niobium for thermionic reactor design consideration and dimensions were altered to improve the thermal design.

RESTRICTED DATA
ATOMIC ENERGY ACT 1954
GROUP 1

LC-7 employed an unfueled emitter to provide baseline performance data with which LC-8 (90UC-10ZrC fuel) and LC-9 (high-work-function emitter) could be compared. The optimum performance for LC-7 was 7.1 W/cm^2 at an emitter temperature average of 1800°C. Work function measurements indicate that the niobium collector was responsible for the output being lower than in converters operated with molybdenum collectors. The output of LC-7 was about the same as was observed in OC-4 (niobium collector) and about 30% below the OC-5 (molybdenum collector) output. The LC-7 test operated stably for 3672 hours before the cesium was lost due to the failure of the cesium tube-cesium reservoir weld joint. The results of the post-operational examination are reported.

(C-RD)(Gp-1) The LC-8 converter has been on test for 6639 hours and has been tested at 1400°, 1600°, and 1800°C emitter temperature. The performance was relatively stable during the operation at 1400°C. The performance at 1600°C decreased, particularly following low temperature diagnostic measurements. The initial performance at 1800°C was identical to that of LC-7 within ±3%. However, the performance soon decreased and was 29% below that of LC-7 by the end of the reporting period but appeared to be stabilizing.

(C-RD)(Gp-1) The observed changes in power output are interpreted to be the result of work function changes due to the accumulation of fuel constituents on the emitter and collector surfaces. The emitter work function data indicates that the value at 1400°C was ~4.7 eV and was ~4.5 eV at 1800°C. Since the latter value is typical of this type of tungsten, some of the performance loss was due to the removal of a high work function material from the emitter surface. The remainder of the power loss appears to be due to the increases in the cesiated collector work function observed during operation.

(C-RD)(Gp-1) The unfueled converter LC-9 contained an emitter prepared by hydrogen reduction of WCl_6 vapor. Its vacuum work function was determined to be 4.8 eV or 0.2 eV higher than found for emitters deposited from WF_6. The initial output power, extrapolated to optimum operating conditions, was 10 W/cm^2 at an 1800°C emitter temperature, which, compared

RESTRICTED DATA
ATOMIC ENERGY ACT 1954
GROUP 1

with LC-7 at equal operating conditions, was 25% greater. Most of the performance increase is attributed to the high-work-function emitter. The power output and efficiency have been stable within ±3% during the 20,696 hours accumulated thus far. Other test parameters, such as collector temperature and cesium reservoir temperature, have remained stable.

5.1. INTRODUCTION

(U) The program objective was to measure the performance stability of electrically heated cesium thermionic converters with refractory metal-clad fueled emitters for test durations up to 10,000 hour at power densities exceeding 5 W/cm^2. Nonfueled converters were tested to obtain performance baseline data with which the fueled converters could be compared and, thereby, to obtain a direct measurement of the effects of fuel diffusion on performance. In addition, a new objective was introduced – to measure performance improvement from high-work-function emitters.

(U) Three converters were placed on test during the report period. All three were diagnostic as well as life test converters. Performance mappings and diagnostic measurements were conducted at approximately 2000 hour intervals during the tests. The converter designations, characteristics, and status are presented in Table 5.2.

(U) The major differences between the converter series from LC-7 to LC-9 and earlier converter series from LC-1 to LC-6[1] were (1) the substitution of niobium for molybdenum as a collector material, (2) the use of a duplex tungsten emitter in LC-9, which consists of a partially (110) oriented chloride tungsten deposited on a fluoride tungsten substrate, and (3) bulk degassing of all converter components prior to assembly. The modification in accessories for LC-7 through LC-9 included the improvement of the design of the electron bombardment filament and the use of a collector heat sink incorporating a variable thermal conductance gas gap. Figure 5.1 shows the converter design configuration. Specific data on design features and fabrication procedures are extensively reported in Reference 2. Converter LC-7 operated for 3672 hours before the test was

RESTRICTED DATA
ATOMIC ENERGY ACT 1954
GROUP 1

Table 5.2

(U) CONVERTER CHARACTERISTICS AND STATUS

(This table is Unclassified)

	LC-7	LC-8	LC-9
Emitter			
Material	Fluoride Tungsten	Fluoride Tungsten	Chloride/Fluoride Tungsten[a]
Orientation	{100}	{100}	{110}
Area cm^2	16.1	16.1	16.1
Interelectral Spacing			
(hot) mil	10	10	10
(cold)	9	9	9
Collector	Nb	Nb	Nb
Fuel	None	90UC-10ZrC[b]	None
Status	Envelope Leak. Terminated Test 3672 hr.	6639 Operating Hours. Test Continuing	20,696 Operating Hours. Test Continuing

[a]Chloride tungsten = tungsten formed by the hydrogen reduction of tungsten hexachloride.
Fluoride tungsten = tungsten formed by the hydrogen reduction of tungsten hexafluoride.

[b]Mole percent

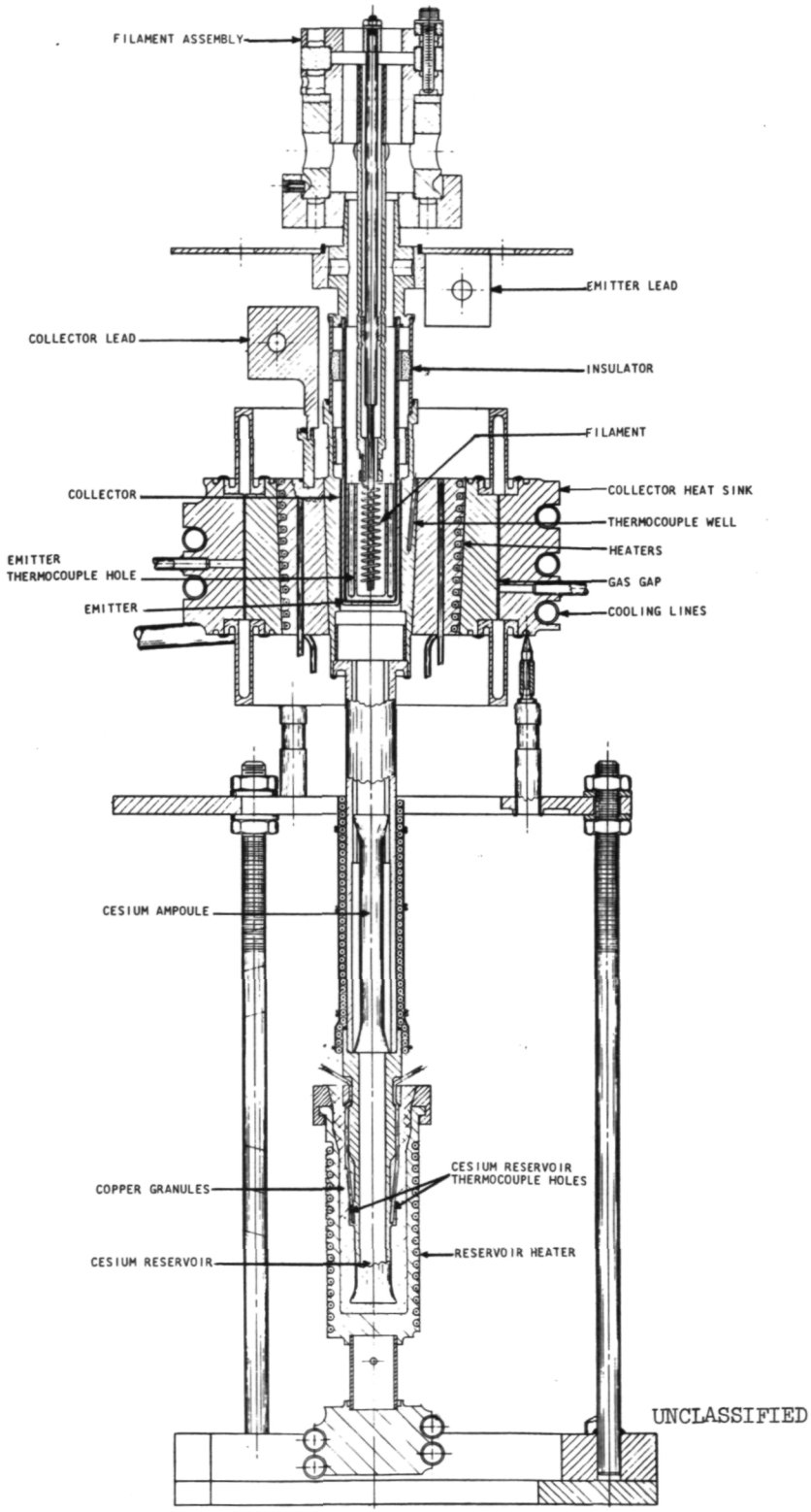

Fig. 5.1--(U) Converter design of LC-7, 8 and 9

terminated because of an envelope leak. LC-8 and LC-9 converters are still in operation and have accumulated 7089 and 20,696 hours respectively.

(U) The test results of LC-7, LC-8, and LC-9 are presented in Sections 5.2, 5.3, and 5.4 using the following format: initial performance, operating history, diagnostic data, and interpretation of results. Emitter temperature profile and vacuum work function data for the LC-7, LC-8, and LC-9 emitters are presented in Appendix 5A. High temperature thermocouple development work is described in Appendix 5B, and the post operational examination results of LC-7 are reported in Appendix 5C.

5.2. LC-7 TEST (UNFUELED CONVERTER)

(U) The purpose of the LC-7 test was to obtain long-term baseline data on an unfueled converter containing a tungsten emitter deposited from WF_6 and a niobium collector. Its performance is to be compared with that of LC-8, which contains 90UC-10ZrC fuel slabs in the emitter wall but otherwise was identical in materials and preparation. Converter LC-7 was the first converter to be prepared using converter parts that were all bulk degassed.

(U) The designs of the emitter and collector heat sink are somewhat different from those of earlier converters. The emitter area was increased to 16.1 cm^2 from the previously used 14.2 cm^2, by extending the coverage of the emitter surface by the collector. The increase eliminated the possibility of overheating the ends of the emitter which could result from poor heat transfer through fuel slabs (in cells that contain fuel). LC-7 is the first cell since LC-4 to be unfueled.

(U) The LC-7 test is the first of the LC series to be conducted in the upgraded ultra high vacuum system. The system includes a water-cooled metal bell jar, sublimation pumping, and ports for optical pyrometry of emitter temperature. Typical operating pressure was about 5×10^{-9} torr.

5.2.1. LC-7 Initial Performance

(U) Operating conditions preselected for LC-7 were the following: 1800°C average emitter temperature, 750°C collector temperature, and optimum cesium pressure and current. The results of the performance mapping are shown in Figs. 5.2, 5.3, and 5.4. The raw data obtained are displayed in Fig. 5.2 in the form of cesium optimization curves at constant cell currents. The maximum voltage on these curves when plotted against the current forms the envelope of current-voltage curves, as shown in Fig. 5.3. Figure 5.4 shows the maximum electrode power point as a function of current density. It is noted that the maximum output power was 7.1 W/cm^2 at T_E = 1800°C and T_C = 750°C. It will be shown later that the optimum collector temperature is actually somewhat in excess of 800°C. The optimum current density appears to be about 12 amp/cm^2.

(U) The maximum output of LC-7 is compared in Fig. 5.4 with that obtained from OC-4, which had the same materials and geometry as did LC-7. Operation of OC-4 was conducted at an average emitter temperature of 1750°C instead of 1800°C. If OC-4 had been run at 1800°C it would have produced ~7 W/cm^2 so it can be concluded that the output of OC-4 and LC-7 were within the experimental uncertainties (estimated to be on the order of 5%) of the LC-7 output.

(U) The initial temperatures of the emitter thermocouples in the assembled cesiated converter are shown in Fig. 5.5 at zero current operation. For comparison temperature profile measurements obtained on the emitter component only (see Appendix 5A) are also shown. The maximum deviation between the two thermocouple profiles was 30°C, which is close to the experimental uncertainties of ±25°C. This means that the temperature profile of the emitter surface for zero-current converter operation was nearly the same as it was during the profile measurements. As noted in Appendix 5A, from measurements on the emitter component alone the thermocouple average and the surface temperature average were within 5°C, which makes it possible to use the average of the thermocouple temperature to estimate the average surface temperature in the operating converter at zero current flow. The emitter surface temperature distribution, as shown in Fig. 5.5, is quite uniform; the difference between the maximum and average is 20°C. It was determined from Fig. 5.5 that over

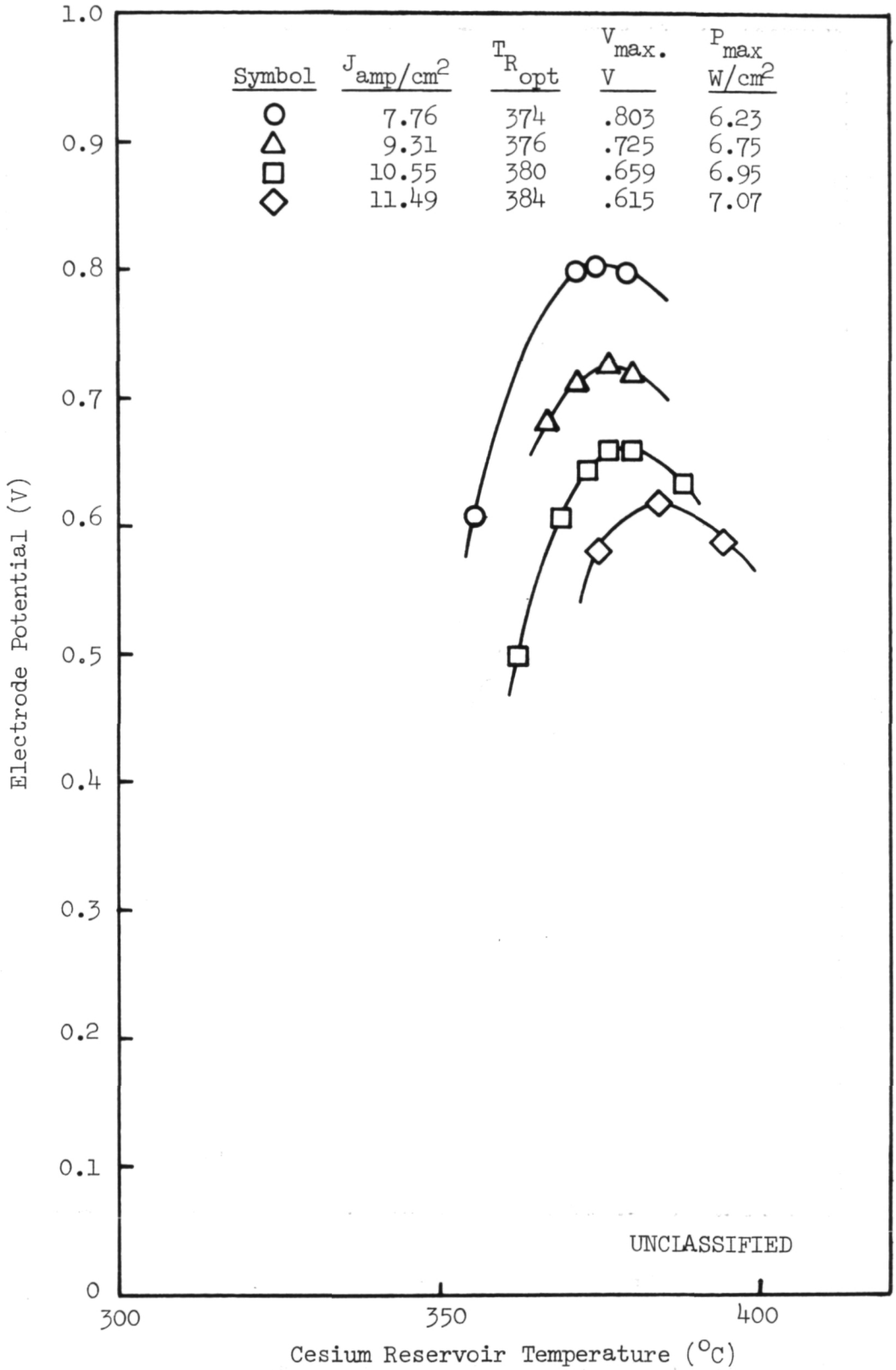

Fig. 5.2--(U) LC-7 cesium reservoir temperature optimization initial data. Emitter temperature 1805°C, collector temperature 750°C

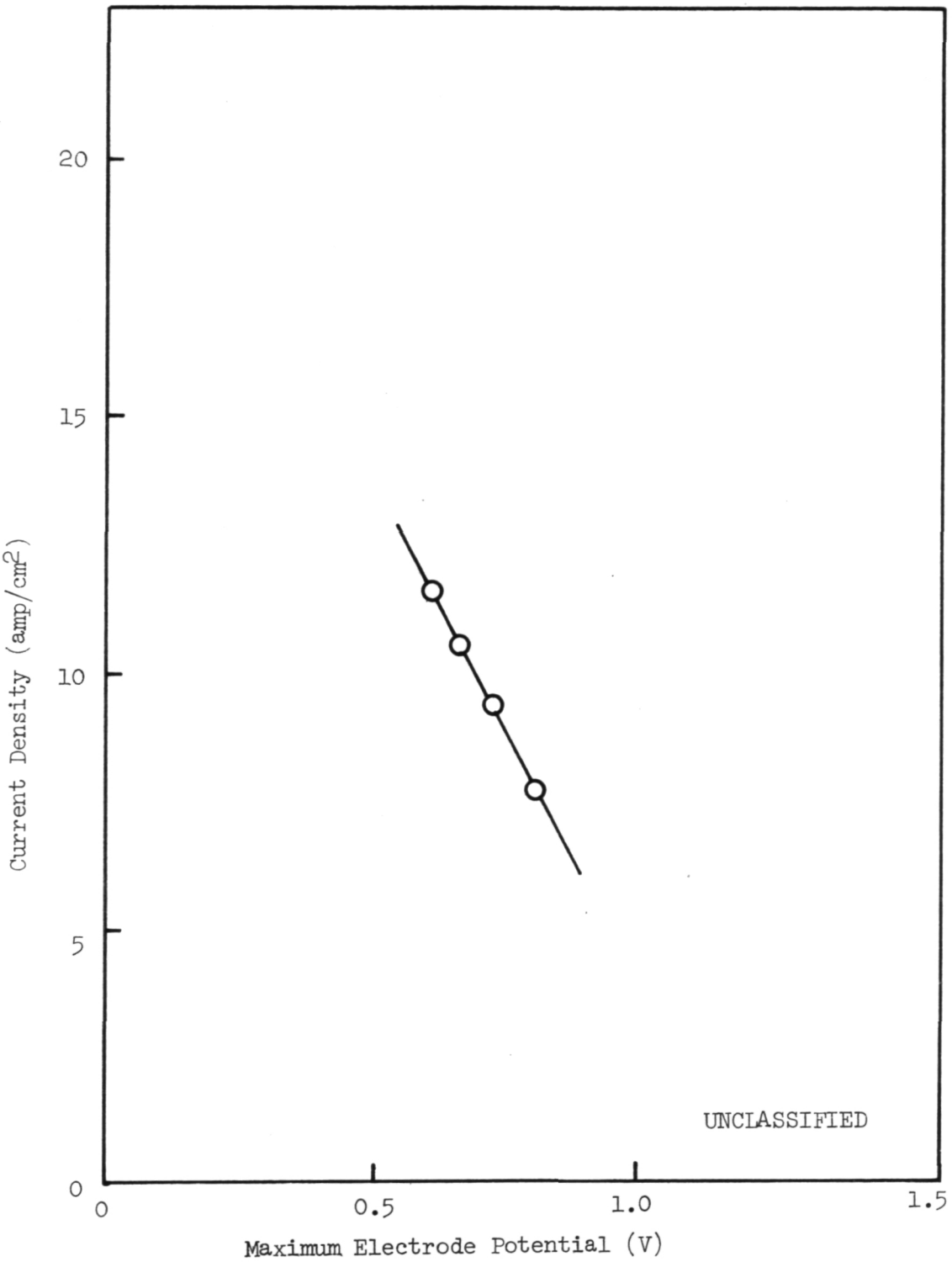

Fig. 5.3--(U) Envelope of I-V characteristics for LC-7 initial data. Emitter temperature 1805°C, collector temperature 750°C

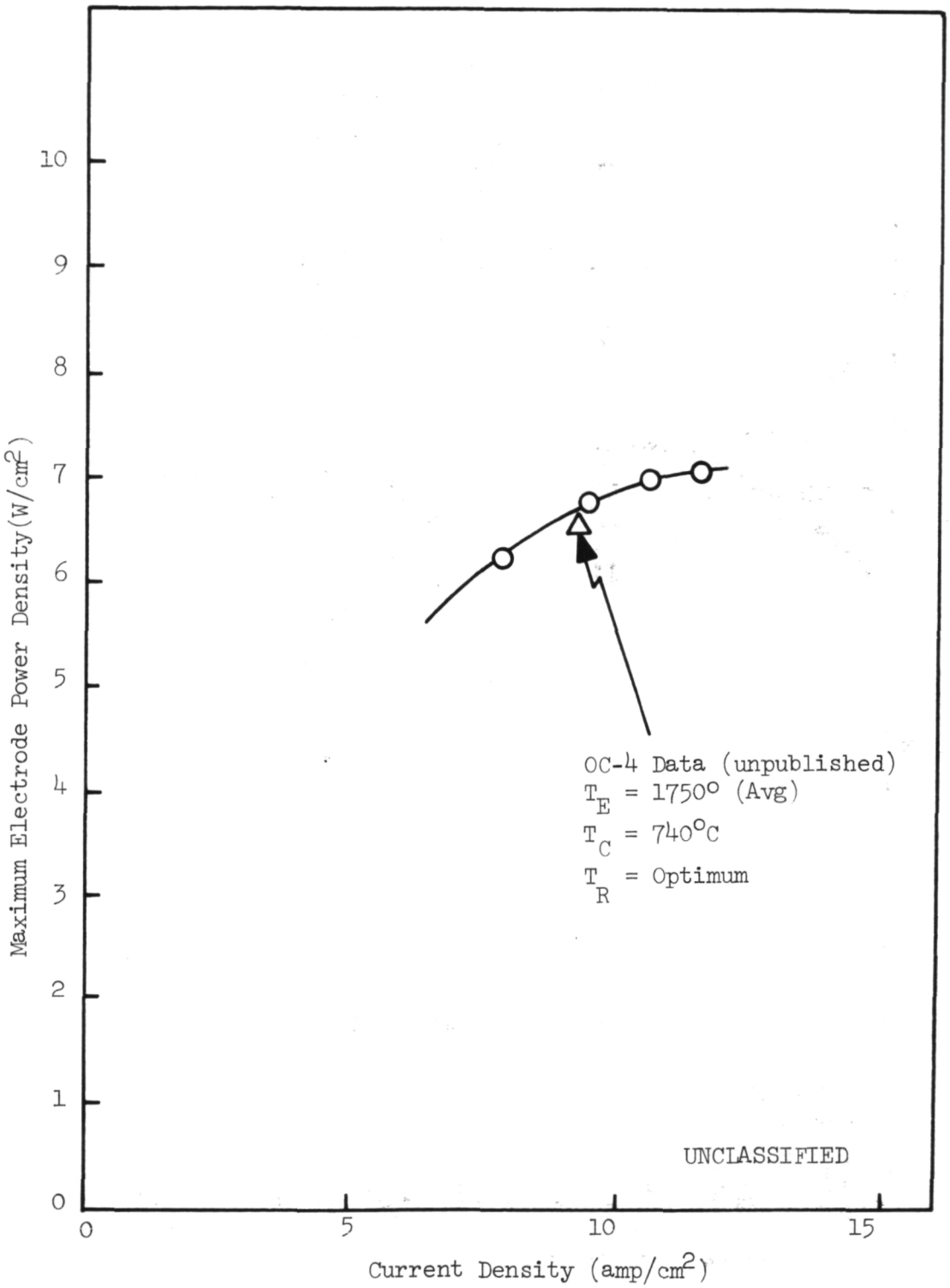

Fig. 5.4--(U) Maximum output power and optimum current determination for LC-7 initial data. Emitter temperature 1805°C, collector temperature 750°C

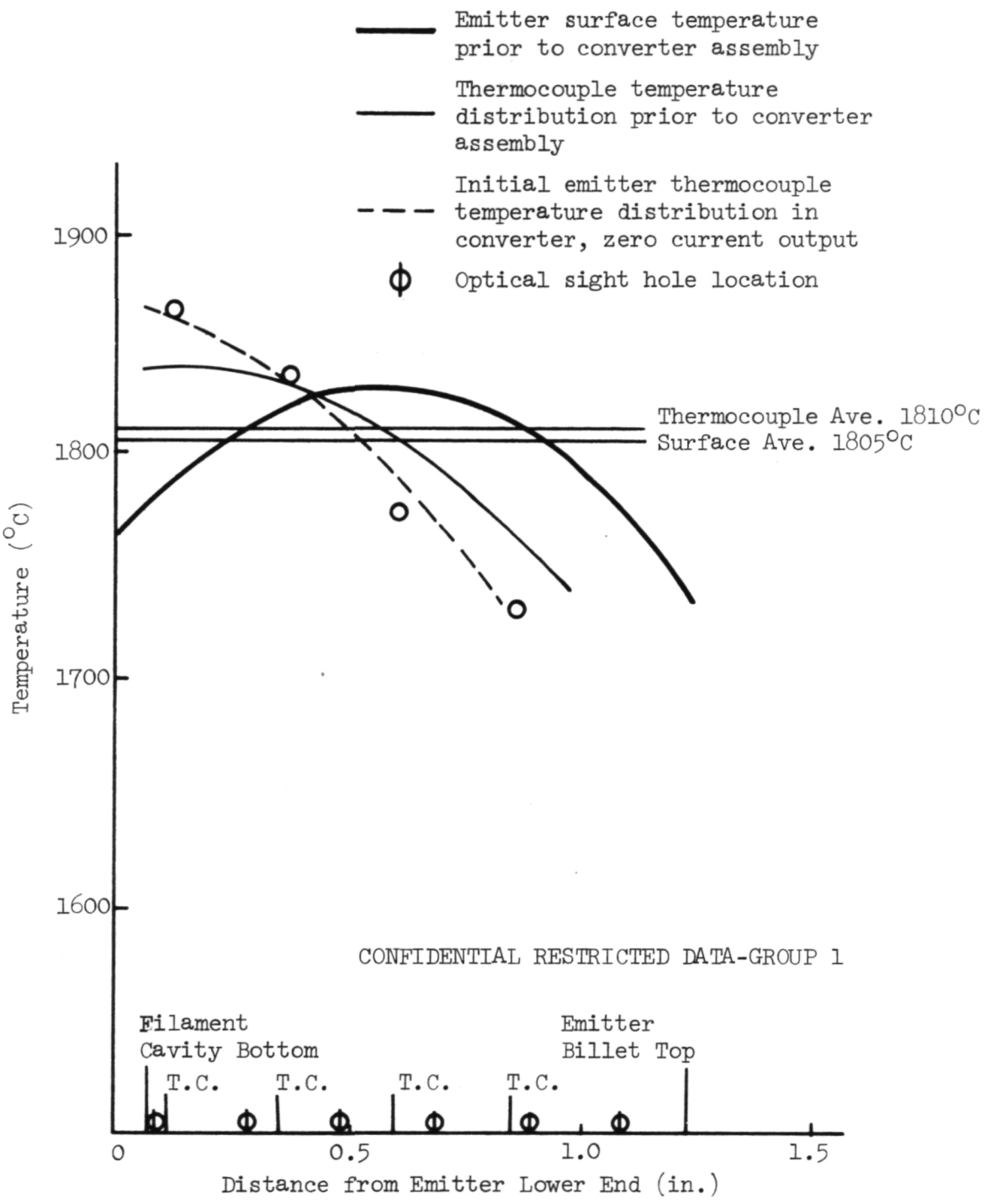

Fig. 5.5--(U) LC-7 emitter temperature profile and thermocouple distribution in converter compared with pre-converter-assembly data

73% of the surface was within 20°C. When current is conducted through the converter, the emitter temperature distribution tends to flatten due to resistance heating of the emitter stem. Therefore, the emitter surface temperature at high current should have been more uniform that the distribution shown in Fig. 5.5.

(U) Following the performance mapping described above, the life test of LC-7 was officially started. The recorded time for the beginning of the test was 0000 on November 8, 1966. Data obtained at that time are given in Table 5.3.

5.2.2. LC-7 Operating History

(U) The operating history of LC-7 is shown in Fig. 5.6 and 5.7 for the test period of 3672 hours. Converter performance and operating parameters at various times during the test as well as average values are listed in Table 5.4. The average power density for the test was 6.72 W/cm^2 with perturbations of $^{+2.0}_{-4.5}$% from initial performance. A comparison of initial and 2096 hour performance mappings is shown in Figs. 5.8 and 5.9. The displacement of the 2096 hour data is less than 4% and is not significant considering the experimental uncertainties estimated to be ±3%.

(U) Collector temperature was maintained at 750°C throughout the test. The optimum collector temperature as discussed in Section 5.2.3 was in excess of 800°C. However, insufficient heat rejection by emitter lead radiation required operation below optimum collector temperature.

(U) The cesium reservoir temperature, which initially optimized at 380°C remained constant until 1293 hours, at which time an increase of optimum to 387°C was observed. The change in optimum followed replacement of the filament at 1081 hours. Similarly, at 1953 hours, following a filament replacement, the optimum reservoir temperature fluctuated down to 381°C but rose to 386°C after 150 hours operation. These changes are attributed to changes in the emitter temperature profile after filament replacements, as discussed in the following paragraph.

Table 5.3

(U) CONVERTER LC-7 (UNFUELED) AT BEGINNING OF LIFE TEST

(This table is Unclassified)

Input power, watts	1040
Electrode	
Output power, watts/cm^2	6.95
Voltage, volts	0.659
Current, amp	170
Temperatures, ^{o}C	
Emitter	
Thermocouple No. 1	1888
Thermocouple No. 2	1867
Thermocouple No. 3	1794
Thermocouple No. 4	1760
Estimated surface avg	1827
Collector	749
Cesium Reservoir	379
Insulator	
Upper sheath	713
Lower sheath	666

UNCLASSIFIED

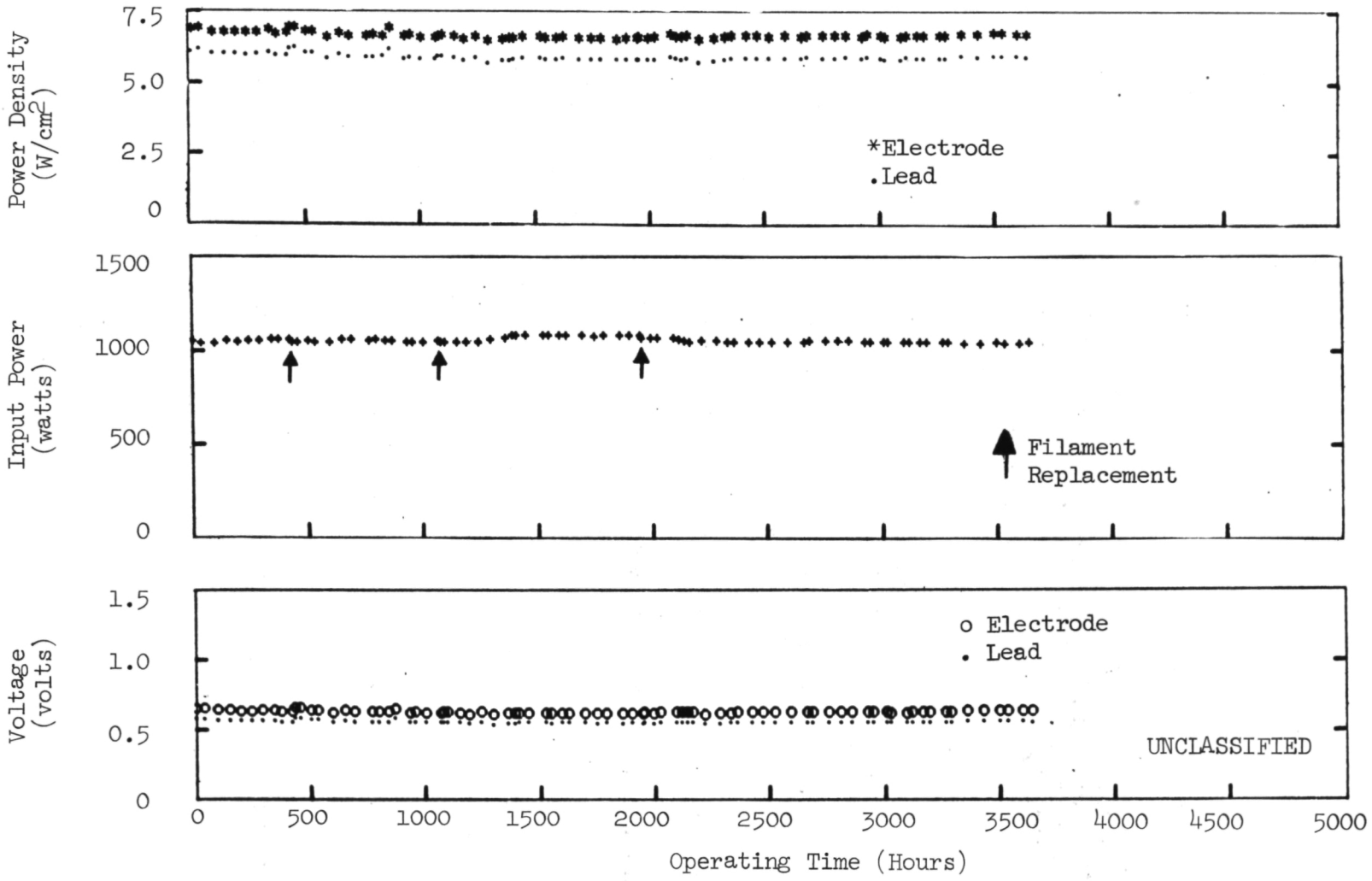

Fig. 5.6--(U) LC-7 performance history

UNCLASSIFIED

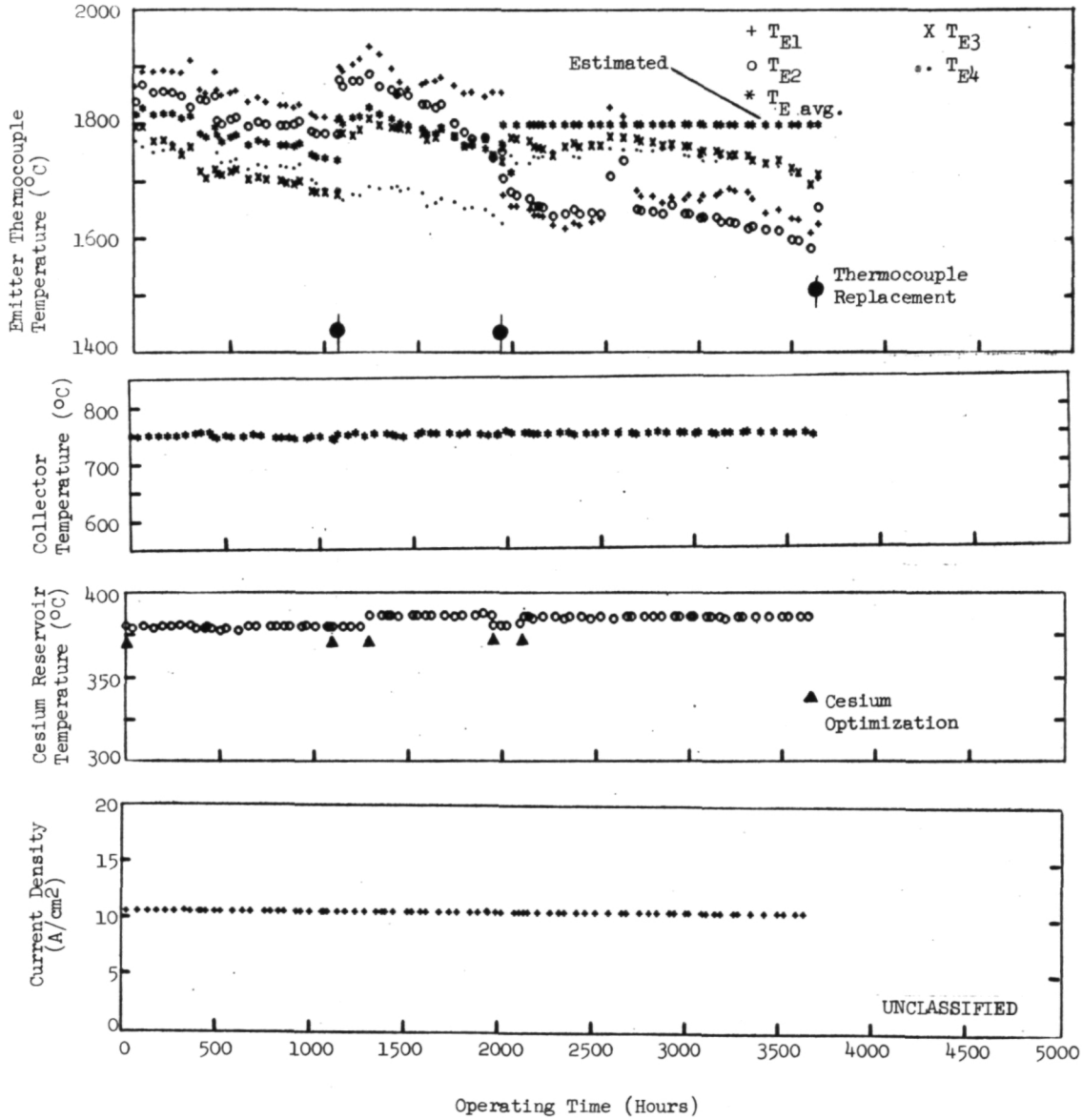

Fig. 5.7--(U) LC-7 performance history

Table 5.4

(U) LC-7 PERFORMANCE AND OPERATING PARAMETERS

(This table is Unclassified)

Operating Time - hours	0	498	1081	3645
Input Power - watts	1040	1048	1048	1044
Output Power (electrode) - W/cm^2	6.95	6.93	6.71	6.79
Voltage (electrode) - volts	.659	.656	.636	.643
Voltage (lead) - volts	.584	.582	.563	.565
Current - amp	170	170	170	170
Current Density - amp/cm^2	10.55	10.56	10.56	10.56
Temperatures - ^oC				
Emitter Thermocouples No. 1	1888	1860	1900	1624
No. 2	1867	1806	1880	1657
No. 3	1794	1712	1785	1713
No. 4	1760	1732	1685	1704
Average	1827	1778	1812	1674
Estimated Surface Average	1827	1800*	1812	1800*
Collector	749	748	743	747
Cesium Reservoir	379	380	380	386

*Thermocouples unreliable - Average Surface Temperature estimated to be 1800^oC based on previous operation at similar conditions.

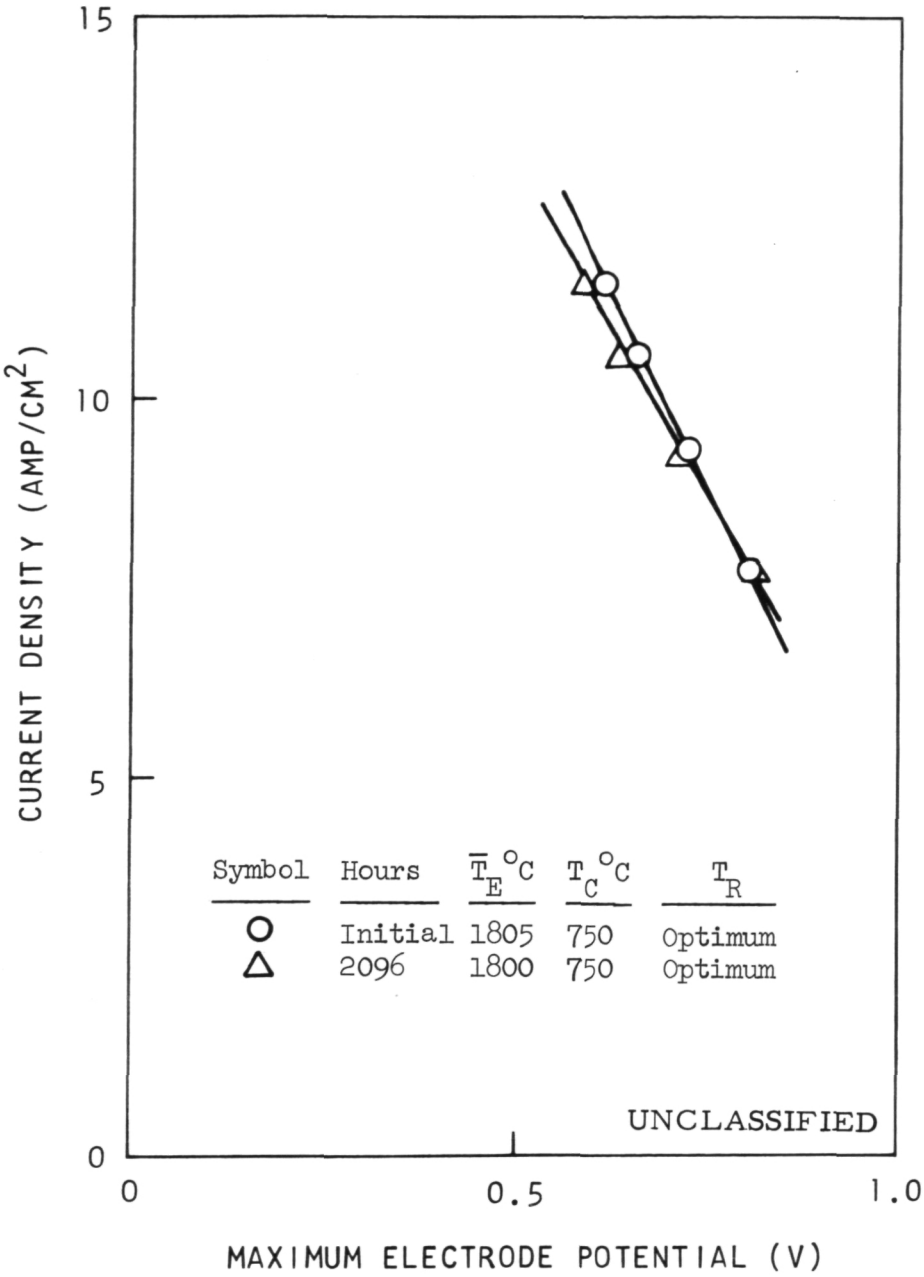

Fig. 5.8 --(U) Envelope of I-V characteristics for LC-7

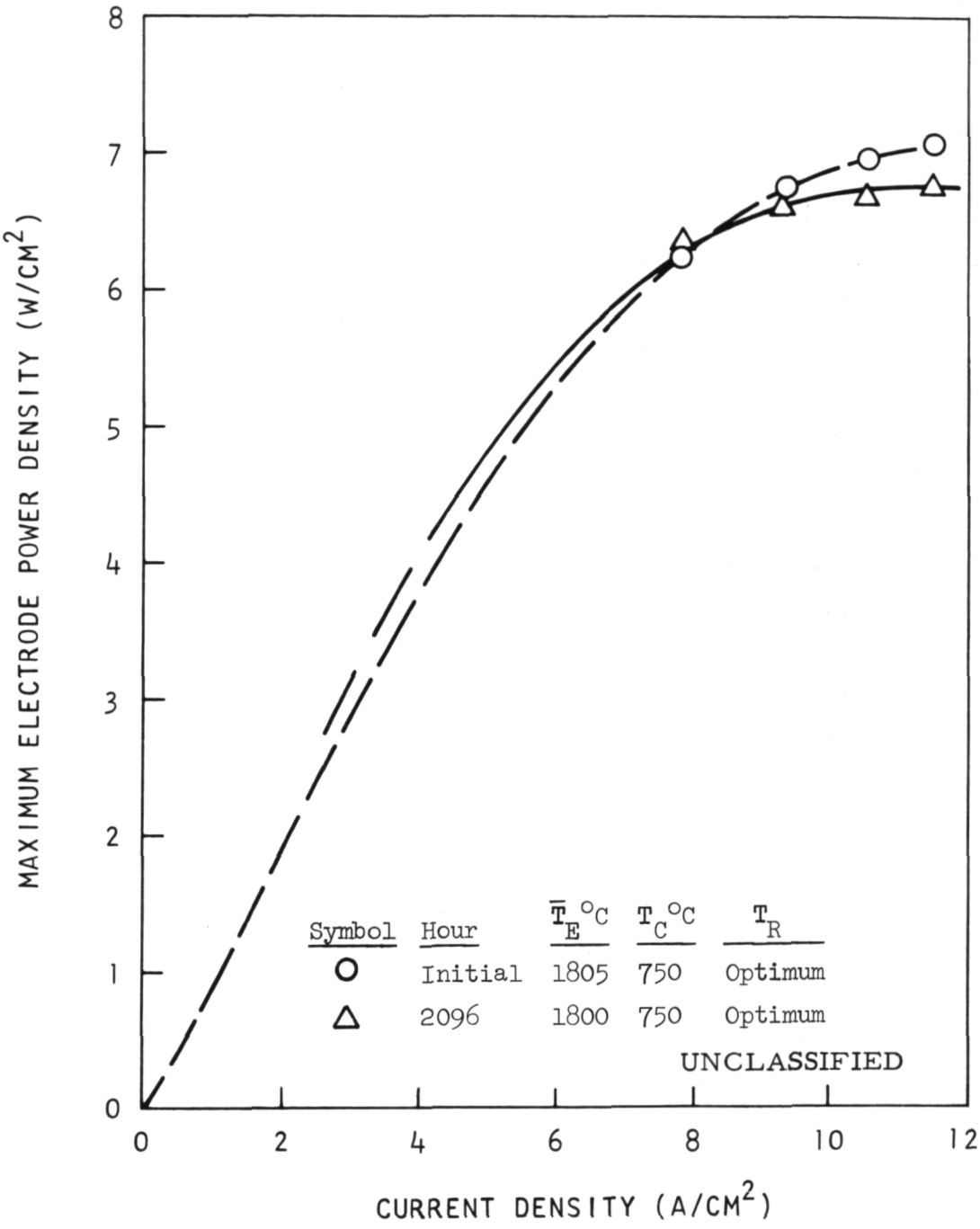

Fig. 5.9 --(U) Maximum output power and optimum current determinations for LC-7

(U) LC-7 emitter thermocouples were replaced twice during the test. At 1081 hours all four thermocouples were replaced, and at 1954 hours only T_{E1} and T_{E2} were changed. As shown in Fig. 5.7, the average temperature reading of the original thermocouples decreased 70°C in the first 1000 hours. The apparent decrease in emitter temperature, however, was not accompanied by changes in converter performance or input power requirements; therefore, it was concluded that the thermocouples were unreliable. The replacement thermocouples installed with a new filament at 1081 hours indicated a change of emitter temperature profile which is related to filament alignment and filament temperature distribution. Localized heating at the lower end of the filament due to contact resistance could contribute to the flattened emitter temperature profile that was observed. Electron beam welding of the filament to the center post and changes in filament operating mode significantly increased lifetime of the filaments used in the test.

(U) The replacement thermocouples for T_{E1} and T_{E2} at 1954 hours were unreliable; therefore, the average temperature was estimated on the basis of the input power for the remainder of the test. Recalibration of emitter thermocouples was not accomplished because of thermocouple failure resulting from embrittlement of W-Re wires. The thermocouples open circuited during removal from the converter or during recalibration. Inspection of thermocouples after removal revealed extensive loss of material from the tantalum crimp plug at the junction end and dark deposits on the beryllium oxide insulation. Subsequent investigation disclosed a film of magnesium on the surface of the BeO which created low resistance shunt paths, resulting in decreased thermocouple output. The magnesium originated from MgO used in the manufacture of the BeO. The results of a thermocouple stability test at temperatures ranging from 1400°C to 1800°C are reported in the Appendix 5B.

(U) A total of five shutdowns occurred during the test: four due to filament problems and one due to a plant power outage.

5.2.3. LC-7 Diagnostic Data

(U) The first measurements obtained after converter startup were the open circuit data to be used in calculation of the relative effective emittance. Data on effective emittance was also taken during the test. No changes in effective emittance outside of the experimental errors were observed during the test. These errors were estimated to be ±0.2 because of problems with the stability of the tungsten-rhenium thermocouples at 1800°C. Using the formulas derived in Reference 1, an error in effective emittance of ±0.1 can be calculated for an error in emitter temperature of ±25°C. The thermocouples were not, even initially, considered more accurate than this.

(U) Collector temperature optimization data were obtained after 181 hours of operation. The data shown in Fig. 5.10 indicates that the collector temperature optimum was in excess of 800°C. At the time the data were obtained, the difference in output between 800°C and 750°C was 0.4 W/cm^2. It appears certain that if the collector temperature had been initially operated near the optimum, the output of LC-7 would have been about 7.5 W/cm^2.

(U) Emitter and collector work function measurements obtained initially and at the 2000 hour performance mapping are shown in Fig. 5.11 and compared to Rasor-Warner curves. The emitter work function remained unchanged at 4.5 eV with experimental uncertainties estimated to be ±.05 eV. The initial and 2000 hour collector work function measured at T_C/T_R ratio of 1.57°C/°C (normal operating conditions) were 1.75 eV and 1.60 eV respectively. The 0.15 eV difference in collector work function is inconsistent with the stable performance history of LC-7. Also, the latter 1.60 eV value is in good agreement with the LC-9 data as discussed later. As a result it was concluded that the initial value of 1.75 eV was inaccurate and that no change in ϕ_C actually occurred. Also, in the interim between the initial and 2000 hour data, collector work function test equipment was modified to improve measurement accuracy.

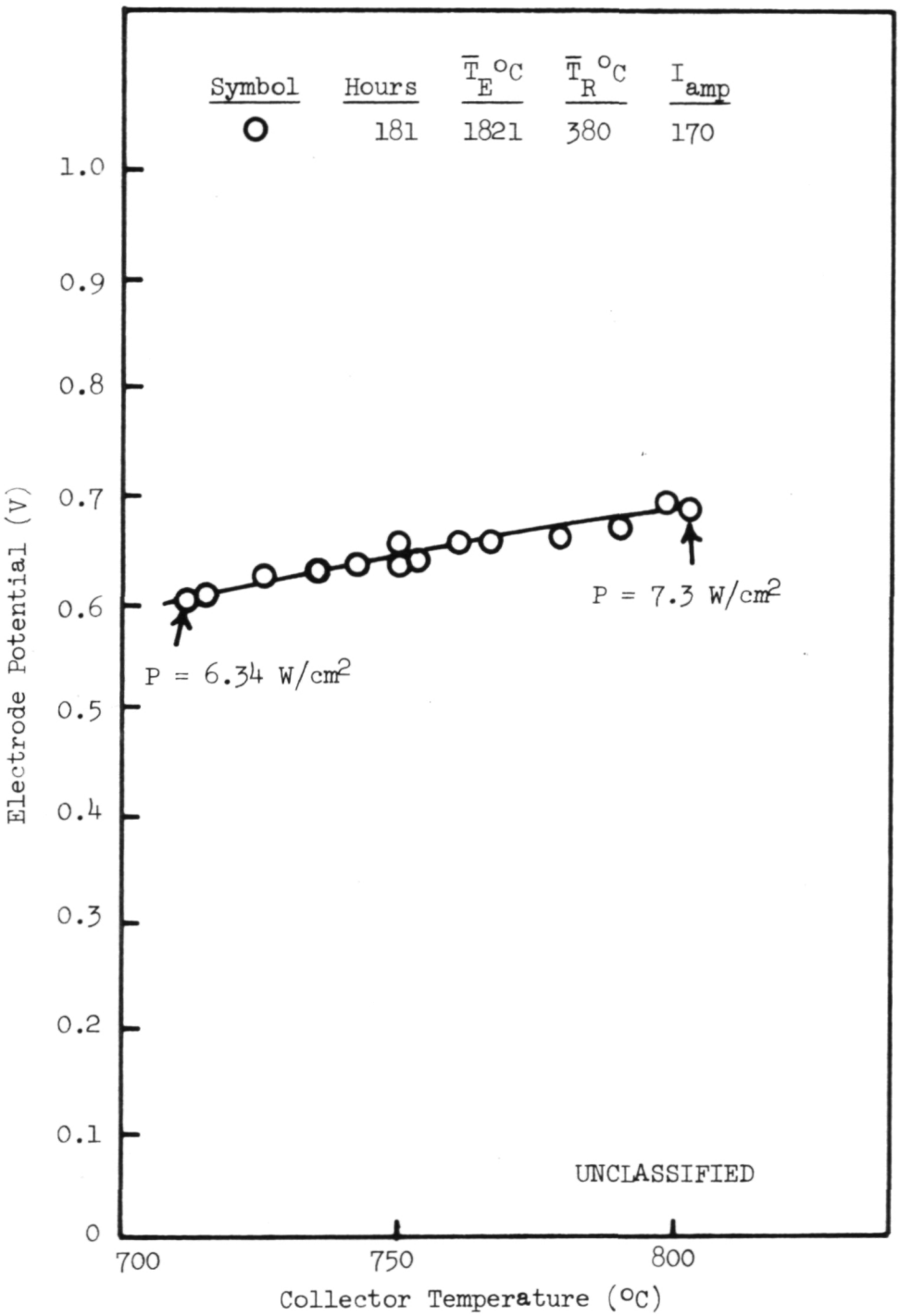

Fig. 5.10--(U) LC-7 collector temperature optimization

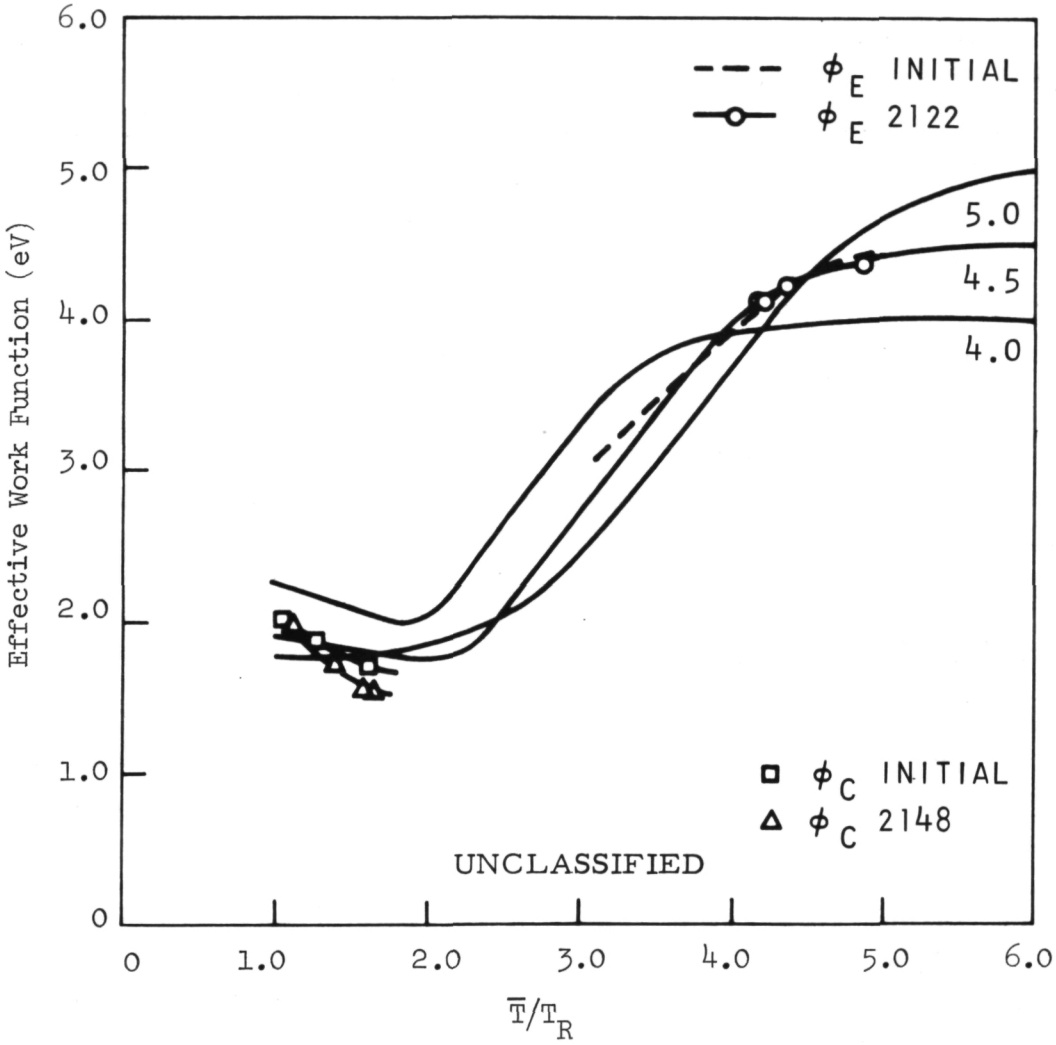

Fig. 5.11--(U) LC-7 emitter and collector work function

RESTRICTED DATA
ATOMIC ENERGY ACT 1954
GROUP 1

5.2.4. Interpretation of the LC-7 Results

(U) LC-7 and OC-4 performed about equally and both produced about 70% of the OC-5 output power. From the levels of performance and work function data it is concluded that the major reason the performance of LC-7 was lower than found for OC-5 is that the cesiated work function for niobium in the operating region is higher than for molybdenum. The higher cesiated work function yields less contact potential for the converter. The emitter work function was close to the expected value and thus is considered to have contributed little to the lower performance of LC-7.

(U) The converter operated stably with maximum perturbation of $^{+2}_{-4.5}\%$ from initial performance throughout its life. Test failure was due to loss of cesium which occurred when the copper-niobium weld joint near the cesium reservoir failed. Details of this joint failure as well as other post-operational results are presented in Appendix 5C. In addition, the results of pre- and post-operational emitter temperature profile and vacuum work function measurements are presented in Appendix 5A.

5.3 LC-8 TEST (90UC-10ZrC)

(C-RD)(Gp-1) The purpose of the LC-8 test was to measure the performance and long term stability of a converter fueled with 90UC-10ZrC at 1400°, 1600°, and 1800°C. The fuel material in LC-8 differed from that used in previous out-of-pile converters in two respects: 4 w/o tungsten was added to the fuel in order to satisfy the fuel's solubility requirement for this material; the carbon to uranium ratio of the fuel was controlled between 1.03-1.05 in order to reduce uranium activity and diminish the amount of uranium diffusion through the tungsten clad.

(C-RD)(Gp-1) Except for the fuel the design and preparation of LC-8 was identical to LC-7. In addition the LC-8 test was also conducted in an all metal, bakeable vacuum station. A typical operating pressure is 5×10^{-8} torr.

5.3.1. LC-8 Initial Performance

(C-RD)(Gp-1) The LC-8 test plan was to operate at optimum output power density for 1000 hours at an emitter temperature of 1400°C, followed by 1000 hours at 1600°C and then life test at 1800°C. Performance mapping (i.e. determining the cesium temperature for optimum converter performance at various values of current density and constant emitter and collector temperatures) and diagnostic measurements were to be obtained at the start and conclusion of the three test periods. Because of this test plan, all of the performance data will be presented in Section 5.3.2.

5.3.2. LC-8 Operating History

(C-RD)(Gp-1) The operating history for LC-8 is shown in Figs. 5.12 and 5.13. Figures 5.14 through 5.21 and Table 5.5 give the results of the performance mappings. A total of 7098 hours have been accumulated since the start of testing on July 18, 1968. The converter was operated from 0 to 1491 hours at 1400°C, 1491 to 3186 hours at 1600°C, and 1800°C thereafter.

1400°C Operation

(C-RD)(Gp-1) Following a 300 hour stabilization period performance mapping and diagnostic measurements were obtained. The power output stabilized by the time of the first performance mapping at a value of 3.1 W/cm^2 at 9 A/cm^2. The converter performance remained stable until a shutdown at 1062 hours. When the converter was returned to power the output was 2.7 W/cm^2. The performance subsequently improved to 2.9 W/cm^2 at 1491 hours, the end of the 1000 hour test period. The performance maps taken at the beginning and end of the test period are shown in Figs. 5.14 and 5.15 and show a net decrease in performance of 6% at the optimum power point.

1600°C Operation

(C-RD)(Gp-1) At 1600°C the converter performance initially improved then stabilized at 1722 hours at which time converter performance mapping and diagnostic measurements were initiated. Maximum power density was 5.77 W/cm^2 at a current density of 11.18 A/cm^2. However, the converter performance failed to return to the prediagnostic level following the diagnostic

RESTRICTED DATA
ATOMIC ENERGY ACT 1954
GROUP 1

CONFIDENTIAL

(This page is Unclassified)

RESTRICTED DATA
ATOMIC ENERGY ACT 1954
GROUP 1

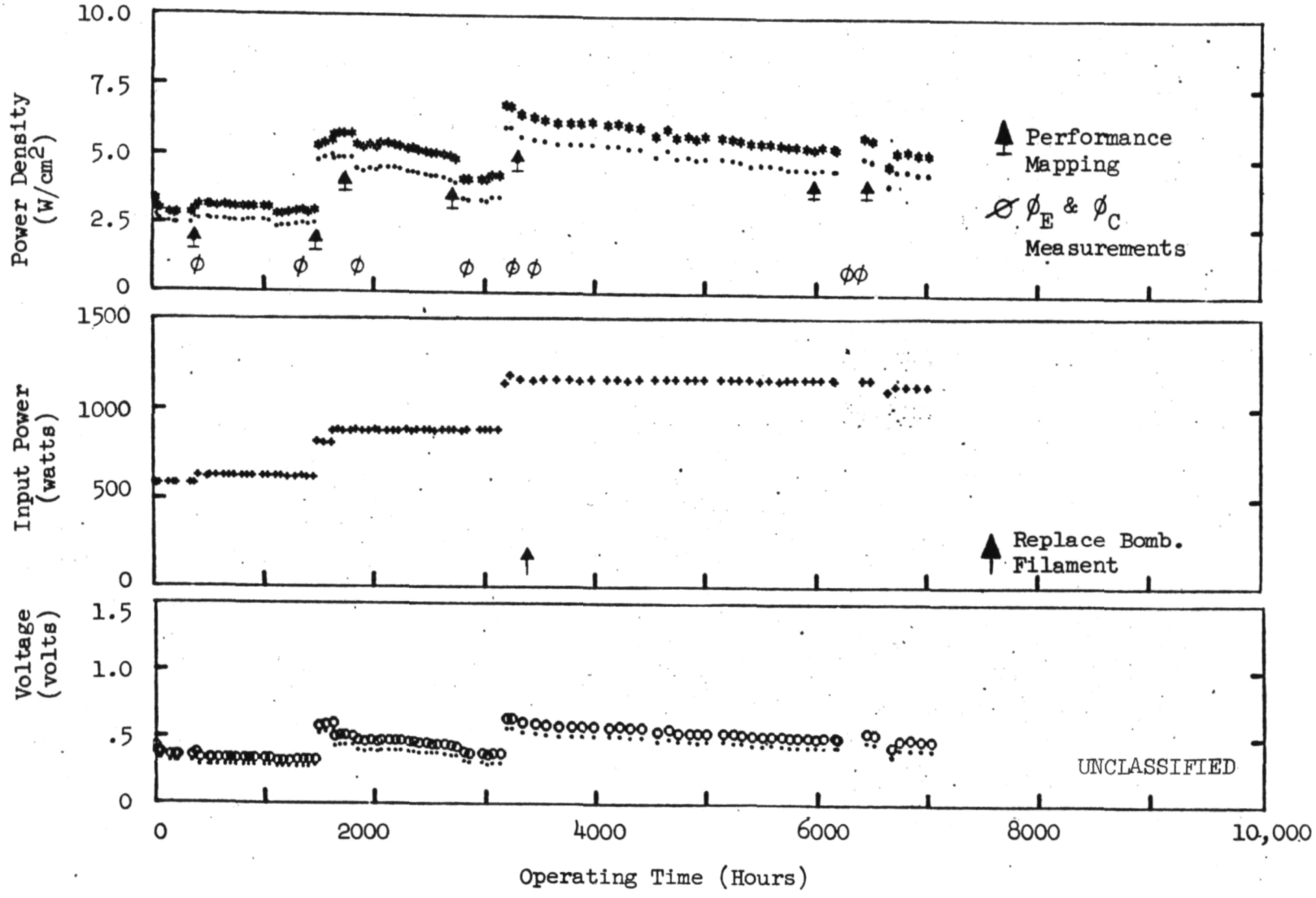

Fig. 5.12--(U) LC-8 performance history

CONFIDENTIAL

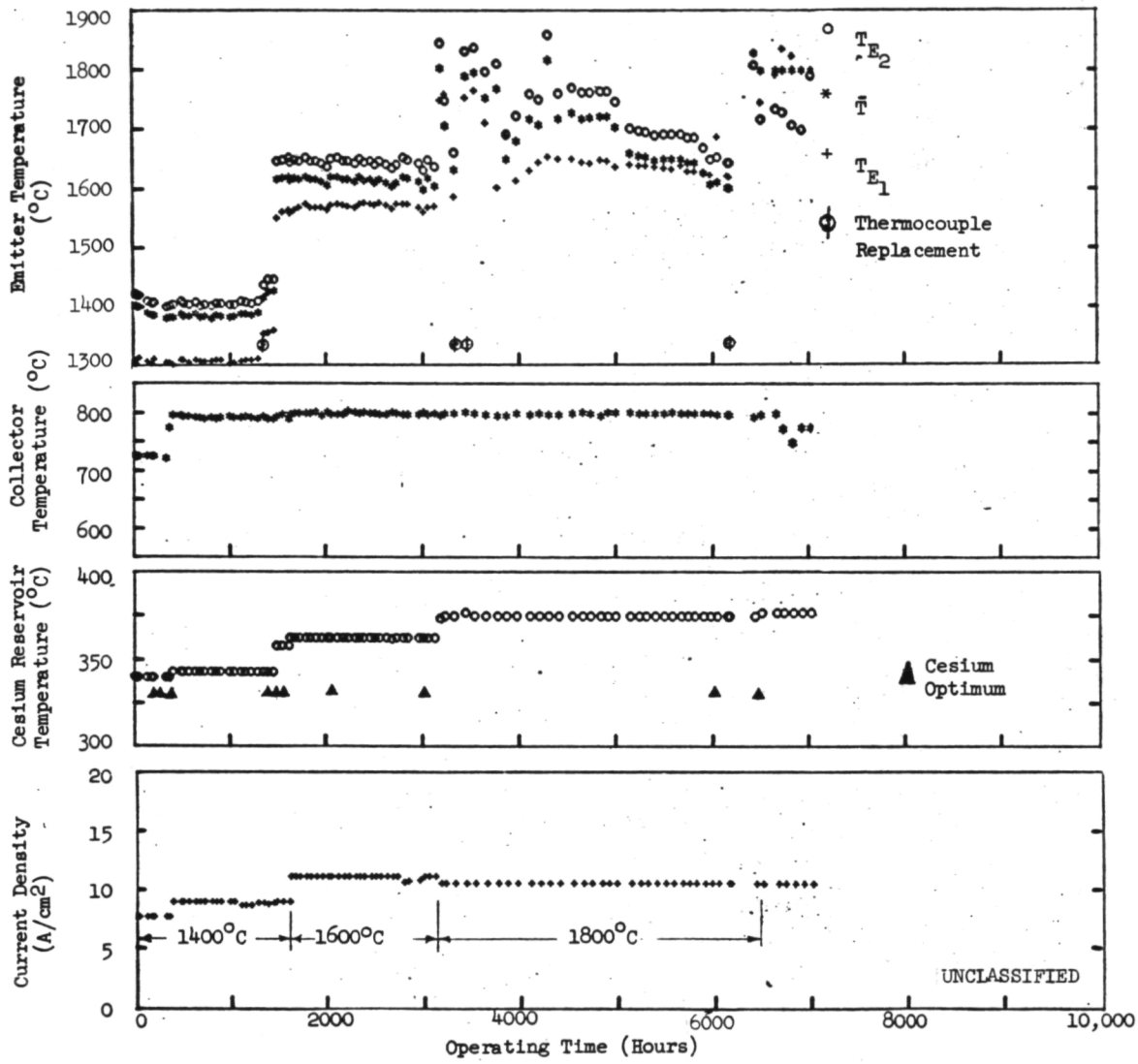

Fig. 5.13--(U) LC-8 performance history

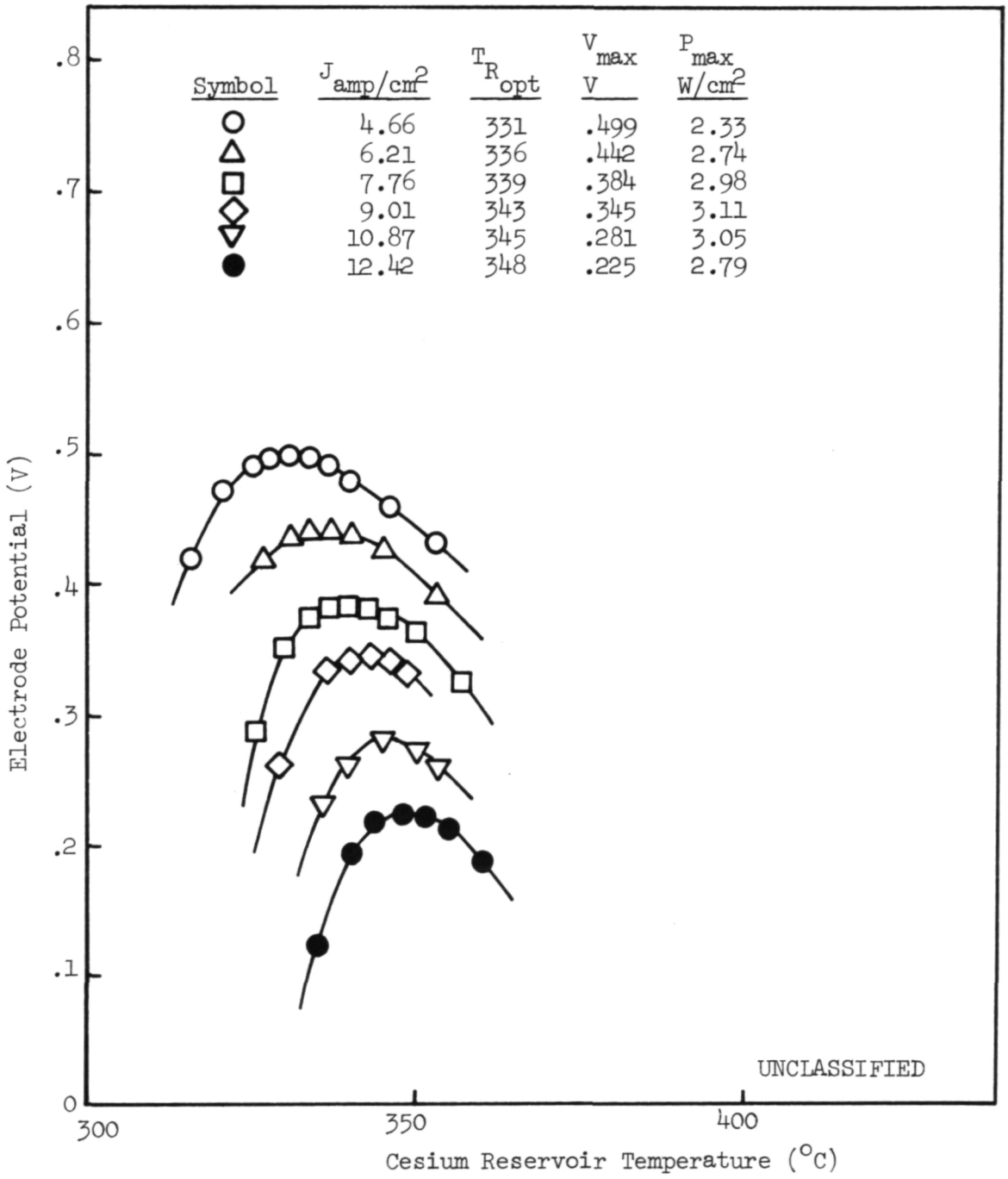

Fig. 5.14--(U) LC-8 cesium reservoir temperature optimization initial data. Emitter temperature 1400°C, collector temperature 775°C, time 353 hours

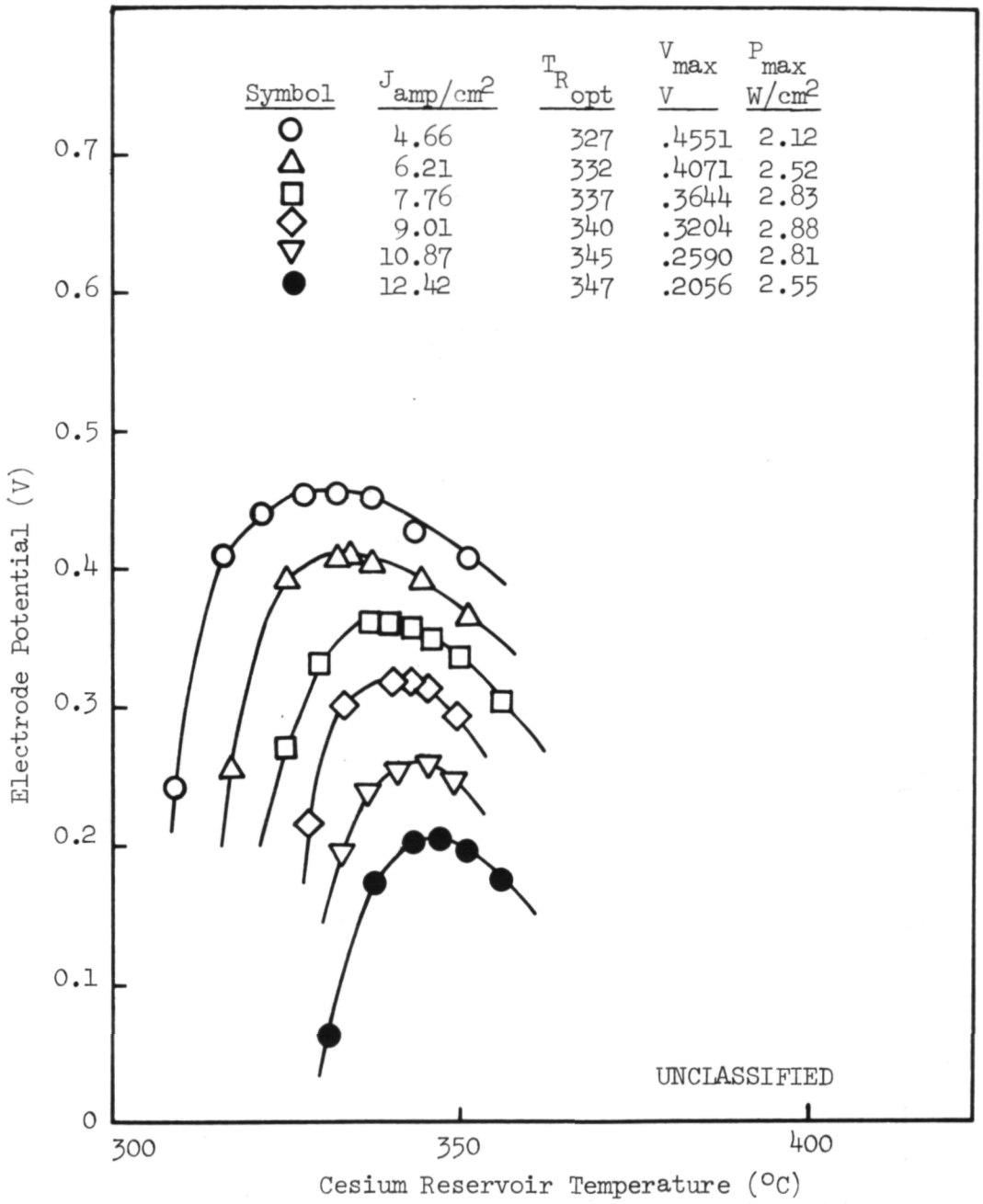

Fig. 5.15--(U) LC-8 cesium reservoir temperature optimization initial data. Emitter temperature 1400°C, collector temperature 790°C, time 1458 hours

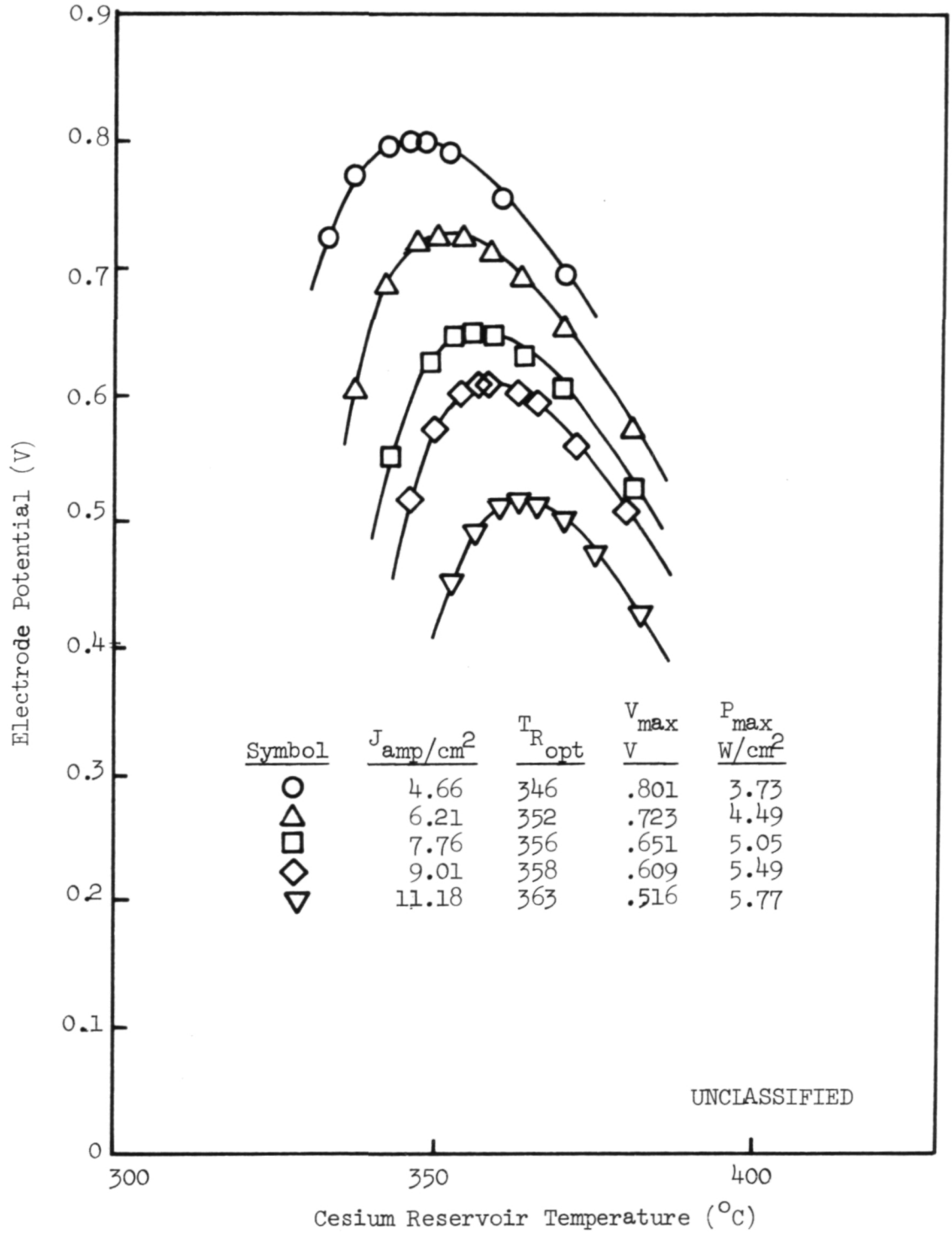

Fig. 5.16--(U) LC-8 cesium reservoir temperature optimization initial data. Emitter temperature 1600°C, collector temperature 800°C, time 1722 hours

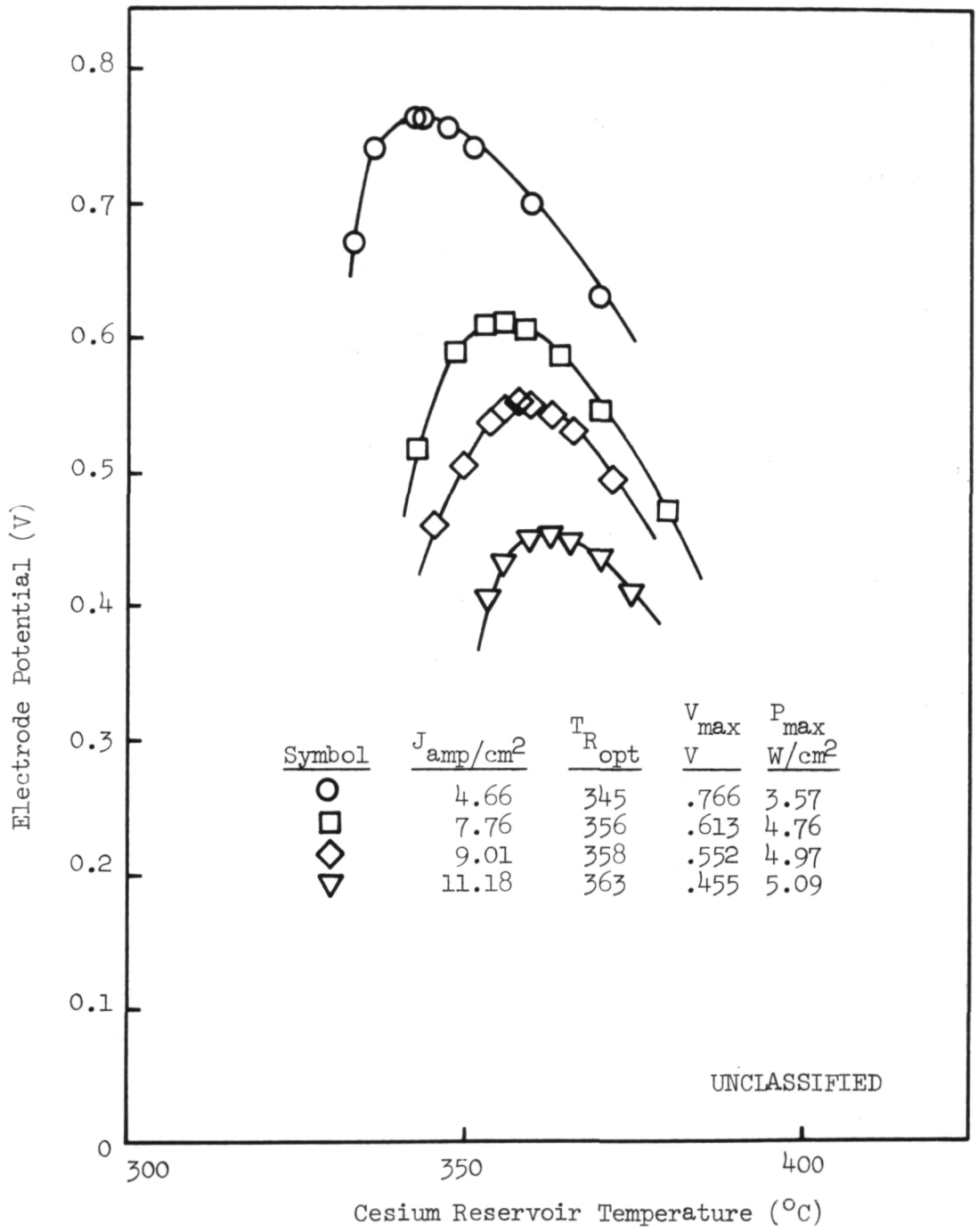

Symbol	J_{amp/cm^2}	$T_{R_{opt}}$	V_{max} V	P_{max} W/cm²
○	4.66	345	.766	3.57
□	7.76	356	.613	4.76
◇	9.01	358	.552	4.97
▽	11.18	363	.455	5.09

Fig. 5.17--(U) LC-8 cesium reservoir temperature optimization initial data. Emitter temperature 1600°C, collector temperature 800°C, time 2683 hours

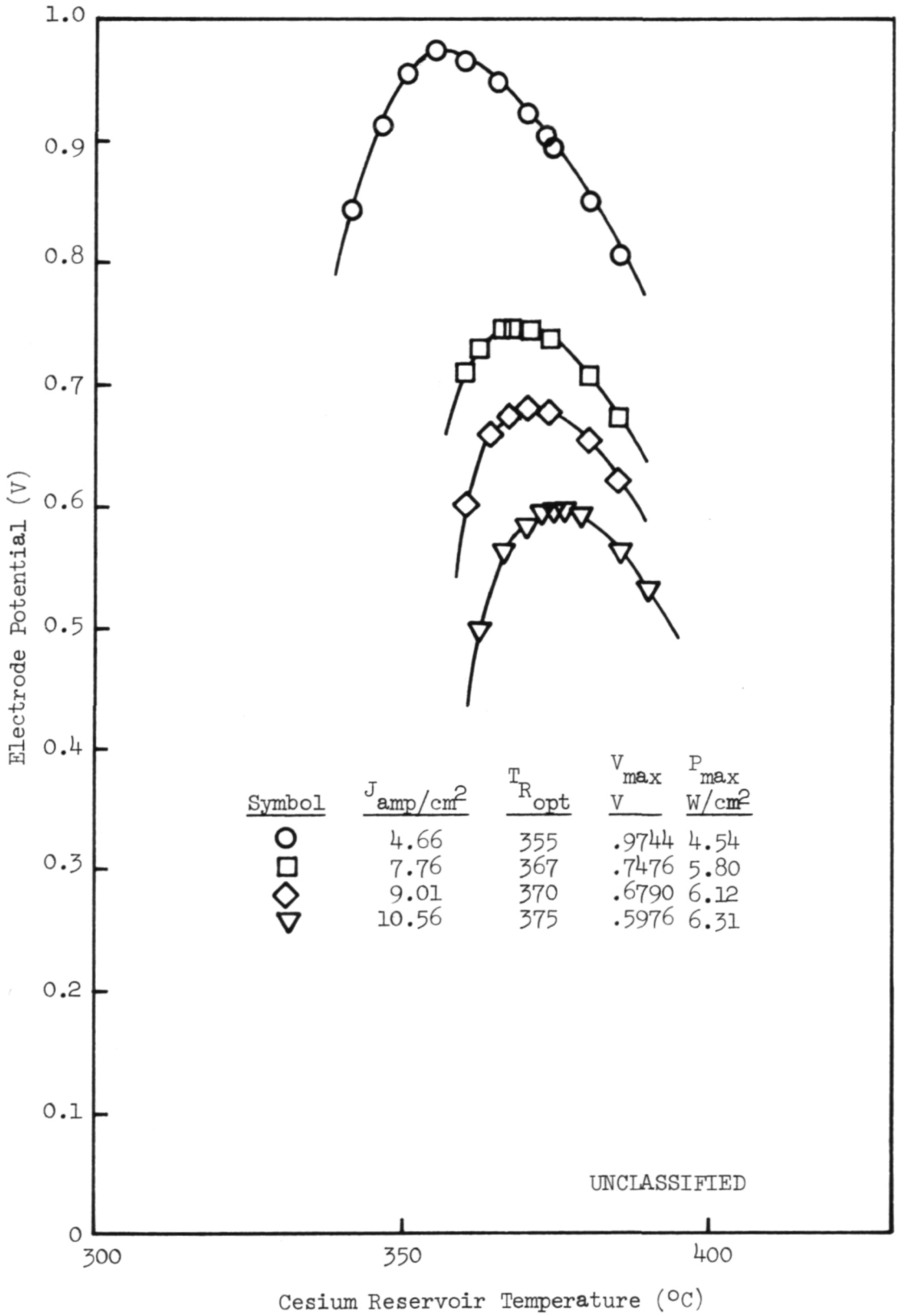

Symbol	J_{amp/cm^2}	$T_{R_{opt}}$	V_{max} V	P_{max} W/cm²
○	4.66	355	.9744	4.54
□	7.76	367	.7476	5.80
◇	9.01	370	.6790	6.12
▽	10.56	375	.5976	6.31

Fig. 5.18--(U) LC-8 cesium reservoir temperature optimization initial data. Emitter temperature 1800°C, collector temperature 800°C, time 3306 hours

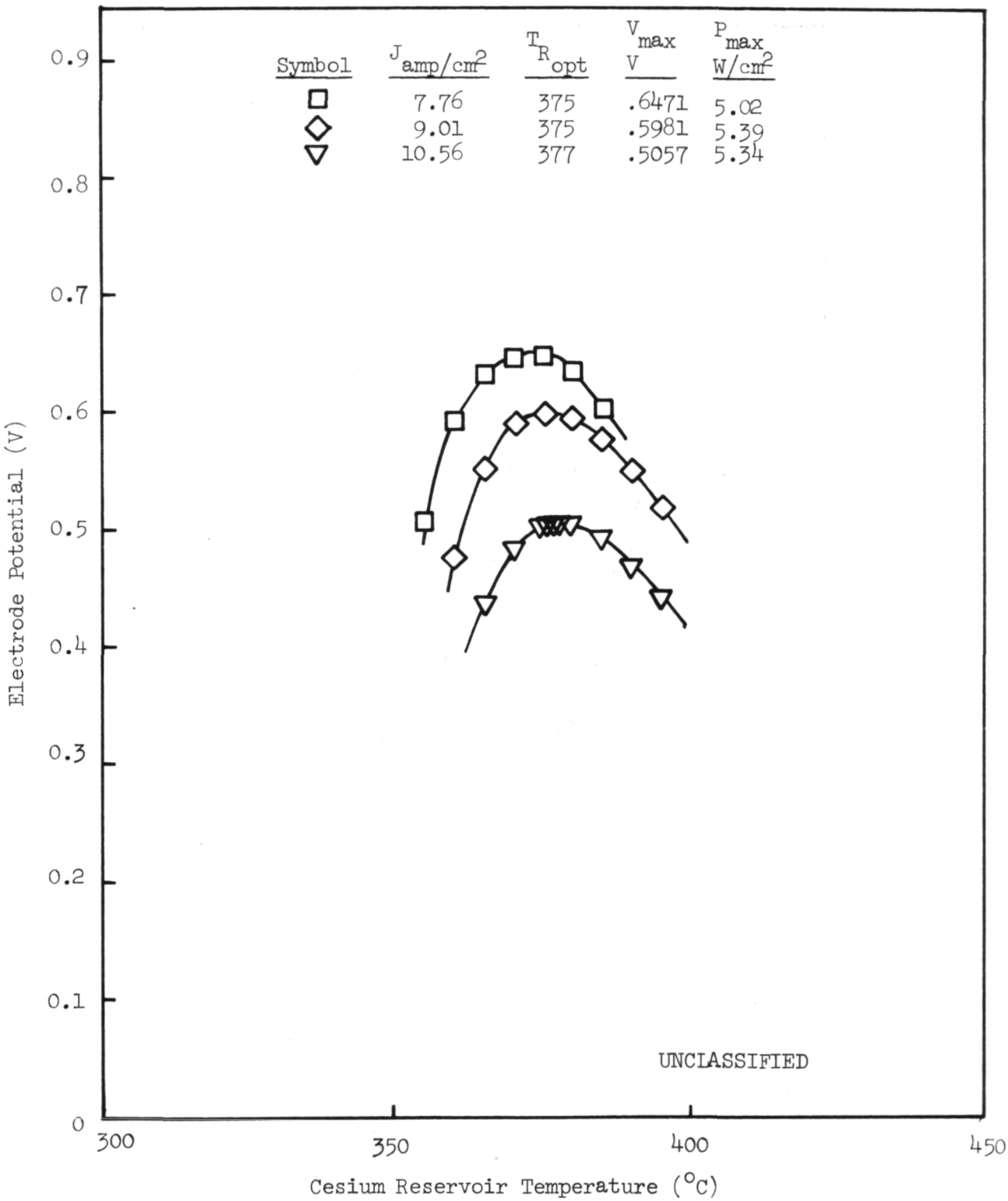

Fig. 5.19--(U) LC-8 cesium reservoir temperature optimization initial data. Emitter temperature 1800°C, collector temperature 800°C, time 5987 hours

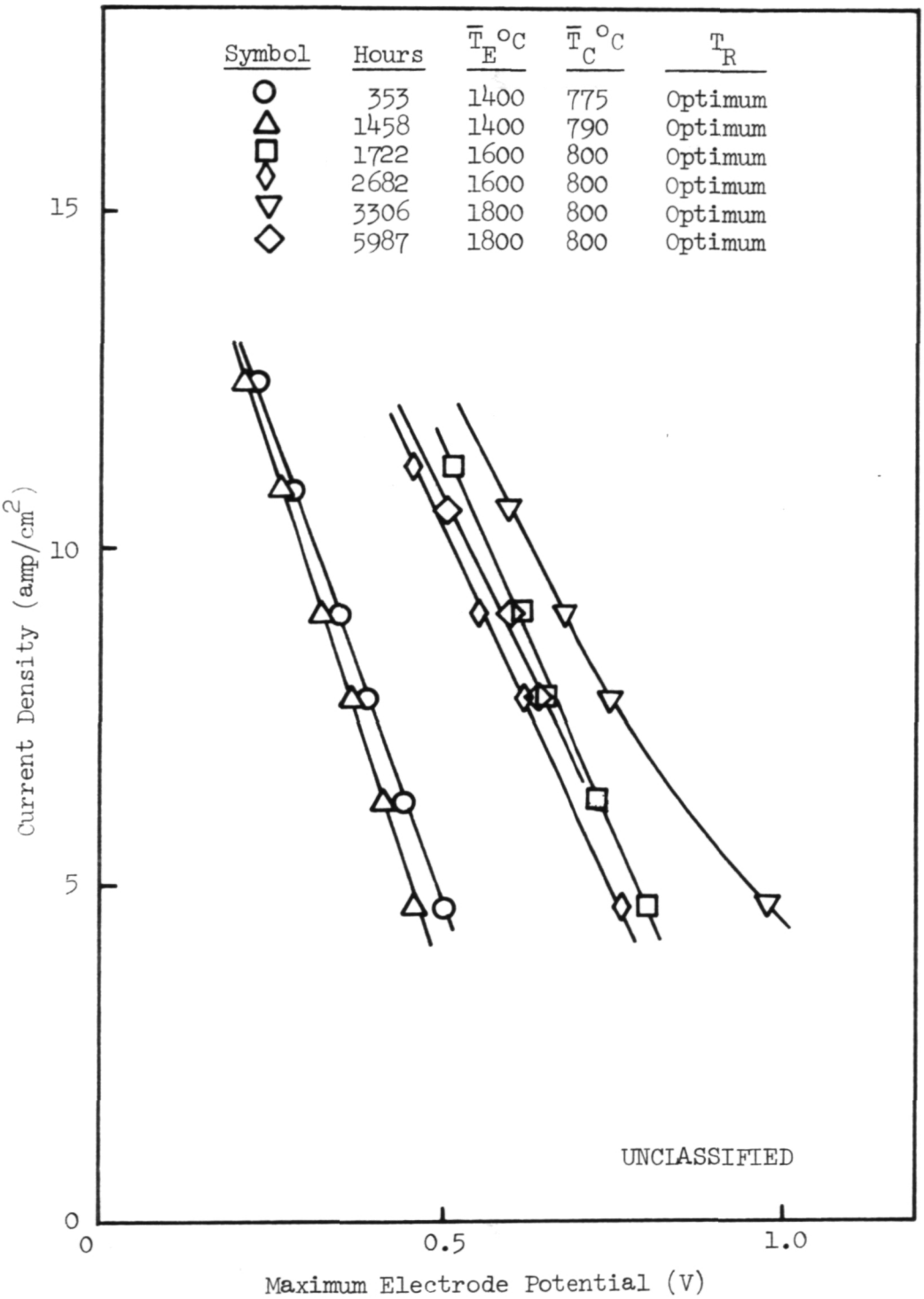

Fig. 5.20--(U) Envelope of I-V characteristics for LC-8

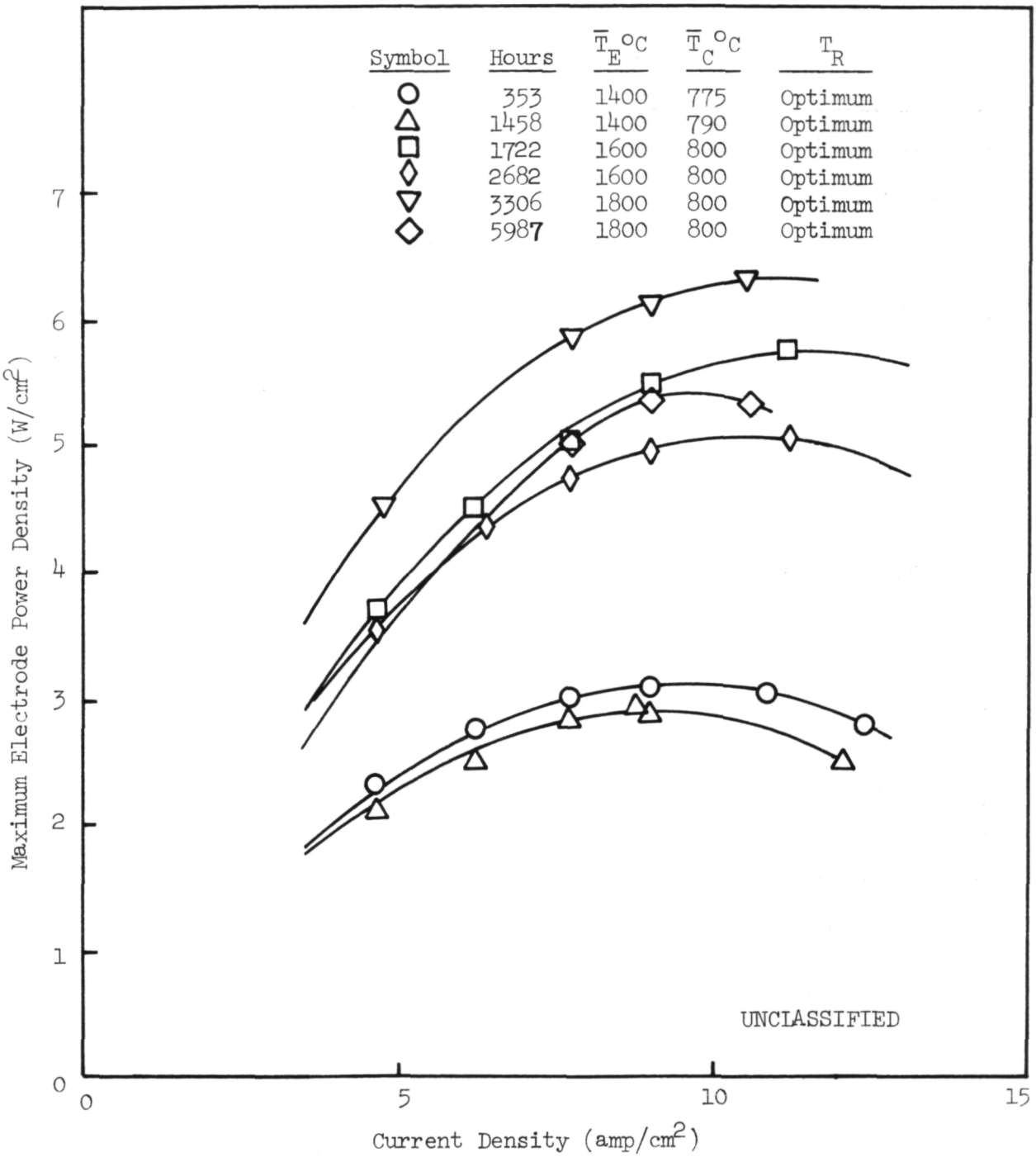

Fig. 5.21--(U) Maximum output power and optimum current determination for LC-8

Table 5.5

(U) LC-8 PERFORMANCE AND OPERATING PARAMETERS

(This table is Unclassified)

Operating Time - hours	353	1458	1722	2682	3306	7098
Input Power - watts	626	622	880	893	1160	1120
Output Power (electrode) - W/cm^2	3.11	2.88	5.77	5.09	6.31	5.07
Voltage (electrode) - volts	.345	.320	.609	.455	.598	.480
Voltage (lead) - volts	.289	.265	.550	.378	.552	.412
Current - amps	145	145	180	180	170	170
Current - density	9.01	9.01	11.18	11.18	10.56	10.56
Temperatures - ^{o}C						
Emitter Thermocouples No. 1	1301	1351	1572	1575	1586	1839
No. 2	1402	1438	1648	1649	1657	1746
Average	1351[2]	1394[2]	1610[2]	1612[2]	1800[2]	1800[2]
Estimated Surface Average	1400[2]	1400[1]	1600[1]	1600[1]	1800[2]	1800[2]
Collector	775	790	800	800	800	775
Cesium Reservoir	343	340	363	363	375	377

[1]Based on emitter temperature profile data.

[2]Based on previous data at similar operating conditions

measurements. Maximum output power decreased to 5.4 W/cm^2. At 2683 hours, the conclusion of the 1600°C emitter test, the maximum output power was 5.10 W/cm^2, a total decrease of 12% during a 1000-hour period. Following the diagnostic measurements at 2683 hours converter performance again decreased. Output power density was 4.16 W/cm^2, 18% below prediagnostic performance. The test was continued at 1600°C to determine if the output power would recover. After 200 hours the performance had not changed significantly, and the emitter temperature was increased to 1800°C. Figures 5.16 through 5.17 show the cesium optimization and performance data.

1800°C Operation

(C-RD)(Gp-1) There was no preliminary stabilization period prior to performance mapping and diagnostic measurements at 1800°C because of short term reliability of emitter thermocouples at that temperature. (High temperature stability of emitter thermocouples is discussed in Appendix 5B.) Output determined from a cursory optimization performed initially at 1800°C was 6.78 W/cm^2 at a current density of 10.56 A/cm^2 (170A). At 3306 hours the maximum output power density was 6.30 W/cm^2 at 10.56 A/cm^2. At 87 hours, maximum output power density was 5.34 W/cm^2, a decrease of 15%. At the end of this reporting period the output power density was 5.41 W/cm^2 and appeared to be stabilizing. Figures 5.18 and 5.19 show the cesium optimization and performance data.

(C-RD)(Gp-1) During work function measurements taken at ~6300 hours an intermittant interelectrode short developed. This short appeared only at certain emitter and collector temperatures and was not present upon returning to power. This behavior will be discussed more fully in Section 5.3.4.

(C-RD)(Gp-1) A total of 14 shutdowns have occurred during the operation thus far, four due to plant power outages, five due to necessary filament or thermocouple replacements, and five due to problems encountered with the control of the electron bombardment power.

(C-RD)(Gp-1) A summary of the preceeding performance data is shown in Figs. 5.20 and 5.21.

RESTRICTED DATA
ATOMIC ENERGY ACT 1954
GROUP 1

5.3.3. LC-8 Diagnostic Data

(C-RD)(Gp-1) Relative effective emittance data was taken periodically during the test at 1400°, 1600°, or 1800°C. The only consistant set of data was that taken at 1400°C. This set indicates a 10% increase in the effective emittance over the test life. Since this change corresponds to a thermocouple error of only 25°C, very little significance can be placed on these results.

(C-RD)(Gp-1) Emitter and collector work function data was obtained periodically during the test and is shown in Fig. 5.22. The cesiated emitter work function data taken at 1400°C indicate that the base work function was about 4.7 eV, a value close to that observed during preoperational vacuum work function measurements (see Appendix 5A). However, the value at 1800°C appeared to be near 4.5 eV, a value close to that expected from tungsten deposited from WF_6.

(C-RD)(Gp-1) The cesiated collector work function at 1400°C taken at the beginning and end of the 1000 hour test are reasonably consistant, as in the first set of data taken at 1600°C. However, the second set of data at 1600°C indicates an increase in the cesiated work function of ~0.1 eV. The cesiated work function continued to increase through the 1800°C operation and ended up ~0.3 eV higher than the original values at 1400°C.

(C-RD)(Gp-1) Collector optimization data was also taken periodically during the test. Optimum curves taken at 1400°, 1600°, and 1800°C are shown in Fig. 5.23 as electrode voltage versus the ratio of collector temperature to cesium reservoir temperature. The value of this ratio which gives the optimum voltage should be the same for the three cases. However, this was not the case for the 1800°C curve. The data at 1800°C was taken at 6230 hours following work function measurement. The optimum collector temperature increased with time and was close to 800°C by the end of this reporting period.

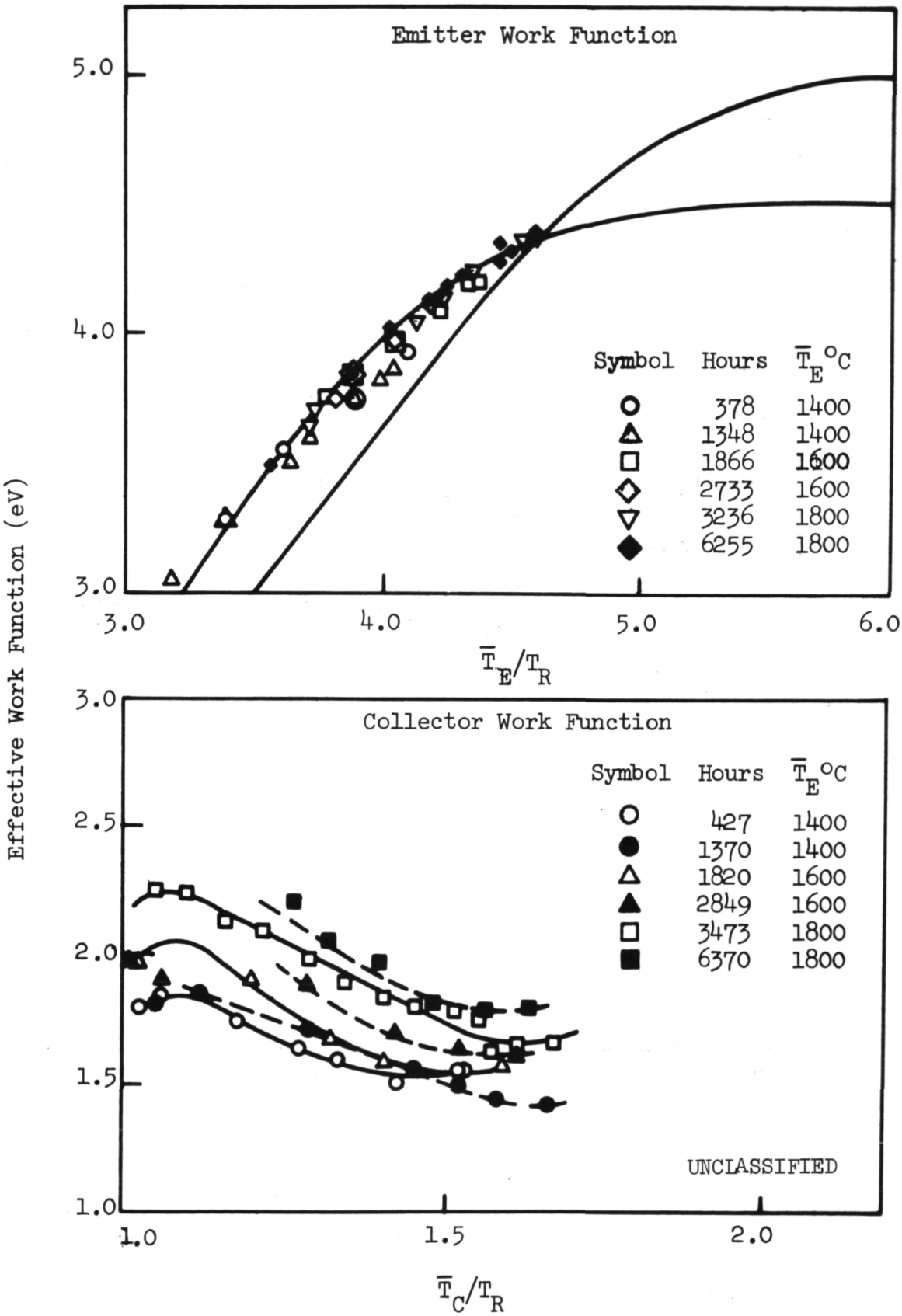

Fig. 5.22--(U) Emitter and collector work function

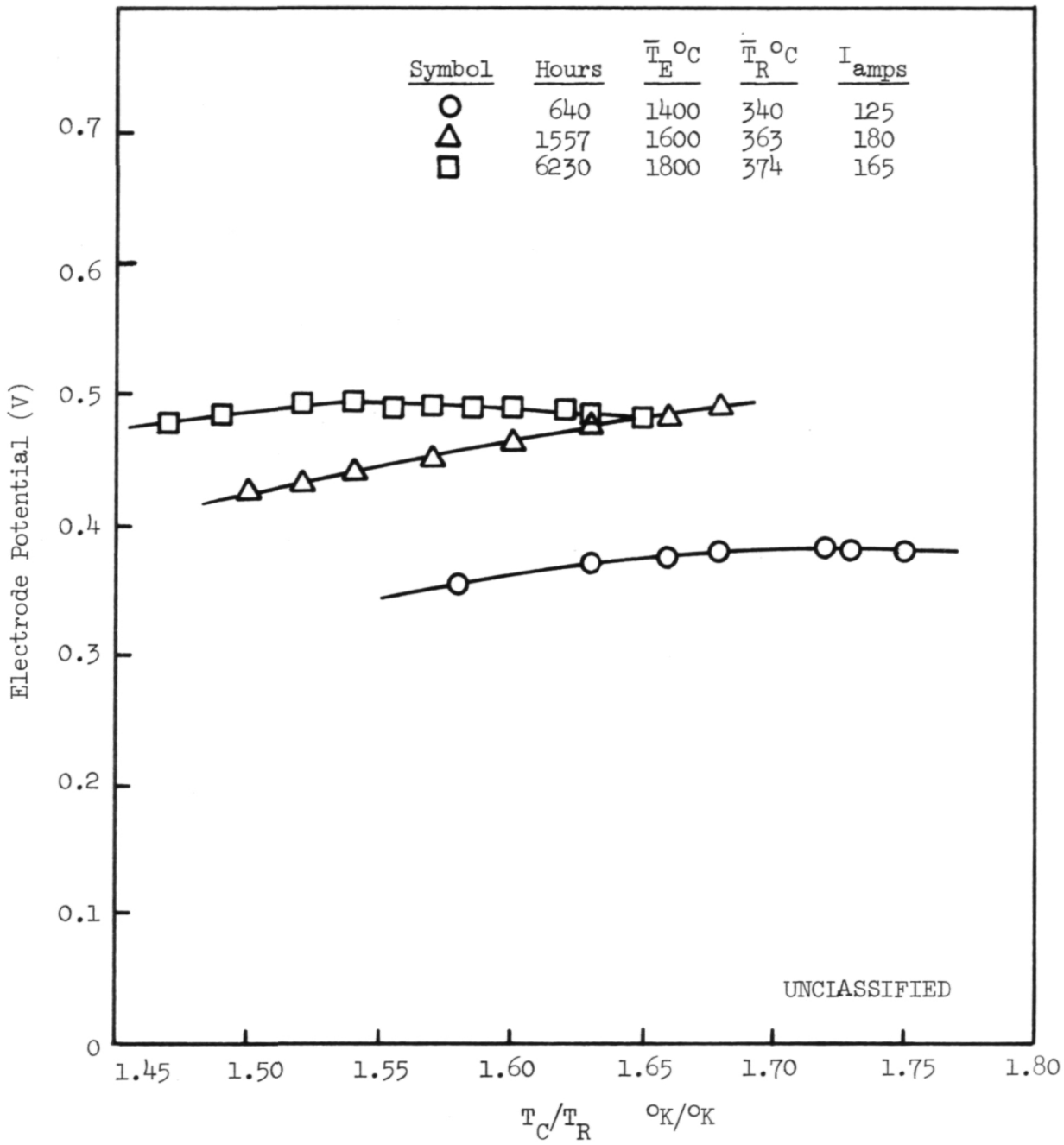

Fig. 5.23--(U) LC-8 collector temperature optimization

CONFIDENTIAL

5.3.4. Interpretation of the LC-8 Results

(C-RD)(Gp-1) The performance of LC-8 at 1800°C is compared to that of LC-7 in Fig. 5.24. The two converters can be compared only at 1800°C because LC-7 was not mapped at any other emitter temperature. The first data point taken on the LC-8 converter falls within 2% of the LC-7 curve. The mapping done at 3306 hours falls about 10% below this curve at 10 amps/cm^2; the point at 5987 hours falls ~25% below this curve.

(C-RD)(Gp-1) The observed changes in power output are interpreted to be the result of work function changes due to the accumulation of fuel constituents on the emitter and collector surfaces. The emitter work function data indicates that the value at 1400°C was ~4.7 eV and was ~4.5 eV at 1800°C. Since the latter value is typical of this type of tungsten, some of the performance loss was due to the removal of a high work function material from the emitter surface. This effect has been observed before in carbon rich fuels.(3),(4) The stabilization time required when the emitter was first taken to 1400°, 1600°, and 1800°C were probably due to the evaporative removal of fuel constituents from the emitter surface as described in Reference 4.

(C-RD)(Gp-1) The observed increases in cesiated collector work function undoubtedly contributed to the observed power losses. In fact, since the emitter work function at 1800°C returned to the normal value of 4.5 eV, all of the power loss at this temperature is probably due to collector effects.

(C-RD)(Gp-1) The interelectrode short which was observed ~6300 hours could be due to cocking of the emitter, emitter (or collector) dimensional changes, or to a buildup of material (such as fuel) in the interelectrode space. Since the diffusion of fuel through the clad should not have caused the observed contamination because of stoichiometry control and tungsten addition, it is possible that the emitter has cracks in it which could introduced a large amount of fuel into the interelectrode space or could cause a tungsten layer to pull away from the emitter surface. The exact reasons for the shorting behavior may only be discovered during the post-operational examination.

CONFIDENTIAL

RESTRICTED DATA
ATOMIC ENERGY ACT 1954
GROUP 1

CONFIDENTIAL

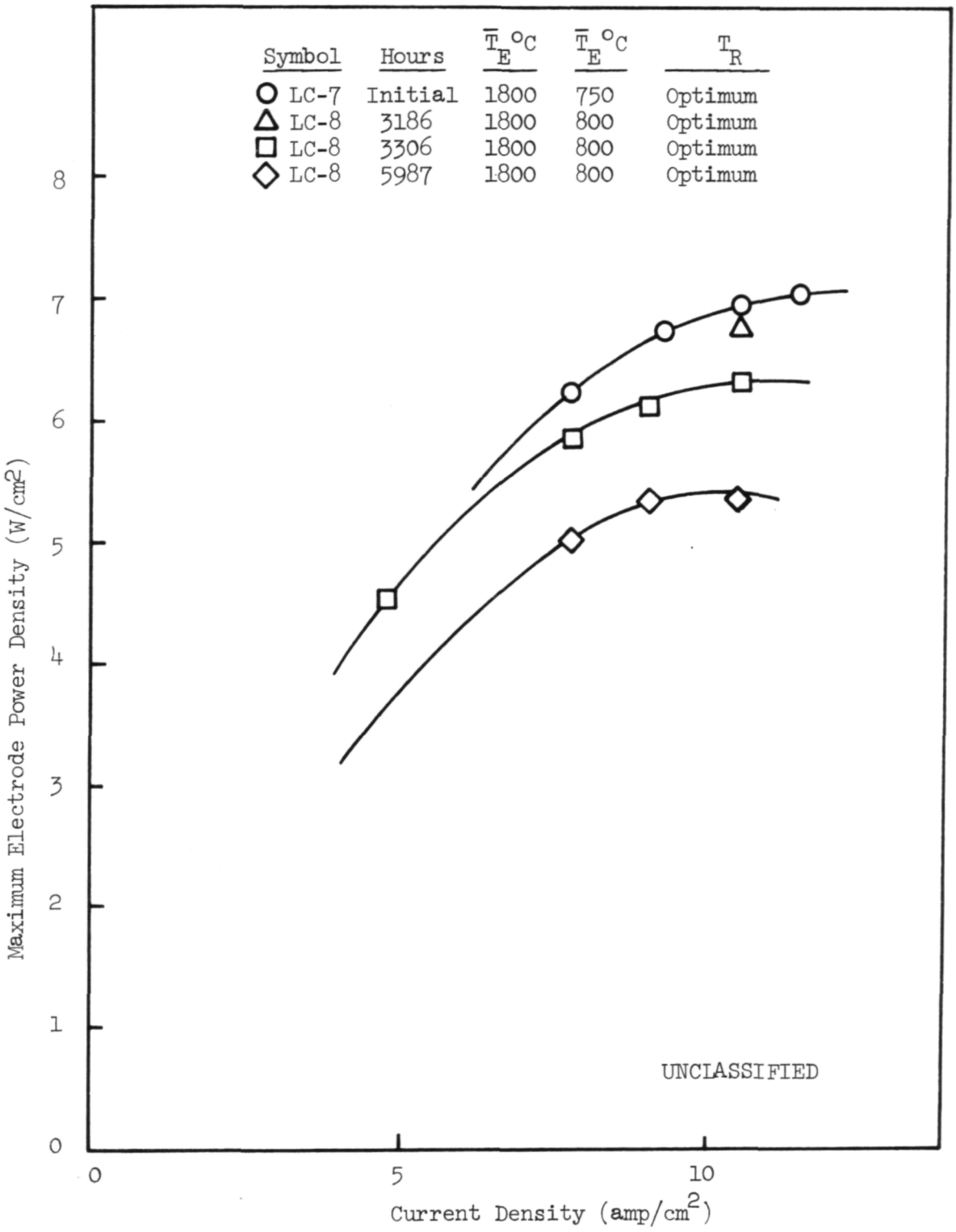

Fig. 5.24--(U) Maximum output power and optimum current determination for LC-7 and LC-8 at 1800°C

CONFIDENTIAL
RESTRICTED DATA
ATOMIC ENERGY ACT 1954
GROUP 1

5.4. LC-9 TEST (UNFUELED HIGH-WORK-FUNCTION EMITTER)

(U) The main purpose of the LC-9 test was to determine the long-term stability of a duplex, high work function emitter. The design of the converter was identical to that of LC-7 except for an 0.0125 inch layer of tungsten deposited from WCl_6 which formed the emitter surface. All components were bulk degassed as in the other two converters, and LC-9 was operated in a glass bell jar vacuum system which had a typical operating pressure of 4×10^{-8} torr.

5.4.1. LC-9 Initial Performance

(U) The initial performance mapping data and work function measurements on LC-9 were obtained over the first three hundred hours of the test.

(U) Three sets of performance data were obtained at 0, 169, and 330 hours, and all were considered to be part of the initial performance mapping. The test was to be at an 1800°C average emitter temperature, T_E, and optimum values for the current density J, cesium reservoir temperature T_R, and collector temperature T_C. The collector temperature maximum was initially set at 750°C.

(U) At startup it was found that collector heat rejection was limited, a condition which in turn limited the current density to values below optimum. The heat rejection capability of the LC-9 heat sink was determined to be 35% less than that found for the LC-7 heat sink. Incomplete wetting of a braze joint is suspected to be the cause of the discrepancy. For the startup measurements, T_E was decreased to 1700°C to obtain a value of J that was nearer optimum. The zero-hour performance mapping data at T_E = 1708°C are shown in Fig. 5.25 in the form of cesium reservoir optimization data with current density a parameter. Figure 5.26 is a plot of the maximum electrode voltage V_{max} (from the curves in Fig. 5.25) versus the current density J, which is the envelope of I-V curves. Other data in that figure will be discussed below. Figure 5.27 shows the maximum electrode output power P_{max} as a function of J for emitter temperatures of 1700°C and 1800°C and collector temperatures of 742-767°C and 800°C. It may be seen that the current for optimum

UNCLASSIFIED

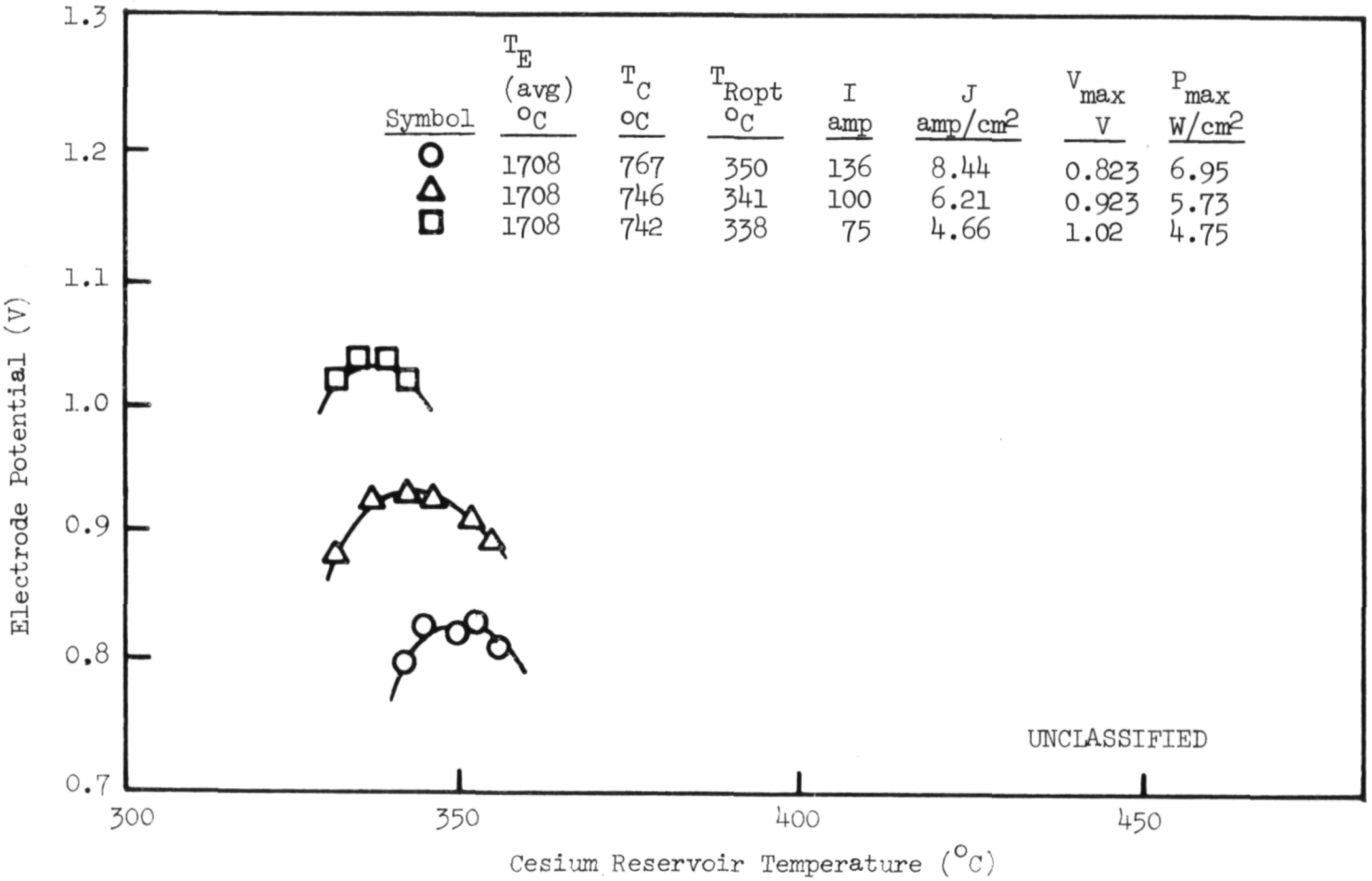

Fig. 5.25--(U) LC-9 initial cesium reservoir temperature optimization data

UNCLASSIFIED

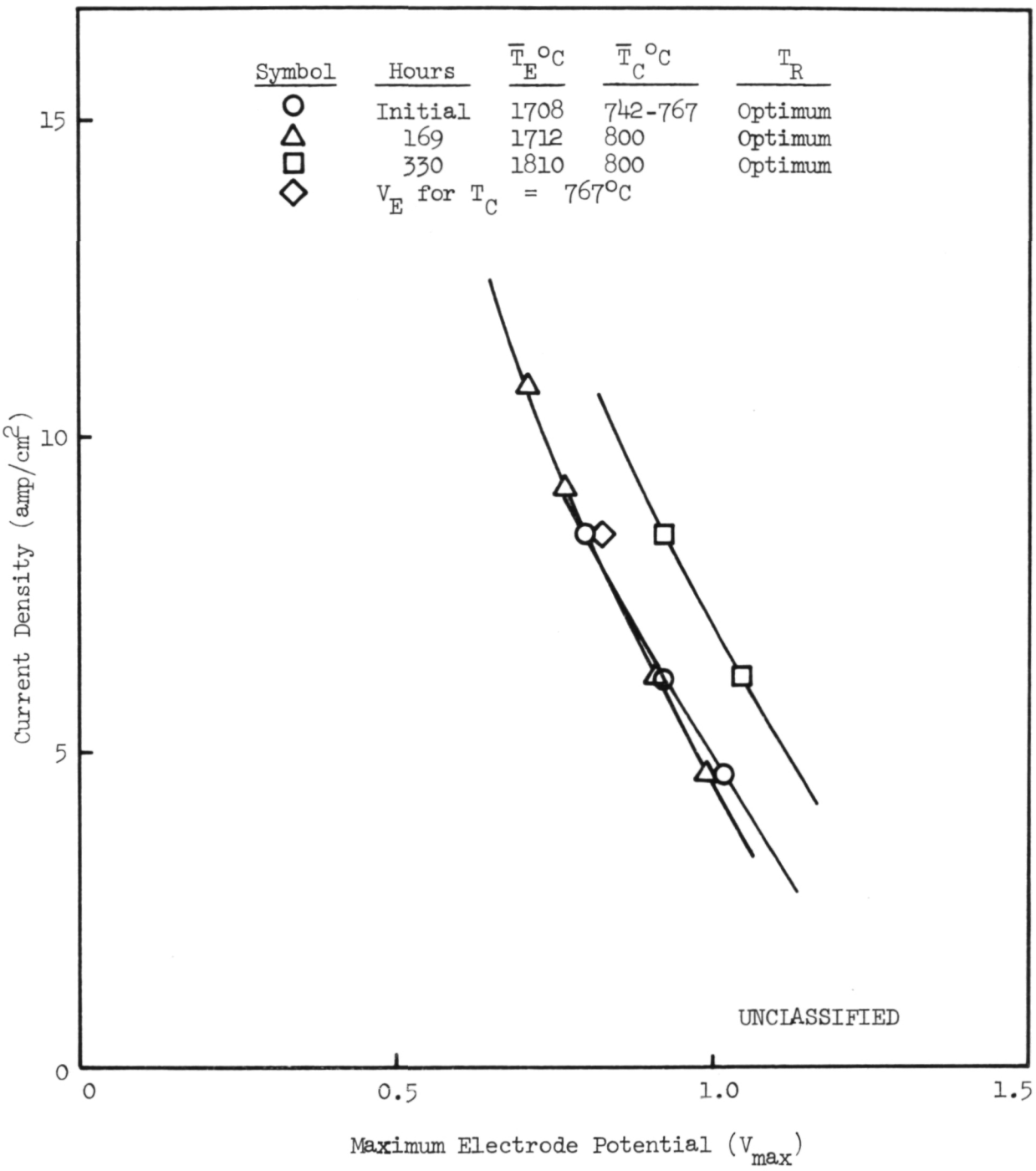

Fig. 5.26--(U) Envelope of I-V characteristics for LC-9

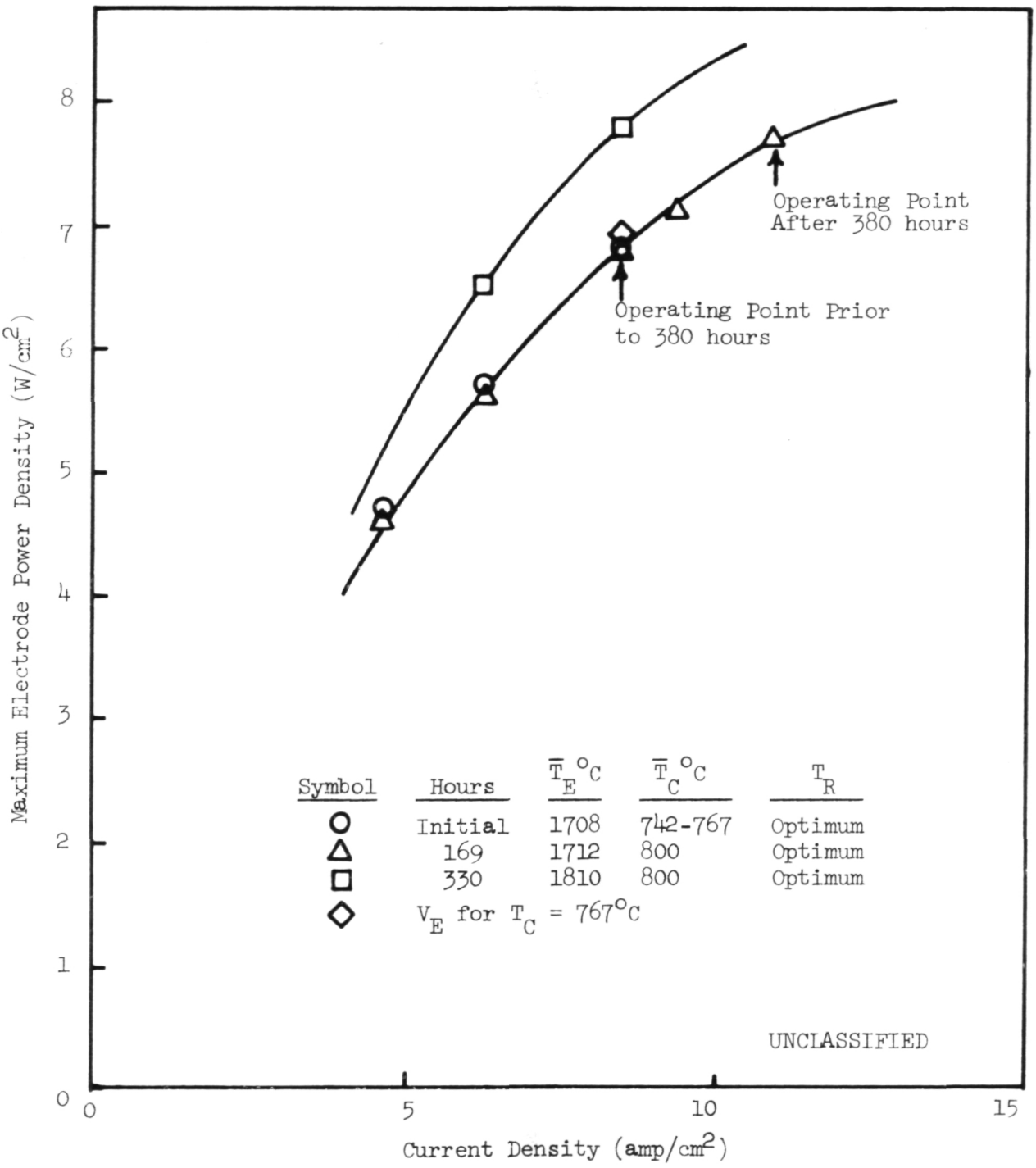

Fig. 5.27--(U) Maximum output power and optimum current determination for LC-9

power could not be reached within the collector temperature limitation initially set (750°C). At a current of 8.44 amp/cm^2, P_{max} was found to be 6.95 W/cm^2 at a T_C value of 767°C. By correcting V_E to T_C value of 745°C, where the other zero-hour data were obtained, P_{max} would have been 6.75 W/cm^2. The voltage correction is based on measurements taken later in the test, as described in the following paragraph.

(U) Collector optimization data, obtained at 162 hours is shown in Fig. 5.28. The curve indicates $T_C$opt. to be above 800°C for a T_E value of 1712°C and a J value of 8.44 amp/cm^2. The shape of the optimization curve closely matches that of the LC-7 curve in Fig. 5.10.

(U) At 169 hours the converter was again performance-mapped at T_E = 1700°C but with T_C increased to 800°C. As shown in Fig. 5.27, P_{max} was 7.71 W/cm^2 at a J value of 10.96 amp/cm^2. Rough extrapolation of the maximum performance data indicates the optimum J to be of the order of 14 amp/cm^2 and P_{max} at J_{opt} to be greater than 8 W/cm^2. Taking into account the collector temperature increase, the initial and 169 hour output powers corresponded within experimental uncertainties.

(U) After 328 hours, the helium used in the collector heat sink gas gap was replaced with hydrogen to try to improve the heat sink rejection capabilities. Heat rejection was only slightly improved by the hydrogen, with the result that optimization at 1800°C was limited to a J_{max} of 8.44 amp/cm^2 at a T_C of 800°C. The electrode output power at those conditions was 7.80 W/cm^2. From the P_{max} curve in Fig. 5.27, it appears that the J_{opt} would have been around 15 amp/cm^2, and P_{max} at J_{opt} would have been between 9.5 and 10 W/cm^2. The P_{max} of LC-9 is compared with the performance of other converters in Section 5.4.4.

(U) The initial temperature distribution of the emitter thermocouple in the converter at zero current is shown in Fig. 5.29, together with the data taken during the emitter temperature profile measurement (see Appendix 5A). The agreement between the emitter thermocouple readings taken in the

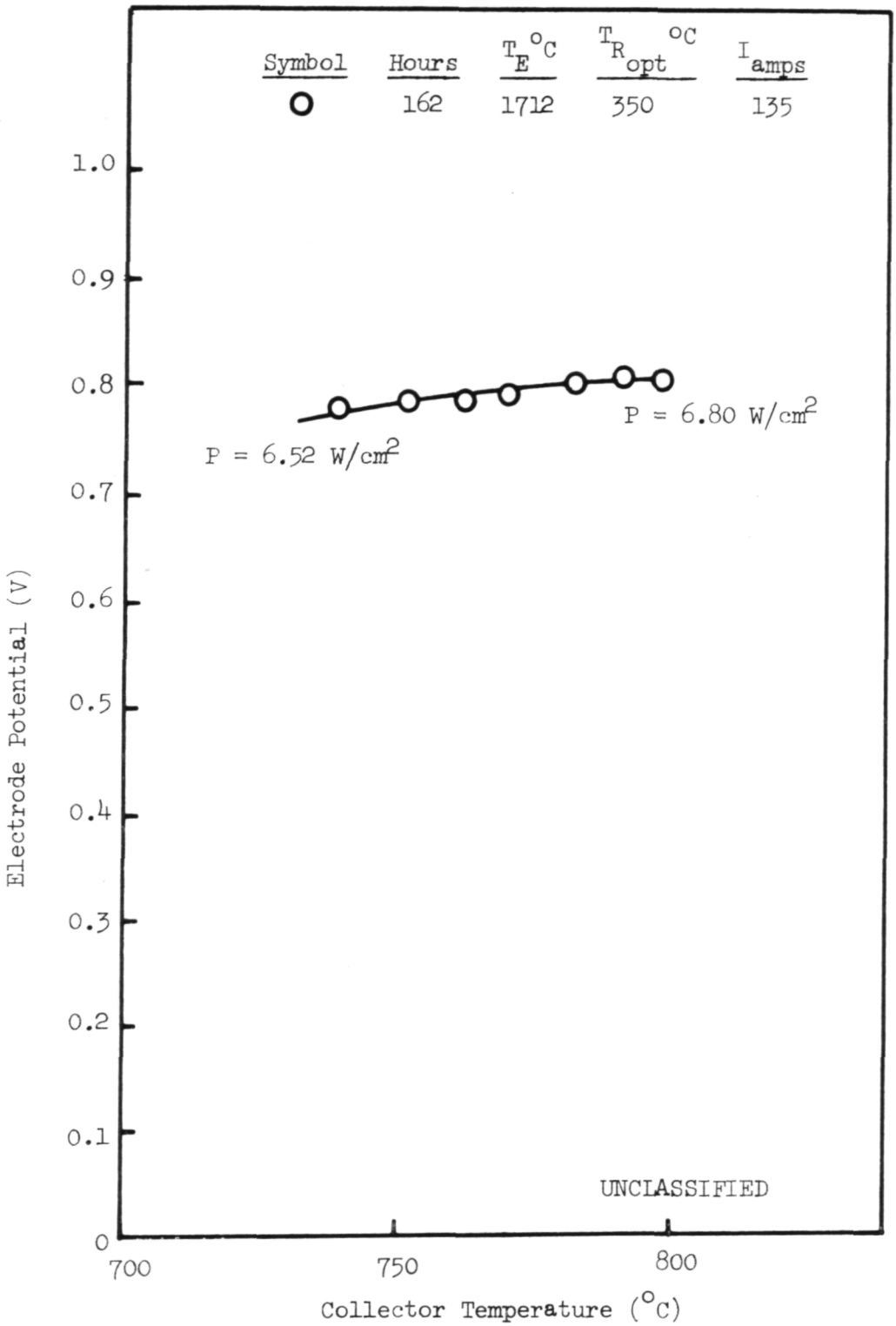

Fig. 5.28--(U) LC-9 collector temperature optimization

CONFIDENTIAL

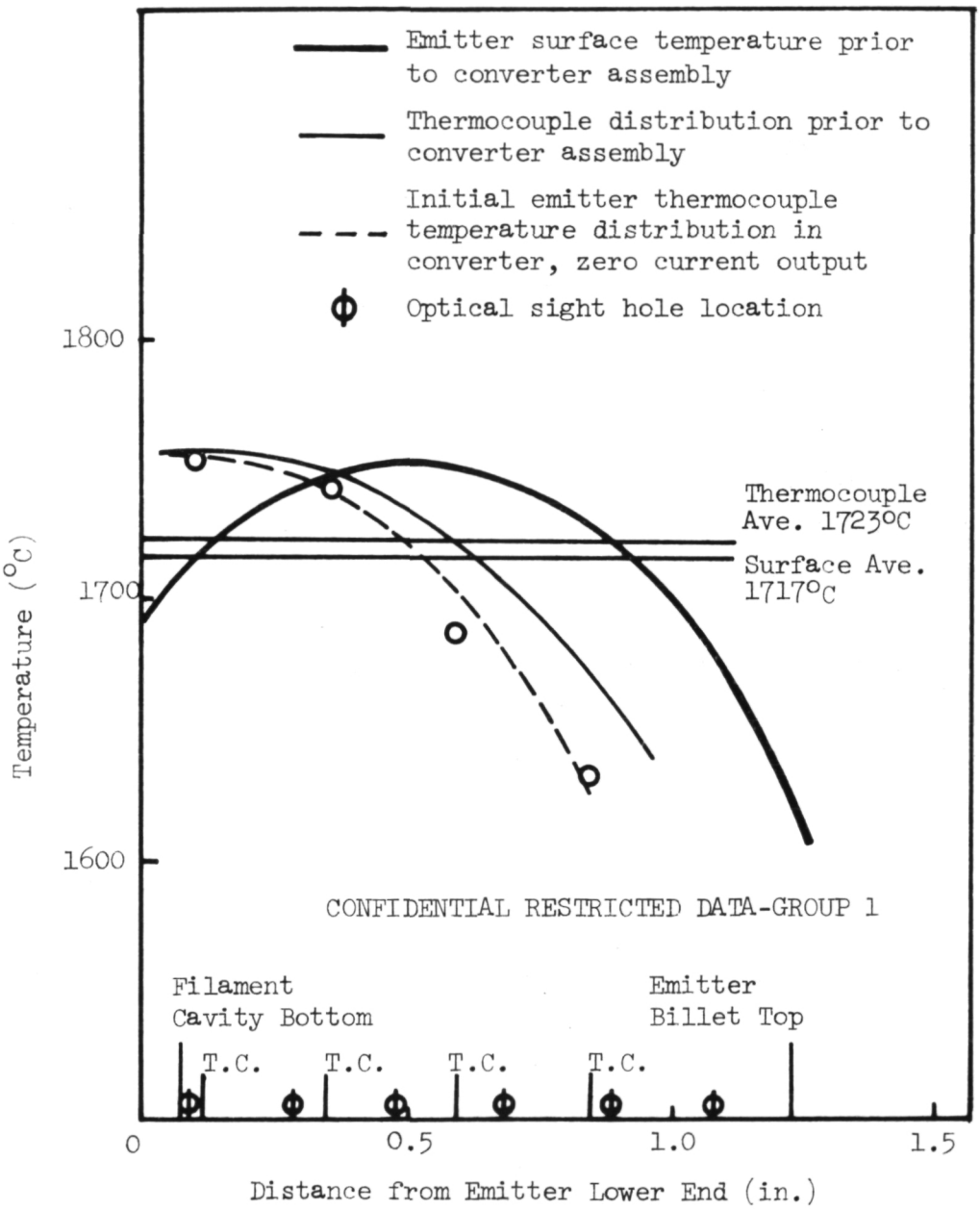

Fig. 5.29--(U) LC-9 emitter temperature profile and thermocouple distribution in converter compared with pre-converter-assembly data

CONFIDENTIAL
RESTRICTED DATA
ATOMIC ENERGY ACT 1954
GROUP 1

converter and those taken during emitter temperature profile measurement is excellent. In Appendix 5A it was found that the average of thermocouple readings was within 5°C of the average surface temperature. Therefore, in the converter the average of the thermocouples could be assumed to be equal to the true surface temperature average.

5.4.2. LC-9 Operating History

(U) Operating history for LC-9 is shown in Figs. 5.30 and 5.31 for total of 20,696 hours accumulated since start of testing on 27 December 1966. Converter performance for initial and at selected times during testing with an emitter surface average temperature of 1700°C is shown in Table 5.6. Operation up to 380 hours continued at initial conditions because of a restriction imposed by the heat rejection capability of the collector heat sink. Prior to 380 hours collector temperature was maintained at 800°C during performance mapping by flowing helium gas through the collector gas gap. However, this technique was not practical for continuous converter operation. Improvement in heat transfer by the addition of hydrogen in the heat sink gas gap permitted operation at higher current density of 10.56 A/cm^2 and a collector temperature of 800°C. At these conditions an output power density of 7.54 W/cm^2 was obtained. Results of several performance mappings are shown with the initial data in Figs. 5.32 and 5.33.

(U) At 2453 hours, following a filament replacement, converter performance increased to 8.00 W/cm^2 and continued at that value within the experimental uncertainties for the remainder of this report period. The only difference in converter operation at that time was a flattening of the emitter temperature profile which is compared in Fig. 5.34 with a previous profile determined at 1170 hours. Only the thermocouple nearest to the emitter top (T_{E4}) had been replaced between profile measurements. The change in profile was probably the result of welding the filament to the center post. Previous filaments were not welded and exhibited a localized heating at the center post contact. The same observation was made on the LC-7 filaments.

UNCLASSIFIED

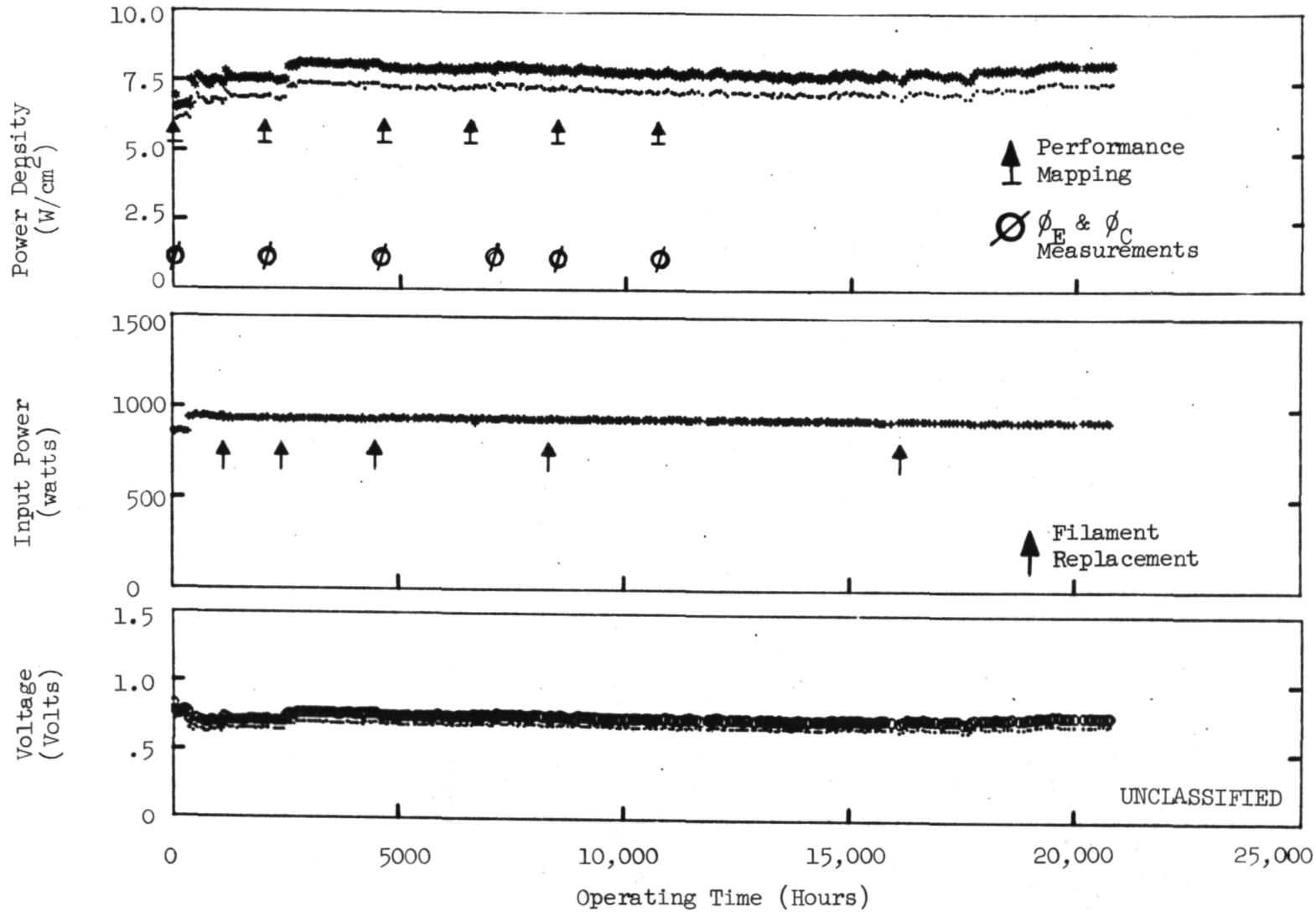

Fig. 5.30--(U) LC-9 Performance history

UNCLASSIFIED

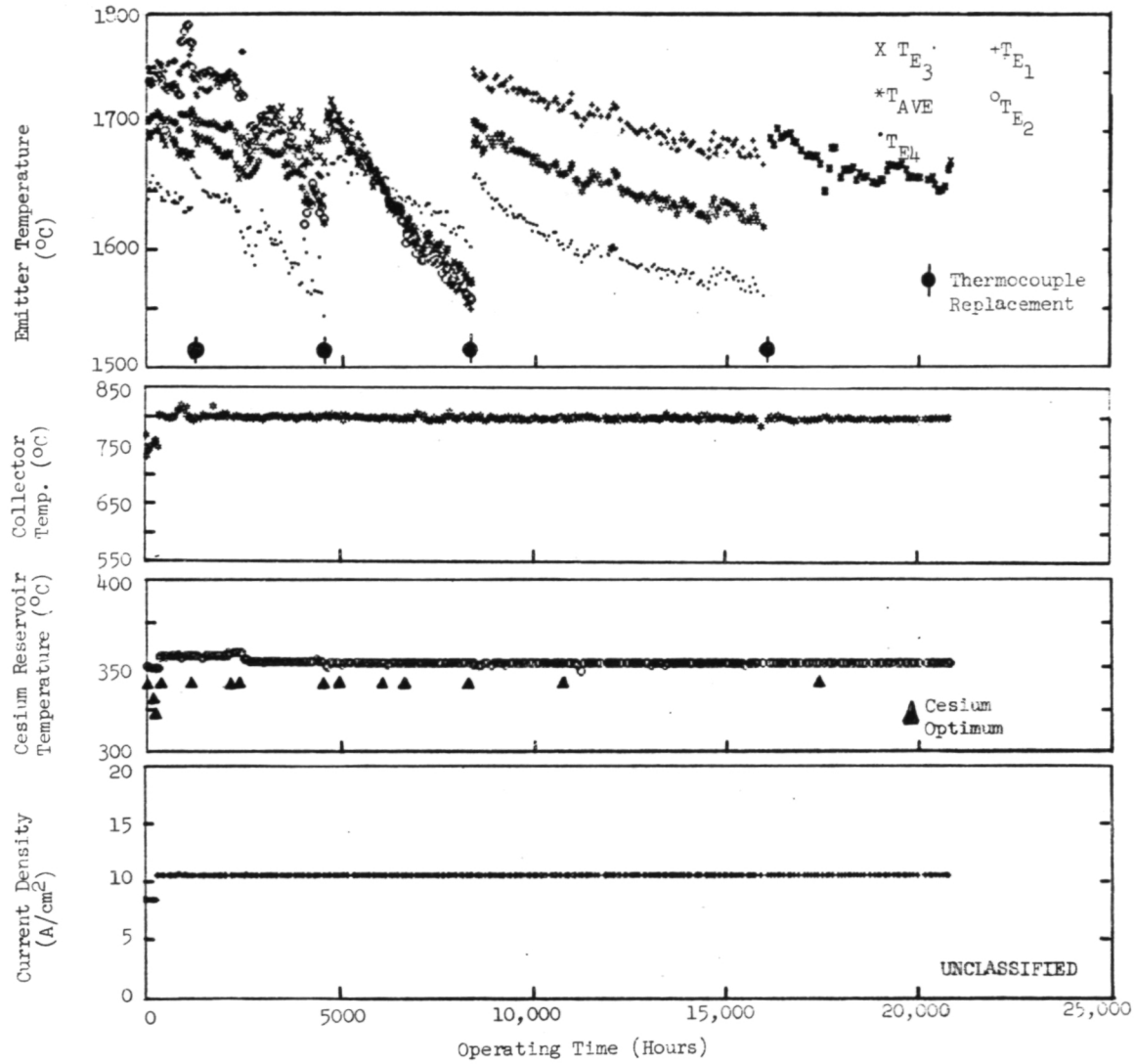

Fig. 5.31--(U) LC-9 performance history

Table 5.6

(U) LC-9 PERFORMANCE AND OPERATING PARAMETERS

(This table is Unclassified)

Operating Time - hours	0	380	2519	20696
Input Power - watts	855	934	931	933
Output Power (electrode) - W/cm^2	6.95	7.54	8.00	8.18
Voltage (electrode) - volts	.823	.714	.756	.775
Voltage (lead) - volts	.770	.646	.687	.709
Current - amp	136	170	170	170
Current Density - amp/cm^2	8.44	10.56	10.56	10.56
Temperatures - ^oC				
Emitter Thermocouples No. 1	1754	1756	1682	None
No. 2	1743	1743	1688	None
No. 3	1696	1696	1682	1667
No. 4	1642	1644	1597	None
Average	1708	1709	1662	1667
Estimated Surface Average	1709	1709	1700[1]	1700[2]
Collector	767	800	797	800
Cesium Reservoir	350	356	353	352

[1]Thermocouple readings unreliable. Average surface temperature estimated to be 1700°C based on previous data at similar operating conditions.

[2]Based on previous data at similar operating conditions

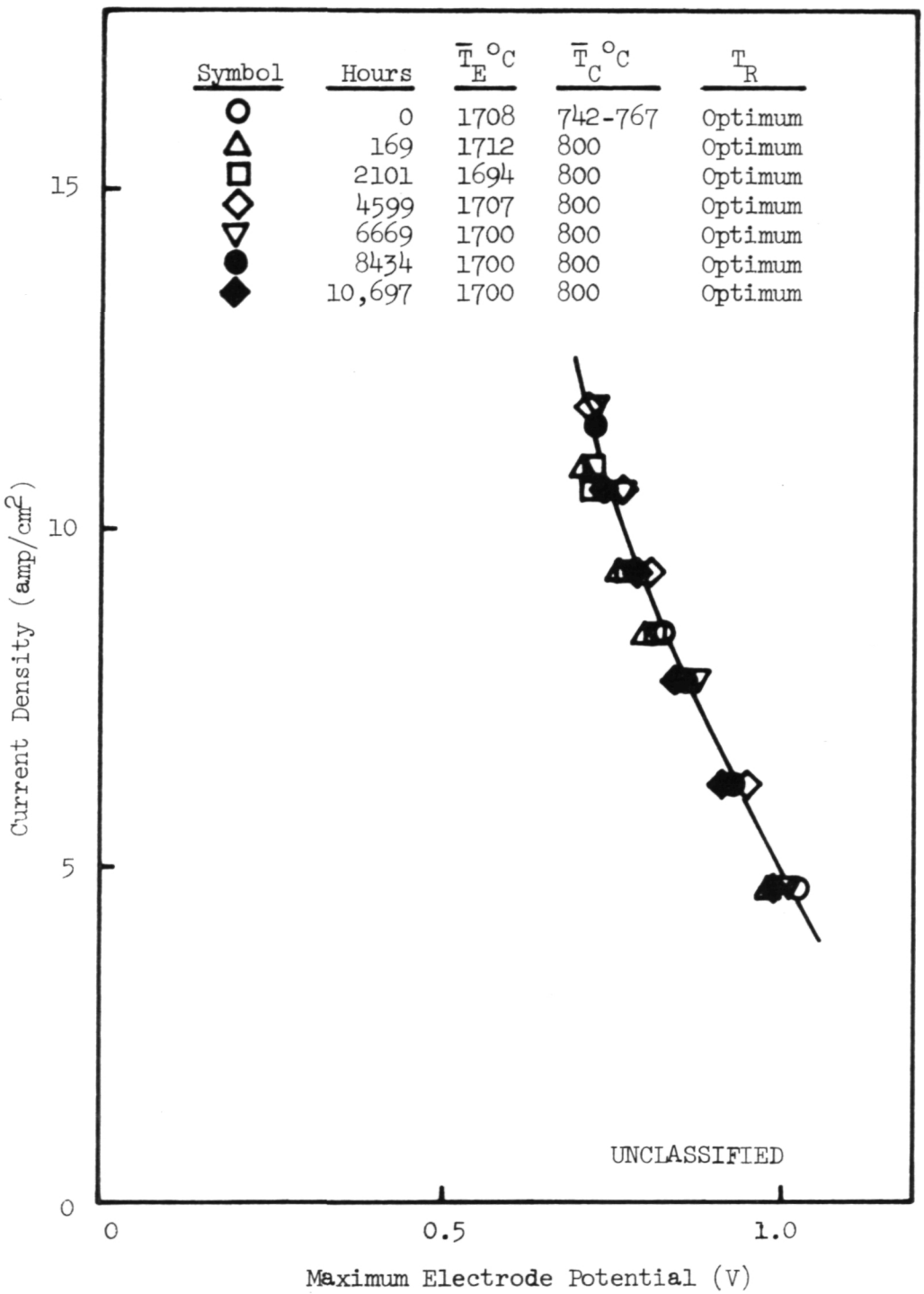

Fig. 5.32--(U) Envelope of I-V characteristics for LC-9

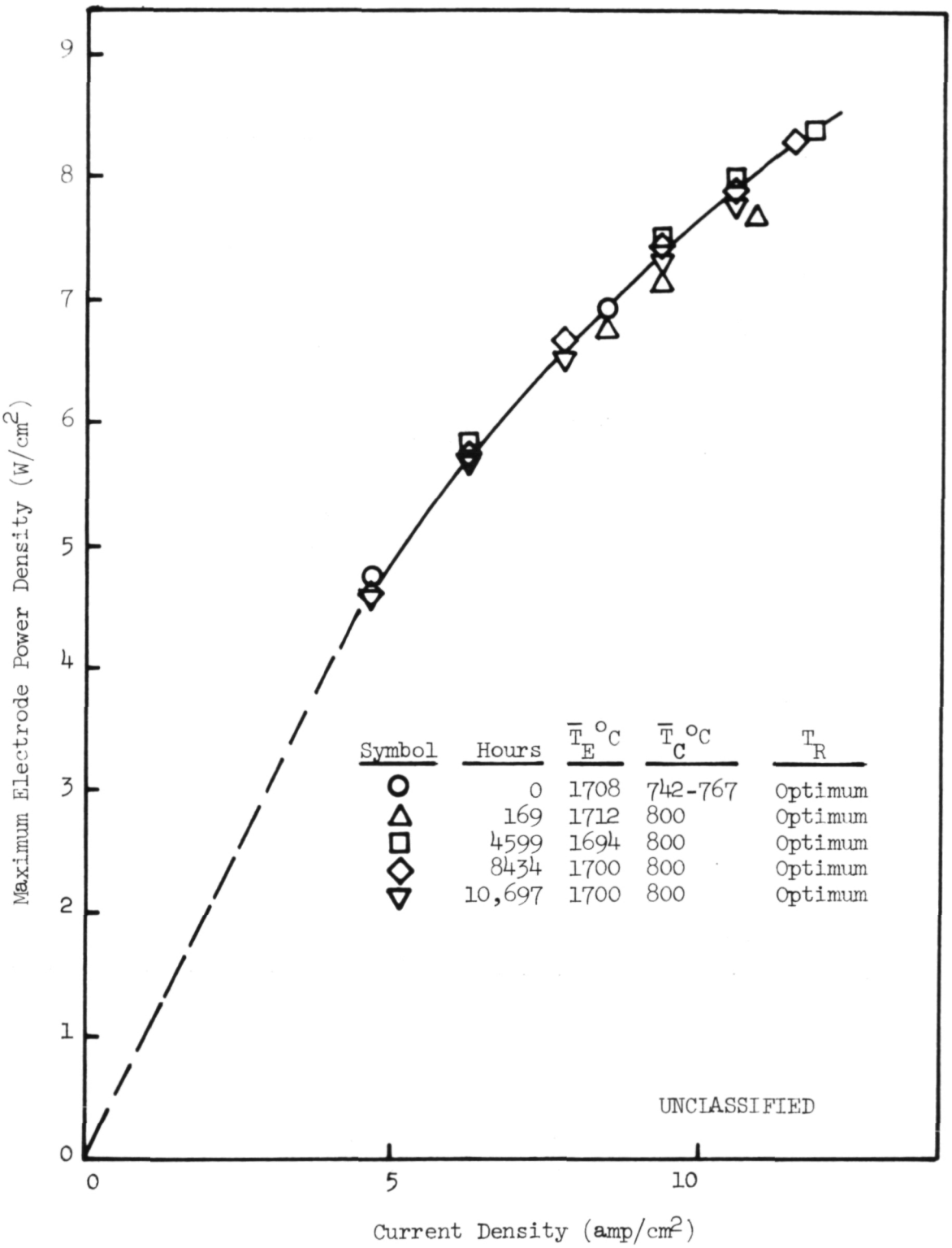

Fig. 5.33--(U) Maximum output power and optimum current determination for LC-9

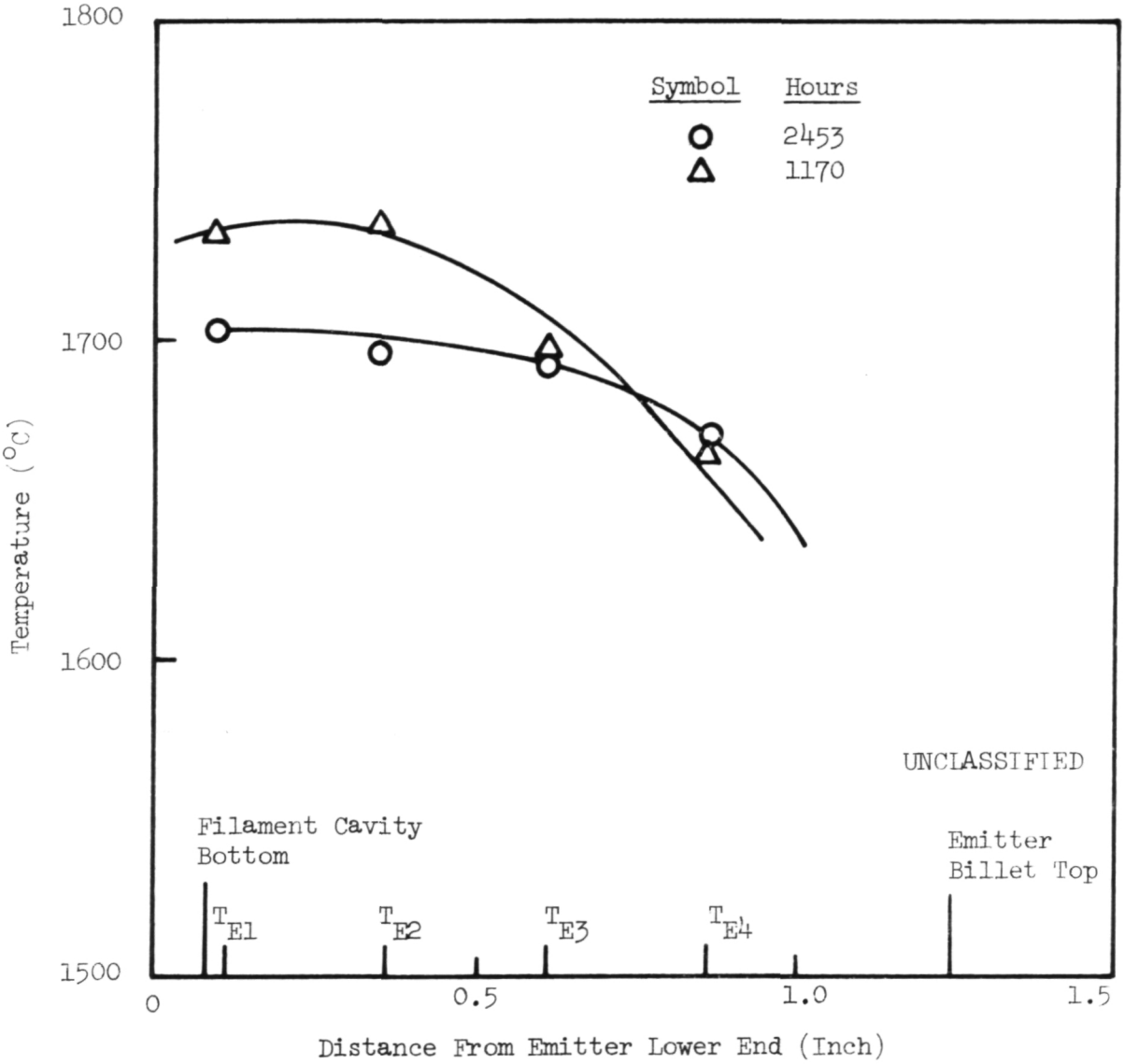

Fig. 5.34--(U) LC-9 emitter temperature profile (power mode)

(U) Prior to the change of profile at 2456 hours the optimum cesium reservoir temperature remained constant at 356°C. Concurrent with the profile change the optimum cesium reservoir temperature was reduced to 353°C and remained at that value within ±1.5°C which is within experimental uncertainties.

(U) A performance map of LC-9 at emitter temperatures of 1400°C and 1500°C was obtained along with the 1700°C data. The results are shown in Fig. 5.35. Maximum output power density for the converter at 1400°C and 1500°C was ~4.5 W/cm^2 and 6.1 W/cm^2 respectively.

(U) LC-9 emitter thermocouple readings shown in Fig. 5.31 were considerably more reliable than those of LC-7 and LC-8. This behavior is due to lower temperature operation and will be discussed further in Appendix 5B. However, the thermocouple emf slowly decreased during the test, dropping the equivalent of 50°C per 5000 hours of operation. Thermocouples installed at 4500 hours degraded faster but this behavior was traced to an impure batch of BeO.

(U) Twenty-seven shutdowns have occurred during the operation, 5 for filament replacement, 12 due to plant power outages, 7 due to instrumentation problems, and 3 for miscellaneous reasons.

5.4.3. LC-9 Diagnostic Data

(U) Relative effective emittance data was taken periodically during the LC-9 test. The data indicated that the effective emittance was constant within experimental errors, which are estimated to be ±0.10.

(U) Emitter and collector work function data are shown in Fig. 5.36. The emitter substrate work function was estimated from the Rasor-Warner plot to be 4.7 eV, which was about 0.08 eV lower than the 4.78 eV value determined by measurements taken during the vacuum emission tests described in Appendix 5A. Except for some anomalous data taken at 8683 hours, the emitter work function data indicate that the electrode surface has remained stable at 4.7 eV.

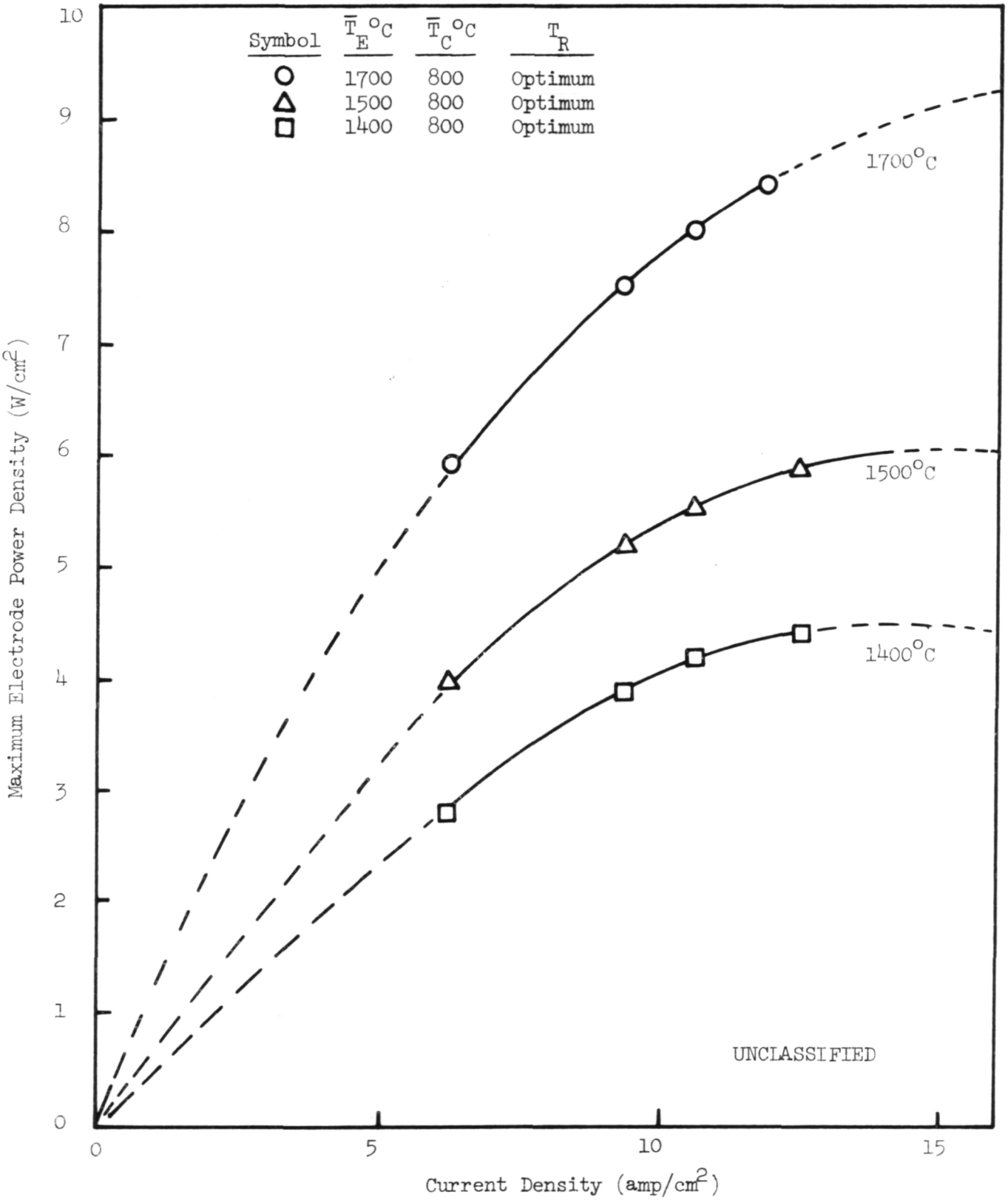

Fig. 5.35--(U) Maximum output power and optimum current determination for LC-9

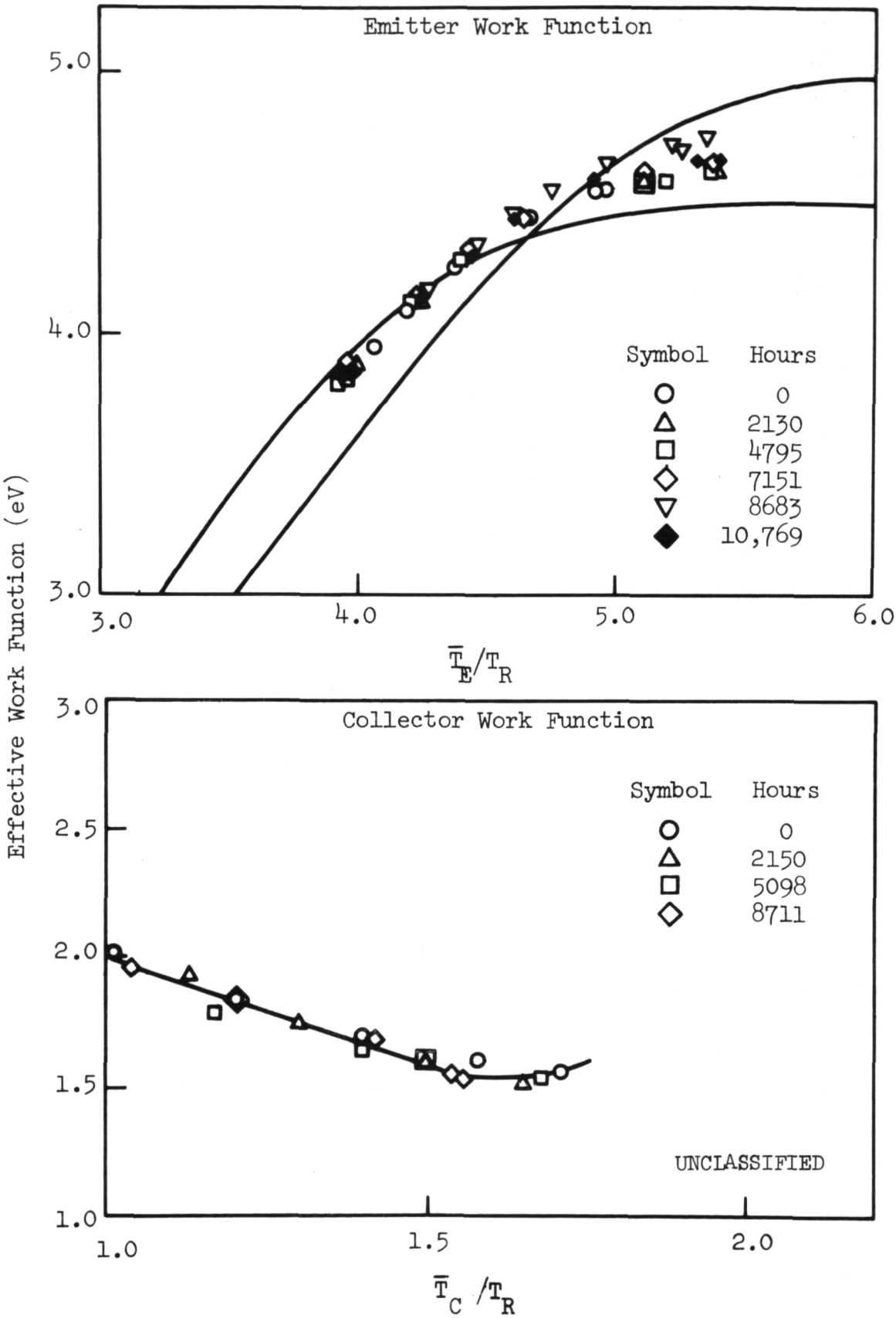

Fig. 5.36--(U) LC-9 work function data

(U) The collector cesiated work function is shown to be 1.58 eV at T_C/T_R = 1.65 (operating conditions), and is about 0.1 eV above that found for molybdenum collectors. The implications of these work function measurements are discussed in Section 5.4.4. The agreement in the work function results at different testing time, indicates that the collector surface is also stable.

5.4.4. Interpretation of the LC-9 Results

(U) Since the purpose of the LC-9 test was to determine the improvement in performance of LC-9 brought by the use of the high-work-function emitter, it is worthwhile to compare LC-9 performance characteristics with those of LC-7 since LC-9 is similar to LC-7 in all respects except the emitter. Such a comparison is shown in Fig. 5.37, where it may be observed that LC-9 would have produced about 10 W/cm^2, while LC-7 produced only 7.1 W/cm^2, both at J_{opt} and T_E = 1800°C. The LC-7 data were for a collector temperature of 750°C, while the LC-9 data were taken at a collector temperature of 800°C. As shown previously, LC-7 would have produced 6% more power if it were run at T_C = 800°C; therefore, LC-9 was capable of producing about 25% more output power than LC-7.

(U) This 25% difference is somewhat more than would have been predicted on the basis of the ϕ_{EO} measurements alone. The ϕ_{EO} for LC-9 was 4.7 eV while ϕ_{EO} for LC-7 was only 4.5 eV, the difference being 0.2 eV. Previous work relating emitter work function changes to changes in performance has shown that a 0.2 eV increase in ϕ_{EO} yields about a 20% increase in performance, which leaves 5% yet to be explained. However, such a difference is probably within the accuracy of the correlation method.

(U) Another comparison that may be made is between the performance of LC-9 and that of OC-5. The latter converter employed a molybdenum collector, which is known to produce lower cesiated ϕ_C and thus higher outputs. At a J of 13 amp/cm^2, LC-9 produced 9.3 W/cm^2, while OC-5 produced 10.9 W/cm^2, or 17% more than LC-9. The work functions of the emitter and collector were not measured in OC-5; therefore no direct correlation is possible between the values of ϕ_C, ϕ_{EO}, and P_{max}. If one compares the ϕ_C values of LC-9

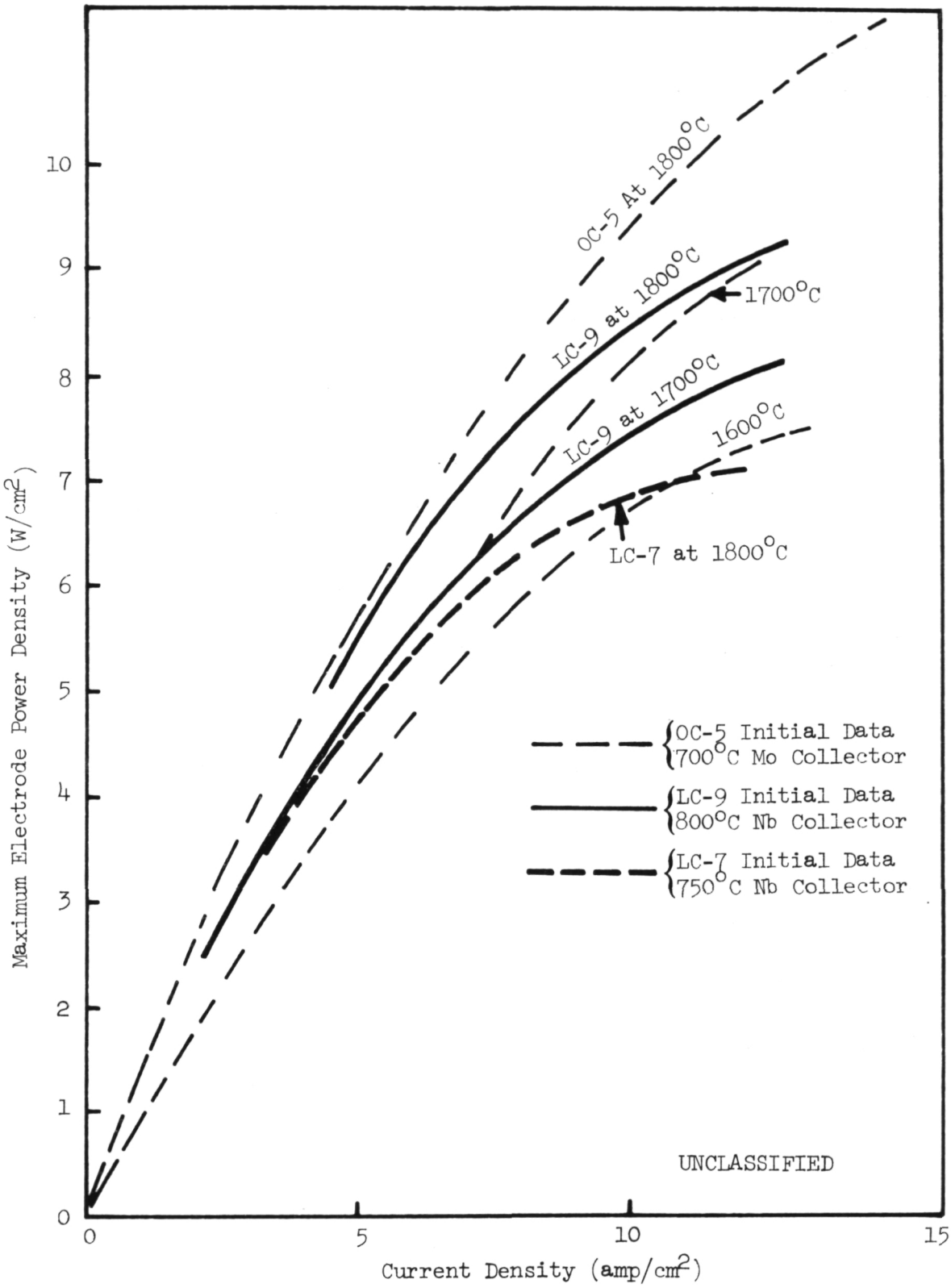

Fig. 5.37--(U) Performance comparison between LC-9 and OC-5

with values reported on molybdenum collector in the literature,[5] however, it is found that molybdenum yields collector work functions of 0.1 to 0.2 eV lower than niobium. That much difference alone would explain the difference between the output of OC-5 and that of LC-9.

(U) One other factor that has not been mentioned before is that the OC-5 emitter temperature distribution was flatter and the electrical resistance of the stem was higher. This means that at the higher currents for the OC-5 operation the emitter temperature distribution became flatter. Improvement in performance is obtained with more uniform emitter temperatures since the cesium pressure will be optimized over a greater fraction of the emitter surface. Thus, it is likely that part of the higher electrode performance was due to the emitter stem design of OC-5. However, the higher electrode output of OC-5 is an artificial gain in performance since the temperature flattening is accomplished at the expense of the power available, because electrical loss in the stem increases as the stem is made thinner. A future problem will be to find the optimum stem design for a desired current taking into account changes in the emitter temperature profile.

(U) Thus, the test results showed that tungsten emitters with a (110) preferred orientation can produce more power output than those with the (100) orientation. Highly oriented and high-work-function emitters are predicted to be inherently more stable since the (110) plane has the lowest surface free energy. The duration and stability of the LC-9 test lend credibility to this prediction. A possible advantage from a systems standpoint is that higher voltages are obtained. Another advantage might be that performance and emitter temperature can be traded off to reduce the problems of fuel diffusion and fission product handling caused by higher temperatures.

REFERENCES

1. "Studies of Thermionic Materials for Space Power Applications," (U) Annual Summary Report for the Period November 23, 1965 - January 31, 1967, GA-7682, NASA-CR-72315. (C/RD)

2. "Studies of Thermionic Materials for Space Power Applications," (U) Annual Summary Report for the Period November 23, 1965 - September 30, 1968, GA-8974, NASA-CR-72517. (C/RD)

3. Hudson, R. G. and L. Yang, "Effect of Operating Temperature on the Vacuum Emission Stability of Vapor-Deposited Tungsten Clad UC-ZrC and UO_2," Presented at the Thermionic Conversion Specialist Conference, Houston, Texas, November 3-4, 1966. GA-7340.

4. Holland, J. W.,and J. Kay, "Effects of Fuel Constituent Diffusion on Emitter Work Functions," (U), Presented at the Thermionic Conversion Specialist Conference, Palo Alto, California, October 30 through November 2, 1967, GA-7751. (C/RD)

5. Kitrilakis, S., et al., "Final Report for the Thermionic Research Program, Task IV, Contract No. 950671, Vol. I," Thermo Electron Corporation Report TE 7-66, August 2, 1965, p. VI-34. (Unclassified)

APPENDIX 5A

EMITTER TEMPERATURE PROFILE AND VACUUM WORK FUNCTIONS

(J. Kay, M. Yates)

(U) Prior to final converter assembly, measurements of emitter effective work function and emitter temperature distribution were conducted for the LC-7, LC-8, and LC-9 emitters. In addition, the same measurements were made on the LC-7 emitter after the converter failed at 3672 hours. These measurements were done using the experimental arrangement shown in Fig. 5A.1. A niobium cylinder which had three sets of eleven optical pyrometry sight holes set at 120° was used as the collector. The emitter-collector gap was 0.020 inch and the outer diameter of the niobium cylinder was 1.5 inch. Stainless steel air lines brazed to the cylinder provided collector cooling. An alumina insulator separated the collector from the emitter support plate. The emitter hung within the collector from the support plate. The emitter in turn supported the filament assembly. The filament assembly and lead cooling collar are the same as those used during life testing of LC-7, LC-8 and LC-9.

(U) The complete assembly was enclosed in an ion pumped glass bell jar vacuum system. A partial pressure gauge was added to the vacuum system to measure the residual oxygen pressure. The total pressure during the experiments was maintained below 5×10^{-7} torr; the oxygen pressure was less than 10^{-9} torr.

(U) Effective work functions were determined from extrapolated short circuit currents and Richardson's equation using $A = 120$ A/cm^2. Axial temperature profiles of the emitter surface were obtained by pyrometry using the sight holes in the collector. The average surface temperature as determined from this profile was used for the effective work function calculations. Errors in the determination of the work function due to experimental uncertainties was estimated to be ±0.03 eV.

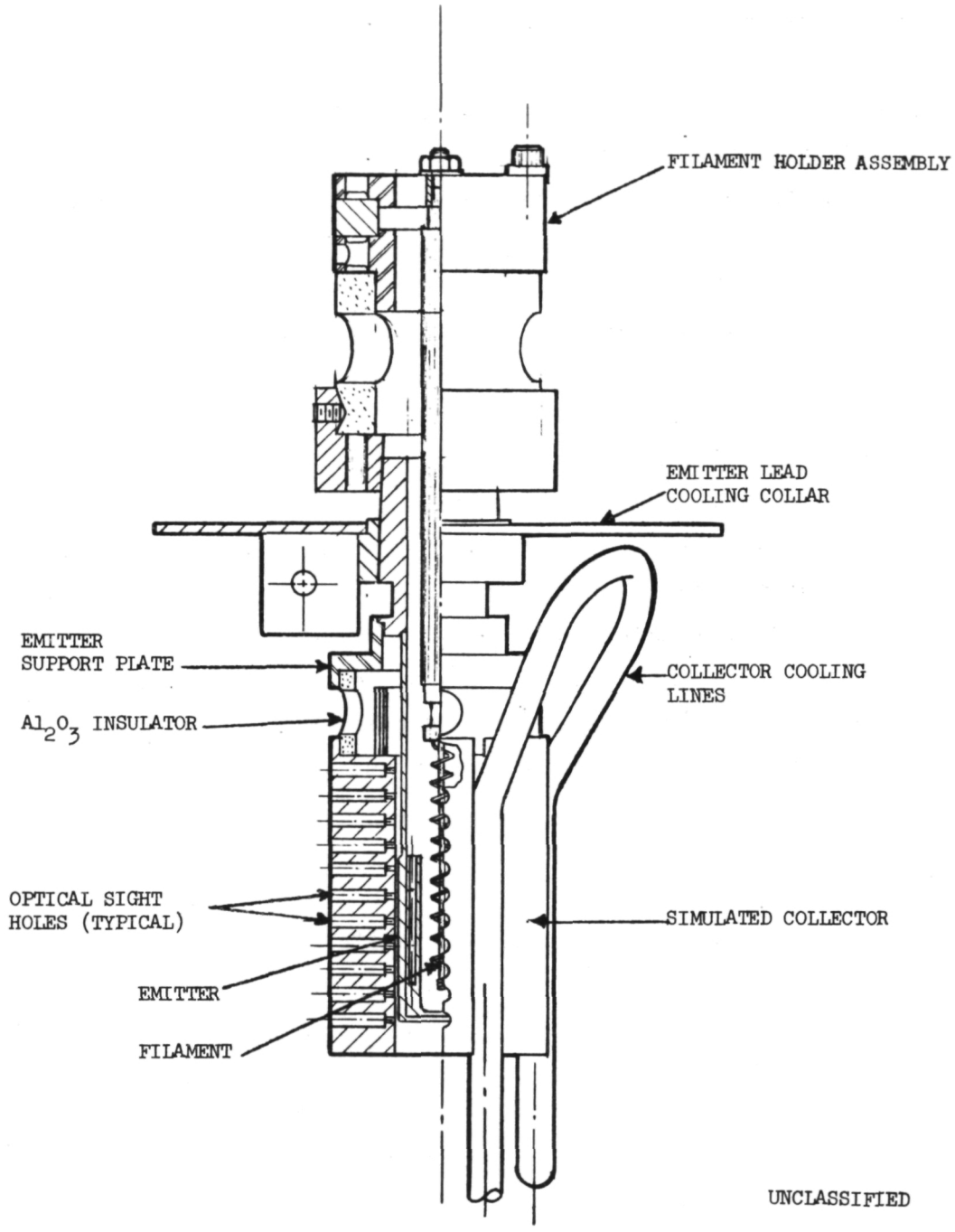

Fig. 5A.1--(U) Vacuum emission test assembly

(U) In addition to work function determinations the vacuum emission apparatus provided a correlation between the emitter surface temperature profile and emitter thermocouple temperature distribution. Both LC-7 and LC-9 converters were instrumented with four emitter thermocouples positioned along the emitter axis. The average surface temperature determined by optical pyrometry and the thermocouple average were found to be within 10°C. Also the maximum deviation between the thermocouple temperature profile obtained from the vacuum emission test and from the open circuit condition during life test was 30°C which made it practical to use the average thermocouple temperature to estimate the average surface temperature of the converter at open circuit. Moreover, when the converter was under going life testing (power mode) the difference between the converter thermocouple temperature distribution and the true cesiated emitter surface temperature distribution was reduced because of the resistance heating of the stem at high currents. For the LC-8 converter which was fueled and instrumented with only two high temperature thermocouples at the same axial location, the readings of thermocouples T_{E1} or T_{E2} were used to estimate the average temperature of the emitter surface in the converter, assuming the observed relationships between these thermocouple readings and the average temperature of the emitter surface remained unchanged after the emitter was incorporated into the converter.

LC-7

(U) The distribution of the emitter surface and the emitter thermocouple temperatures prior to assembly are shown in Fig. 5A-2. The temperature distribution gives a maximum to average of 20°C, and over 73% of the surface is within 20°C. The average of the thermocouple temperatures corresponds within 5°C of the surface average and since the two temperature profiles were not markedly disimiliar in shape it was possible to substitute the thermocouple average for the true surface average.

(U) The initial value of the vacuum function was 4.65 eV, but after 16 hours at 1800°C, this reduced to 4.56 eV. A final value for the work function obtained after 19 hours was 4.55 eV. A substrate work function of 4.5 eV was determined in the cesiated converter at the start of the life test; this compares quite well with the stable values obtained for the vacuum work function during the emitter temperature profile work.

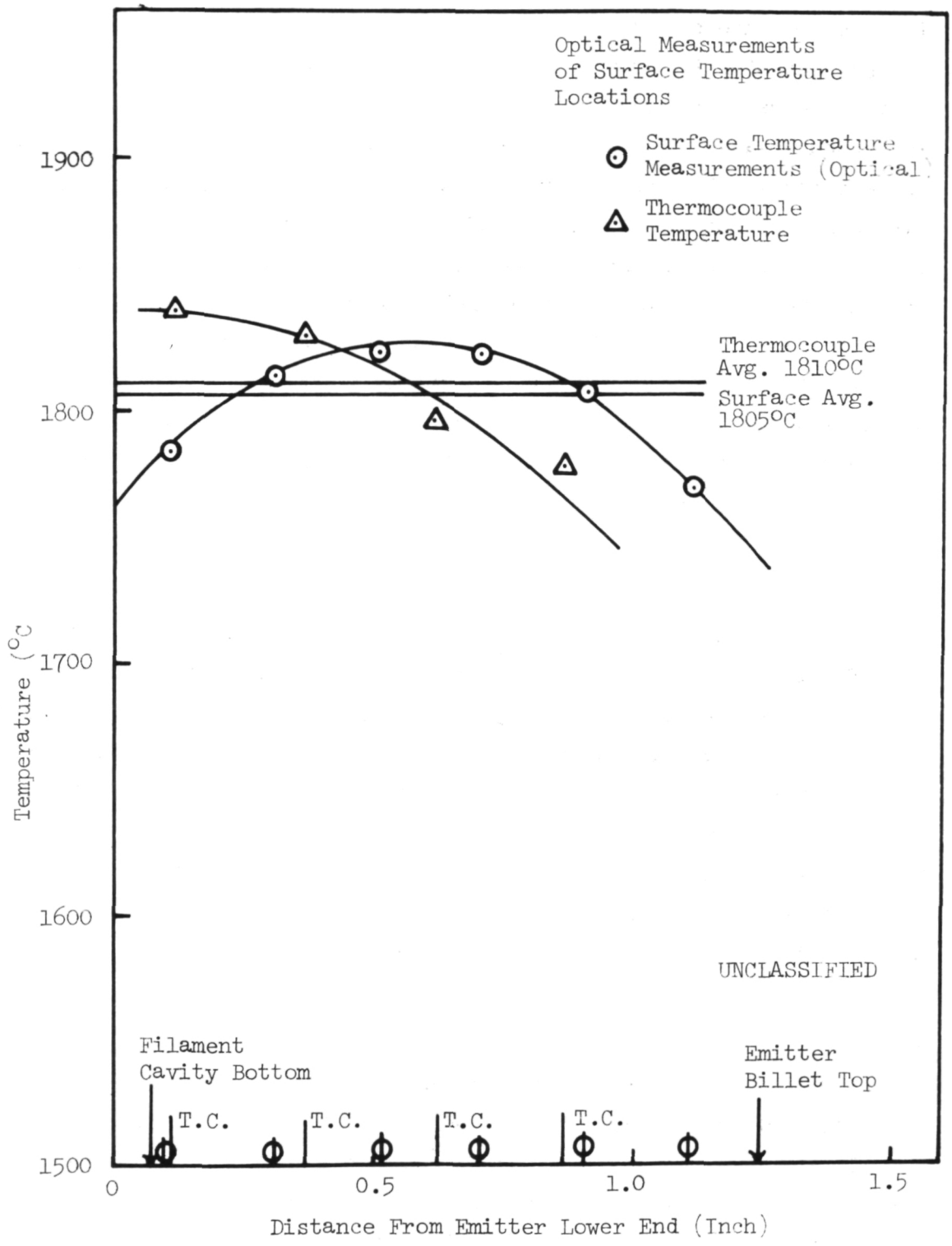

Fig. 5A.2--(U) LC-7 emitter temperature profiles prior to converter assembly

(U) Post operational emitter temperature profile and vacuum work function measurements were obtained after the converter was disassembled. Typical emitter temperature profile data is shown in Fig. 5A.3 and is similar to data obtained prior to operation. Only three emitter thermocouples were used because one hole was obstructed by a broken thermocouple sheath. Differences in the profiles are probably due to slightly different filament placement resulting from the use of a different emitter support. LC-7 was broken at the stem to transition piece joint during post operation machining and required a special fixture to hold the emitter in place. The emitter was held at temperature for 225 hours to ensure that the work function was stable. The effective work function as a function of time is plotted in Fig. 5A.4 and indicates good stability. The average value, 4.51 eV, is in good agreement with the pre-assembly value of 4.55 eV and the Rasor-Warner correlation during converter life test.

LC-8

(U) Figure 5A.5 shows the emitter temperature profile measured on LC-8 for three different temperatures. The difference between maximum and average temperatures is between 30° to 55°C, and about 80% of the surface is within ±30°, ±40°, and ±55°C for the three emitter temperatures shown. The effective work function was measured at temperatures of 1800°, 1600°, and 1400°C over a period of 113 hours. The results are plotted in Fig. 5A.6 and show that the work function was stable at 4.69 within ±0.03 eV at all three temperatures. This value compares very well with the values obtained during initial operation of the converter.

LC-9

(U) The LC-9 emitter temperature profile and vacuum work functions were also determined prior to converter assembly. The surface temperature profile and the emitter thermocouple profile are shown in Fig. 5A.7. The temperature distribution gives a maximum to average of 30°C, and 85% of the surface is within 33°C. As for LC-7 the average of the thermocouple temperatures corresponds within 5°C to the surface average temperature.

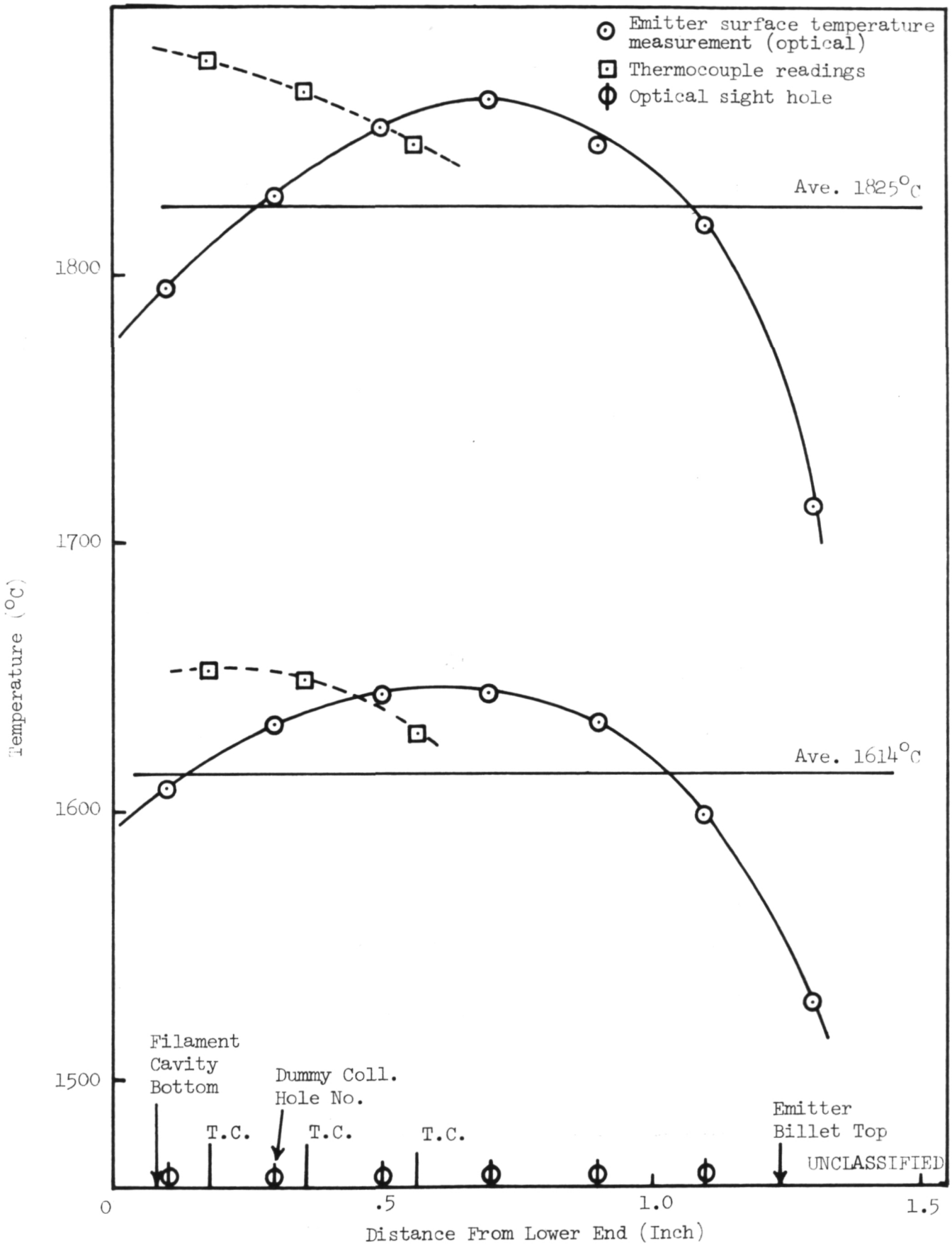

Fig. 5A.3--(U) LC-7 post operational emitter profiles

UNCLASSIFIED

UNCLASSIFIED

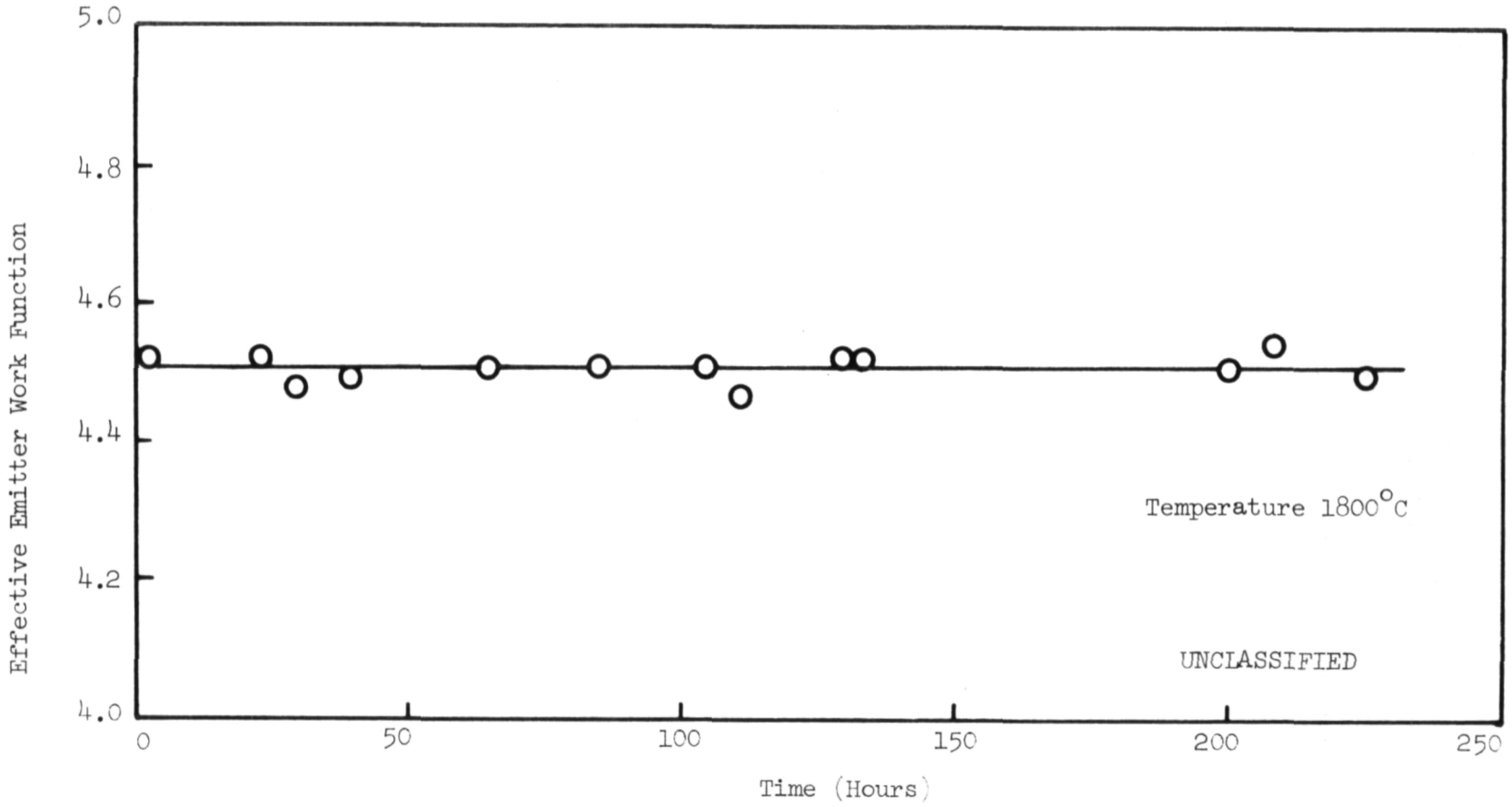

Fig. 5A.4--(U) LC-7 vacuum emitter work function (post operative)

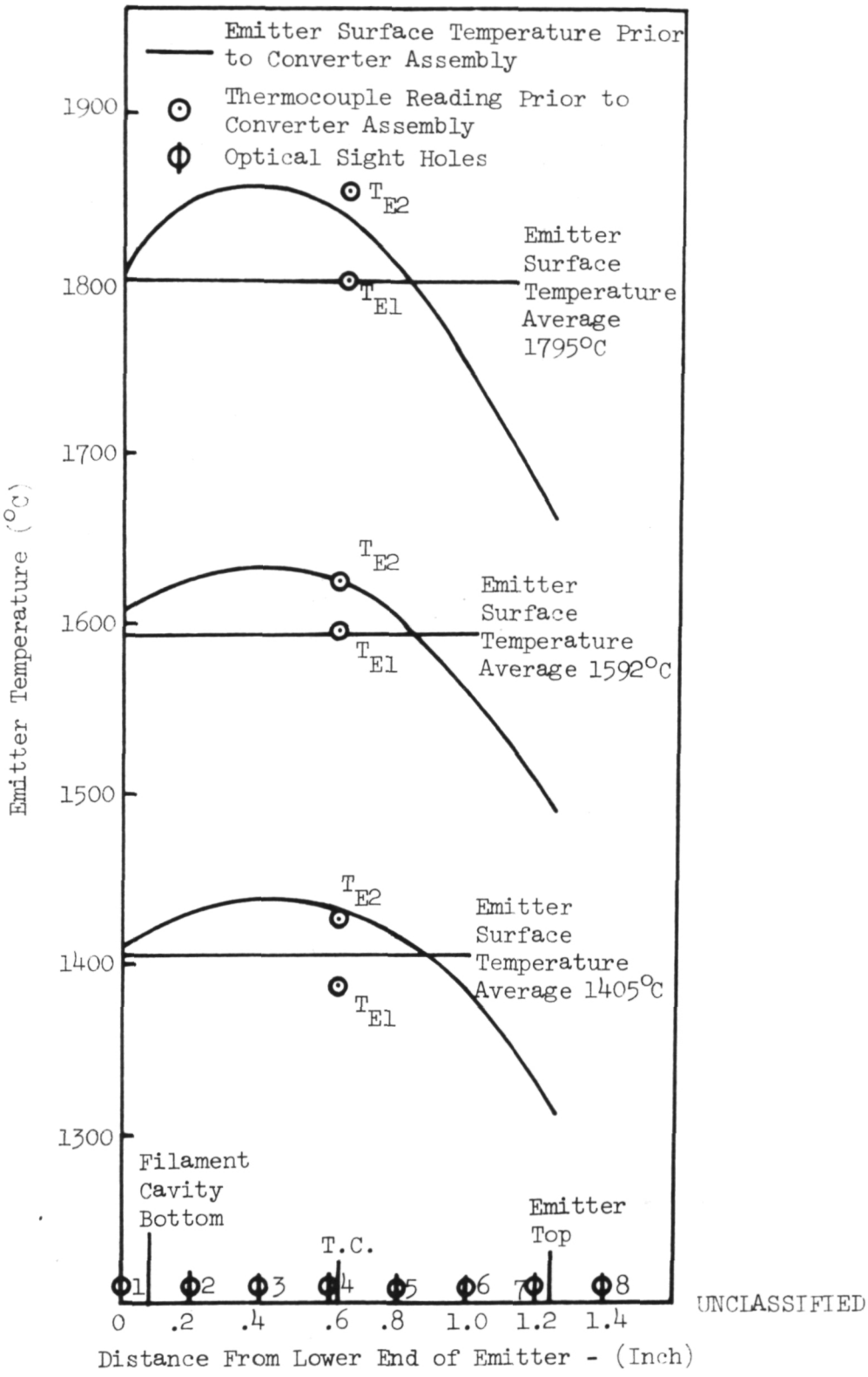

Fig. 5A.5--(U) LC-8 emitter temperature profile and thermocouple reading prior to converter assembly

UNCLASSIFIED

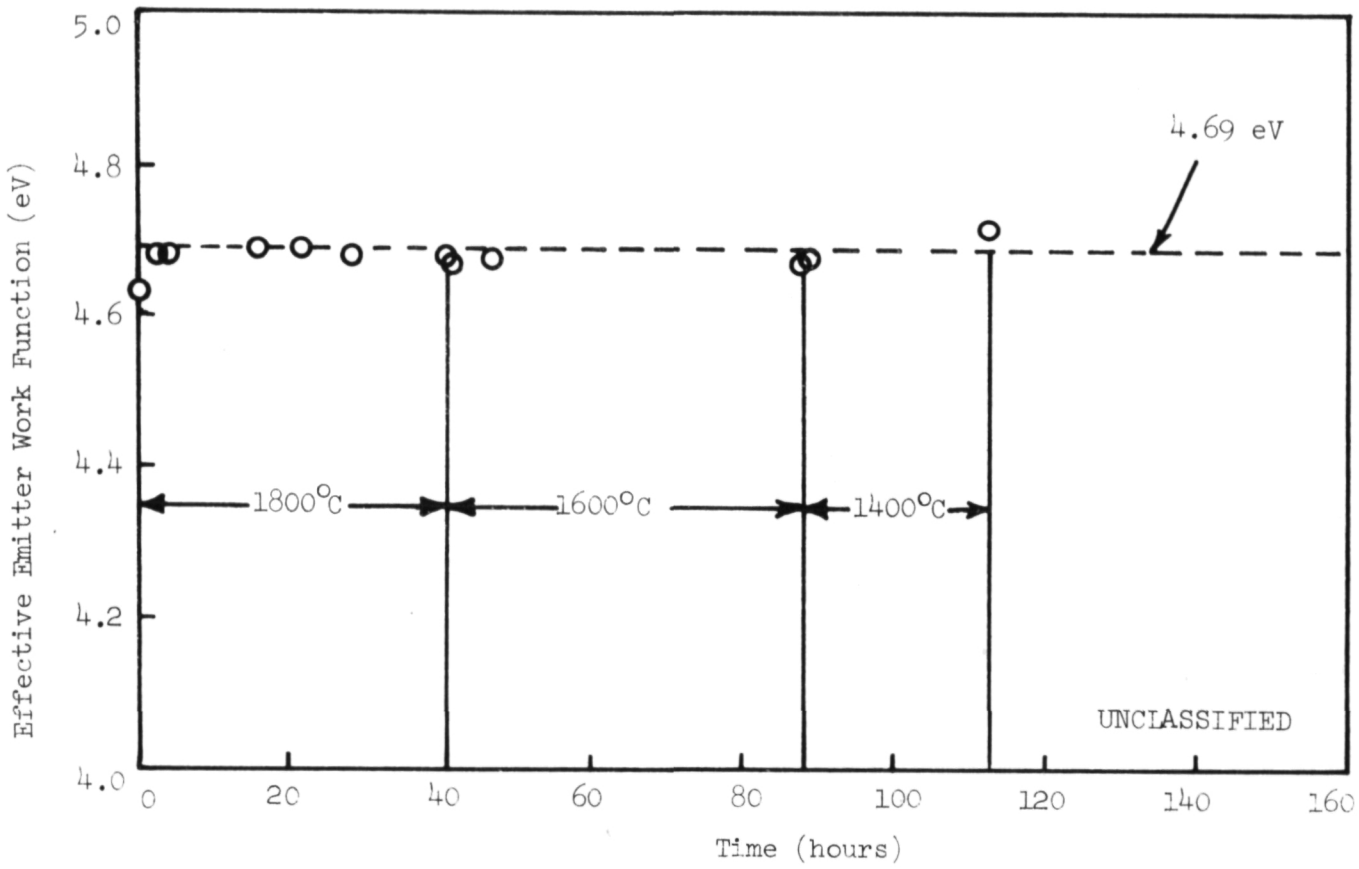

Fig. 5A.6--(U) LC-8 vacuum emitter work function

UNCLASSIFIED

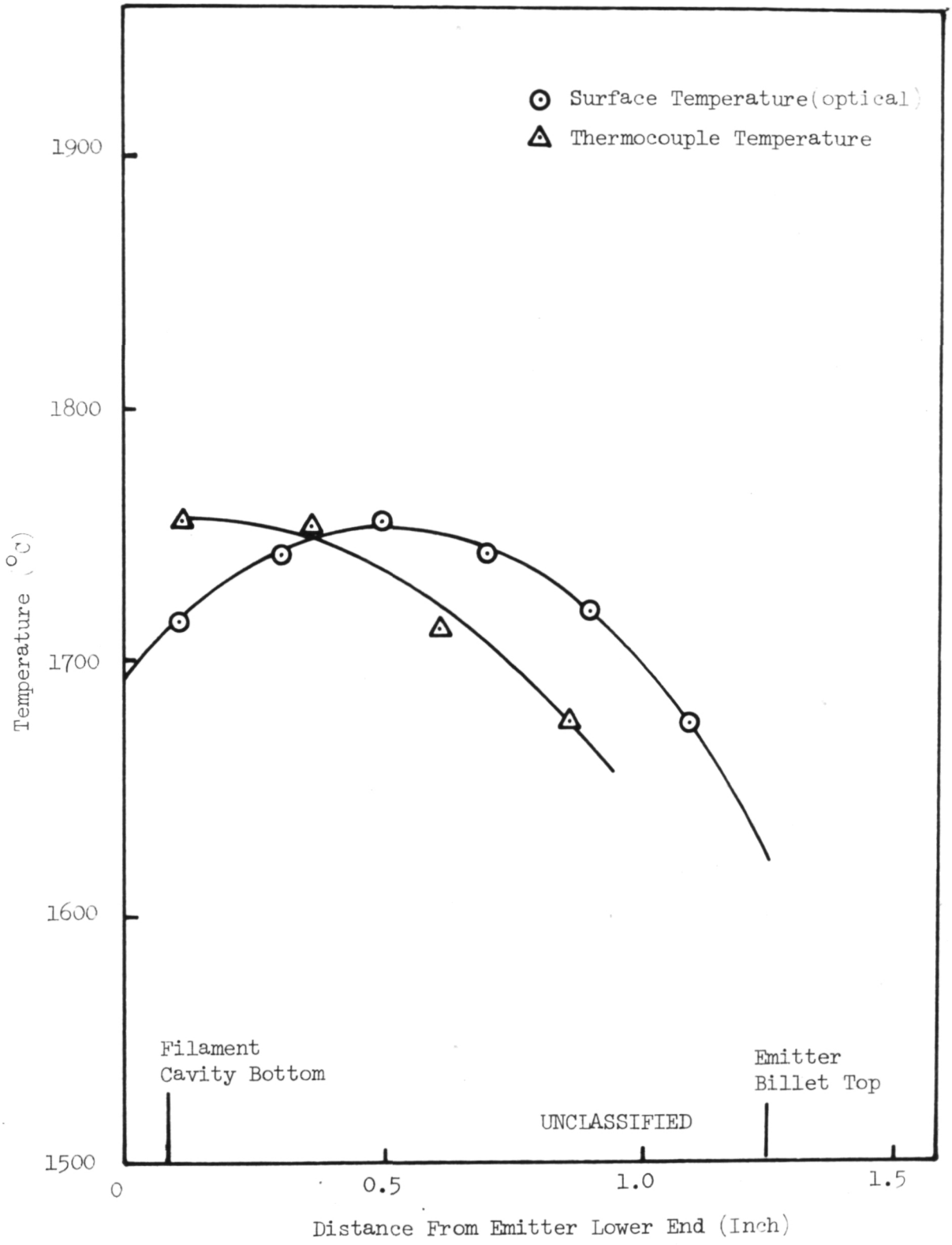

Fig. 5A.7--(U) LC-9 emitter temperature profiles prior to converter assembly

(U) After the emitter profile determinations, the vacuum work function was monitored for 45 hours. The results are shown in Fig. 5A.8, where it may be observed that the initial value of ϕ_E was 4.81 eV. Determinations of ϕ_E at 40, 42, and 45 hours were 4.81 eV, and 4.79 eV, respectively, so that the conclusion would be made that the vacuum work function was stable within the experimental uncertainties, estimated to be ±0.03 eV.

(U) After converter assembly, the vacuum emission work function obtained during outgassing was 4.78 eV; this is in good agreement with the pre-assembly value of 4.79 eV. The cesiated work function determined at the start of the converter life test was 4.7 eV.

LC-6

(C-RD)(Gp-1) LC-6 converter had a (100) oriented WF_6 clad emitter fueled with 50UC-50ZrC. The converter operated at an average emitter temperature of 1650°C for 2800 hours. The test was terminated because of cesium leakage. Fuel diffusion effects were observed and verified by work function measurements obtained during the test.(1)

(C-RD)(Gp-1) Post operative emitter temperature profile and vacuum emission measurements are shown in Figs. 5A.9 and 5A.10. Temperature profile and vacuum emission data were not obtained prior to converter testing. The emitter surface temperature profile in Fig. 5A.9 are in good agreement with those previously reported for LC-3, 4 and 5.(1) During converter operation the average emitter surface temperature was estimated to be ~50° lower than the average of the emitter thermocouple readings. The post operative profile data indicates that the estimate was reasonably accurate.

(C-RD)(Gp-1) Vacuum work function measurements for LC-6 are compared in Fig. 5A.10 with those of LC-5 which also contained UC-ZrC fuel material. The results are almost identical to LC-5 and are believed to be the effects of fuel diffusion. The dependence of work function on temperature and the effects of fuel diffusion on LC-6 converter performance is discussed extensively in an earlier report.(1)

RESTRICTED DATA
ATOMIC ENERGY ACT 1954
GROUP 1

UNCLASSIFIED

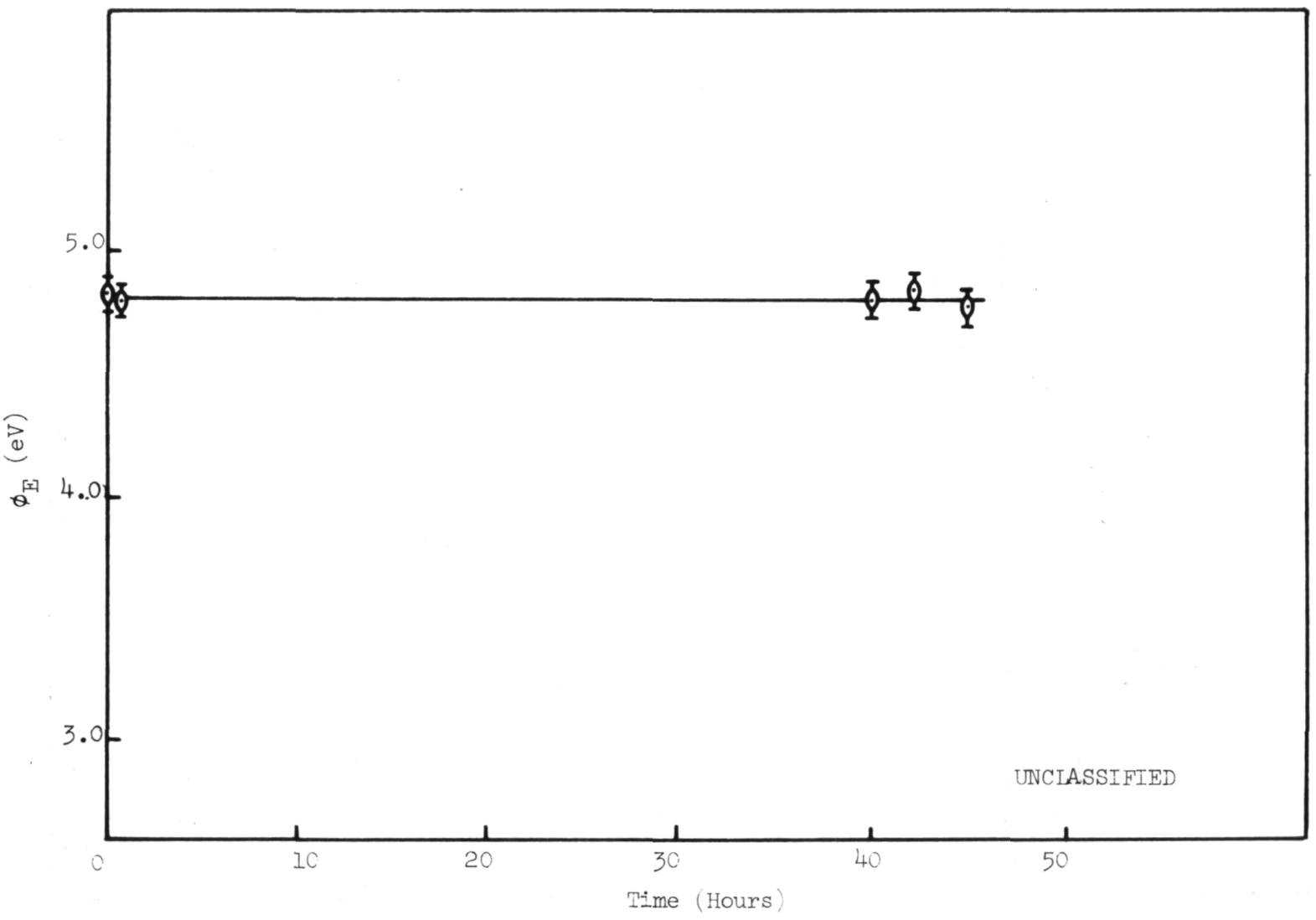

Fig. 5A.8--(U) LC-9 emitter vacuum work function

UNCLASSIFIED

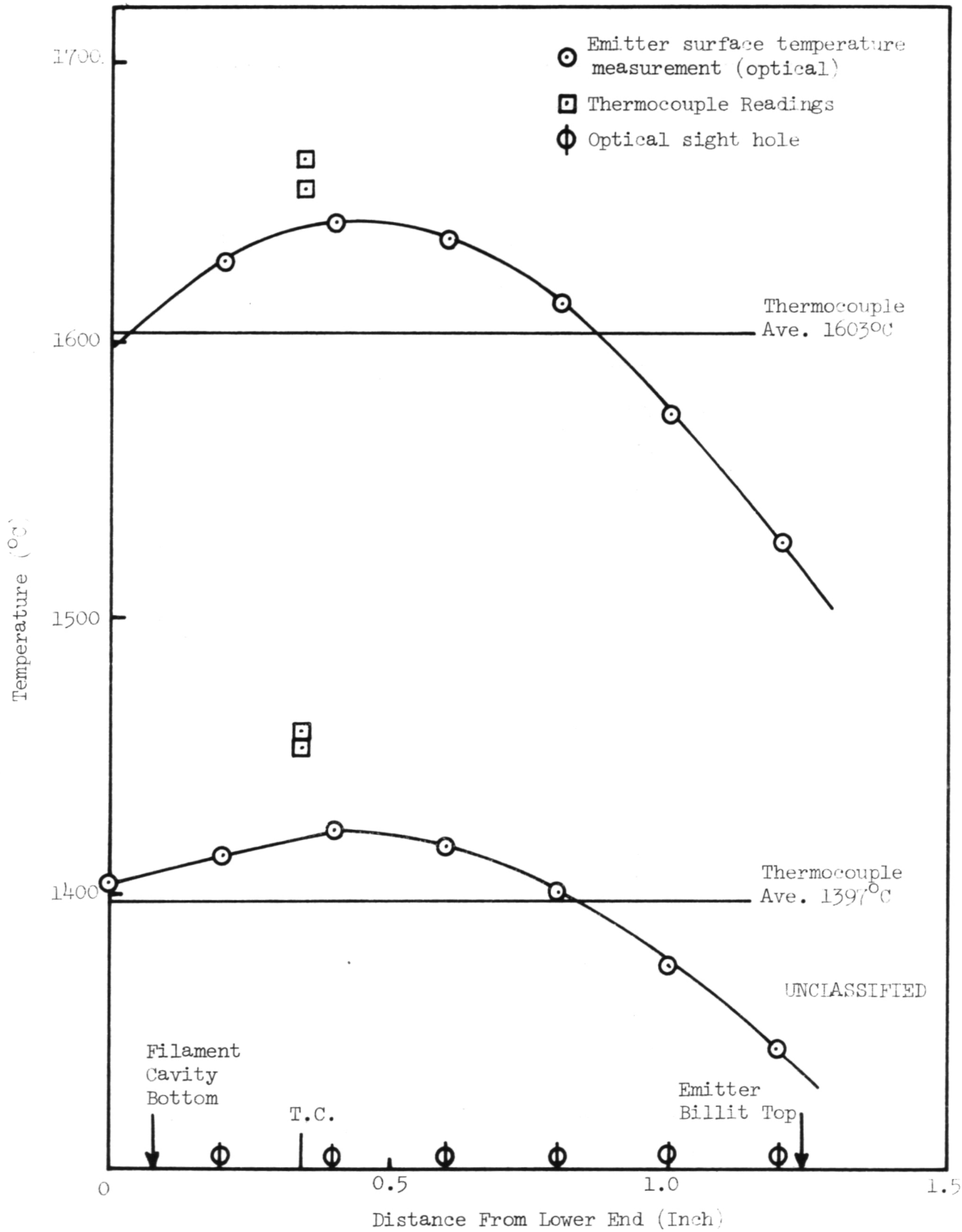

Fig. 5A.9--(U) LC-6 emitter profile data

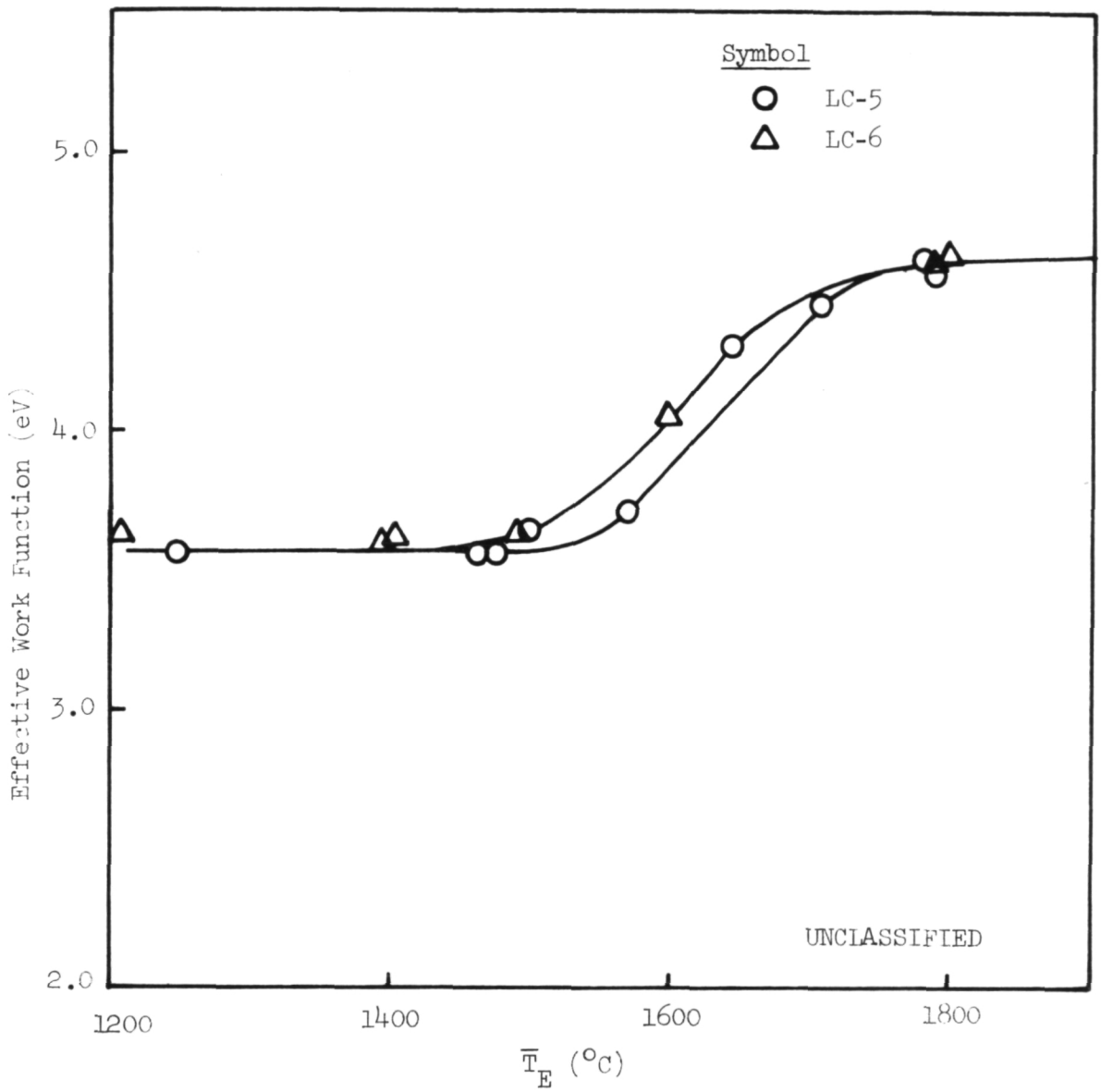

Fig. 5A.10--(U) LC-5 and LC-6 emitter vacuum emission determinations

REFERENCE

1. "Studies of Thermionic Materials for Space Power Applications," (U) Annual Summary Report for the Period November 23, 1965 - January 31, 1967, GA-7682, NASA-CR-72315. (C/RD)

APPENDIX 5B

STABILITY OF HIGH TEMPERATURE THERMOCOUPLES

(U) A special test was set up to evaluate the stability of the type of tungsten-rhenium thermocouples used in LC-7, 8, and 9. Three thermocouples were installed in the calibration assembly shown in Fig. 5B.1. This assembly is the same one that is used to calibrate thermocouples prior to installation in converters.

(U) The three thermocouples were run for 200 hour periods at 1500, 1600, 1700, 1800, and 1830°C. The temperature as read by an optical pyrometer was held constant during each 200 hour period and the emfs of the thermocouples monitored. The results are shown in Fig. 5B.2. All thermocouples were stable until 800 hours when the temperature was raised to 1830°C. Their emf began dropping as soon as this temperature was reached. After a shutdown around 900 hours for filament replacement, the emfs dropped further and were from 50 - 150°C below the optical readings at the end of the test.

(U) These results confirmed the observation made in the LC-7, 8, and 9 tests that this type of thermocouple is relatively stable at temperatures less than 1800°C; but soon degrades at temperatures above 1800°C.

UNCLASSIFIED

UNCLASSIFIED

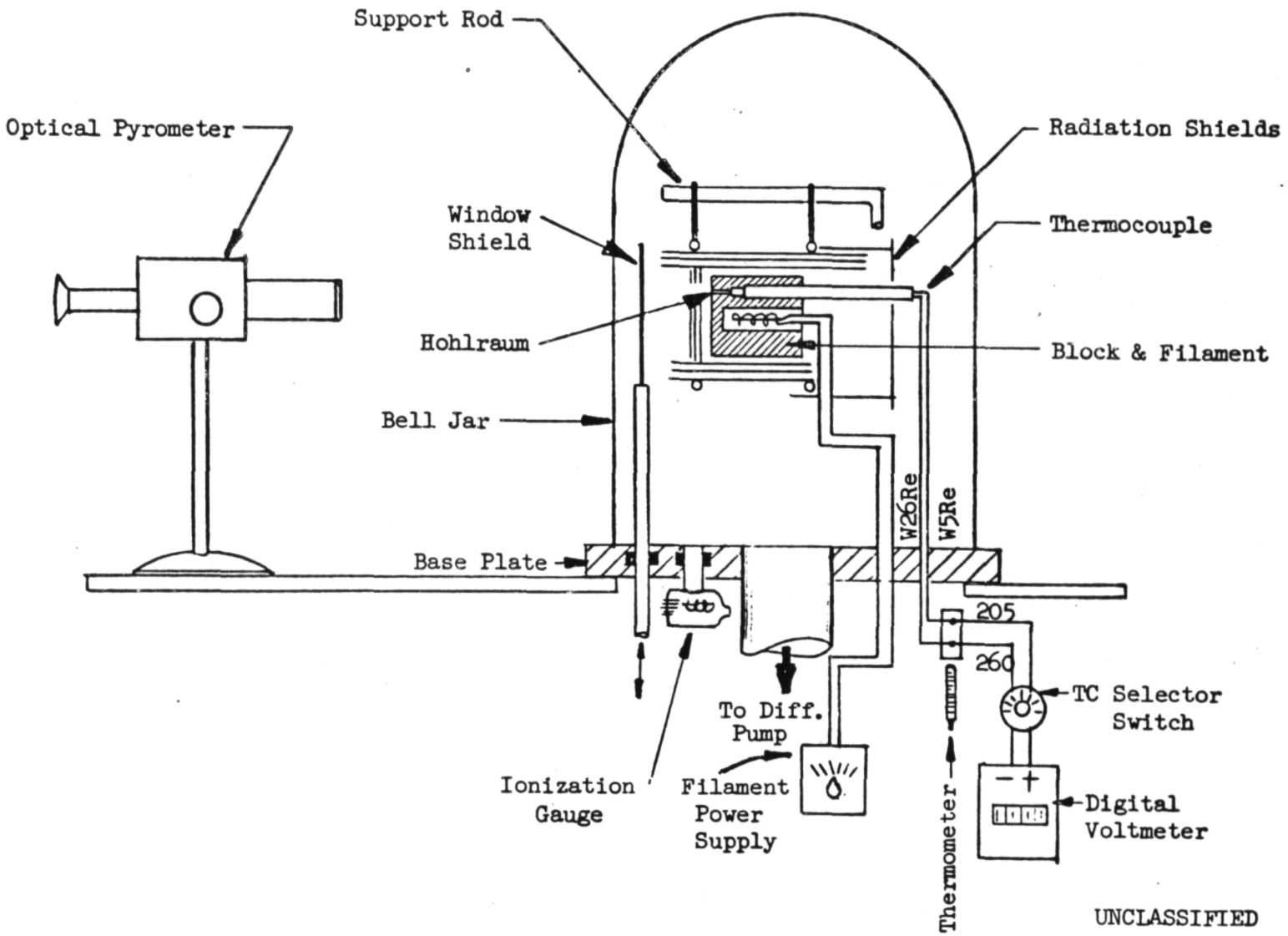

Fig. 5B.1--(U) Calibration and test assembly schematic

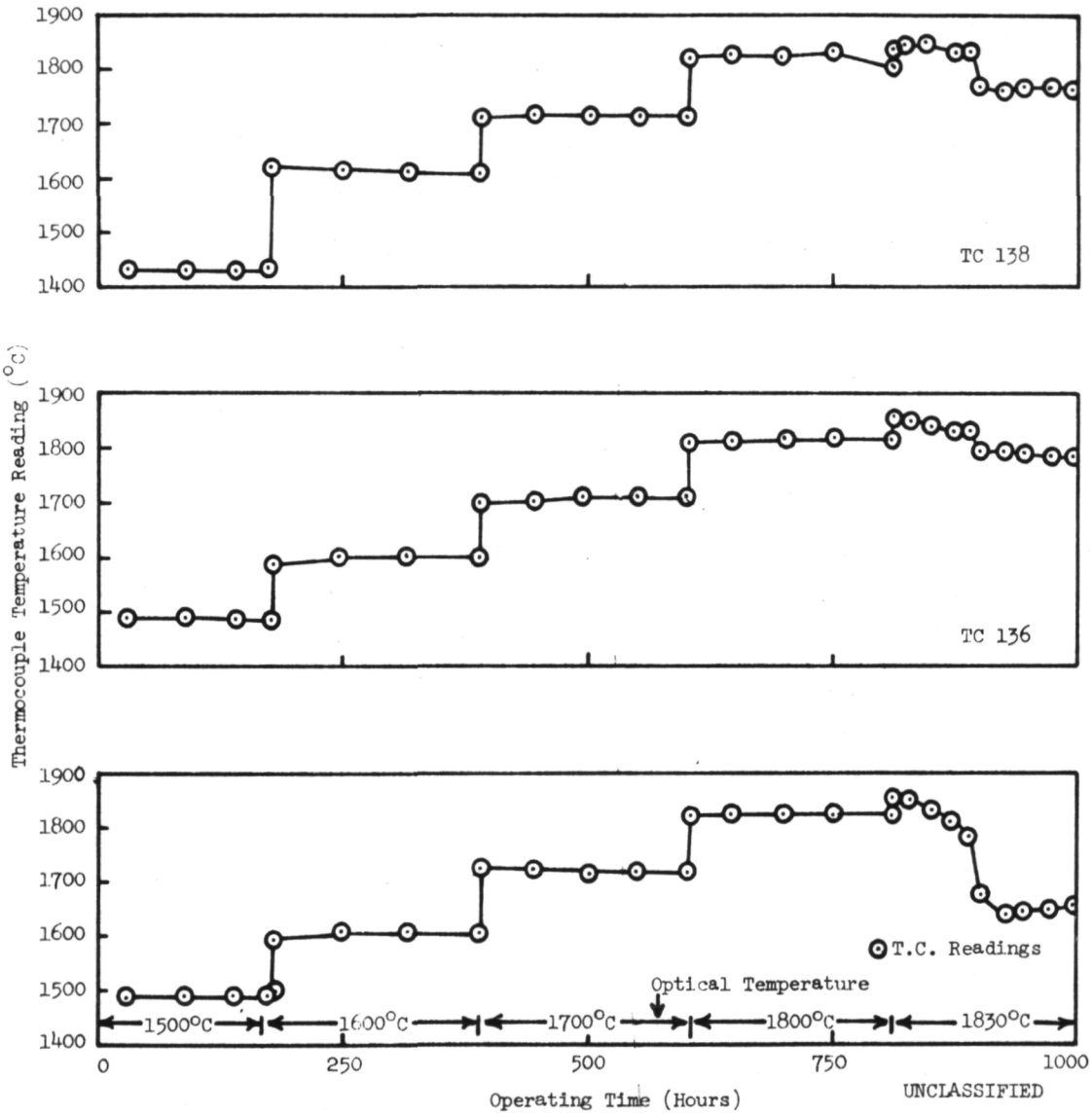

Fig. 5B.2--(U) 1000 hour test of three tungsten rhenium thermocouples

APPENDIX 5C

POST-OPERATIONAL METALLOGRAPHIC EXAMINATION OF LC-7 CONVERTER

(U) Figure 5C.1 shows the macroscopic appearance of the LC-7 fluoride tungsten emitter after testing in the cesiated environment. There does not appear to be any visible surface contamination. Measurements made with a micrometer indicated no significant change in its diameter from the pre-test value.

(U) Figure 5C.2 shows the microstructure of a cross section of the emitter. It can be seen that numerous voids are present in the region facing the electron bombardment filament and fine porosities exist in the region near the emitting surface. Considerable grain growth has occurred in the former region while the grains in the latter region still remain small and columnar. It is believed that these voids and fine porosities were formed by the coalescence of small bubbles containing fluorine or fluorine compounds. In the region near the electron bombardment filament, the temperature was much higher than that near the emitting surface; therefore the bubbles became coalesced into much bigger sizes, and in the absence of small bubbles at the grain boundaries, grain growth occurred. Similar void formation has been observed near the fuel-clad interface in in-pile converters containing tungsten claddings of high fluorine contents. The emitter of LC-7 was fabricated with fluoride tungsten containing 42 ppm fluorine at a time when the importance of controlling the fluorine content of tungsten emitter cladding was just beginning to be appreciated. The current limit of acceptance of fluorine concentration, 5-15 ppm, is much lower than this.

(U) Fig. 5C.3 shows the macroscopic appearance of the post-test collector surface which was shiny and free from any deposits.

(U) Fig. 5C.4 shows the post-test microstructures of the niobium collector. The large grain size is probably due to the high temperature

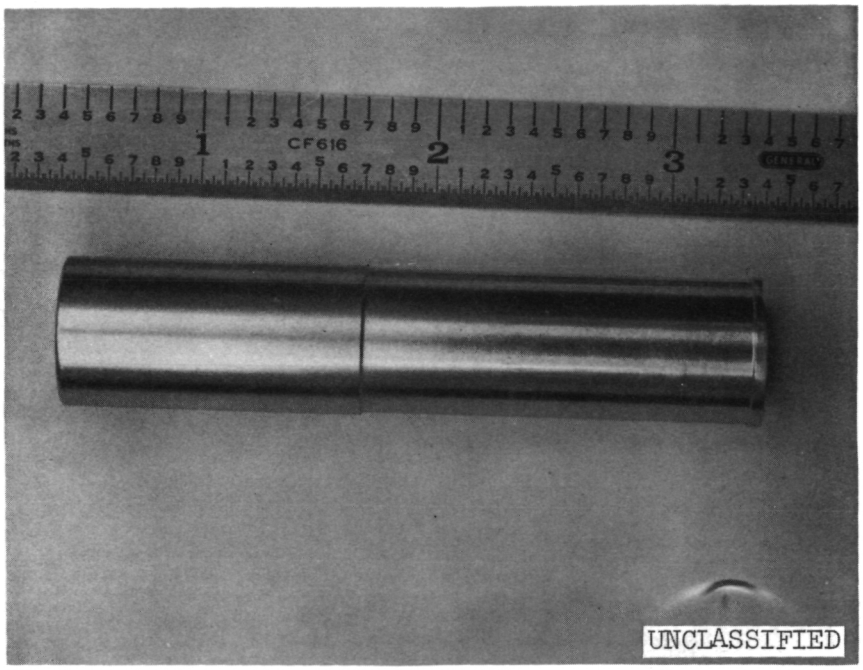

Fig. 5C.1--(U) Post-test macroscopic appearance of LC-7 emitter

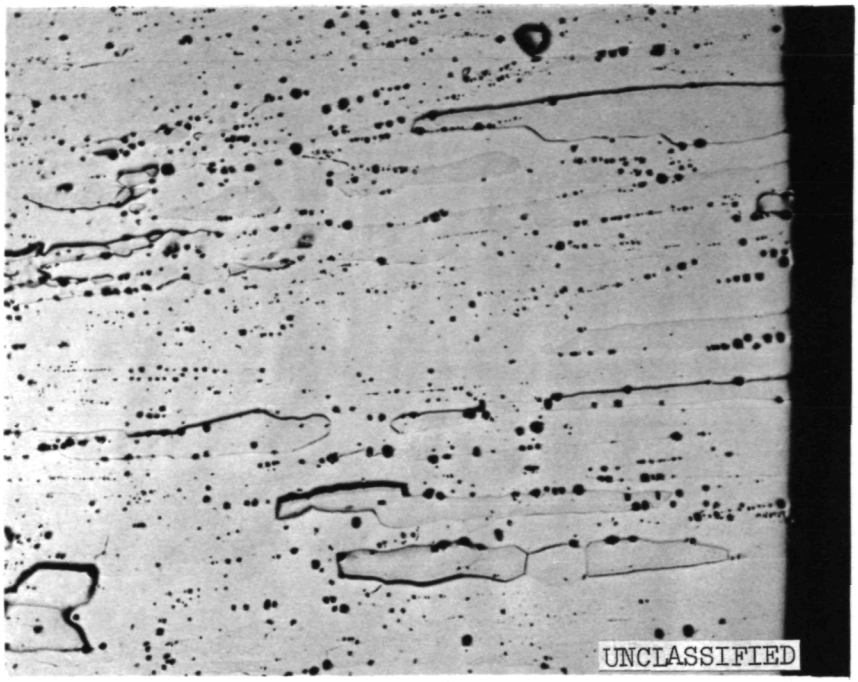

M 31589-3 75X

(a) Near the emitting surface

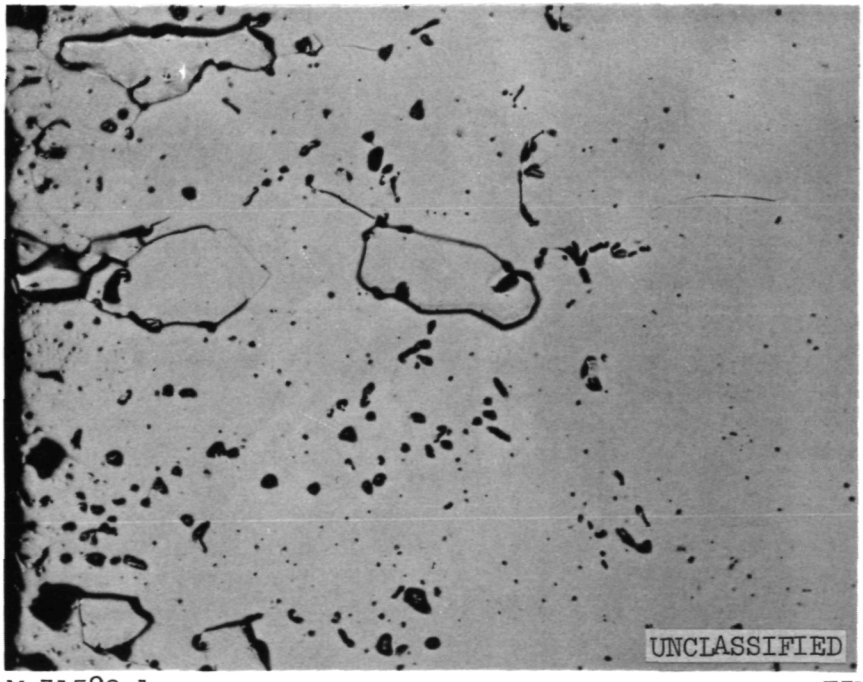

M 31589-1 75X

(b) Near the electron gun side

Fig. 5C.2--(U) Post-test microstructures of a cross section of the fluoride tungsten emitter of LC-7 converter

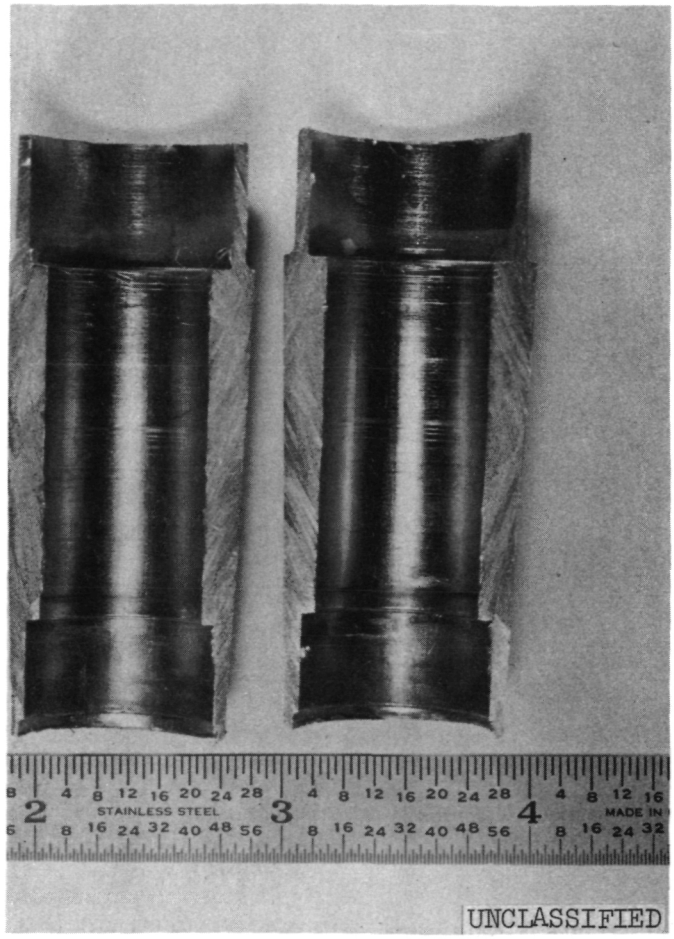

Fig. 5C.3--(U) Post-test macroscopic appearance of LC-7 collector surface

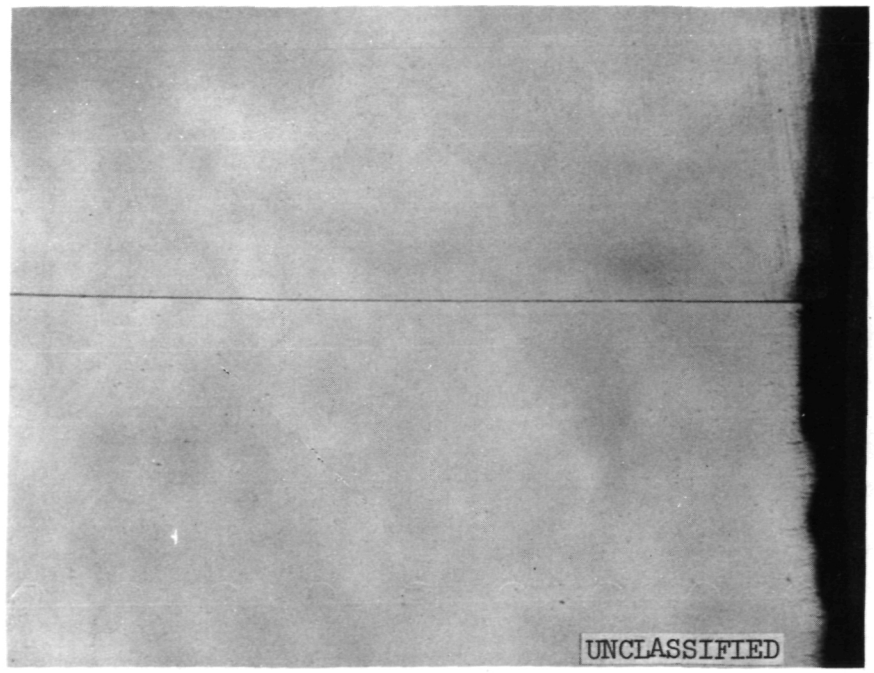

M 29597-6 40X

Fig. 5C.4--(U) Post-test microstructures of the niobium collector of LC-7 converter

bulk outgassing operation at 1800°C rather than operation at 750°C during converter testing. The microhardness results at the O.D. and the I.D. and that along the grain boundary showed no significant difference, indicating no significant contamination by the testing environment. Chemical analysis yielded the following interstitial impurity concentrations (in ppm): C, 28; O, 110; and N, 44; which are of the same order of magnitude as that in the niobium material used for the fabrication of the collector.

(U) Figure 5C.5 shows the post-test appearance of the Cu-Ti final closure braze between the lower sleeve of the Al_2O_3 insulator and the top of the niobium collector. Although there seems to be a diffusion layer formed between the braze and the niobium collector, the joint remained intact. The improved testing environment (5×10^{-9} torr vacuum) probably contributed to the absence of any significant deterioration of the braze, which was observed for the LC-4 and LC-5 converters.

(U) Figures 5C.6(a) and (b) show respectively the post-test appearances of the interface between the Al_2O_3 and the niobium sleeve of the insulator seal, at a location near the cesium vapor and at a location further away from the cesium vapor. It can be seen that at a location near the cesium vapor, the metallizing layer has been corroded severely (Fig. 5C.6(a)), although the metallizing layer appears to be intact at a location further away from the cesium vapor (Fig. 5C.6(b)). The reliability of insulator seals using such a metallizing layer is therefore open to question.

(U) Figure 5C.7 shows the macroscopic appearance of the cesium reservoir tube and its niobium to copper joint made by TIG welding. The location where the failure of the joint occurred is indicated.

(U) After determining that the location of the cesium leak in the converter was in the niobium cesium lead tube to copper cesium reservoir weld as shown in Fig. 5C.7, a sample was cut from the area of the leak location and mounted so that a microstructural examination could be made on a plane coincident with the exterior penetration of the leakage path and along a radius of the cesium lead tube. Examination of the microstructures revealed:

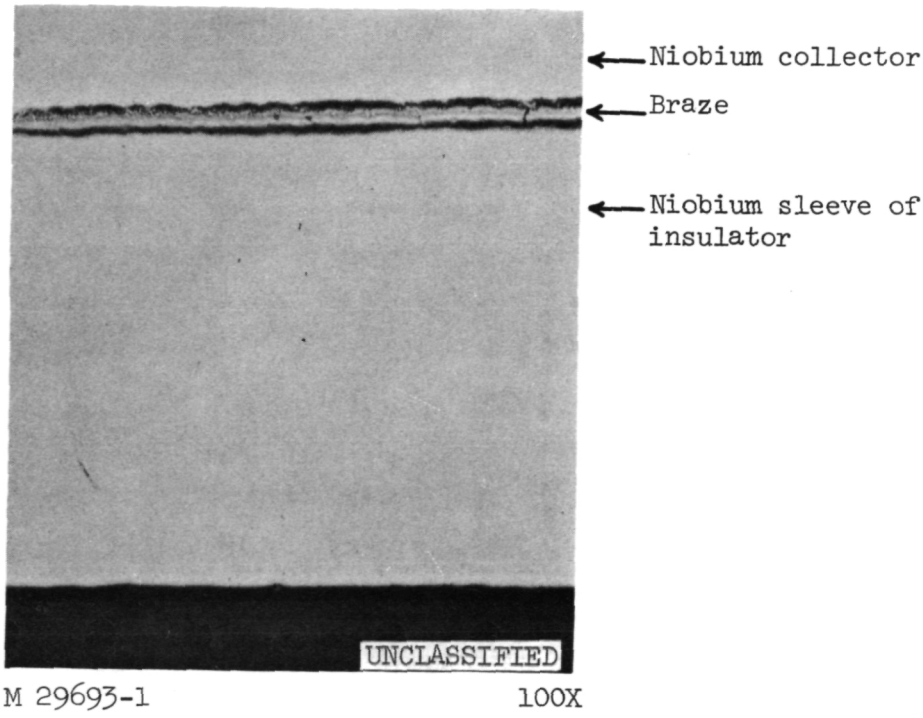

Fig. 5C.5--(U) Post-test appearance of the final closure braze of LC-7 converter

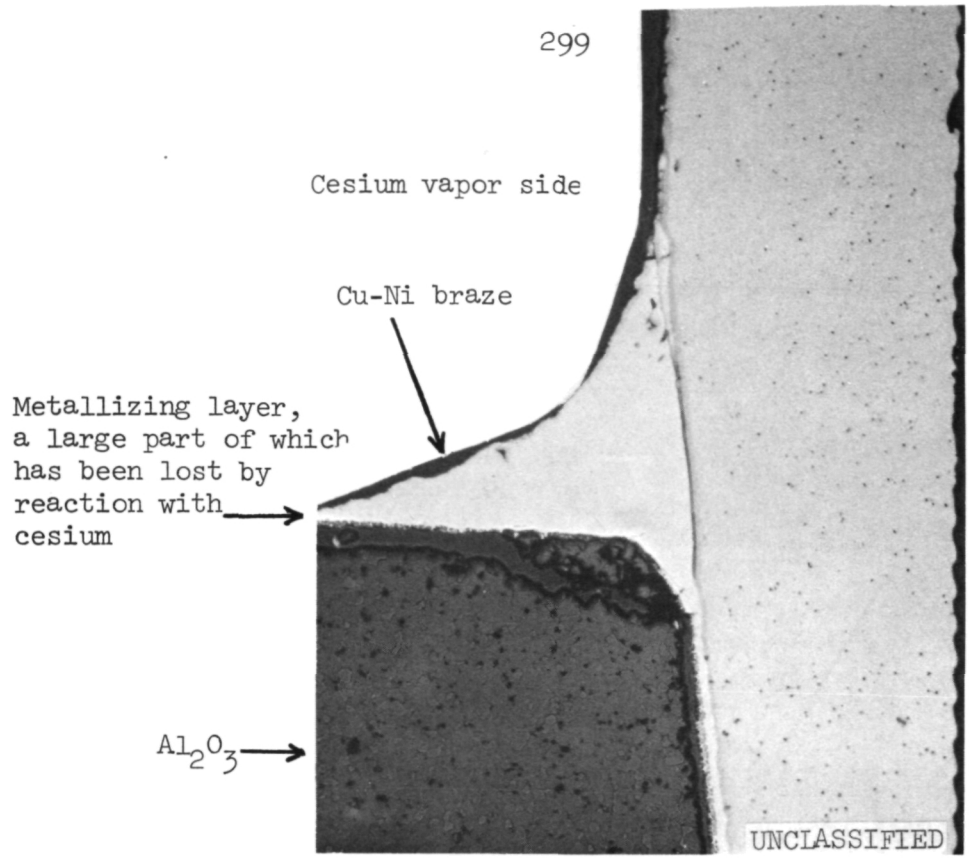

M 29715-1 75X

(a) At a location near cesium vapor

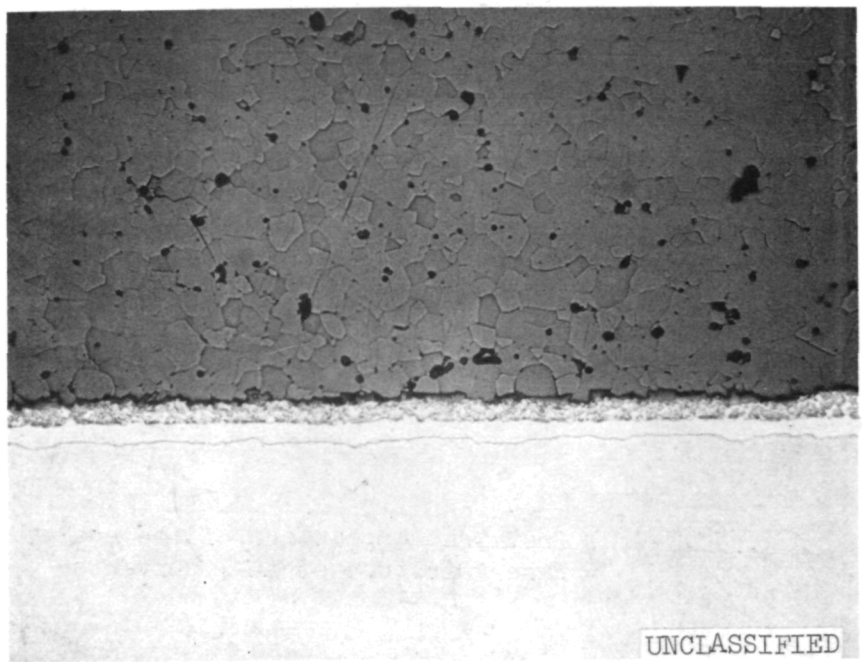

M 29716-1 250X

(b) At a location further away from cesium vapor

Fig. 5C.6--(U) Post-test appearance of the Al_2O_3-niobium interface of the insulator seal of LC-7 converter

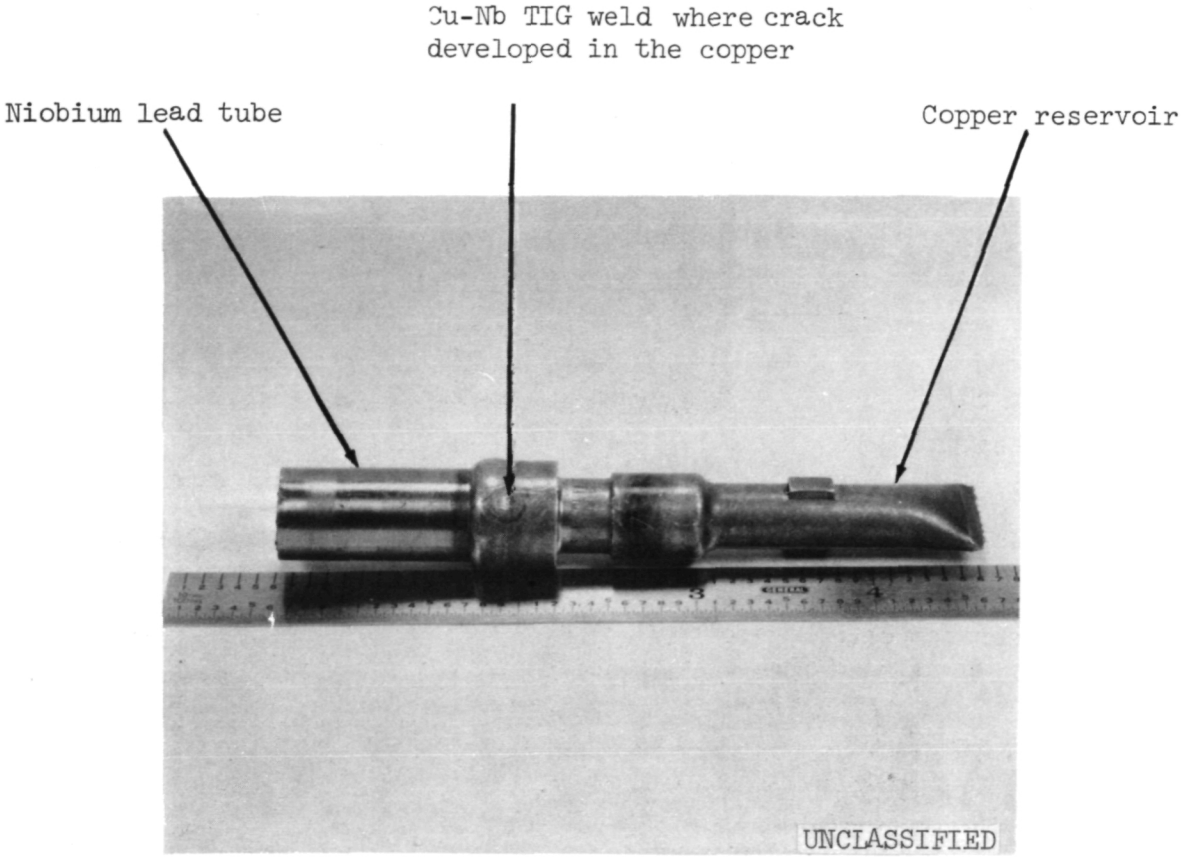

Fig. 5C.7--(U) Post-test appearance of the cesium reservoir tube of LC-7 converter

(a) The niobium to copper interface extended for its full intended length, indicating that the weld had been satisfactorily performed with respect to welding power and electrode position.

(b) The microstructure of the copper weld zone showed a localized concentration (in the region of the leak) of interconnected grain boundary inclusions. These inclusions appeared to be an oxide of copper and in some cases showed evidence of having been leached from the grain boundaries. Example of etched and unetched microstructures of the inclusions are shown in Figs. 5C.8(a), (b) and (c).

(c) There was evidence of mechanical deformation in the region of the inclusions in that there were mechanical or annealing twins present in the structure that showed distortion.

(U) Interpretation of the microstructure yields the conclusion that the cesium leakage path was through the network of oxide inclusions in the copper. A contributing factor was a mechanical working of the structure (already weakened by the presence of oxide in the grain boundaries) resulting from differential thermal stresses because of the thermal expansion difference between copper and niobium.

(U) The volume of oxide present, and its distribution indicated that, if the source of oxygen was the OFHC copper used for the cesium reservoir fabrication the oxygen was present in the form of an isolated inclusion in the raw material. If the source of oxygen was the argon cover gas used for welding, one would expect a more general distribution of oxide that that observed because of the welding technique employed.

(U) In conclusion, the failure of LC-7 was directly attributable to the presence of copper oxide inclusions in the copper of the cesium reservoir to cesium lead tube weld zone which rendered that zone susceptable to cesium corrosion. Another contributing factor was the weld joint design which allowed cyclic thermal stresses to operate in the region of the oxide inclusions. An improved copper-niobium weld joint design should be employed for future converter fabrication. In addition, a hydrogen

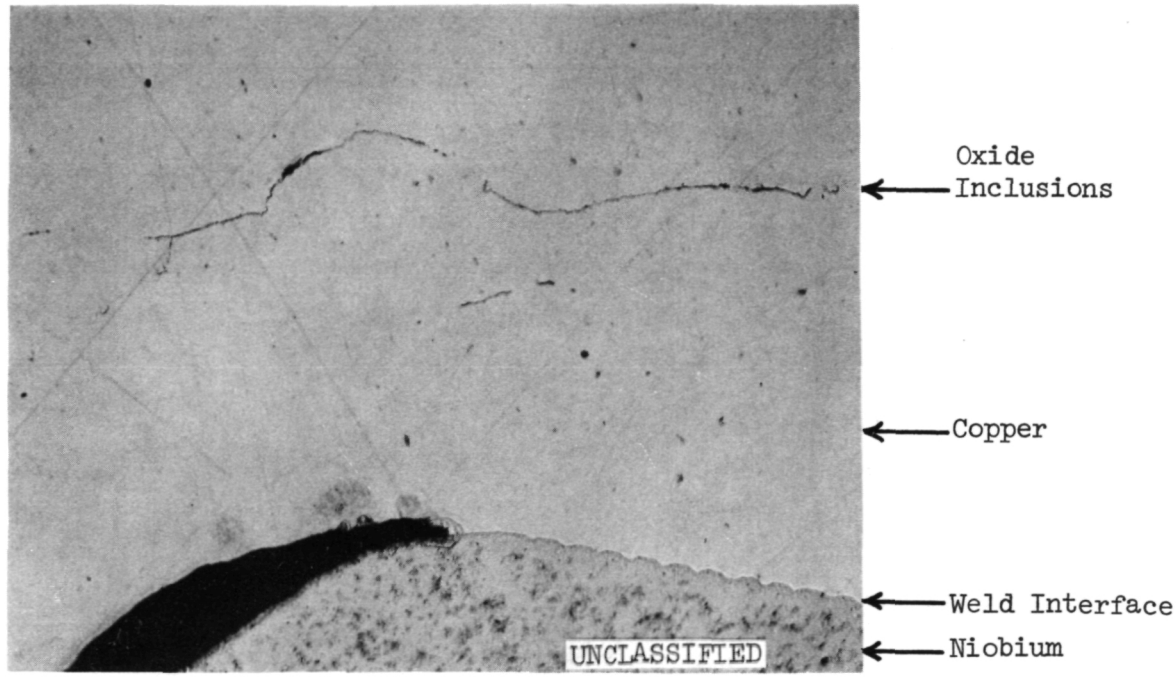

M 52654-1 X75

Fig. 5C.8(a)--(U) Grain boundary oxide inclusions in the LC-7 copper cesium reservoir to niobium lead tube weld. Note the niobium-copper interface integrity

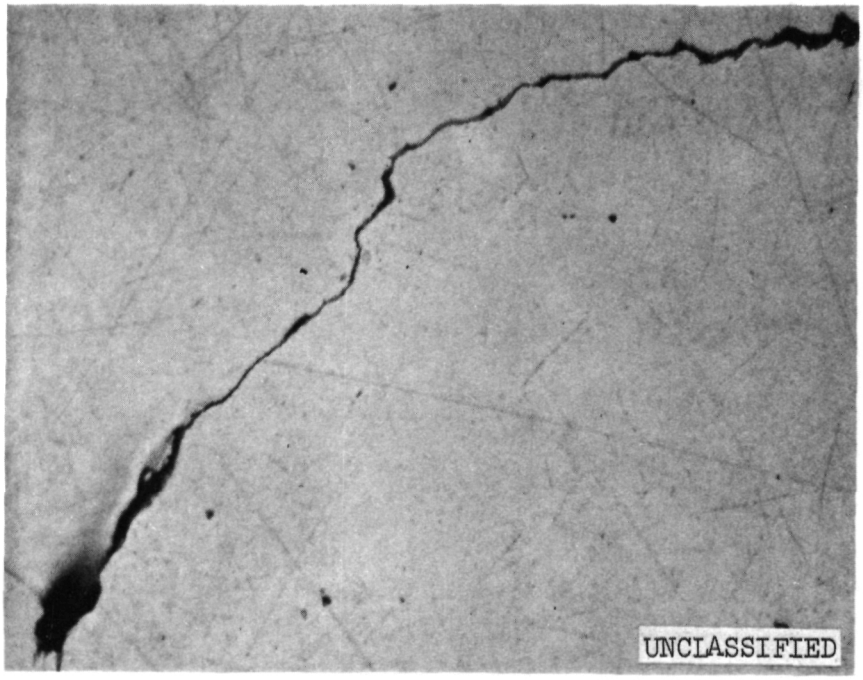

M 25654-4 X500

Fig. 5C.8(b)--(U) Same area as in Fig. 5C.8(a) at higher magnification. The oxide inclusions in the copper grain boundary are visable. In the lower left and upper right hand portions of the view, porosity is apparent

M 25654-8 X75

Fig. 5C.8(c)--(U) Etched microstructure of a portion of Fig. 5C.8(b). Evidence of plastic deformation is shown by the structure of the twins

prefiring at 750°C (followed by a leak check) of all machined copper envelope components should be initiated to insure that components with an isolated oxide inclusion are not employed for converter fabrication. This prefiring at 750°C should preceed the normal 750°C degassing treatment presently employed. It is believed that the subject copper-niobium joints should be electron beam welded to eliminate the possibility of contamination by impure argon cover gas during welding.

DISTRIBUTION LIST

1. NASA Lewis Research Center
Attn: Librarian
21000 Brookpark Road
Cleveland, Ohio 44135
For: J. E. Dilley, MS 302-1 (1)
J. W. R. Creagh, MS 49-2 (1)
J. R. Smith, MS 49-2 (1)
R. Breitwieser, MS 302-1 (1)
R. Mather, MS 500-309 (1)
N. Saunders, MS 105-1 (1)
Technology Utilization Office, MS 3-19 (1)
R. Migra, MS 49-2 (1)
J. Ward, MS 302-1 (1)
R. Forman, MS 302-1 (1)
B. Lubarsky, MS 500-201 (1)
T. A. Moss, MS 500-201 (1)
Report Control, MS 5-5 (1)
Library, MS 3-7 (1)
V. Hlavin, MS 3-14 (1)

2. NASA Washington
Attn: Document Control
600 Independence Avenue, S.W.
Washington, D. C. 20546
For: James J. Lynch, Code RNP (1)
Fred Schulman, Code RNP (1)

3. Jet Propulsion Laboratory
California Institute of Technology
Attn: Central Document Control
4800 Oak Grove Drive
Pasadena, California 91103
For: Jerry Davis (1)
Peter Rouklove (1)

4. NASA Manned Spacecraft Center
Attn: Technical Information Program Division
Houston, Texas 77058
For: Bobby Bragg (1)

5. NASA Electronics Research Center
Attn: Librarian
575 Technology Square
Cambridge, Massachusetts 02139
For: F. C. Schwarz, Code CP (1)

6. NASA Ames Research Center
Attn: Document Control Section
Moffett Field, California 94035
For: Library (1)

7. NASA Goddard Space Flight Center
Attn: Security Officer 236
Greenbelt, Maryland 20771
For: Joseph Epstein (1)
Library (1)

8. NASA Langley Research Center
Attn: Librarian
Langley Field, Virginia 23365
For: Library (1)

9. NASA Marshall Space Flight Center
Attn: Library
Huntsville, Alabama 35812
For: Library (1)

10. NASA Scientific Technical Information Facility
Attn: NASA Representative
P. O. Box 33
College Park, Maryland 20740
For: NASA Representative(2 + Repro)

11. Battelle Memorial Institute
Columbus Laboratories
Attn: Security Officer
505 King Avenue
Columbus, Ohio 43201
For: Don Kizer (1)
Don Keller (1)

12. Battelle Memorial Institute
Pacific Northwest Laboratories
Attn: Technical Information Center
P. O. Box 999
Richland, Washington 99352
For: Library (1)

13. The Boeing Company
Attn: Aerospace Library 8K38
P. O. Box 3999
Seattle, Washington 98124
For: Library (1)

14. Naval Ship Systems Command
Department of the Navy
Washington, D.C. 20360
For: B. B. Rosenbaum, Code 3422 (1)
E. P. Lewis, Code 08 (1)

15. McDonnell Douglas Aircraft Corporation
Missile & Space Engineering Nuclear Research (A2-260)
Attn: Library
3000 Ocean Park Boulevard
Santa Monica, California 90405
For: Library (1)

16. Electro-Optical Systems, Inc.
Attn: Security
300 North Halstead Avenue
Pasadena, California 91107
For: A. Jensen (1)

17. General Electric Company
Missile & Space Division
Attn: Document Control Center
P. O. Box 8555
Philadelphia, Pennsylvania 19101
For: ANSE (1)

18. General Electric Company
Knolls Atomic Power Laboratory
Attn: Document Custodian
P. O. Box 1072
Schenectady, New York 12301
For: R. Ehrlich (1)

19. General Electric Company
Nuclear Systems Program
Attn: J. W. Stephenson
P. O. Box 15132
Cincinnati, Ohio 42515
For: J. A. McGurty (1)

20. General Electric Company
Research Development Center
Attn: Document Control Center
P. O. Box 8
Schenectady, New York 12301
For: Volney C. Wilson (1)

21. General Electric Company
Electronic Components Division
Attn: Document Control
One River Road
Schenectady, New York 12301
For: D. A. Wilbur, Mgr., Tube Research (1)

22. General Electric Company
Atomic Power Equipment Department
Attn: Alleen Thompson
P. O. Box 1131
San Jose, California 95108
For: J. Danko (1)
B. G. Voorhees (1)
J. Van Hoomissen (1)

23. North American Aviation, Inc.
S&ID Division
Attn: Document Control
12214 Lakewood Boulevard
Downey, California 90241
For: C. L. Gould (1)

24. North American Aviation, Inc.
Atomics International
Attn: Document Control
P. O. Box 309
Canoga Park, California 91304
For: Robert C. Allen (1)
Charles K. Smith (1)

25. Oak Ridge National Laboratory
Attn: Library
Oak Ridge, Tennessee 37831
For: Library (1)

26. Office of Naval Research
Power Branch
Department of the Navy
Attn: Code 429
Washington, D. C. 20360
For: CDR O. J. Loper (1)

27. United Aircraft Corporation
Pratt & Whitney Division
Attn: Document Control
400 Main Street
East Hartford, Connecticut 06108
For: Library (1)

28. The Rand Corporation
Attn: Correspondence Control
1700 Main Street
Santa Monica, California 90406
For: Ben Pinkel (1)

29. Republic Aviation Corporation
Fairchild Hiller Division
Attn: Engineering Library
Farmingdale, L. I., New York 11735
For: Alfred Schock (1)
B. Wolk (1)

30. Aerojet General Corporation
San Ramon Plant
Attn: Sandra Johnson
P. O. Box 86
San Ramon, California 94583
For: Library (1)

31. Aerospace Corporation
Attn: Reports Acquisition Group
P. O. Box 95085
Los Angeles, California 90045
For: Library (1)

32. AF Cambridge Research Laboratory
Attn: Chief S&TIS
L. G. Hanscom Field
Bedford, Massachusetts 01730
For: CRZAP (1)

33. AFWL (WLIL)
Kirtland AFB New Mexico 87117
For: WLIL (1)

34. Flight Vehicle Power Branch
AF Aero Propulsion Laboratory
Wright-Patterson AFB Ohio 45433
For: A. E. Wallis (1)

35. Headquarters
Space & Missile Systems Org. (SMTS)
AF Unit Post Office
Los Angeles, California 90045
For: SMTS (1)

36. General Motors Corporation
Research Laboratories
Attn: Security Officer
P. O. Box 866
Warren, Michigan 48090
For: F. E. Jamerson (1)

37. Institute for Defense Analyses
Attn: Document Control
400 Army-Navy Drive
Arlington, Virginia 22202
For: R. C. Hamilton (1)

38. Radio Corporation of America
Attn: Master Document Control
P. O. Box 1140
Lancaster, Pennsylvania 17601
For: Fred Block (1)

39. Babcock & Wilcox Company
Boiler Division
Attn: Document Custodian
5061 Fort Avenue
Lynchburg, Virginia 24505
For: Library (1)

40. Los Alamos Scientific Laboratory
Attn: Mail & Records Group
P. O. Box 1663
Los Alamos, New Mexico 87544
For: G. M. Grover (1)
R. Salmi (1)

41. Marquardt Corporation
Attn: Document Control Station
16555 Saticoy Street
P. O. Box 2013
Van Nuys, California 91409
For: A. N. Thomas (1)

42. Lockheed Missile & Space Company
Attn: Document Control Station
P. O. Box 504
Sunnyvale, California 94088
For: H. H. Greenfield (1)

43. TRW Systems
Attn: Manager Technical Information Center
One Space Park
Redondo Beach, California 92078
For: M. N. Sloane, Chief Librarian (1)

44. U. S. Army ERDL
Attn: Security Officer
Fort Monmouth, New Jersey 07703
For: Emil Kittl (1)

45. Mr. Donald S. Beard
Space Nuclear Systems Division
U. S. Atomic Energy Commission
Washington, D. C. 20545 (1)

46. Mr. Patrick O'Riordan
Space Nuclear Systems Division
U. S. Atomic Energy Commission
Washington, D. C. 20545 (1)

47. Mr. J. M. O'Leary
U. S. Atomic Energy Commission
Technical Reports Library
Washington, D. C. 20525 (3)

48. U. S. Atomic Energy Commission
Division of Technical Information Extension
P. O. Box 62
Oak Ridge, Tennessee 37831 (3)

49. Varian Associates
Attn: Document Control
611 Hansen Way
Palo Alto, California 94303
For: Ira Weismann (1)

50. Westinghouse Electric Corporation
Astro-Nuclear Laboratory
Attn: Document Custodian
P. O. Box 10864
Pittsburgh, Pennsylvania 15236 (1)

51. Thermo Electron Engineering Corporation
Attn: Security Officer
P. O. Box 482
Waltham, Massachusetts 02154
For: George Hatsopoulos (1)
Robert Howard (1)

CONFIDENTIAL

CONFIDENTIAL

RESTRICTED DATA
ATOMIC ENERGY ACT 1954
GROUP 1